Continuous Radial Flow Chromatography

A thesis submitted in partial fulfilment

of the requirements for the degree of

Doctor of Philosophy

in Materials and Process Engineering

by

Mark Lay

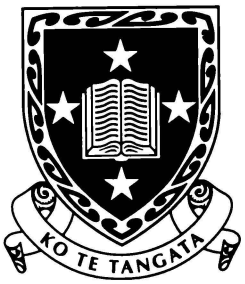

The
University
of Waikato
Te Whare Wānanga
o Waikato

Hamilton, New Zealand

March 2005

Abstract

A prototype of a continuous radial flow chromatograph (CRFC) was developed consisting of a rotating annular bed (14.6 cm O.D., 8.6 cm I.D. and 2 cm deep). A protein-laden feed, equilibration and elution buffer flow radially inwards from a feed chamber at the periphery towards an exit chamber at the axis. Bed movement past fixed feed and exit points allows continuous separation of components from a feed mixture.

Continuity equations describing CRFC performance were developed using two resin-solute interaction models. Adsorption was described in both models by the multicomponent Langmuir-Freundlich isotherm (MLF). In the first model (NP) the resin was treated as non-porous and in the second (FD) the resin was porous and mass transfer between flowing solution and resin pores was described by film-diffusion. These models were solved using a finite difference method.

Adsorption isotherm and rate parameters were obtained from batch equilibrium, kinetic and axial flow column breakthrough and elution experiments using bovine serum albumin (BSA) and DEAE Sepharose Fast Flow resin. Because MLF caused model instability in breakthrough simulations, the multicomponent Langmuir isotherm (ML) was used. Good agreement was found with axial column breakthrough and elution experiments. NaCl breakthrough was best described by the FD-ML model. Bed dispersion was masked by extra-column dispersion effects.

Breakthrough and elution experiments showed that the CRFC had poor resolution when operated in batch mode, due to slow solute distribution in the feed and exit chambers. BSA uptake rates determined by curve fitting were 30 times lower than those found in axial column experiments, indicating poor resolution.

FD-ML parameters obtained from continuous extraction of BSA agreed well with data from axial column experiments. CRFC performance can be predicted from small axial column data.

The CRFC was used to continuously separate BSA from lactoferrin. 85% of BSA was recovered from the mixture at 94% purity, with a separation factor of 4.8.

Acknowledgements

I would like to thank my supervisor, Assoc-Prof. Conan Fee, for letting me embark on this project and giving me wide latitude, encouragement, jobs and lots of time for editing. Assoc-Prof. Janis Swan for her extremely valuable editing and writing tips. Everyone from the Co-operative Education Unit, in particular, Dr Richard Chapman, for giving me a job for three years that enabled me to do my PhD and Assoc-Prof. Richard Coll for conspiring with people in high places for PhD funding and for providing interesting little black science education projects. Professor Richard Price for agreeing to fund me for the rest of my PhD. Sarah Tofield, for making life entertaining with stories of credit card abuse, car crashes and so on. Karsten Zegwaard, an avid Christian who shared my office for several years, for keeping the old intellect sharp in big debates over who was going to go to hell first and creationism. The science workshop crew, for letting me run amok in the workshop, Chris Sistern for building and repairing the CRFC and teaching me how to dimension technical drawings properly, Brian Clark for letting Chris spend so much time on the CRFC and giving me jobs, and Callum Turnbull for brightening lunchtime and tea breaks with his sordid tales of sin and debauchery. The beloved secretaries, Mary Dalbeth, Lesley Falconer and Cathy Shaw, the department technicians, namely Brett Nichols, Jijian Lu, Lisa Lee, and computer support, Brett Loper and Ai-Phing Wood for their most excellent services. Dr Rob Torrens, for providing this poor student with plenty of jobs to do. The department academics, namely Dr Kim Pickering, Dr Johan Verbeek and Dr Brian Gabbitas for their cheerful encouragement, advice and extra-curricular activities. All the students, namely Amita Chand, Marion Buckley-Smith, Zuben Weeds, Meme Nilawongsee, and Darin Sutherland, for their entertaining philosophical tea-room conversation and support.

The Edwards, Lau and Salehi families, surrogate parents and providers of many meals. All the Baha'i youth for keeping life entertaining and Masood Masoodian for keeping weekends busy with home improvement, and providing tasty food.

And last but not least, my beloved family, without whom I would not have existed, who kept me fed and clothed and did all the good things that good parents do.

Contents

List of Figures

List of Tables

Nomenclature

A_b	Solute A bound to packed bed
A_f	Solute A free in solution
A_r	Area in radial direction (cm^2)
A_{re}	Area in radial direction for an annular segment (cm^2)
A_R	Total spherical area of resin particles (cm^2)
A_{RP}	Spherical area of a resin particle (cm^2)
A_z	Area in axial direction (cm^2)
A_θ	Area in angular direction (cm^2)
C_A	Solution concentration of solute A in solution (mg/ml)
C_A^*	Solution concentration of solute A at equilibrium (mg/ml)
$C_{elution}$	Elution buffer concentration (mg/ml)
C_{exA}	Exit concentration of solute A (mg/ml)
C_{feed}	Feed concentration (mg/ml)
C_{RPA}	Resin pore concentration of solute A (mg/ml)
C_{RA}	Resin phase concentration of solute A (mg/ml)
C_{RA}^*	Resin phase concentration of solute A at equilibrium (mg/ml)
C_{RAmax}	Resin phase concentration of solute A at saturation (mg/ml)
d_p	Resin particle diameter (cm)
D	Number of sections in the feed and exit chambers
D_{Ar}	Dispersion in radial direction (cm^2/s)
D_{Az}	Dispersion in axial direction (cm^2/s)
$D_{A\theta}$	Dispersion in angular direction (cm^2/s)
D_{eff}	Effective solute pore diffusivity (cm^2/s)
D_{mA}	Molecular diffusivity (cm^2/s)
D_{pA}	Pore diffusivity (cm^2/s)
D_{sA}	Surface diffusivity (cm^2/s)
H	Packed bed height (cm)

J	Time divider (dimensionless)
J_A	Mass flux due to diffusion (mg/cm^2.s)
$J_{A\theta}$	Mass flux due to diffusion /dispersion in angular direction (mg/cm^2.s)
J_{Ar}	Mass flux due to diffusion/dispersion in radial direction (mg/cm^2.s)
J_{Az}	Mass flux due to diffusion/dispersion in axial direction (mg/cm^2.s)
k_{fA}	Film mass transfer coefficient (cm/s)
k_{ext}	External film mass transfer coefficient (cm/s)
k_{int}	Internal pore mass transfer coefficient (cm/s)
k_{A1}	Solute uptake rate by packed bed (ml/mg.s) (has the dimensions of 1/s when used as a first order rate constant)
k_{A2}	Solute desorption rate from packed bed (1/s)
K_A	Equilibrium constant (ml/mg), subscripts s and p refer to salt and protein respectively. (dimensionless when used in equations by Huang, Lee *et al.* (1988a), Howard *et al.* (1988) and Carta *et al.* (1989))
K_d	Desorption parameter (ml/mg)
L	Axial bed depth (cm)
m	Time or angular step (dimensionless)
M	Total number of time or angular steps (dimensionless)
M_{ad}	Angular position of dividers in terms of angular steps (dimensionless)
M_{rev}	Number of time or angular steps per revolution (dimensionless)
$M_{section}$	Number of time or angular steps per section (dimensionless)
M_{secfin}	Time or angular step at which a section finishes (dimensionless)
$M_{secstart}$	Time or angular step at which a section starts (dimensionless)
n	Stage number (dimensionless)
n_A	Fitting parameter (dimensionless)
N	Total number of stages (dimensionless)
N_{as}	Total number of angular segments (dimensionless)
N_{max}	Maximum number of stages (dimensionless)
Q	Flow-rate (ml/s)
Q_e	Flow-rate through an element (ml/s)
r	Radius (cm)

r_1	Outside radius of annular packed bed (cm)
r_2	Inner radius of annular packed bed (cm)
r_A	Annular column radius (cm)
r_c	Axial column radius (cm)
R	Radial position in a resin particle (cm)
Re	Reynolds number (dimensionless)
R_p	Resin particle radius (cm)
s	Angular segment (dimensionless)
S_{ad}	Position of dividers in terms of angular segment position (dimensionless)
S_{secfin}	Angular segment at which a section finishes (dimensionless)
$S_{secstart}$	Angular segment at which a section starts (dimensionless)
Sc	Schmidt number (dimensionless)
Sh	Sherwood number (dimensionless)
t	Time (s)
t_{run}	Simulation run time (s)
T	Sintered wall thickness (cm)
u	Superficial velocity (cm/s)
v	Interstitial velocity (cm/s)
V	Volume (ml)
V_e	Element volume (cm^3)
V_R	Resin volume (cm^3)
V_{Rp}	Resin particle volume (cm^3)
w	Rotational speed (degrees per second)
y_1	Molecular diffusion coefficient (dimensionless)
y_2	Turbulent dispersion coefficient (dimensionless)
z	Axial position (cm)

Greek

ε_o	Void fraction of resin in stirred tank (dimensionless)
ε_P	Internal pore fraction of resin (dimensionless)

ε_R	External void fraction of resin (dimensionless)
ε_{sw}	Pore fraction of sintered wall (dimensionless)
ϕ	Angle rotated (degrees)
ϕ_{div}	Angle of outer divider relative to inner divider (degrees)
ϕ_p	Angular position (degrees)
γ	Resin pore tortuousity (dimensionless)
η	Viscosity (kg/m.s)
λ	Dispersion coefficient
π	Constant (3.142)
θ	Angle (radians or degrees)
θ_{max}	Total angle of annulus in radians (2π) or degrees
ρ	Density (g/ml)

Subscripts

A	Solute A
B	Solute B
est	Estimate
FM	Flow manifold
IEC	Inner exit chamber
isw	Inner sintered wall
osw	Outer sintered wall
OFC	Outer feed chamber
P	Resin pores
r	Radial direction
R	Resin
z	Axial direction
θ	Angular direction

Chapter 1

Introduction

1.1 Background

As the fields of biotechnology, genetics, and medicine advance, many new biologically derived compounds of medicinal or nutritional value have become available. These compounds are isolated from feedstocks such as fermentation broth, animal blood or milk. Separation and purification of these compounds may take many steps for a product that meets with regulatory approval. Purification and recovery can amount to half the capital expenditure in processing equipment and 80% of the total cost of manufacturing.

Chomatography is a mainstream process in the biotechnology, pharmaceutical and food industries because of its separating power and versatility. Separation of compounds from a mixture is achieved on the basis of their different rates of migration through a separating medium. Such rates are influenced by factors such as the size and charge of a molecule and its affinity for the separating media.

When chromatographic systems are scaled up from traditional laboratory-scale columns (2 ml – 2 l) to pilot or large scale (two to several thousand litres) they can suffer from low throughput, high pressure drops, fouling, low resolution and inefficient use of the separating medium.

Several innovative strategies have been developed to overcome these issues. These include:

- Alternate flow geometries such as radial flow chromatography to allow greater throughput.
- Fluidised and expanded bed chromatography to reduce pressure drops and column fouling.
- Continuous chromatographic techniques, such as simulated moving bed and rotating annular bed chromatography, to obtain continuous separation and purification of a product and more efficient use of the separation media.

Lay (1998) developed a new technology named continuous radial flow chromatography (CRFC). This combines radial flow and rotating annular bed chromatography into one

system (Figure 1-1). The CRFC is operated like a rotating annular bed chromatographic system, except that solution flows radially through the annular bed rather than axially. It has the advantages of batch radial flow columns and a continuous process, and eliminates the need for complex control systems typically associated with automated batch chromatographic systems and simulated moving bed chromatography. The main features distinguishing CRFC from rotating annular bed chromatography are

- Shorter bed depth reducing pressure drop, allowing greater throughput and/or the use of soft gels.
- Easier packing because the fluid distribution system does not need to be removed to pack the bed. Also the CRFC can be pump packed whilst rotating annular bed chromatographic systems can only be slurry packed.

Several proposals for technologies similar in principle to the CRFC exist in the patent literature (see Mosier 1963; Sussman 1970; Tuthill 1970), but only one, called continuous disc chromatography, was developed to a prototype stage (Sussman and Rathore 1975; Sussman 1976). This used rotating solvent coated glass discs to continuously separate gaseous mixtures applied at the centre of the apparatus. Differences between the CRFC and continuous disc chromatography are shown in Table 1-1.

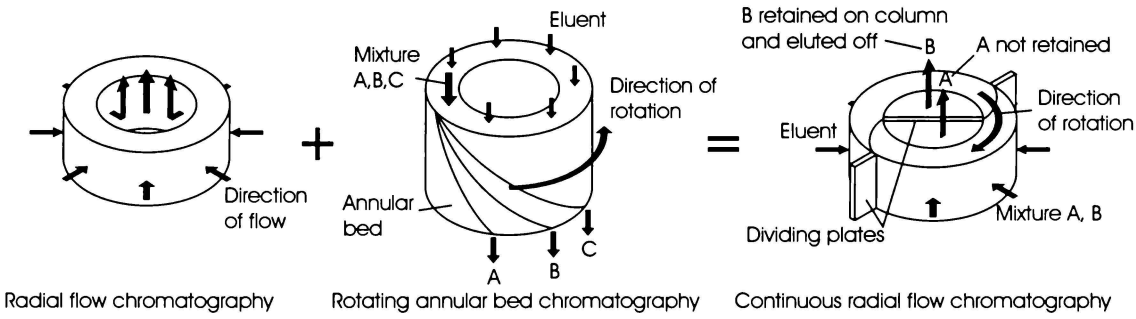

Figure 1-1. Combination of radial flow and annular rotating bed chromatography to develop the concept of the CRFC.

Table 1-1. Differences between continuous disc chromatography and continuous radial flow chromatography.

	Continuous disc chromatography	Continuous radial flow chromatography
Mobile phase	Gas	Liquid
Separation media	Solvent coated glass discs	Resin packed annular bed
Separation type	Isocratic	Step elution
Separation	Volatile organics	Water soluble compounds
Flow direction	Outward	Inward

1.2 Problem statement

An initial prototype of the CRFC was constructed and tested (Lay 1998), from which a number of engineering problems were identified which needed solving:

- The prototype was not robust and prone to mechanical failure. Additionally, the motors used did not have sufficient torque to rotate the annulus at low rotation speeds because of the friction generated by sealing the moving parts of the system.
- Low separation capability due to a short bed depth and fast rotation speeds.
- The feed and exit chamber configuration only allowed binary separations
- Bed channelling could not be detected because of large feed and exit chamber volumes.

When developing a new technology it is useful to simulate it using mathematical models. This allows the process to be optimised and enables predictions on how the technology will perform under different conditions without expending resources in extensive experimentation. Although both radial and rotating annular bed chromatography have been modelled (Bloomingburg and Carta 1994; Gu 1995; Tsaur and Shallcross 1997b), no mathematical models exist for the CRFC. In addition, radial

flow models have only been verified using salts, none have been tested using proteins. This is surprising given that chromatography is commonly used to separate protein mixtures, and that mass transfer resistances are likely to be higher for proteins due to the their large size, low diffusivity and high visocosity as compared to salt.

1.3 Research objectives

Based on the areas identified in the problem statement, the objectives of this thesis were threefold:

1. To develop and construct a new prototype of the CRFC which was more robust, performed better than the first prototype, and could be used in separating proteins.

2. To model the new prototype using finite difference techniques. The interaction of protein with the separation media would be modelled using well-established equations such as the Langmuir isotherm. The overall model would be used to predict CRFC performance under different operating conditions.

3. To apply the CRFC to extracting and eluting a model protein and separating a binary mixture of proteins.

1.4 Organisation of this thesis

A review of technologies upon which the CRFC is based is presented in Chapter Two. These include radial flow and rotating annular bed chromatography. Applications and modelling of these technologies are examined. In addition, similar mooted concepts are presented and compared to the CRFC.

The first CRFC prototype and problems encountered during testing are described in Chapter Three. Design features of the new prototype are detailed and comparisons between the two prototypes are discussed.

Continuity equations for the CRFC are developed in Chapter Four as well as additional equations relevant to the experimental work. Two approaches are presented in

modelling solute interaction with the chromatographic media. The first considers the media as solid spheres while second treats them as porous. Both use a multicomponent Langmuir-Freundlich isotherm to describe uptake of solute between solution and resin matrix. The second accounts for film diffusion of solute between the bulk solution and the resin pores. Conversion of the continuity equations into finite difference models is also presented.

The experimental methods used to test the new CRFC design are presented in Chapter Five. The interaction of a model protein with chromatographic media was investigated using adsorption isotherm, rate kinetic and small column breakthrough and elution experiments. The CRFC was operated in batch and continuous modes. Breakthrough and elution experiments were performed in batch mode. The extraction of a model protein from solution and the separation of two proteins were then studied in continuous mode.

Experimental results and model comparisons are given in Chapter Six and implications of findings and suitability of the models used are discussed. Model predictions of CRFC performance are shown to be comparable to experimental results and one set of model parameters could be used for a range of continuous operating conditions.

Conclusions obtained from this research are presented in Chapter Seven, along with recommendations for future work.

Chapter 2

Literature Review

2.1 Introduction

Traditionally, chromatographic separations are performed in axial flow columns. These columns are scaled-up for pilot and large scale separations by increasing column length and diameter. When scaling-up, the increase in back-pressure with bed length needs to be addressed. This back-pressure comes from forcing fluid through interstices between packed bed resin particles. Robust columns and resin are needed to withstand the high pressures; otherwise flow through the column must be reduced. Several approaches can be used to reduce bed back-pressure, such as using larger resin particles or macro-porous resin, and having short bed depths and large column diameters.

One development in chromatography is radial flow systems. These systems have an annular bed with solution flowing radially from the periphery to the centre or vice versa. They have a short bed depth and large area available for flow, allowing fast separations and low pressure drops. A variety of separations have been performed using radial flow.

Chromatography is traditionally a batch-wise technique involving sequential application of equilibration buffer, feedstock, and a series of elution buffers. Unless the process is highly optimised, batch operation means only a small section of the packed bed is used for the separation while the rest acts as a conduit, an inefficient use of the separation medium (Barker and Ganetsos 1988).

The bed can be used more efficiently by converting chromatography into a continuous process. A continuous process can be achieved by moving a chromatographic bed counter-current, co-current or cross-current to fluid flow (Sussman and Rathore 1975; Sussman 1976; Bridges and Barker 1993). Bed motion relative to the feed and exit points translates the time-dependent migration of a mixture of compounds into a physical displacement. This allows individual compounds to be collected at different positions along the column. Rotating annular bed chromatography is one example of a successfully developed cross-current apparatus. It has been widely applied and its behaviour is well understood.

The CRFC combines radial flow and rotating annular bed chromatography into one system. Therefore, this chapter reviews the development, application and modelling of

these two technologies so design factors for the CRFC, CRFC performance, and how it might be modelled can be understood.

Radial flow chromatography can be categorised into four types, based on configuration. The first three (fixed-bed; thin-layer; and spinning disc/bed radial flow chromatography), are batch techniques involving sequential application of feed and elution buffers. Fixed-bed systems use pump pressure to push solution through the bed; thin-layer uses capillary action; and spinning disc/bed systems use centrifugal forces generated when the bed is rapidly rotated about its axis. The fourth type, which includes CRFC and continuous disc chromatography, is a continuous cross-current technique where the bed rotates past stationary feed and elution points. Fixed bed and continuous radial flow techniques, along with rotating annular bed chromatography are the main focus of this literature review. Thin-layer and spinning disc systems are briefly mentioned for completeness. Modelling aspects of radial flow and rotating annular bed chromatography are discussed and specific examples of models are presented.

2.2 Fixed bed radial flow chromatography

Fixed bed radial flow chromatography systems consist of three concentric annular chambers: a feed chamber, a packed bed, and exit chamber, separated by two porous cylinders that contain the resin bed (Figure 2-1). Solution is applied under pressure at the top of the system and directed to the feed chamber through a series of spreaders, before flowing radially through the bed into the exit chamber at the centre, and out through the base of the column. Flow direction can be reversed depending on processing requirements (Saxena and Dunn 1989). The annular bed can be packed with chromatographic resin, continuous or monolithic chromatographic media (Podgornik *et al.* 2000; Gustavsson and Larsson 2001), or membrane material with chromatographic ligands attached (Sun *et al.* 2000c).

Fixed bed radial chromatography is well established with several companies marketing these systems, including LKB, Sweden (Jungbauer *et al.* 1988), Cuno Inc. (Huang *et al.* 1988b; Lee *et al.* 1990), Convection Interaction Media by BIA Separations, Slovenia

(Podgornik *et al.* 1999), Sartorius (Demmer and Nussbaumer 1999) and Sepragen (Akoum *et al.* 1989).

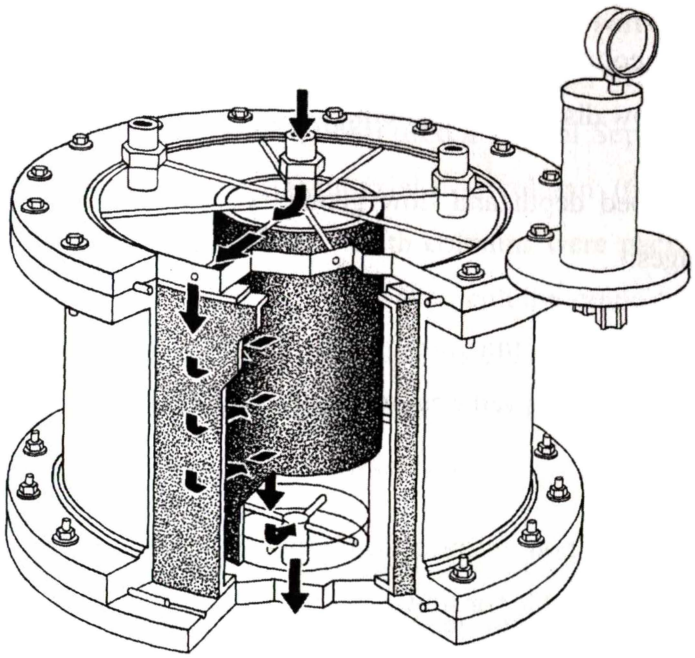

Figure 2-1. Sepragen radial flow Superflo chromatography column (Saxena and Dunn 1989).

The main features distinguishing radial flow systems from traditional axial flow columns are short bed depth, high cross-sectional area normal to solution flow and flow geometry. These result in low pressure drop through the bed which provides the following advantages (Ponzi and Kaye 1979; Saxena and Dunn 1989; Levison 2003):

- Allows the use of soft gel or compressible resin.
- Gives greater throughput per unit volume of column bed, hence faster process times.
- Reduces capital costs because smaller columns can be used.
- Allows biological compounds sensitive to proteolysis to be separated and purified quickly.

- Allows easy scale-up. Column height can be increased without altering performance provided column diameter and overall superficial velocity of solution through the bed is not changed.

- Allows easy column packing. The column can be packed without having to remove the flow distribution system.

The short effective bed depth and flow geometry of radial flow columns also have several disadvantages:

- Column resolution, a function of bed depth, is lower than conventional axial flow columns, which reduces separation capability in isocratic and gradient elutions.

- The possiblity of non-uniform flow around the annular bed increases because greater area is available for flow.

- Channelling at the top of the bed can occur due to resin settling.

- The changing superficial velocity in the bed can affect uptake kinetics and dispersion.

In the following sections the effects of short bed depth, flow geometry, scale-up, packing and elution type on column performance are reviewed. Applications of fixed bed radial flow chromatography are also reviewed.

2.3 Short bed depth

Short bed depths and large cross sectional areas are used in radial flow chromatography to reduce back-pressure and increase throughput. This allows high flowrates, which reduces processing times and capital costs. Quick processing times decrease losses due to protein degradation. However, flowrate is limited by solute diffusion and adsorption kinetics in the resin, which are dependent on separation media and feedstock. Fast flowrates can lead to early breakthrough and low resolution at low diffusion and adsorption rates.

2.3.1 Rapid separation

Radial columns operate at low pressures because of their short bed depth and large cross-sectional area available for flow. This allows the use of soft compressible gels or high flowrates, which result in faster separations (Saxena and Weil 1987; Saxena and Dunn 1989). For example, Lane *et al.* (1990) used a 100-ml Sepragen Superflo radial flow column (3 cm bed depth) and a 100-ml axial flow column (6.6 cm long by 4.4 cm I.D.) to separate protein from egg whites. Both columns were packed with Whatman DE52 and QA52 resin. They found the radial flow column could be run at five times the flowrate of the axial column (Table 2-1) (also cited by Levison 2003), but the axial flow column, having a longer bed depth than the radial flow column, exhibited better resolution under gradient elution conditions (Figure 2-2).

Table 2-1. Pressure/flowrate data for chromatography of egg-white proteins on DE52 and QA52 under axial and radial flow conditions (Levison 2003).

Flowrate (ml/min)	Pressure (kPa)			
	DE52 column		QA52 column	
	Axial	Radial	Axial	Radial
5	7	-	7	7
15	34	7	34	28
25	97	7	117	28
50	>310	7	>310	28
100	-	41	-	124
150	-	41	-	138

Planques *et al.* (1991) adapted an axial flow technique for radial flow purification of plasminogen from human plasma for radial flow. They used a Zetaffinity 250-ml radial flow membrane cartridge with lysine as the ligand and recovered greater than 85% of the plasminogen with a 110-fold increase in specific activity. Flowrates of 20 ml/min were achieved compared with 1.25 ml/min obtained by Deutsch and Mertz (1970) with an axial flow column.

Faster separation times mean smaller columns can be used, which reduces capital cost, and increases the separation cycles that can be performed in a day (Table 2-2) (Saxena and Dunn 1989; Podgornik *et al.* 2000).

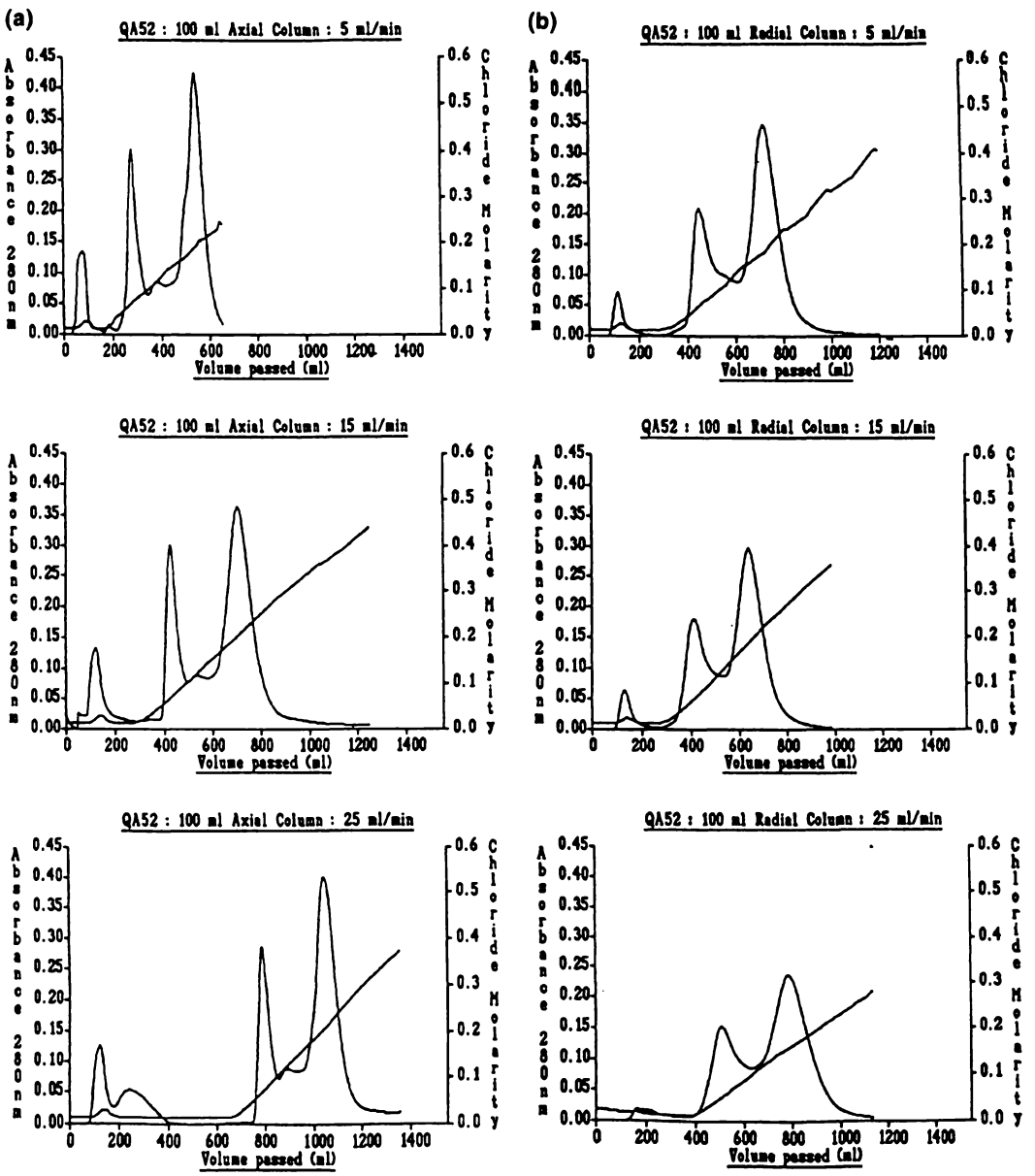

Figure 2-2. Chromatography of hen egg-white proteins on QA52 in 0.025M Tris-HCL buffer, pH 7.5 at flowrates of 5-25ml/ml in (a) 100 ml axial flow column (6.6 cm I.D.) and (b) 100 ml Superflo-100 radial flow column (Levison 2003).

Table 2-2. Comparison of production economics of radial and axial flow columns on pilot and large scale (Saxena and Dunn 1989).

	Axial Flow Column	Radial Flow Column
Pilot scale		
Flow rate (L/hr)	25	75-95
Production rate (L/shift)	117	350
Column size (L)	16	20
Large scale		
Flow rate (L/hr)	200	200
Production rate (L/shift)	1000	1000
Column size (L)	160	60

2.3.2 Limiting protein degradation

Short separation times reduce protein degradation due to proteolysis (Jungbauer *et al.* 1988; Saxena and Dunn 1989). This was demonstrated by Akoum *et al.* (1989) and by analysing data from Sun *et al.* (2000 a,b,c) detailed below.

Akoum *et al.* (1989) used a 400-ml Sepragen radial flow column and an 80-ml axial flow column (16 cm long by 2.5 cm I.D.) packed with Sepharose-4B, a soft gel matrix, with a histidine ligand, to purify myxalin. Flowrates for the radial and axial flow columns were 1200 ml/hr and 80 ml/hr respectively and the residence time for the radial flow column was one third that of the axial flow column. They obtained faster separation times, higher percentage activity yields and higher specific activity when myxalin was purified in radial flow columns.

Sun *et al.* (2000 a,b) used a 50-ml Sepragen Superflo radial flow column (1.2 cm bed depth) and a XK26/20 (2.5 cm bed depth) and 5ml HiTrap (3 cm bed depth) axial flow column (Amersham Biosciences, Uppsala, Sweden) packed with Q sepharose and DEAE sepharose to separate human prothombin from Nitschmann fraction III. They varied the flowrates, loading volumes and packing type, and found loading capacity per unit volume media was independent of flow geometry. They concluded radial flow showed good potential for separating prothombin.

An analysis of Sun *et al.*'s (2000 a,b) data in terms of specific activity, loading times and superficial velocities showed that faster separation times gave greater prothombin activity (Figure 2-3). The HiTrap column packed with Q Sepharose gave greater prothombin activity, faster separation times, and eluted three to four times more concentrated prothombin (Figure 2-4) than the radial flow column with the same packing. The specific activities were similar when DEAE Sepharose packing was used, but the XK26/20 column gave better elution concentrations than the radial flow column. These results showed that the radial flow column had poor resolution. Also, only a small range of superficial velocities were used for the radial flow columns, suggesting loading flowrates had to be kept low to prevent early breakthrough.

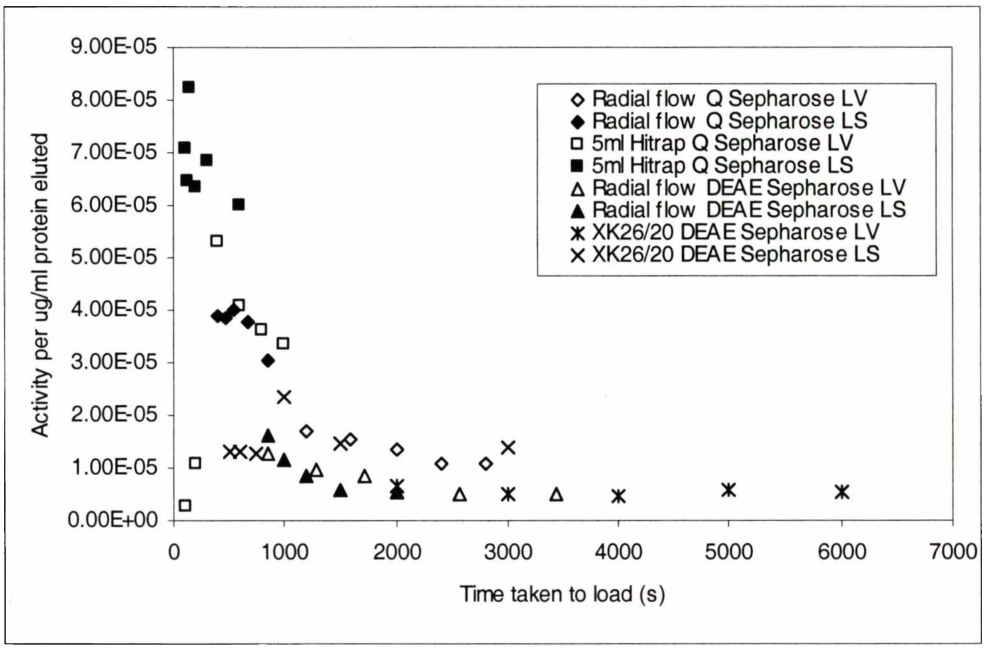

Figure 2-3. Effect of sample loading time on specific activity of human prothrombin extracted from Nitschmnann fraction III in radial flow and axial flow columns packed with Q sepharose and DEAE sepharose (LV: loading volume varied, LS: loading flowrate varied). Calculations based on data from Sun *et al.* (2000a,b).

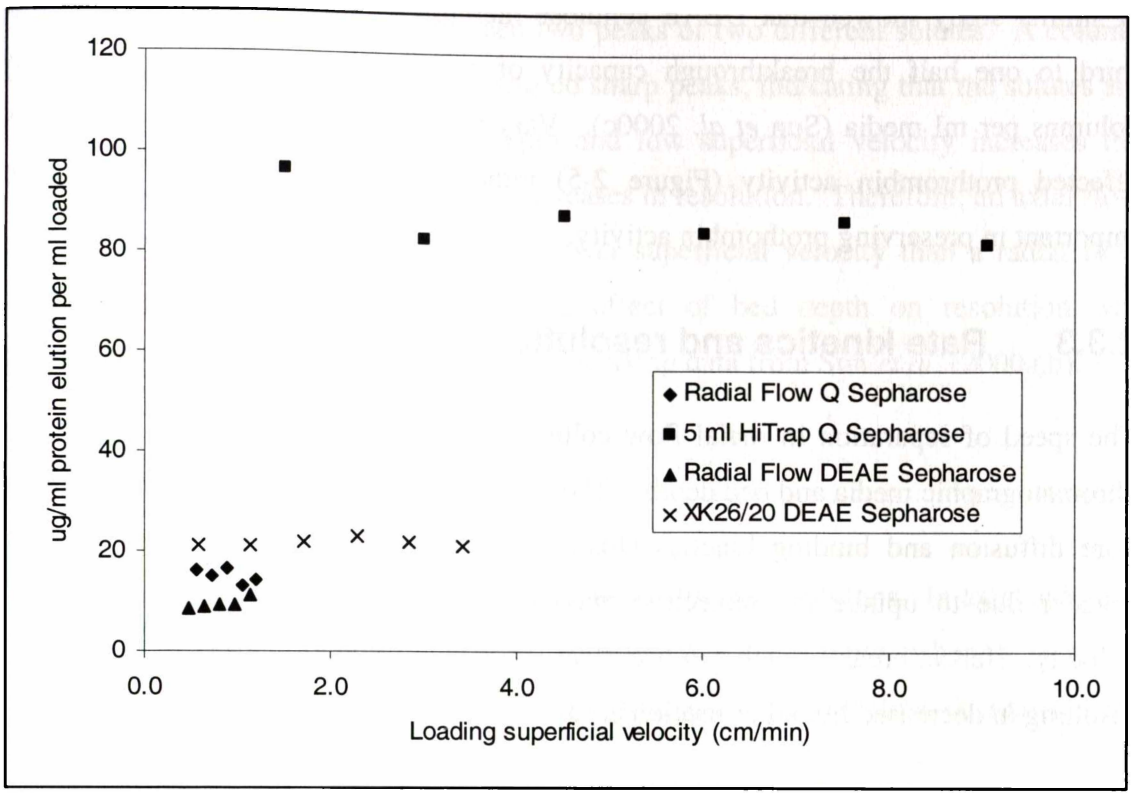

Figure 2-4. Effect of superficial velocity on concentration of prothrombin eluted in radial flow and axial flow columns packed with Q Sepharose and DEAE Sepharose. Calculations based on data from Sun *et al.* (2000b; 2000a).

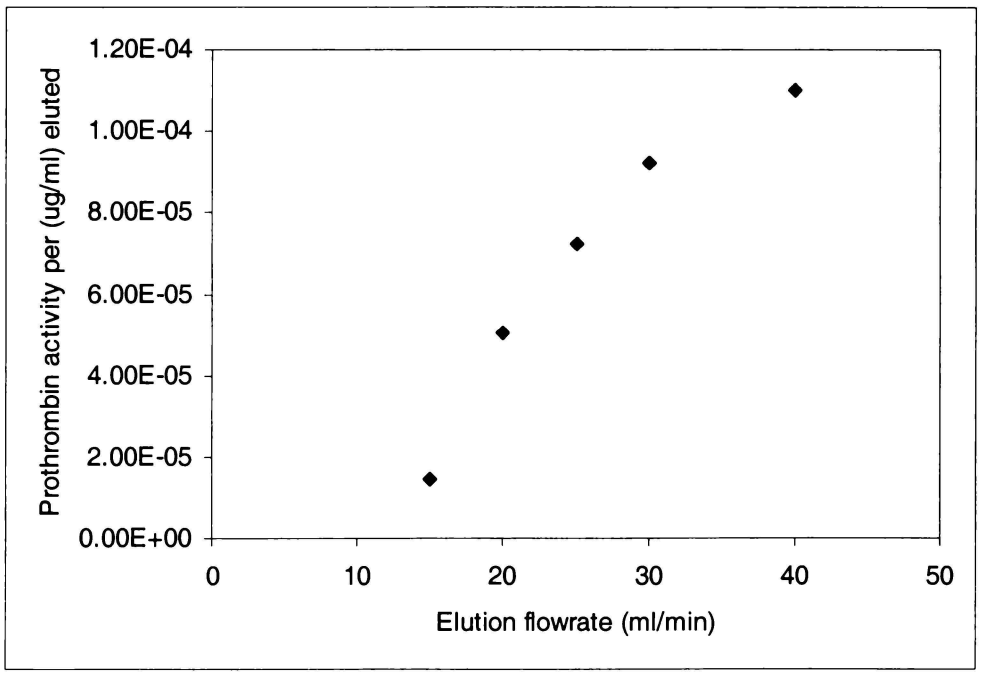

Figure 2-5. Effect of elution flowrate in a DEAE membrane radial flow column on prothrombin activity. Calculations based on data from Sun *et al.* (2000c).

A similar study showed that DEAE cellulose membrane radial flow column had one third to one half the breakthrough capacity of resin packed radial and axial flow columns per ml media (Sun *et al.* 2000c). Varying the elution flowrates dramatically affected prothrombin activity (Figure 2-5) indicating that elution speed was also important in preserving prothombin activity.

2.3.3 Rate kinetics and resolution

The speed of separation in radial flow columns depends on solute uptake rate of the chromatographic media and bed depth. The solute uptake rate is dependent on film and pore diffusion and binding kinetics (Josic and Strancar 1999). The ratio of mass transfer due to uptake to convective mass transfer decreases with increasing fluid velocity. Hence, breakthrough can occur earlier at high flowrates and short bed depths, resulting in decreased ligand utilisation at low uptake rates.

Several examples of decreased breakthrough capacity are reported:

- Hou *et al.* (1991) showed that a 250-ml Protein A affinity membrane radial flow cartridge operated at 200 ml/min retained 90% of its binding capacity for human immunoglobulin but retained 100% at 20 ml/min.

- Chen and Hou (1985) found a Cuno (formerly AMF) Zetaprep-250 DEAE membrane radial flow column adsorbed 58% of BSA in a feedstock at 150 ml/min compared to 88% at 50 ml/min.

- Tsaur and Shallcross (1997a) found that the breakthrough capacity of a radial flow column packed with Dowex MSC-1 cation exchanger for calcium and sodium ions decreased slightly with increasing flowrate.

Liapis (1989) recommended that recycling column effluent would prevent solute loss due to early breakthrough when the radial flow column is loaded at high flowrates.

Short bed depth, high flowrate and rate kinetics also affect column resolution. Column resolution can be measured as the height equivalent to a theoretical plate (HETP), with each plate representing a theoretical equilibrium stage (Giddings 1962). Resolution can also be expressed as the height to width ratio of a peak of an eluted solute in a

chromatogram and the distance between two peaks of two different solutes. A column with high resolution produces widely spaced sharp peaks, indicating that the solutes are completely separated. A long bed depth and low superficial velocity increases the number of theoretical plates, and hence increases in resolution. Therefore, an axial flow column with a greater bed depth and/or lower superficial velocity than a radial flow system will give better resolution. The effect of bed depth on resolution was demonstrated by Lane *et al.* (1990) and by analysing data from Sun *et al.* (2000a,b).

2.4 Flow geometry

The flow geometry in radial flow columns differs from axial columns. In axial columns the superficial velocity remains constant with repect to bed depth, whereas in radial flow the superficial velocity changes as the area available for flow decreases with decreasing radial position (Figure 2-6).

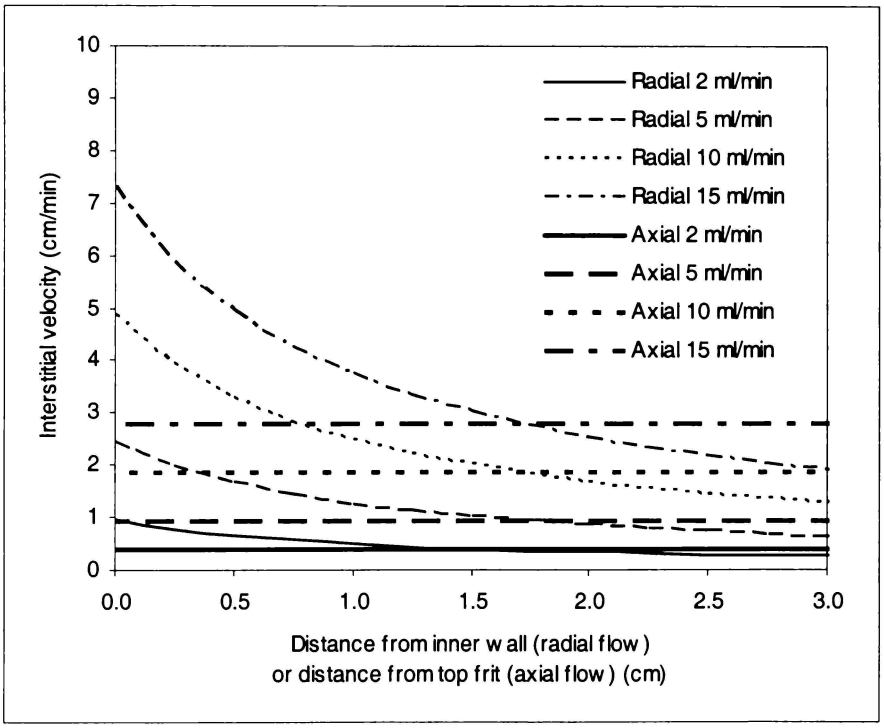

Figure 2-6. Interstitial velocities through a 50-ml radial flow column (ID 2.3 cm, OD 8.3 cm, height 0.95 cm and bed depth 3 cm), and a 50-ml axial flow column (ID 4.8 cm and bed depth 2.8 cm), both with a void fraction of 0.3.

The changing flow velocity affects column dispersion and chromatographic performance. Solution can flow through radial flow columns towards the axis (inward flow) or towards the periphery (outward flow). However, flow direction appears to have little or no impact on performance, apart from inward flow giving better flow uniformity.

2.4.1 Effect of flow geometry on dispersion

Changing fluid velocity in radial flow packed beds has important consequences for column resolution and peak spreading. The ratio of mass transfer due to pore diffusion and adsorption to convective mass transfer decreases with increasing fluid velocity. Eddy dispersion in the interstices of the packed bed is also affected, but the ratio of eddy dispersion to convective mass transfer remains constant if a linear relationship between eddy dispersion and velocity is assumed (Gu 1995). Therefore dispersive effects in radial flow columns are primarily due to diffusive and adsorptive mass transfer, and are greatest near the inner wall (where interstitial velocity is highest) and lowest at the periphery. Non-uniform flow, flow distributors and experimental equipment attached to the column can also contribute to peak spreading.

Tharakan and Belizaire (1995b) investigated the impact of flow geometry in chromatographic performance by comparing the height to width ratio (HTW) of peaks for a range of flowrates and concentrations in radial and axial flow columns for gel filtration of bovine serum albumin. Both columns had the same bed depth and volume. The axial flow column gave HTWs up to 10 times greater than those obtained from the radial flow column for the same flowrate and feed concentration. The behaviour of blue dextran moving through the columns eliminated the possibility that the difference was due to non-uniform flow. Tharakan and Belizaire (1995b) concluded peak broadening was due to greater dispersion in radial flow columns because fluid velocity through the packed bed was up to 2.7 times that of the axial flow column at the inner wall and 0.7 at the outer wall (Figure 2-6). The greater dispersion could also be due to the radial flow distributors. For example, the flow distributors may have a greater open volume than those in axial flow columns, contributing to peak spreading. Tharakan and Belizaire (1995b) do not discuss this possibility however.

Tsaur (1996) on the other hand, found that a radial flow column (O.D. 60 cm, I.D. 3 cm, height 1.5 cm, 30 degree wedge) packed with Dowex cation exchange resin for absorbing sodium and calcium ions exhibited less dispersion than an axial flow column (ID 2.65 cm, length 53.5 cm). The decrease in dispersion was attributed to outward flow, with fluid velocity decreasing with increasing radial position. The chromatographic equipment and solute Tsaur (1996) used could have also caused the differences:

- Bed height (1.5 cm) was very short compared to annulus bed depth (28.5 cm).
- Solute was introduced to the annulus near its axis.
- Effluent exited the column through a series of tubes connected to a multichannel peristaltic pump, unlike typical radial flow columns, which have an inner or outer chamber with one exit port.
- Salts, which have much higher diffusivities than bovine serum albumin, were used. This would decrease dispersive effects because salts diffuse between solution and resin pores more rapidly.

All four factors would reduce dispersive effects, with the first two also reducing the effects of non-uniform solute distribution.

Kim and Lee (1996) separated recombinant hepatitis B surface antigen using a 100-ml (I.D. 2.54 cm I.D. and height 19.74 cm) axial column to a 100-ml (O.D. 8.56 cm O.D., I.D. 1.56 cm I.D and height 1.8 cm) radial flow column (Sepragen, San Leandro, CA, USA) packed with Toyopearl-650 resin using step elution. Although the axial column had 5.6 times the bed depth of the radial column, both columns gave similar resolutions (measured in number of theoretical plates). However, interstitial velocities through the radial flow column were on average four times lower than the axial flow column (Figure 2-7), hence dispersive effects in the radial column were greatly reduced. If similar interstitial velocities were used, the axial flow column would have shown much greater resolution.

There were no reports in the literature about the effect of flow distributors on dispersion in packed bed radial flow chromatographic columns.

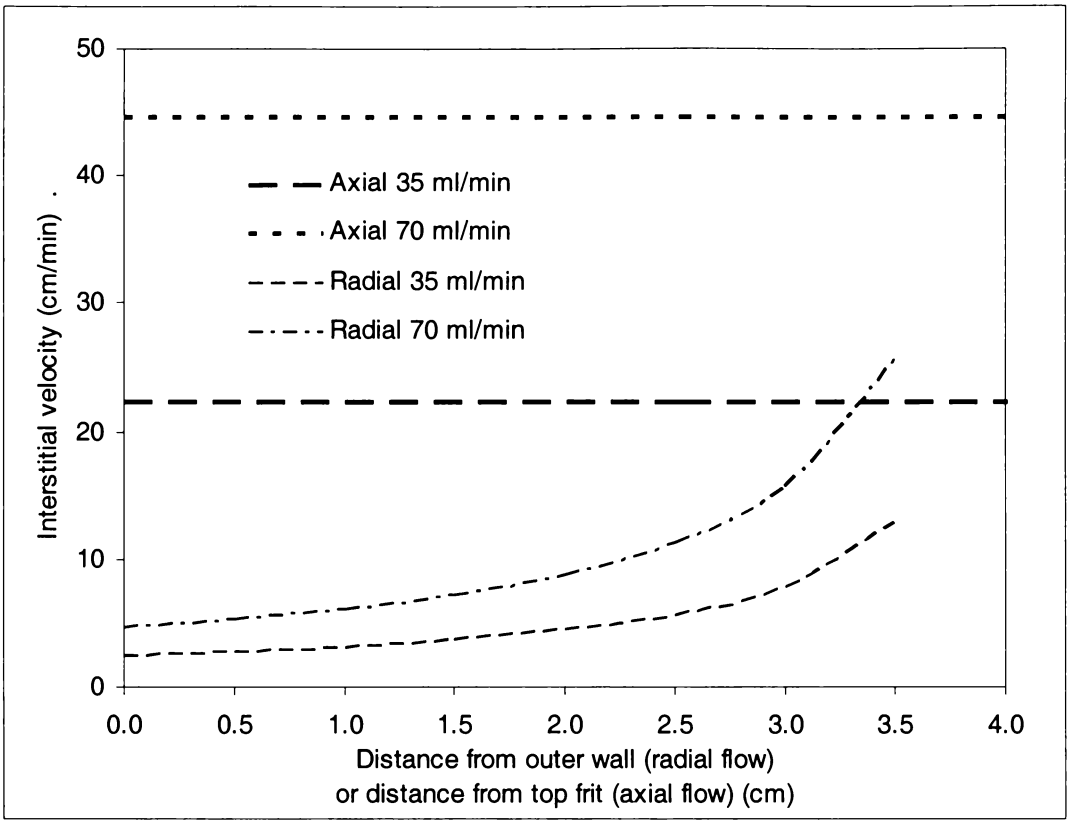

Figure 2-7. Interstitial velocities through a 100-ml (I.D. 2.54 cm and height 19.74 cm) axial column and a 100-ml (O.D. 8.56 cm, I.D. 1.56 cm and height 1.8 cm) radial flow column, calculated using a void fraction of 0.31.

2.4.2 Reducing dispersive effects

The dispersive effects in radial flow columns due to changing fluid velocity can be reduced by decreasing the outer wall to inner wall diameter ratio (Figure 2-8) (Podgornik *et al.* 2000). This is done by having a large inner wall diameter and a short bed depth. Monolithic radial flow columns typically have very short bed depths ranging between 6.5 mm and 21 mm for 8-ml and 800-ml columns respectively (Milavec Zmak *et al.* 2003), reducing dispersion due to changing velocity.

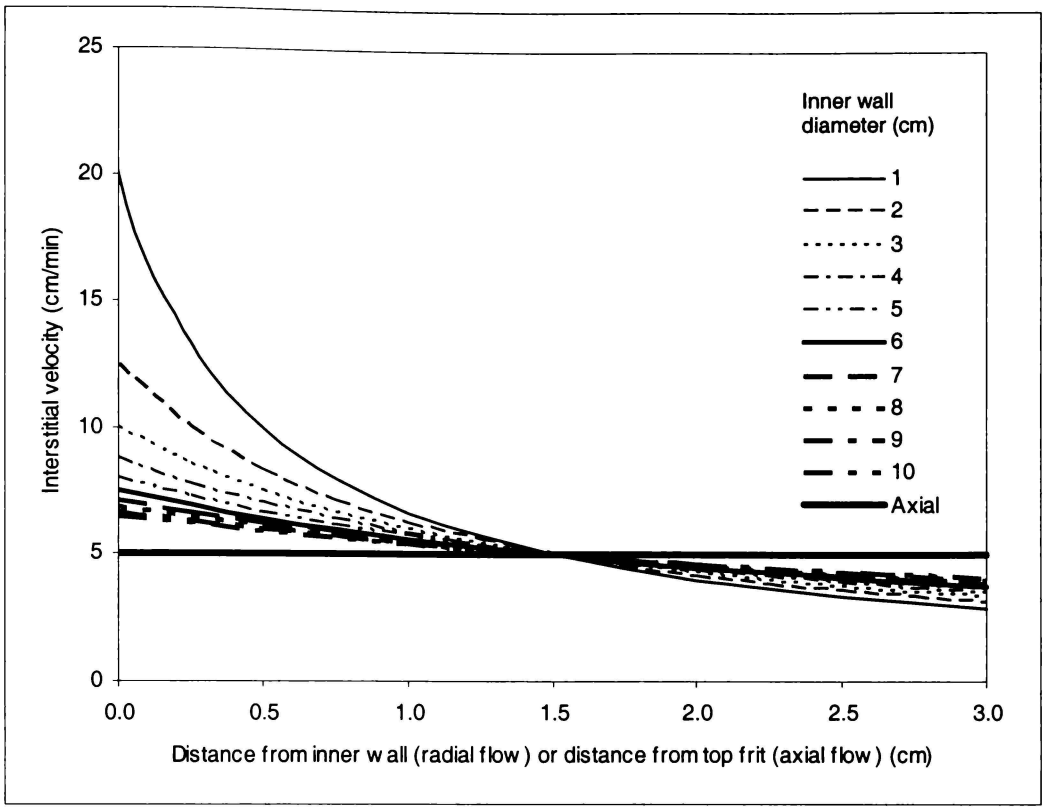

Figure 2-8. Interstitial velocities through a 100-ml radial flow column of different inner wall diameters, and a 100-ml axial flow column. For all columns: bed depth is 3 cm, void fraction is 0.3, and flowrate is 50 ml/min.

2.4.3 Direction of flow

Solution can flow through radial flow columns towards the axis (inward flow) or towards the periphery (outward flow). Inward flow is typically used in radial flow chromatographic systems marketed by Cuno, Sepragen, and CIM. Exceptions are spinning bed radial flow systems, such as the Chromatotron by Harrison Research, where centrifugal forces generated by spinning the bed propel solution outwards.

Inward flow in gas radial flow chromatography gives greater flow uniformity because of the increasing resistance to flow with decreasing radial position (Kaye 1978; Yee 1987). Kaye (1978) also found that a small inner wall diameter and a greater bed depth reduced flow maldistribution.

Yee (1987) reported theoretical work on the impact of flow direction on chemical conversion in radial flow reactors and concluded that flow direction only slightly

affected conversion. For constant volume isothermal systems, first order reactions were independent of flow direction, inward flow was better for reaction orders less than one and outward flow better for reaction orders greater than one. Yee (1987) also cites work done by Medellin (1976), who found flow direction did not affect extraction of sulphur dioxide and nitrogen oxides from flue gas in a 60 degree wedge shape radial flow reactor. Theoretical studies of a resin packed radial flow chromatographic bed found that inward flow gave slightly sharper concentration profiles than outward flow in liquid chromatography (Gu *et al.* 1991) and gas chromatography (Heft 1991).

Tharakan and Belizaire (1995a) used radial and axial flow columns packed with Sepharose with monoclonal antibody as the ligand to isolate coagulation factor IX. They varied flow direction, flowrate (0.3-15 ml/min) and feed concentration (1.7-6.9 mg/ml) and found the resin capacity was independent of all three factors. The volume of feedstock loaded was not stated, however, and breakthrough data was not provided. They collected column effluent in four fractions; loading, wash, elution and regeneration, which was assayed for total protein concentration using a UV spectrophotometer at 280 nm. It is likely that the loading volume of feedstock was high enough so any effect of the factors listed above would not be observed because the resin was loaded to capacity. Effects of the three variables would have been more readily observed if protein concentration had been measured instantaneously using an inline UV spectrophotometer coupled directly to the column effluent stream.

Inward flow appears to be the best flow direction for radial flow columns as it gives better flow uniformity and slightly better theoretical chromatographic performance. Thorough investigation in this area for different kinds of separations and solutes of different diffusivities would greatly increase the understanding of radial flow column performance.

2.5 Scale-up

Scale-up of radial flow columns is straight forward (Saxena and Dunn 1989). Methods optimised for pilot scale separations can be scaled provided only the column height is increased and the volumetric flowrate increased so radial velocities are unchanged.

Jungbauer *et al.* (1988) investigated scaling a Zetaprep 15 laboratory scale QAE anion exchange membrane radial flow column to Zetaprep 100 and 800 pilot scale columns (Cuno) for separating monoclonal antibodies from murine hybridoma culture supernatant. A two-step process of membrane filtration and radial chromatography was used to purify the antibody. Scaling up the system did not affect the chromatograms produced or product purity. However, they were unable to use experimental values from the laboratory scale to calculate buffer volumes required and process times for the larger scale systems because the larger columns had greater diameters.

Ngo and Khatter (1991) used 100-ml and 500-ml AvidPak radial flow columns packed with an affinity gel to produce 2.5 to 10 g of purified IgG from goat serum. The columns had the same diameter and bed depth but different bed height and were operated at 10 and 50 ml/min respectively. They found that both columns behaved similarly.

So far, the impact of scale-up on radial flow column resolution has not been investigated. A general trend in preparative axial flow columns is that HETP increases with increasing bed width (Giddings 1962), reducing resolution. Whether or not a similar trend occurs in radial flow columns has not been investigated and may be important in understanding column performance.

2.6 Packing

Three kinds of packing can be used in radial flow chromatography: spherical resin packed beds, monolithic or continuous resin, and membranes with chromatographic ligands attached. Resin packed beds have the advantage of high surface areas giving high capacities, but have problems with shrinking and swelling, compacting and settling and channelling. Monolithic and membrane beds are more stable, but do not have the high loading capacities of resin beds and must be replaced when blocked.

2.6.1 Influence of packing type on kinetics

The type of packing affects the operational flowrate of a radial flow column, breakthrough capacity and column resolution. Uptake is influenced by film and pore diffusion and solute binding rate to the chromatographic ligands (Podgornik *et al.*

2000). Resin particles are highly porous with stagnant zones that solute must diffuse through to reach the chromatographic ligand. Hence, pore diffusion is often rate limiting. Macroporous resins and monolithic beds have macropores allowing convective flow through the resin, reducing the stagnant zones and increasing the rate of solute uptake (Josic *et al.* 2001). Breakthrough capacity is largely unaffected by flowrate in monolithic radial flow beds, (Figure 2-9) (Podgornik *et al.* 2004). Non-porous resin and membrane beds have also been developed, eliminating pore diffusion. However, all these packings have lower surface areas than conventional resin for attaching chromatographic ligands and therefore have lower loading capacities per ml of media.

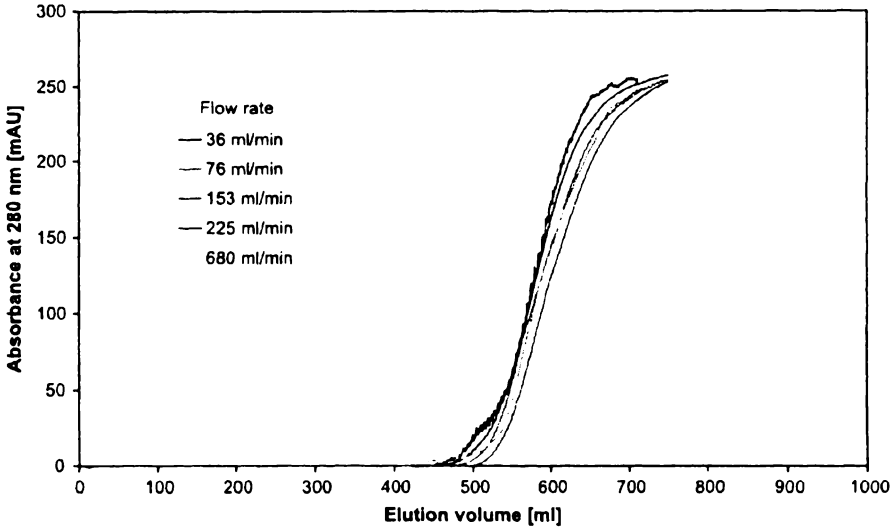

Figure 2-9. Effect of flowrate on dynamic binding capacity of an 80-ml CIM DEAE monolithic column. Sample: 3 mg/ml BSA in 20 mM TrisHCl buffer, pH 7.4 (Podgornik *et al.* 2004).

2.6.2 Resin packed beds

Radial flow and axial flow columns are typically packed using highly porous spherical resin with chromatographic ligands attached. This packing has a large surface area and high loading capacities. Axial columns are usually packed by removing the top flow distributor, adding resin slurry and allowing the resin to settle under flow. A recent innovation is side packing, allowing axial columns to be pump packed. Radial flow columns can be pump packed without removing the flow distributors, and reproducible

packs can be achieved (Levison 2003). The packing can be easily changed for different types of separation.

Disadvantages of packed beds are the tendency of resin particles to shrink and swell when exposed to different solutions, wall effects, uneven packing density, settling, compaction under pressure, and channelling. All contribute to non-uniform flow and affect column resolution.

2.6.2.1 Wall effects and shrinkage

Preferential flow close to the walls in packed beds can occur, affecting column resolution. This occurs because interstices between the resin and wall are greater than amongst the tightly packed resin, giving less resistance to flow. Wall effects have been observed in studies of axial flow beds (Fahien and Smith 1955). Tsaur (1996) attributed slight deviations between model and experimental results to wall effects in his study of radial flow chromatography. Shrinkage and swelling of the ion exchange resin when exposed to salt solutions of different concentrations also contributed to wall effects. Mueller (1999) examined the impact of walls in annular packed beds on void fraction and found that the largest void fraction occurred between the wall and a distance from the wall equal to the radius of the resin particle.

Wall effects can be neglected if the aspect ratio, which is the ratio of bed width (axial) or height (radial) to resin particle diameter, exceeds twenty (Fahien and Smith 1955; Yee 1987). Tsaur (1996) used a radial flow column with a bed height of 15 mm packed with resin 0.3 to 0.8 mm in diameter, giving aspect ratios between 50 and 18.75 respectively. Medellin (1976) found no significant wall effects on his experimental radial flow reactor, which had an aspect ratio of 13.

Effects of resin shrinkage and swelling due to different ionic strength solutions can be eliminated by immersing the resin in a high ionic strength elution buffer before packing the column.

2.6.2.2 Packing uniformity

Achieving uniform packing density is difficult in large diameter columns (Rice and Heft 1990). Yee (1987) attributed band development during iodine tracer tests in a gas radial flow chromatograph to non-uniform flow due to uneven packing density.

Bed compression can reduce non-uniform flow (Yee 1987; Rice and Heft 1990). Rice and Heft (1990) compressed a radial flow packed bed of alumina to 34 MPa to perform experiments on methane. However, bed compression is not feasible for large scale liquid radial flow columns as the porous walls have to be significantly reinforced, robust chromatographic media must be used to prevent resin collapsing, and hydraulic rams are needed to compress the bed.

2.6.2.3 Bed settling and compaction

A packed bed can compact and/or settle during column operation. This compaction creates a void between the bed and the porous wall or distributor, which reduces column resolution. Bed compaction can be avoided by pump packing the column to greater pressures than operating pressure (Levison 2003).

Bed settling in radial flow systems can create a channel at the top of the column for fluid to flow through. Munson-McGee (2000) performed a theoretical study of flow profiles with axial position in a partially packed and completely packed Sepragen Superflow 1500 radial flow column (bed height 28.45 cm). He predicted that 9% of the fluid would flow through the headspace of a partially packed where the top 2% (0.57 cm) was empty headspace (Figure 2-10) and recommended that the top 10% of the porous walls containing the bed should be impermeable to prevent non-uniform flow. His theoretical flow studies showed that flow in that region of the packed bed would be zero. However, this solution is not feasible for columns used to separate and purify biological compounds because the stagnant zone would be a source of bacterial contamination and because the column could not be cleaned adequately after a separation is performed.

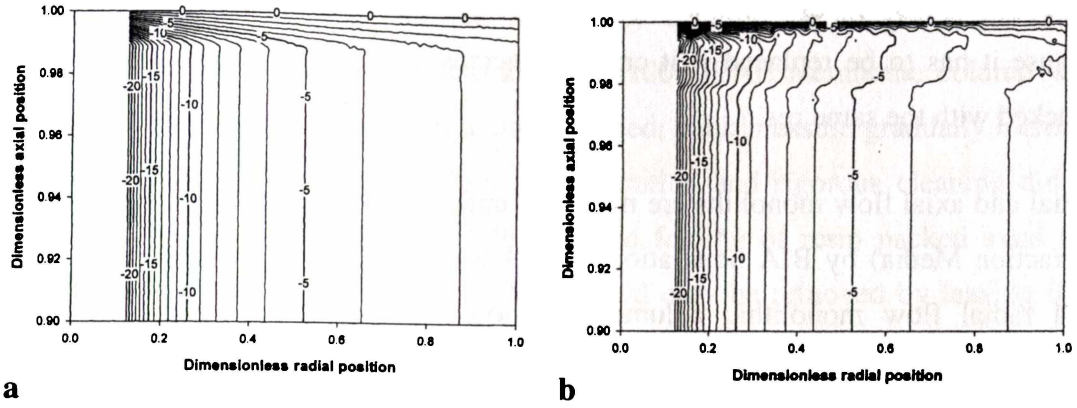

Figure 2-10. Simulated flow velocity profiles (cm/s) through (a) a completely packed column and (b) a partially packed radial flow column where the top 2% is empty headspace (Munson-McGee 2000).

2.6.3 Monolithic Packing

Continuous or monolithic chromatographic beds are produced from materials such as acrylates, silica, polystyrene and agarose. Monolithic columns are highly porous and have low pressure drops. They are easier to manufacture than columns packed with discrete resin particles (Svec and Frechet 1999). However, monolithic columns typically have smaller loading capacities per unit volume of media than resin packed beds because they have less surface area available for attaching chromatographic ligands. For example, a DEAE monolithic column has a capacity of 25 mg BSA per ml of support (Podgornik *et al.* 2004) compared with 80-90 mg/ml for DEAE sepharose FF media (Amersham Biosciences) (James and Do 1991).

Scale up of monolithic axial flow columns is difficult because of column cracking and non-uniform pore size due to uneven cooling during bed polymerisation (Peters *et al.* 1997; Podgornik *et al.* 2004). Gustavsson and Larson (2001) found the annular format and short bed depth of radial flow columns allowed more uniform cooling. They produced a 60-mm diameter radial flow continuous agarose bed derivatised with Cibracon Blue 3GA and successfully extracted lactate dehydrogenase from bovine heart extract. Podgornik *et al.* (2000) manufactured an 80-ml radial flow monolith made from several concentric annular columns. The radial flow format also overcame other difficulties in scaling up monolith discs such as sample distribution, leakage, rapid blocking and pressure resistance (Strancar *et al.* 1997; Josic and Strancar 1999).

Mechanical stability of a monolithic column is important (Podgornik *et al.* 2000) because it has to be replaced if it cracks, whereas a resin packed bed can simply be repacked with the same resin.

Radial and axial flow monoliths are marketed under the trademark of CIM (Convective Interaction Media) by BIA Separations (Ljubljana, Slovenia) (Podgornik *et al.* 2000). CIM radial flow monolithic columns are now manufactured in sizes up to 8 L (Podgornik *et al.* 2004).

2.6.4 Membrane columns

Cuno, LKB, Satorius and Pall market radial flow membrane chromatographic systems that consist of spiral-wrapped membrane sheets with attached ligands. While these systems have the advantage of low pressure drops and high flowrates (Plaigin *et al.* 1989), they have lower protein binding capacities than packed resin beds (see Sun *et al.* 2000c). The exception is monodisperse resin, which has lower capacities than membrane beds (Ghosh 2002). Therefore, membrane beds are only suitable if the feedstock has low concentrations of the component of interest. Membrane beds also have problems of uneven inlet flow distribution, broad membrane pore size distribution, and uneven membrane thickness, which impair flow dynamics and chromatographic performance (Ghosh 2002).

2.6.5 Fouling

Fouling is a serious problem with all three packings. It gives high back pressures and impairs chromatographic performance. Feedstocks such as fermentation media, milk or cheese whey contain particulates that can cause monolithic columns to block (Strancar *et al.* 1997). Feedstocks need to be very clean to obtain reasonable life from monolithic and membrane columns, because the column cannot be reused once blocked. On the other hand, resin beds can be unpacked, cleaned and repacked.

Guard columns, commonly used in HPLC, can be used to remove contaminants (McGregor *et al.* 1986). Lacoste-Bourgeacq et al. (1991), for example, used a cationic depth filter to protect their Cuno Zetaprep 100 SP and DEAE radial membrane columns when separating albumins from Kistler and Nitschmann's faction IV.

Fouling can also occur with clarified feed. For example McGregor *et al.* (1986) reported visible fouling on their Cuno Zetaprep-100 DEAE membrane column when isolating a recombinant protein from a clarified feed; back pressure gradually increased with each subsequent separation cycle. Regeneration and rigorous cleaning did not remove the fouling. Levison *et al.* (1991) found fouling of resin packed axial flow columns when separating egg white proteins could only be removed by leaving 0.5M NaOH in the column overnight.

2.7 Elution type

The importance of radial flow column resolution in a separation depends on whether isocratic, gradient, and step elution is used to separate the solutes. Isocratic elution uses a single elution buffer and separation depends on differences in solute migration rate. Gradient elution uses a gradual change in ionic strength and/or pH of the elution buffer to effect separation. Low column resolution for either technique can give poor separation.

Altering the rate of change in elution buffer's ionic strength in gradient elution can compensate for loss of resolution in radial flow columns. This was done by Milavec Zmak *et al.* (2003) when they used four same diameter, different volume axial flow and three different volume and bed thickness radial flow DEAE CIM monolith columns to separate two mixtures of proteins; myoglobin, conalbumin, and soybean trypsin inhibitor; and lignin and manganese peroxidase from *Phanerocaete chrysoporium* medium. They found similar column resolutions for both column types were achieved, and the separations could be scaled without loss of resolution.

In step elution, ionic strength and/or pH are changed step-wise to elute different solutes adsorbed to the column. Usually one solute is completely removed before another step change is implemented, so column resolution is not as important (Levison 2003). Hence, radial flow columns are better for step elutions. However, good resolution is still beneficial as less buffer is required and the eluted solutes are more concentrated and require less downstream processing.

2.8 Applications

Many applications of fixed bed radial flow chromatography have been reported (Table 2-3). Membrane or resin packed beds were used in the majority of applications reported until the year 2000, when more applications using continuous or monolithic beds began to be reported.

Sepragen has commissioned large scale and pilot scale plants with several major food industries for removing bitterness and acidity from grapefruit juice, and isolating whey proteins for use in food products (Sepragen 1998).

2.9 Alternate forms of radial flow chromatography

Two alternate forms of radial flow chromatography are thin layer and spinning disc/bed radial flow chromatography. These are discussed briefly to complete the literature review on radial flow chromatography.

2.9.1 Thin layer radial flow chromatography

In thin layer radial flow chromatography, a sample is spotted at the centre of a disk of absorbent paper or chromatographic media on a glass plate and eluted outwards by applying a solvent (Brown 1939; Williams 1947; Mackenzie and Truesdale 1990). Although it has high resolution this technique has extremely low throughput, so it is limited to analytical rather than preparative purposes.

2.9.2 Spinning disc/bed radial flow chromatography

Spinning disk/bed systems use centrifugal forces generated by spinning an annular bed at great speeds to propel solution outwards. Examples are the Chromatofuge (Hopf 1947; Heftmann *et al.* 1972), the Cyclograph (Analtech Inc.), and the Chromatotron (Harrison Research Inc.). The Chromatofuge and its successors, such as those

Table 2-3. Separations reported for fixed bed radial flow chromatography (1952-2004).

Date	Fractionation/Separation/Purification	Column	Supplier	Resin/Membrane	Flowrate	Reference
1952	Adsorption of KCl Adsorption of CuSo4 and HAc	Radial disc	Built by researchers	Dowex 50 resin Al_2O_3 granules	5.6-21.5 ml/min	(Lapidus and Amundson 1952)
1985	Breakthrough using BSA	Zetaprep-250	AMF	DEAE cellulose membrane	50 ml/min 100 ml/min 150 ml/min	(Chen and Hou 1985)
	Separation of nucleotides AMP, ADP and ATP	Zetaprep-250	AMF	DEAE cellulose membrane	46 ml/min	(Chen and Hou 1985)
	Transferrin from gamma globulin	Zetaprep-250	AMF	DEAE cellulose membrane	20 ml/min	(Chen and Hou 1985)
	Separation of HAS, human gamma globulin and cytochrome	Zetaprep-100	AMF	SP cellulose membrane	10 ml/min	(Chen and Hou 1985)
1986	Fractionation of human plasma	Zetaprep-HP 3200	Cuno	QAE membrane	Not stated	(Hou and Mandaro 1986)
	Breakthrough using BSA	Zetaprep-250	Cuno	DEAE membrane	40-150 ml/min	(Hou and Mandaro 1986)
	Isolation of recombinant protein	Zetaprep-100 Zetaprep-8000	Cuno	DEAE cellulose membrane	50 ml/min 6-8 L/min	(McGregor *et al.* 1986)
1987	Immunoglobulins from animal sera	N/S	Cuno	Membrane derivatized with recombinant protein A and G	Not stated	(Mandaro *et al.* 1987)
	Antibodies from ascites fluid	Superflo-100 Superflo-1500	Sepragen	Fibrous DEAE cellulose	10 ml/min 150 ml/min	(Saxena and Weil 1987) (Saxena *et al.* 1987)

Table 2-3 continued. Separations reported for fixed bed radial flow chromatography (1952-2004).

Date	Fractionation/Separation/Purification	Column	Supplier	Resin/Membrane	Flowrate	Reference
1987	Ethane and air in helium carrier gas	Gas radial flow column	Built by researcher	Compressed and uncompressed alumina packing	0-140 ml/min	(Yee 1987)
	Ricin A from ricin toxin	Superflo-200	Sepragen	Agarose with anti-ricin B anitbody	45 ml/min	(Saxena and Weil 1987)
	Riboflavin-binding protein from egg whites	Superflo-1500	Sepragen	Riboflavin immobilized on sepharose 4B	350 ml/min	(Saxena and Weil 1987)
	IgG from cell culture fluid	Superflo-100 Superflo-5000	Sepragen	Not stated	10 ml/min 500 ml/min	(Saxena and Weil 1987)
	Enzymes from bacterial cell culture extract	Superflo-1500	Sepragen	DEAE sepharose FF	350 ml/min	(Saxena and Weil 1987)
	CMP, UMP, ATP from nucleotide mixture	Superflo-250s	Sepragen	Nu-Gel C-18 Silica	30 ml/min	(Saxena and Weil 1987)
	Plasma fractionation	20L Superflo	Sepragen	Herapin Sepharose	95 L/hr load and 75 L/hr elution	(Saxena and Weil 1987) (Saxena *et al.* 1989)
	Mouse monoclonal antibodies from hybridoma culture	AMF Zetaprep 250 ml SP cartridge	LKB	Cellulose SP membrane	150 ml/hr	(Menozzi *et al.* 1987)
1988	Purification of trypsin	250 ml 800 ml 3200 ml Zetaffinity cartridge	LKB	Cellulose membranes derivatised with p-aminobenzamidine and soybean trypsin inhibitor	31 ml/min 100 ml/min 400 ml/min	(Huang *et al.* 1988b)

Table 2-3 continued. Separations reported for fixed bed radial flow chromatography (1952-2004).

Date	Fractionation/Separation/Purification	Column	Supplier	Resin/Membrane	Flowrate	Reference
1988	Monoclonal antibodies from murine hybridoma culture	Zetaprep-15 Zetaprep-100 Zetaprep-800	LKB	QAE anion exchange membrane	0.24 L/hr 1.90 L/hr 7.30 L/hr	(Jungbauer *et al.* 1988)
1989	Myxalin from myxococcus cell culture supernatant Desalting Myxalin	Superflo-400	Sepragen	Histidyl-Sepharose Sephadex G-25	20 ml/hr 162 ml/hr	(Akoum *et al.* 1989)
	Anti-human ferritin IgG from rabbit, monkey, baboon, horse, bovine, and porcine	Zetaprep-250	Cuno	QAE cellulose membrane	40 ml/min	(Plaigin *et al.* 1989)
	Kallikrein and thrombin from human plasma	Zetaprep-800	Cuno	Membrane derivatized with p-aminobenzamidine	100 ml/min	(Plaigin *et al.* 1989)
	Breakthrough using BSA	Zetaprep-100 Zetaprep-150 Zetaprep-800 Zetaprep- 3200 Zetaprep-MGS Zetaprep-30L	Cuno	DEAE cellulose membrane	15 ml/min 30 ml/min 150 ml/min 600 ml/min 4 L/min 5-11 L/min	(Plaigin *et al.* 1989)
	Trypsin activity	Zetaprep-250 Zetaprep-800 Zetaprep-3200	Cuno	Membrane derivatized with p-aminobenzamidine	40 ml/min not stated not stated	(Plaigin *et al.* 1989)
	Egg white	50 ml Superflo 20 L Superflo	Sepragen	DE-52	5 ml/min 2 L/min	(Saxena *et al.* 1989)
1990	Desalting bovine serum albumin	100 L Superflo	Sepragen	Biogel P-6DG	5 L/min	(Saxena *et al.* 1989)
	Egg white	Superflo-100	Sepragen	Whatman DE52 and QA52	150 ml/min	(Lane *et al.* 1990)

Table 2-3 continued. Separations reported for fixed bed radial flow chromatography (1952-2004).

Date	Fractionation/Separation/Purification	Column	Supplier	Resin/Membrane	Flowrate	Reference
1990	Breakthrough using trypsin	Zetaffinity 250 ml cartridge	Cuno	Cellulose membrane derivatized with p-aminobenzamidine	18-80 ml/min	(Lee *et al.* 1990)
	Purification of urokinase from human urine	Radial membrane cartridge	Cuno	SP cellulose membrane Zinc chelated affinity membrane	100 ml/min 50 ml/min	(Hou and Zaniewski 1990)
	Methane pulse in helium carrier gas	Gas radial flow column	Built by researcher	Compressed alumina packing	60-100 ml/min	(Rice *et al.* 1989)
1991	Plasminogen from human plasma	Zetaffinity 250 cartridge	Cuno	Cellulose membrane with immobilised L-lysine	20 ml/min	(Planques *et al.* 1991)
	IgG from goat serum	100ml and 500 ml Avid Pak radial	BioProbe International	Avid AL™ affinity gel	10-50 ml/min	(Ngo and Khatter 1991)
	Albumin from Kistler and Nitschmann's fraction IV	Zetaprep-100	Cuno	DEAE cellulose membrane SP cellulose membrane	40 ml/min 38 ml/min	(Lacoste-Bourgeacq *et al.* 1991)
	Immunoglobulins from animal plasma	250 ml Radial membrane cartridge	Cuno	Cellulose and acrylic membrane derivatized with protein A	20 ml/min 200 ml/min	(Hou *et al.* 1991)
1995	Factor IX from coagulation FIX	50 ml Superflo	Sepragen	MAb coupled to Sepharose CL2B	0.3-15 ml/min	(Tharakan and Belizaire 1995a)
	Gel filtration of bovine serum albumin	50 ml Superflo	Sepragen	S-200 Sephacryl gel filtration	2-15 ml/min	(Tharakan and Belizaire 1995b)

Table 2-3 continued. Separations reported for fixed bed radial flow chromatography (1952-2004).

Date	Fractionation/Separation/Purification	Column	Supplier	Resin/Membrane	Flowrate	Reference
1996	Extraction of recombinant hepatitis B surface antigen from crude extract	100 ml Superflo	Sepragen	Toyopearl-650	35-140 ml/min	(Kim and Lee 1996)
1997	Breakthrough using Na+ and Ca+ ions	30° Wedge column 30 mm ID, 300 mm OD, 15 mm deep	Built by research institute	0.3-0.85 mm DOWEX MSC-1	380-1014 ml/hr	(Tsaur 1996) (Tsaur and Shallcross 1997b) (Tsaur and Shallcross 1997a)
	Isolation of clotting factor VIII and IX from human plasma	8 ml column	BIA	QA GMA-EDMA monolithic column	6-9 ml/min	(Strancar *et al.* 1997)
2000	Human prothrombin from Nitschmann fraction III	50 ml Superflo	Sepragen	Q Sepharose FF DEAE sepharose FF	7-15 ml/min 6-14 ml/min	(Sun *et al.* 2000a) (Sun *et al.* 2000b)
		50 ml radial column	Chinese Academy of Sciences	DEAE cellulose membrane	15-40 ml/min	(Sun *et al.* 2000c)
2000	Separation of myoglobin, conalbumin, and soybean trypsin inhibitor	80 ml column	Built by researchers	DEAE GMA-EDMA monolithic column	200 ml/min	(Podgornik *et al.* 2000)
	Separation of factor IX and vitronectin	8 ml	CIM, BIA	DEAE monolithic column	8 ml/min	(Branovic *et al.* 2000)
2001	Lactate dehydrogenase from bovine heart extract	61 mm ID, 80 mm OD, 100 mm long radial column	Built by research institute	Continuous agarose gel derivatised with cibacron blue 3GA	10 ml/min load and 5 ml/min elution	(Gustavsson and Larsson 2001)
	Removal of lactose from milk	61 mm ID, 80 mm OD, 100 mm long radial column	None	Continuous agarose gel derivatised with immobilised B-Galactosidase	86 ml/min	(Gustavsson and Larsson 2001)

Table 2-3 continued. Separations reported for fixed bed radial flow chromatography (1952-2004).

Date	Fractionation/Separation/Purification	Column	Supplier	Resin/Membrane	Flowrate	Reference
2003	Separation of myoglobin, conalbumin, and soybean trypsin inhibitor	8 ml 80 ml 800 ml	CIM, BIA	DEAE GMA-EDMA monolithic columns	16 ml/min 160 ml/min 800 ml/min	(Milavec Zmak *et al.* 2003)
	Lignin and manganese peroxidase from *Phanerocaete chrysoporium* medium	8 ml 80 ml	CIM, BIA	DEAE GMA-EDMA monolithic columns	45 ml/min 215 ml/min	(Milavec Zmak *et al.* 2003)
2004	Breakthrough using BSA	80 ml column	Built by researchers	DEAE GMA-EDMA monolithic column	36-680 ml/min	(Podgornik *et al.* 2004)
	Separation of myoglobin, conalbumin, and soybean trypsin inhibitor	8 ml 80 ml 800 ml	CIM, BIA	DEAE GMA-EDMA monolithic columns	16 ml/min 160 ml/min 800 ml/min	(Podgornik *et al.* 2004)

AMF (Meriden, Connecticut) Sepragen (San Leandro, CA), LKB (Sweden) Cuno (Cergy-Pontoise, France; Meriden, Connecticut), CIM - Convective Interaction Media - BioProbe International (Tustin, CA)

mentioned by Weil (1949) and Mitchell *et al.* (1953), were used primarily for preparative separations such as extracting carotene from dyhdrated alfalfa meal; separating vanadium, iron, nickel and zinc; oleic acid and ricinoleic acid; octan-2-ol and methyl hexyl ketone; and purifying caster oil (Hopf 1947). Similar systems were used by Stauffer Chemical Co., Rochester, Minnesota (Delaney *et al.* 1973), where basket centrifuges filled with gel filtration media were used to separate lactose and three grades of protein for human consumption from cheese whey. The plant had a rated capacity of 453 tonne per day. These systems were physically large and cumbersome (Heftmann *et al.* 1972) and were expensive because of the rapidly rotating equipment (like centrifugation).

The Cyclograph and Chromatotron are thin layer variants of the Chromatofuge. They are widely used for preparative separation of organic compounds with typical flow rates of approximately 2-3 ml/min per millimeter of adsorbent thickness. These systems are difficult to scale up however, because the bed thickness is restricted to maintain high resolution and prevent bed thickness varying due to centrifugal forces deforming the bed.

2.10 Rotating annular bed chromatography

Annular chromatography was first suggested by Martin (1949). He proposed a rotating annular chromatographic column with stationary feed and exit points through which solution flowed axially (Figure 2-11). The solutes exit at different angles around the base of the annulus depending on their rate of migration through the column. Considerable work has been done on developing annular chromatography, but it has not been as widely applied as technologies such as simulated moving bed chromatography (Thiele *et al.* 2001). Equipment development up to modern day variant, the P-CAC (pressurized continuous annular chromatograph marketed by Prior Separation Technology, Austria), is reviewed in this section. Disadvantages of the P-CAC are discussed and variations on rotating annular bed systems are described.

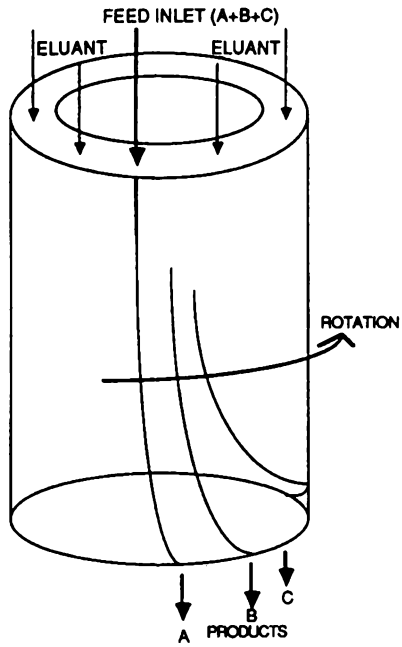

Figure 2-11. Concept of rotating annular chromatography (Bridges and Barker 1993).

2.10.1 Equipment development

During the 1950s work on annular chromatography led to the development of systems consisting of circular arrays of chromatographic tubes (Solms 1955; Svensson *et al.* 1955). However it was difficult to get uniform flow through each of the tubes due to slight variations in packing density.

Several groups proposed pressurized annular gas chromatographic systems (Hall and Cole 1959; Dinelli *et al.* 1962; Giddings 1962; Luft 1962; Heaton 1963; Taramasso and Dinelli 1964), which Giddings (1962) argued would have better resolution and higher throughput than a conventional axial flow column of the same cross sectional area. Dinelli *et al.* (1962) developed equipment consisting of a rotating array of tubes to separate n-heptane and toluene, and n-hexane and acetone. The efficiency of the system was similar to an equivalent batch system. A similar device developed by Taramasso and Dinelli (1964) was used to separate 3-chloro-2-methyl-propene and 1-chloro-2-methyl-propene, α and β pinene, isomers of 1-3 pentadine, and to purify 2-5 dimethyl-hexa-2,4 diene and n-hexane. They usually achieved greater than 99% purity.

Fox *et al.* (1969) developed a gravity-fed liquid annular chromatograph that could rotate at 0.4 to 2 rpm. A level detector maintained the solvent level in the column and the fractions were collected at the base of the annulus (Fox 1969). The annulus was packed with Sephadex gel (size 40-120 μm) and used to separate myoglobin at 97% purity from haemoglobin in beef heart extracts (Nicholas and Fox Jr 1969). However, ten times the solvent used in a conventional column was needed for the separation because the process had not been optimised.

Scott *et al.* (1976) developed a pressurized liquid annular chromatograph. The top of the annulus was sealed using double o-rings and the head space was pressurized using an inert gas (Figure 2-12). Six inlets supplied the feed and elution buffers. Spacers at the top and bottom of the annular bed segmented the annulus into different regions, which allowed gradient elution and prevented backmixing at the exit points. Distribution coefficients for isocratic separation of blue dextran and $CoCl_2$ using Sephadex G-25 resin and nickel and colbalt using Dowex 50W-X8 were 25% less than those obtained in an analytical column and they found their system had low resolution.

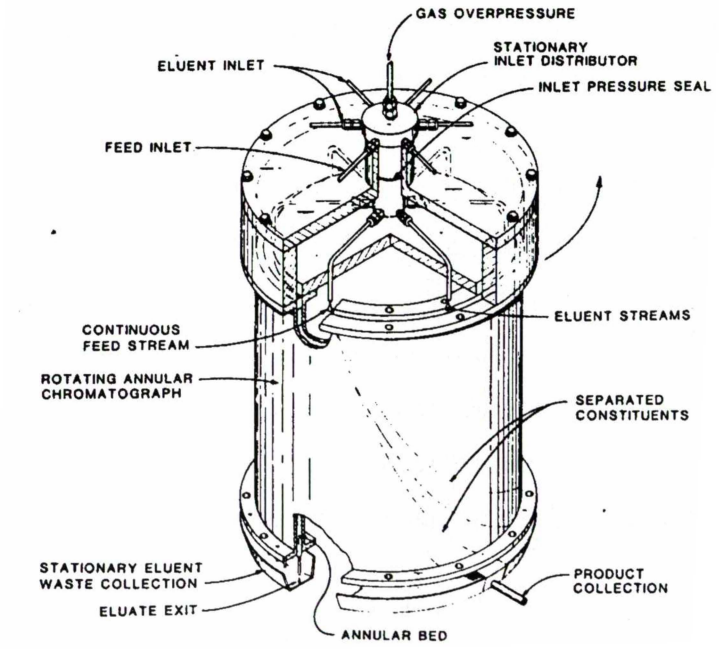

Figure 2-12. Pressurised annular chromatograph (Scott *et al.* 1976).

Canon and Sisson (1978) improved the device used by Scott *et al.* (1976) by adding four manifolds to distribute different eluents over sections of the annulus for step elution. The upper spacers segmenting the top of the annulus were replaced with two layers of different sized glass beads and the feed and eluent tubes were arranged so solution exited beneath the surface of the glass beads. Liquid level was kept below the surface of the glass beads to prevent circumferential mixing in the head space. Backmixing as solution exited the annulus was eliminated by attaching 180 exit tubes with porous plugs to the base. This system has been used for separating nickel and cobolt; iron and aluminium; zirconium and hafnium (Canon *et al.* 1980; Begovich *et al.* 1983; Begovich and Sisson 1984), colbalt and blue dextran (Sisson *et al.* 1988), and sugars (Howard *et al.* 1988).

Canon and Sisson's (1978) system was further improved by removing the gas overpressure system was removed from the rotating annular bed apparatus and flooding the entire headspace with eluent. This improved system has been used to separating sugars (Byers *et al.* 1989; Byers *et al.* 1990; Bart *et al.* 1996), metals (Carta *et al.* 1989), amino acids (DeCarli *et al.* 1990; Kitakawa *et al.* 1997), and proteins, (Bloomingburg *et al.* 1991; Bloomingburg and Carta 1994), fractionating beet molasses (Bridges and Barker 1993), and desalting bovine serum albumin (Reissner *et al.* 1997).

The P-CAC (pressurized continuous annular chromatograph) marketed by Prior Separation Technology, Austria, is based on the above system. It can be packed to various bed depths, the annular bed has the dimensions of 15 cm O.D. and 13-14 cm I.D., and rotates at 60-600 degrees per hour (Schlegl *et al.* 2003). The base of the annulus has 90 evenly spaced exit ports. The P-CAC system has been used for the isolating antibodies (Giovannini and Freitag 2001), fluorescent proteins (Uretschlager *et al.* 2001) and plasmid DNA (Giovannini and Freitag 2002) from cell culture supernatants; purifying immunoglobulins (Iberer *et al.* 2001) and clotting factor IX (Iberer *et al.* 2002); removing protein aggregates (Buchacher *et al.* 2001) and refolding of proteins (Schlegl *et al.* 2003; Lanckriet and Middelberg 2004).

Buchacher *et al.* (2001) used the P-CAC to remove protein aggregates from an IgG preparation. They intended to carry out the separation and column regeneration at the same time, but found that the entire column was needed to separate the protein aggregates, therefore the process had to be stopped periodicially to regenerate the

column. The column could operate continuously for five hours before requiring regeneration and four cycles were completed before the column fouled. Fouling was eliminated by diluting the feedstock. The P-CAC had double the productivity of conventional axial columns. However, high feed flowrates resulted in feed migrating into the headspace, contaminating other regions of the annulus. This effect depended on feed concentration and diluted feeds could be applied at greater flowrates.

Giovannini and Freitag (2002) isolated plasmid DNA from *e.coli* cell lysate using hydroxyapatite and a step gradient elution in a P-CAC, an analytical column of the same length and a preparative column of the same length and volume. The pDNA yield from the P-CAC was 84% compared with 92% for the analytical column and 89% for the preparative column. The P-CAC resolution in terms of HETP was lower than the analytical and preparative columns at low rotation speeds but increased with rotation speed. Giovannini and Freitag (2002) explained that this was an artefact of the equipment because the base of the annulus had 90 outlets spaced at four degrees. At low speeds the purified sample would elute over a few outlets so peaks would appear much broader than what they actually were. At higher speeds, the purified sample would elute over a greater number of outlets and the peak will approach more closely the actual concentration profile.

Iberer *et al.* (2002) used the P-CAC to separate and purify factor IX from vitronectin, a commonly found impurity in factor IX concentrates. The feed nozzles arrangement on the P-CAC prevented the conventional axial column method for purifying factor IX from being translated directly to the P-CAC, so the productivity of the P-CAC was lower than the conventional method. They also had the same problem as Buchacher *et al.* (2001) of not being able to apply feed solution at high flowrates without feed solution contaminating the headspace.

Schlegl *et al.* (2003) used the P-CAC to continuously refold denatured bovine α-lactalbumin using a size exclusion medium and obtained a yield of 41% of reactivated protein compared to 30% in an equivalent batch process. Lanckriet and Middelberg (2004) used the P-CAC to refold denatured lysozyme. They studied flow distribution and found significant variation in flowrate from each outlet, ranging between zero to twice the average flow. However, this did not appear to affect the performance of the P-CAC as the lysozyme eluted over several outlets. The P-CAC behaved as a series of

batch columns, so its performance could be predicted by experimenting with an equivalent length batch column.

2.10.2 Disadvantages of P-CAC

The P-CAC system has several disadvantages if it is used for a range of different separations with different chromatographic media. Firstly, setting up is complicated because the top of the system has to be removed to unpack and pack the annular bed. Secondly, a stratified packing system is used consisting of the chromatographic medium and two layers of different size glass beads at the top of the annulus. The glass beads and media need to be removed and sieved. Packing is time consuming because the annulus has to be slurry packed and the resin carefully levelled before the glass beads are layered on top.

2.10.3 Variations on the P-CAC

Two variations on the P-CAC have been reported. The first had two multichannel peristaltic pumps to control flow through the annulus (Yonemoto *et al.* 1993; Kitakawa *et al.* 1995). One pump was stationary above the rotating annular bed and supplied feed and eluent buffers to the top of the annulus. The top of the annulus was partitioned into 36 sections to prevent the different solutions mixing before entering the bed. The other pump on a rotating table under the annular bed was connected to exit ports at the bottom of the annulus and pulled solution through the bed. Flow from the bottom pump was collected in stationary sample tubes arrayed in a circle about the base of the system. The annular bed was 0.5 cm wide, 47 cm long and 15 cm I.D. This system was used to separate two amino acids. It was also used with a partial effluent recycle to completely separate of glutamic acid and valine with 30% greater recovery (Kitakawa *et al.* 1997) (Figure 2-13).

The advantages of Yonemoto *et al.*'s system over the P-CAC are that the peristaltic pump ensures flow exiting the annulus is uniform, and having 36 feed nozzles gives greater separation possibilities such as using gradient elution. Because the top of the annulus does not need to be pressurized to push solution through the bed, it can be divided up into sections, which the feed and elution buffer drip into. This also simplifies set-up as a stratified packing system used in the P-CAC is not needed. The

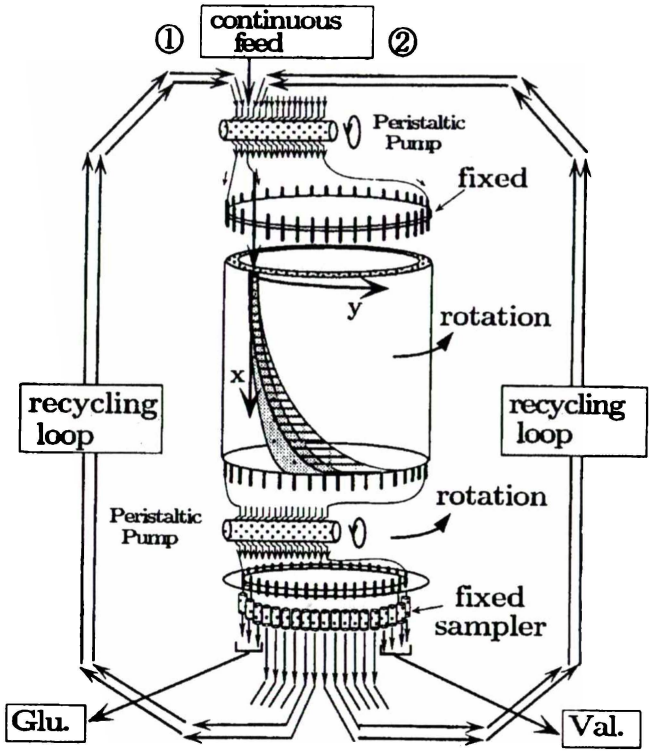

Figure 2-13. Schematic of annular chromatograph with partial effluent recycling (Kitakawa *et al.* 1997).

sections also prevent circumferential mixing of solution, a problem in the P-CAC. However, this set-up has two disadvantages. Firstly, power has to be supplied to the bottom peristaltic pump, which is rotating with the bed. Secondly, the negative pressure near the base can produce air bubbles in the bed if the solutions have not been degassed, which can affect flow and column performance.

The second variant of the P-CAC used a pressurised system with a stationary annular bed, and stepper motor rotating the feed and eluent nozzles at the top and sample collectors at the base (Goto and Goto 1987). This system has been used to concentrate valine (Takahashi and Goto 1991a), separate amino acids (Takahashi and Goto 1991c; Takahashi and Goto 1991b), separate methanol and sodium chloride (Goto and Takahashi 1993), and fractionate fructooligosaccharides (Takahashi and Goto 1994). Takahashi and Goto (1994) argued that this system would be easy to scale up because the bed does not rotate. However, an obvious disadvantage of such a system is that the

rotating feed and eluent system and sample collectors become very complex if more than three different solutions were being applied to the annulus.

2.11 Continuous radial flow chromatographic systems

Technologies similar to the CRFC are reviewed in this section. Several are proposed technologies which were not developed, two of which were for practical reasons. Another technology called continuous disc chromatography was developed and tested, but research did not continue beyond the 1970s. Several other variations are briefly mentioned.

2.11.1 Continuous radial flow packed bed proposals

The first continuous radial flow chromatographic system was proposed by Mosier (1963) who suggested a rotating annular gas chromatographic system with a carrier gas flowing radially from a feed chamber at the axis to the periphery. Sample is introduced at a point near the inner edge of the annular bed and separated into its components as it progresses through the packed bed. The different components are collected at different angles around the outer periphery of the annular bed, with the angle depending components rate of migration through the bed. The first system proposed consisted of a standard annular bed where carrier gas velocity decreased with increasing distance from the axis (Figure 2-14). The second system had a tapered annular packed bed so carrier gas velocity remained constant with radial position. There were no published reports on either system being constructed or tested.

Tuthill (1970) patented a similar system to Mosier (1963) except the sample was introduced and removed from the top of the annular bed through ports near the axis and periphery. No reports were found in the scientific literature on constructing and testing this system. In an engineering sense, this proposed system was similar to another concept based on the multiple layer chromatographic system developed by Wolf and Vermeulen (1976). Selective packings are layered in a column, and product is removed by a series of cross-flows with the axial flow temporarily stopped. Wankat (1977) suggested this system could be made continuous by using a rotating annulus. The

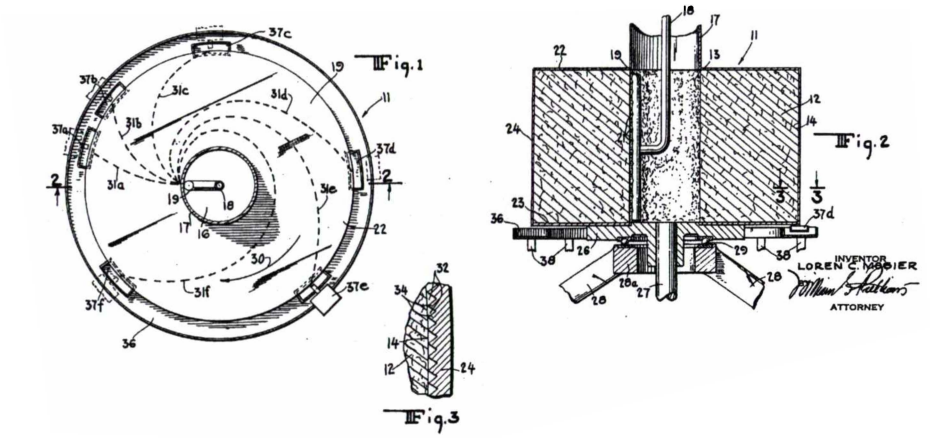

Figure 2-14. Continuous gas chromatographic system (Mosier 1963).

annulus is divided into segments with vertical dividers to prevent angular dispersion and packed with several layers of selective adsorbents. Sample is continuously applied to the top of the column and flows axially through the bed, with each component being selectively bound to a particular adsorbent. The annulus rotates past a fixed section where axial flow is stopped and components are eluted using radial flow. Tuthill's (1970) system does the opposite, the components are separated radially and removed axially. It would be extremely difficult to build these systems. The inner and outer walls and top and base of the annulus would need to be porous. The outer and inner walls would need to be sealed, except where radial flow occurs, to prevent sample flowing axially exiting through the outer and inner walls. The top and bottom would also need to be sealed except where axial flow occurs to prevent the radially flowing phase exiting axially. In addition, the annulus would be moving against these seals. Not surprisingly, these systems were not developed.

2.11.2 Continuous disc chromatography

Sussman and co-workers (Sussman and Huang 1967; Sussman 1970; Sussman *et al.* 1972; Sussman *et al.* 1974) developed a continuous gas chromatographic system, which used two solvent coated glass discs held apart by precision spacers rather than an annular packed bed (Figure 2-15). Solvent-coated discs eliminated problems of packing uniformity. This system was used to continuously separate mixtures of methane and propane and methane and butane using glass discs sprayed with 5%

silicone grease in benzene (Figure 2-16) at flowrates up to 180 ml/min and rotation speeds up to 1 rpm.

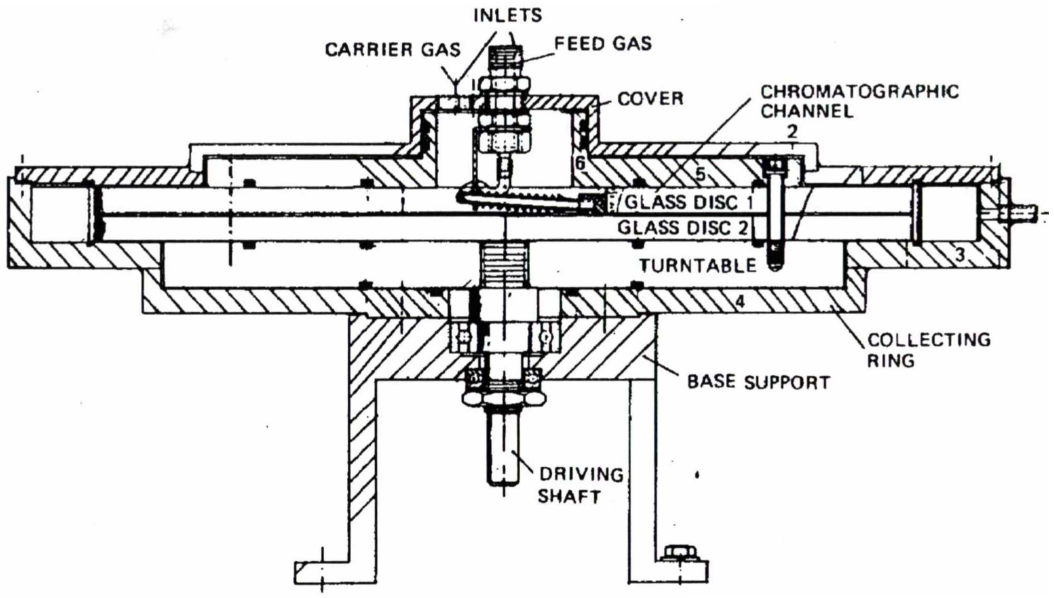

Figure 2-15. Continuous surface chromatograph (Sussman *et al.* 1972).

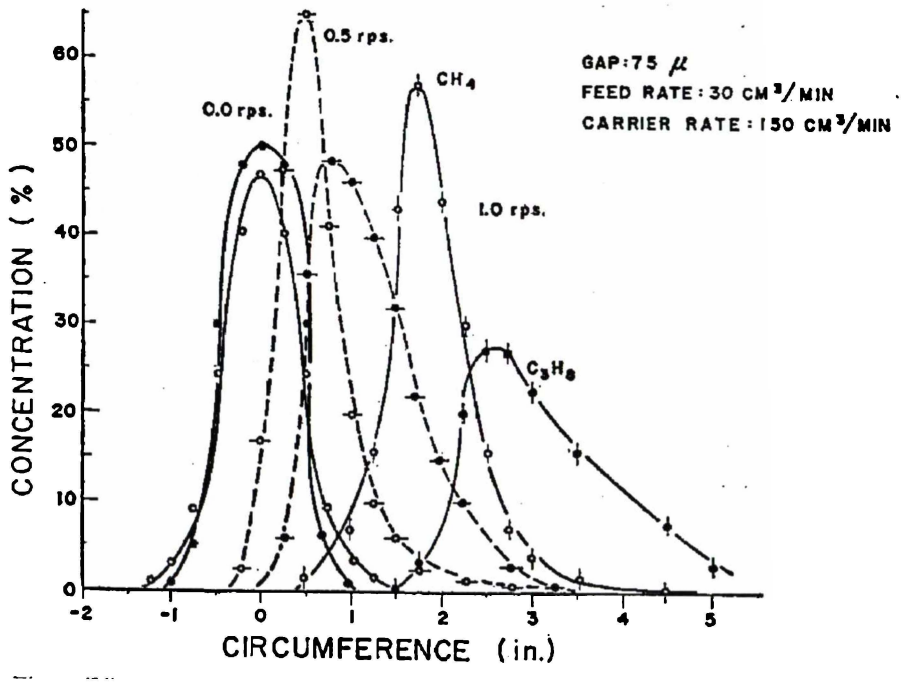

Figure 2-16. Effect of rotation speed on effluent exit concentration with distance around the periphery when separating methane and propane at 30 ml/min (Sussman and Huang 1967).

This system was modelled using an analytical solution presented by Sussman *et al.* (1972) that accounted for the angle the component of interest exited the outer periphery of the glass discs, the distance the component travelled, diffusion factors, and gas solubility in the solvent coating the glass discs. The model agreed with experimental results for separating methane and butane, predicting the exit positions, but underestimated butane peak spreading.

Differences between continuous disc chromatography and the CRFC described in this thesis are summarised in Table 2-4. Although the CRFC and continuous disc chromatography are similar in principle, their intended use and separation method are quite different.

Table 2-4. Differences between continuous disc chromatography and continuous radial flow chromatography.

	Continuous disc chromatography	Continuous radial flow chromatography
Mobile phase	Gas	Liquid
Separation media	Solvent-coated glass discs	Resin packed annular bed
Separation type	Isocratic	Step elution
Separation	Volatile organics	Water soluble compounds
Flow direction	Outward	Inward

2.11.3 Absorbent wheels for gas separation

Modified versions of systems proposed by Mosier (1963), Sussman (1970) and Wankat (1977) are used commercially for treating waste gas for volatile organic compounds (Figure 2-17). Most of these systems are axial flow but some have a radial flow format (LeVan *et al.* 1997). Most of the adsorbent bed is exposed to the gas being treated, while a small section is regenerated. The adsorbent wheels rotate step-wise indexing to a new position, instead of rotating continuously. These systems have low efficiency due to the short contact time of the gas with the resin bed, mechanical leakage at the seals and from allowing the adsorbent wheel to exceed breakthrough to increase packed bed utilisation.

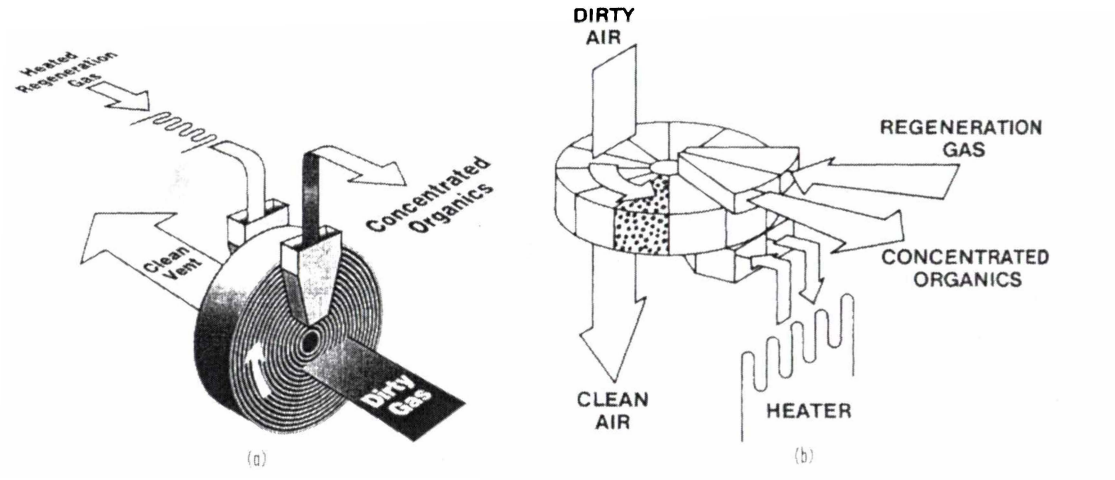

Figure 2-17. Absorbent wheels for gas separation: (a) horizontal with fixed beds; (b) vertical monolith (LeVan *et al.* 1997).

2.11.4 Other variations

Radial flow moving bed reactors used in the continuous catalytic reforming of UOP and IFP are one other variation of continuous radial flow systems (Song *et al.* 1994). Rather than using a rotating packed bed, the catalyst bed moves down through a radially flowing gas stream (Figure 2-18).

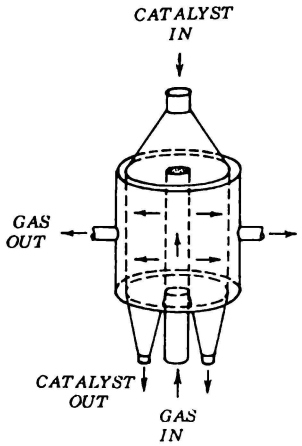

Figure 2-18. Typical arrangement of a moving bed reactor with outward radial flow of reactant gas (Song *et al.* 1994).

2.12 Modelling of radial flow and rotating annular bed chromatography

Surprisingly, very little work has been reported in modelling liquid radial flow packed bed chromatography compared with conventional chromatography. Most were theoretical only, with only three comparisons to experimental results:

- K^+ uptake on cation exchange resin (Lapidus and Amundson 1952).
- $CuSO_4$ and HAc on Al_2O_3 granular particles (Lapidus and Amundson 1952).
- Exchange of Na^+ and Ca^{2+} ions and H^+ on cation exchange resin (Tsaur 1996; Tsaur and Shallcross 1997).

Radial flow packed bed models have not yet been tested for ion-exchange of proteins, which is unusual considering that large scale radial flow processes have been developed for separating whey proteins and other foodstuffs. An experimentally verified model for separating proteins in a radial flow chromatography system would be useful as it could be used to predict performance and operating conditions.

In contrast to radial flow chromatography, models for rotating annular bed liquid chromatography have been applied to a wide range of separations, including one novel application (Table 2-5). Because the CRFC is intended for step-elution separation of a mixture of proteins, the review of annular chromatography models will be limited to step elution models.

This section will describe general models for radial flow and rotating annular bed chromatography. Specific examples for modelling packed bed radial flow chromatography and approaches taken to model step-elution separations in rotating annular bed chromatography will be discussed.

Table 2-5. Separations modelled in rotating annular bed chromatography.

Separation	Type	Reference
Size exclusion of blue dextran	Isocratic	(Scott *et al.* 1976)
Metals	Isocratic	(Begovich *et al.* 1983; Begovich and Sisson 1984)
	Step elution	(Carta *et al.* 1989)
Sugars	Isocratic	(Howard *et al.* 1988; Byers *et al.* 1989; Byers *et al.* 1990; Takahashi and Goto 1994; Bart *et al.* 1996)
Amino acids	Isocratic	(Takahashi and Goto 1991c; Goto and Takahashi 1993; Yonemoto *et al.* 1993; Kitakawa *et al.* 1995; Kitakawa *et al.* 1997)
	Concentration	(Takahashi and Goto 1991a; Goto and Takahashi 1993)
	Step-elution	(De Carli *et al.* 1990; Goto and Takahashi 1993)
Sodium chloride and methanol	Isocratic	(Goto and Takahashi 1993)
Desalting of BSA	Isocratic	(Reissner *et al.* 1997)
Separation of proteins	Isocratic	(Bloomingburg *et al.* 1991)
	Step-elution	(Bloomingburg and Carta 1994)
Removal of protein aggregates	Isocratic	(Buchacher *et al.* 2001)
Refolding of proteins	Isocratic	(Schlegl *et al.* 2003)

2.12.1 General equations

The continuity equation for a radial flow column is

$$\frac{\partial C_A}{\partial t}+\left(\frac{1-\varepsilon_R}{\varepsilon_R}\right)\frac{\partial C_{RA}}{\partial t}=\frac{1}{r}\frac{\partial}{\partial r}\left(rD_{Ar}\frac{\partial C_A}{\partial r}\right)-\frac{Q}{\varepsilon_R A_r}\frac{\partial C_A}{\partial r} \qquad (1)$$

where C_A is interstitial solute concentration, t is time, ε_R is external void fraction of the chromatographic media, C_{RA} is the concentration of solute in the resin, D_{Ar} is radial dispersion coefficient, Q is flowrate, and A_r is area of the radial column perpendicular to the direction of flow (Gu *et al.* 1991; Tsaur and Shallcross 1997b).

The continuity equation for rotating annular bed chromatography can be obtained by adapting the mass balance equation for an axial flow column,

$$\frac{\partial C_A}{\partial t}+\left(\frac{1-\varepsilon_R}{\varepsilon_R}\right)\frac{\partial C_{RA}}{\partial t}=D_{Az}\left(\frac{\partial^2 C_A}{\partial z^2}\right)-\frac{Q}{\varepsilon_R A_z}\frac{\partial C_A}{\partial z} \tag{2}$$

where z is axial position, D_{Az} is the axial dispersion coefficient and A_z is cross sectional area perpendicular to flow. The transformation given by Wankat (1977)

$$t=\frac{\theta}{w} \tag{3}$$

where θ is angular position and w is rotation speed, can be used to give

$$w\frac{\partial C_A}{\partial \theta}+w\left(\frac{1-\varepsilon_R}{\varepsilon_R}\right)\frac{\partial C_{RA}}{\partial \theta}=D_{Az}\left(\frac{\partial^2 C_A}{\partial z^2}\right)-\frac{Q}{\varepsilon_R A_z}\frac{\partial C_A}{\partial z} \tag{4}$$

Angular dispersion may be significant as concentration changes with angular position in rotating annular beds. When angular dispersion is included equation (4) becomes

$$w\frac{\partial C_A}{\partial \theta}+w\left(\frac{1-\varepsilon_R}{\varepsilon_R}\right)\frac{\partial C_{RA}}{\partial \theta}=D_{Az}\left(\frac{\partial^2 C_A}{\partial z^2}\right)+\frac{D_{A\theta}}{r_A{}^2}\left(\frac{\partial^2 C_A}{\partial \theta^2}\right)-\frac{Q}{\varepsilon_R A_z}\frac{\partial C_A}{\partial z} \tag{5}$$

where $D_{A\theta}$ is angular dispersion coefficient and r_A is radius of the annular bed (Buchacher *et al.* 2001). The change in concentration due to angular dispersion can take two different forms depending on how the mass balance is done. It is either

$$\frac{D_{A\theta}}{r_A{}^2}\left(\frac{\partial^2 C_A}{\partial \theta^2}\right) \quad \text{or} \quad D_{A\theta}\left(\frac{\partial^2 C_A}{\partial \theta^2}\right) \tag{6}$$

where $\partial\theta$ is in radians for the first (Buchacher *et al.* 2001), and in cm for the second (Thiele *et al.* 2001).

Area normal to flow A_r in a radial column changes with radial position and is given by

$$A_r=2\pi rH \tag{7}$$

Axial cross sectional area A_z is constant with axial position

$$A_z=\pi\left(r_1{}^2-r_2{}^2\right) \tag{8}$$

2.12.2 Dispersion

Column dispersion can be due to convective mixing or eddy dispersion and diffusion of solute in the interstices of the packed bed. The interstitial dispersion coefficient can be set empirically or calculated by

(Gu *et al.* 1991) $$D_{Ar} = y_1 D_{mA} + y_2 (2R_p) v_r \tag{9}$$

(Thiele *et al.* 2001) $$D_{Az} = y_1 D_{mA} + y_2 (2R_p) v_z \tag{10}$$

(Thiele *et al.* 2001) $$D_{mA} \leq D_{A\theta} \leq D_{Az} \tag{11}$$

where $y_1 D_{mA}$ represents molecular diffusion and $y_2 (2R_p) v$ represents eddy dispersion, y_1 and y_2 are constants with values of approximately 0.7 and 0.5 respectively (Gu *et al.* 1991), D_m is molecular diffusivity, R_p is radius of the resin particle and v is interstitial velocity given by

$$v_r = \frac{Q}{A_r \varepsilon_R} \text{ and } v_z = \frac{Q}{A_z \varepsilon_R} \tag{12}$$

Eddy dispersion is much larger than molecular diffusion for liquids flowing through packed beds, so molecular diffusion can be neglected. In gas radial flow chromatography, molecular diffusion dominates (Rice and Heft 1991), so eddy dispersion can be neglected. Tsaur (1996) used $D_{Ar} = \lambda v_r$ to determine the radial dispersion coefficient and characterised λ from experimental work.

The assumption implicit in equations (9) and (10) is that eddy dispersion has a linear relationship with interstitial velocity. Results from work on an axial flow column confirm an approximate linear dependency (see Tsaur 1996). Therefore D_{Az} and $D_{A\theta}$ remain constant with axial and angular position for annular chromatography, while D_{Ar} changes with radial position in radial columns. This has certain implications that are described by Gu (1995).

Gu (1995) defines the radial Peclet number, the ratio of convective to dispersive mass transfer as

$$Pe_r = \frac{v_r(r_1 - r_2)}{D_{Ar}} \tag{13}$$

where $(r_1 - r_2)$ is the radial bed depth. This equates with the definition of the Peclet number for axial flow columns

$$Pe_z = \frac{v_z L}{D_{Az}} \tag{14}$$

where the L is length of the column or axial bed depth.

When molecular diffusion is neglected, equation (9) reduces to

$$D_{Ar} = y_2(2R_p)v_r \tag{15}$$

Substituting this into equation (13) gives

$$Pe_r = \frac{(r_1 - r_2)}{y_2(2R_p)} \tag{16}$$

Therefore the Peclet number is constant with radial position and is independent of interstitial velocity through the column (Gu 1995). It should therefore be the same regardless of what flowrate is applied to the column.

Dispersion can also occur due to diffusion of solute between resin interstices and resin pores. This can be modelled using film diffusion and is incorporated into solute uptake equations described in the next section.

2.12.3 Solute uptake

Several approaches can be used to describe solute uptake by ion exchange resin. The simplest is to treat the ion exchange resin bed as a continuous porous network, where solute is in equilibrium between solution and the resin matrix. If the equilibrium is assumed to be instantaneous, for example where mass transfer resistances are negligible, a linear isotherm can be used to describe exchange. The linear isotherm is the simplification of the Langmuir isotherm for very weak absorbers or early stages of an adsorption

$$C_{RA} = K_A C_A \tag{17}$$

where C_{RA} is the resin phase solute concentration, and K_A is the ratio of forward and reverse rate constants k_{A1} and k_{A2}

$$K_A = \frac{k_{A1}}{k_{A2}} \tag{18}$$

The Langmuir isotherm is commonly used for non-linear adsorption. This allows equilibrium resin concentration to be calculated through to saturation

$$C_{RA}^{*} = \frac{K_A C_{RAMax} C_A^{*}}{1 + K_A C_A^{*}} \tag{19}$$

For multicomponent separation in radial flow, Gu *et al.* (1991) used the multicomponent Langmuir isotherm

$$C_{Ri} = \frac{K_i C_{RiMax} C_{Ri}}{1 + \sum_{j=1}^{Ns} K_j C_{Rj}} \tag{20}$$

where *Ns* is the number of solutes in competition for binding sites on the resin.

When mass transfer resistances are significant, equilibrium is not instantaneous and the linear iostherm becomes

$$\frac{\partial C_A}{\partial t} = \left(\frac{1-\varepsilon_R}{\varepsilon_R}\right)\frac{\partial C_{RA}}{\partial t} = k_{A1} C_A - k_{A2} C_{RA} \tag{21}$$

or

$$\frac{\partial C_A}{\partial t} = \left(\frac{1-\varepsilon_R}{\varepsilon_R}\right)\frac{\partial C_{RA}}{\partial t} = K_A C_A - C_{RA} \tag{22}$$

and the Langmuir isotherm converts to

$$\frac{\partial C_A}{\partial t} = \left(\frac{1-\varepsilon_R}{\varepsilon_R}\right)\frac{\partial C_{RA}}{\partial t} = k_{A1} C_A \left(C_{RAMax} - C_{RA}\right) - k_{A2} C_{RA} \tag{23}$$

For a binary mixture, equation (13) becomes

$$\frac{\partial C_A}{\partial t} = \left(\frac{1-\varepsilon_R}{\varepsilon_R}\right)\frac{\partial C_{RA}}{\partial t} = k_{A1}C_A\left(C_{RAMax} - C_{RA}\right) - k_{A2}\left(1 + K_B C_B\right)C_{RA} \tag{24}$$

where the reverse rate constant k_{A2} is increased by increasing concentrations of a competing solute.

These equations can be modified to incorporate additional rate controlling mechanisms such as film diffusion or solid diffusion. For example, equation (17) can be modified to

$$\frac{\partial C_A}{\partial t} = \left(\frac{1-\varepsilon_R}{\varepsilon_R}\right)\frac{\partial C_{RA}}{\partial t} = k_{fA}\left(K_A C_A - C_{RA}\right) \tag{25}$$

where k_f is a film diffusion rate coefficient (see for example Lapidus and Amundson 1950; Rice 1982).

Another common method is to treat the resin particles as porous spheres. Solute diffuses from flowing solution into the resin pores and exists in equilibrium between the stagnant solution in the pores and the resin matrix. This method has varying degrees of complexity. The simplest is to use an averaged pore concentration (Kaczmarski *et al.* 2001), while a more complex method involves discretising the resin particle into spherical layers (Gu *et al.* 1991). The change in solute concentration due to diffusion into the resin pores is given by

$$\frac{\partial C_A}{\partial t} = \left(\frac{1-\varepsilon_R}{\varepsilon_R}\right)\frac{\partial C_{RA}}{\partial t} = \frac{3k_{fA}\left(1-\varepsilon_R\right)}{\varepsilon_R R_p}\left(C_A - C_{RPA}\right) \tag{26}$$

where C_{RPA} is solute concentration in the resin pores near the surface if using a layered model, or average solute concentration in the pores over the entire resin particle. k_f can be calculated using equations presented by, for example, Nelson and Galloway (1975) or Kaczmarski *et al.* (2001).

Gu *et al.* (1991), in developing a radial flow model, used a general mass balance equation to describe the solute diffusing through the pores of the resin,

$$\frac{\partial}{\partial t}\left[\left(1-\varepsilon_p\right)C_{RA}+\varepsilon_p C_{RPA}\right]-\varepsilon_p D_{eff}\left[\frac{1}{R^2}\frac{\partial}{\partial R}\left(R^2\frac{\partial C_{RPA}}{\partial R}\right)\right]=0 \tag{27}$$

where ε_p is resin porosity, C_{RPA} and D_{eff} is concentration and effective diffusivity of solute in the pores, and R is radial position in the resin. Alternatively, a simple mass balance can be used for the entire resin particle (Kaczmarski *et al.* 2001)

$$\frac{\partial C_{RPA}}{\partial t}+\frac{\left(1-\varepsilon_p\right)}{\varepsilon_p}\frac{\partial C_{RA}}{\partial t}=\frac{3k_{fA}}{R_p\varepsilon_p}\left(C_A-C_{RPA}\right) \tag{28}$$

Exchange of solute between the pores and resin matrix can be described by adapting the linear and Langmuir isotherm equations by substituting C_A for solute concentration in the resin pores C_{RPA}. For example, using a linear isotherm, the uptake equation becomes

$$\frac{\partial C_{RPA}}{\partial t}=\frac{\left(1-\varepsilon_p\right)}{\varepsilon_p}\frac{\partial C_{RA}}{\partial t}=K_A C_{RPA}-C_{RA} \tag{29}$$

2.12.4 Radial flow models

This section briefly reviews several gas and liquid radial flow chromatographic models developed for packed annular beds. Other models have been developed for thin layer and paper radial flow chromatography (for example, Rachinskii 1968) but are not considered here.

Lapidus and Amundson (1952) compared a range of different adsorption mechanisms including kinetic mechanisms of various orders (for example the Langmuir isotherm), and liquid and solid diffusion equations for predicting uptake of KCl onto Dowex 50 resin, and $CuSO_4$ and HAc onto Al_2O_3 granular particles, in an outward flowing radial flow bed. Radial dispersion was neglected. They found that a liquid diffusion-linear isotherm model was best for KCl onto Dowex 50 and the solid diffusion-linear isotherm model was best for $CuSO_4$ and HAc onto Al_2O_3. Lapidus and Amundson (1952) used both numerical and analytical approaches to solve their models.

Rice (1982) presented an analytical solution for a model of outward flowing radial flow gas chromatography, where radial dispersion was neglected and negligible inner

chamber diameter was assumed. A parabolic concentration profile for solute inside a resin particle was adoped for calculating average resin phase concentration, and a film diffusion-linear isotherm was used for solute uptake. Yee (1987) adapted Rice's model to account for the inner chamber. Ethane and air response tests were performed on a compressed outward flowing radial flow bed packed with activated alumina. It was found that radial dispersion was needed in the model to to achieve a good fit with experimental data.

Rice *et al.* (1989) modified his original model to account for eddy dispersion and molecular diffusion in the packed bed interstices. Film diffusion was neglected and a linear isotherm was used to describe uptake. The model was solved numerically using an explicit finite different method and a good fit was achieved for response tests using methane pulses in a helium carrier gas. The dispersion coefficients obtained compared well to helium diffusivity in methane so Rice *et al.* (1989) concluded that molecular diffusion was the main contributor to peak spreading in gas radial flow chromatography and that intraparticle resistances were small. An analytical solution to this model was developed (Rice and Heft 1990) and an excellent fit with experimental data was achieved for response tests using methane and butane (Rice and Heft 1991). Theoretical work showed inward flow would give slighter sharper peaks (Heft 1991). Rice and Heft (1991) point out that while molecular diffusion dominates eddy dispersion in gas chromatography, in liquid chromatography it becomes small in comparison to eddy dispersion, which is dependent on interstitial velocity.

Huang *et al.* (1988a) used a film diffusion linear isotherm model, and included radial dispersion but assumed D_{Ar} to be constant with radial position. Therefore, the dispersion part of equation (1) becomes

$$\frac{D_{Ar}}{r}\frac{\partial}{\partial r}\left(r\frac{\partial C_A}{\partial r}\right) \tag{30}$$

In gas chromatography, a constant D_{Ar} can be assumed as molecular diffusion is much larger than eddy dispersion (Rice and Heft 1991). In liquid chromatography, assuming a constant D_{Ar} is questionable as it neglects the impact of changing velocity on eddy dispersion (Tsaur and Shallcross 1997b). Huang *et al.* (1988a) referred to bioseparation so clearly their model was intended for liquid chromatography. A constant D_{Ar} may be

suitable for annular beds with large inner diameters and short bed depths where change in velocity across the bed is not great, but could produce erronous results in radial columns of small inner diameters and large bed depths. Huang *et al.*'s (1988a) model was solved numerically using finite differences. Column breakthrough for a single solute was simulated using different values for the equilibrium constant K_A, film diffusion coefficient k_{fA} and dispersion constant D_{Ar}. They showed that high K_A values gave earlier breakthrough, k_{fA} became rate controlling at low values, and high D_{Ar} values increased breakthrough curve tailing.

Gu *et al.* (1991) presented a multicomponent radial flow model that included radial dispersion, film and pore diffusion and a multicomponent Langmuir isotherm for solute uptake. The resin particle was discretized into spherical layers, and diffusion of solute through the resin pores modelled. D_{Ar} and k_{fA} was assumed to be dependent on radial interstitial velocity. The model was made dimensionless, solved using a finite element method and orthogonal collocation. Simulations were run using Fortran for a two-component separation. They found that inward flow gave slightly sharper concentration profiles, decreasing Peclet numbers reduced resolution, and increasing k_{fA} and pore diffusion coefficients increased resolution. Gu *et al.* (1992) adapted this model for simulating affinity radial flow chromatography where solute was eluted by reacting it with a soluble ligand. They found increasing the soluble ligand concentration eluted the solute more rapidly.

Tsaur and Shallcross (1997b) examined the exchange of sodium and calcium ions on radial and axial flow columns and used an elaborate binary cation exchange thermodynamic equilibrium model to describe solute uptake by the resin (fully described in Tsaur 1996). An instantaneous equilibrium was assumed, film diffusion was not considered and radial dispersive effects were treated as dependent on interstitial velocity. An explicit finite difference technique was used to solve the model. Simulations were run in Fortran and there was excellent agreement between experimental data and the model.

Examination of Tsaur's (1996) data from dispersion experiments with an axial flow column indicates that a linear correlation for dispersion can be used, although it is not as accurate as the empirical correlation Tsaur obtained using curve fitting methods (Figures 2-18 and 2-19).

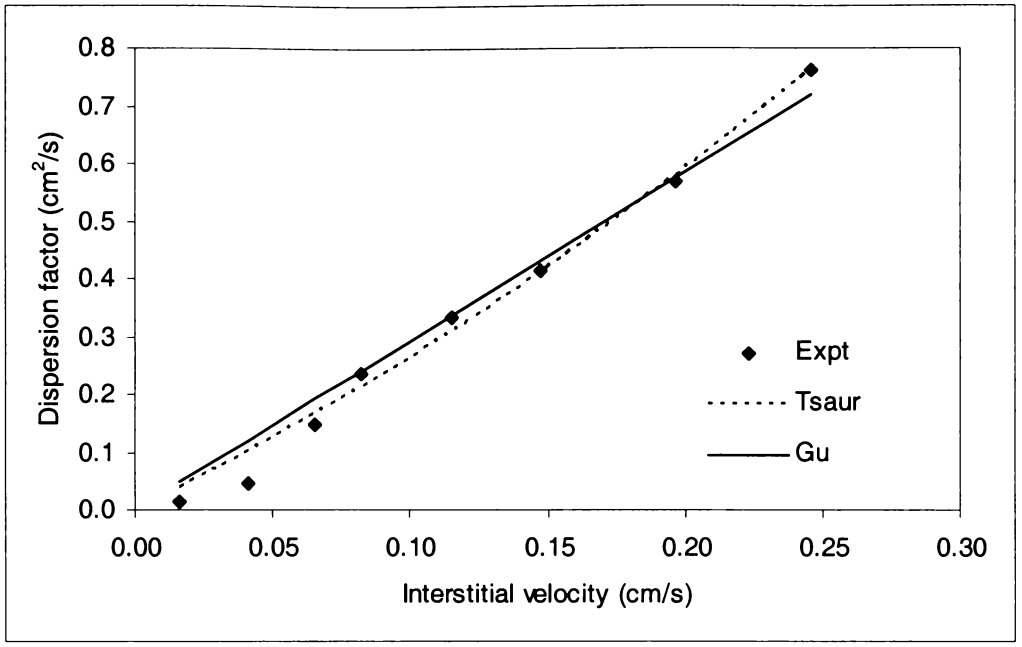

Figure 2-19. Experimentally determined dispersion factors for a 53.5-cm long 2.65-cm I.D. axial flow column packed with Dowex resin in Na form (porosity 0.307, resin diameter 0.3-0.85 mm) (using data from Tsaur 1996).

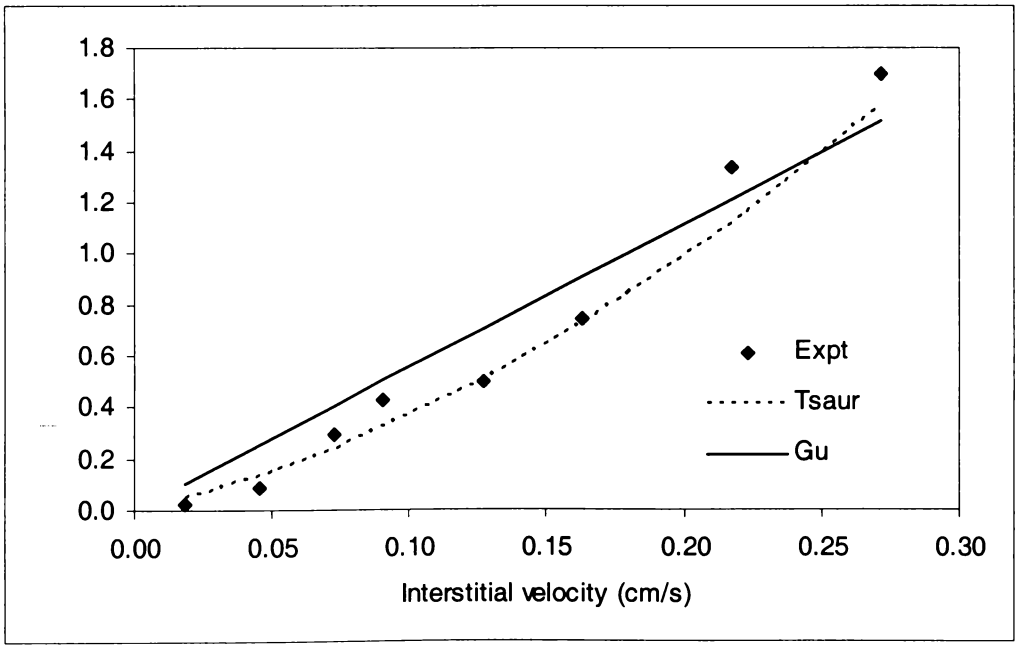

Figure 2-20. Experimentally determined dispersion factors for a 53.5-cm long 2.65-cm I.D. axial flow column packed with Dowex resin in H form (porosity 0.275, resin diameter 0.3-0.85 mm) (using data from Tsaur 1996).

Tsaur (1996) only performed dispersion experiments for two flowrates in the radial flow column, so there is not enough data to indicate whether a linear correlation for dispersion can be used. The Peclet number for the higher flowrate was two thirds that of the lower flowrate, which implies that the relationship $D_{Ar} = \lambda v_r$ was incorrect, or that other factors within or outside the column were not considered. Tsaur (1996) assumed an instantaneous equilibrium and did not consider film diffusion. This could make the dispersion coefficient appear to increase with interstitial velocity, even though increased band spreading could be due to film diffusion.

2.12.5 Annular step elution models

Carta *et al.* (1989) modelled continuous separation of iron and chromium and used equation (4) for the overall model of the annular chromatograph. The uptake of solute was described using a linear isotherm coupled with solid diffusion (equation (25)) instead of film diffusion. They used a general dispersion coefficient that combined axial and angular dispersive contributions. Equation (4) was used to model the eluent, but interaction with the resin was neglected. The distribution coefficient K for each metal in equation (25) was calculated as

$$K = \alpha(C_S)^{\beta} \tag{31}$$

where C_S is the concentration of the eluent and α and β are fitted parameters. This allowed the two continuity equations for the metal solution and eluent to be coupled. The model was solved numerically using orthogonal collocation. Model parameters were obtained from fixed bed experiments. They found that bed dispersion was negligible and that there was an excellent fit with experimental results.

DeCarli *et al.* (1990) modelled continuous separation of three amino acids in a rotating annular bed chromatograph using cation exchange and step elution using different concentrations of NaOH. Four continuity equations were developed, one for each amino acid and one for sodium. Angular and axial dispersion, mass transfer resistances and accumulation of solutes in the resin bed interstices were neglected. Amino acid uptake was based on ionic concentrations of amino acid cations and hydrogen ions, dissociation constants and exchange selectivities. Displacement was modelled on sodium ions adsorbing preferentially to the amino acids as well as the high pH making

the overall charge of the amino acid negative. The model was solved using finite differences, where the column was divided along the axis into N equilibrium stages and the concentrations of each stage calculated for each time step. N was adjusted so model curves would fit the experimental data. A lower N gives greater peak spreading, simulating bed dispersion. The model and experimental data was in reasonable agreement except peak spreading was underestimated. The model predicted NaOH would elute earlier than what occurred experimentally, because solute accumulation in the bed interstices was neglected.

Bloomingburg and Carta (1994) modelled the continuous separation of bovine serum albumin and haemoglobin. Cation exchange resin was used and conditions set so only haemoglobin would bind. Haemoglobin adsorption in different concentrations of NaCl was modelled using the Langmuir isotherm

$$C_{RA}^{*} = \frac{AC_A^{*}}{1+BC_A^{*}} \tag{32}$$

where $A = K_A C_{RAMax}$ and $B = K_A$. The Langmuir isotherm was fitted to adsorption data for each salt concentration by adjusting parameters A and B to obtain an empirical correlation. Uptake kinetics were studied using stirred tank experiments and modelled assuming transport within the resin occurred through surface and pore diffusion. Data were then used to develop a model for continuous separation. The concentration of bovine serum albumin, haemoglobin and NaCl in the rotating annular bed was modelled using equation (4). Axial dispersion was neglected and uptake was modelled using

$$\left(\frac{1-\varepsilon_R}{\varepsilon_R}\right)\frac{\partial C_{RA}}{\partial t} = k_{fA}\left(C_A - C_A^{*}\right) \tag{33}$$

where C_A^{*} was calculated using equation (32), and k_{fA} was calculated as a function of surface and pore diffusion for each component

$$k_{fA} = \frac{15}{R_p^{\,2}}\left(D_{pA} + D_{sA}\frac{\partial C_{RA}}{\partial C_A}\right)_{C_A = C_A^{*}} \tag{34}$$

D_{pA} and D_{sA} are the pore and surface diffusivities respectively and R_p is the outer radius of the resin particle. For BSA and NaCl, resin phase concentrations were taken as $C_{RA} = \varepsilon_p C_A^*$ and D_{sA} was set to zero assuming no surface diffusion. This allowed the model to be solved analytically. For haemoglobin, the model was solved numerically using orthogonal collocation, using the calculated NaCl concentrations from the analytical solution to determine parameters A and B in equation (32). The model gave good predictions for a range of flowrates and rotation speeds.

Goto and Takahashi (1993) modelled the step elution of amino acids using a change in pH in a rotating annular bed chromatograph. Film diffusion was used to describe the mass transfer of solute between the bed interstices and the resin pores, and a film diffusion-linear isotherm was used to describe exchange of solute between solution in the pores and resin matrix. Angular dispersion was neglected. The annular bed was modelled as having two zones, a loading zone and an elution zone. The positions of these were based on the expected helical profile the elution buffer would take through the rotating annulus. The linear isotherm equilibrium constant K_A was set to zero or nearly zero when solute was in the elution zone, simulating the desorption of solute by the elution buffer. Adsorption isotherms of each amino acid were measured for the loading pH and elution pH to determine K_A. Two amino acids were eluted isocratically and the third was eluted in the elution zone. Excellent fits were achieved for the isocratically eluted amino acids, but the model overestimated the peak height for the third amino acid and underestimated peak width. This was because the dispersive effects in the bed were neglected for the elution zone, which would produce a pH gradient rather than a step change.

2.13 Conclusions

In this chapter, technologies relevant to continuous radial flow chromatography, namely radial flow chromatography, annular chromatography and radial flow continuous chromatographic systems, have been reviewed.

Radial flow columns can operate at greater flowrates enabling faster separations, but they are limited by the short bed depth and dispersive effects of changing fluid velocity through a resin packed bed. They are better suited to step-elution separations where

column resolution is not as important. Alternate packings such as monolithic beds can be used, which allow faster separations because of the faster rate kinetics. However, such packings have lower loading capacities and need to be replaced once fouled or blocked.

The separation requirements and impact of lower column resolution in packed bed radial flow columns need to be balanced against the benefits of faster separation times. Rapid separations are beneficial for proteins sensitive to proteolysis, so resolution is not as important as retaining protein activity. In biotechnology, there are multiple steps in purifying a protein or enzyme. Therefore, using rapid, but low resolution techniques in the early purification stages may help reduce costs, increase yields and speed up processing.

The effect of flow direction, scale-up and flow distributors on performance and resolution in radial flow chromatography has not been thoroughly investigated. Some theoretical work has been done on the effect of flow direction on performance, but needs to be supported by experimental evidence. Several researchers have developed models for packed bed radial flow chromatography, but these have only been tested in liquid chromatography using salts and in gas chromatography. Models have not yet been tested for protein separations.

Moving bed cross flow systems such as annular chromatography and continuous radial flow chromatography are capable of multicomponent separation and are simple to operate. A batch chromatographic method can be adapted to annular chromatography and in some cases similar or better productivities can be achieved. The extent to which a method can be adapted is limited by the physical arrangement of the feed and eluent nozzles of the annular chromatograph and the flowrates that can be applied. Resolution appears to be an artefact of the way the exit ports are positioned at the base of the annulus. Models of annular chromatography have been applied to a wide range of separations.

Continuous disc chromatography has been developed that is similar in principle to the CRFC. However, its intended use and separation method is quite different because it uses solvent-coated glass discs to separate gaseous mixtures, whereas the CRFC uses a packed bed to separate protein mixtures.

Chapter 3

Prototype Design

3.1 Introduction

In previous work (Lay 1998) a continuous radial flow chromatograph (CRFC) was developed by combining two technologies, radial flow and rotating annular bed chromatography (Figure 3-1). The prototype consisted of a rotating annular bed through which two solutions, a protein laden feed and an elution buffer, flowed simultaneously in a radial direction cross-current to the movement of the bed. This configuration gave the following advantages:

- The short bed depth low reduces overall pressure drop.
- The cross-current regime enables multicomponent separations, unlike counter-current regimes which can only separate two or three components.
- The complex valve and control systems of other continuous processes, such as simulated moving bed chromatography, are not needed.

Several engineering problems were identified when testing the first prototype. One objective of this thesis was to design and construct a new prototype that minimised or eliminated these problems.

This chapter reviews the first CRFC prototype and describes an improved design.

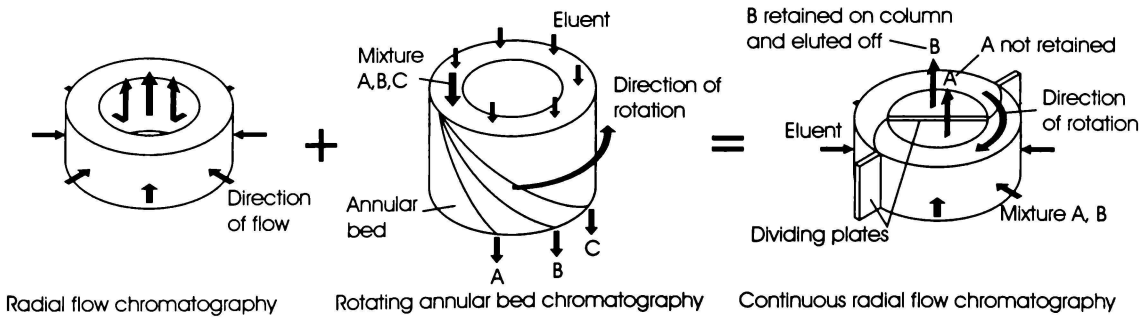

Figure 3-1. The CRFC concept, a combination of radial flow and annular rotating bed chromatography.

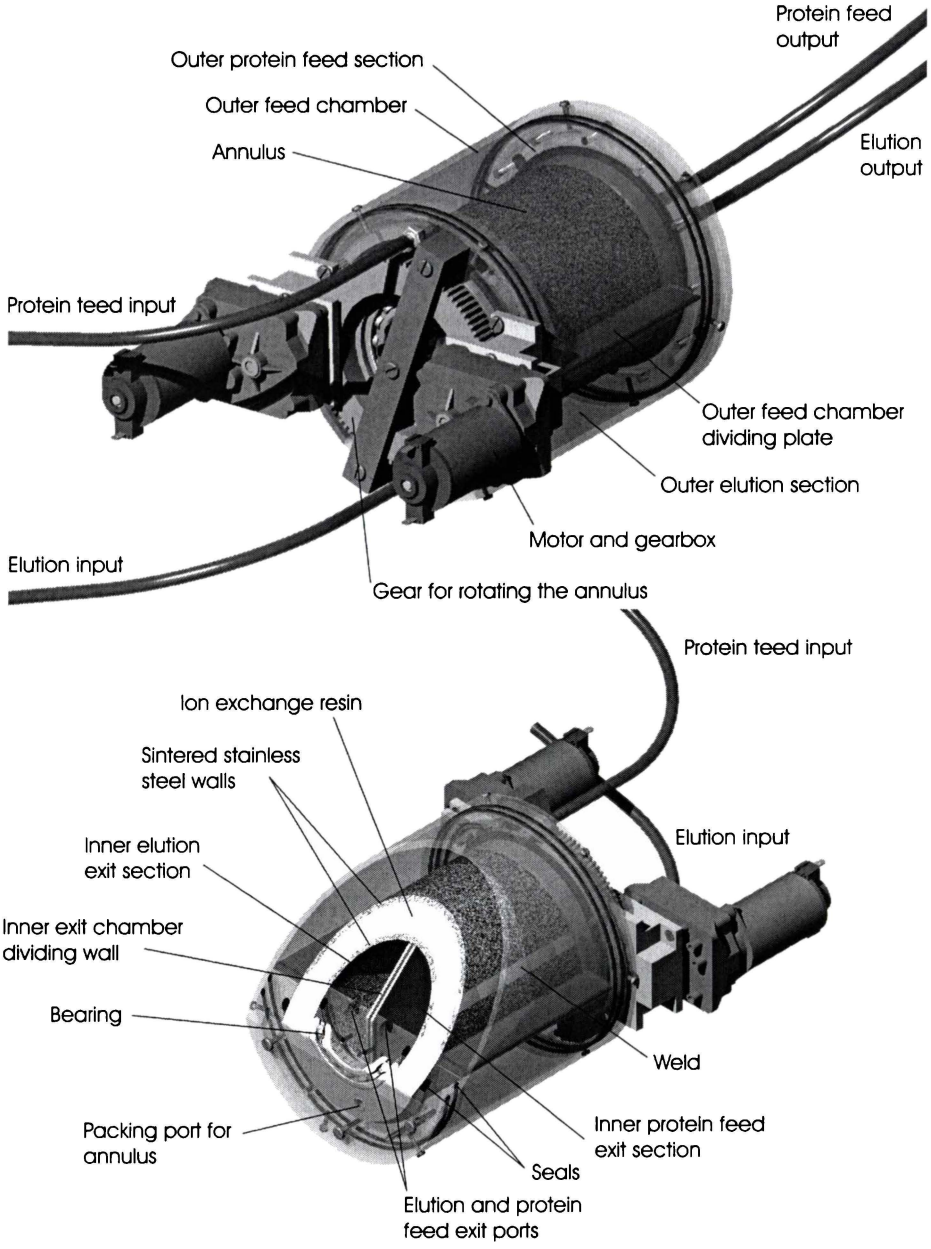

Figure 3-2. The first CRFC prototype (Lay 1998).

3.2 Construction of first CRFC prototype

The first CRFC prototype (Figure 3-2) consisted of an annular packed bed (I.D. 8.6 cm, O.D. 11.6 cm and length 12 cm) enclosed by two concentric porous cyclinders. The cylinders formed the outer and inner walls of the annulus and were constructed by rolling and welding sintered stainless steel sheet. These were sealed at each end to form an annular space which could be filled with chromatographic media through packing

ports at one end. A gear was attached to the other end so the annulus could be rotated using two D.C. motors.

Solution was pumped under pressure into an outer feed chamber surrounding the outer wall of the annulus, radially through the annular bed, and into an inner exit chamber at the axis of the CRFC. These chambers were constructed out of Perspex and were sealed at each end of the annulus using O-rings.

The feed and exit chambers were divided lengthwise into two sections so two solutions, a protein laden feed and elution buffer, could be applied to the annulus simultaneously. The target protein would bind to the resin in the loading zone and be transported by the rotation of the annulus to the elution zone where it would be eluted (Figure 3-3). The exit chamber dividing plate could be set to different angular positions to allow for angular displacement of the solutions as they passed through the annulus. The inner plate was fixed in position using a cross-bar and disc with angular slots attached to the outer chamber.

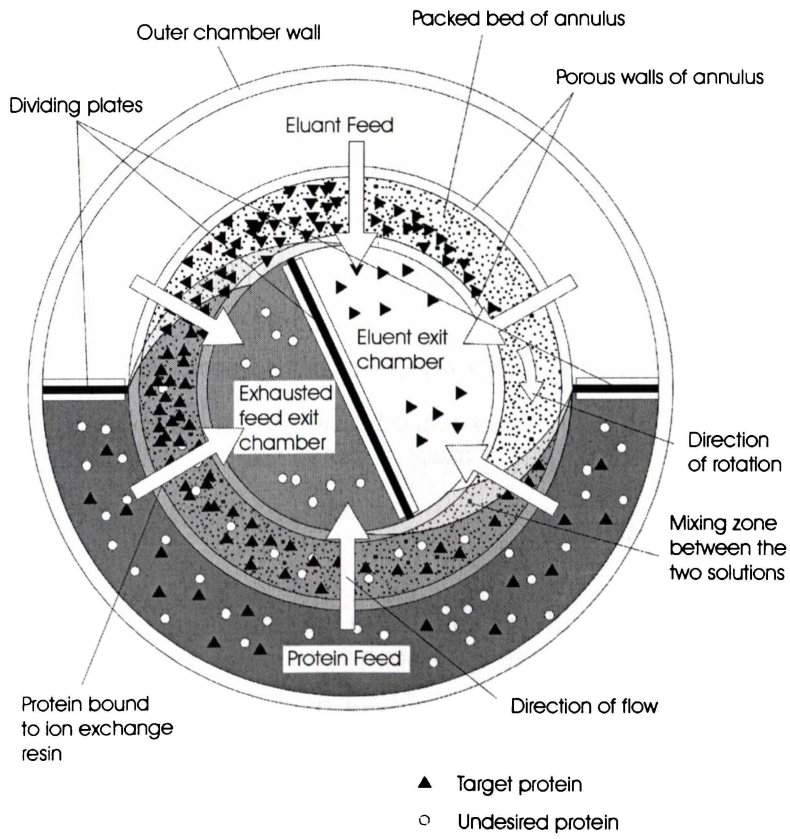

Figure 3-3. Cross-section of the first CRFC prototype.

3.3 Problems of the first prototype

Several problems associated with the feed and exit chambers, the annulus bed construction, and the gearing and motors were encountered during testing (Lay 1998).

3.3.1 Feed and exit chambers

There were several areas of concern with the feed and exit chambers.

- The feed and exit chambers had large open volumes, which resulted in low broad peaks and extended tailing. This concealed evidence of channelling in chromatograms during batch operation and increased the time to reach steady state during continuous experiments.

- The Perspex used for the outer chamber was not strong enough to withstand pressures greater than 345 kPa and cracked where the O-rings were housed. In addition, when one of the motors failed, the end of the feed chamber where the motors were attached deformed due to the force being exerted by the other motor, causing leakage around the seals.

- The O-rings used to seal the feed and exit chambers around the inner and outer circumferences of the annulus required a substantial amount of force to rotate the annulus. This force increased with lower rotation speeds. The annulus could not be reliably rotated at speeds less than 0.3 r.p.m.

- The bearings housed in the inner chamber adjacent to the O-rings were exposed to solution when the O-rings leaked, resulting in corrosion.

3.3.2 The annulus

There were four concerns with the annulus in the first prototype:

- Welds in the annulus walls obstructed flow and generated oscillations in the exit solute concentrations when the annulus was rotating.

- The limited access to the annulus interior via the packing ports made unpacking of the annulus difficult and it was not possible to verify that all the resin had been removed from the interior.

- The annulus had a bed volume of 600 ml, so large quantities of buffer and feed solution were needed to operate the CRFC for extended times.

- The short bed depth would impact on column resolution resulting in broader peaks and reduced separating power.

3.3.3 General set-up

- The CRFC was constructed as a single entity with a horizontal axis of rotation. The unit had to be dismantled when making modifications, which was time consuming. In addition, the annulus had to be held vertically during packing.

- The annulus tended to move along its central axis when rotating if it was slightly out of alignment.

- Flowrates through the annular bed were much higher than ideal. The CRFC was operated at a total flowrate of 9 ml/s and 0.3 to 0.4 r.p.m. Annulus rotation speed and flowrate had to be decreased to minimise angular displacement of solution as it passed through the annular bed, but the motors could not operate reliably at under 0.3 rpm.

- The high rotation speeds would result in broad elution peaks.

- Brass gears for rotating the annulus were found to wear quickly and were subsequently replaced with steel gears.

- Pinion gears were held in position at one end only. This allowed the pinion gear shafts to flex due to the high resistance of the annulus to rotation, which caused the gears to mesh incorrectly. A more robust set-up was used when steel gears were installed which involved fixing the shaft position at both ends.

3.4 Design considerations for the second prototype

Based on the problems identified with the first prototype, the second prototype was designed with the following criteria:

- Components built from stainless steel.
- Withstand pressures of greater than 690 kPa.
- Withstand corrosive solutions.
- Minimise or eliminate flow obstructions in the porous walls of the annulus.
- Divide the CRFC into separate modules that fit together. For example: a top bearing housing; a separation module containing the annulus and outer feed and inner exit chambers; and a bottom bearing housing.
- A vertical axis of rotation for ease of assembly and disassembly of modules.
- Position of dividing plates in the inner exit chamber easily adjustable to allow for angular displacement of solutions flowing through the rotating annulus.
- Removable annulus lid to expose the packed bed for easy unpacking.
- A greater effective bed depth to allow for greater resolution.
- Shorter annulus axial length to decrease the volumes of solution, overall flowrates, and resin volume required for operation.
- Motors and gearing sufficiently robust so the annulus could be rotated for long periods without wear.
- Annulus to rotate at speeds from 0.02 to 0.5 r.p.m.
- A combination of deep groove and angular contact bearings to prevent sideways or axial movement when the annulus is rotating.

3.5 Design and construction of the second CRFC

The second CRFC was designed as a modular system consisting of a top bearing housing; separation module; bottom bearing and gear housing; and stand mounted motor (Figure 3-4).

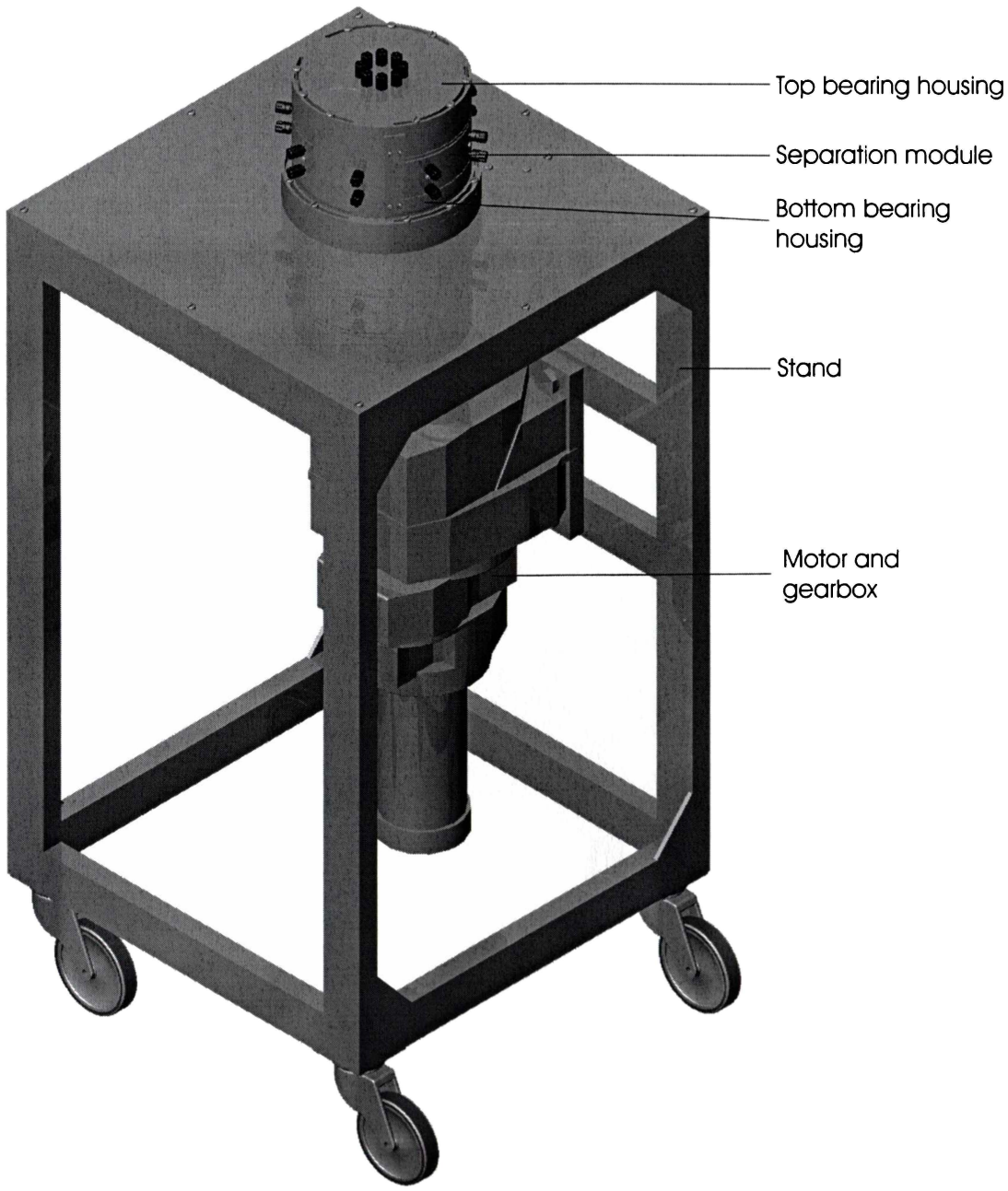

Figure 3-4. Fully assembled new CRFC prototype.

The four modules are stacked vertically so the central axis of rotation is vertically aligned. The vertical arrangement and modular approach has the following advantages:

- Compact and easy to assemble and modify. For example, greater throughput could be achieved by increasing the axial length of the separation module, while the other units remained the same.
- Easy access to the feed and effluent ports.
- Easy to purge air from the system.
- Better protection of bearings. The primary seals in the separation module retain solution under high pressures while secondary, looser fitting, seals in the bearing housings protect the bearings from leakage from the separation module.

The modules slot into each other via keys and pins and are locked in place using screws on the CRFC exterior. Three angular slots at the base and top of the CRFC allow for the angular position of the outer feed chamber to be set relative to the inner feed chamber. This design also allowed easy removal of the upper bearing housing to access the separation module.

3.5.1 Separation module

The separation module consists of the annulus, and inner and outer chambers. The design is illustrated in Figures 3-5 to 3-7.

3.5.1.1 The annulus

The annulus (Appendix A.2) has two parts: the casing (which contains the separation media) and the lid (Figure 3-7). The casing consists of a base to which two concentric sintered stainless steel cylinders are welded. Braces are welded to the cyclinders and are used to attach the lid. The lid is designed so that it sits flush with the top of the resin bed and is sealed using o-rings. The annulus can be pump-packed through four ports in the lid. The lid can be easily removed for unpacking the annulus.

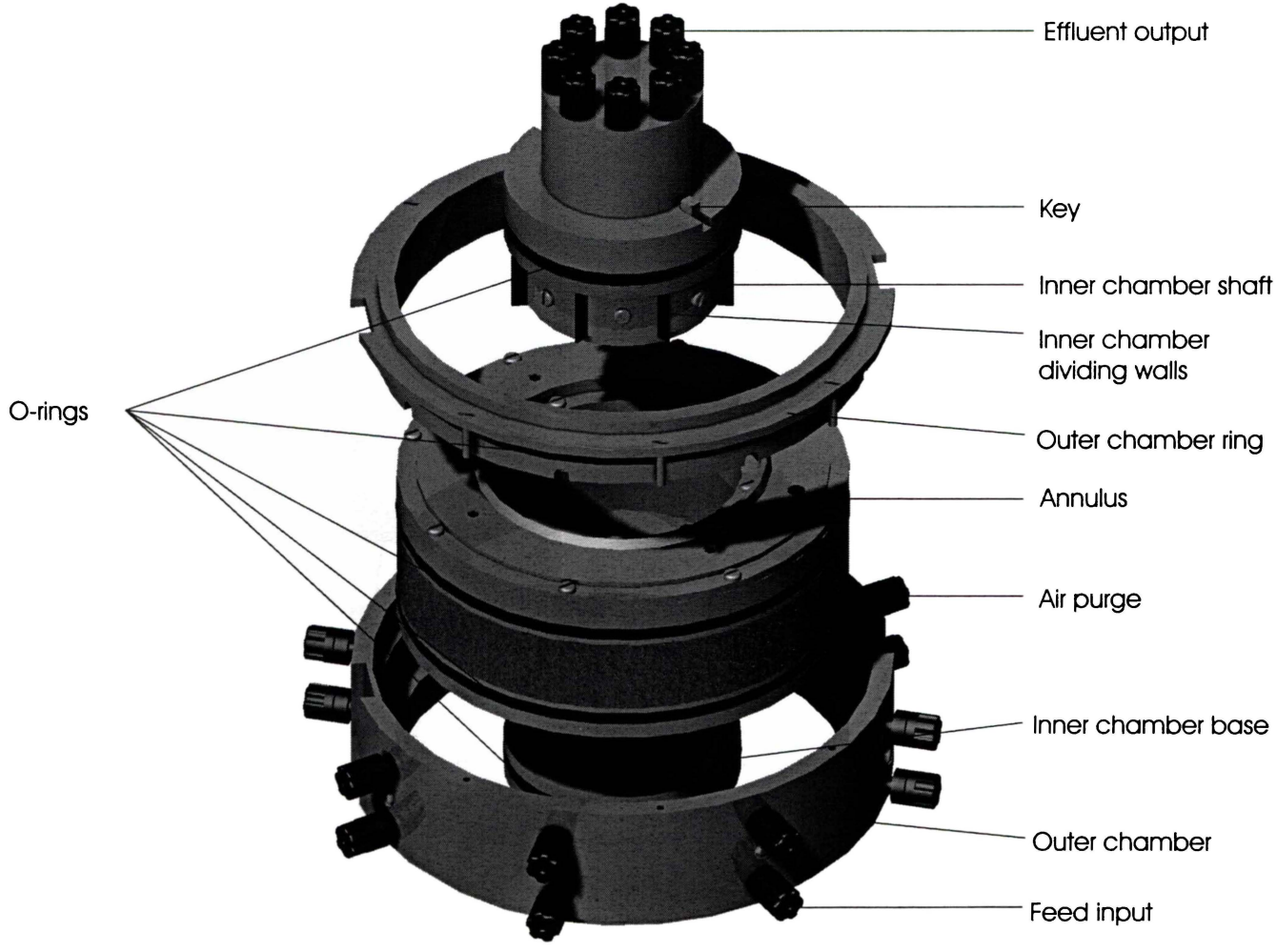

Figure 3-5. Exploded view of the separation module.

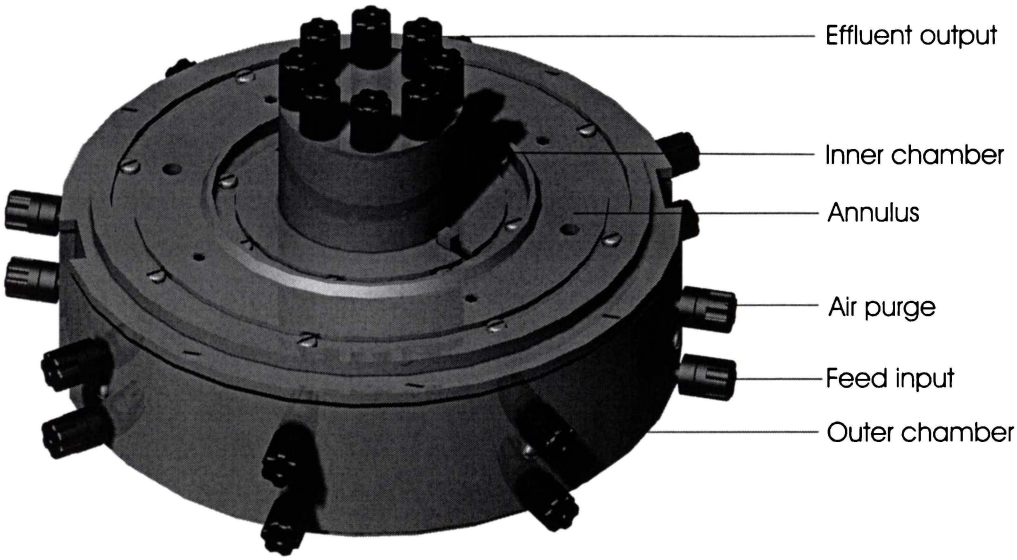

Figure 3-6. Separation module: Annulus and inner and outer chambers assembled.

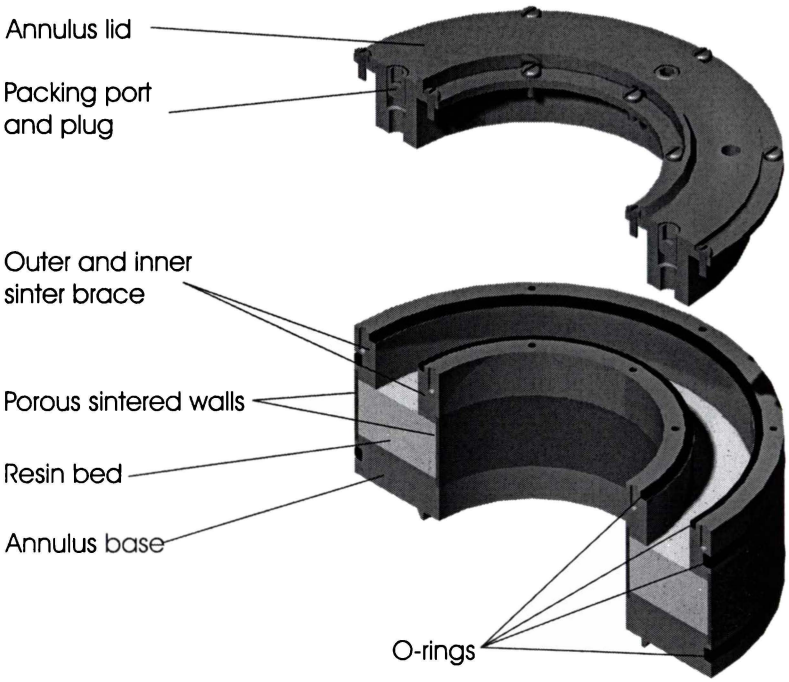

Figure 3-7. Exploded and sectioned view of annulus.

Ideally, there should be no flow obstructions in the sintered stainless steel walls. However, it was not possible to obtain a uniformly porous cylinder of the dimensions required for the annulus. Pall New Zealand (Hamilton), a supplier of sintered stainless

steel and filters, was asked to construct the cylinders from sintered stainless sheet to minimise the width of the flow obstruction due to welding.

O-rings near the top and bottom of the annulus seal the outer chamber. O-rings generate high resistance to rotation, requiring a powerful motor for rotating the annulus. However, they provide a reliable seal and occupy a small space, simplifying construction. Mechanical seals, for example, would require much more space and are more complex.

Pins are used to transmit rotational motion from the bottom bearing housing to the annulus and from the annulus to the top bearing housing. Circular grooves in the top and bottom bearing housings keep the axis of rotation of the annulus coincident to those of the bearing housings.

3.5.1.2 Wall effects in the annulus

Preferential flow close to the walls in packed beds can occur, affecting column resolution. This occurs because interstices between the resin and wall are greater than amongst the tightly packed resin, giving less resistance to flow. Wall effects have been observed in studies of axial flow beds (Fahien and Smith 1955) and radial flow columns (Tsaur 1996).

As shown in Section 2.6.2.1, wall effects can be neglected if the aspect ratio, defined as the height of the bed divided by the average particle diameter for radial flow columns, exceeds 20. Table 3-1 shows the aspect ratio is well in excess of this value, even for a bed height of 10mm.

Table 3-1. Effect of height and diameter of radial and axial flow columns on aspect ratio and area affected for 100μm diameter resin.

CRFC			Axial Flow Column		
Bed height (mm)	Aspect ratio	Area affected (%)	Bed diameter (mm)	Aspect ratio	Area affected (%)
10	100	1.00	10	100	1.99
20	200	0.50	20	200	1.00
120	1200	0.08	120	1200	0.17

Mueller (1999) examined the impact of walls in annular packed beds on void fraction. He found that the largest void fraction was within a region between the wall and a distance from the wall equal to the radius of the resin particle. The cross-sectional area perpendicular to flow that is affected by wall effects was calculated for radial and axial flow columns and was found to be negligible for the CRFC (Table 3-1).

3.5.1.3 The inner chamber

The inner chamber has two main parts: the inner chamber shaft and inner chamber base (Figure 3-5 and Appendix A.4).

O-rings seal the inner chamber around the inner wall of the annulus. The O-rings between the annulus and the inner and outer chamber have a crush of 0.75 mm (i.e. a 4 mm thick O-ring is compressed to 3.25 mm). This crush was sufficient to retain solution even under high pressures and high rotation speeds (Lay 1998).

During assembly, the inner chamber shaft slides down centrally through the annulus until it contacts the inner chamber base, which slides up centrally through the annulus base. A key prevents the base rotating independently of the shaft, and screws are used to fix both parts together. This arrangement prevents lubricating grease on the O-rings blocking pores in the sintered stainless steel of the annulus. During dismantling the inner chamber base can be separated from the shaft by inserting screws in threaded holes in the inner chamber base. The screws push against the shaft as they are wound in, forcing the two components apart.

Eight flexible rubber seals in the inner chamber are held in place by plates attached to the inner chamber shaft. These seals divide the inner chamber into eight equal sections, segregating flow from the annulus. Standard liquid chromatography fittings (Amersham Biosciences, Uppsala, Sweden) are used for all outlet connections.

The inner chamber is held in position relative to the top and bottom bearing housings using keys. This prevents the inner chamber rotating with the annulus when the CRFC is in operation.

3.5.1.4 The outer chamber

The outer chamber has two main parts: the outer chamber wall and outer chamber ring (Figure 3-5 and Appendix A.3). O-rings on the outside of the annulus seal around the outer chamber.

The outer chamber wall slides up from the base of the annulus while the outer chamber ring slides down from the top of the annulus. Both parts are held together by screws. The outer chamber is locked in location relative to the bottom and top bearing housings using braces, which fit into slots running the length of the CRFC exterior.

Eight flexible rubber seals divide the outer chamber into eight equal sized sections. These are held in place with plates attached to the interior of the outer chamber. Each section has its own feed input and air purge. Up to eight different solutions can be applied simultaneously to the annulus.

3.5.1.5 Flow distribution

Two important considerations when designing the outer chamber are flow distribution and jet effects. Uneven flow distribution reduces column resolution. Jet effects are generated in axial flow columns by the sudden change in cross-sectional area for flow as fluid exits the inlet port into the column.

Axial flow columns have a flow distributor at the top and base of the bed to reduce jet effects. Even flow distribution is achieved by ensuring the radial back-pressure of the distributor is negligible compared with the axial back-pressure at the column inlet. A commonly-used method is to place a coarse mesh net between the column end-pieces and a fine mesh net retaining the bed to create channels for radial distribution. This may be combined with multiple inlet/outlet ports depending on column diameter (Pharmacia 1983).

In Sepragen (Hayward, CA) radial flow columns, the outer feed chamber is used to distribute the solution around the periphery of the bed. Solution is applied at the top of the column and directed to the outer feed chamber via radial distribution channels. From there it passes through the outer porous wall into the packed bed, and out through the inner porous wall into the inner exit chamber. Radial flow packed bed back-

pressure allows for even flow distribution. Jet effects are dissipated in the feed chamber as the solution is introduced axially rather than radially.

The CRFC uses a similar method to the Sepragen radial flow columns for flow distribution. However, solution is supplied to different sections of the outer feed chamber via an external flow splitter (Section 5.6). Solution is introduced radially near the base of the outer feed chamber sections and deflected upwards into the chamber (Figure 3-8).

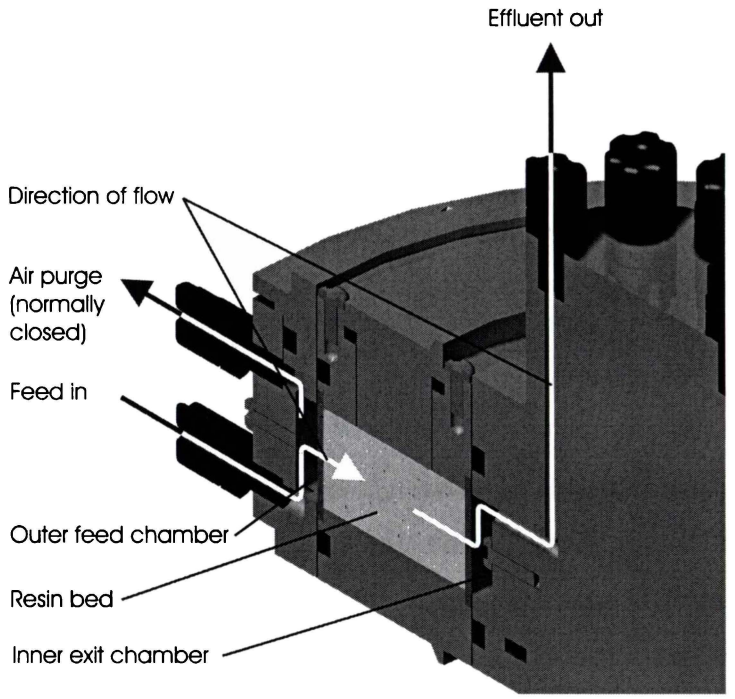

Figure 3-8. Cross section of separation module showing direction of flow.

3.5.2 Bearing units

For ease of assembly and disassembly, the bearings are distinct sealed units (Figure 3-9 and 3-10). The CRFC has two bearing units: one above and one underneath the separation module (Appendix A.5 and A.6). The bearings hold the annulus in position axially and radially. Angular contact bearings take any axial loading while deep groove bearings take the radial loads. Axial loading can be generated if the annulus is misaligned causing it to shift along its axis during rotation. Radial loading is generated by the pinion gear pushing against the main gear as it rotates the annulus. The bottom

bearing unit has a dual role of load bearing and transmitting rotational motion from the motor to the annulus. The centre of the top bearing unit is hollow to allow the top of the inner chamber to fit through, giving access to the tube fittings.

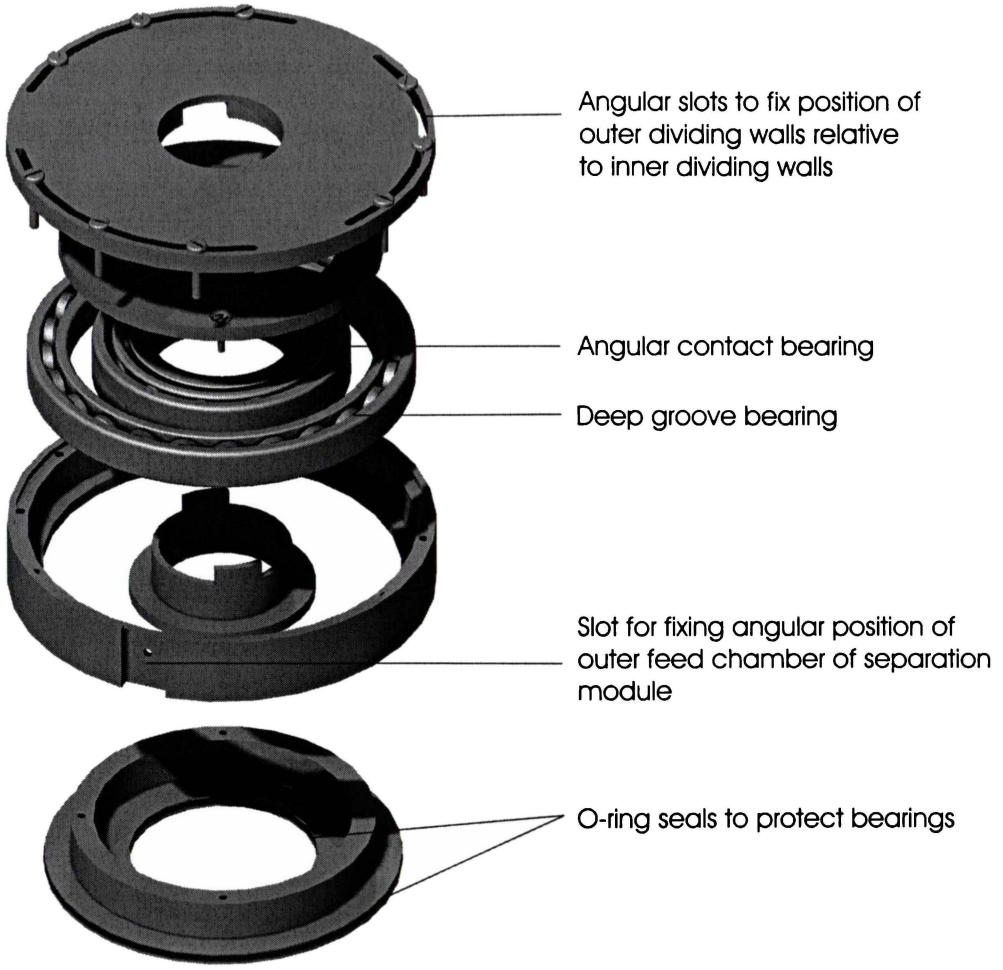

Figure 3-9. Bearing unit for top of the CRFC.

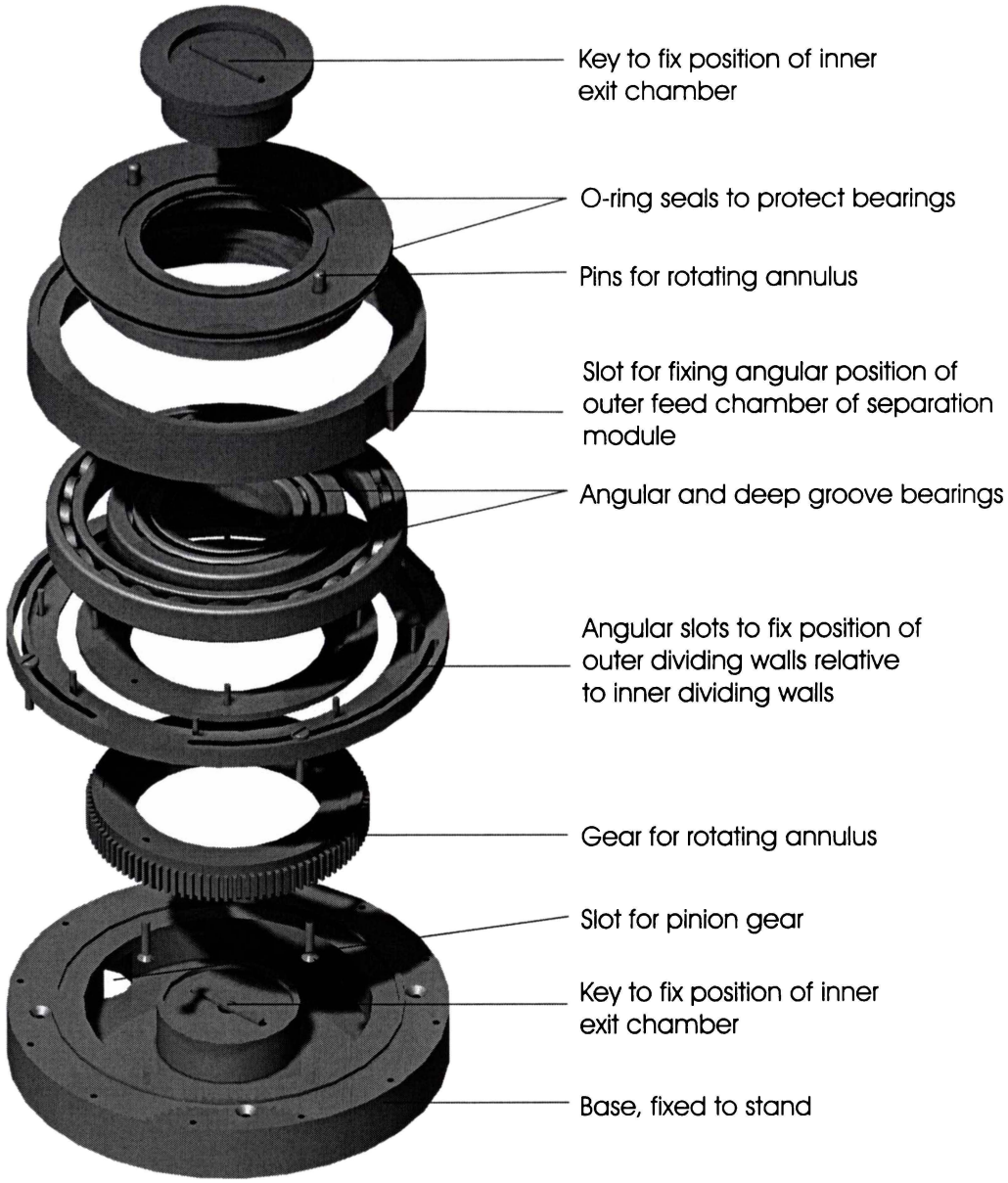

Figure 3-10. Exploded view of bearing housing.

3.5.3 Stand and motor

A 1.8 kW 1800 r.p.m. permanent magnet DC Lesson motor coupled to an quadruple reduction gearbox with a gear ratio of 347:1 (both supplied by Eric Paton Ltd., Auckland, New Zealand) was used to rotate the annulus at 0.02-0.5 r.p.m. The motor/gearbox was mounted vertically inside a stand made of standard 50 by 25-mm rectangular section steel tube (Appendix A.7). The motor came as a sealed unit to prevent potential problems of oil leakage from the gearbox. The motor/gearbox was

positioned with the shaft vertical and the motor located underneath the gearbox. This allowed for compact assembly and convenient access to the CRFC to attach tubes and fittings and make adjustments.

The motor/gearbox was connected by a flexible coupling to a 15-mm diameter shaft mounted on two pillow block bearings. This arrangement allowed for any misalignment of the motor/gearbox, which weighed approximately 40 kg and was over 600 mm long. A 1-inch, 20-diametral pitch pinion gear was mounted on the end of the shaft and was used to drive the 5-inch gear on the bottom bearing housing. The 5-inch gear from the first CRFC prototype was reused in the second prototype. The 1-inch pinion gear was constructed specifically for the second prototype.

The stand was mounted on four trolley wheels so the CRFC could be easily moved. A splash plate covered the top of the stand protecting the motor/gearbox, coupling and pillow bearings from any solutions leaking from the CRFC or nearby fittings. The CRFC was fixed in position on the splash plate using screws.

3.6 Comparison of prototypes

Specifications of the two CRFC prototypes are given in Table 3-2. CRFC 2 has several advantages over CRFC 1:

- It has one-third the bed volume and twice the bed depth, giving greater resolution.
- It requires less resin, buffer and protein solution for experiments.
- It operates at lower flowrates allowing it to be coupled to standard chromatography systems such as the AKTAexplorer100™ (Amersham Biosciences) available in the laboratory.
- The maximum operating pressure is much greater giving greater flexibility in terms of the range of operating flowrates that can be used.

- The outer feed chamber and inner exit chamber volumes are smaller, reducing the total open volume tenfold. This will reduce peak spreading in chromatograms during batch experiments.

- CRFC 2 has four times as many sections in the outer and inner chambers, which provides greater flexibility in terms of separation possibilities.

- The minimum operational r.p.m. is 15 times lower, reducing peak spreading.

Table 3-2. Comparison of the first and second prototypes of the CRFC.

Specifications	CRFC 1	CRFC 2
Bed volume (ml)	615.25	226.62
Bed height (cm)	12.00	2.00
Effective bed depth (cm)	1.60	3.15
Bed capacity (g BSA on DEAE sepharose FF)	34.9	12.8
Typical flowrate (ml/s)	9	0.67
Flow velocity through bed at typical flowrates (cm/s)	0.055 - 0.075	0.020 - 0.035
Typical operating pressure (kPa)	276	138 - 276
Max pressure[1] (kPa)	345	2068
Outer feed chamber volume (ml)	1358.87	47.08
Inner exit chamber volume (ml)	628.32	23.56
Total open volume[2] (ml)	2373.45	220.12
Residence time of solution at typical flowrate (s)	263.72	328.53
Number of sections	2	8
Rotational speed (rpm)	0.30 - 2.70	0.02 - 0.75

1 Before mechanical failure occurs
2 Includes void space in the resin bed and sintered walls

3.7 Conclusions

The new prototype design has solved many of the problems identified in the first prototype. The comparison shown in Table 3-2 shows that the second prototype has significantly lowered total volume, increased bed depth, slower rotation rates and reduced feed and exit chamber volumes in comparison to the first prototype, increasing chromatographic performance. The improved mechanical robustness will make the second prototype a more reliable tool for experimental work.

Chapter 4

Modelling

4.1 Introduction

Continuity equations for batch radial and axial flow chromatography are derived in this chapter. The radial flow equation includes both radial and angular dispersion while the axial flow model includes axial dispersion only. Dispersion equations are developed from equations analoguous to Fick's first law of diffusion. Solute uptake by the chromatographic media is modelled in two ways. Both use a multicomponent Langmuir-Fruendlich isotherm (MLF) to describe ion-exchange of solute between solution and the resin matrix. The first treats the media as non-porous spheres (NP-MLF), while the second treats the media as porous and accounts for film diffusion of solute between flowing solution and the resin pores (FD-MLF). The radial flow equations are then converted to continuity equations for the CRFC using a transformation given by Wankat (1977).

The models are solved using an explicit finite difference method for batch and continuous operation of the CRFC and for axial flow chromatography. The continuous operation model is solved neglecting angular dispersion, allowing the CRFC to be modelled as a two dimensional matrix of radial position and time. Time is converted to angular position so solute concentrations in the CRFC exit streams can be calculated. This gives a simple model so simulations can be run quickly.

The continuous model is also solved including angular dispersion. This requires the CRFC to be modelled as a three dimensional matrix of radial and angular position and time. This model is more complex so no simulations were run. However, it will be useful for future research in radial flow chromatography.

4.2 Radial flow annular packed bed

The CRFC consists of an annular resin bed that is packed between two concentric porous walls (Figure 4-1). Around the periphery is a feed chamber that is divided into eight sections, each with an input port. At the axis is an exit chamber, also divided into eight sections, each with an output port. Solution flows radially from the feed to the exit chamber.

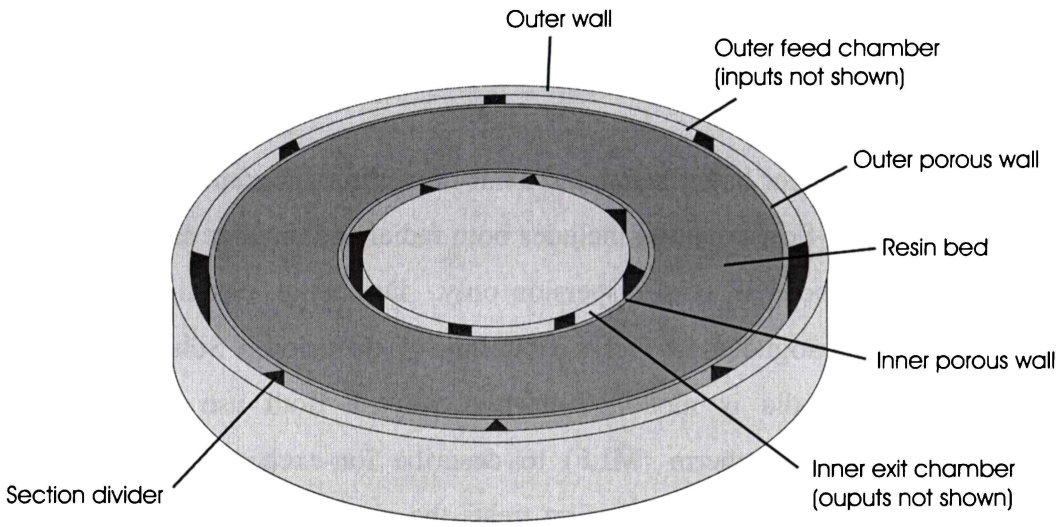

Figure 4-1. Cross section of the CRFC.

The CRFC has two modes of operation: fixed bed and moving bed. In fixed bed operation, the CRFC is operated like a conventional batch column to perform a separation, i.e. a sequence of equilibration, loading, wash, elution and regeneration steps. Solute concentration is assumed to be constant with angle, but changes with packed bed radial position and time. The elution profile is therefore time dependent. Dispersive effects due to concentration gradients are assumed to occur in the radial direction only.

In moving bed or continuous operation, the annulus rotates perpendicular to flow direction. Each section in the outer feed chamber can independently supply feed, equilibration, wash or elution buffers simultaneously to the annulus. Therefore solute concentration changes with respect to both angular and radial position and depends also on the location of the feed, equilibration, elution and wash input sections. Concentration is constant with respect to time during steady state continuous operation. The elution profile is thus independent of time but dependent on angular position. Dispersive effects will occur in both radial and angular directions.

The assumptions implicit in both modes of operation are:

- the packing is of uniform density;

- liquid and solid phases are incompressible;
- flow through the annulus is uniform with respect to angular position;
- in the continuous mode the annulus is rotating at a uniform velocity;
- there are no concentration or velocity changes with respect to height;
- temperature is constant.

If a differentially small element of the annular packed bed with dimensions Δr, $\Delta\theta$ and H (Figure 4-2) is examined under batch operation, or followed as the bed rotates during continuous operation, liquid and solid phase solute concentrations change due to:

- convection in the radial direction;
- dispersion in the radial (batch and continuous operation) and angular (continuous operation only) direction;
- adsorption and desorption of solute by the resin.

These changes are accounted for in the following sections and then incorporated into an overall mass balance for the element.

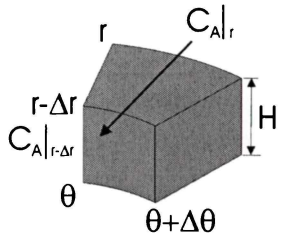

Figure 4-2. An element of the annular bed.

4.2.1 Concentration changes due to radial convection

From a flow perspective, the annular bed is considered to be a continuous porous phase. It is assumed that there is no convective flow of solution in the angular direction within the bed; all flow is in the radial direction towards the axis (Figure 4-2).

A mass balance on solute A in the fluid phase of the element gives,

$$C_A\big|_{t+\Delta t} V_e \varepsilon_R = C_A\big|_t V_e \varepsilon_R + C_A\big|_r Q_e \Delta t - C_A\big|_{r-\Delta r} Q_e \Delta t \tag{35}$$

where C_A is concentration of solute A in solution, ε_R is voidage of the packed bed, Δt is change in time, V_e is volume of the element given by,

$$V_e = \left(r^2 - (r-\Delta r)^2\right)\pi H \frac{\Delta\theta}{\theta_{\max}} \tag{36}$$

Equation (36) can be simplified by expanding $r^2 - (r-\Delta r)^2$ and neglecting Δr^2 to give

$$V_e = 2r\Delta r \pi H \frac{\Delta\theta}{\theta_{\max}} \tag{37}$$

where $\Delta\theta$ is the angular width of the element and $\theta_{\max}$ is total angular distance (360 degrees or 2π radians for an annular packed bed). Q_e, the flowrate through the element, is given by

$$Q_e = Q \frac{\Delta\theta}{\theta_{\max}} \tag{38}$$

where Q is the total flowrate through the packed bed. Dividing equation (35) by $V_e \Delta t \varepsilon_R$, substituting in equations (37) and (38) and rearranging gives

$$\frac{C_A\big|_{t+\Delta t} - C_A\big|_t}{\Delta t} = \frac{Q}{2\pi r H \varepsilon_R} \frac{\left(C_A\big|_r - C_A\big|_{r-\Delta r}\right)}{\Delta r} \tag{39}$$

Taking the limits as Δt and Δr approaching zero gives the change in concentration with respect to time due to convection

$$\frac{\partial C_A}{\partial t} = \frac{Q}{2\pi r H \varepsilon_R} \frac{\partial C_A}{\partial r} \tag{40}$$

4.2.2 Change in concentration due to radial dispersion

Radial dispersion effects can be accounted for by adapting the method presented in Bird *et al.* (2002), pp 564-565, for determining diffusion in a porous sphere, as well as the method used by Tsaur and Shallcross (1997b). A porous element is considered of dimensions H, Δr, $\Delta\theta$ (Figure 4-3).

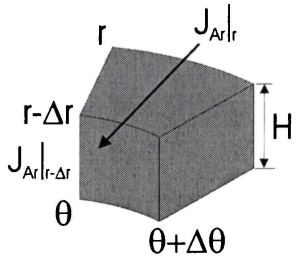

Figure 4-3. A porous element with solute A diffusing in the radial direction.

Solute A disperses into the element at r and exits at r-Δr. No reaction or adsorption takes place in the element. A mass balance on solute A gives

$$C_A|_{t+\Delta t} V_e \varepsilon_R = C_A|_t V_e \varepsilon_R + J_{Ar}|_r A_{re}|_r \varepsilon_R \Delta t - J_{Ar}|_{r-\Delta r} A_{re}|_{r-\Delta r} \varepsilon_R \Delta t \tag{41}$$

Equation (41) can be simplified to

$$\frac{C_A|_{t+\Delta t} - C_A|_t}{\Delta t} = \frac{J_{Ar}|_r A_{re}|_r - J_{Ar}|_{r-\Delta r} A_{re}|_{r-\Delta r}}{V_e} \tag{42}$$

where $J_{Ar}|_r$ is mass of solute A moving through the boundary of the element at r per unit time and $A_{re}|_r$ is the area of the element at r. $A_{re}|_r$ is given by

$$A_{re}|_r = 2\pi r H \frac{\Delta\theta}{\theta_{\max}} \tag{43}$$

Substituting equations (37) and (43) into equation (42) and simplifying gives

$$\frac{C_A|_{t+\Delta t} - C_A|_t}{\Delta t} = \frac{J_{Ar}|_r r - J_{Ar}|_{r-\Delta r}(r-\Delta r)}{r\Delta r} \tag{44}$$

When Δr and Δt approach zero equation (44) becomes

$$\frac{\partial C_A}{\partial t} = \frac{1}{r}\frac{\partial}{\partial r}(rJ_{Ar}) \tag{45}$$

Gu *et al.* (1991) and Tsaur and Shallcross (1997b) determined radial dispersion flux using an equation analoguous to Fick's first law of diffusion,

$$J_{Ar} = D_{Ar}\frac{\partial C_A}{\partial r} \tag{46}$$

where D_{Ar} is the radial dispersion coefficient. Gu *et al.* (1991) assumed dispersion was primarily due to turbulent mixing or eddy diffusion and ignored contributions by molecular diffusion. The dispersion coefficient was calculated by

$$D_{Ar} = y_2(2R_p)v \tag{47}$$

where y_2 is a constant and has a value of approximately 0.5, R_p is the radius of the resin particle and v is the interstitial solution velocity given by

$$v = \frac{Q}{2\pi r H \varepsilon_R} \tag{48}$$

Substituting equation (46) into equation (45) gives

$$\frac{\partial C_A}{\partial t} = \frac{1}{r}\frac{\partial}{\partial r}\left(rD_{Ar}\frac{\partial C_A}{\partial r}\right) \tag{49}$$

If we let

$$y = \left(rD_{Ar}\frac{\partial C_A}{\partial r}\right) \tag{50}$$

the derivative of equation (50) can be found using the product rule

$$\frac{\partial y}{\partial r} = \frac{\partial e}{\partial r}.f.g + e.\frac{\partial f}{\partial r}.g + e.f.\frac{\partial g}{\partial r} \tag{51}$$

where

$$e = r \tag{52}$$

$$f = D_{Ar} \tag{53}$$

and

$$g = \frac{\partial C_A}{\partial r} \tag{54}$$

and where

$$e'.f.g = D_{Ar}\frac{\partial C_A}{\partial r} \tag{55}$$

$$e.f'.g = r\frac{\partial D_{Ar}}{\partial r}\frac{\partial C_A}{\partial r} \tag{56}$$

and

$$e.f.g' = rD_{Ar}\frac{\partial^2 C_A}{\partial r^2} \tag{57}$$

Substituting equations (55), (56) and (57) back into equation (51) gives

$$\frac{\partial y}{\partial r} = \left(D_{Ar} \frac{\partial C_A}{\partial r} + r \frac{\partial D_{Ar}}{\partial r} \frac{\partial C_A}{\partial r} + r D_{Ar} \frac{\partial^2 C_A}{\partial r^2} \right) \tag{58}$$

Substituting equation (58) back into (49) gives

$$\frac{\partial C_A}{\partial t} = \frac{1}{r} \left(D_{Ar} \frac{\partial C_A}{\partial r} + r \frac{\partial D_{Ar}}{\partial r} \frac{\partial C_A}{\partial r} + r D_{Ar} \frac{\partial^2 C_A}{\partial r^2} \right) \tag{59}$$

and simplifying yields the rate of change in concentration due to radial dispersion

$$\frac{\partial C_A}{\partial t} = \left(D_{Ar} \frac{\partial^2 C_A}{\partial r^2} + \frac{D_{Ar}}{r} \frac{\partial C_A}{\partial r} + \frac{\partial D_{Ar}}{\partial r} \frac{\partial C_A}{\partial r} \right) \tag{60}$$

Equation (60) is the same as that presented by Tsaur (1996) and Tsaur and Shallcross (1997b) for radial dispersion.

4.2.3 Concentration changes due to angular dispersion

During batch operation, solute concentration is uniform with respect to angle so angular dispersion can be neglected. However, during continuous operation, solute concentration varies with angle so angular dispersion must be considered. An equation for angular dispersion is derived in this section.

Solute A diffuses through an element from a region of high concentration to one of low concentration (Figure 4-4). No reaction or adsorption takes place between the element and the solute.

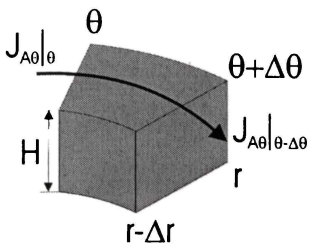

Figure 4-4. A porous element with solute A diffusing in the angular direction θ.

A mass balance on solute A on an element of dimensions Δr, Δθ and H over a period Δt gives

$$C_A\big|_{t+\Delta t} V_e \varepsilon_R = C_A\big|_t V_e \varepsilon_R + J_{A\theta}\big|_\theta A_\theta \varepsilon_R \Delta t - J_{A\theta}\big|_{\theta+\Delta\theta} A_\theta \varepsilon_R \Delta t \tag{61}$$

where $J_{A\theta}\big|_\theta$ is flux of solute A moving through the boundary at angle θ in a given time period Δt and A_θ is the area the solute moves through, given by

$$A_\theta = \Delta r H \tag{62}$$

Substituting equations (37) and (62) into equation (61) and simplifying yields

$$\frac{C_A\big|_{t+\Delta t} - C_A\big|_t}{\Delta t} = \frac{1}{r}\frac{J_{A\theta}\big|_\theta - J_{A\theta}\big|_{\theta+\Delta\theta}}{\Delta\theta} \tag{63}$$

When Δr and Δt approach zero, equation (63) becomes

$$\frac{\partial C_A}{\partial t} = \frac{1}{r}\frac{\partial}{\partial \theta}\left(J_{A\theta}\right) \tag{64}$$

Angular dispersion flux is determined using an equation analoguous to Fick's first law,

$$J_{A\theta} = D_{A\theta}\frac{\partial C_A}{r\partial\theta} \tag{65}$$

Substituting equation (65) into equation (64) gives

$$\frac{\partial C_A}{\partial t} = \frac{1}{r}\frac{\partial}{\partial \theta}\left(D_{A\theta}\frac{\partial C_A}{r\partial\theta}\right) \tag{66}$$

Dispersion is primarily due to turbulent mixing or eddy diffusion and is dependent on velocity. Because fluid velocity through the packed bed does not change with angular position, $D_{A\theta}$ is independent of angular position. Therefore, equation (66) becomes

$$\frac{\partial C_A}{\partial t} = \frac{D_{A\theta}}{r^2}\frac{\partial^2 C_A}{\partial\theta^2} \tag{67}$$

When modelling rotating bed annular chromatography, Thiele *et al.* (2001) assumed angular dispersion would be within the range

$$D_{mA} \leq D_{A\theta} \leq D_{Az} \tag{68}$$

where D_{mA} is the dispersion coefficient due to molecular diffusion and D_{Az} is the axial dispersion coefficient. If the same assumption is made for determining angular dispersion in the CRFC, then

$$D_{mA} \leq D_{A\theta} \leq D_{Ar} \tag{69}$$

4.2.4 Concentration changes due to solute adsorption and desorption

Solute uptake by the chromatographic media is modelled in two ways. Both use a multicomponent Langmuir-Fruendlich isotherm (MLF) to describe ion-exchange of solute between solution and the resin matrix. The first treats the media as non-porous spheres (NP-MLF), while the second treats the media as porous and accounts for film diffusion of solute between flowing solution and the resin pores (FD-MLF).

4.2.4.1 NP-MLF

In the resin bed, solute A exists in equilibrium between being bound to the resin and free in solution (shown in Figure 4-5 as A_b and A_f respectively, with forward and reverse binding rate constants k_{A1} and k_{A2}).

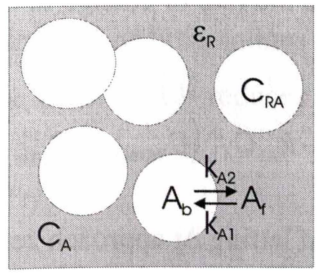

Figure 4-5. Solute A in contact with ion exchange resin.

The resin particle, the solution in the pores of the resin, and the stagnant zone surrounding the resin particle are considered as a single sphere. At equilibrium the solute and resin concentrations are related using the Langmuir isotherm,

$$C_{RA}^{*} = \frac{C_{RA\max} K_A C_A^{*}}{1 + K_A C_A^{*}} \tag{70}$$

where C_A* and C_{RA}* are the solution phase and resin phase solute concentrations at equilibrium, C_{RAmax} is the maximum adsorption capacity of the adsorbent, and K_A is the equilibrium constant given by

$$K_A = \frac{k_{A1}}{k_{A2}} \tag{71}$$

C_{RAmax} can be evaluated from isotherm measurements at high solute concentrations where C_{RA}* approaches C_{RAmax}. k_{A1} can be evaluated from batch adsorption experiments to determine the initial rate of uptake of solute, which then allows k_{A2} to be computed as k_{A1}/K_A (Cowan *et al.* 1989).

Substituting equation (71) into equation (70), the Langmuir isotherm can be rearranged to give

$$k_{A2} C_{RA}^{*} = k_{A1} C_A^{*} \left(C_{RA\max} - C_{RA}^{*} \right) \tag{72}$$

The above equation is for the system at equilibrium. For a protein solution flowing through a packed bed, mass transfer between solution and resin can be rate-controlling. A mass balance is performed on solute A in the void space of an element (Figure 4.2) using equation (72) to determine the rate of change in concentration when the system is not at equilibrium.

$$C_A\big|_{t+\Delta t} \varepsilon_R V_e = C_A\big|_t \varepsilon_R V_e - k_{A1} C_A\big|_t \left(C_{RA\max} - C_{RA}\big|_t \right) V_e \varepsilon_R \Delta t + k_2 C_{RA}\big|_t V_e \varepsilon_R \Delta t \tag{73}$$

Dividing through by $V_e \varepsilon_R \Delta t$ and letting Δt approach zero gives

$$\frac{\partial C_A}{\partial t} = -k_{A1} C_A \left(C_{RA\max} - C_{RA} \right) + k_{A2} C_{RA} \tag{74}$$

which is the same result as Cowan *et al.* (1989).

Performing a mass balance on solute A in the resin phase yields

$$C_{RA}\big|_{t+\Delta t}(1-\varepsilon_R)V_e = C_{RA}\big|_t(1-\varepsilon_R)V_e + k_{A1}C_A\big|_t\left(C_{RA\max} - C_{RA}\big|_t\right)V_e\varepsilon_R\Delta t$$

$$- k_{A2}C_{RA}\big|_t V_e\varepsilon_R\Delta t \tag{75}$$

Dividing through by $V_e(1-\varepsilon_R)\Delta t$ and letting Δt approach zero gives

$$\frac{\partial C_{RA}}{\partial t} = \left(k_{A1}C_A\left(C_{RA\max} - C_{RA}\right) - k_{A2}C_{RA}\right)\frac{\varepsilon_R}{1-\varepsilon_R} \tag{76}$$

During elution, solute A is displaced or eluted from the resin by solute B. The effect of elution conditions on rate constants k_{A1} and k_{A2} can be described using a multicomponent Langmuir-Freundlich isotherm (MLF) that accounts for solute B concentration. For a binary mixture (subscripts A and B respectively), MLF is

$$C_{RA}^{\ *} = \frac{C_{RA\max}K_A{C_A}^{*1/n_A}}{1 + K_A{C_A}^{*1/n_A} + K_B{C_B}^{*1/n_B}} \tag{77}$$

The non-equilibrium form of equation (77) for the solution phase is

$$\frac{\partial C_A}{\partial t} = -k_{A1}C_A^{1/n_A}\left(C_{RA\max} - C_{RA}\right) + k_{A2}\left(1 + K_BC_B^{1/n_B}\right)C_{RA} \tag{78}$$

and for the resin phase

$$\frac{\partial C_{RA}}{\partial t} = \left(k_{A1}C_A^{1/n_A}\left(C_{RA\max} - C_{RA}\right) - k_{A2}\left(1 + K_BC_B^{1/n_B}\right)C_{RA}\right)\frac{\varepsilon_R}{1-\varepsilon_R} \tag{79}$$

This model requires the concentrations of both solutes A and B throughout the packed bed to be calculated at the same time. MLF reduces to a multicomponent Langmuir (ML) rate equation when n_A and $n_B = 1$.

4.2.4.2 FD-MLF

When comparing model curves to experimental results for NaCl breakthrough it was found that NP-MLF predicted earlier breakthrough than was observed. A film diffusion equation was therefore developed to describe NaCl-resin interaction.

Change in concentration of solute in solution flowing past the resin due to diffusive flux into the resin is given by

$$\frac{\partial C_A}{\partial t} = -\frac{J_A A_R}{V_e \varepsilon_R} \tag{80}$$

where

$$J_A = k_{fA}\left(C_A - C_{RPA}\right) \tag{81}$$

k_{fA} is the film diffusion coefficient for solute A. Solute migrates from the resin periphery to the centre by pore diffusion. The resin particle would need to be discretizd into spherical layers to model pore diffusion, which would make the overall model more complex. Therefore for simplicity it was assumed that C_{RPA} is the average concentration of solute A in the resin pores.

If resin particles are spherical, A_R is the total surface area of resin, given by

$$A_R = A_{Rp}\frac{V_R}{V_{Rp}} \tag{82}$$

A_{Rp} is the surface area of a resin particle

$$A_{Rp} = 4\pi R_p^{\,2} \tag{83}$$

V_R is the volume of resin in an element

$$V_R = V_e\left(1-\varepsilon_R\right) \tag{84}$$

and V_{Rp} is the volume of a resin particle

$$V_{Rp} = \frac{4}{3}\pi R_p^{\,3} \tag{85}$$

Substituting equations (83) to (85) into equation (82) gives

$$A_R = \frac{3V_e(1-\varepsilon_R)}{R_p} \tag{86}$$

Substituting equations (81) and (86) into equation (80) yields

$$\frac{\partial C_A}{\partial t} = -\frac{3k_{fA}(C_A - C_{RPA})(1-\varepsilon_R)}{R_p \varepsilon_R} \tag{87}$$

The change in concentration of solute in solution in the resin pores is found by multiplying equation (87) by

$$\frac{\varepsilon_R}{(1-\varepsilon_R)\varepsilon_p} \tag{88}$$

where ε_p is the internal porosity of the resin particle, giving

$$\frac{\partial C_{RPA}}{\partial t} = \frac{3k_{fA}(C_A - C_{RPA})}{R_p \varepsilon_p} \tag{89}$$

k_{fA}, the overall film diffusion coefficient, is a function of both the external and internal mass transfer coefficients k_{ext} and k_{int} respectively (Kaczmarski *et al.* 2001),

$$k_{fA} = \left[\frac{1}{k_{ext}} + \frac{1}{k_{\text{int}}}\right]^{-1} \tag{90}$$

k_{ext} can be calculated as a function of the Sherwood number *Sh* from the Wilson-Geankoplis correlation,

$$Sh = \frac{k_{ext} d_p}{D_m} = \frac{1.09}{\varepsilon_R} Sc^{1/3} \,\mathrm{Re}^{1/3} \tag{91}$$

where d_p is the resin particle diameter. D_{mA} is the solute molecular diffusivity, which can be obtained from Tyn and Gusek (1990) for proteins. *Sc* and *Re* are the Schmidt number and particle Reynolds number respectively

$$\mathrm{Sc} = \frac{\eta}{\rho D_{mA}} \text{ and } \mathrm{Re} = \frac{u d_p \rho}{\eta} \tag{92}$$

η and ρ are buffer viscosity and density respectively, and u is the buffer superficial velocity (flowrate divided by the column cross sectional area). k_{int} can be calculated using

$$k_{int} = \frac{10 D_{eff}}{d_p} \tag{93}$$

D_{eff} is the effective diffusivity

$$D_{eff} = \frac{\varepsilon_p D_{mA}}{\gamma} \tag{94}$$

γ is pore tortuousity

$$\gamma = \frac{(2-\varepsilon_p)^2}{\varepsilon_p} \tag{95}$$

Loss of solute in the resin pores due to adsorption by the resin matrix is described by including the multicomponent Langmuir-Fruendlich isotherm in equation (89), giving

$$\frac{\partial C_{RPA}}{\partial t} = \frac{3k_{fA}(C_A - C_{RPA})}{r_p \varepsilon_p} - k_{A1} C_{RPA}^{1/n_A}(C_{RA\max} - C_{RA}) + k_{A2}\left(1 + K_B C_{RPB}^{1/n_B}\right) C_{RA} \tag{96}$$

Change in solute concentration for the resin matrix is given by

$$\frac{\partial C_{RA}}{\partial t} = \frac{\varepsilon_p}{(1-\varepsilon_p)}\left(k_{A1} C_{RPA}^{1/n_A}(C_{RA\max} - C_{RA}) - k_{A2}\left(1 + K_B C_{RPB}^{1/n_B}\right) C_{RA}\right) \tag{97}$$

C_{RA} in equation (97) is resin matrix solute concentration rather than overall resin solute concentration. Calculating an overall resin solute concentration, neglecting solute in the resin pores, allows resin capacities from other work to be used. Therefore, equation (97) becomes

$$\frac{\partial C_{RA}}{\partial t} = \varepsilon_p\left(k_{A1} C_{RPA}^{1/n_A}(C_{RA\max} - C_{RA}) - k_{A2}\left(1 + K_B C_{RPB}^{1/n_B}\right) C_{RA}\right) \tag{98}$$

4.2.5 Final continuity equations

When solute-resin interaction is modelled using NP-MLF, combining equations (40), (60), (67) and (78) gives the final continuity equation for the buffer concentration of solute A in a packed bed element.

$$\frac{\partial C_A}{\partial t} = \frac{Q}{2\pi r H \varepsilon_R}\frac{\partial C_A}{\partial r} + \left(D_{Ar}\frac{\partial^2 C_A}{\partial r^2} + \frac{D_{Ar}}{r}\frac{\partial C_A}{\partial r} + \frac{\partial D_{Ar}}{\partial r}\frac{\partial C_A}{\partial r} \right) + \frac{D_{A\theta}}{r^2}\frac{\partial^2 C_A}{\partial \theta^2}$$

$$- k_{A1} C_A^{1/n_A} \left(C_{RA\max} - C_{RA} \right) + k_{A2} \left(1 + K_B C_B^{1/n_B} \right) C_{RA} \tag{99}$$

The resin phase solute concentration is given by equation (79).

When solute-resin interaction is modelled using FD-MLF, equations (40), (60), (67) and (87) are combined to give the final continuity equation for the buffer concentration of solute A in a packed bed element.

$$\frac{\partial C_A}{\partial t} = \frac{Q}{2\pi r H \varepsilon_R}\frac{\partial C_A}{\partial r} + \left(D_{Ar}\frac{\partial^2 C_A}{\partial r^2} + \frac{D_{Ar}}{r}\frac{\partial C_A}{\partial r} + \frac{\partial D_{Ar}}{\partial r}\frac{\partial C_A}{\partial r} \right) + \frac{D_{A\theta}}{r^2}\frac{\partial^2 C_A}{\partial \theta^2}$$

$$- \frac{3k_f \left(C_A - C_{RPA} \right)\left(1 - \varepsilon_R \right)}{R_p \varepsilon_R} \tag{100}$$

Resin pore and resin phase solute concentrations are given by equations (96) and (98),

For batch conditions, the angular dispersion component is neglected in equations (99) and (100).

Equations (99) and (100) can be transformed for continuous operation with a rotating bed using the relation from Wankat (1977),

$$\Delta\phi = \Delta t \cdot w \tag{101}$$

where $\Delta\phi$ is change in angle due to rotation and w is rotational speed. This gives

$$\frac{\partial C_A}{\partial \phi} w = \frac{Q}{2\pi r H \varepsilon_R}\frac{\partial C_A}{\partial r} + \left(D_{Ar}\frac{\partial^2 C_A}{\partial r^2} + \frac{D_{Ar}}{r}\frac{\partial C_A}{\partial r} + \frac{\partial D_{Ar}}{\partial r}\frac{\partial C_A}{\partial r} \right) + \frac{D_{A\theta}}{r^2}\frac{\partial^2 C_A}{\partial \theta^2}$$

$$- k_{A1} C_A^{1/n_A} \left(C_{RA\max} - C_{RA} \right) + k_{A2} \left(1 + K_B C_B^{1/n_B} \right) C_{RA} \tag{102}$$

$$\frac{\partial C_A}{\partial \phi} w = \frac{Q}{2\pi r H \varepsilon_R} \frac{\partial C_A}{\partial r} + \left(D_{Ar} \frac{\partial^2 C_A}{\partial r^2} + \frac{D_{Ar}}{r} \frac{\partial C_A}{\partial r} + \frac{\partial D_{Ar}}{\partial r} \frac{\partial C_A}{\partial r} \right) + \frac{D_{A\theta}}{r^2} \frac{\partial^2 C_A}{\partial \theta^2}$$

$$- \frac{3 k_{fA} (C_A - C_{RPA})(1 - \varepsilon_R)}{R_p \varepsilon_R} \tag{103}$$

Equations (102) and (103) cannot be solved analytically due to the angular and radial dispersion components (Tsaur 1996) and must be solved numerically (Section 4.4).

4.3 Axial flow model

An axial flow column model was developed for small column experimental work to determine rate parameters that could be applied to the radial flow models. Axial flow is easier to model than radial flow because cross-sectional area and fluid velocity does not change with respect to bed depth. A mass balance on a thin section of height Δz of an axial flow column of radius r_c for the change in concentration due to convection gives

$$C_A\big|_{t+\Delta t} \pi r_c^{\,2} \Delta z \varepsilon_R = C_A\big|_t \pi r_c^{\,2} \Delta z \varepsilon_R + C_A\big|_z Q \Delta t - C_A\big|_{z-\Delta z} Q \Delta t \tag{104}$$

Simplifying gives

$$\frac{\left(C_A\big|_{t+\Delta t} - C_A\big|_t\right)}{\Delta t} = \frac{\left(C_A\big|_z - C_A\big|_{z-\Delta z}\right)}{\Delta z} \frac{Q}{\pi r_c^{\,2} \varepsilon_R} \tag{105}$$

Letting Δt and Δz approach zero gives

$$\frac{\partial C_A}{\partial t} = \frac{\partial C_A}{\partial z} \frac{Q}{\pi r_c^{\,2} \varepsilon_R} \tag{106}$$

The change in concentration due to dispersion is given by

$$C_A\big|_{t+\Delta t} \pi r_c^{\,2} \Delta z \varepsilon_R = C_A\big|_t \pi r_c^{\,2} \Delta z \varepsilon_R + J_{Az}\big|_z \pi r_c^{\,2} \varepsilon_R \Delta t - J_{Az}\big|_{z-\Delta z} \pi r_c^{\,2} \varepsilon_R \Delta t \tag{107}$$

which can be simplified to

$$\frac{\left(C_A\big|_{t+\Delta t} - C_A\big|_t\right)}{\Delta t} = \frac{\left(J_{Az}\big|_z - J_{Az}\big|_{z-\Delta z}\right)}{\Delta z} \tag{108}$$

Letting Δt and Δz approach zero gives

$$\frac{\partial C_A}{\partial t} = \frac{\partial J_{Az}}{\partial z} \tag{109}$$

Using Fick's first law to approximate dispersion equation (109) becomes

$$\frac{\partial C_A}{\partial t} = \frac{\partial}{\partial z}\left(D_{Az} \frac{\partial C_A}{\partial z} \right) \tag{110}$$

If the axial dispersion coefficient D_{Az} is dependent on velocity, which does not change with bed depth in an axial flow column, then equation (110) becomes,

$$\frac{\partial C_A}{\partial t} = D_{Az} \frac{\partial^2 C_A}{\partial z^2} \tag{111}$$

The solute-resin interaction can be described using NP-MLF, equation (78), or FD-MLF, equation (87). For NP-MLF, combining equations (106), (111) and (78) gives,

$$\frac{\partial C_A}{\partial t} = \frac{\partial C_A}{\partial z}\frac{Q}{\pi r_c^{\,2}\varepsilon_R} + D_{Az}\frac{\partial^2 C_A}{\partial z^2} - k_{A1} C_A^{1/n_A}\left(C_{RA\max} - C_{RA}\right) + k_{A2}\left(1 + K_B C_B^{1/n_B}\right) C_{RA} \tag{112}$$

Equation (79) is used for the resin phase. For FD-MLF, the axial flow column continuity equation is

$$\frac{\partial C_A}{\partial t} = \frac{\partial C_A}{\partial z}\frac{Q}{\pi r_c^{\,2}\varepsilon_R} + D_{Az}\frac{\partial^2 C_A}{\partial z^2} - \frac{3k_{fA}\left(C_A - C_{RPA}\right)\left(1-\varepsilon_R\right)}{R_p \varepsilon_R} \tag{113}$$

The resin pore and resin phase solute concentrations are given by equations (96) and (98).

4.4 Finite difference models

The radial and axial flow continuity equations are solved using an explicit finite difference method. The finite difference method is a simple numerical procedure that can be directly applied to solving an entire model (Gu 1995). Finite difference modelling can be easily done in Microsoft Excel spreadsheets, Matlab or Fortran.

Finite difference models were developed from the two continuity equations for the following applications:

1. Rate kinetics in stirred tanks
2. Batch axial flow column operation
3. Batch operation of the CRFC
4. Continuous operation of the CRFC neglecting angular dispersion
5. Continuous operation of the CRFC including angular dispersion

The first four were used for comparison to experimental work. The fifth model is a logical extension of the fourth and has some useful applications for future work. All five finite difference models are are presented in the following sections.

4.4.1 Rate kinetics experiments in stirred tanks

Rate kinetic studies are typically done in stirred tanks with a known starting concentration of solute and known volume of resin. The buffer concentration is monitored over time. As there is no convective or dispersive mass transfer, the continuity equations for the radial and axial flow columns reduce to the change in concentration due to uptake. Therefore, in finite difference form

$$C_A\big|_m = C_A\big|_{m-1} + \Delta C_A \text{Uptake}\big|_m \tag{114}$$

Uptake is modelled over M time steps where time is given by

$$\text{for } 1 \le m \le M+1 \qquad t\big|_m = (m-1)\Delta t \tag{115}$$

Starting conditions at m=1 are

$$C_A\big|_m = C_{AStart},\ C_{RPA}\big|_m = 0,\ C_{RA}\big|_m = 0,\ \Delta C_A\text{Uptake}\big|_m = 0 \tag{116}$$

Where uptake is calculated using NP-MLF, equation (78) for a single component buffer becomes

$$\Delta C_A\text{Uptake}\big|_m = k_{A1} C_A\big|_{m-1}^{1/n_A} \left(C_{RA\max} - C_{RA}\big|_{m-1}\right)\Delta t - k_{A2} C_{RA}\big|_{m-1}\Delta t \tag{117}$$

and for the resin phase

$$C_{RA}\big|_m = C_{RA}\big|_{m-1} + \Delta C_A\text{Uptake}\big|_m \frac{\varepsilon_0}{1-\varepsilon_0} \tag{118}$$

Where uptake is modelled using FD-MLF, equation (87) becomes

$$\Delta C_A\text{Uptake}\big|_m = \frac{3k_{fA}\left(C_A\big|_{m-1} - C_{RPA}\big|_{m-1}\right)(1-\varepsilon_0)\Delta t}{R_p \varepsilon_0} \tag{119}$$

For the resin pores

$$C_{RPA}\big|_m = C_{RPA}\big|_{m-1} + \Delta C_A\text{Uptake}\big|_m \frac{\varepsilon_0}{(1-\varepsilon_0)\varepsilon_p} - \Delta C_{RPA}\text{Exchange}\big|_m \tag{120}$$

where

$$\Delta C_{RPA}\text{Exchange}\big|_m = k_{A1} C_{RPA}\big|_{m-1}^{1/n_A} \left(C_{RA\max} - C_{RA}\big|_{m-1}\right)\Delta t - k_{A2} C_{RA}\big|_{m-1}\Delta t \tag{121}$$

and for the resin phase

$$C_{RA}\big|_m = C_{RA}\big|_{m-1} + \Delta C_{RPA}\text{Exchange}\big|_m \varepsilon_p \tag{122}$$

ε_0 in equations (118)-(120) is the resin volume to buffer volume ratio. Model parameters are obtained by fitting model curves to experimental data.

4.4.2 Fixed bed axial flow

An axial flow column bed is divided into N stages along the axis. Each stage is modelled as a well-mixed tank. Under ideal conditions, the maximum number of stages required can be calculated by

$$N_{\max} = \frac{L}{4d_p} \tag{123}$$

where L is the axial bed length and d_p is the diameter of the resin particles (Levenspiel 1993). Simulations showed that

$$N \approx \frac{N_{\max}}{2} \tag{124}$$

was sufficient for finite difference modelling and reduced processing time. No significant differences in concentration profile were observed between using N or $N_{\max}$. N is rounded to the next integer.

The height (Δz), cross sectional area (A_z), volume of each stage (V_e), interstitial velocity (v_z) and change in time (Δt) are given by

$$\Delta z = \frac{L}{N} \tag{125}$$

$$A_z = \pi r_c^{\,2} \tag{126}$$

$$V_e = A_z \Delta z \tag{127}$$

$$v_z = \frac{Q}{A_z \varepsilon_R} \tag{128}$$

$$\Delta t = \frac{V_e \varepsilon_R}{QJ} \tag{129}$$

Normally J, a dimensionless parameter for reducing Δt for each time step, is set to 3, but is increased if the model became unstable when adsorption, desorption, film diffusion or dispersion rates were high.

Total time steps M is given by,

$$M = \frac{t_{run}}{\Delta t} \tag{130}$$

where

$$t_{run} = \sum_{i=1}^{NSteps} \frac{V_i}{Q} \tag{131}$$

NSteps is the total number of steps taken in a run and V_i is the volume applied for *i*th step. A run might normally include equilibration, loading, and wash and elution (a total of four steps).

The axial flow column is modelled as a two dimensional matrix with dimensions of n stages and m time steps. An additional stage is used to set input concentrations, giving N+1 stages. If necessary, additional stages of different volumes can be included before and after the model column to simulate dispersive effects of surrounding equipment.

For boundary conditions of $1 \le n \le (N+1)$ and m=1

$$C_A\big|_{n,m} = 0,\ C_{RPA}\big|_{n,m} = 0,\ C_{RA}\big|_{n,m} = 0 \tag{132}$$

Feed input concentrations change with time. Initially there is an equilibration step, followed by a loading step where solute A is applied to the system, followed by wash and elution steps. The specific volume of solution applied during each step is used to calculate the time for each step. These times are then used to set the input concentration for the first stage n=1 (Table 4-1).

The resin and interstitial buffer concentrations for each stage in the bed and each time step are calculated using,

for $$1 < n \le (N+1) \text{ and } 1 < m \le M+1$$

$$C_A\big|_{n,m} = C_A\big|_{n,m-1} + \Delta C_A \text{Convection}\big|_{n,m} + \Delta C_A \text{Zdisp}\big|_{n,m} - \Delta C_A \text{Uptake}\big|_{n,m} \tag{133}$$

Convection is given by equation (105)

$$\Delta C_A \text{Convection}\big|_{n,m} = \frac{\left(C_A\big|_{n-1,m-1} - C_A\big|_{n,m-1}\right) Q \Delta t}{V_e \varepsilon_R} \tag{134}$$

Table 4-1. Time calculations and input concentrations for a four step method.

Step	Volume applied (ml)	Time for step to end (s)	Condition	Input concentrations
Equilibration	V_1	$t_1 = \frac{V_1}{Q}$	$0 < t\|_m \le t_1$	$C_A\|_{n=1,m} = 0$ $C_B\|_{n=1,m} = 0$
Loading	V_2	$t_2 = \frac{V_2}{Q} + t_1$	$t_1 < t\|_m \le t_2$	$C_A\|_{n=1,m} = C_{feed}$ $C_B\|_{n=1,m} = 0$
Wash	V_3	$t_3 = \frac{V_3}{Q} + t_2$	$t_2 < t\|_m \le t_3$	$C_A\|_{n=1,m} = 0$ $C_B\|_{n=1,m} = C_{elution}$
Elution	V_4	$t_4 = \frac{V_4}{Q} + t_3$	$t_3 < t\|_m \le t_4$	$C_A\|_{n=1,m} = 0$ $C_B\|_{n=1,m} = 0$

Dispersion is given by equation (107)

$$\Delta C_A \text{ZDisp}|_{n,m} = \frac{A_z \left(J_{Az}|_{n-1,m-1} - J_{Ar}|_{n,m-1} \right) \Delta t}{V_e} \tag{135}$$

Substituting the axial flow finite difference form of the dispersion equivalent of Fick's Law, equation (46), into equation (135) gives

$$\Delta C_A \text{ZDisp}|_{n,m} = \frac{D_{Az} A_z \Delta t}{V_e \Delta z} \left(C_A|_{n-1,m-1} - 2C_A|_{n,m-1} + C_A|_{n+1,m-1} \right) \tag{136}$$

Equations (47) and (128) for calculating the dispersion coefficient and interstitial velocity are then substituted into equation (136), giving

for within the bed $2 < n < N+1$

$$\Delta C_A \text{ZDisp}|_{n,m} = \frac{y_2 (2R_p) Q \Delta t}{V_e \varepsilon_R \Delta z} \left(C_A|_{n-1,m-1} - 2C_A|_{n,m-1} + C_A|_{n+1,m-1} \right) \tag{137}$$

and at the bed boundaries

n=2
$$\Delta C_A \text{ZDisp}\big|_{n,m} = -\frac{y_2(2R_p)Q\Delta t}{V_e \varepsilon_R \Delta z}\left(C_A\big|_{n,m-1} - C_A\big|_{n+1,m-1}\right) \tag{138}$$

n=N+1
$$\Delta C_A \text{ZDisp}\big|_{n,m} = \frac{y_2(2R_p)Q\Delta t}{V_e \varepsilon_R \Delta z}\left(C_A\big|_{n-1,m-1} - C_A\big|_{n,m-1}\right) \tag{139}$$

Where uptake is modelled using NP-MLF, equation (78) becomes

$$\Delta C_A \text{Uptake}\big|_{n,m} = k_{A1} C_A\big|_{n,m-1}^{1/n_A}\left(C_{RA\max} - C_{RA}\big|_{n,m-1}\right)\Delta t$$

$$- k_{A2}\left(1 + K_B C_B\big|_{n,m-1}^{1/n_B}\right) C_{RA}\big|_{n,m-1}\Delta t \tag{140}$$

For the resin phase

$$C_{RA}\big|_{n,m} = C_{RA}\big|_{n,m-1} + \Delta C_A \text{Uptake}\big|_{n,m}\frac{\varepsilon_R}{1-\varepsilon_R} \tag{141}$$

Where uptake is modelled using FD-MLF, equation (87) becomes

$$\Delta C_A \text{Uptake}\big|_{n,m} = \frac{3k_{fA}\left(C_A\big|_{n,m-1} - C_{RPA}\big|_{n,m-1}\right)(1-\varepsilon_R)\Delta t}{R_p \varepsilon_R} \tag{142}$$

For the resin pores

$$C_{RPA}\big|_{n,m} = C_{RPA}\big|_{n,m-1} + \Delta C_A \text{Uptake}\big|_{n,m}\frac{\varepsilon_R}{(1-\varepsilon_R)\varepsilon_p} - \Delta C_{RPA}\text{Exchange}\big|_{n,m} \tag{143}$$

where
$$\Delta C_{RPA}\text{Exchange}\big|_{n,m} = k_{A1} C_{RPA}\big|_{n,m-1}^{1/n_A}\left(C_{RA\max} - C_{RA}\big|_{n,m-1}\right)\Delta t$$

$$- k_{A2}\left(1 + K_B C_{RPB}\big|_{n,m-1}^{1/n_B}\right) C_{RA}\big|_{n,m-1}\Delta t \tag{144}$$

For overall resin phase concentration

$$C_{RA}\big|_{n,m} = C_{RA}\big|_{n,m-1} + \Delta C_{RPA}\text{Exchange}\big|_{n,m}\varepsilon_p \tag{145}$$

For solutions containing more than one solute, the concentrations of other solutes are calculated in the same way as for solute A.

4.4.3 Fixed bed radial flow

The CRFC is modelled as a series of well mixed tanks, each tank representing a stage. The annular bed is divided into N stages in the radial direction, while the outer and inner sintered stainless steel walls are divided into N_{osw} and N_{isw} stages respectively (Figure 4-6).

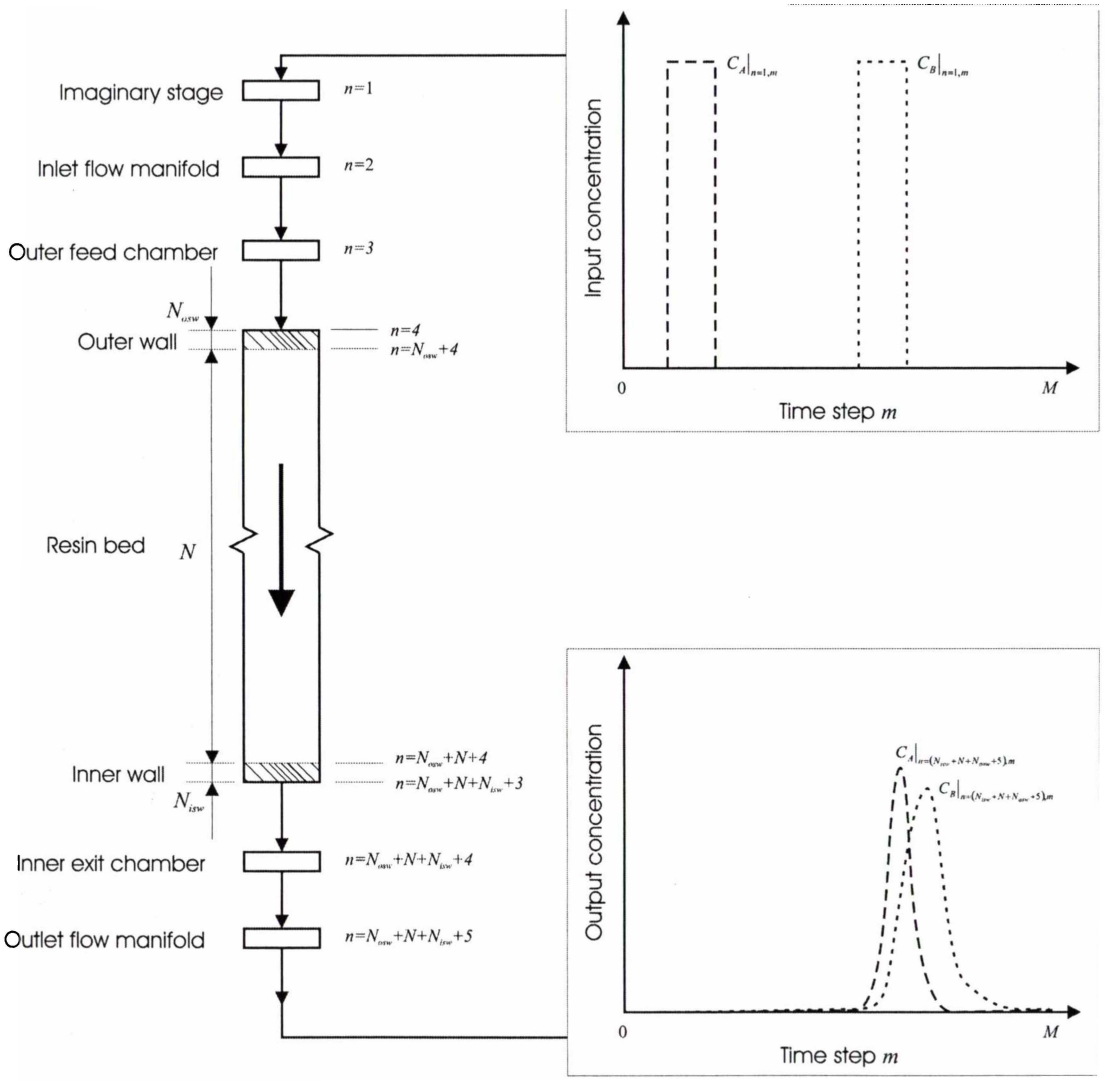

Figure 4-6. Set-up of finite difference model for fixed bed operation of CRFC.

The maximum number of bed stages required can be determined using

$$N_{\max} = \frac{r_1 - r_2}{4d_p} \tag{146}$$

Where r_1 and r_2 are the outer and inner radii of the annular bed respectively and d_p is the diameter of the resin particles. During simulations it was found that

$$N = \frac{N_{max}}{2} \tag{147}$$

was sufficient for the finite difference modelling as no significant differences were observed between using N or N_{max}.

The change in radius for each stage in the bed is given by

$$\Delta r = \frac{r_1 - r_2}{N} \tag{148}$$

The change in radii for the outer and inner sintered walls are given by

$$\Delta r_{osw} = \frac{T_{osw}}{N_{osw}} \tag{149}$$

$$\Delta r_{isw} = \frac{T_{isw}}{N_{isw}} \tag{150}$$

where T is the wall thickness and subscripts *osw* and *isw* are outer sintered wall and inner sintered wall respectively.

As well as stages for the bed and sintered walls, three stages are required before the annulus for setting feed input concentrations, the flow inlet manifold, and the CRFC outer feed chamber. Two stages are required after the bed and walls for the inner exit chamber and flow outlet manifold (Figure 4-6). It is assumed that no dispersion occurred between these stages or in the annulus walls.

Calculations for radii and volume for each stage are shown in Table 4-2. For convenience the volume calculations for the sintered walls include the wall void fraction. This allows the same equation to be used to calculate concentration with each time step for all stages except for the feed stage and resin bed stages.

Table 4-2. Calculation of radius and volume with respect to stage n. V is volume, ε is void fraction and subscripts *FM*, *OFC*, *IEC* and *sw* are flow manifold, outer feed chamber, inner exit chamber and sintered wall respectively.

	Stage n	Annular radius $r\|_n$	Volume $V_e\|_n$
Feed input	1	N/A	0
Inlet flow manifold	2	N/A	$V_e\|_n = V_{FM}$
Outer feed chamber	3	N/A	$V_e\|_n = V_{OFC}$
Outer sintered wall	$4 \le n \le (N_{osw} + 3)$	$r\|_n = r_1 + T_{osw} - (n-4)\Delta r_{osw}$	$V_e\|_n = \pi\left(r\|_n^{\,2} - \left(r\|_n - \Delta r_{osw}\right)^2\right)H\varepsilon_{sw}$
Resin bed	$(N_{osw} + 4) \le n \le (N + N_{osw} + 3)$	$r\|_n = r_1 - (n - N_{osw} - 4)\Delta r$	$V_e\|_n = \pi\left(r\|_n^{\,2} - \left(r\|_n - \Delta r\right)^2\right)H$
Inner sintered wall	$(N + N_{osw} + 4) \le n \le (N_{isw} + N + N_{osw} + 3)$	$r\|_n = r_2 - (n - N - N_{osw} - 4)\Delta r_{isw}$	$V_e\|_n = \pi\left(r\|_n^{\,2} - \left(r\|_n - \Delta r_{isw}\right)^2\right)H\varepsilon_{sw}$
Inner exit chamber	$(N_{isw} + N + N_{osw} + 4)$	N/A	$V_e\|_n = V_{IEC}$
Outlet flow manifold	$(N_{isw} + N + N_{osw} + 5)$	N/A	$V_e\|_n = V_{FM}$

A further simplification to the volume calculations can be made if Δr^2 is neglected, but this depends on the number of stages being sufficiently large so significant errors are not generated. There are errors for example, if the annular bed is divided into 70 stages (using bed dimensions of 14.6-cm OD, 8.6-cm ID and 2-cm high). The difference in volume neglecting Δr^2 is 0.3% to 0.6% of the actual volume. This would have a culmulative effect, therefore for modelling purposes Δr^2 was not neglected.

The change in time for a calculation was given by the residence time of solution in the inner most stage of the annular bed ($n = (N + N_{osw} + 3)$) divided by J,

$$\Delta t = \frac{V_e\big|_{n=(N+Nosw+3)} \varepsilon_R}{QJ} \tag{151}$$

The total number of time steps M was obtained by equation (131).

4.4.3.1 Boundary conditions and feed input concentrations

The intial solution and resin phase solute concentrations are set to zero, i.e.

for $$1 \le n \le (N_{isw} + N + N_{osw} + 5) \text{and } m=1$$

$$C_A\big|_{n,m} = 0,\ C_{RPA}\big|_{n,m} = 0,\ C_{RA}\big|_{n,m} = 0 \tag{152}$$

Table 4-1 is used to set the input concentrations with respect to time.

4.4.3.2 Concentration in stages outside the bed

Solute concentration for each stage outside the resin bed for each time step is calculated assuming no adsorption or reaction.

For $2 \le n \le (N_{osw} + 3)$ and $(N + N_{osw} + 4) \le n \le (N_{isw} + N + N_{osw} + 5)$,

and $$2 \le m \le (M + 1)$$

$$C_A\big|_{n,m} = C_A\big|_{n,m-1} + \frac{(C_A\big|_{n-1,m-1} - C_A\big|_{n,m-1})Q\Delta t}{V_e\big|_n} \tag{153}$$

4.4.3.3 Concentration in bed stages

For $(N_{osw}+4) \le n \le (N+N_{osw}+3)$ and $2 \le m \le (M+1)$

interstitial solute concentration for each stage in the resin bed is given by

$$C_A|_{n,m} = C_A|_{n,m-1} + \Delta C_A \text{Convection}|_{n,m} + \Delta C_A \text{Rdisp}|_{n,m} - \Delta C_A \text{Uptake}|_{n,m} \quad (154)$$

Each term is calculated from the mass balances used to derive the continuity equations. For convection, equation (35) becomes

$$\Delta C_A \text{Convection}|_{n,m} = \frac{(C_A|_{n-1,m-1} - C_A|_{n,m-1})Q\Delta t}{V_e|_n \varepsilon_R} \quad (155)$$

Dispersion is calculated by adapting equation (42) and substituting in the dispersion equivalent of Fick's Law, (equation (46)), the dispersion coefficient (equation (47)) and interstitial velocity (equation (48)).

Within the bed $(N_{osw}+5) \le n \le (N+N_{osw}+2)$

$$\Delta C_A \text{RDisp}|_{n,m} = \frac{y_2(2R_p)Q\Delta t}{V_e|_n \varepsilon_R \Delta r}(C_A|_{n-1,m-1} - 2C_A|_{n,m-1} + C_A|_{n+1,m-1}) \quad (156)$$

At the bed boundaries $n = (N_{osw}+4)$

$$\Delta C_A \text{RDisp}|_{n,m} = -\frac{y_2(2R_p)Q\Delta t}{V_e|_n \varepsilon_R \Delta r}(C_A|_{n,m-1} - C_A|_{n+1,m-1}) \quad (157)$$

$$n = (N_{osw}+N+3)$$

$$\Delta C_A \text{RDisp}|_{n,m} = \frac{y_2(2R_p)Q\Delta t}{V_e|_n \varepsilon_R \Delta r}(C_A|_{n-1,m-1} - C_A|_{n,m-1}) \quad (158)$$

The only difference between equations (156) to (158) and their axial dispersion equivalents (equations 137 to 139) is that volume is changing with radial position.

$\Delta C_A \text{Uptake}|_{n,m}$ is calculated using equations (140) and (141) for NP-MLF and equations (142) to (145) for FD-MLF.

4.5 Moving bed

The CRFC can be modelled for continuous operation in two ways. The first neglects angular dispersion or lumps it with radial dispersion by increasing the radial dispersion coefficient. This allows a thin section of the resin bed to be modelled as a two dimensional matrix with dimensions of radial position and time in a similar manner to the method for fixed bed operation. The section then experiences cyclical inputs of equilibration, feed, wash and elution. The timing of each depends on the angular width of the sections supplying the solution and the rotation speed of the annulus. The section of the bed, in effect, appears to be moving past the different feed and exit sections of the outer feed and inner exit chambers. Solute concentration with respect to angular position is averaged within the boundaries of each exit chamber section to obtain solute concentrations in the CRFC exit streams. This model was used to simulate CRFC operation.

The second method includes angular dispersion and requires the annular bed to be modelled as a three dimensional matrix with dimensions of radial and angular position and time. It is a logical extension of the two dimensional model. Although it requires greater processing time, it has some useful applications for future research in modelling radial flow chromatography.

4.5.1 Two dimensional model

Continuous operation of the CRFC where angular dispersion is neglected is modelled by following a thin segment of the annulus as the annulus revolves about its axis. The segment is exposed to repeating loading, wash, elution and equilibration cycles, each step at a different angular position in the CRFC (Figures 4-7 and 4-8). The resulting elution profiles are then mapped with respect to angular position to determine solute concentration exiting each section of the inner exit chamber (Figure 4-9).

The annular bed is divided into N stages along the radial direction (similar to the fixed bed model) and N_{as} segments in the angular direction. N_{as} has to be divisible by D, the number of sections in the outer feed and inner exit chambers, and give an integer if this model is extended to include angular dispersion (Section 4.5.2). Similarly, the outer and inner sintered stainless steel walls are divided into N_{osw} and N_{isw} stages respectively

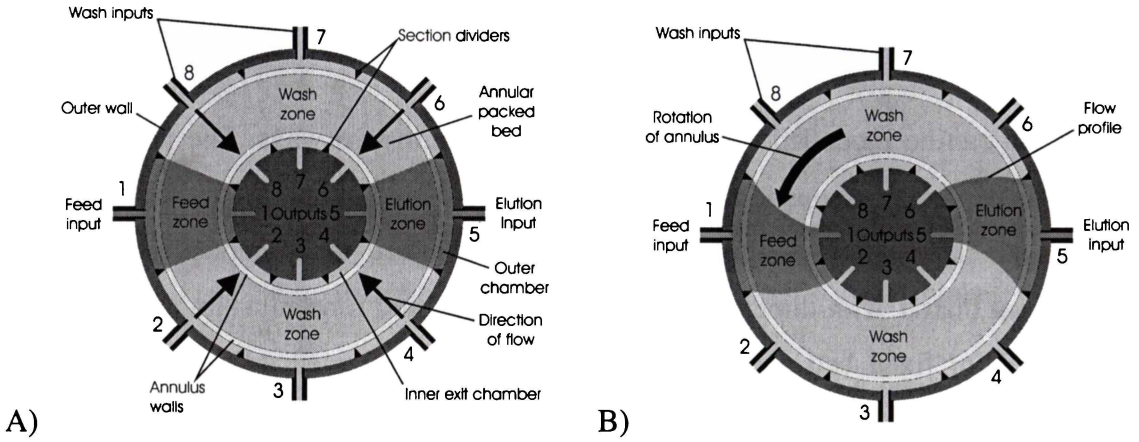

Figure 4-7. Flow profiles through the CRFC when A) the bed is stationary and B) whe the bed is rotating.

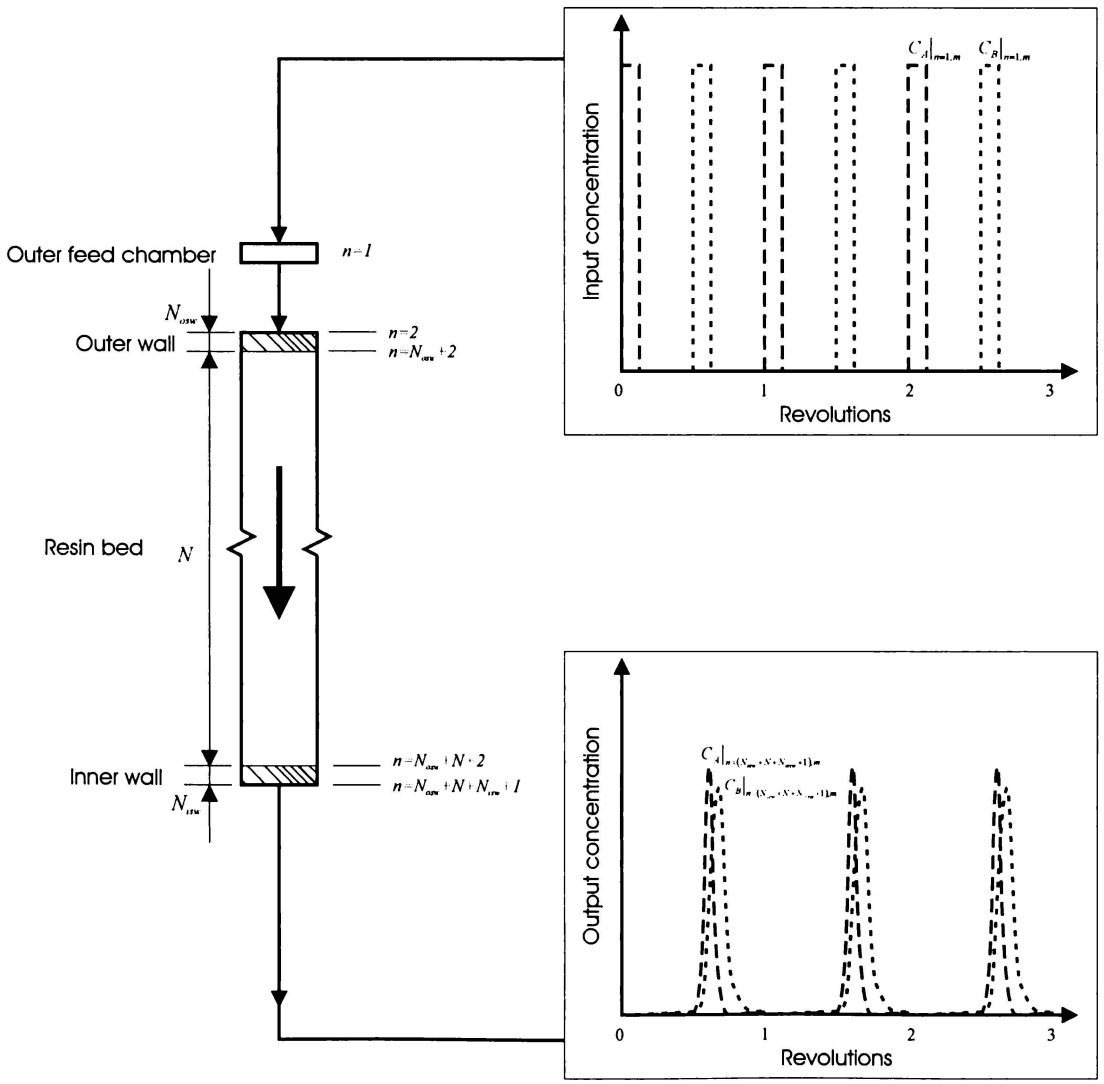

Figure 4-8. Set-up of two dimensional CRFC finite difference model.

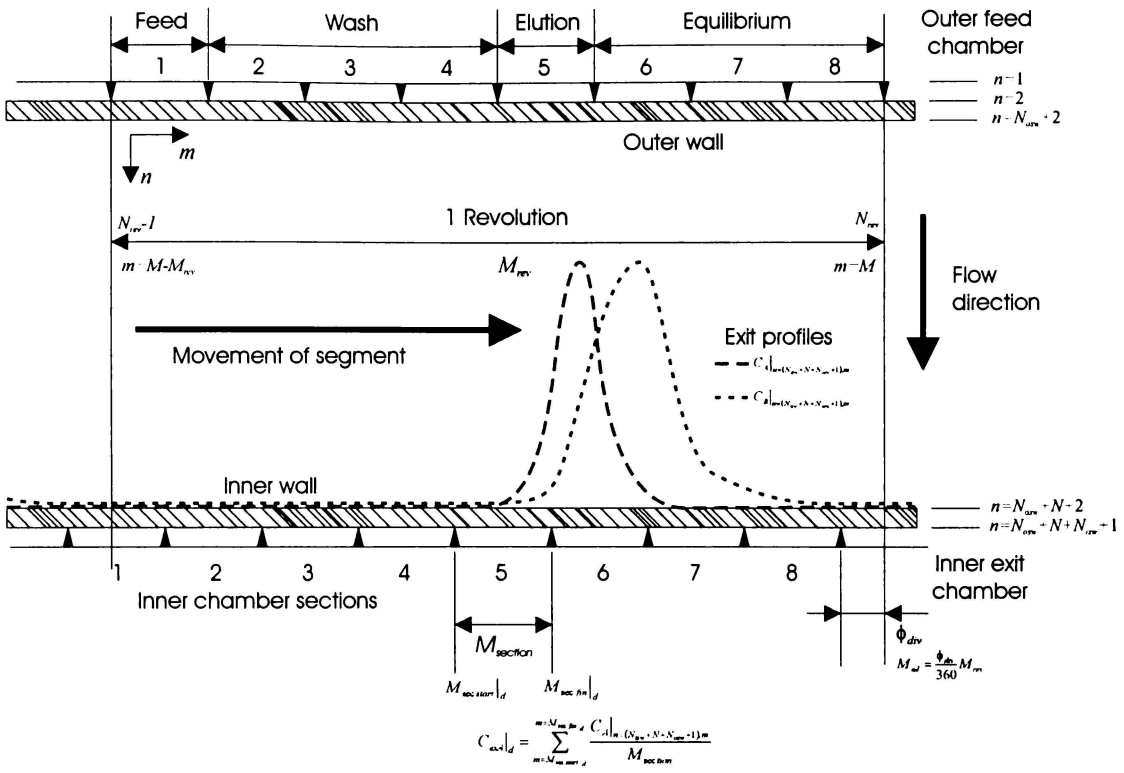

Figure 4-9. Mapping of concentration history with respect to angular position to calculate solute concentration exiting each inner exit chamber section.

and N_{as} segments in the angular direction. The inlet and outlet flow manifolds and outer feed and inner exit chambers are neglected because concentration will not change with time during continuous operation. The outer feed chamber is used to set the feed input concentrations.

Volumes of elements for each stage can be calculated for:

the outer sintered wall $$2 \le n \le (N_{osw} + 1)$$

$$r|_n = r_1 + T_{osw} - (n-2)\Delta r_{osw}$$

$$V_e|_n = \frac{\pi\left(r|_n^{\,2} - \left(r|_n - \Delta r_{osw}\right)^2\right) H \varepsilon_{sw}}{N_{as}} \tag{159}$$

the resin bed $$(N_{osw} + 2) \le n \le (N + N_{osw} + 1)$$

$$r|_n = r_1 - (n - N_{osw} - 2)\Delta r$$

$$V_e|_n = \frac{\pi\left(r|_n^{\,2} - \left(r|_n - \Delta r\right)^2\right)H}{N_{as}} \tag{160}$$

and the inner sintered wall

$$\left(N + N_{osw} + 2\right) \le n \le \left(N_{isw} + N + N_{osw} + 1\right)$$

$$r|_n = r_2 - \left(n - N - N_{osw} - 2\right)\Delta r_{isw}$$

$$V_e|_n = \frac{\pi\left(r|_n^{\,2} - \left(r|_n - \Delta r_{isw}\right)^2\right)H\varepsilon_{sw}}{N_{as}} \tag{161}$$

Flowrate through each element is given by

$$Q_e = \frac{Q}{N_{as}} \tag{162}$$

The estimated time interval for a calculation is given by the residence time of solution in the innermost stage of the annular bed $\left(n = N + N_{osw} + 1\right)$ divided by J,

$$\Delta t_{est} = \frac{V_e|_{n=(N+Nosw+2)}\,\varepsilon_R}{Q_e J} \tag{163}$$

The actual Δt is found by

$$\frac{360}{wM_{section}D} = \Delta t \le \Delta t_{est} \tag{164}$$

where w is rotation speed and D is the number of sections in the feed and exit chambers of the CRFC. $M_{section}$ is a positive integer and is the number of rotation steps per section. It is adjusted so that $\Delta t \le \Delta t_{est}$ and is used to calculate the total number of rotation steps per revolution,

$$M_{rev} = M_{section}D \tag{165}$$

Total time and angular steps M is given by

$$M = M_{rev}N_{rev} \tag{166}$$

where N_{rev} is the number of revolutions of the annulus that the simulation is run for.

The angular position of the segment with respect to rotation step m is given by

$$\phi_p\big|_m = 360 \cdot \left(0.5 + a\tan\left(\tan\left(\frac{\phi\big|_m}{360}\pi + \frac{\pi}{2} \right) \right) \frac{1}{\pi} \right) \tag{167}$$

where $$\phi\big|_m = (m-1)w\Delta t \tag{168}$$

The angular position is used to determine input concentrations into the segment.

4.5.1.1 Boundary conditions and feed input concentrations

Solute concentrations in the solution and resin phases are initially set to zero, i.e.

for $$1 \le n \le (N_{isw} + N + N_{osw} + 1) \text{ and } m=1$$

$$C_A\big|_{n,m} = 0,\ C_{RPA}\big|_{n,m} = 0,\ C_{RA}\big|_{n,m} = 0 \tag{169}$$

The outer feed and inner exit chambers are divided into eight equal sized sections. Each section in the outer feed chamber can independently supply solution to the annulus. For example, one section can supply a protein-laden feed, three sections remove unbound protein, one section to elute and three sections to equilibrate the resin (Figure 4-7). Input concentrations into the annular segment at n=1 with respect to angular position are calculated using conditions in Table 4-3.

4.5.1.2 Sintered wall concentrations

Solute concentration with respect to angular step for the outer and inner sintered wall stages is given by,

when $$2 \le n \le (N_{osw} + 1),\ (N + N_{osw} + 2) \le n \le (N_{isw} + N + N_{osw} + 1)$$

and $$2 \le m \le (M + 1)$$

$$C_A\big|_{n,m} = C_A\big|_{n,m-1} + \frac{\left(C_A\big|_{n-1,m-1} - C_A\big|_{n,m-1}\right) Q_e \Delta t}{V_e\big|_n} \tag{170}$$

Table 4-3. Segment input concentrations at n=1 with respect to angular position and feed chamber section.

Feed chamber sections	Solution	Start and finish of section (degrees)	Input concentrations
1	Protein-laden feed	$0 < \phi_p\|_m \leq 45$	$C_A\|_{n=1,m} = C_{feed}$, $C_B\|_{n=1,m} = 0$
2-4	Wash	$45 < \phi_p\|_m \leq 180$	$C_A\|_{n=1,m} = 0$, $C_B\|_{n=1,m} = 0$
5	Elution	$180 < \phi_p\|_m \leq 225$	$C_A\|_{n=1,m} = 0$, $C_B\|_{n=1,m} = C_{elution}$
6-8	Equilibration	$225 < \phi_p\|_m \leq 360$	$C_A\|_{n=1,m} = 0$, $C_B\|_{n=1,m} = 0$

4.5.1.3 Annular bed concentrations

The overall solution concentration for stages in the resin bed is given by equation (154),

for $$(N_{osw}+1) \leq n \leq (N+N_{osw}+1) \text{ and } m > 1$$

$$C_A|_{n,m} = C_A|_{n,m-1} + \Delta C_A\text{Convection}|_{n,m} + \Delta C_A\text{Rdisp}|_{n,m} + \Delta C_A\text{Uptake}|_{n,m}$$

$\Delta C_A\text{Convection}|_{n,m}$ is obtained by modifying equation (155) for flow through a narrow segment,

$$\Delta C_A\text{Convection}|_{n,m} = \frac{\left(C_A|_{n-1,m-1} - C_A|_{n,m-1}\right)Q_e\Delta t}{V_e|_n \varepsilon_R} \tag{171}$$

$\Delta C_A\text{Uptake}|_{n,m}$ is calculated using equations (140) and (141) for NP-MLF and equations (142) to (145) for FD-MLF.

$\Delta C_A\text{RDisp}|_{n,m}$ within the bed, $(N_{osw}+2) \leq n \leq (N+N_{osw})$, is given by

$$\Delta C_A\text{RDisp}|_{n,m} = \frac{y_2(2R_p)Q_e\Delta t}{V_e|_n \varepsilon_R \Delta r}\left(C_A|_{n-1,m-1} - 2C_A|_{n,m-1} + C_A|_{n+1,m-1}\right) \tag{172}$$

and at the boundaries $n = (N_{osw} + 1)$

$$\Delta C_A \text{RDisp}|_{n,m} = -\frac{y_2(2R_p)Q_e\Delta t}{V_e|_n \varepsilon_R \Delta r}\left(C_A|_{n,m-1} - C_A|_{n+1,m-1}\right) \tag{173}$$

$$n = (N + N_{osw} + 1)$$

$$\Delta C_A \text{RDisp}|_{n,m} = \frac{y_2(2R_p)Q_e\Delta t}{V_e|_n \varepsilon_R \Delta r}\left(C_A|_{n-1,m-1} - C_A|_{n,m-1}\right) \tag{174}$$

4.5.1.4 Average concentration leaving exit chamber sections

An exit solute concentration profile with respect to rotation step m can be determined using the solute concentration history for the last stage of the annulus inner wall, $n = (N_{isw} + N + N_{osw} + 1)$. If steady state is assumed once the last annulus revolution has begun the solute concentration with angular position will be constant over time. The solute concentration exiting the annulus segments within each exit chamber section can be averaged to determine solute concentration in the section at steady state.

The inner chamber section dividers are adjusted to a given angular distance ϕ_{div} clockwise relative to the outer chamber section dividers. This is converted to the number of angular steps M_{ad},

$$M_{ad} = \frac{\phi_{div}}{360} M_{rev} \tag{175}$$

The start and finish points for each section are determined in terms of angular step m. These points are then used for the calculation of the exit solute concentration, which is the average concentration exiting the annulus between the two points.

For $1 \le d \le D$

$$M_{\text{sec}\,start}|_d = (N_{rev} - 1)M_{rev} + (d-1)M_{\text{sec}\,tion} - M_{ad} + 2 \tag{176}$$

$$M_{\text{sec}\,fin}|_d = (N_{rev} - 1)M_{rev} + d \cdot M_{\text{sec}\,tion} - M_{ad} + 1 \tag{177}$$

$M_{\sec start}\big|_d$ and $M_{\sec fin}\big|_d$ are rounded up to the nearest integer, and the concentration is given by

$$C_{exA}\big|_d = \sum_{m=M_{\sec start}\big|_d}^{m=M_{\sec fin}\big|_d} \frac{C_A\big|_{n=(N_{isw}+N+N_{osw}+1),m}}{M_{\sec tion}} \tag{178}$$

4.5.2 Three dimensional model

Including angular dispersion requires the annular bed to be modelled as a three dimensional matrix with dimensions of radial (n) and angular position (s) and time (m). The annulus is discretized as described in Section 4.5.1, but all segments (rather than a single segment) are simulated. Volumes, run times and Δt are calculated as shown in Section 4.5.1.

Initially, solute concentrations in the solution and resin phases are set to zero.

For $1 \le n \le (N_{isw} + N + N_{osw} + 1)$, $1 \le s \le N_{as}$ and $m = 1$

$$C_A\big|_{n,s,m} = 0\,,\; C_{RPA}\big|_{n,s,m} = 0\,,\; C_{RA}\big|_{n,s,m} = 0 \tag{179}$$

Angular position for each segment s for each rotation step m is given by

for $1 \le s \le N_{as}$ and $1 \le m \le M + 1$

$$\phi_p\big|_{s,m} = 360 \cdot \left(0.5 + a\tan\left(\tan\left(\left(\frac{\phi\big|_m}{360} + \frac{s}{N_{as}}\right)\pi + \frac{\pi}{2}\right)\right)\frac{1}{\pi}\right) \tag{180}$$

where $\phi\big|_m$ is given by equation (168). $\phi_p\big|_{s,m}$ is used to determine the each segment's position relative to the sections in the outer feed and inner exit chambers using Table 4-4.

Table 4-4. Input concentrations at n=1 for each annulus segment with respect to angular position and feed chamber section.

Feed chamber sections	Solution	Start and finish of section (degrees)	Input concentrations
1	Protein-laden feed	$0 < \phi_p\big\|_{s,m} \le 45$	$C_A\big\|_{n=1,s,m} = C_{feed}$, $C_B\big\|_{n=1,s,m} = 0$
2-4	Wash	$45 < \phi_p\big\|_{s,m} \le 180$	$C_A\big\|_{n=1,s,m} = 0$, $C_B\big\|_{n=1,s,m} = 0$
5	Elution	$180 < \phi_p\big\|_{s,m} \le 225$	$C_A\big\|_{n=1,s,m} = 0$, $C_B\big\|_{n=1,s,m} = C_{elution}$
6-8	Equilibration	$225 < \phi_p\big\|_{s,m} \le 360$	$C_A\big\|_{n=1,s,m} = 0$, $C_B\big\|_{n=1,s,m} = 0$

4.5.2.1 Sintered wall concentrations

Solute concentration with respect to angular step for elements in the outer and inner sintered wall is calculated by

for $2 \le n \le (N_{osw}+1)$, $(N+N_{osw}+2) \le n \le (N_{isw}+N+N_{osw}+1)$,

$$1 \le s \le N_{as} \text{ and } m>1$$

$$C_A\big|_{n,s,m} = C_A\big|_{n,s,m-1} + \frac{\left(C_A\big|_{n-1,s,m-1} - C_A\big|_{n,s,m-1}\right) Q_e \Delta t}{V_e\big|_n} \tag{181}$$

4.5.2.2 Annular bed concentrations

The resin bed interstitial solution concentration is obtained by adapting equation (154) to include angular dispersion

for $(N_{osw}+1) \le n \le (N+N_{osw}+1)$, $1 \le s \le N_{as}$, and $m>1$

$$C_A\big|_{n,s,m} = C_A\big|_{n,s,m-1} + \Delta C_A \text{Convection}\big|_{n,s,m} + \Delta C_A \text{Rdisp}\big|_{n,s,m}$$

$$+ \Delta C_A \text{Adisp}\big|_{n,s,m} + \Delta C_A \text{Uptake}\big|_{n,s,m} \tag{182}$$

$\Delta C_A\text{Convection}|_{n,s,m}$, $\Delta C_A\text{Uptake}|_{n,s,m}$, and $\Delta C_A\text{Rdisp}|_{n,s,m}$ are calculated by adapting equations in Section 4.5.1.3 to three dimensions. For example, equation (171) becomes

$$\Delta C_A\text{Convection}|_{n,s,m} = \frac{\left(C_A|_{n-1,s,m-1} - C_A|_{n,s,m-1}\right)Q_e\Delta t}{V_e|_n\,\varepsilon_R} \tag{183}$$

Angular dispersion is calculated using the finite difference forms of equations (61) and (65) and substituting in equation (62), to give

$$\Delta C_A\text{Adisp}|_{n,s,m} = \frac{D_{A\theta}|_n\,\Delta r H \Delta t}{V_e|_n\left(r|_n - \frac{\Delta r}{2}\right)\Delta\theta}\left(C_A|_{n,s-1,m-1} - 2C_A|_{n,s,m-1} + C_A|_{n,s+1,m-1}\right) \tag{184}$$

$\left(r|_n - \frac{\Delta r}{2}\right)$ is used instead of $r|_n$ for angular dispersion because angular distance between the two elements over which dispersion occurs is taken from the centre of the elements rather than one edge.

Equation (47) for radial dispersion is converted to give angular dispersion

$$D_{A\theta}|_n = y_{2\theta}\left(2R_p\right)v|_n \tag{185}$$

where $y_{2\theta}$ is a constant and can be adjusted so

$$D_{mA} \le D_{A\theta} \le D_{Ar} \tag{186}$$

$v|_n$ is the interstital solution velocity at the centre of the element

$$v|_n = \frac{Q_e N_{as}}{2\pi\left(r|_n - \frac{\Delta r}{2}\right)H\varepsilon_R} \tag{187}$$

and $\Delta\theta$ is given by

$$\Delta\theta = \frac{2\pi}{N_{as}} \tag{188}$$

Equation (184) is valid for $1 < s < N_{as}$. For the angular boundary where $s = 1$ and $s = N_{as}$, equation (184) becomes

for $s = 1$

$$\Delta C_A \text{Adisp}\big|_{n,s,m} = \frac{D_{A\theta}\big|_n \Delta r H \Delta t}{V_e\big|_n \left(r\big|_n - \frac{\Delta r}{2} \right) \Delta\theta} \left(C_A\big|_{n,N_{as},m-1} - 2C_A\big|_{n,s,m-1} + C_A\big|_{n,s+1,m-1} \right) \quad (189)$$

and for $s = N_{as}$

$$\Delta C_A \text{Adisp}\big|_{n,s,m} = \frac{D_{A\theta}\big|_n \Delta r H \Delta t}{V_e\big|_n \left(r\big|_n - \frac{\Delta r}{2} \right) \Delta\theta} \left(C_A\big|_{n,s-1,m-1} - 2C_A\big|_{n,s,m-1} + C_A\big|_{n,1,m-1} \right) \quad (190)$$

4.5.2.3 Average concentration leaving exit chamber sections

The concentrations over specific regions of the last stage of the annulus can be averaged to determine the concentration of solute exiting each section of the inner exit chamber (Figure 4-10). The CRFC inner exit chamber is divided into D sections. Elements per section is given by

$$S_{section} = \frac{N_{as}}{D} \quad (191)$$

The inner chamber section dividers are adjusted to a specific angular distance ϕ_{div} clockwise to the outer chamber section dividers. ϕ_{div} is converted to the number of angular segments S_{ad} by

$$S_{ad} = \frac{\phi_{div}}{360} N_{as} \quad (192)$$

The start and finish points for each section are determined in terms of angular step m. These points are then used to calculate the exit solute concentration, which is the average concentration exiting the annulus between the two points.

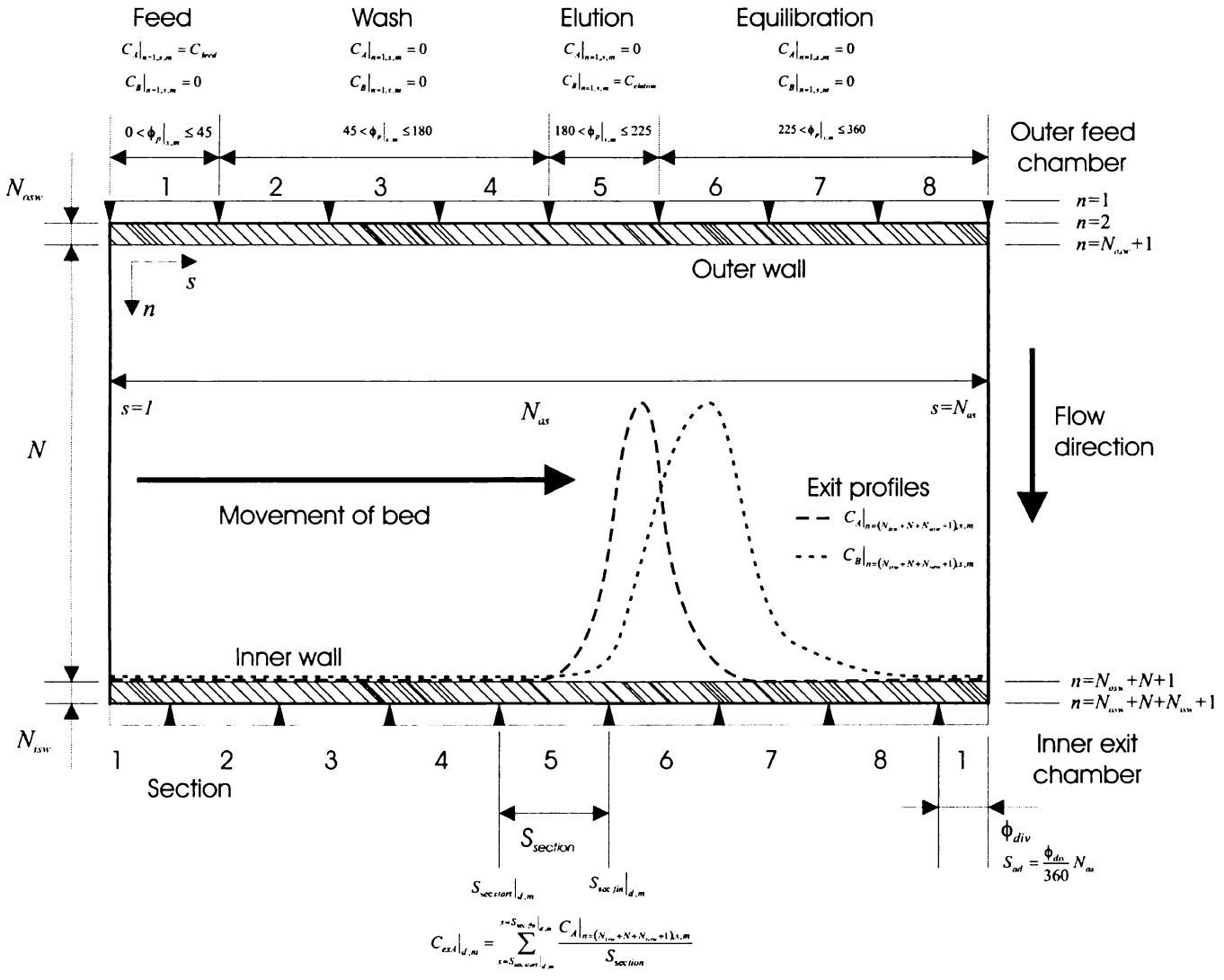

Figure 4-10. Set-up of angular dispersion model for continuous operation of CRFC.

For $1 \le d \le D$ and $m \ge 1$

$$S_{\sec start}\big|_{d,m} = N_{as} \cdot \left(0.5 + a\tan\left(\tan\left(\left(\frac{\phi|_m}{360} + \frac{(d-1)S_{section} - S_{ad} + 1}{N_{as}} \right)\pi + \frac{\pi}{2} \right) \right) \frac{1}{\pi} \right) \quad (193)$$

$$S_{\sec fin}\big|_{d,m} = N_{as} \cdot \left(0.5 + a\tan\left(\tan\left(\left(\frac{\phi|_m}{360} + \frac{d \cdot S_{section} - S_{ad}}{N_{as}} \right)\pi + \frac{\pi}{2} \right) \right) \frac{1}{\pi} \right) \quad (194)$$

$S_{\sec start}\big|_{d,m}$ and $S_{\sec fin}\big|_{d,m}$ are rounded up to the nearest whole integer.

where $$S_{\sec start}\big|_{d,m} < S_{\sec fin}\big|_{d,m} \quad (195)$$

$$C_{exA}\big|_{d,m} = \sum_{s=S_{\sec start}|_{d,m}}^{s=S_{\sec fin}|_{d,m}} \frac{C_A\big|_{n=(N_{isw}+N+N_{osw}+1),s,m}}{S_{section}} \quad (196)$$

where $$S_{\sec start}\big|_{d,m} > S_{\sec fin}\big|_{d,m}$$

$$C_{exA}\big|_{d,m} = \frac{\sum_{s=S_{\sec start}|_{d,m}}^{s=N_{as}} C_A\big|_{n=(N_{isw}+N+N_{osw}+1),s,m} + \sum_{s=1}^{s=S_{\sec fin}|_{d,m}} C_A\big|_{n=(N_{isw}+N+N_{osw}+1),s,m}}{S_{section}} \quad (197)$$

At steady state, $C_{exA}\big|_{d,m}$ will become constant with time step m.

4.5.2.4 Possible applications of the 3D model

The 3D model would be useful for examining situations in batch radial flow chromatography such as non-uniform flow, channelling and uneven solute distribution in the flow distributors. The non-uniform flow and channelling modelling could be done by making flow through the resin bed dependent on angular position, and input concentrations time rather than position dependent. The effects of non-uniform flow on column resolution and performance could then be investigated.

Uneven solute distribution modelling could be done by discretizing the feed and exit chambers and modelling solute distribution in the chambers over time. The effects of solute distribution on column resolution and performance could then be determined.

The data may explain why radial flow columns have much lower resolution than axial flow columns. This could be explored further by expanding the 3D model to 4D. Concentration with respect to height, depth, angular position and time could be calculated, and the effects of different distributor set-ups could be investigated. Data from this model would provide valuable information for designing radial flow chromatographic columns.

4.6 Conclusion

Finite difference models were developed to simulate batch adsorption of protein, axial and radial flow breakthrough and elution, and continuous separation using the CRFC. These models will allow experimental results obtained to be analysed in terms of uptake kinetics, pore diffusion and dispersion, by fitting model curves to experimental data.

Chapter 5

Methodology

5.1 Introduction

This chapter presents the methods used for the experiments reported in this thesis.

There are four main areas of experimental work.

1. Determining uptake and desorption kinetic properties of the ion exchange resin used for the CRFC and small column work. This includes adsorption isotherm experiments and rate kinetic experiments in stirred beakers, and breakthrough and elution experiments on small axial flow columns. Experimental apparatus used for small column work is characterised to determine extra column effects that may affect fitting the models to experimental results.

2. Batch operation of the CRFC at different loading flowrates and loading concentrations to compare experimental and model results. Apparatus used external to the CRFC is characterised to determine extra column effects that may affect fitting the models to experimental results.

3. Obatining elution profiles for continuous operation of the CRFC at different rotation speeds and different divider angles, using a single protein and comparing experimental and model results.

4. Continuous operation of the CRFC to separate two proteins.

5.2 Reagents

The following reagents were used:

- Ion exchange resin: DEAE Sepharose Fast Flow anion exchanger (Amersham Biosciences, Uppsala, Sweden) (Appendix B).

- Feed solutions: Bovine serum albumin (BSA) (Fraction V, low endotoxin) (Life Technologies GibcoBRL) and bovine lactoferrin (Tatua Co-operative Dairy Company Ltd., Morrinsville, New Zealand), dissolved in equilibration buffer and adjusted to pH 7 (Appendix B).

- Equilibration buffer: Tris(hydroxymethyl)methylamine (BDH Laboratory Supplies or AppliChem Biochemica, GmbH), made to 0.02 M, pH 7.
- Elution buffer: NaCl (University of Waikato) made to 1 M in equilibration buffer, pH 7.
- Regeneration solutions: NaOH (Scharlau Chemic S.A.), made to 0.5 M and 1 M; and sodium acetate (Lancaster and Prolabo), made to 1 M, pH 3.
- Packing buffer: NaCl made to 1 M.
- Resin storage buffer: Ethanol, analytical grade, (Ajax FineChem), diluted to 20% vol/vol.

All solutions up to 2 L were freshly made in B grade volumetric flasks. Solutions greater than 2 L were prepared in appropriate sized containers. All solutions, except the protein solution which foamed easily, were degassed with helium for ten minutes. pH adjustments were made using concentrated sulphuric acid (Scharlau Chemic S.A.). Absorbencies of feed solutions greater than 2 L were checking using a UV spectrophotometer at 280nm, and concentrations calculated from calibration data (Appendix C).

5.3 Equipment

In addition to the CRFC, the following equipment was used:

Chromatography work

- AKTAexplorer100, an automated liquid chromatography system, equipped with a 1-ml Hi-Trap DEAE Sepharose Fast Flow column (Amersham Biosciences, Uppsala, Sweden).

Lactoferrin assay

- Surface Plasmon Resonance system (SPR), equipped with a CM5 chip with lactoferrin antibody (Biacore, Uppsala, Sweden).

pH, conductivity and pressure

- Cyberscan pH 100 (Alphatech Systems Ltd & Co, Auckland, New Zealand).
- Cyberscan Con 100 (Alphatech Systems Ltd & Co, Auckland, New Zealand).
- Wika pressure gauge (0-1000 kPa) (Wholesale Industrial Supplies, Hamilton, New Zealand).

Protein absorbance

- Ultraspec 2000 UV/visible spectrophotometer (Amersham Biosciences, Uppsala, Sweden).
- Inline Optical and Control Unit UV-1 spectrophotometer (Amersham Biosciences, Uppsala, Sweden).

Pumps

- Peristaltic pump P-1 (Amersham Biosciences, Uppsala, Sweden).
- Pro-Spense pump (Cole-Palmer, Illinois, USA).
- P-6000 and P-500 syringe pumps (Amersham Biosciences, Uppsala, Sweden).

5.4 Batch adsorption experiments

Equilibrium isotherm and rate kinetic experiments were done to validate the multicomponent Langmuir-Freundlich isotherm for modelling uptake of BSA by DEAE Sepharose Fast Flow media.

5.4.1 Equilibrium adsorption isotherms

Adsorption equilibrium experiments of BSA on DEAE Sepharose Fast Flow media were done using a stirred batch adsorption method. Six to eight 250-ml beakers were set up containing a known volume of equilibration buffer (0.02M pH 7 Tris solution)

with different concentrations of BSA (0.5-2 mg/ml). Starting concentrations were checked using a UV spectrophotometer at 280nm. Absorbances were compared to calibration data (Figure C-1) and concentrations determined. Known volumes of resin (pre-equilibrated and settled overnight in 5 ml measuring cylinders) in known volume of buffer were added to each of the beakers. The beakers were agitated for 18 hours under overhead stirrers. Agitation was stopped and the resin allowed to settle for 15-30 min before solution concentrations were determined. The solutions were agitated for another hour, and concentrations remeasured to ensure equilibrium had been achieved. Trials were done for 0, 0.02, 0.4 and 0.1M NaCl in equilibration buffer to observe the effect of salt concentration on protein adsorption.

Resin solute concentration was determined by mass balance and data plotted as mass of protein bound per ml of resin against concentration of unbound protein in solution at equilibrium. The multicomponent Langmuir-Freundlich isotherm (equation (77) in Chapter 4) was fitted to experimental data to obtain isotherm parameters.

5.4.2 Batch kinetics

Batch kinetic experiments of BSA on DEAE Sepharose Fast Flow media were done using a stirred batch adsorption method. The set-up consisted of a magnetic stirrer, 500-ml beaker, a peristaltic pump and in-line UV spectrophotometer connected with 1-mm ID plastic tubing (Figure 5-1). The BSA solution and resin was well mixed with a magnetic flea and circulated at 2 ml/min. Tubing length and diameter were selected to minimize residence time in the circuit. A filter at the inlet prevented resin flowing through the spectrophotometer. The signal from the spectrophotometer was recorded on a chart recorder.

The spectrophotometer was zeroed using equilibration buffer. Air was then pumped through the spectrophotometer and tubing to clear the equilibration buffer. The spectrophotometer and chart recorder were then calibrated with standard solutions (Figure C-4). DEAE sepharose ion exchange resin was pre-equilibrated and settled in a 20-ml measuring cylinder. BSA solution was prepared in a 500-ml B grade volumetic flask using 0.02M Tris HCL pH 7 equilibration buffer. The BSA solution was added to the beaker and pumped through the UV spectrophotometer to obtain the initial reading. 20ml of resin (pre-equilibrated, settled in a measuring cylinder overnight and excess

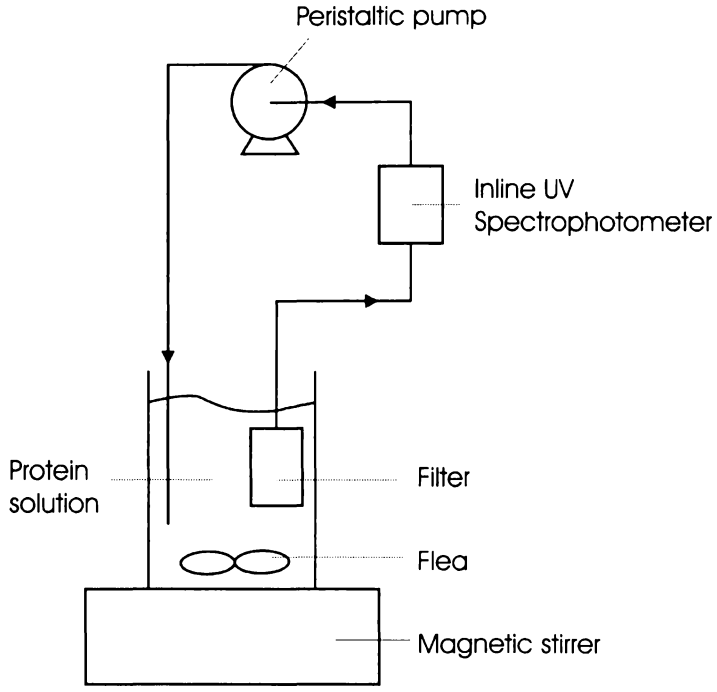

Figure 5-1. Setup for determining BSA uptake rates by DEAE sepharose FF.

equilibration buffer removed) was added to the beaker. Changes in protein concentration were measured until equilibrium was achieved. This procedure was repeated for six different initial BSA concentrations.

The chart recorder readings were converted to concentration (mg/ml) using calibration data (Figure C-4). The concentration of protein adsorbed to resin with time was determined by mass balance (taking into account the external void fraction of the resin and the equilibration buffer added with the resin to the bulk solution). Resin protein concentration was plotted against time and the two rate kinetics finite difference models (Section 4.4.1) were fitted.

5.5 Small column experiments

Breakthrough and elution experiments were performed on a 1-ml DEAE Sepharose FF axial flow column coupled to an AKTAexplorer100 liquid chromatography system (Amersham Biosciences). The data were used to determine the validity of uptake and desorption models presented in Chapter 4. Preliminary work investigated extra-column effects that would influence breakthrough and elution profiles.

5.5.1 AKTA set-up

All small column work and batch experiments using the CRFC were performed using the Amersham Biosciences AKTAexplorer100 (Figure 5-2). The AKTAexplorer100 has two primary pumps which can supply two different solutions to the column. Up to 11 solutions can be used in a single trial through the primary pumps. A step or continuous change in buffer concentration for step or gradient elution can be achieved by combining different ratios of two solutions via the two primary pumps and mixing the two solutions using a gradient mixer. The gradient mixer is a 2-ml vessel with two inlets and one outlet and contains a small magnetic flea.

Feed can be loaded directly onto a column with one of the primary pumps, or by using a 50-ml graduated glass syringe (a "Superloop"), which is loaded by injecting feed solution through an injection port in the injection valve with a hand held syringe (Figure 5-3). Feed solution is applied to the column by diverting flow from the primary pumps to the superloop to drive a plunger that pushes feed solution into the column (Figure 5-3). Smaller samples can be loaded into sample loops, either with a hand-held syringe or automatically with a sample pump (Figure 5-4). Eight different samples can be applied to the column using the sample valve.

Up to seven columns can be attached to the AKTAexplorer100. The column is selected using a column selection valve. Flow through the column can be reversed using a column flow direction valve (Figure 5-2). Effluent from the column passes through an inline UV spectrophotometer, conductivity meter and pH sensor before being directed to different collection vessels or fraction collector using the outlet valve. Tubing in the AKTA are 0.5 mm I.D. to minimise residence time of solution in the system. The system can be replumbed to cater for different experiments. The AKTAexplorer100 is operated by a PC using Unicorn software and can be programmed for automated operation. Data from each run are stored in the PC for later use.

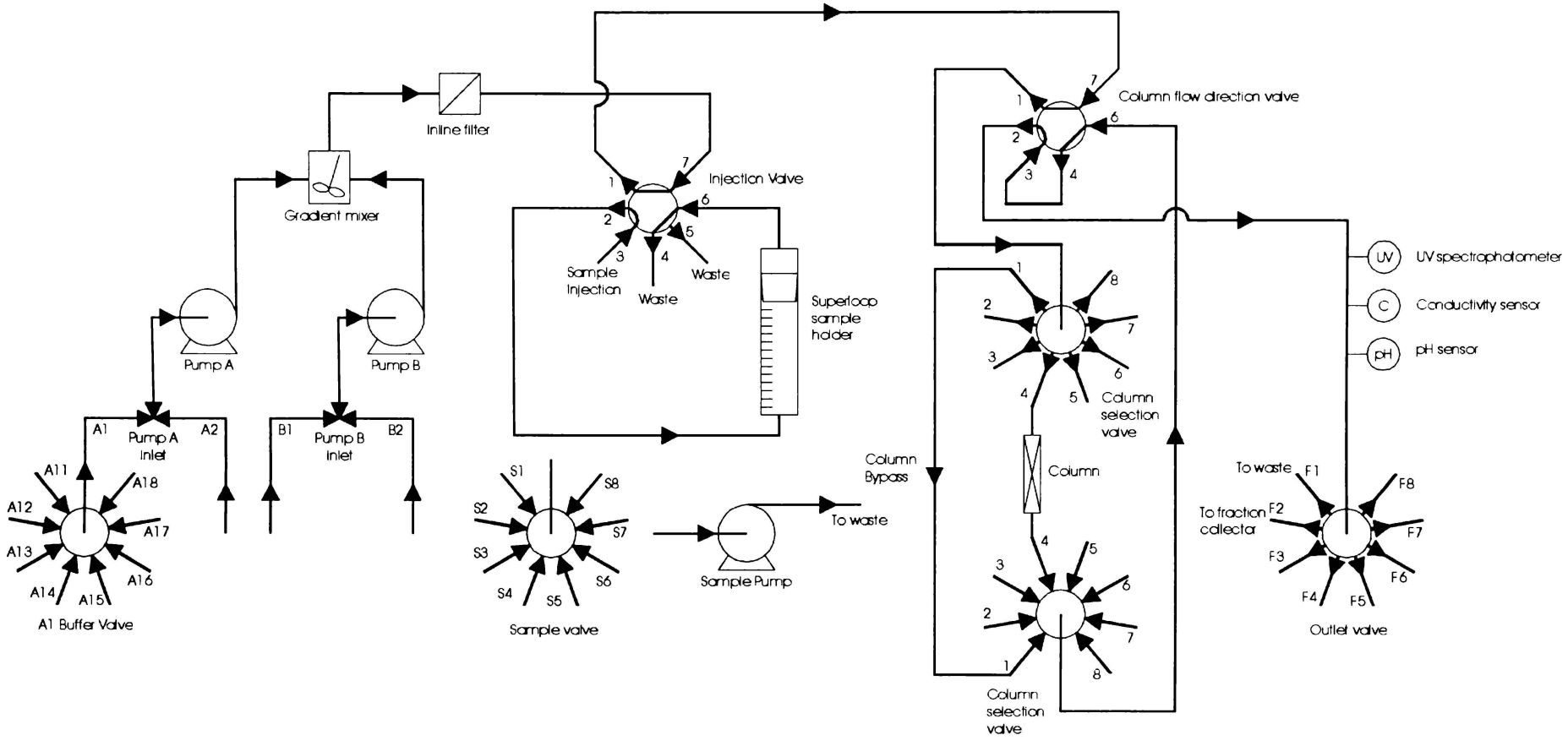

Figure 5-2. Flow diagram of the AKTAexplorer100. The sample pump and sample valve are not connected.

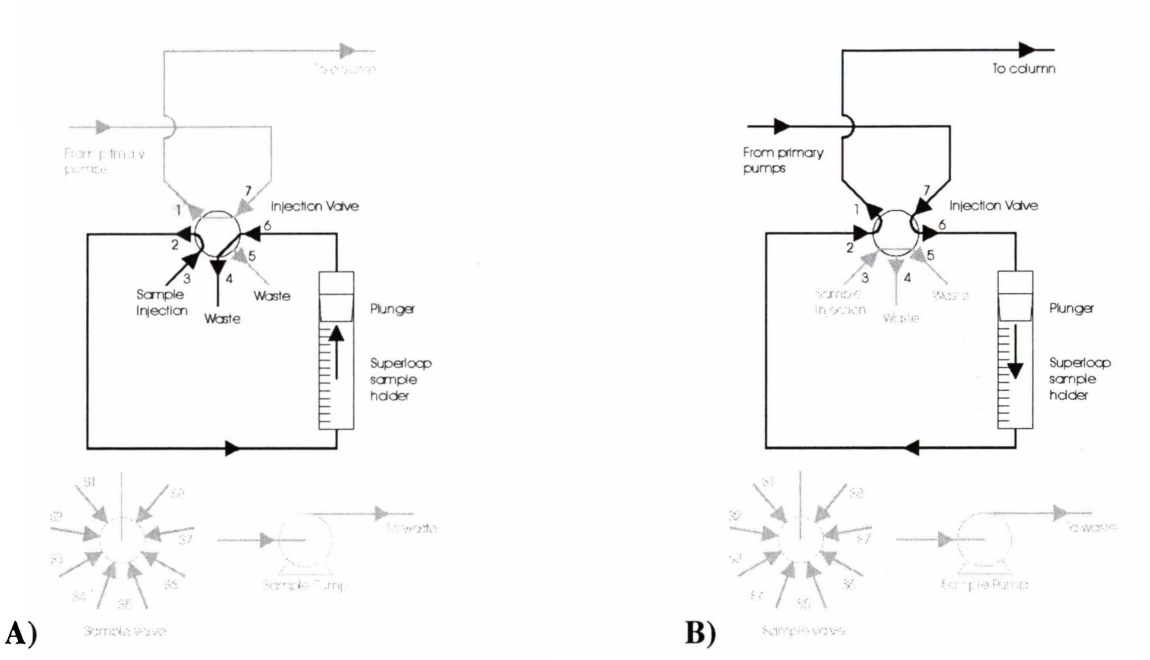

Figure 5-3. A) Loading of superloop on the Akta-100 when the injection valve is in loading position. B) The primary pump is used to drive the plunger of the superloop down pushing the sample into the column when the injection valve in inject position.

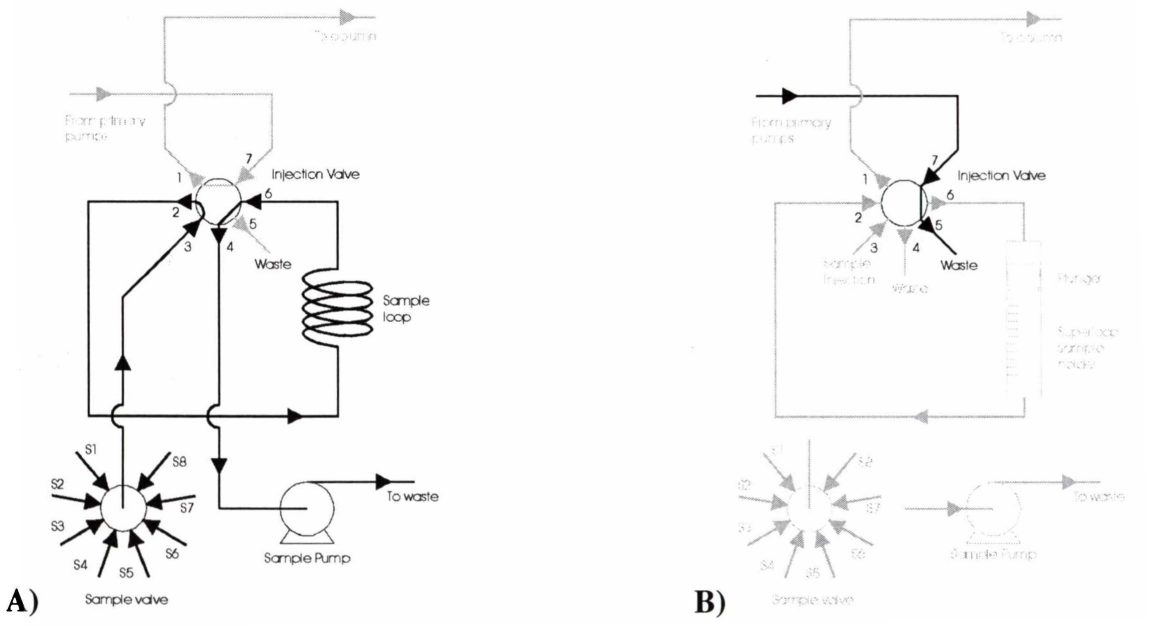

Figure 5-4. A) A sample pump can be used to draw solution from the sample valve through the sample loop when the injection valve is in loading position and then inject the sample into the column when the injection valve is in inject position for repeated automated runs using small volumes of different samples. B) The injection valve can be set to waste so all flow from pumps is discarded allowing flushing of the pumps.

5.5.2 AKTA characterisation

The gradient mixer influences the data collected for modelling. A step change in concentration generated by the primary pumps becomes a gradient change due to mixing in the gradient mixer. This can give the appearance of the column having greater dispersion. There is also a delay between introducing a step change in concentration and it being detected by the inline conductivity probe and UV adsorbance detector because of the residence time in the tubing and valves. The values for rates of desorption and adsorption, column capacity, and dispersion can be incorrect if the set-up of the AKTA is neglected in any modelling done.

Three experiments were done to investigate the impact of the AKTA setup on concentration profiles. The 1-ml column, which is used in later experiments, was removed from column position 3 of the AKTA and the female and male unions were joined. An equilibration buffer, a 1M NaCl solution in equilibration buffer and a 1.5 mg/ml BSA solution in equilibration buffer were prepared. The AKTA was programmed to mix different ratios of BSA solution and equilibration buffer to produce step concentration changes and the resulting solutions were passed through column position 3 (Appendix E.4). The trial was done at different flowrates and with NaCl solution to determine whether the concentration profile changed due to the different flowrates or solution. A similar experiment was performed using the superloop to produce a single step change in concentration (Appendix E.5). The superloop should give a rectangular step change in concentration because the solute is being applied directly rather than through the gradient mixer.

The resulting data was exported to an Excel spreadsheet and concentrations obtained from calibration data (Figures C-3 and C-6, conductivity results were corrected for equilibration buffer conductivity (1.5-1.7 mS/cm)). The AKTA performance was then simulated using a Matlab model, which treated the system as a series of small well mixed tanks to model the effects of the setup (Appendix H.1).

5.5.3 Small column breakthrough work

Breakthrough trials were performed on a 1-ml HiTrap DEAE sepharose FF axial flow column at different flowrates to validate the uptake models presented in Chapter 4. An equilibration buffer, a 1M NaCl solution in equilibration buffer and a 1.5 mg/ml BSA solution in equilibration buffer were prepared. The AKTA system was flushed and the inline UV spectrophotometer zeroed using equilibration buffer. The first primary pump on the AKTA was used for the equilibration buffer and the second for the protein solution. Protein solution was passed through the UV spectrophotometer to determine the maximum adsorption. The lines were then flushed again with equilibration buffer. The column was equilibrated with 5 ml equilibration buffer, loaded with 120 ml protein solution, and then washed with 5 ml equilibration buffer. The protein was eluted using 10 ml elution buffer and the column was then re-equilibrated with 5 ml equilibration buffer (AKTA program given in Appendix E.6). Data was exported to an Excel spreadsheet and UV absorbance readings converted to protein concentration using calibration data from Figure C-3. Breakthrough times were performed for five flowrates (Table 5-1).

The axial flow models presented in Section 4.4.2 were fitted to experimental data and rate and dispersion factors calculated. The column was simulated using the Matlab model in Appendix H.2 and H.3.

Table 5-1. Flowrates used for breakthrough work on the 1-ml HiTrap DEAE Sepharose FF column and equivalent flowrates and velocities for the CRFC. Linear velocities were calculated using a void fraction of 0.31.

Axial Flow, 1-ml HiTrap DEAE Sepharose FF column, OD 0.7cm, L 2.5cm		CRFC, OD 14.6cm, ID 8.3cm, L 2cm		
Flowrate (ml/min)	Linear Velocity (cm/min)	Flowrate (ml/min)	Outer LV (cm/min)	Inner LV (cm/min)
0.10	0.87	18.20	0.67	1.16
0.20	1.73	36.39	1.32	2.32
0.30	2.60	54.59	1.99	3.49
0.50	4.33	90.98	3.31	5.81
1.00	8.67	181.97	6.61	11.63

5.5.4 Desorption experiments

Experiments were performed on a 1-ml HiTrap DEAE sepharose FF column to determine the impact of NaCl concentration in the elution buffer on desorption kinetics of BSA. The pre-equilibrated column was loaded with 50 ml of 1.5 mg/ml BSA in equilibration buffer at 0.5 ml/min. The column was washed with 10 ml equilibration buffer, and then protein eluted at 0.2 ml/min (to give a similar interstitial velocity through the column to that in the CRFC annulus) at a set dilution of a stock elution buffer consisting of 1M NaCl in equilibration buffer, and the remainder finally eluted with 10 ml of undiluted stock elution buffer. The two primary pumps on the AKTA were used to mix the elution buffer and equilibration buffer at different ratios (AKTA program given in Appendix E.7). The experiment was repeated for nine different dilutions of elution buffer.

In this trial three different solutions were passed through the column. This experiment needed to be uninterrupted so elution data would not be affected by protein diffusing from or adsorbing to the resin when the run was paused to change solutions in one of the two primary pumps on the AKTA. Therefore, protein solution was pre-loaded into a superloop attached to the injection valve. Normally the superloop is loaded manually, but as the experiments were run over several days, the AKTA was configured to load the superloop automatically. One of the primary pumps was used to load the superloop because the sample pump did not exert sufficient pressure to move the plunger. The superloop was loaded by connecting the injection port of the injection valve to position 3 of the column valve (Figure 5-5).

Conductivity and absorbance at 280 nm for each run was recorded and exported to an Excel spreadsheet for analysis. Concentrations were calculated using calibration data from Figures C-4 and C-7. The model developed in Section 4.4.2 was fitted to elution data to determine rates of desorption. Matlab programs in Appendix H.4 and H.5 were used for simulations.

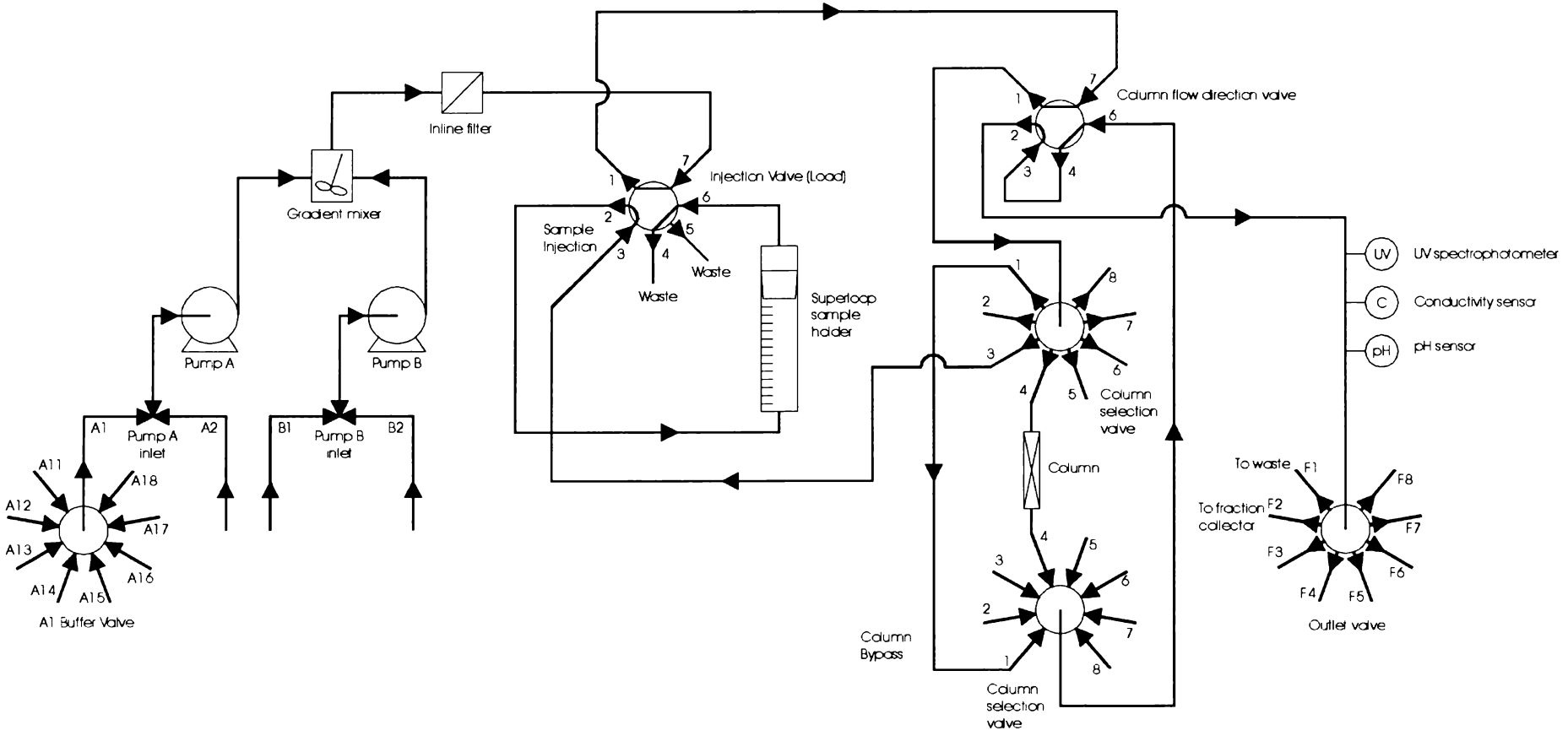

Figure 5-5. Setup of Akta for loading the superloop using one of the primary pumps. The sample valve and sample pump is not shown.

5.6 Batch CRFC trials

The AKTAexplorer100 was used to pump various solutions through the CRFC during batch operation and monitor effluent concentrations (Figure 5-6). A flow manifold split the solution into eight streams which entered the CRFC outer feed chamber inlets (Figure 5-7) and passed through the packed bed. The eight streams were then recombined in an exit manifold.

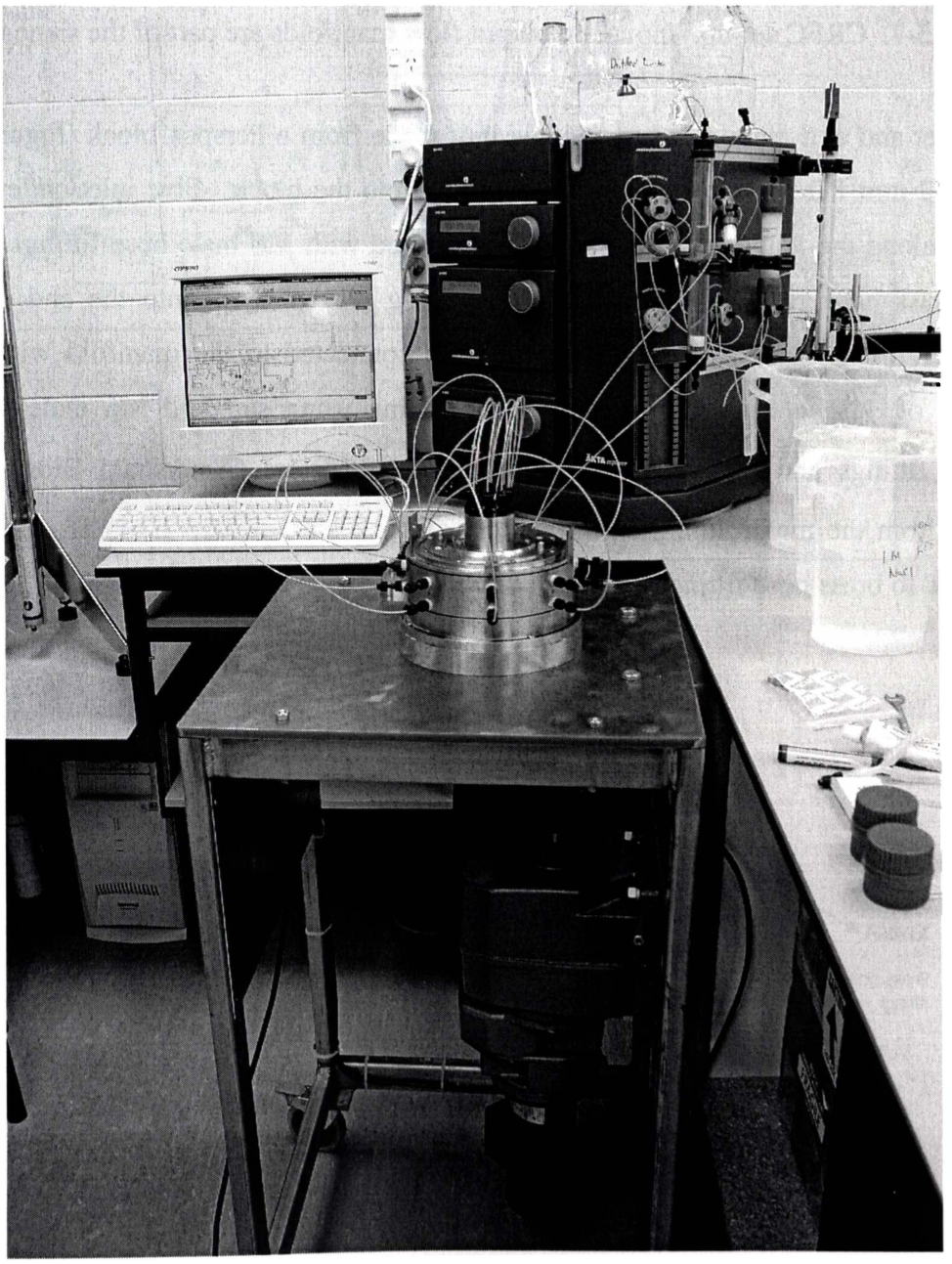

Figure 5-6. CRFC connected to AKTAexplorer100.

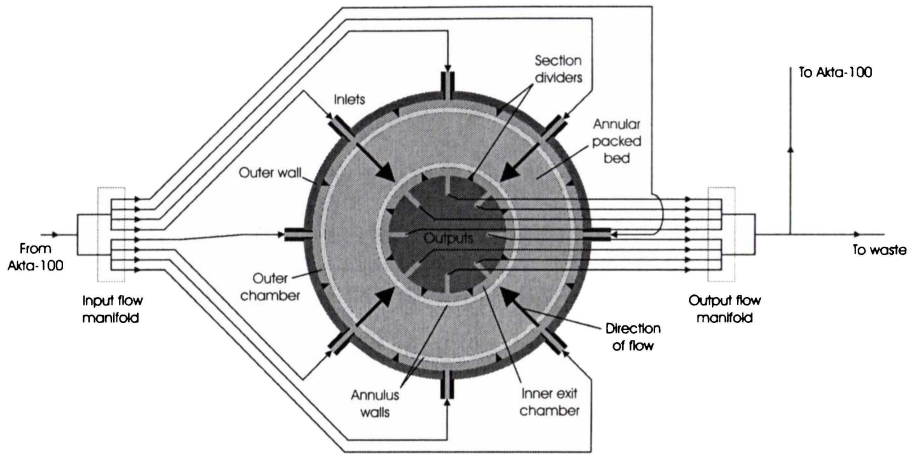

Figure 5-7. CRFC set-up. Input and output flow manifolds are part of the same unit.

The inlet and exit manifolds are a single unit made from a Perspex block (Figure 5-8). Eight 12-mm I.D., 9-ml chambers were drilled into the block. Five inlet/outlets were drilled along the length of each chamber and fitted with M6 male hose fittings. A ¼-inch brass hose fitting or ½-inch SP brass plug was screwed into the end of each chamber. The CRFC inlets and outlets were connected to the manifold with equal lengths of $\frac{1}{16}$-inch O.D., 1 mm I.D. peek tubing using standard M6 male-$\frac{1}{16}$-inch female fittings and $\frac{1}{16}$-inch 'fingertight' hose connectors (Amersham Biosciences). Waste from the manifold exited through Swagelock LT-3-5 3/16 ID, 5/16 OD tubing attached to brass hose fittings.

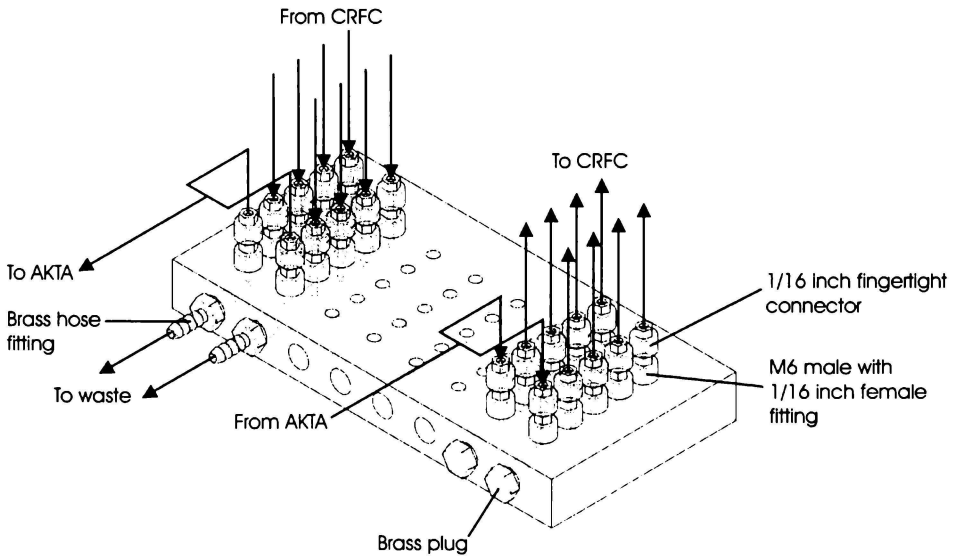

Figure 5-8. Set-up of CRFC flow manifold.

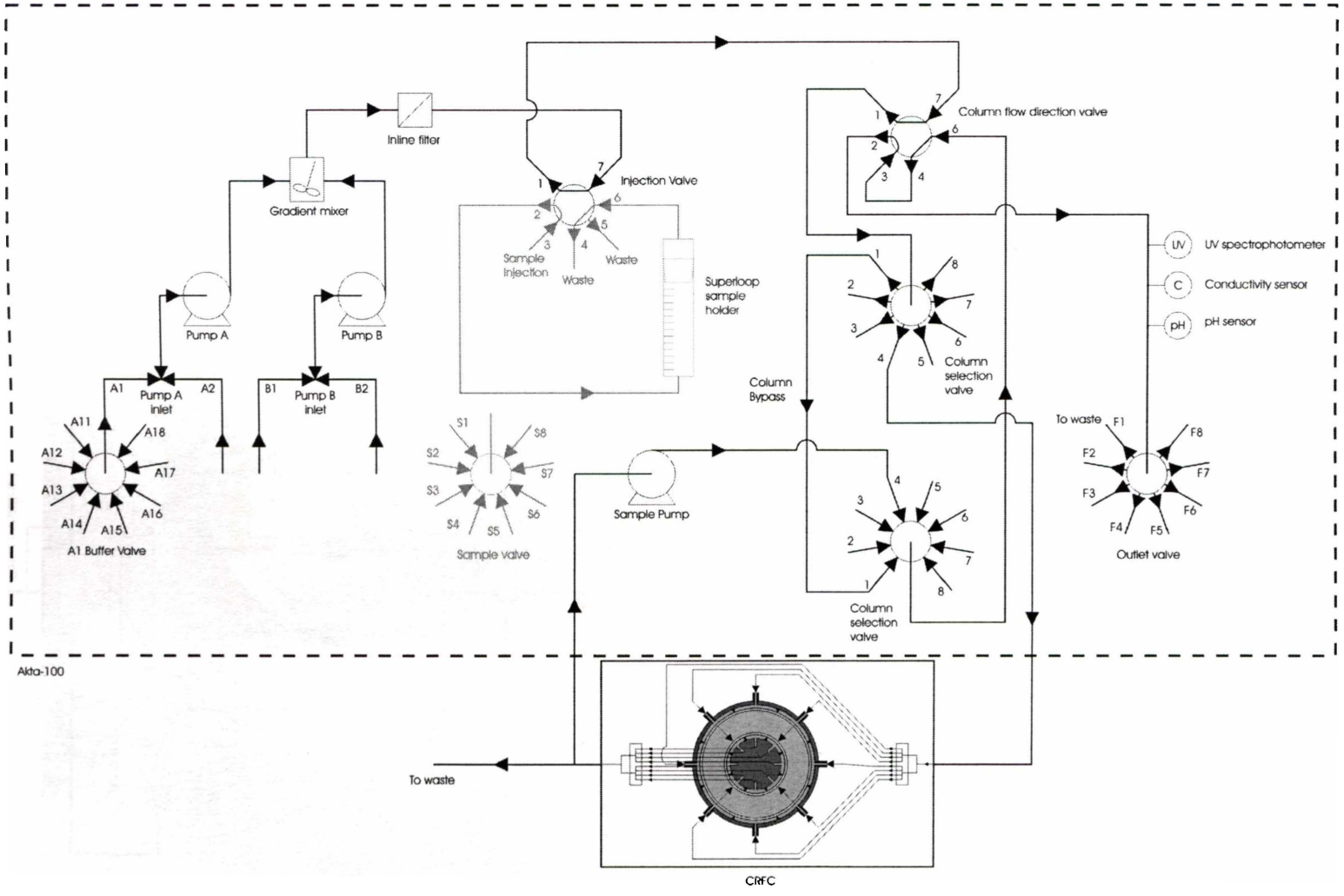

Figure 5-9. CRFC connected to the AKTAexplorer100.

The manifold was initially set so all flow from the CRFC went through the AKTA. However, the backpressure generated by the tubing connecting the AKTA to the manifold, the plumbing inside the Akta and fouling in the CRFC packed bed, caused the welds joining the porous cylinders to the top and bottom of the annulus to fail. Therefore, the flow was split. The sample pump on the AKTA was used to draw solution from the CRFC manifold exit stream at 5 ml/min, and pump it through the AKTA. The remainder of the effluent went to waste (Figures 5-7 and 5-9). The CRFC back-pressure was monitored using a Wika pressure gauge (0-1000 kPa) connected to an air purge fitting on the outer chamber.

5.6.1 CRFC packing

The CRFC was set up for pump-packing using a closed circuit (Figure 5-10). A Cole-Palmer Pro-Spense pump circulated at 50 ml/min a 1M NaCl packing solution into the CRFC through packing ports and through the flow manifold to a 3-L stirred tank at 50 ml/min. Swagelock LT-3-5 3/16 ID, 5/16 OD tubing connected the manifold, the stirred tank, pump and packing ports. A Wika pressure gauge (0-1000 kPa) was used to monitor pressure.

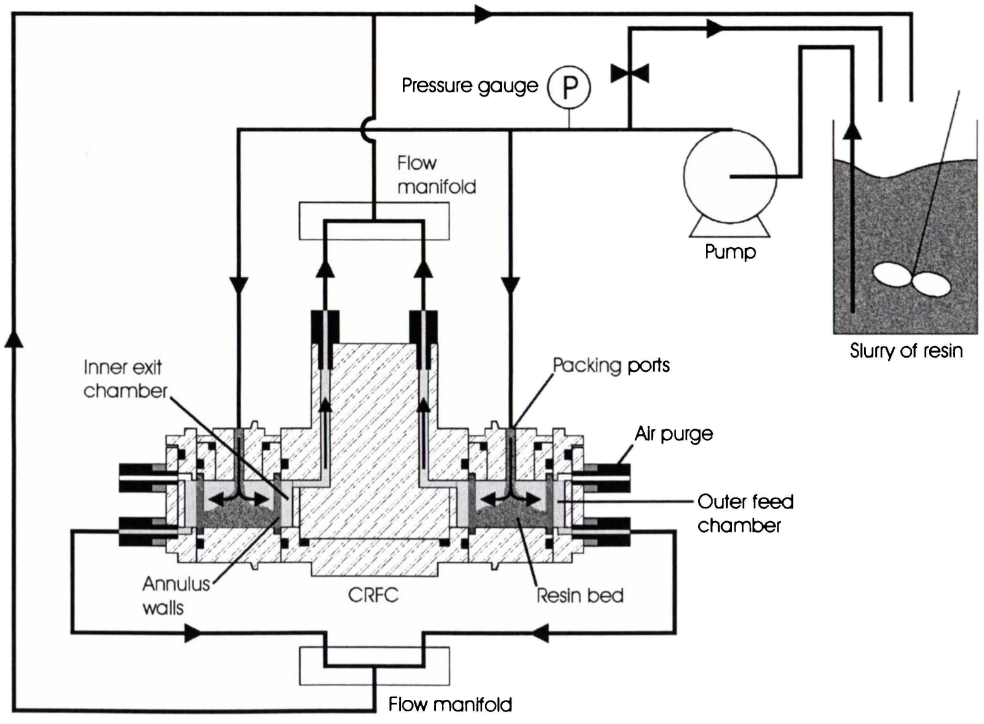

Figure 5-10. Set-up for packing the CRFC annulus.

Air was vented from the outer feed chamber through air purge fittings and removed from the annulus by reversing pump flow.

The flow was stopped and 500 ml of fresh or cleaned resin that had been decanted and rinsed with distilled water was added to the stirred tank and equilibrated with the packing solution for 15 minutes. The slurry was then pumped into the annulus and retained by the porous walls. As the annulus filled, the pressure gradually increased and flowrate from the pump dropped. Packing was stopped once the annulus was completely packed, indicated by a rapid increase in pressure (packing was stopped at about 345 kPa) and resin filling the tubes connected to the packing ports.

Tubes from the flow manifold to the tank were clamped, hose fittings for the annulus packing ports removed and the packing ports sealed with grub screws. The CRFC was then connected to the AKTA (Figure 5-9) and packing solution flushed out using distilled water. Bed integrity was then checked as described in Section 5.6.3.

The CRFC was unpacked by removing the annulus top (Figure 5-11) and scooping out the resin with a spatula. The resin was cleaned using the method given in Appendix F.

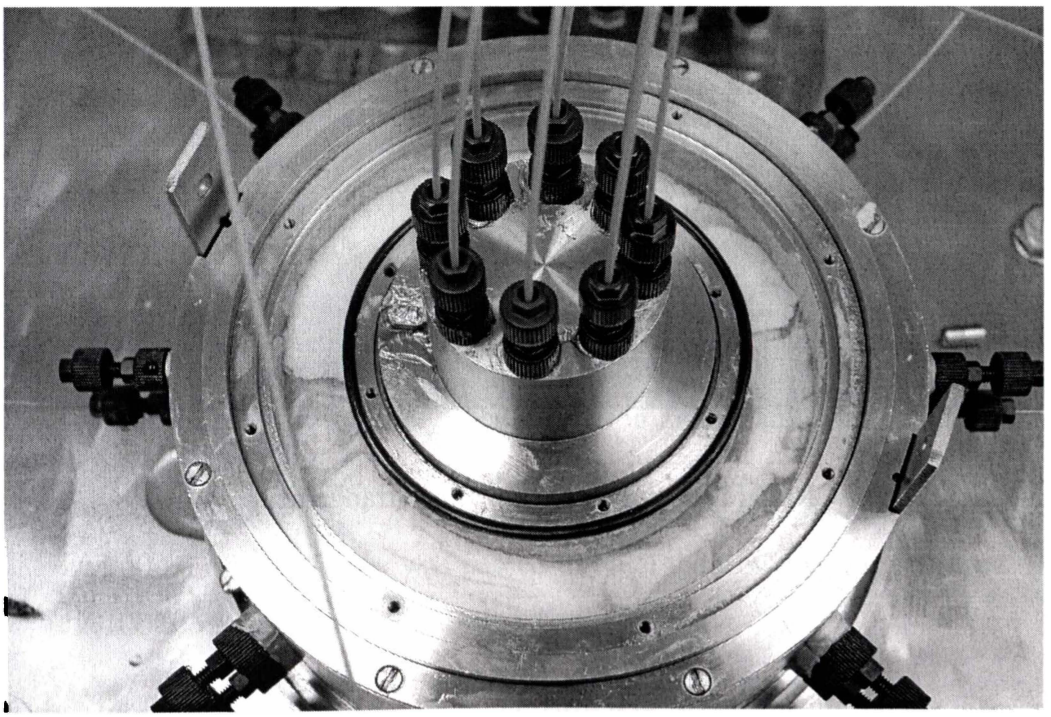

Figure 5-11. CRFC with bed exposed.

5.6.2 Set-up of flow manifold

Several different flow arrangements could be used for the flow manifold, depending on the position of the feed inlets and exits for each chamber. The effect of the manifold flow arrangement on peak shape was examined using a column bypass, which enabling the inlet chambers to be coupled directly to the outlet chambers of the flow manifold, and by passing a salt pulse through the system for three different flow arrangements (Figure 5-12 and 5-13).

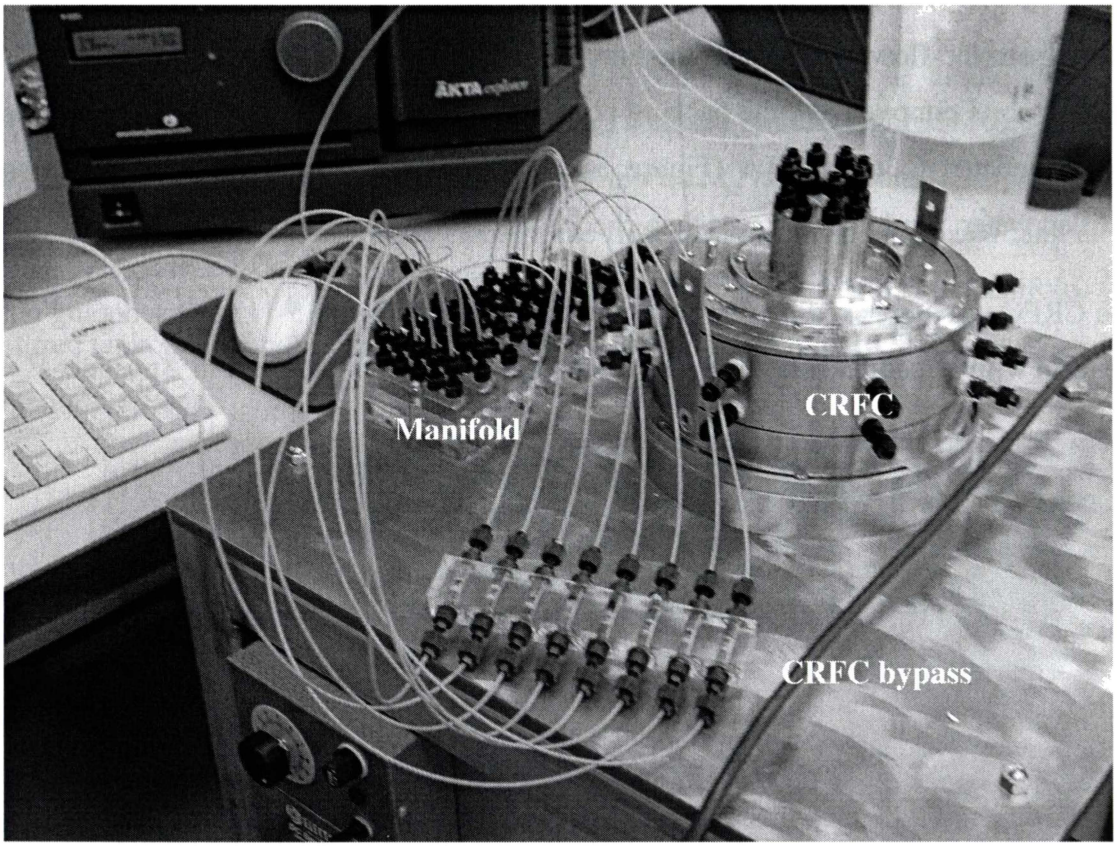

Figure 5-12. Set up of CRFC for testing impact of flow arrangement.

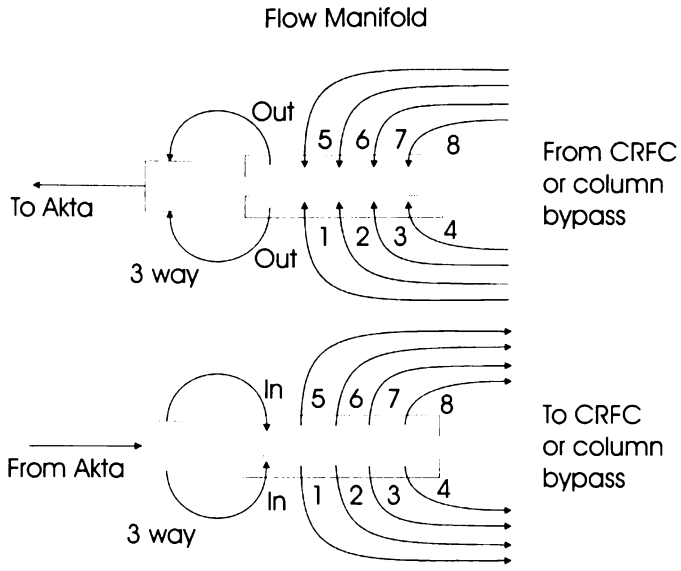

Figure 5-13. Set up of flow manifold for CRFC.

Distilled water and 40 mg/ml NaCl in distilled water were used for the trials

Experimental steps for each run included (See Appendix E.8 for AKTA program)

- Akta lines cleared with 100 ml distilled water.
- 50-ml aliquots of 20%, 40%, 60%, 80% dilutions of NaCl solution were passed through the conductivity detector. The two primary pumps on the AKTA were used to mix the NaCl solution and distilled water at different ratios. This was followed by 110 ml 100% NaCl solution and 90 ml distilled water. Flow was then switched to the CRFC input manifold.
- 200 ml distilled water was passed through the flow bypass, followed by 300 ml 100% NaCl solution and 800 ml distilled water.

This procedure was repeated for three different arrangements of the flow manifold (Figure 5-14).

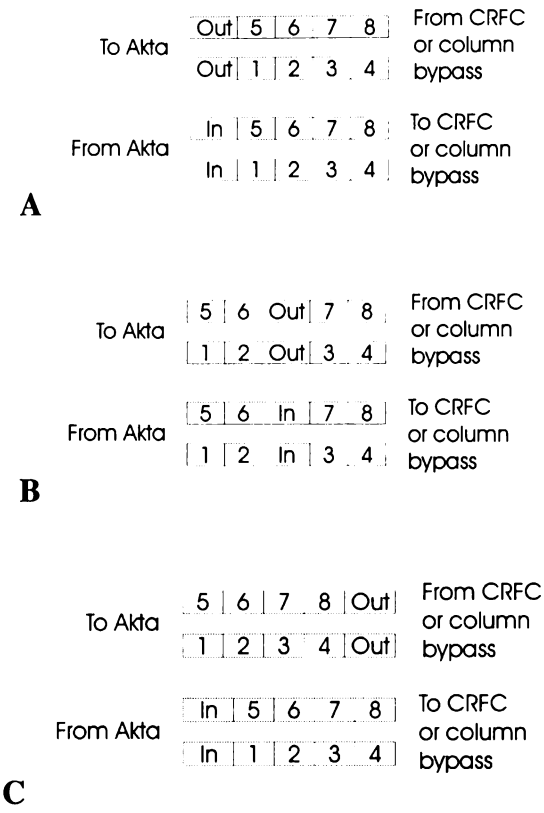

Figure 5-14. Manifold flow arrangement. "In" is the input from the Akta, "out" is the output to the Akta for analysis. Numbers 1-8 represent the hoses, with 1 connected to 1 and so on.

Calibration data in Figure C-7 was used obtain concentrations from conductivity data. The manifold inlet and exit chambers were modelled as well-mixed tanks, and experimental data used to validate modelling the chambers as single tanks (Appendix H.6).

5.6.3 Bed integrity

CRFC bed integrity was tested before a series of experiments and after packing by passing a salt slug through the annulus. Conductivity of the effluent stream was monitored and the resulting peak was examined for evidence that solution was bypassing the bed. A shoulder on the leading edge of the peak indicated fluid bypassing. Bed integrity was tested using the same method given in Section 5.4.2 except that flow went through the annular bed instead of the column bypass (See Appendix E.8 for AKTA program).

5.6.4 Breakthrough and elution

A series of breakthrough and elution experiments were performed on the CRFC to generate data for fitting the fixed bed CRFC model to.

Five solutions were prepared for each run:

- Equilibration buffer: 6 L 0.02M TrisHCl in distilled water, pH 7
- Loading solution: 9 L BSA at different concentrations in 0.02M TrisHCl buffer, pH 7
- Elution buffer: 5 L 1M NaCl in 0.02M TrisHCl buffer, pH 7
- Regeneration: 2 L 0.5M NaOH in distilled water
- Storage solution: 2 L 20% ethanol in distilled water
- 2 L distilled water

The following are the steps for each run (See Appendix E.9 for AKTA program).

1. Lines were cleared with 150 ml equilibration buffer, after which the UV spectrophotometer was zeroed.
2. 200 ml of loading solution was passed through the UV spectrophotometer to obtain an adsorbence of the loading solution.
3. Lines were cleared with 200 ml equilibration buffer and then flow was directed to the CRFC.
4. The CRFC was equilibrated with 800 ml equilibration buffer.
5. 8 L loading solution was passed through the CRFC.
6. Unbound protein was removed with 4 L equilibration buffer.
7. Bound protein was eluted with 4 L elution buffer.
8. The resin was regenerated with 1 L NaOH solution.

9. The resin was rinsed with 1.5 L distilled water and 1.5 L 20% ethanol solution.

The conductivity and absorbance at 280nm of the effluent stream was measured. Data obtained was converted to concentration using calibration data (Figures C.4 and C.7).

This procedure was repeated for three flowrates (20, 45 and 80 ml/min at 4.5 mg/ml loading concentration) and three loading concentrations (2, 4.5 and 9 mg/ml at 45 ml/min).

Bed integrity was tested after each run (see Section 5.6.3). If channelling had occurred, the CRFC was repacked (see Section 5.6.1), bed integrity was rechecked and the experiment repeated. When pressure drops were high due to fouling, the CRFC was unpacked and the resin cleaned (Appendix F).

Because large quantities of BSA were needed for the trials, it was recycled (see Appendix G).

The fixed bed CRFC model (Section 4.4.3) was fitted to experimental data and comparisons made. The Matlab program used to run simulations is given in Appendix H.9.

5.7 Continuous adsorption and elution of BSA

Trials were done to investigate the effect of changing divider angle and changing rotation speed on BSA elution profile with angular position around the annulus of the CRFC.

The annulus was packed with fresh Amersham Biosciences Sepharose Fast Flow DEAE ion exchange resin for these trials (Section 5.6.1) and tested for bed integrity (Section 5.6.3).

Five solutions were prepared for each run:

- Equilibration buffer: 10 L 0.02M TrisHCl in distilled water, pH 7
- Feed solution: 2 L BSA at 1.5 mg/ml in 0.02M TrisHCl buffer, pH 7
- Elution buffer: 4 L 1M NaCl in 0.02M TrisHCl buffer, pH 7

- Regeneration solution: 2 L 0.5 and 1M NaOH in distilled water

The CRFC was configured for batch operation before each trial. All inputs on the CRFC were connected to the input flow manifold, which was attached to the AKTAexplorer100. The ouput tubing of the CRFC was disconnected from the flow manifold and directed to a 5 L container. The flow from each CRFC exit stream was restricted using equal lengths of 0.02 mm ID tubing to produce sufficient back-pressure so flowrates from each tube were similar. Back-pressure developed by the tubing was approximately 165 kPa. The CRFC was equilibrated with two litres of equilibration buffer at 40 ml/min.

The CRFC was then configured for continuous operation. The input for section 1 of the CRFC was connected to an Amersham Pharmacia P-6000 syringe pump, which was used to supply feed solution at 5 ml/min. The input for section 5 of the CRFC was attached to an Amersham Pharmacia P-500 syringe pump which was used to supply the elution buffer at 5 ml/min. The remaining six inputs remained connected to the flow manifold which supplied equilibration buffer, using the AKTAexplorer100, at a total flowrate of 30 ml/min. These six inputs provided wash zones between the feed and elution zones (Figure 5-15).

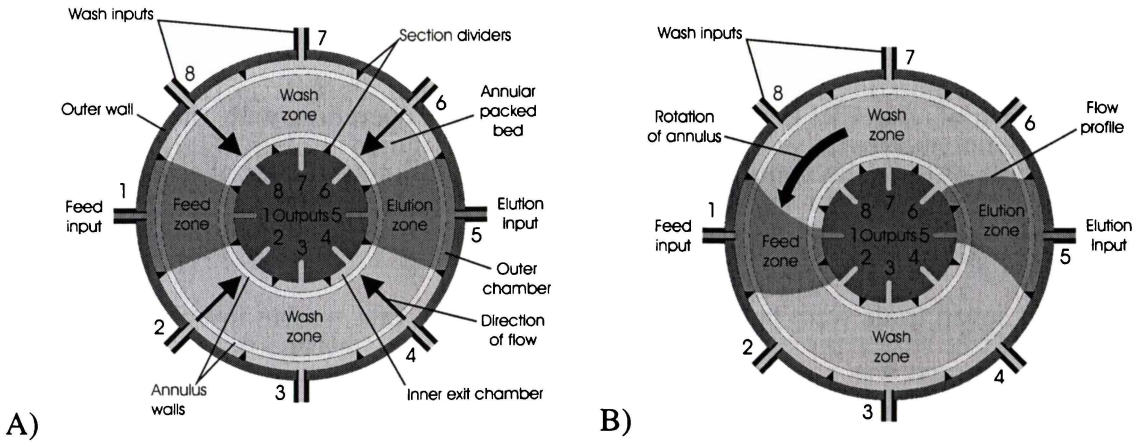

Figure 5-15. Cross section of the CRFC with three solutions: feed, wash (equilibration) and elution buffers being applied simultaneously at a total flowrate of 40 ml/min. A) The flow paths through the CRFC when the annulus is stationary. B) The expected flow profiles when the annulus is rotating at 48 min/rev.

The annulus was set rotating and the feed solution, elution and equilibration buffer applied simultaneously to the CRFC. BSA was loaded onto fresh resin as it rotated past section 1, unbound BSA was removed in sections 2-4, the bound BSA eluted in section 5, and the elution buffer removed and resin re-equilibrated in sections 6-8 (Figure 5-15). Flowrates into the CRFC for each solution are given in Table 5-2.

Table 5-2. Flowrates into the CRFC.

Solution	Supply pumps	Flow (ml/min)
Equilibration	AKTA	30.00
Elution	P-500	4.96
Feed	P-6000	4.97

The CRFC was operated for three hours to allow it to reach steady state. The outflows from each exit section were then collected individually in 1-L Shott bottles for three hours. At the end of each trial, the solution in each bottle was well mixed to ensure consistency and measured for protein and NaCl concentration. Data was converted to concentrations using calibration data (Figures C-1 and C-8). Flow into each bottle was checked by measuring the volume of solution in a 1-L measuring cylinder and dividing by the time over which solution was collected. Mass and volume balances were then calculated.

After each trial, the CRFC was configured for batch operation with the AKTA and protein remaining in the annulus eluted with 1.8 L of elution buffer, the resin cleaned with 1.5 L regeneration solution, and the CRFC flushed with 4 L of distilled water.

A total of seven trials were performed (Table 5-3). The first was an initial six hour run where the effluent was collected from each output stream for the last three hours. The second run was a twelve hour run where the effluent from each stream was collected in three hour batches after the first three hours to observe if the system reached steady state. When it was noted mass balances were not closing within 10%, the remaining five runs were six hour runs where all the effluent was collected, including the effluent from cleaning, and concentrations and volumes measured for mass balance purposes.

The CRFC was operated at different divder angles and rotation speeds to observe the effect of these factors on effluent concentrations. The outer dividers were set to 0, 15

and 30 degrees anticlockwise relative to the inner dividers, and rotation speeds were approximately 12.5, 31 and 48 minutes per revolution.

An extra trial was done between the third and forth trials, which involved separating two proteins (See Section 5.8).

Table 5-3. Conditions for continuous adsorption and elution trials

Run	Rotation Speed (min/rev)	Divider angle (degrees)	Outlet sample collection time (hr)	Effluent collected
1	48	0	3	Sample only
2	48	0	12	Sample only
3	48	0	3	All
4	48	15	3	All
5	48	30	3	All
6	12.5	0	3	All
7	31	0	3	All

The cleaning regime was changed after the third run because the CRFC operating pressure increased from 165 kPa for the first run up to 345 kPa for the fourth run. This indicated that the cleaning regime was not adequate and the column was fouling. The regeneration buffer strength was increased to 1M NaOH and the solution left in the column overnight before being flushed. The pressure was closely monitored during runs thereafter. Operating pressures dropped back to 165 kPa after the regime was changed.

The continuous experiments were simulated using the model presented in Section 4.5.1 and Matlab program in Appendix H.10. Comparisons of model data to experimental data were made.

5.8 Continuous separation of BSA and lactoferrin

One trial was done where a two-component feed of 0.53 mg/ml bovine lactoferrin and 1.6 mg/ml BSA was continually separated using the same methodology as for adsorption and elution of BSA. The annulus was rotated at 49 min/rev and the outer

dividers were set at 0 degrees relative to the inner dividers. The CRFC was operated continuously for 3 hours, after which sample from each effluent stream was collected individually for a further 3 hours. All effluent was collected.

Effluent was analysed for total protein absorbance at 280nm, lactoferrin activity using Surface Plasmon Resonance (SPR) (Indyk and Filonzi 2004), and conductivity. 5 ml samples were taken from the effluent for analysis using SPR. These were diluted by mixing 0.5 μL of sample in 500 μL of analyte solution (HBS-EP buffer, Biacore Uppsala, Sweden). 100 μL of each were analyzed using SPR, the remainder stored with the rest of the samples at -10 degrees C. Lactoferrin activity was compared to calibration data to determine concentration (Figure C-6).

A calibration curve of UV absorbance against lactoferrin concentration was prepared (Figure C-2). Once concentration of lactoferrin in the samples collected had been obtained, the concentration was converted to absorbance using the calibration curve and the absorbance of lactoferrin subtracted from the total absorbance of the solution to obtain the absorbance for BSA. The concentration of BSA was calculated from calibration data (Figure C-1). Mass and volume balances were then performed.

The continuous experiments were simulated using the model presented in Section 4.5.1 and Matlab program in Appendix H.10. Comparisons of model data to experimental data were made.

Chapter 6

Results and Discussion

6.1 Introduction

Experimental work to obtain parameters for and verify NP-MLF and FD-MLF finite difference models developed in Chapter 4 are presented in this chapter. Model modifications are discussed and one model is chosen to simulate batch and continuous separations. Results are discussed in terms of goodness of fit, parameters obtained, and simulation and CRFC performance.

6.2 Batch adsorption experiments

6.2.1 Adsorption isotherm results

Experimental data and predictions using the multicomponent Langmuir-Freundlich isotherm (MLF) (equation 77, Section 4.2.4.1) agreed well (Figure 6-1). Curve fitting showed DEAE sepharose FF has a C_{RAmax} of 110 mg/ml in the absence of salt, which is the same as the manufacturer's stated capacity for human serum albumin (Amersham Biosciences, Uppsala, Sweden). Small concentrations of NaCl reduced equilibrium capacity.

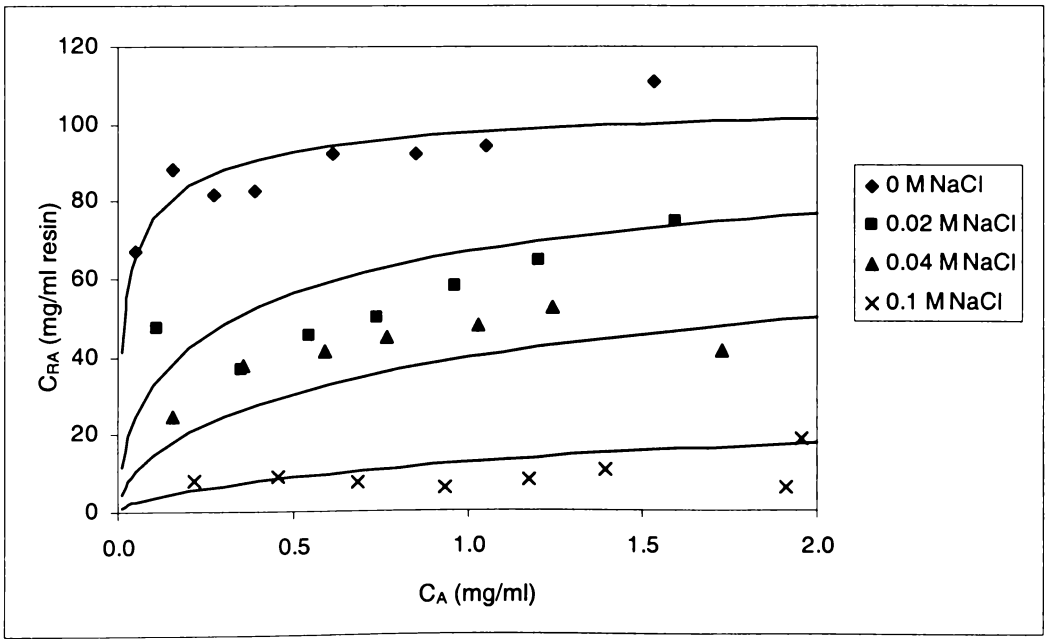

Figure 6-1. Effect of NaCl concentration on BSA adsorption on DEAE Sepharose Fast Flow resin. Model parameters are C_{RAmax} = 110 mg/ml, K_A = 8 ml/mg.s, K_B = 3.2 ml/mg.s, n_B = 0.6, and n_A = 1.78.

Other researchers reported binding capacities of about 85 mg/ml at pH 8.1-8.5 (James and Do 1991; Liu *et al.* 2001). Because model parameters from James and Do (1991) (Table I.1-1) were not directly comparable to those in current work, the MLF model was fitted to their experimental data (Table 6.1, Figures I.1-1 and I.1-2). MLF parameters calculated from their data were the same as those from current work except for n_B and n_A at pH 9.1 and C_{RAmax}. Differences in C_{RAmax} may be due to different times allowed for equilibrium.

Breakthrough simulations showed MLF caused finite difference solution instability at n_A>1 and low protein concentrations (Section 6.3.2.1). This instability was resolved by setting n_A=1, reducing MLF to ML. Therefore isotherm parameters were recalculated for n_A=1 (column 4, Table 6-1).

Table 6-1. BSA adsorption isotherm parameters.

Adsorption Parameters	Model			
	MLF			ML
	From current work, pH 7	James and Do (1991) pH 8.1	James and Do (1991) pH 9.1	From current work, pH 7
C_{RAmax} (mg/ml resin)	110	84	120	94
K_A (ml/mg.s)	8	8	8	47
K_B (ml/mg.s)	3	3.2	3.2	15
n_B	0.6	0.6	0.8	0.6
n_A	1.78	1.78	16	1

6.2.2 Batch kinetics

Excellent agreement was found between the NP-MLF and FD-MLF batch kinetic finite difference models (Section 4.4.1) and batch kinetic experimental data (Figure 6-2).

6.2.2.1 NP-MLF model

The NP-MLF model fits experimental data well with R^2 = 0.98 using parameters from isotherm experiments (Table 6-2); only C_{RAmax} needed adjusting for a good fit. When n_A = 1, k_{A1} increased with decreasing concentration (Figure 6-3), possibly because BSA diffusivity increased as solution viscosity decreased. A fixed k_{A1} and n_A = 1.78 gave

good agreement, but finite difference instability occurred for $n_A > 1$ in breakthrough simulations (Section 6.3.2.1) and could not be used.

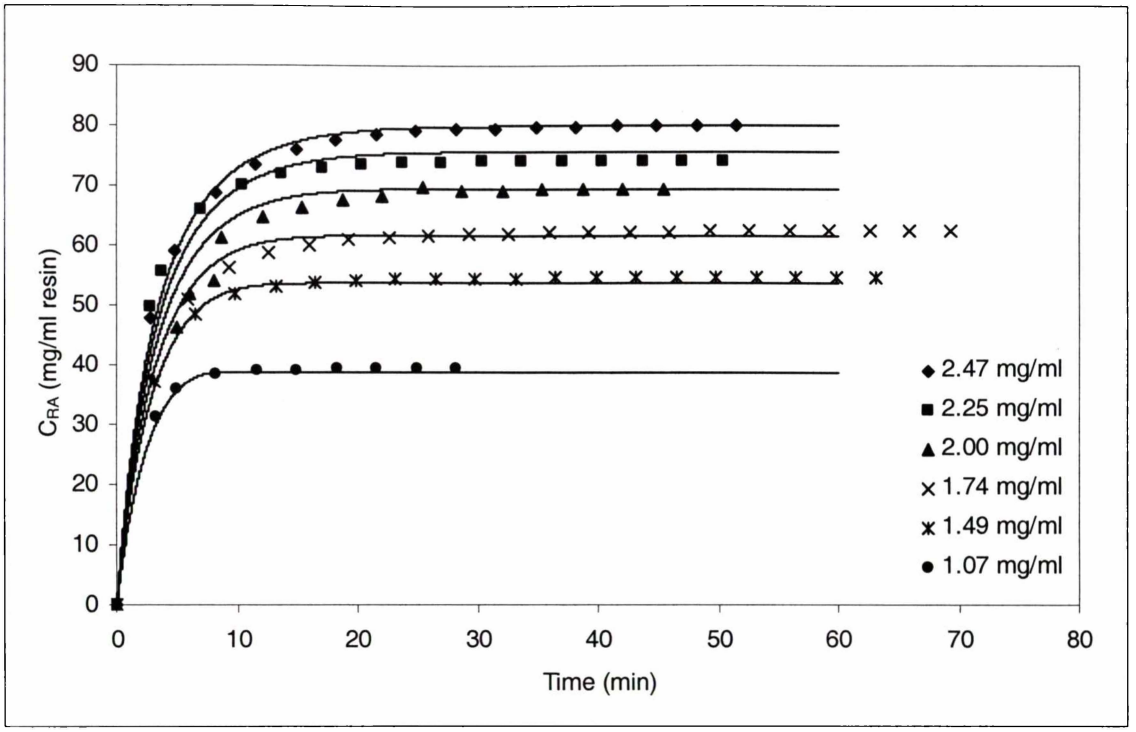

Figure 6-2. Effect of BSA concentration in uptake kinetics and comparison of NP-MLF and FD-MLF model results. Solid lines are from the models (NP-MLF parameters are in Tables 6-2 and I.2-1, and FD-MLF parameters in Tables 6-3 and I.2-2).

Table 6-2. Fixed NP-MLF model parameters for data in Figure 6-2. R^2 values are regression coefficients indicating goodness of fit. Overall void fraction is the ratio of solution volume to resin volume.

Parameter	$n_A=1$	$n_A=1.78$
Void fraction ε_o	0.973	0.973
C_{RAmax} (mg/ml resin)	86	100
K_A (ml/mg)	47	8
k_{A1} (ml/mg.s)	8.20E-05	7.20E-05
R^2	0.98	0.98

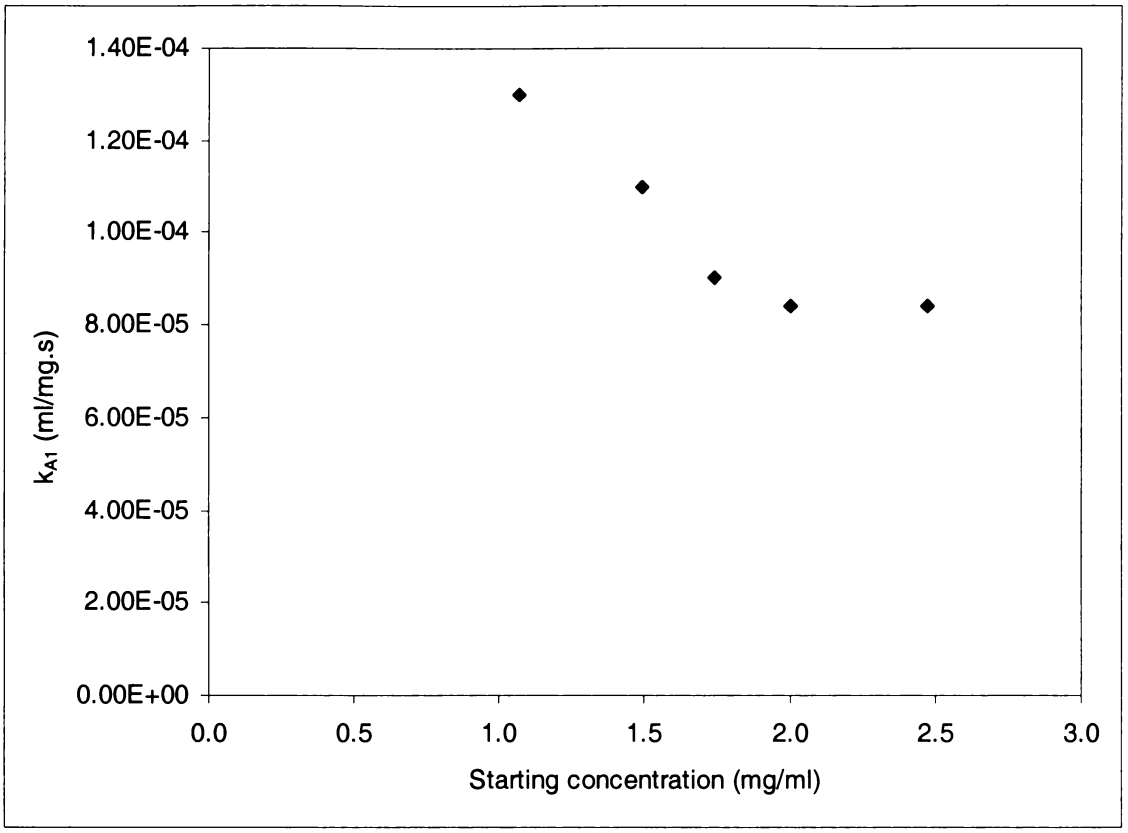

Figure 6-3. Effect of initial feed concentrations on k_{A1} at n_A=1.

6.2.2.2 FD-MLF model comparison

The FD-MLF model was fitted to kinetic data by fixing k_{A1} and varying k_{fA}, the film diffusion coefficient, for different starting concentrations (fixed parameters shown in Table 6-3). k_{fA} decreased with increasing starting concentration (Figure 6-4), possibly due to BSA diffusivity decreasing as viscosity increased.

Table 6-3. Fixed parameters used in FD-MLF model.

Parameter	Value
Overall void fraction ε_o	0.97
Resin pore fraction ε_p	0.72
Resin radius R_p (μm)	45
C_{RAmax} (mg/ml resin)	86
K_A (ml/mg)	47
k_{A1} (ml/mg.s)	8.50E-03
n_A	1

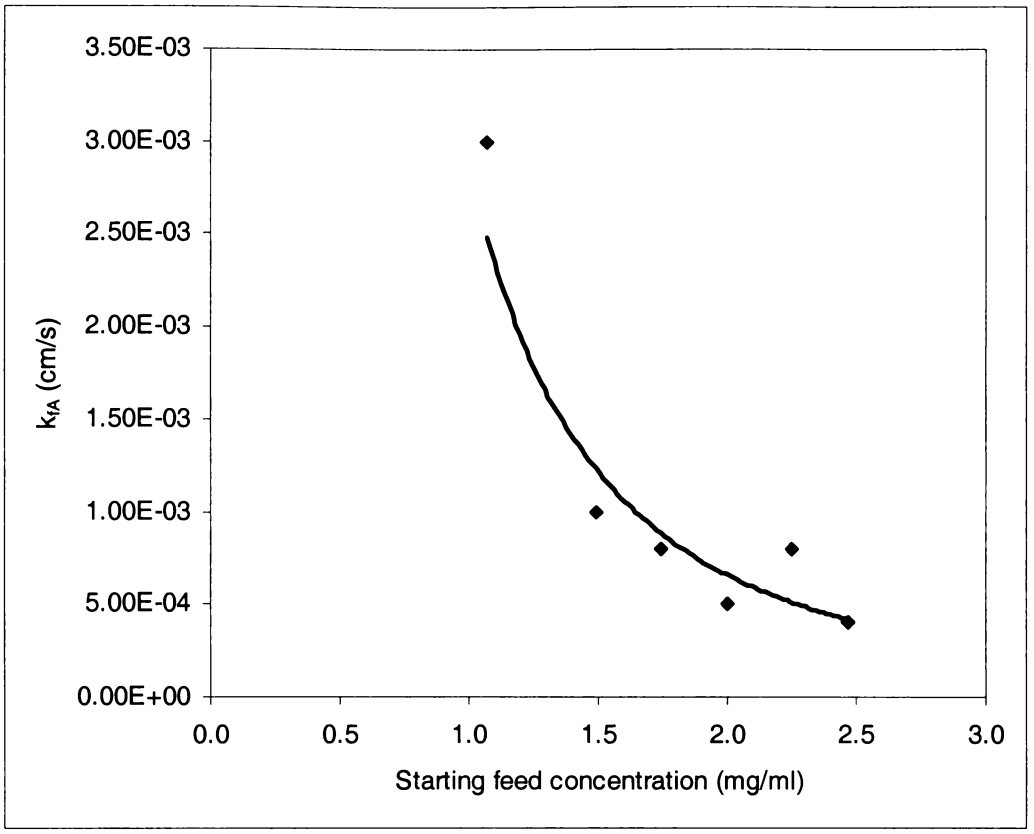

Figure 6-4. Effect of different starting feed concentration on k_{fA} .

6.3 Small column experiments

6.3.1 Extra-column dispersion

The extra–column dispersive effects for small column breakthrough and elution studies were investigated by passing salt pulses (using a superloop) through the AKTAexplorer100. Band spreading due to dispersion within the valves, connectors and tubing was simulated using a series of well-mixed tanks. The superloop was assumed to give a step input and a volume delay accounted for system residence time. A good fit was achieved with five 0.13-ml tanks in series and a volume delay of 1.33 ml solution applied (Figure 6-5).

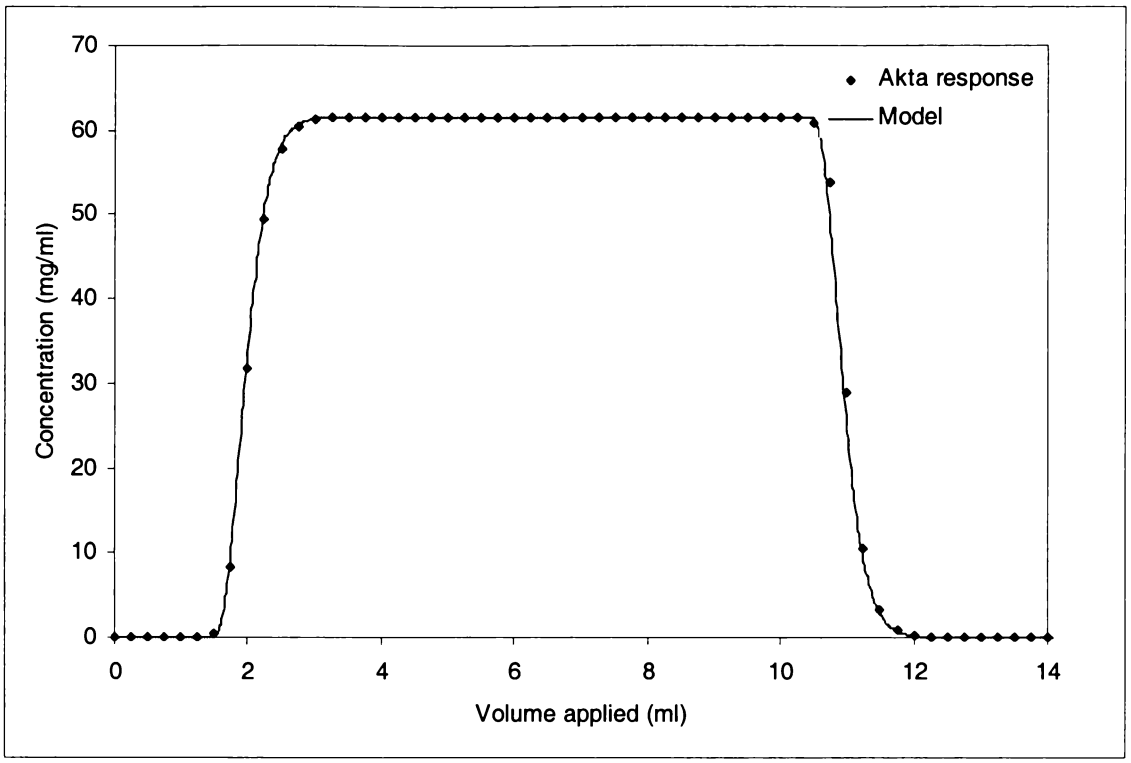

Figure 6-5. Concentration profile from the AKTAexplorer100 using step NaCl injection from the superloop at 1 ml/min.

The model was then modified to simulate sequential step inputs from the AKTA's primary pumps by including an additional 2.2-ml tank to represent the gradient mixer (compared with the actual mixer volume of 2 ml). The volume delay was increased to 2 ml to account for the longer path length. BSA (Figure 6-6) and NaCl (Figure I.3-1) gave similar profiles. This model was incorporated into the batch axial flow finite difference solution. The gradient mixer was included as a tank before the column while dispersion occurring after the superloop was approximated as five tanks after the column.

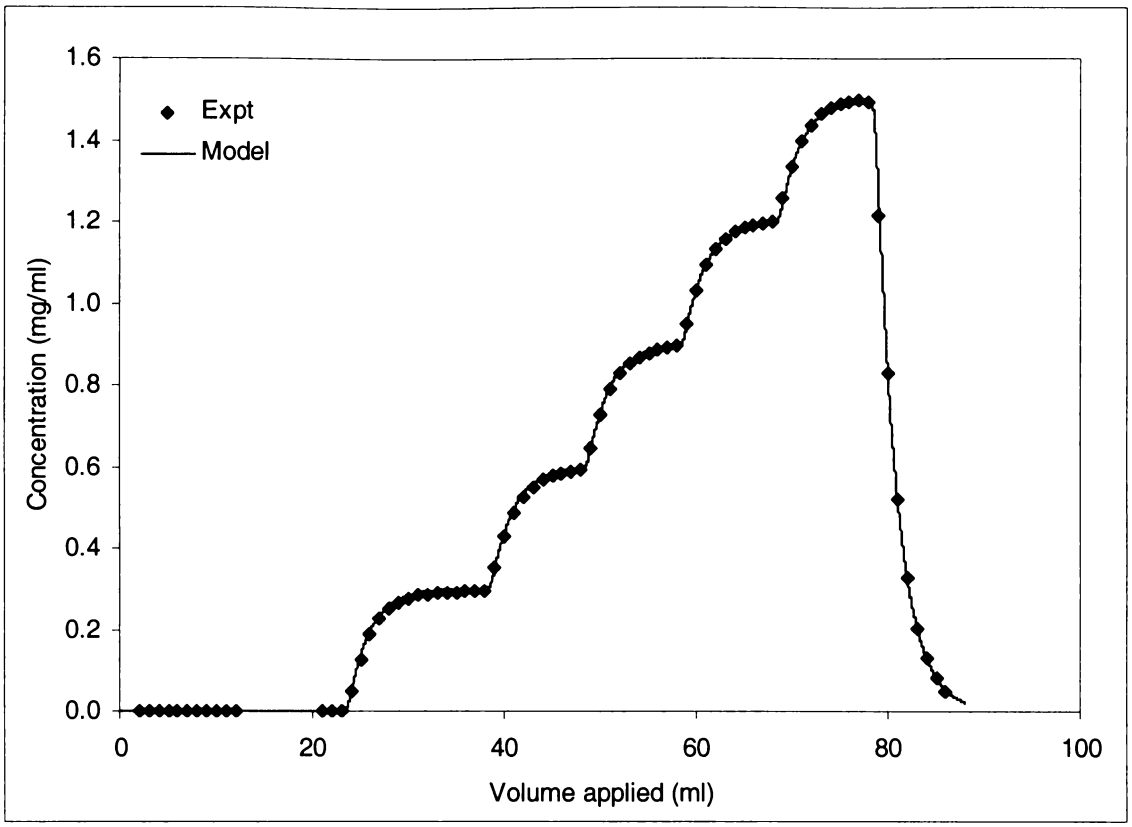

Figure 6-6. BSA concentration profiles using the AKTAexplorer100 gradient mixer and solutions from primary pumps.

6.3.2 BSA breakthrough results

Typical data from breakthrough experiments on a 1-ml DEAE sepharose FF column are shown in Figures 6-7 to 6-8 with additional results in Figures I.4-1 to I.4-3. Parameters for fitted breakthrough curves, simulated using NP-MLF and FD-MLF finite difference models for axial columns (Section 4.4.2), are in Tables I.4-2 and I.4-3. Breakthrough occured when the easily accessible binding sites on or near the resin surface were occupied at $C_{RA} \approx 71$ mg/ml. This is 15 mg/ml lower than C_{RAmax} from rate kinetic experiments and 23 mg/ml lower than obtained from adsorption isotherm experiments. There was extended tailing, indicating that BSA was slowly adsorbing on the resin after breakthrough.

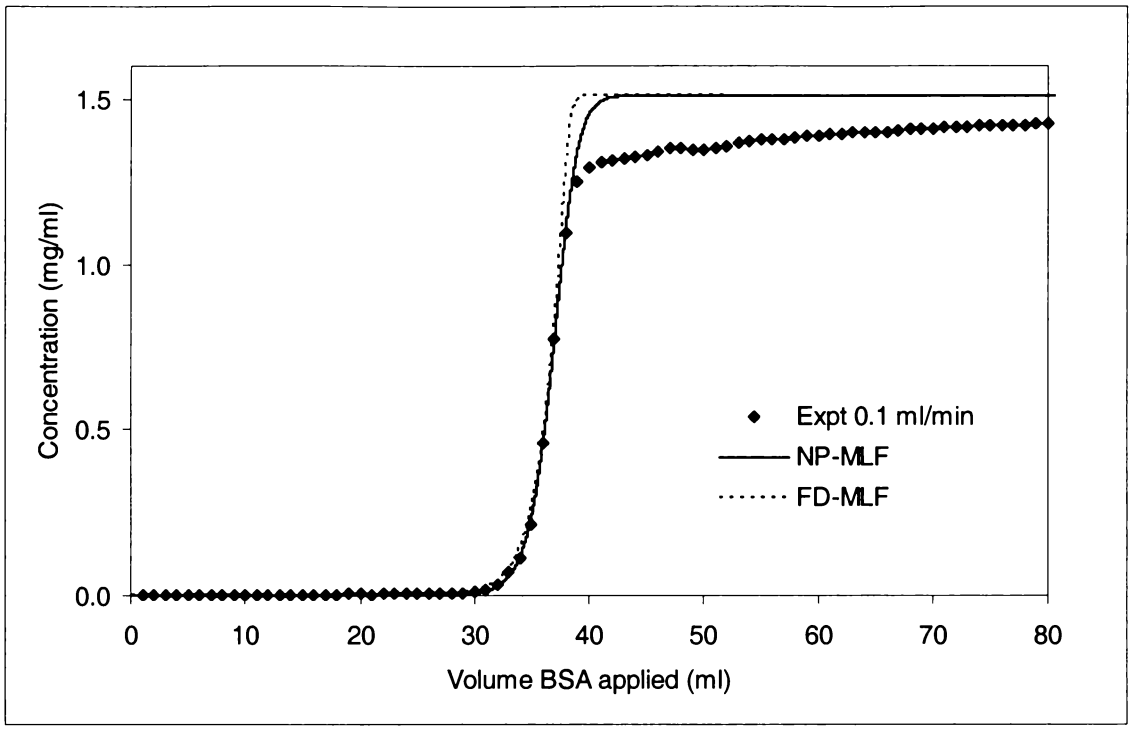

Figure 6-7. Breakthrough curve for 1-ml DEAE Sepharose FF Hitrap column for a flowrate of 0.1 ml/min. Model parameters shown in Table I.4-2 and I.4-3.

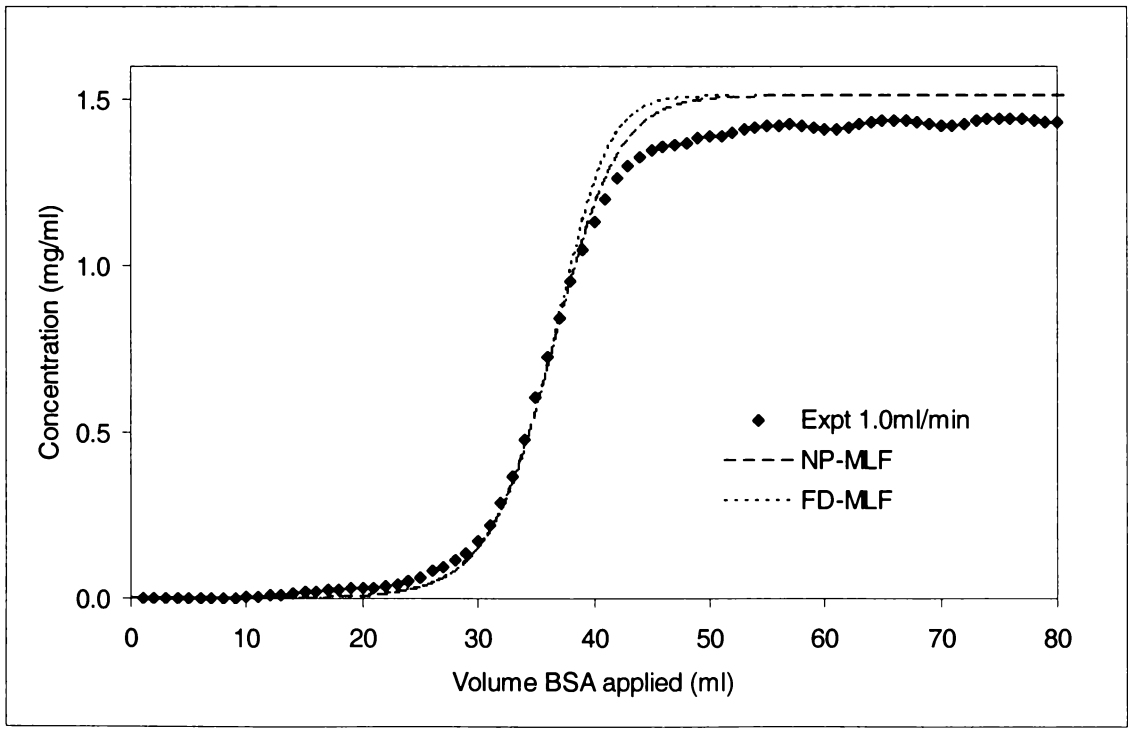

Figure 6-8. Breakthrough curve for 1ml DEAE Sepharose FF Hitrap column for a flowrate of 1 ml/min. Model parameters shown in Table I.4-2 and I.4-3.

BSA mass retained by the column after 80 and 120 ml of feed was applied was calculated by integrating the breakthrough curve. This was divided by the resin volume in the column (accounting for resin external void fraction) to give resin concentration C_{RA} (Table 6-4). After 120 ml had been applied C_{RA} approached adsorption isotherm values. There was a 5% decrease in resin concentration between 0.1 and 0.5 ml/min loading rates.

Table 6-4. BSA resin concentration in a 1-ml DEAE sepharose Fast Flow column (volume=0.962 ml, ε_R=0.31) after applying 80 ml and 120 ml of feed solution.

	After 80 ml		After 120 ml	
Flowrate (ml/min)	Effluent concentration (mg/ml)	Resin concentration (mg/ml)	Effluent concentration (mg/ml)	Resin concentration (mg/ml)
0.1	1.42	91.62	1.44	95.90
0.2	1.42	89.16	1.46	93.32
0.3	1.44	88.70	1.45	92.66
0.5	1.45	87.55	1.46	90.91
1	1.46	87.17	-	-

Other researchers have found tailing (Conder and Hayek 2000; Hunter and Carta 2000; Hunter and Carta 2001b; Kaczmarski *et al.* 2001; Tong *et al.* 2003), which has been attributed to dimers present in commercially available BSA (Hunter and Carta 2001a). The dimer binds more strongly to anion exchange resin, resulting in monomer breaking through before the dimer and tailing. Tailing can be eliminated by removing the dimer (Hunter and Carta 2001a).

Because BSA is modelled as as a single compound with one set of adsorption characteristics in the NP-MLF and FD-MLF models, the models diverge from experimental data. However, excellent fits with the first half of breakthrough curves were obtained for all flowrates.

6.3.2.1 NP-MLF model

NP-MLF solution instability occurred at low solute concentrations at $n_A > 1$ because concentration was raised to the power of $1/n_A$. This resulted in a change in concentration much greater than interstitial concentration, giving negative

concentrations for the next finite difference iteration. Lowering Δt for each time step did not overcome this as it gave even lower concentrations when feed is first introduced to the column. Therefore $n_A = 1$ was used for all finite difference models.

The NP-MLF uptake parameter k_{A1} increases with interstitial velocity to a maximum where presumably pore and uptake rates become controlling (Figure 6-9). k_{A1} values from breakthrough experiments were one to two orders of magnitude greater than from the batch kinetics study because of experimental conditions. Interstitial solute concentration is low at the start of breakthrough experiments, but high in the batch kinetics study. The k_{A1} values come within one order of magnitude if the line from Figure 6-3 is extrapolated to a starting concentration of zero. Also, the resin moved with solution in the batch studies, so the solute had to diffuse through an increasingly larger stagnant zone, slowing uptake.

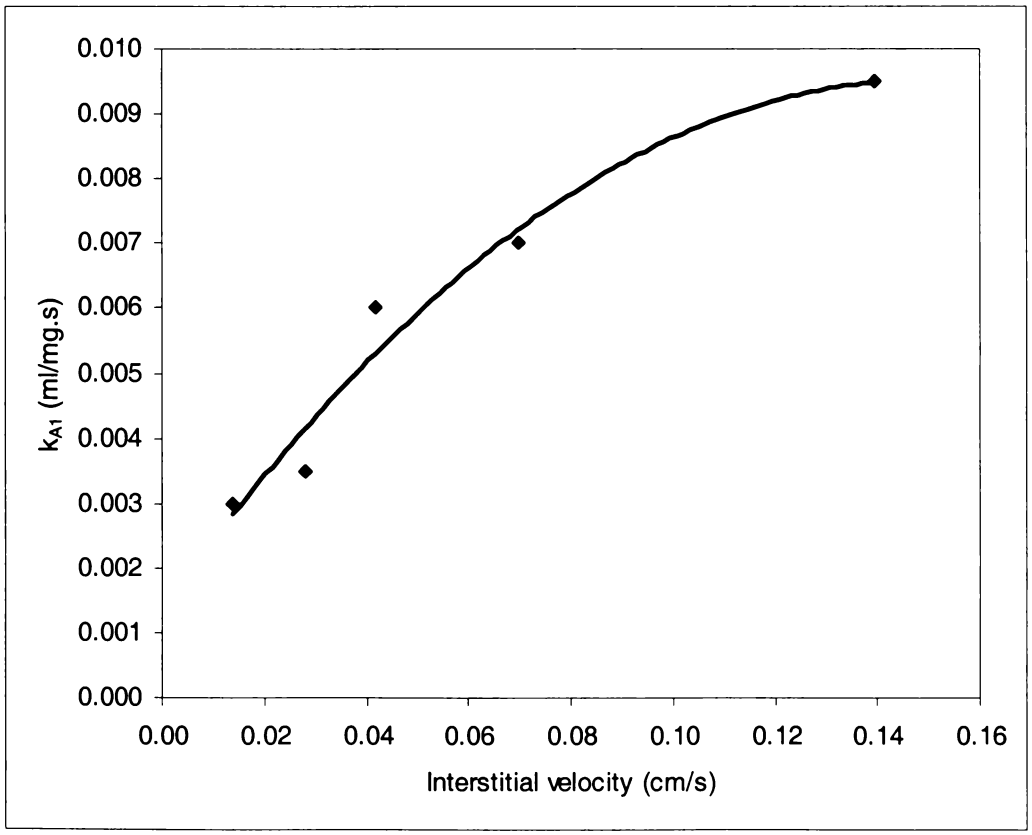

Figure 6-9. Uptake parameter k_{A1} as a function of interstitial velocity.

Axial dispersion was ignored, i.e. $y_2 = 0$, when obtaining model parameters from curve fitting. Simulated breakthrough slope did not change for $y_2 = 0.5$ (suggested by Gu

1995) (Figure I.4-4). Breakthrough slope decreased slightly for y_2 = 10 (Figure I.4-5), but this value is 20 times that recommended by Gu (1995). Column dispersion appears to be masked by the extra-column dispersive effects, which are included in the model. Extra-column dispersion effects are explored in more detail in Section 6.3.4.

The column was divided into 30 stages (N) for all NP-MLF simulations. The effect of higher resolution on breakthrough profile was investigated for N = 70. Higher resolution made breakthrough profiles slightly sharper, requiring k_{A1} for each flowrate for N = 30 to be reduced by up to 0.0005 for a good fit. Although the higher resolution model more closely approximates an analytical solution, simulation times are four times longer. 8.8 million calculations were needed for N = 70 compared to 1.8 million for N = 30. For convenience simulations were kept at N = 30.

6.3.2.2 FD-MLF model

The FD-MLF model matched the first half of the breakthrough curves well (Figures 6-7 and 6-8) using parameters in Table I.4-3. The uptake parameter k_{A1} was fixed at 0.0085 ml/mg.s, n_A = 1, and the film mass transfer coefficient k_{fA} varied. k_{fA} increased with flowrate (Figure 6-10) and values at lower flowrates correlated well with predictions from published equations (Kaczmarski *et al.* 2001) (Section 4.2.4.2). Experimentally-determined k_{fA} values are close to or between calculated values of k_{fA} and k_{ext}, suggesting that surface diffusion predominates at higher flowrates. This is not surpising given that breakthrough occurs when BSA has occupied the binding sites near the resin particle surface. Viscosity and density were based on water values at 20°C. Varying these had little effect on k_{fA} and k_{ext}. The k_{fA} values obtained from breakthrough experiments similar to those in the rate kinetic studies.

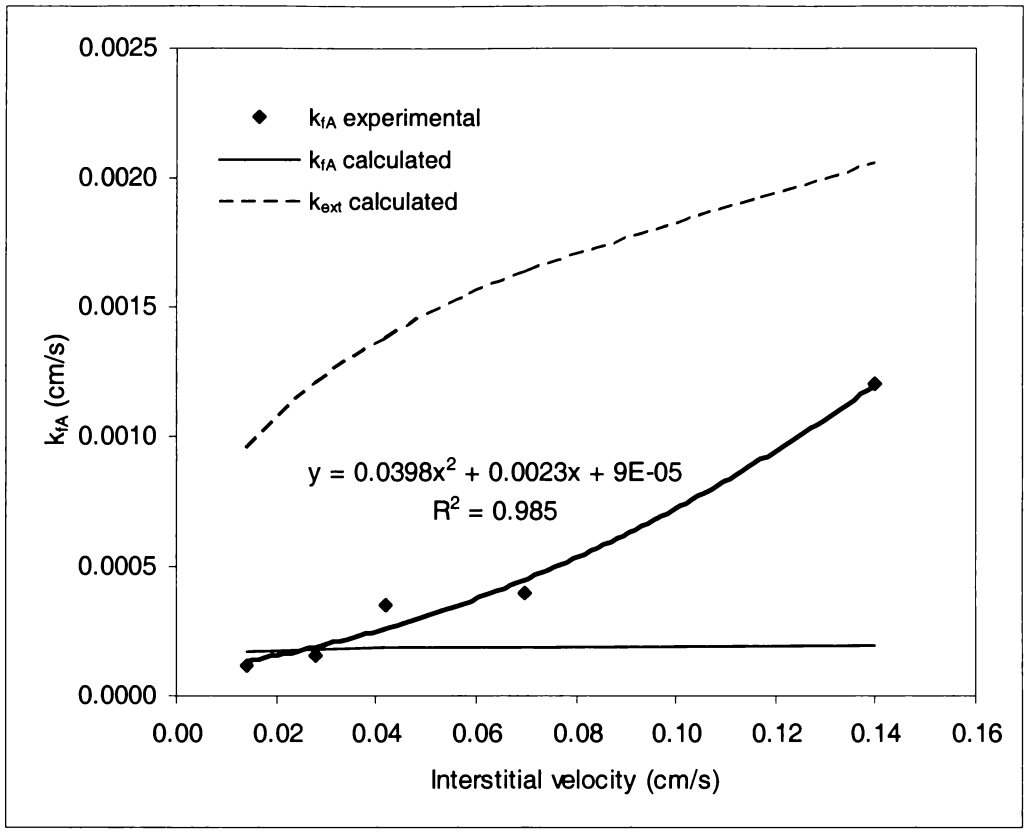

Figure 6-10. k_{fA} as a function of interstitial velocity. Equations for the calculation of k_{fA} and k_{ext} are presented in Section 4.2.4.2 and parameters used are given in Table I.4-1. The equation shown is used in Section 6.4.3.

6.3.3 Desorption

Elution data are shown in Figures 6-11 and 6-12 and Figures I.5-1 to I.5-7. At low NaCl concentrations there was a small BSA peak in the elution profile followed by extended tailing (Figure 6-11). Tailing disappeared at elution concentrations > 0.2M NaCl. The small peak could be loosely bound BSA desorbing before more strongly bound BSA. The BSA elution peak sharpened with increasing NaCl concentrations (for example Figure 6-12), showing that desorption rate was increasing.

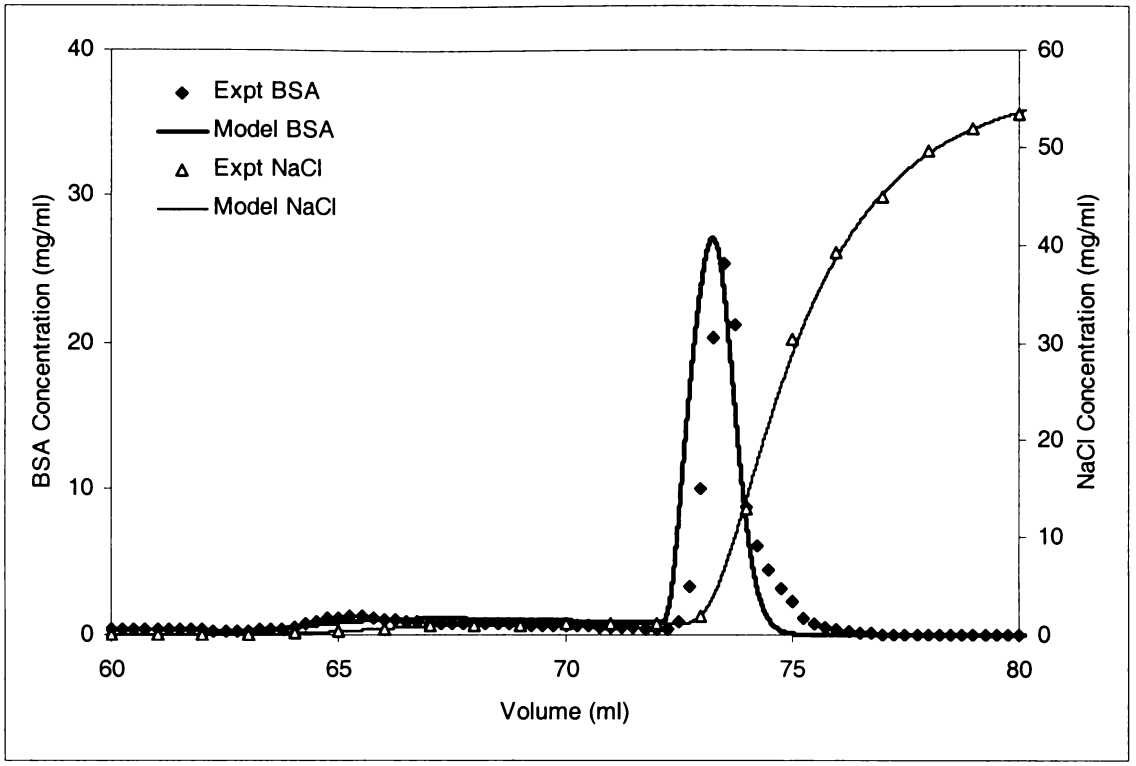

Figure 6-11. Elution profiles at 0.02M NaCl for the first step in elution and 1M NaCl for the second step. Parameters shown in Table 6-5.

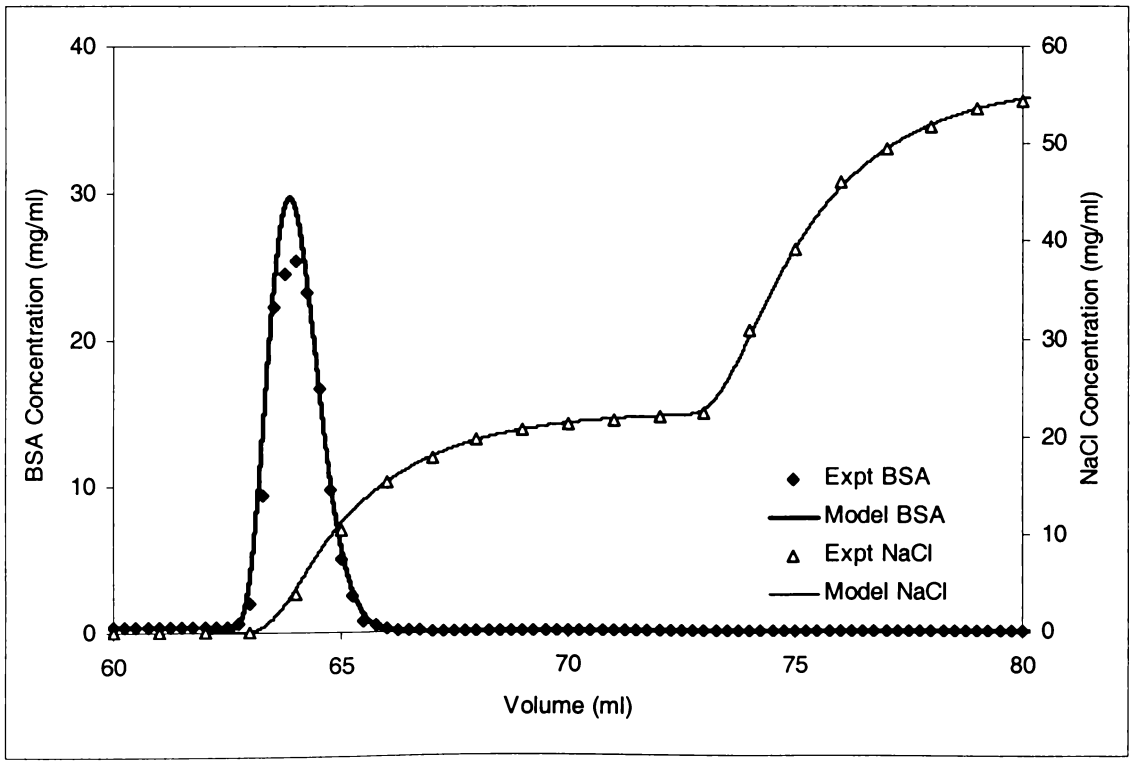

Figure 6-12. Elution profiles at 0.4M NaCl for the first step in elution and 1M NaCl for the second step. Parameters shown in Table 6-5.

There was a very small conductivity peak immediately after the AKTA changed from loading the column with BSA to washing with equilibration buffer (Figure 6-13). A small volume of elution buffer, possibly retained in a valve, had been introduced to the column as the injection valve changed the flow from the primary pumps to the superloop to the column. This also gave a small peak in the BSA profile. Flushing the system failed to prevent the NaCl peak. The concentration profile until the first elution step was integrated to calculate BSA mass retained on the column. The finite difference simulation was adjusted so that simulated BSA mass retained was approximately the same by altering C_{RAmax} and simulating salt contamination effects. Salt contamination did not affect NaCl elution profile modelling as all contaminant was removed before starting elution.

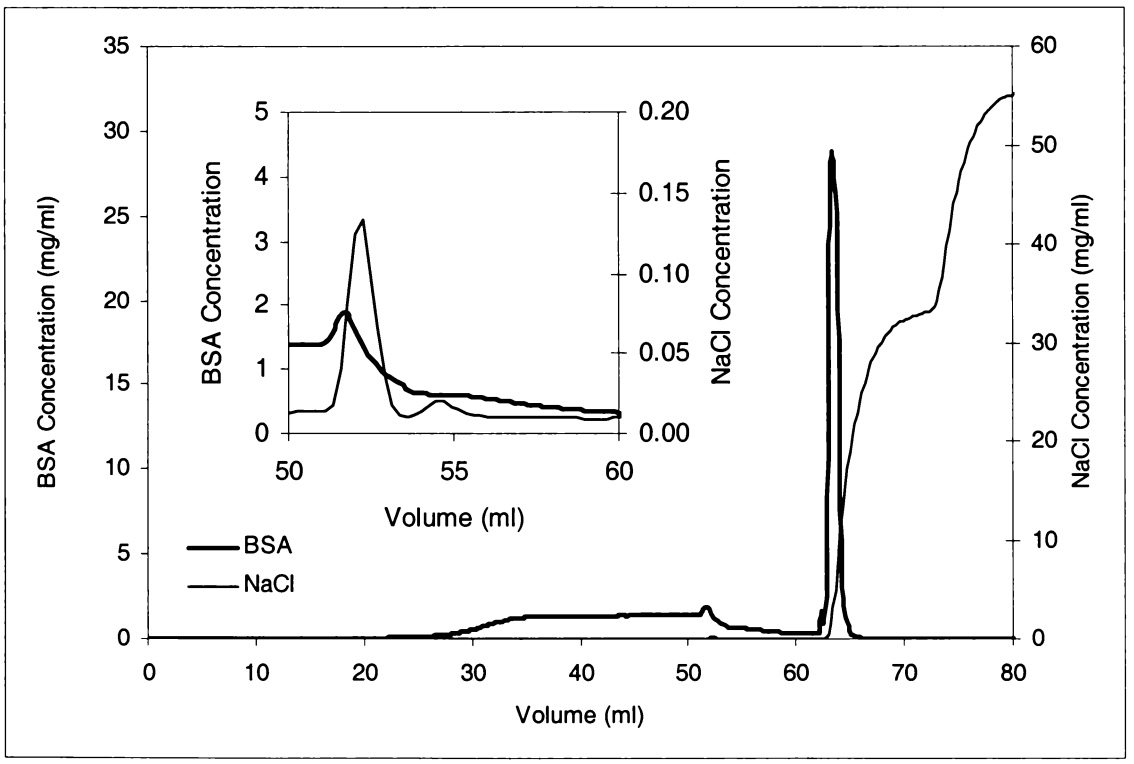

Figure 6-13. Chromatogram for elution strength experiment, first elution step 33.84 mg/ml NaCl in the elution buffer (approximately 0.6M NaCl). Point of interest is the small peak in NaCl concentration at approximately 52.5 ml reaching a peak height of 0.13 mg/ml.

The first step in modelling the effect of NaCl concentration on BSA elution profile was to model the NaCl breakthrough profile. There were two step changes in NaCl

concentration; the first was to a NaCl concentration at which BSA elution was being measured, and the second was to 1M NaCl to remove tightly bound material. Initially, it was assumed that NaCl concentration was high enough so any interaction would not affect NaCl breakthrough profiles. It was assumed that NaCl remained in the resin interstices, did not diffuse into the resin pores and no binding of Cl^- occured. The simulated NaCl breakthrough occurred earlier than observed experimentally (Figure 6-14) indicating the resin retained some NaCl.

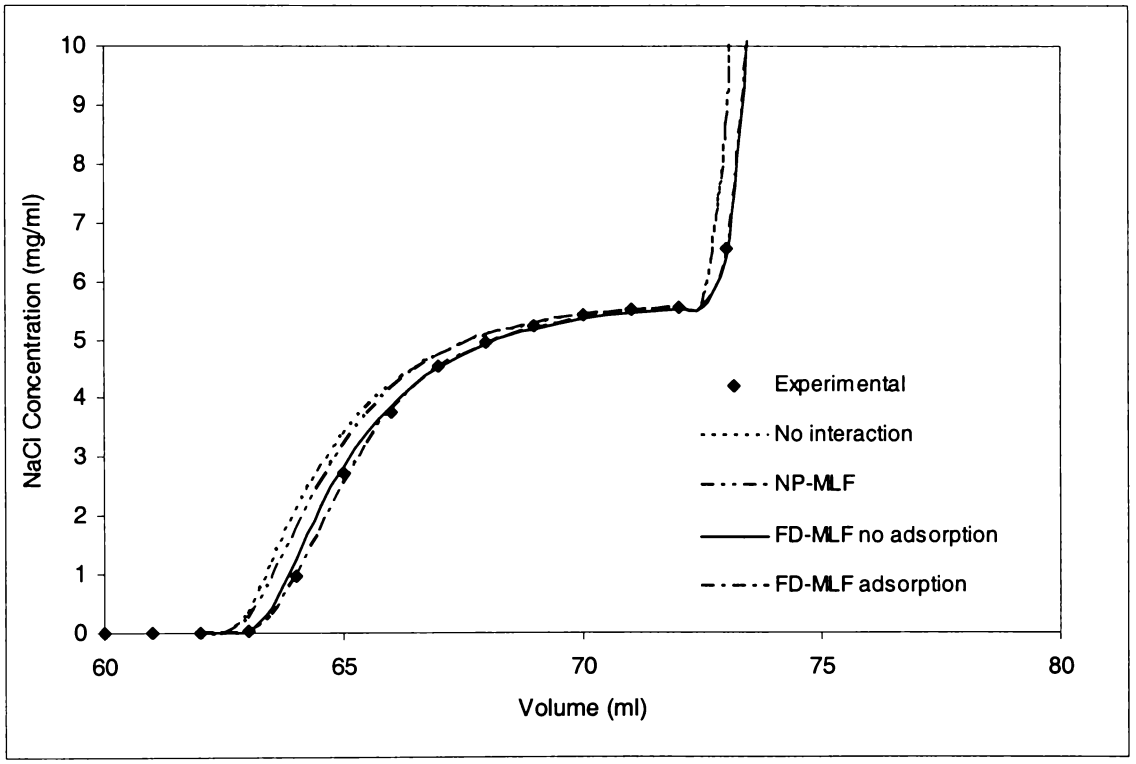

Figure 6-14. Comparison of different NaCl models with experimental data for 0.1M NaCl for the first elution step and 1M NaCl for the second. Model parameters are C_{RBmax} = 1 mg/ml, K_B =15 ml/mg, k_{BI} = 0.003 mg/ml.s, k_{fB} = 0.0001 cm/s, n_B = 1, ε_R = 0.31, and ε_p = 0.72.

The NaCl profile was then modelled using NP-MLF. Competition between BSA and Cl^- for resin binding sites was neglected assuming that Cl^- would dominate binding because it is smaller, more mobile and has a much larger molar concentration. The simulated and experimental data for the first step change agreed well for NaCl concentrations < 0.06M but the simulation predicted earlier breakthrough at higher

concentrations and for the second step change. Therefore NaCl was diffusing into resin pores at a sufficient rate to affect breakthrough.

FD-MLF was then used to simulate NaCl breakthrough, and simulated and experimental data were in good agreement for all concentrations and elution steps (Figure 6-14). Varying K_B values had little effect on NaCl concentration profile, but k_{B1} was more important, requiring slight adjustments for increasing salt concentrations up to 0.08M. C_{RBmax} was important at NaCl < 0.1M where it was 1 mg/ml, but had little effect on NaCl breakthrough curves at higher concentrations. Values for C_{RBmax} were low considering the resin has a Cl^- ion capacity of 3.4-5.7 mg/ml resin (Amersham Biosciences, Uppsala, Sweden). However, assuming Cl^- ions dominate binding may not be valid at these low salt concentrations. Using $n_B = 0.6$ (from the adsorption isotherm experiments, Section 6.1) gave a bad fit for salt profiles < 0.1M, so it was consequently fixed at 1. Dispersion effects were neglected because data from BSA breakthrough experiments indicated that column dispersion was not significant.

It was intended to develop a general model to predict BSA elution profiles for different NaCl concentrations. The FD-MLF model was initially used where protein desorption was given by

$$\Delta C_{RPA(desorption)} = k_{A2}\left(1 + K_B C_{RPB}\big|_{t-1,n}^{1/n_B}\right) C_{RA}\big|_{t-1,n}\,\Delta t \tag{198}$$

$\left(1 + K_B C_{RPB}\big|_{t-1,n}^{1/n_B}\right)$ increases the protein desorption rate as a function of salt concentration, giving an effective desorption rate

$$k_{A2(eff)} = k_{A2}\left(1 + K_B C_{RPB}\big|_{t-1,n}^{1/n_B}\right) \tag{199}$$

K_B and n_B values from adsorption isotherm data (section 0) were initially used. When n_B was used to control desorption rate, the simulations predicted that the BSA elution peak coincided with NaCl breakthrough. However, the BSA peak in experimental runs appeared before NaCl breakthrough, even at very low NaCl concentrations (< 1 mg/ml). This indicated that the Cl^- ion competed very strongly with BSA for resin binding sites, resulting in rapid desorption. Using $n_B = 0.6$ gave simulated elution peak widths greater than experimental peaks at salt concentrations > 0.2M, indicating that desorption rate

was much more rapid than predicted. Lowering n_B increased desorption rate, but the simulation became unstable at high NaCl concentrations because $k_{A2(eff)}$ was high (Table I.5-1). Reducing the time interval in the simulation 10 to 100 fold overcame this but simulations took over a day to run (5 million time steps instead of 50 thousand for a simulation, resulting in over a billion calculations). For practicality, n_B was set to 1, and K_B used to fit BSA elution curves for each salt concentration. K_B was redefined as K_d, a desorption parameter, so it would not be confused with K_B, the equilibrium value for NaCl. Therefore, equations (198) and (199) became,

$$\Delta C_{RPA(desorption)} = k_{A2}\left(1 + K_d C_{RPB}\big|_{t-1,n}\right) C_{RA}\big|_{t-1,n} \Delta t \tag{200}$$

and

$$k_{A2(eff)} = k_{A2}\left(1 + K_d C_{RPB}\big|_{t-1,n}\right) \tag{201}$$

Simulated and experimental BSA elution results are shown in Figures 6-11 to 6-12 and Figures I.5-1 to I.5-7 (model parameters in Table 6-5). The simulation did not predict the small BSA elution peak that occured for low NaCl concentrations. However, simulated and experimental elution curves agreed better at ≥ 0.1M NaCl concentrations because Cl^- concentration was sufficient to displace both weakly and strongly bound BSA. K_d increased rapidly with NaCl concentration but could not be raised above 2000 for 0.8M NaCl because the simulation became unstable.

6.3.4 Model results for interstitial dispersion

Interstitial dispersion was simulated for a step pulse of solute through a 1-ml column (2.5 cm long and 0.7 cm diameter) for three different AKTAexplorer100 set-ups: column injection, superloop injection and pump injection. In column injection (CO) a step input of solute is injected directly into the column and effluent concentration measured directly after the column. In superloop injection (SI) a step input of solute from the AKTA superloop is injected into the column and extra-column dispersion (Section 6.3) is accounted for. In pump injection (PI) a step input of solute is injected from one AKTA primary pump, through the gradient mixer and into the column, and accounts for extra-column dispersion. Simulations were run for each configuration for a range of dispersion factors (y_2). Solute adsorption and pore diffusion was neglected. Results are shown in Figure 6-15.

Table 6-5. Parameters for simulating NaCl and BSA elution profiles for elution strength experiments.

Dilution	NaCl concentration (mg/ml)	k_{B1} (ml/mg.s)	k_{B2} (1/s)	K_d (ml/mg)	$k_{A2(eff)}$ (1/s)
0.02	1.13	0.008	0.00053	8	0.00181
0.04	2.26	0.005	0.00033	10	0.00426
0.06	3.38	0.004	0.00027	12	0.00753
0.08	4.51	0.003	0.00020	15	0.01242
0.1	5.64	0.003	0.00020	25	0.02568
0.2	11.28	0.003	0.00020	150	0.30618
0.4	22.56	0.003	0.00020	350	1.42818
0.6	33.84	0.003	0.00020	2000	12.2402
0.8	45.12	0.003	0.00020	2000	16.3202

$Q_{loading}$ = 0.5 ml/min, Q_{elute} = 0.2 ml/min, k_{fB} = 0.0001 cm/s, C_{RBmax} = 1 mg/ml resin, K_B = 15 ml/mg, n_B = 1, k_{fA} = 0.00016 cm/s, C_{RAmax} = 69 mg/ml resin, K_A = 47 ml/mg, k_{A1} = 0.0085 ml/mg.s, k_{A2} = 0.000181 1/s, n_A = 1, ε_R = 0.31, and ε_p = 0.72.

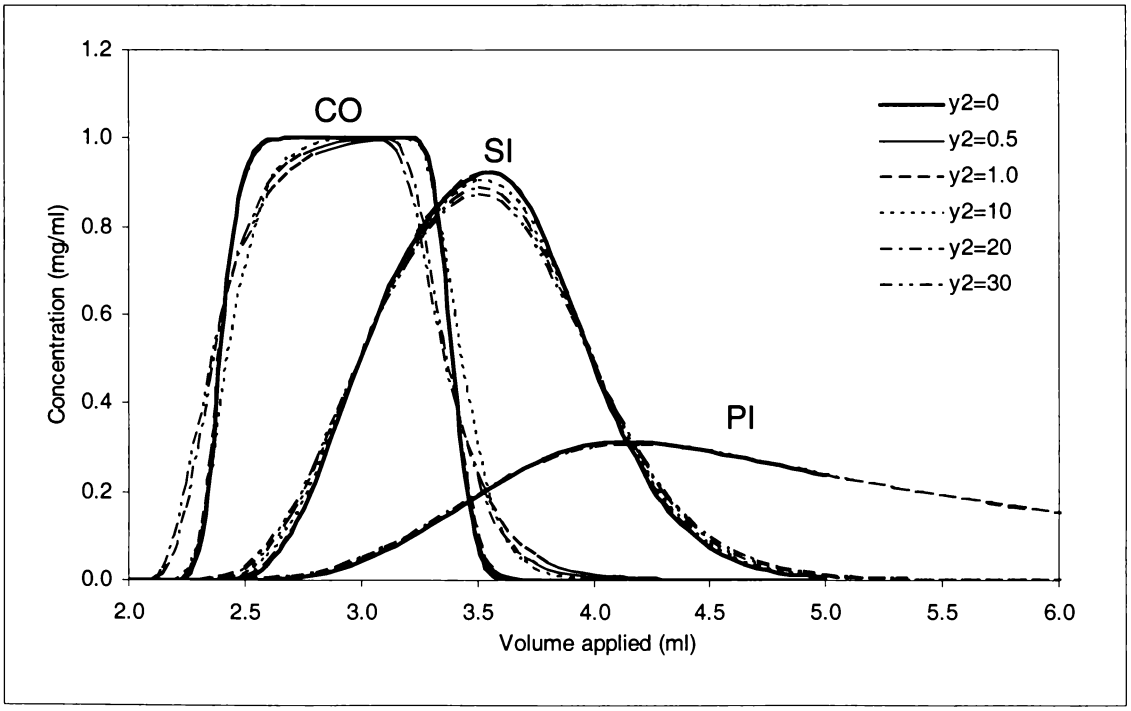

Figure 6-15. Effect of different configurations and y_2 on peak profiles for a 1 ml square input of solute through a 2.5-cm long, 0.7-cm I.D. column, at a flowrate of 0.5 ml/min, number of stages N = 30, time divider J = 12. CO = column only, SI = superloop injection, PI = pump injection.

A dispersion value of $y_2 = 0.5$, suggested by Gu (1995), gave very little difference in peak profile (Figure 6-15). High y_2 values of 10-30 gave a significant difference in peak shape for the CO configuration, but had little or no effect for SI and PI configurations. This indicated that extra-column dispersion was the main cause of peak spreading in the AKTA and interstitial dispersion could be neglected.

Column dispersion becomes more important as column length increases for CO configuration, with peak shapes becoming Guassian (Figure 6-16). A 2.5-cm column is too short for dispersion to be significant, particularly at low y_2.

The effect of changing model resolution on peak shape and height for CO configuration was investigated by varying the stages (N) a 4-ml, 10-cm long column was divided into. There was a significant difference in peak profile for $N = 30$ as compared to $N = 90$ to 240 which showed little difference (Figure 6-17). Levenspiel (1993) recommended $N = 250$ for a 10-cm long column packed with 0.01 cm diameter resin particles (Section 4.4.2). The finite difference model developed is reliable for one quarter to half the recommended N with minimal impact on peak profile.

The time divider (J) was varied for a 30-stage, 10-cm, 4-ml column, to observe the impact of the number of time steps (M) and change in time (Δt) on simulated profiles (see Section 4.4.2 for calculation of M and Δt using J). Increasing J increases the simulation time steps, effectively making the finite difference solution more closely approximate an analytical solution, but requires longer processing times. The peak profile was slightly sharper for J=6 (Δt = 0.51 seconds for 0.5ml/min), as compared to J=48 (Δt = 0.06 seconds) (Figure 6-18). The finite difference solution can be reliably used at low J values provided the dispersion (or elution and adosprtion) rates are not high, which can produce negative concentration values and an unstable model.

Varying the flowrate did not affect peak profile for $y_2 = 30$ (Figure 6-19). The finite difference solution automatically adjusted Δt so time steps M were constant for different flowrates. Simulations were run with Δt fixed at 0.02 s and $y_2 = 10$ (to ensure model stability) for two flowrates. To do this M was set to 6750 at 4 ml/min and 27000 at 1 ml/min. Again, no difference in peak shape was found (Figure 6-19), which be explained by using the finite difference equations for convection and dispersion to determine the Peclet number.

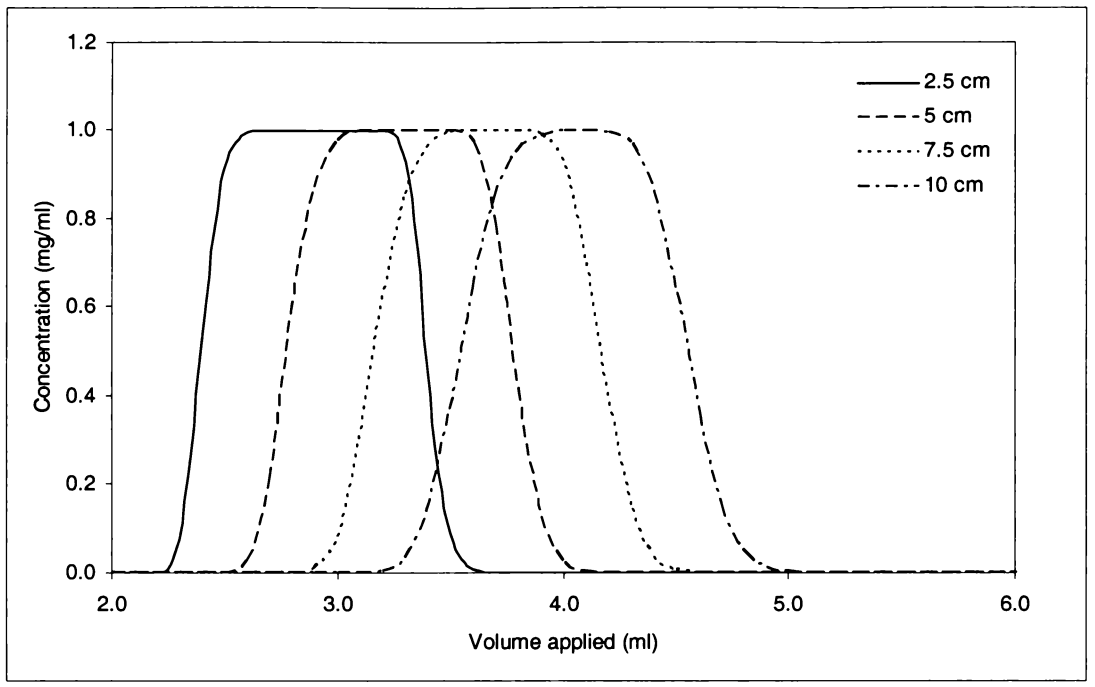

A

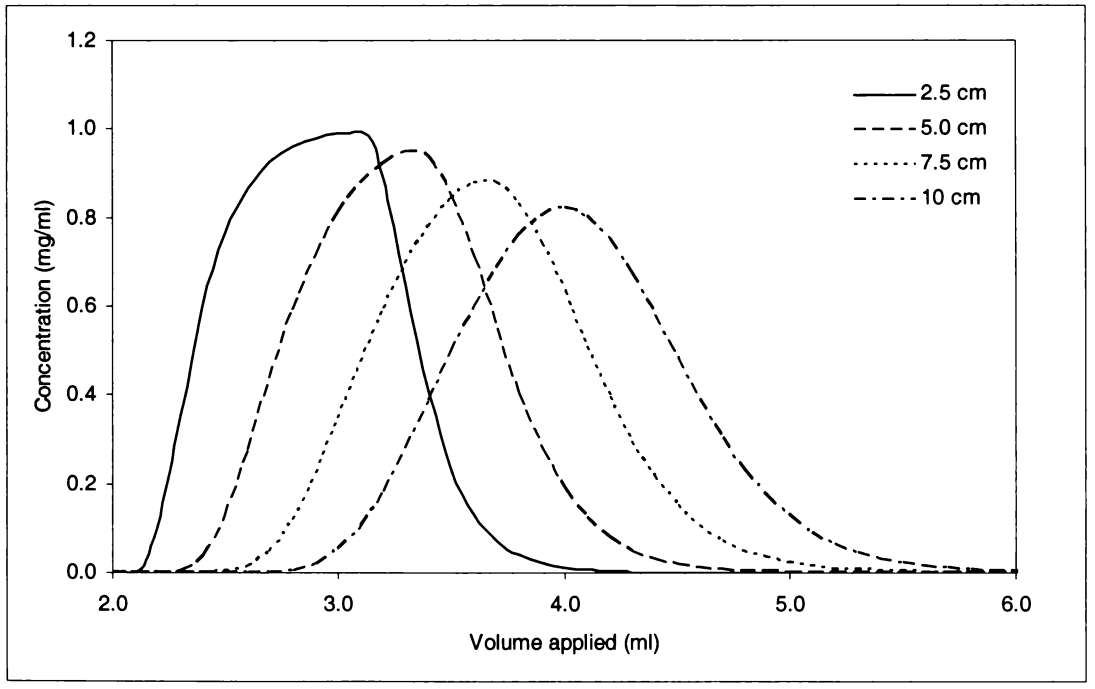

B

Figure 6-16. Effect of column length on peak profile for A) $y_2 = 0.5$ and B) $y_2 = 30$, for a 0.7cm ID column, at a flowrate of 0.5ml/min, number of stages = 30, 60, 90 and 120 for 2.5, 5, 7.5 and 10cm columns respectively, time divider J = 12. The column was modelled.

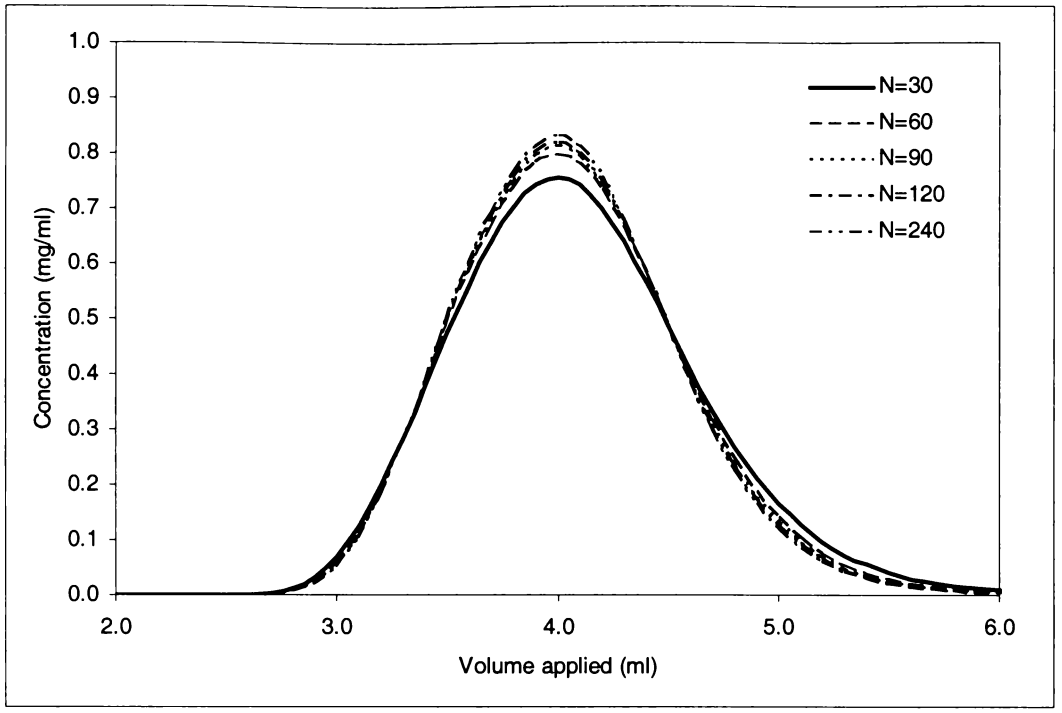

Figure 6-17. Effect of model resolution on peak profile for a 1 ml square input of solute through a 10-cm long and 0.7-cm I.D. column, at a flowrate of 0.5ml/min, N = 30-240, time divider J = 12 and y_2 = 30.

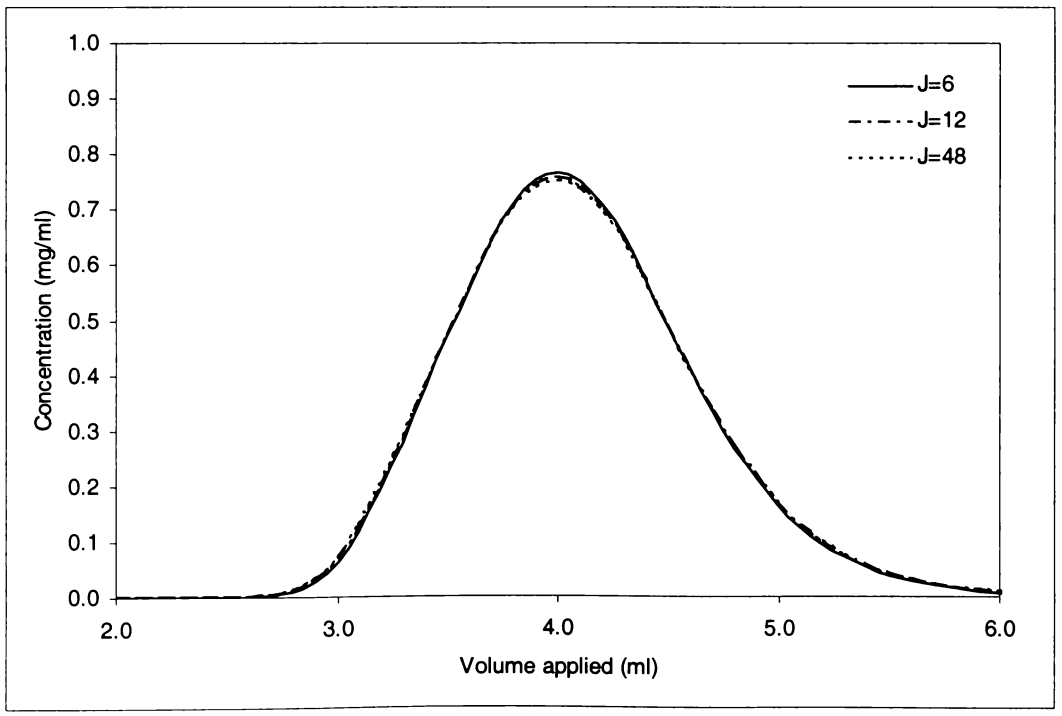

Figure 6-18. Effect of J on simulated peak profile for a 4 ml column, 10 cm in length and 0.7 cm ID, at a flowrate of 0.5 ml/min, N = 30, and y_2 = 30.

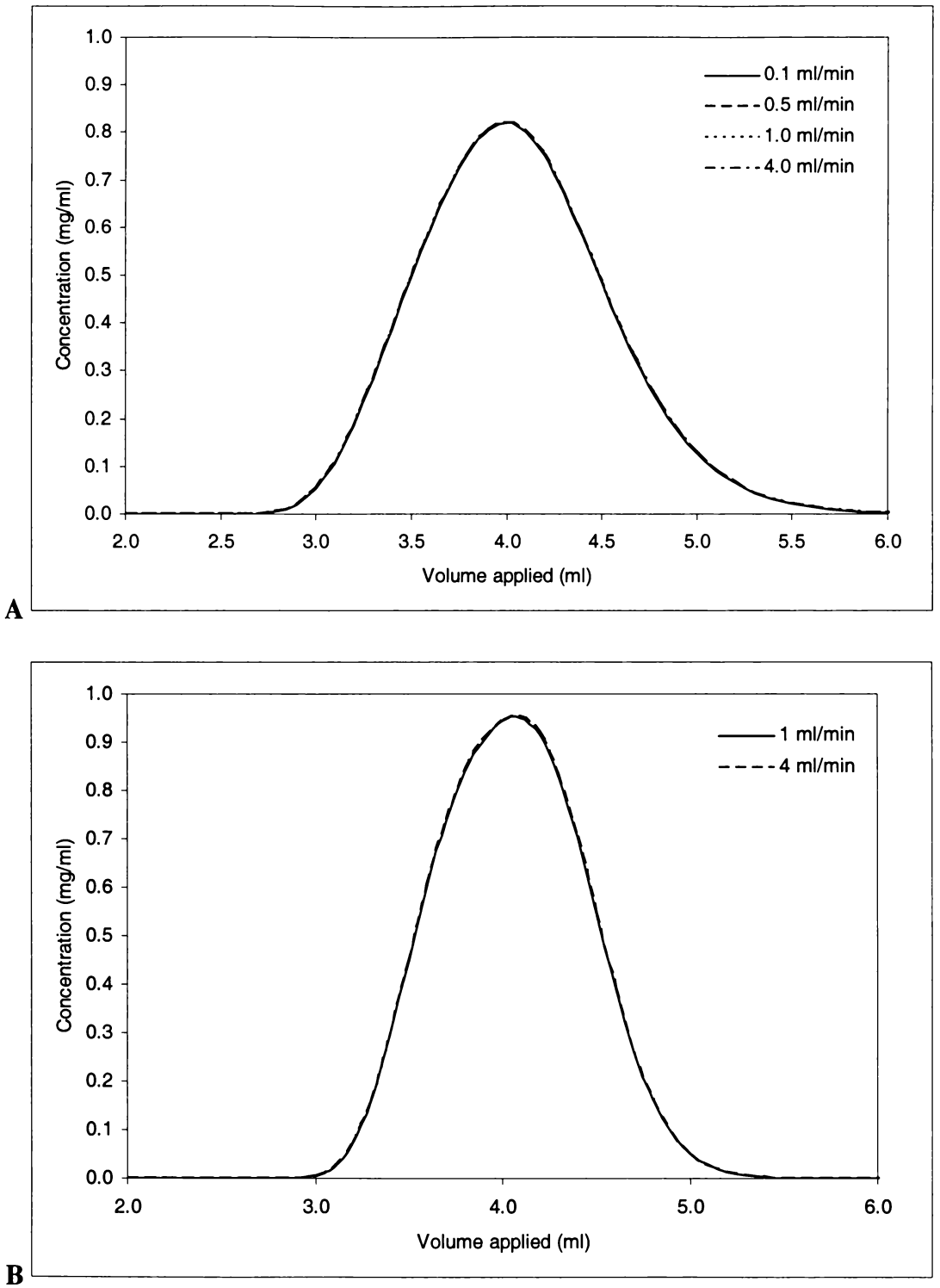

Figure 6-19. Effect of flowrate on simulated peak profile from a 10-cm long, 0.7-cm ID column, input of 1 ml at 1 mg/ml, N = 120. A) Fixed M and y_2 = 30. B) Fixed Δt, y_2 = 10.

Substituting equation (129) for calculating Δt into the axial dispersion equation (137) gives

$$\Delta C_A \text{ZDisp}\big|_{n,m} = \frac{y_2(2R_p)}{\Delta z J}\left(C_A\big|_{n-1,m-1} - 2C_A\big|_{n,m-1} + C_A\big|_{n+1,m-1}\right) \tag{202}$$

Therefore, concentration change for each time step due to dispersion is independent of flowrate but is dependent on Δz. As Δz decreases, the change in concentration due to dispersion increases, but this will be compensated by the concentration difference between stages decreasing with Δz. Increasing J will decrease the concentration change due to dispersion for each time step.

Substituting equation (129) into the convection equation (134) gives

$$\Delta C_A \text{Convection}\big|_{n,m} = \left(C_A\big|_{n-1,m-1} - C_A\big|_{n,m-1}\right)\frac{1}{J} \tag{203}$$

The Peclet number is the ratio of dispersive to convective mass transfer. Therefore dividing equation (202) by (203) gives

$$\frac{\Delta C_A \text{ZDisp}\big|_{n,m}}{\Delta C_A \text{Convection}\big|_{n,m}} \frac{\Delta z}{y_2(2R_p)} = \frac{\left(C_A\big|_{n-1,m-1} - 2C_A\big|_{n,m-1} + C_A\big|_{n+1,m-1}\right)}{\left(C_A\big|_{n-1,m-1} - C_A\big|_{n,m-1}\right)} \tag{204}$$

Substituting equations (202) and (203) into (204) gives

$$\frac{\Delta z}{y_2(2R_p)} = \frac{\left(C_A\big|_{n-1,m-1} - 2C_A\big|_{n,m-1} + C_A\big|_{n+1,m-1}\right)\left(C_A\big|_{n-1,m-1} - C_A\big|_{n,m-1}\right)\frac{1}{J}}{\left(C_A\big|_{n-1,m-1} - C_A\big|_{n,m-1}\right)\left(C_A\big|_{n-1,m-1} - 2C_A\big|_{n,m-1} + C_A\big|_{n+1,m-1}\right)\frac{y_2(2R_p)}{\Delta z J}} \tag{205}$$

Symplifying equation (205) gives the Peclet number for an axial flow column,

$$\frac{\Delta z}{y_2(2R_p)} = \frac{\Delta z}{y_2(2R_p)} = Pe_z \tag{206}$$

A similar result is found for a radial flow column (using equations (151), (155) and (156)),

$$\frac{\Delta r}{y_2(2R_p)} = Pe_r \tag{207}$$

which is the same as equation (16) (Section 2.12.2, Gu (1995)) when Δr is taken as the annular bed depth. Therefore, column dispersion is independent of flowrate, and is a

function of bed depth and dispersive properties of the resin and solution used. Band spreading at different flowrates is due to pore diffusion, not interstitial dispersion.

6.3.5 General conclusions

MLF described adsorption equilibria of BSA with ion exchange resin in different concentrations of NaCl. However, it proved unsuitable when incorporated into NP and FD models to simulate BSA adsorption and elution in small columns. This was because fitting factors n_B and n_A affected breakthrough profiles and position of the eluted peaks giving poor fits, and made the finite difference solutions unstable. n_B and n_A were set to 1, reducing MLF to ML. The FD-ML model best described NaCl breakthrough profiles and gave good correlation between uptake rates from batch kinetic and breakthrough experiments.

The FD-ML model is unsuitable when the column is loaded past breakthrough due to BSA's tailing effects. Resin loading capacity has to be underestimated to obtain a correct breakthrough volume, which means total mass eluted will also be underestimated. The model is suitable for when the column is not loaded past breakthrough such as in continuous separation or standard practice in batch chromatographic separations. Predictions past breakthrough may be improved by using a more complex pore diffusion model where the resin particle is discretized into layers, BSA pore diffusion simulated and binding kinetics of BSA variants accounted for. However, this would considerably increase computation time for little or no gain at the loadings used in practice.

Interstitial dispersion is masked by extra-column effects and only becomes significant when simulating columns with large bed depths. Therefore, band spreading is primarily due to solute diffusion in and out of the resin pores and binding kinetics.

6.4 Batch CRFC results

6.4.1 Extra-column dispersion

Salt pulse experiments to investigate extra-column dispersion show that flow arrangement of the manifold has little or no impact on peak profile (Figure 6-20). The flow manifold was modelled as two 13-ml well mixed tanks with a 21-ml volume delay, thus giving a total open volume of 47 ml that compares well with the calculated open volume (Table 6-6). The gradient on the leading edge decreased when the manifold was modelled as two 18-ml tanks. This, together with peak tailing, indicates the manifold had regions of low mixing. Any dispersive effects in the AKTA set-up did not affect peak profile, and was therefore neglected when modelling the CRFC.

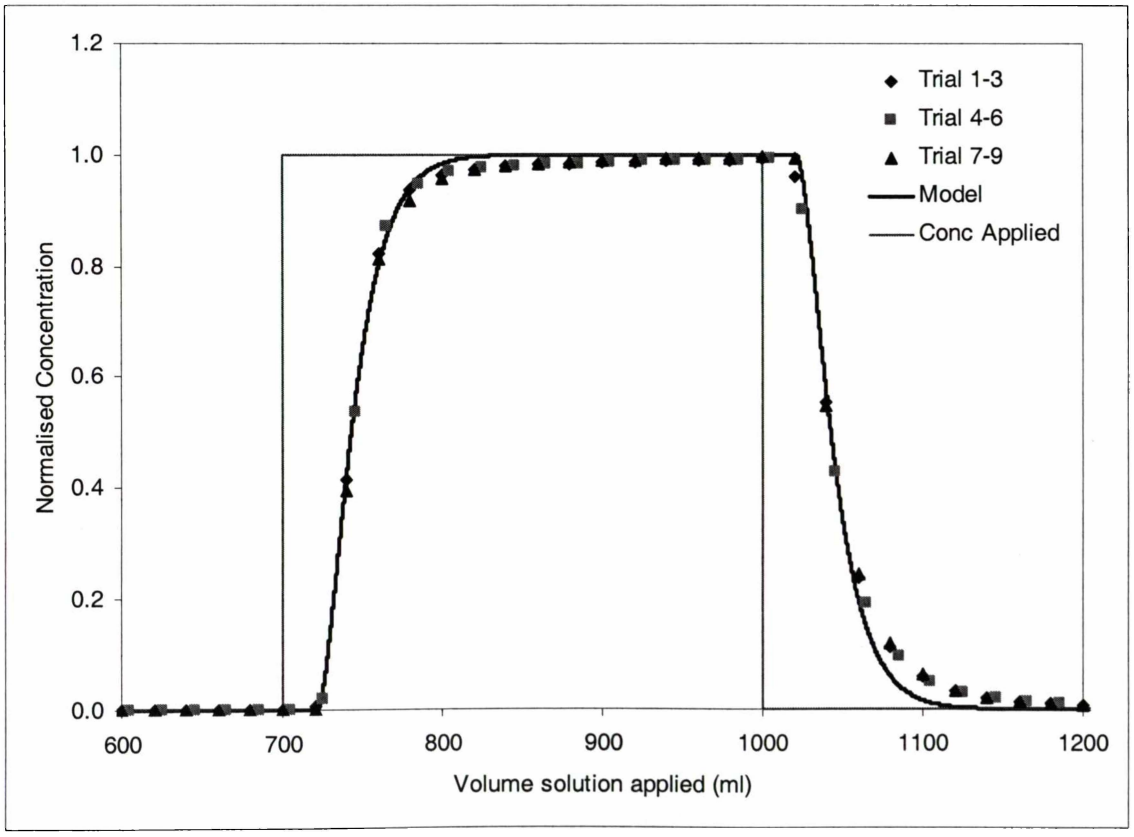

Figure 6-20. Effect of flow manifold arrangement on concentration profile. Trials 1-3 are for flow arrangement A, 4-6 flow arrangement B, and 7-9 flow arrangement C in Figure 5-14.

Table 6-6. Open volume and residence time for 45 ml/min.

Item	Length (mm)	Diameter (mm)	Number	Volume (ml)	Time (min)
From Akta to flow splitter	760	1	1	0.597	0.013
Flow splitter	21	5	1	0.412	0.009
Flow splitter to manifold	200	1	2	0.314	0.007
Manifold chamber	80	12	2	18.096	0.402
Manifold to flow bypass	660	1	8	4.147	0.092
Flow bypass to manifold	450	1	8	2.827	0.063
Manifold chamber	80	12	2	18.096	0.402
Manifold to flowsplitter	240	1	2	0.377	0.008
Flow splitter	21	5	1	0.412	0.009
Flow splitter to Akta	1200	1	1	0.942	0.021
			Total	**46.221**	**1.027**

The CRFC breakthrough experiments required buffer in one primary pump to be changed from equilibration buffer to loading buffer. Because the trial could not be paused while this was done, the effects of changing solution mid-run were determined by analysing the peak profile from the initial pulse of loading solution through the AKTA. The model in Section 6.3.1 was used, except that an additional 2-ml well-mixed tank to represent the pump was included and the volume delay was adjusted to 5 ml. The simulation was run using a Matlab program (Appendix H.7) and agreed well with experimental data (Figure 6-21). Because dispersive effects from changing solution in the primary pump during a trial were small, they were neglected in the overall CRFC model. The volume delay could be adjusted to reflect buffer residence time in the pump. However, the 5-ml delay was very small in comparison with the 20 L applied to the CRFC during batch operation and would not significantly affect results.

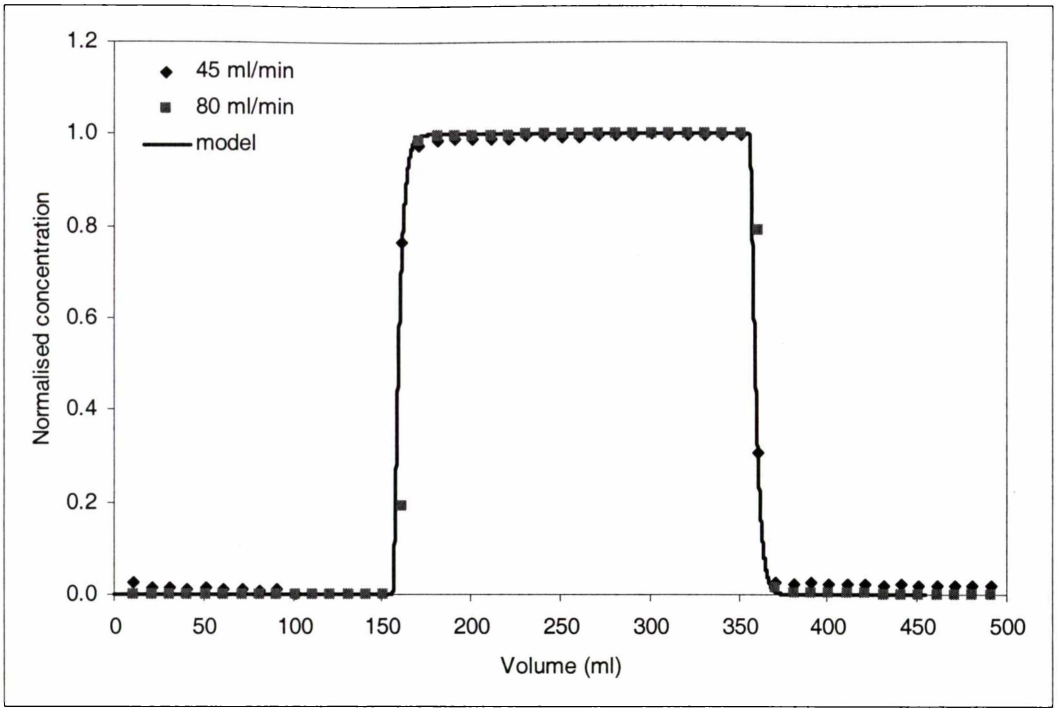

Figure 6-21. Modelling of dispersion arising from changing solution in the primary pump.

Effluent from the CRFC was split into two streams, one going to waste and the other going to the AKTA for analysis. The sample pump withdrew solution at 5 ml/min from the effluent. The AKTA conductivity calibration data was used to determine dispersive effects due to the sample pump. The concentration change was simulated by adapting the superloop model (Section 6.3.1) and increasing the volume delay from 1.3 to 3.3 ml (Appendix H.8). Simulations agreed well with experimental data (Figure 6-22), indicating very little dispersion, so the effects of the sample pump were also neglected in the CRFC model.

6.4.2 Bed integrity

Data from bed integrity tests done after channelling had occurred and after the resin had been cleaned and repacked show channelling can be experimentally determined using the new CRFC prototype (Figure 6-23). This is an important design requirement. Peaks prior to repacking are taller and show little tailing compared with peaks after repacking. A significant proportion of the resin was 3-4 mm diameter hard aggregates when removed from the CRFC and sieved. These aggregates would have affected NaCl pore diffusion, possibly giving the appearance of better performance.

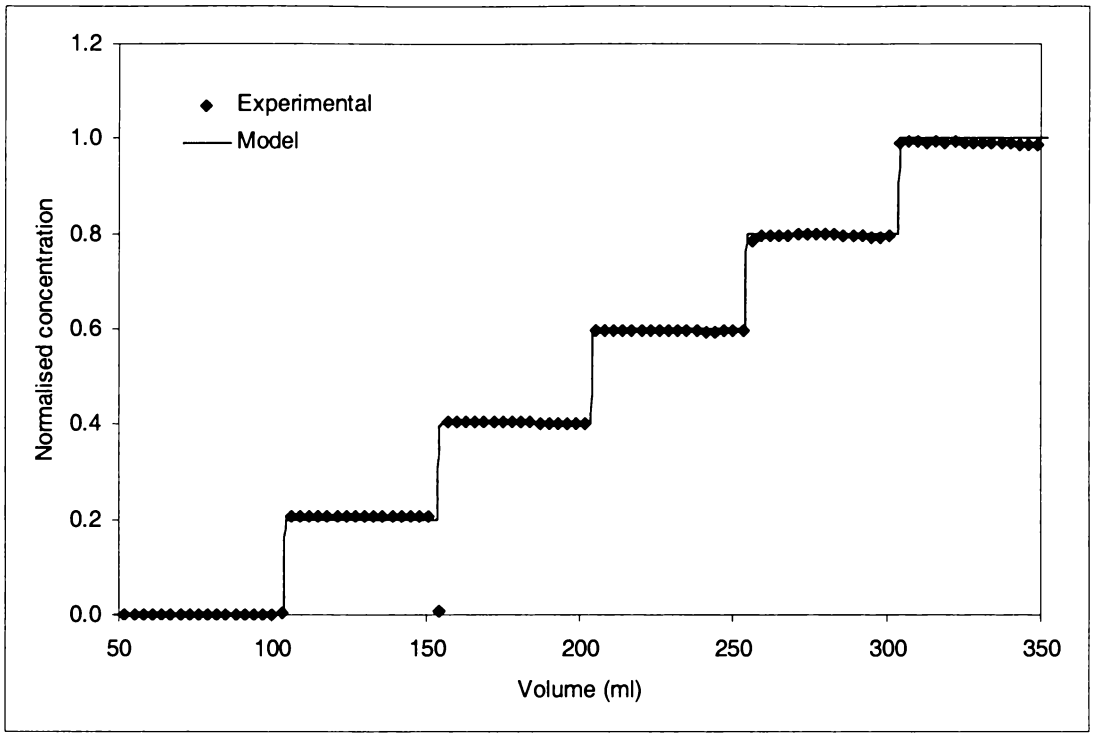

Figure 6-22. Modelling of dispersion arising from using the sample pump.

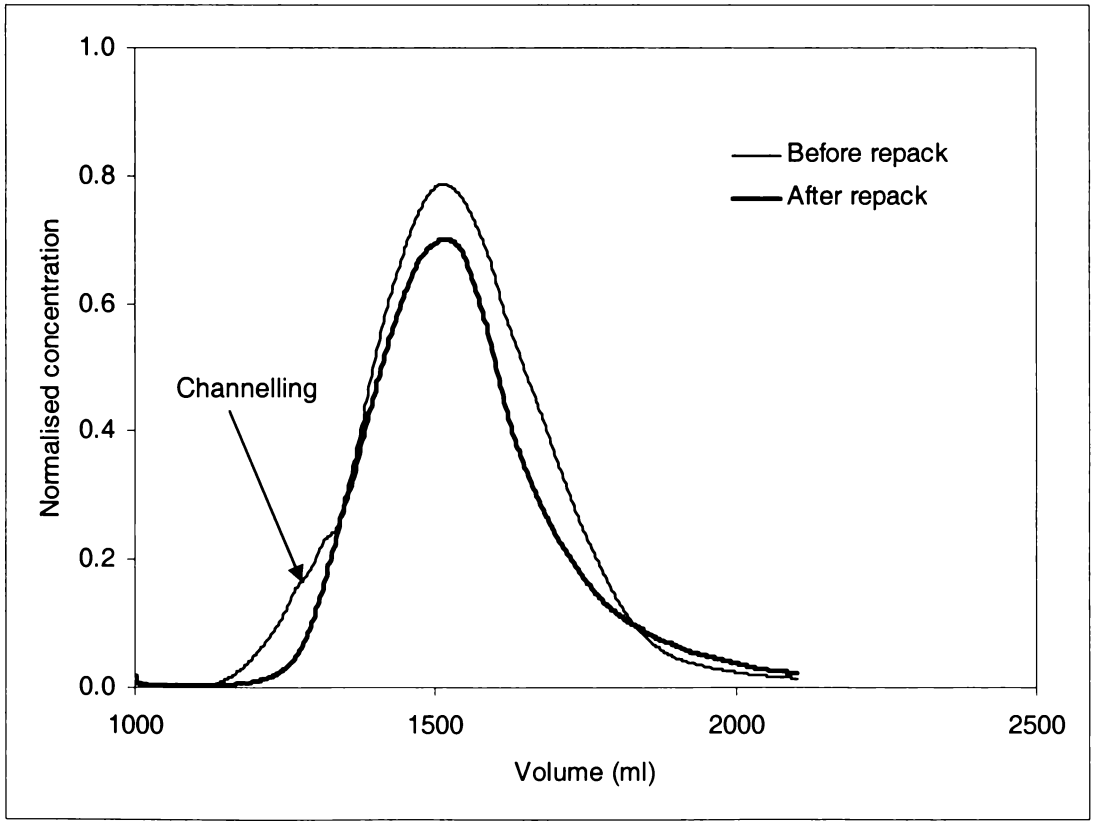

Figure 6-23. Example of channelling. Salt concentration profile in effluent before and after repacking the CRFC annulus.

6.4.3 CRFC breakthrough and elution

CRFC performance was poor for batch breakthrough and elution trials (Figures 6-24 to 6-26 and Figures I.6-1 to I.6-2). The breakthrough profile had a shallow gradient for all trials indicating that the CRFC had much lower resolution than the axial flow column used in Section 6.3. The FD-ML model (modified from Section 4.4.3) was fitted to BSA experimental results and parameters obtained (Table 6-7). The rates required to fit the model were about 30 times lower than those obtained for the axial column, confirming poor resolution. There was a good fit if k_{A1} was used as the rate controlling parameter. Values for desorption parameter K_d were about 44 times smaller than the maximum used in elution experiments, again due to the low CRFC resolution giving broader elution peaks. Simulated breakthrough profiles were unaffected by dispersion factors $y_2 \leq 20$ (40 times higher than recommended by Gu (1995)). NaCl profiles were simulated using data from axial column experiments (Table 6-5).

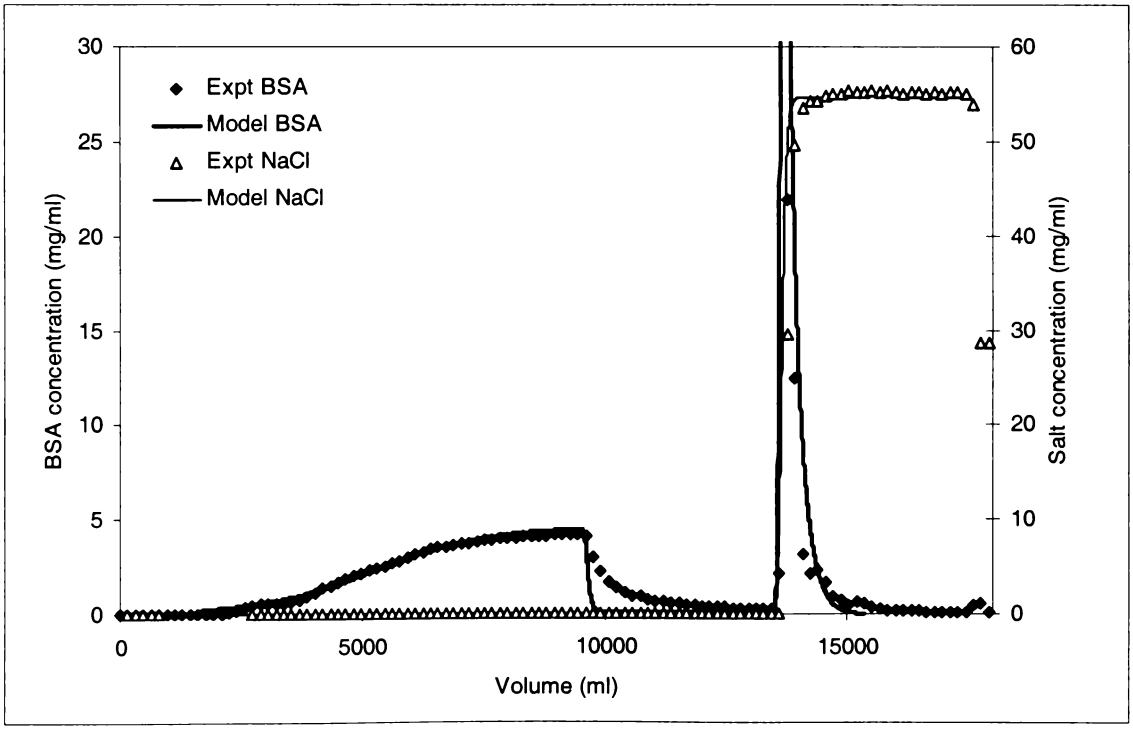

Figure 6-24. Breakthrough and elution profile for feed concentration of 4.5 mg/ml and 45 ml/min (Column 1 of Table 6-7).

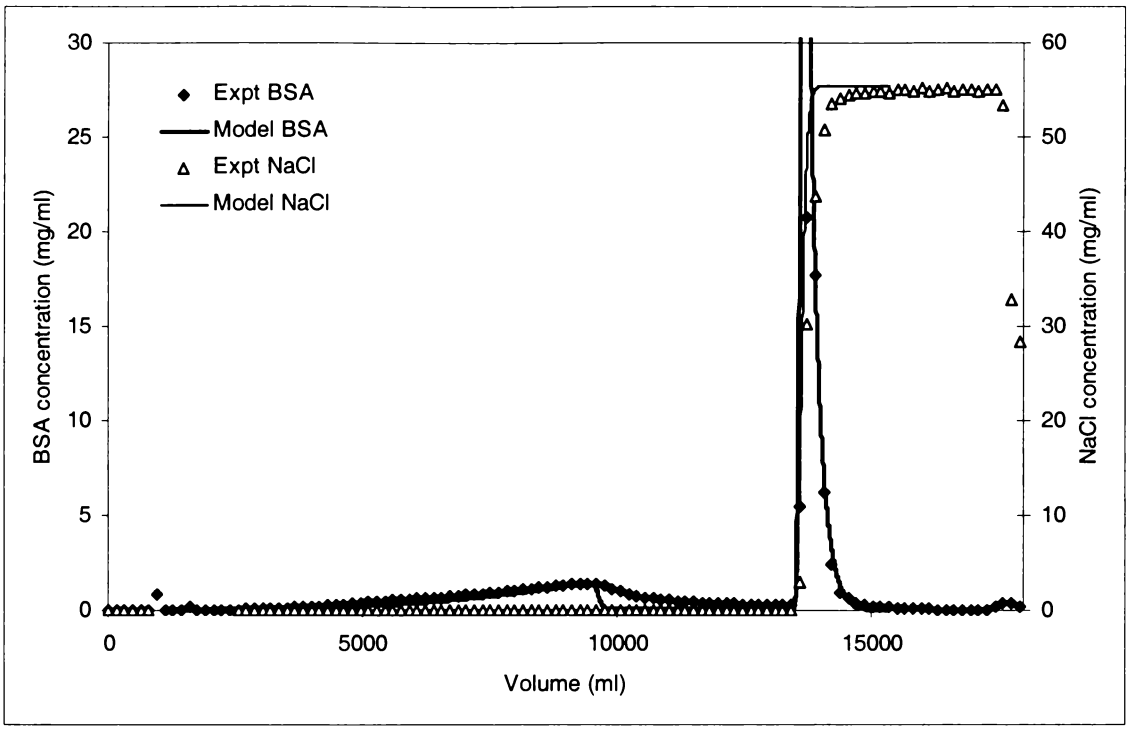

Figure 6-25. Breakthrough and elution profile for feed concentration of 2.3 mg/ml and 45 ml/min (Column 4 of Table 6-7).

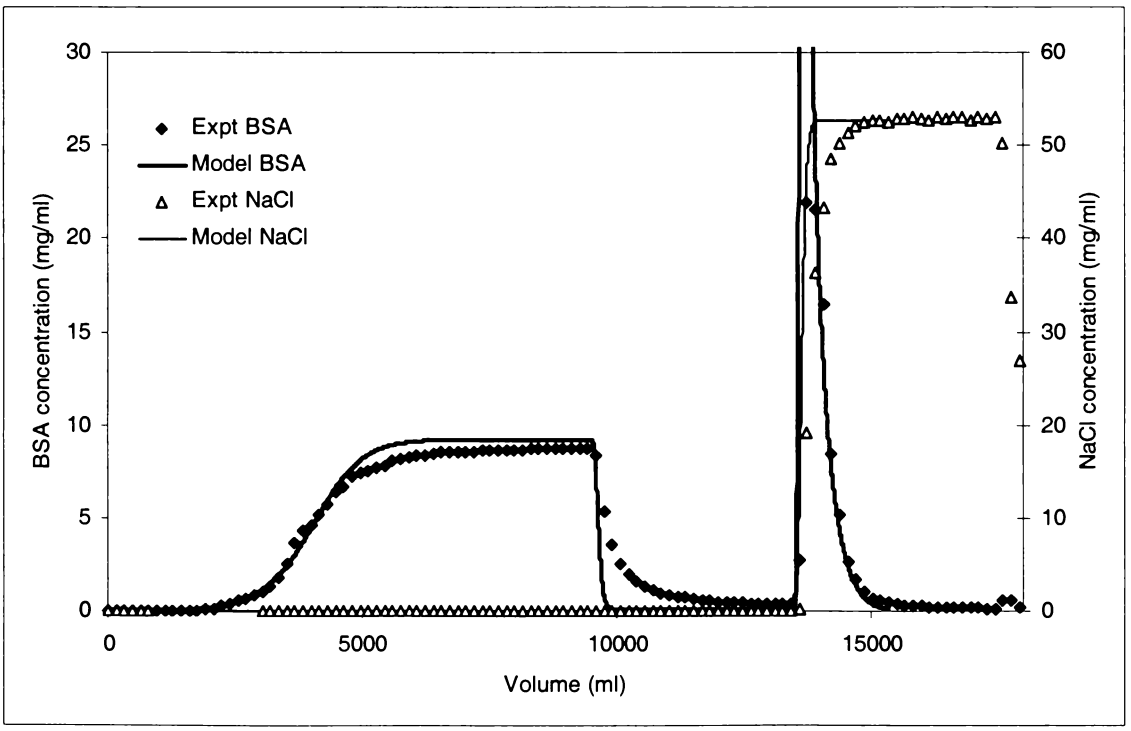

Figure 6-26. Breakthrough and elution profile for feed concentration of 9.3 mg/ml and 45 ml/min (Column 5 of Table 6-7).

Table 6-7. CRFC batch experimental conditions, model parameters obtained by curve fitting, and comparison of experimental and model results.

	Trial					
	1	2	3	4	5	6
Experimental conditions						
Flowrate (ml/min)	20	45	80	45	45	45
C_{feed} (mg/ml)	4.78	4.59	4.76	2.33	9.25	4.59
Mass loaded (mg)	38267	36696	38099	18646	73348	36696
Model parameters						
K_A (ml/mg.s)	47	47	47	47	47	47
k_{A1} (ml/mg)	0.00015	0.0002	0.00035	0.0003	0.00025	0.0085
C_{RAmax} (mg/ml)	115	110	100	110	145	110
k_{fA} (cm/s)	0.00005	0.0005	0.0006	0.0005	0.0005	0.0002
K_d (ml/mg.s)	45	45	45	45	40	60
Experimental results						
Mass fraction						
In breakthrough effluent	0.52	0.51	0.55	0.25	0.63	0.51
In wash effluent	0.10	0.10	0.12	0.12	0.10	0.10
Retained by column	0.39	0.39	0.33	0.63	0.27	0.39
Model results						
Mass fraction						
In breakthrough effluent	0.51	0.52	0.57	0.18	0.67	0.51
In wash effluent	0.05	0.04	0.04	0.03	0.04	0.08
Retained by column	0.44	0.44	0.39	0.78	0.29	0.40

Experimental and model concentration profiles were integrated to estimate BSA mass in effluent during loading (1350 to 9350 ml in Figure 6-26) and wash (9350-13350 ml) (Table 6-7). Mass retained on the column was then determined by mass balance. Predicted effluent mass during breakthrough was up to 4% greater than experimental results, except for loading 2.3 mg/ml feed where simulated mass loss was 7% lower than found experimentally. Low k_{A1} values caused the simulation to underestimate protein desorption during the wash step, so predicted wash effluent mass was two to four times lower than found experimentally. Predicted mass retained by the column was 2-6% higher than experimental results, except for loading 2.3 mg/ml, which was 15% higher.

A simulation using BSA parameters obtained from axial column work (column 6 in Table 6-7) predicted that the CRFC should exhibit excellent performance (Figure 6-27). This simulation correctly estimated protein desorption rate during the wash step and mass estimates were within 2% of experimental data.

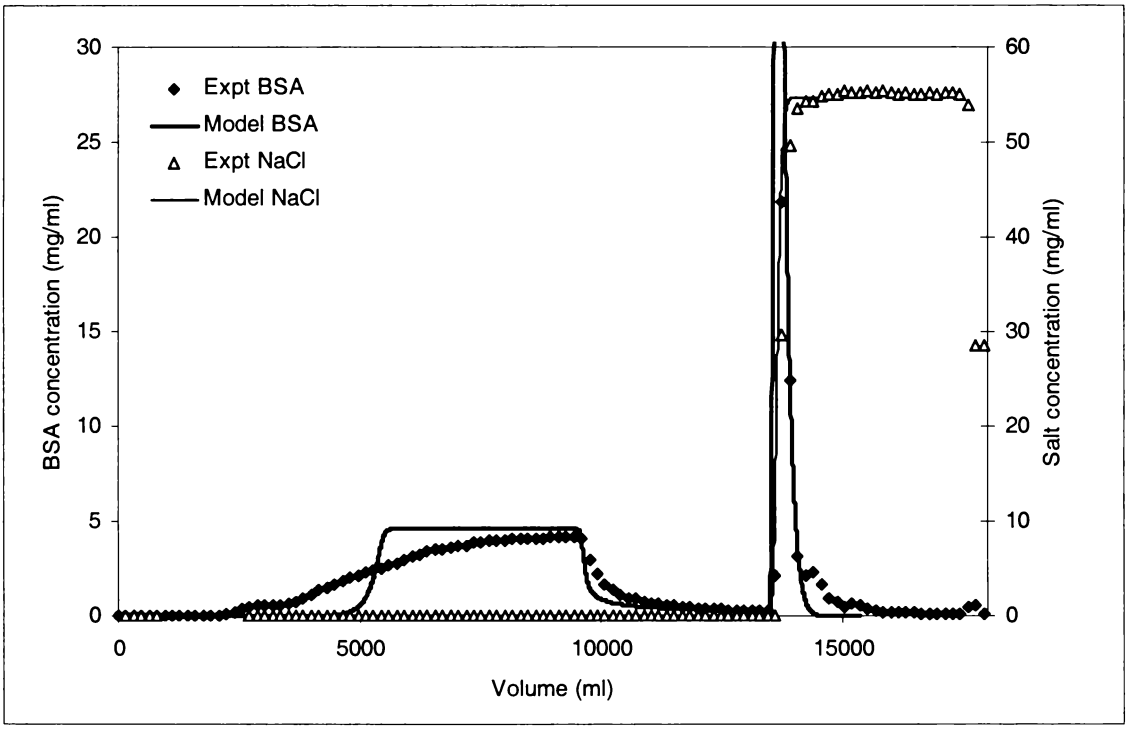

Figure 6-27. Breakthrough and elution profile for feed concentration of 4.5 mg/ml and 45 ml/min (Column 6 of Table 6-7), comparison with model parameters obtained from small column breakthrough experiments.

Fluid velocity and bed depth did not contribute to the decrease in column resolution. Average interstitial velocities were similar to those in the axial column, and did not vary greatly with radius (Figure 6-28). Predicted k_{fA} values also did not change greatly with radial position (Figure 6-29) except for the 80 ml/min trial (A constant k_{fA} was assumed for simulations). CRFC breakthrough curves were only slightly affected by flowrate, indicated by k_{A1} increasing slightly with flowrate (Table 6-7). The CRFC bed depth was 0.5 cm longer than the axial flow column. Extra-column dispersive effects, except for the flow manifold, were negligible. Bed integrity tests after each trial eliminated channelling as a possibility. If channelling occurred, the resin was removed and cleaned, the annulus repacked and the trial repeated.

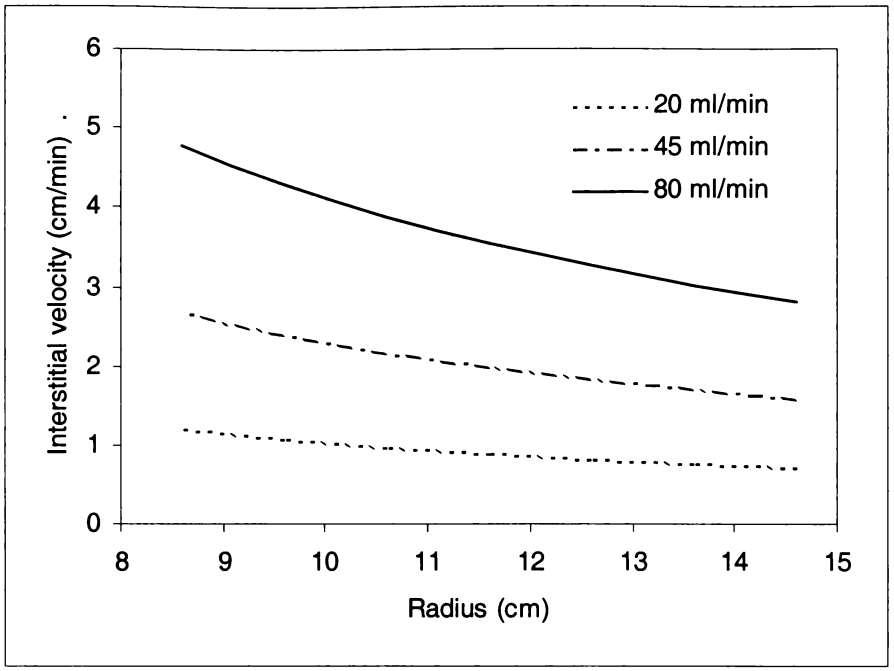

Figure 6-28. Interstitial velocities in the annular bed for three flowrates used in batch CRFC trials.

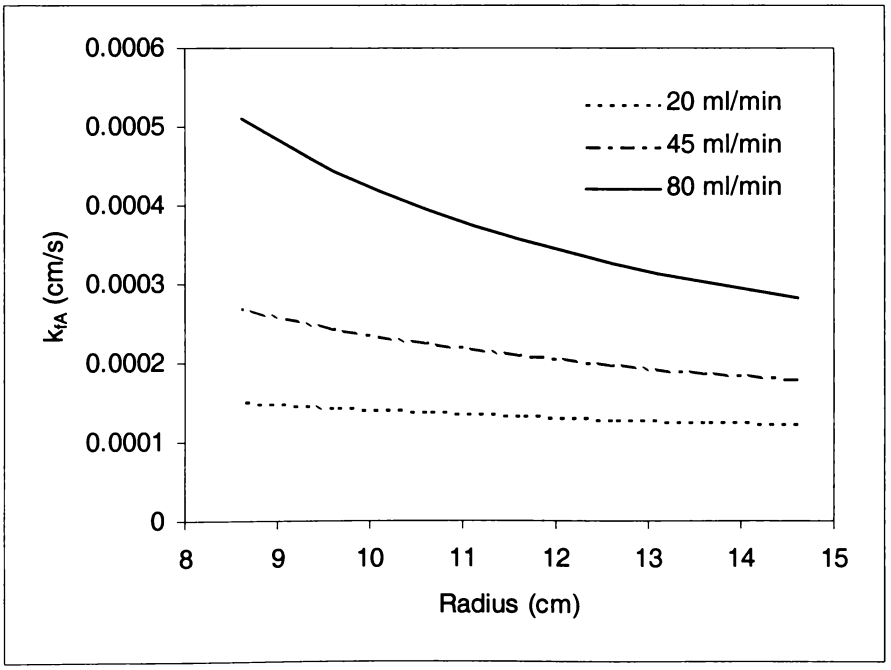

Figure 6-29. k_{fA} values with radial position for three flowrates used in batch CRFC trials (calculated from Figure 6-10).

Decrease in resolution could be because flow in the CRFC is distributed over 140 - 238 times the axial column area (Table 6-8). Giddings (1966) noted that axial column resolution decreases with increasing diameter. The CRFC half-way through the annulus has an area the equivalent of a 9.6-cm diameter axial column, so it is not suprising that resolution was affected. Fouling and wall effects could also contribute to the decrease in resolution.

Table 6-8. Comparison of areas normal to flow for CRFC and axial flow column.

	Column diameter (cm)	Area normal to flow (cm^2)	Ratio annulus area to area axial column	Diameter of axial flow column with same area (cm)
O.D. annulus	14.6	91.7	238.4	10.81
Mid.D. annulus	11.6	72.9	189.4	9.63
I.D. annulus	8.6	54.0	140.4	8.29
I.D. axial column	0.7	0.4	1.0	0.7

6.4.4 Flow distribution

The differences between rate parameters obtained in the small column batch experiments and radial flow experiments may be due to solute and flow distribution in the CRFC outer feed and inner exit chambers. Extending tailing during wash indicates stagnant zones in the chambers. Instantaneous solute distribution was assumed for CRFC simulations, which may be incorrect.

Solute distribution throughout a section during a step change in concentration was simulated by assuming sideways flow was constant with height, and modelling the section as a series of 19 well-mixed tanks of equal volume (Figure 6-30) (Appendix J). The volume of each outer chamber section is approximately 6 ml. Solution enters the bottom of the section at the centre through a 3-mm by 3-mm hole at 5 ml/min (40 ml/min total), at approximately 1 cm/s. Therefore buffer near fluid entry should be well mixed. If the resin bed and annulus walls generate sufficient back pressure so flow into the annulus is uniform with angle, then buffer flows to the section ends and fluid velocity decreases with distance from the fluid entry point.

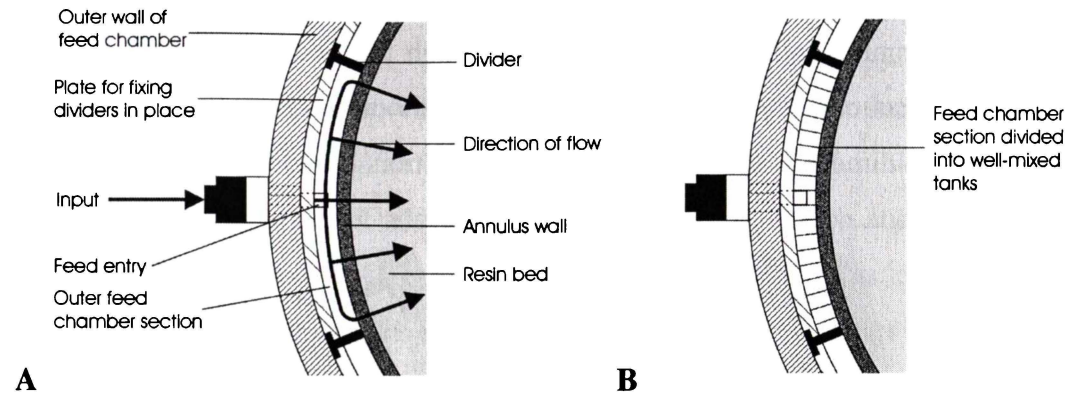

Figure 6-30. A) Cross section of feed chamber section. B) Division of feed chamber section into well mixed tanks for modelling solute distribution.

Buffer took longer to reach the feed input concentration as distance from feed entry increased (Figure 6-31), so assuming instantaneous solute distribution was incorrect. Therefore feed and exit chambers contribute to differences in model rate parameters between the small axial column and the CRFC. The CRFC should perform better with smaller volume outer feed and inner exit chambers because solute distribution will be faster.

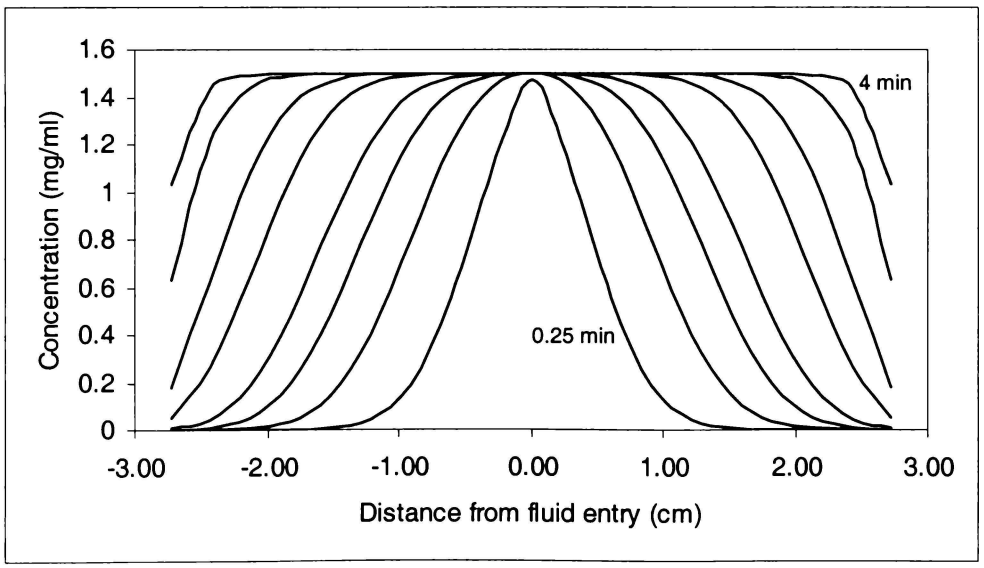

Figure 6-31. Concentration profile in a feed chamber section at different times for a step change in solute concentration.

Future investigation on CRFC flow distribution could be readily done using plates with different profiles in the feed and exit chamber sections (Figure 6-32). The effect of the

feed chamber sections on flow distribution could be examined through a transparent lid on the CRFC annulus, allowing dye passage through the bed to be observed. Flow distribution effects could be incorporated into models of radial flow by adapting the continuous three-dimensional model developed in Section 4.5.2 for batch operation.

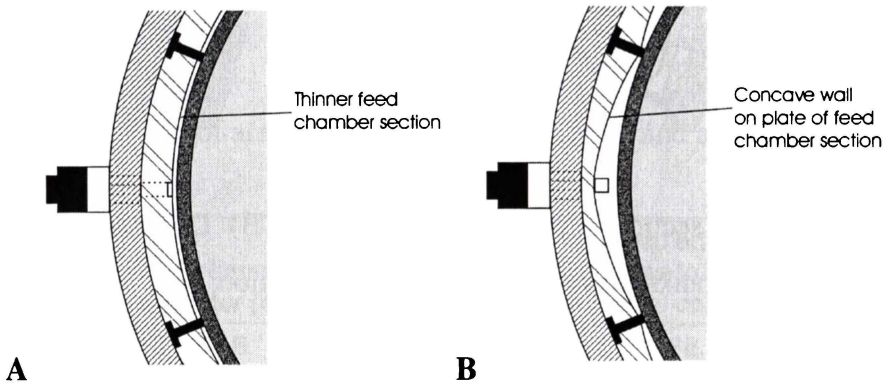

Figure 6-32. Feed chamber sections with: A. reduced volume by having thicker plates holding the dividers in place or B. concave plates.

6.4.5 Wall effects

Wall effects, where solution flows faster between the resin and top and the bottom of the annulus, because interstices are larger in those regions could explain the difference between model parameters obtained for the small axial flow column and the CRFC. This was discounted however as the CRFC had a much greater aspect ratio (defined in Section 2.6.2.1) than the axial column (Table 6-9). If wall effects predominate, CRFC performance would be better than the axial flow column because it has a greater aspect ratio.

Table 6-9. Aspect ratios for the 1-ml axial flow column and the CRFC packed with 90-μm diameter resin.

	Axial Column	CRFC
OD (cm)	0.70	14.60
ID (cm)	0.00	8.60
Height/Length (cm)	2.50	2.00
Volume (ml)	0.96	218.65
Volume affected (ml)	0.02	0.98
Percentage affected	2.55	0.45
Aspect ratio	77.78	222.22

6.4.6 Resin fouling

Resin fouling could also cause differences in performance between the CRFC and axial flow column. Clean resin gave better CRFC performance than fouled resin (Figure 6-33). Resin fouling was not addressed in batch CRFC operation and extremely high back-pressures occurred (1586 kPa), resulting in the annulus welds cracking. Regeneration with 0.5M NaOH did not remove the fouling. However, fouling was removed when 1M NaOH solution was left in the CRFC overnight between continuous separation experiments.

Resin was discoloured in regions near corroding stainless steel by welds and around one packing port. This corrosion was attributed to chromium depletion in regions that had overheated during machining and welding the annulus. While ferrous ions would colour the resin, ion exchange performance should not be affected because the resin is an anion exchanger. Annulus corrosion would be more important if cation exchange resin was used.

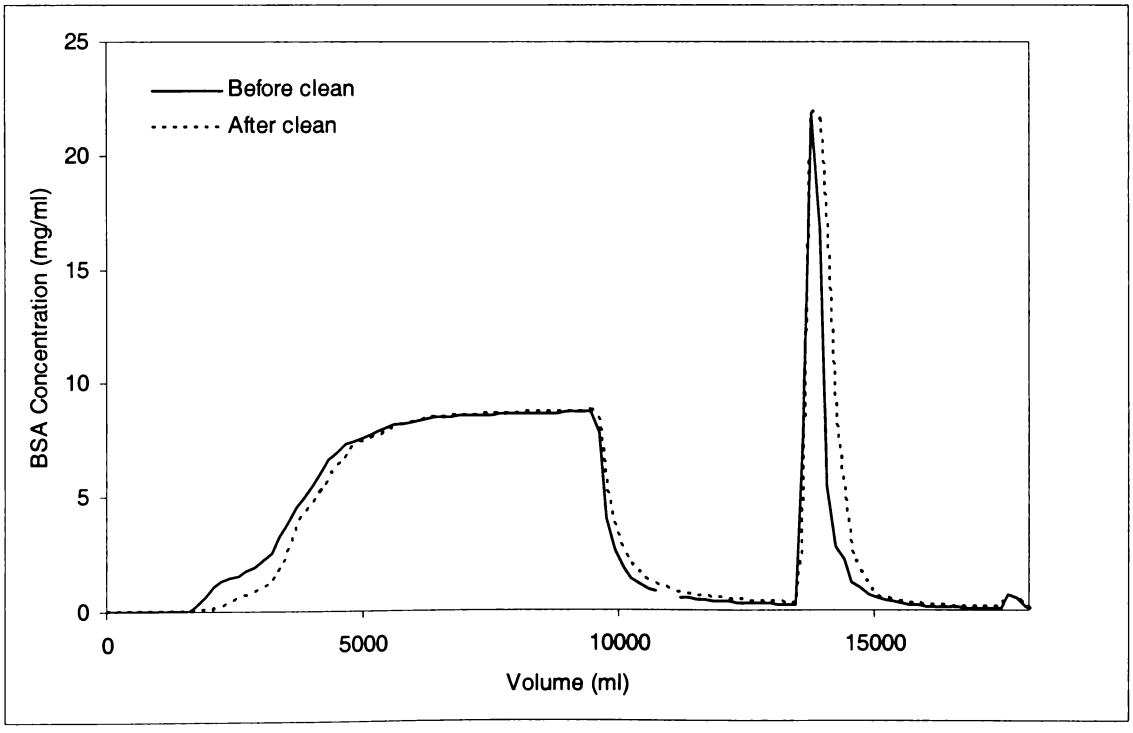

Figure 6-33. Breakthrough and elution profile before and after unpacking and cleaning resin for loading with 9.3 mg/ml feed at 45 ml/min.

6.5 Single component continuous extraction

Seven continuous trials were done to investigate the effect of rotation speed, divider angle and repeated operation on CRFC performance for BSA adsorption and desorption. The first three trials used the same conditions; in trials four and five the outer divider angles were changed relative to the inner exit chamber dividers; and different rotation speeds were used in trials six and seven (Table 6-10). Usually all the volume and NaCl applied and 70-93% of the BSA could be accounted for during sample collection (Table 6-11). BSA profiles show the CRFC could continuously extract BSA from feed applied to one section and elute it in another section.

6.5.1 Initial trials

BSA was applied to section 1 (Position 1) and eluted in section 5 (Position 5) in the first three trials (Figure 6-34). Concentrations were averaged over 45 degrees for each section. The CRFC was operated at 46-49 minutes per revolution (7.3 to 7.8 degrees per minute) and the outer feed chamber dividers were aligned with the inner exit chamber dividers (i.e. 0 degrees).

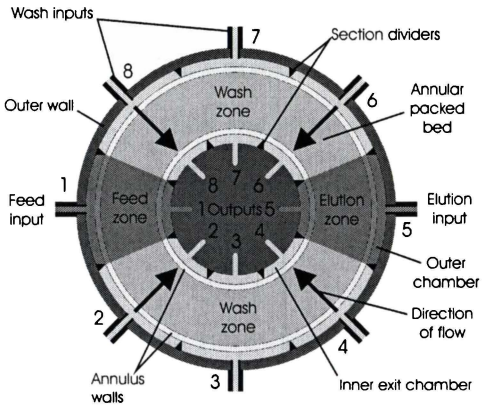

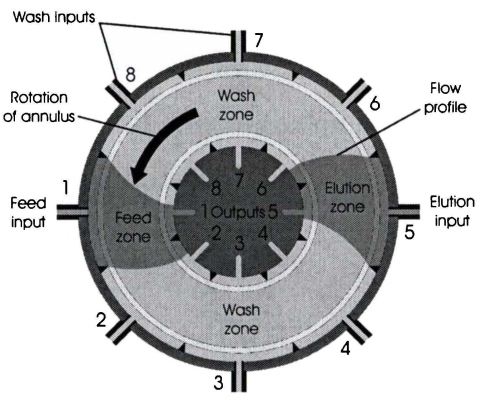

Figure 6-34. Expected buffer flow profiles at 40 ml/min for A) when the annulus is stationary and B) the annulus is rotating at 48 min/rev.

Table 6-10. Summary of run data for continuous single component adsorption and elution.

Trial	BSA (mg/ml)	NaCl (mg/ml)	Rotation speed (min/rev)	Divider angle (degrees)	Run time before collection (min)	Collection time (min)	Total run time (min)	Revolutions completed during collection
1	1.53	59.1	45.5	0	160.2	181.8	342.0	4.0
2a	1.50	58.7	48.0	0	203.5	182.5	386.0	3.8
2b	1.50	58.7	48.0	0	-	190.0	576.0	4.0
2c	1.50	58.7	48.1	0	-	190.0	766.0	4.0
3	1.51	59.0	49.2	0	180.0	194.3	374.3	4.0
4	1.50	56.3	47.9	15	175.7	188.7	364.4	3.9
5	1.50	59.4	46.4	30	180.3	183.7	364.0	4.0
6	1.50	58.5	12.6	0	180.0	188.1	368.1	15.0
7	1.50	58.4	31.1	0	180.0	186.5	366.5	6.0

Table 6-11. Volume and mass fraction results from continuous single component adsorption and elution experiments.

Trial	Recovery						
	Volume	NaCl		BSA			
		Before collection	During collection	Before collection	During collection	Total before overnight clean	Total after overnight clean
1	1.00	-	0.99	-	0.70	-	-
2a	1.01	-	0.97	-	0.75	-	-
2b	1.01	-	0.96	-	0.86	-	-
2c	1.00	-	0.98	-	0.87	-	-
3	1.00	0.94	1.00	0.66	0.93	1.03	1.11
4	1.00	0.95	1.01	0.74	0.92	1.05	1.08
5	1.01	0.92	1.01	0.66	0.79	0.98	1.00
6	1.01	0.91	0.96	0.71	0.91	1.01	1.03
7	1.00	0.92	1.03	0.66	0.86	0.98	1.00

The BSA peak begins at position 4 and finishes at position 7, showing that adsorption had occurred (Figure 6-35). If no binding was occurring, BSA would exit at positions 1 and 2 given a buffer residence time of 2 min at 40ml/min (Table 6-12) (angular displacement is 14.5-15.4 degrees). Tailing before the peak is due to low concentrations of NaCl in the resin (Figure 6-35). BSA exiting at position 4 is possibly due to solute contamination from feed and exit section 5. The NaCl peak occurred over positions 5 to 7, reaching 38% of the starting elution concentration in position 6, and showed tailing in the remaining sections. This suggests some NaCl is retained in the resin and gradually diffuses out with time.

Table 6-12. Dimensions and volumes of the CRFC annulus (2 cm high).

	O.D. (cm)	I.D. (cm)	Volume (ml)	ε	Void volume (ml)
Outer wall	15.2	14.6	28.09	0.25	7.02
Resin bed	14.6	8.6	218.65	0.31	67.78
Inner wall	8.6	8	15.65	0.25	3.91
				Total volume (ml)	78.72
			Residence time (min) (at 40 ml/min)		1.97

NaCl mass balances close within 4%. However, only 70% of BSA applied during sampling was recovered indicating that BSA was accumulating in the annulus. A twelve hour trial (trial 2) showed that the CRFC had not reached steady state with an 87% mass recovery (trial 2c). In further trials all CRFC effluent, including from cleaning, was collected and analysed. Mass recoveries before cleaning overnight closed with 5%. Improving sample collection recovery over trials 1-3 may be an artefact of declining resin capacity due to BSA fouling. Fouling caused CRFC backpressure to steadily increase until trial 3, after which regeneration solution was left in the column overnight. Because the resin was in the elution zone for only six minutes each cycle, not all the BSA was eluted. Mass recovery may be improved by increasing elution zone size and reducing rotation speed.

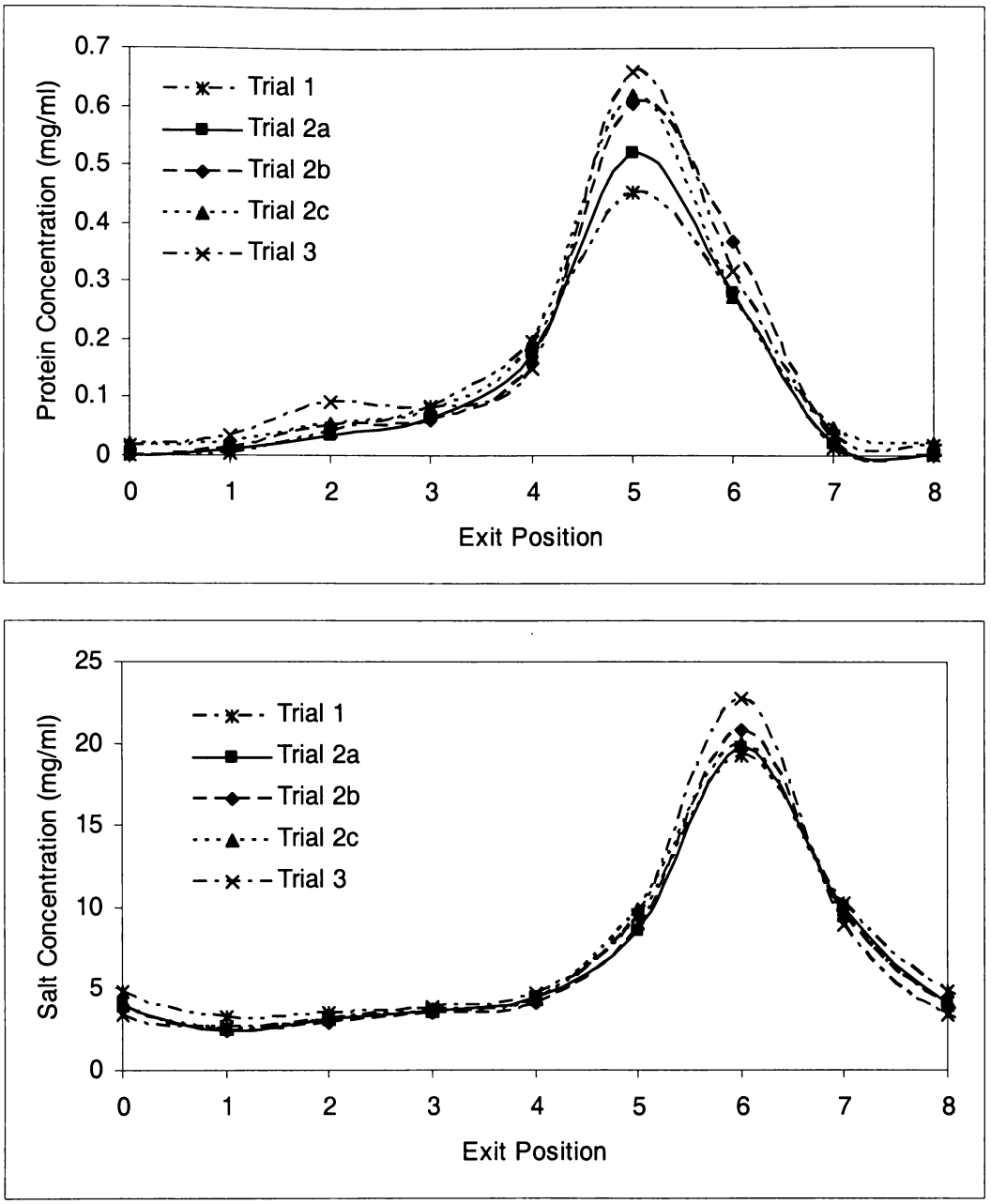

Figure 6-35. BSA and NaCl concentration profiles for trials 1 to 3 at 46-49 min/rev, 0 degree divider angle, flowrate 40 ml/min, 1.5 mg/ml BSA feed, 58 mg/ml NaCl elution.

6.5.2 Changing divider angles and rotation speed

The BSA elution profile shifted when outer dividers were moved 15 and 30 degrees (trials 4 and 5 respectively) anticlockwise to the inner exit chamber dividers (Figure 6-36). The majority of protein eluted in section 6 rather than section 5 (Figure 6-37) indicating the BSA peak occurred close to the divider separating exit sections 5 and 6 for 0 degree divider angle. The majority of NaCl eluted in section 6 at 0 degree divider angle (Run 3), probably near the middle of section 6, so when the divider angle was adjusted, more NaCl entered section 7 (Figure 6-37). Slight differences in rotation speeds between trials 3-5 (Table 6-10) should not affect results, because there was only 0.9 degrees difference in angular displacement between trials.

The BSA and NaCl elution peaks broadened with increasing rotation speed. An increase in angular displacement due to higher rotation speed (31 min/rev, trial 7) caused the majority of BSA to elute in position 6 compared to position 5 for 48 min/rev. The BSA and NaCl elution profile was spread out over five sections for 12.5 min/rev (trial 6).

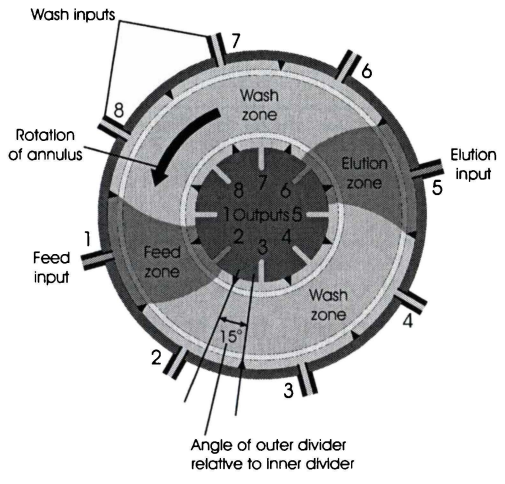

Figure 6-36. Expected buffer flow profiles through the CRFC for 48 min/rev and 40 ml/min for A) 15 degree and B) 30 degree divider angle.

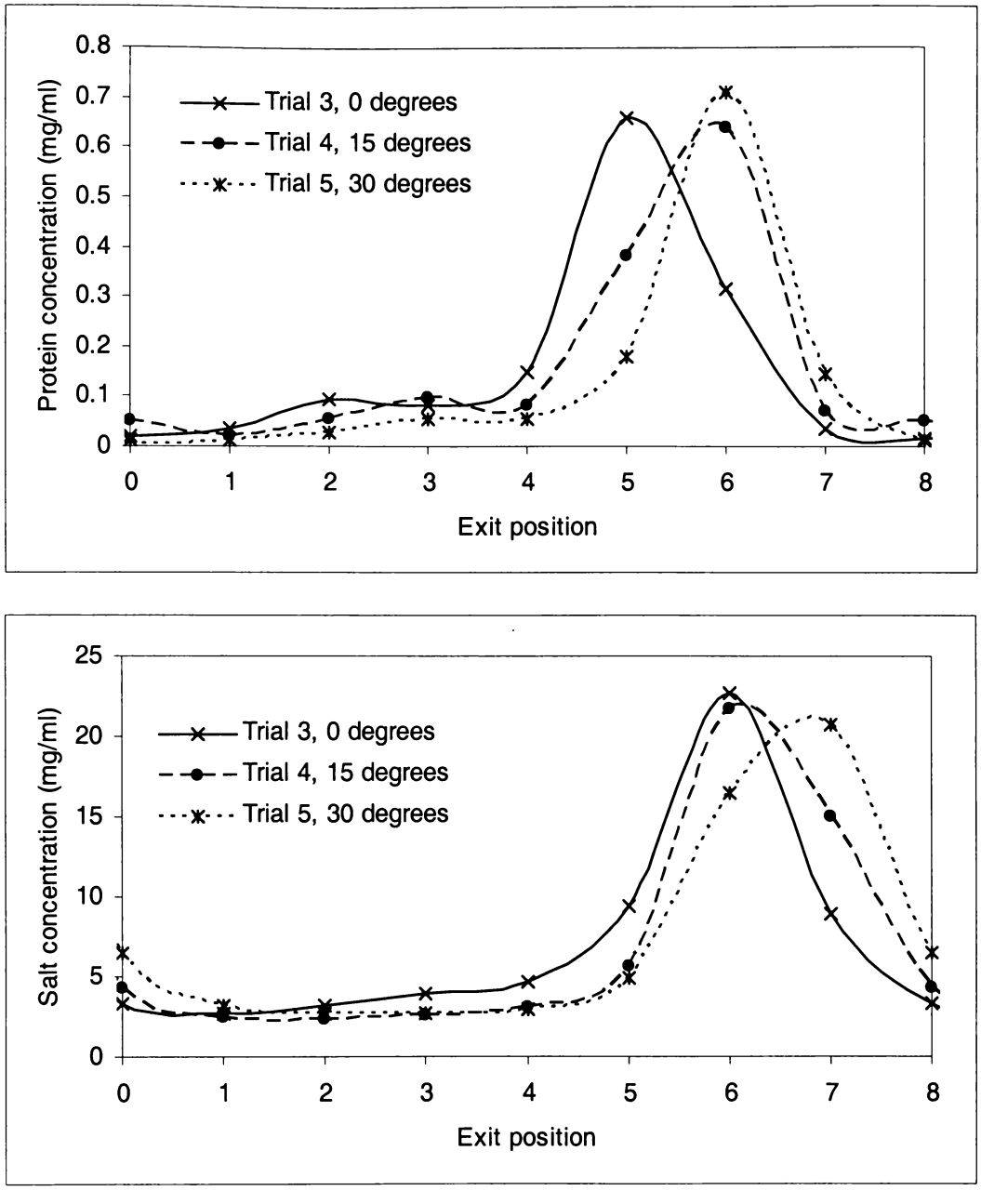

Figure 6-37. Effect of divider angle of concentration profiles for A) BSA and B) NaCl. Trials 3 to 5 at 49-46 minutes per revolution, different divider angles, total flowrate 40 ml/min, feed 1.5mg/ml BSA, elution 58 mg/ml NaCl.

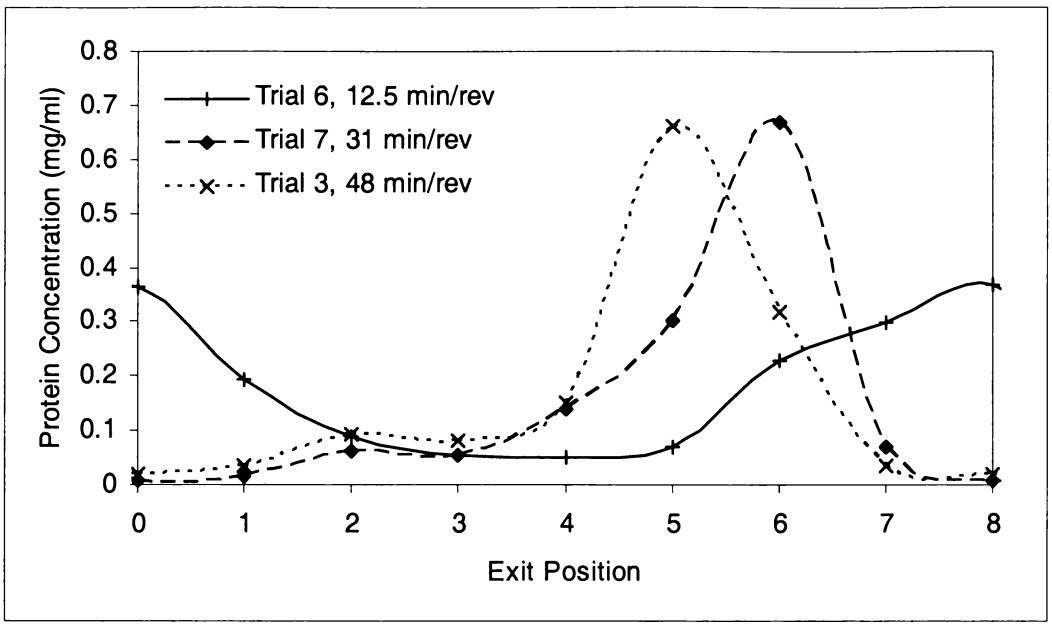

A)

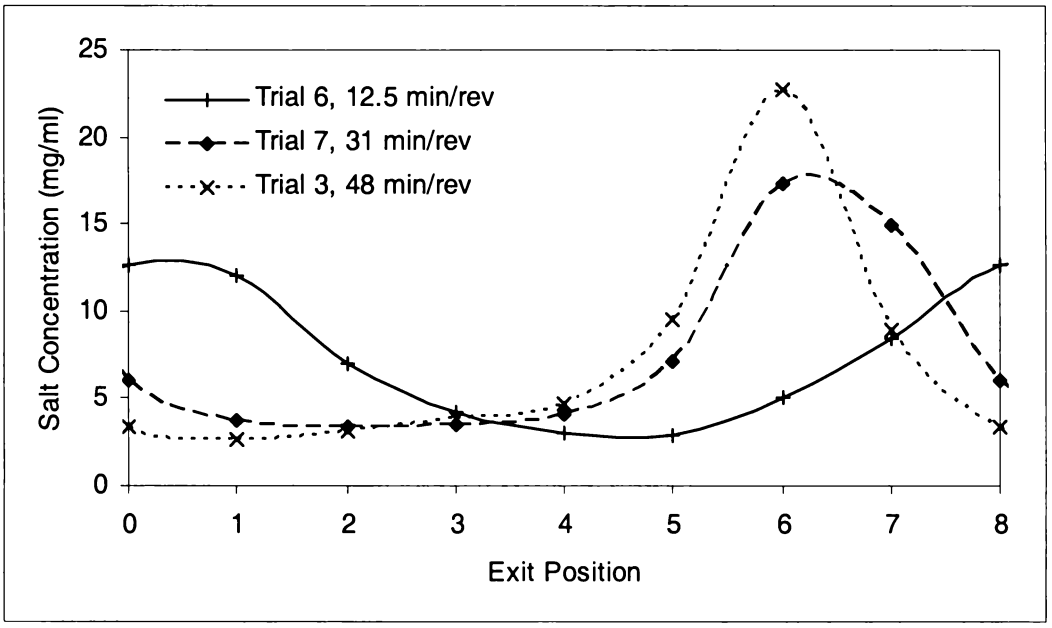

B)

Figure 6-38. Effect of rotation speed on concentration profiles for A) BSA and B) NaCl. Trials 3, 6 and 7, 0 degree divider angle, total flowrate 40ml/min, feed 1.5 mg/ml BSA, elution 58 mg/ml NaCl.

6.5.3 Operational aspects of the CRFC

The CRFC performed consistently well during continuous trials, showing that the prototype was robust and reliable, an important requirement for experimental work. Aspects of CRFC operation such as fouling, exit flowrates, bed integrity, rotation speed and surface pitting around seals are discussed in the following sections.

6.5.3.1 Fouling

The CRFC operating pressure steadily increased with each run due to BSA fouling the resin. The pressures during the third run reached 345 kPa. Regeneration buffer strength was increased to 1M NaOH and left in the column overnight to remove accumulated BSA. This cleaning step resulted in more BSA being recovered than was applied, but the excess gradually decreased in subsequent trials (Table 6-11) and operating pressure only reached 227 kPa.

Fouling will reduce the CRFC operation time between CIP cycles. The resin, feedstock and feed concentration will influence the extent of fouling. To prevent significant fouling, feedstocks such as fermentation media, milk or whey would need to be clarified before being processed by the CRFC.

6.5.3.2 Exit flowrates

Flowrates of solution leaving each exit section were consistently within 4.75 to 5.25 ml/min (Figure 6-39). There were outliers at positions 1, 5 and 8 for runs 2, 3 and 7. For runs 2 and 7, reduced flowrates through positions 1 and 8 would not affect elution results as no BSA was eluting through those positions. For run 5, the flowrate of 4.5 ml/min in section 5 should not significantly affect results at it only results in a displacement difference of 2.5 degrees at 31 min/rev.

6.5.3.3 Bed Integrity

The CRFC was operated for a total of 55 hours for continuous operation and 31 hours for equilibration and regeneration (not including overnight cleaning) without channels forming. Bed integrity tests indicated bed dynamics had changed (Figure 6-40).

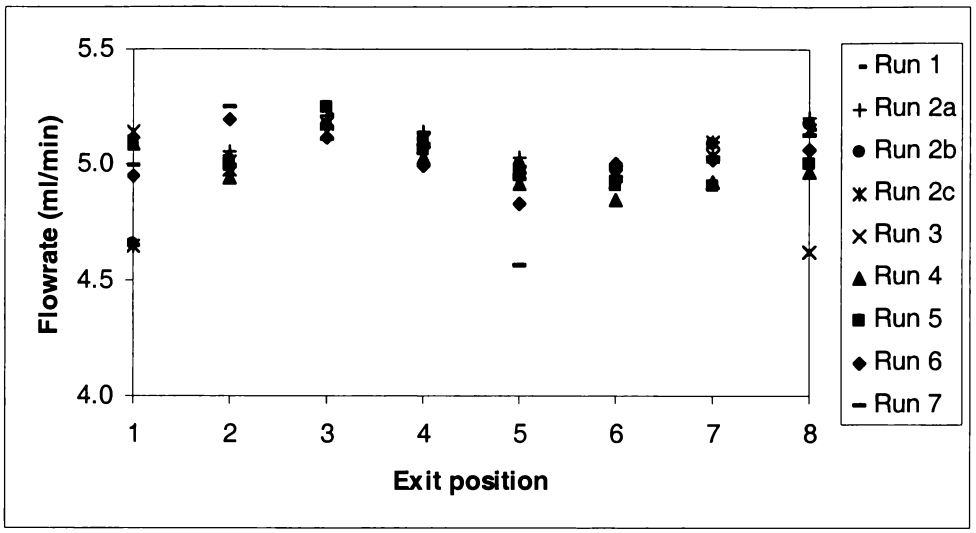

Figure 6-39. Effluent flowrate data for the continuous runs.

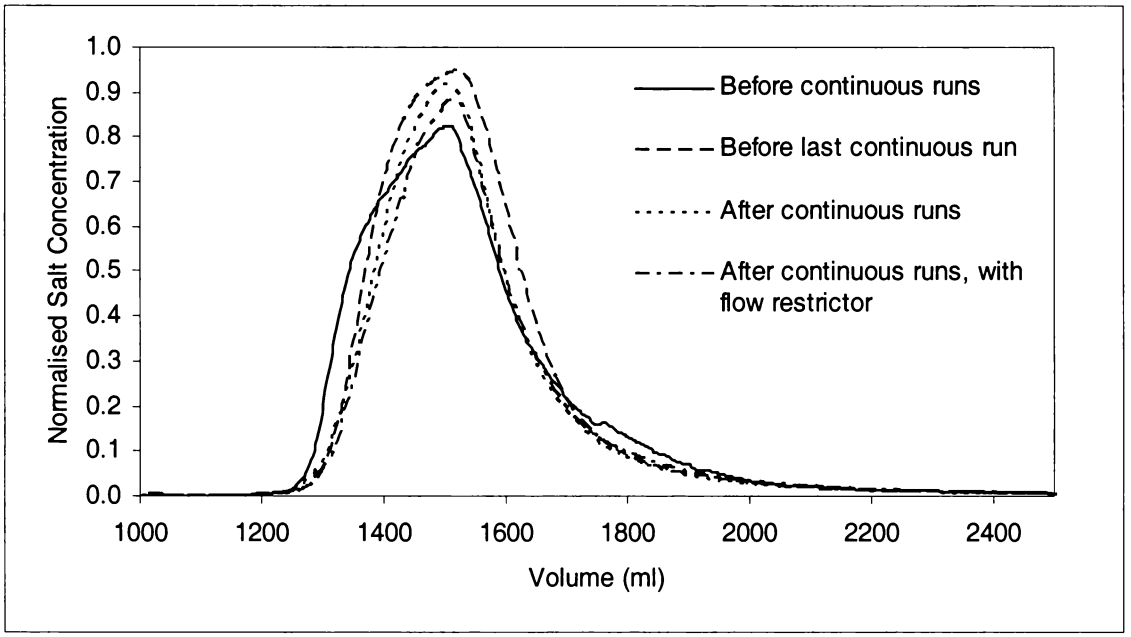

Figure 6-40. Bed integrity tests before and after continuous experiments.

Peak profiles had improved after CRFC operation, presumably because the bed settled after packing. The flow restricting tubes used to control flow from the exit section had little effect on performance.

Bed stability is very importance for preparative applications because column repacking takes valuable processing time. The short bed height of the annulus in the CRFC prototype prevented settling forming a significant channel at the top of the bed.

Channeling from bed settling may occur more readily in a large scale column due to the greater bed height. Alternate packings such as monolithic beds, which have good bed stability but low loading capacity, could be used in a large scale CRFC.

6.5.3.4 Rotation speed and seal surface pitting

Annulus rotation speeds was constant after an hour of operation (Figure 6-41) indicating that the mechanism for rotating the CRFC annulus was reliable and consistent.

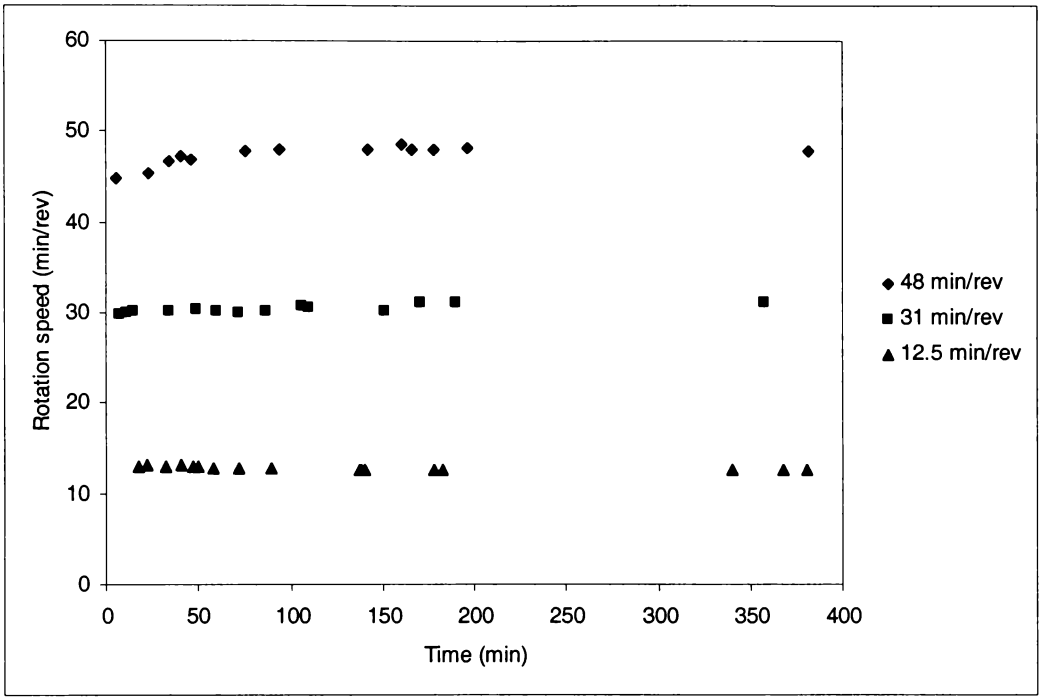

Figure 6-41. Rotation speed of annulus over time.

During initial testing, the annulus began shuddering while rotating and seals around the annulus began to seep under pressure. Visual inspection of the dismantled CRFC revealed that the stainless steel surfaces in contact with the o-rings were pitted. The shuddering was due to the o-rings gripping the pitted surfaces briefly slowing annulus motion. Seal contamination and an acidic environment around the seals probably caused the pitting. Pitting did not occur during the continuous experiments, presumably because the alkaline regeneration solution left in the CRFC overnight prevented corrosion. The pitting was easily removed by polishing the surfaces. Pitting is not desirable for large scale CRFC and future prototypes would need a different sealing system that prevented seal contamination and pitting from occuring.

6.5.4 Comparison of simulation and experimental data

The FD-ML model for continuous extraction using the CRFC (Section 4.5.1) was fitted to experimental data. One set of parameters was obtained that gave good agreement for the operating conditions used (Table 6-13). Radial and angular dispersion was neglected. Comparisons of simulated and experimental data are shown in Figures 6-42 to 6-43 and Figures I.7-1 to I.7-12.

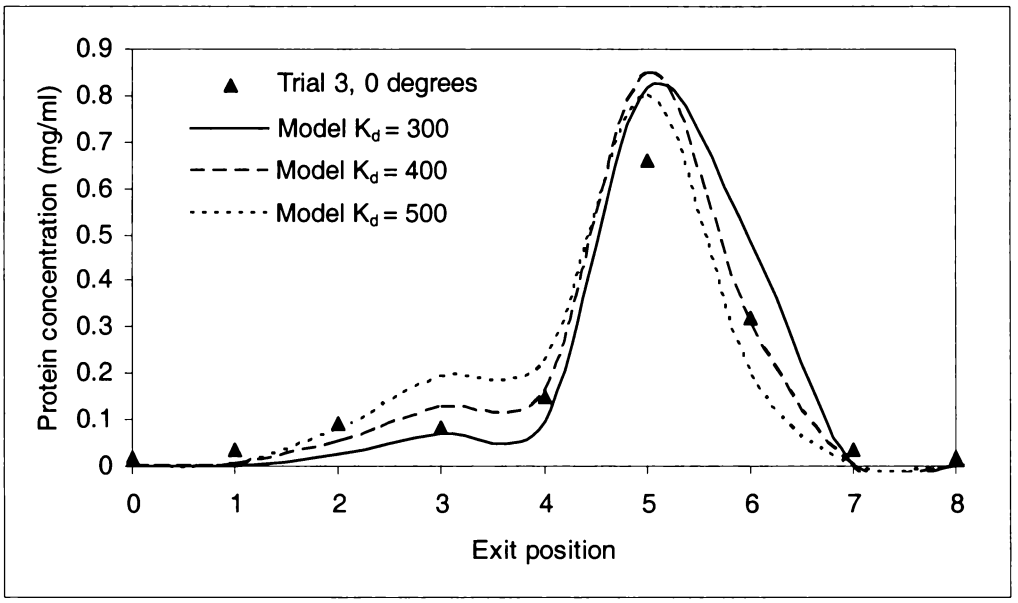

A)

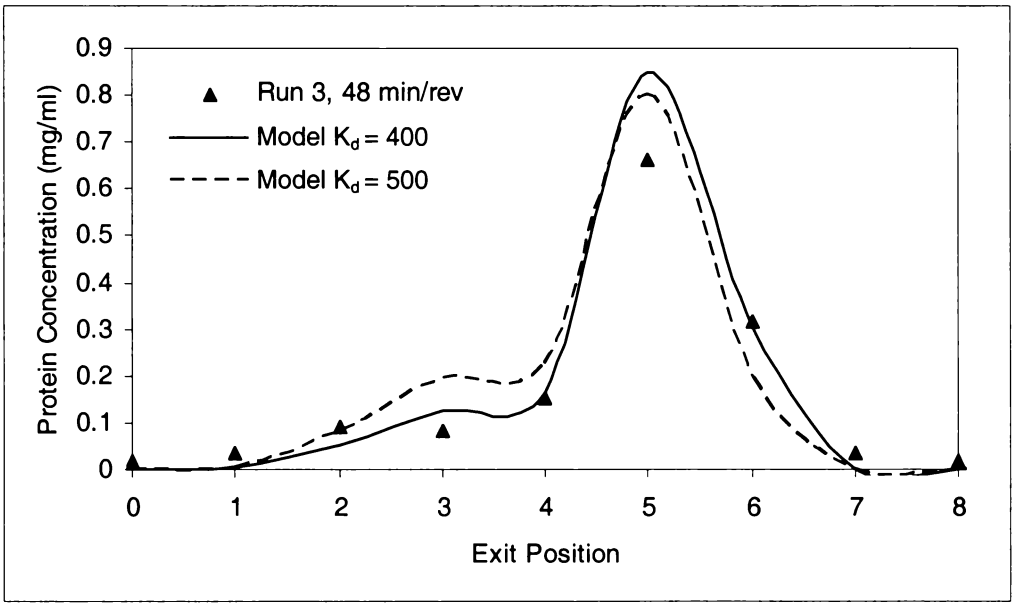

B)

Figure 6-42. Effect of changing ε_p on predicted profiles for BSA elution profiles for 48 min/rev and 0 degree outer divider angle, A) ε_p = 0.72, B) ε_p = 0.9. Model parameters given in Table 6-13.

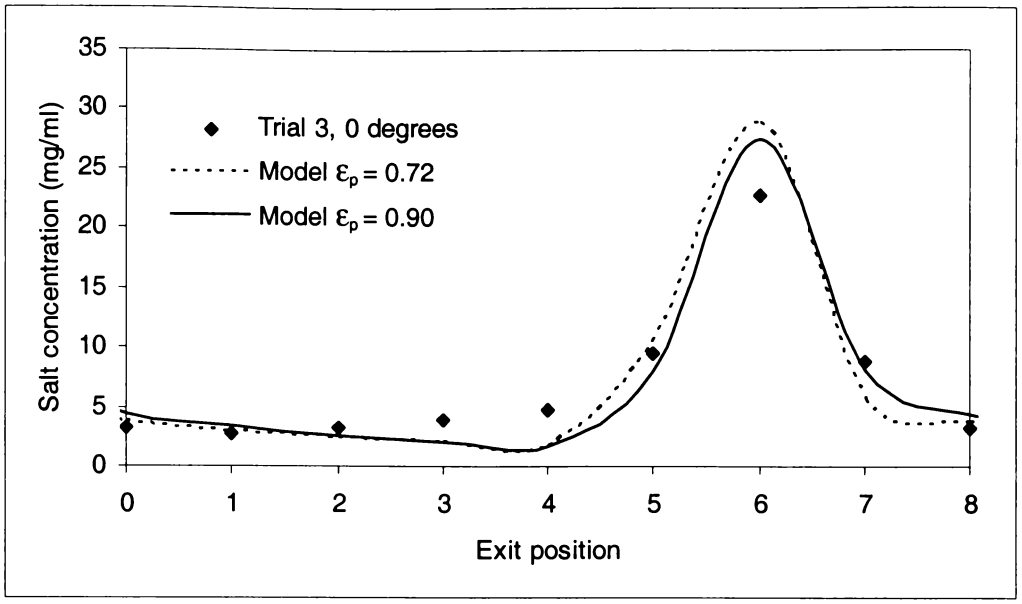

Figure 6-43. Effect of ε_p on NaCl elution profile for 48 min/rev and 0 degree outer divider angle, ε_p = 0.72 and 0.9. Model parameters given in Table 6-13.

Table 6-13. Parameters for simulating BSA and NaCl concentration profiles from continuous experiments and comparison to axial column parameters from small column batch experiments.

BSA				NaCl		
Parameters	Continuous	Axial		Parameters	Continuous	Axial
k_{fA} (cm/s)	0.0001	0.00016		k_{fB} (cm/s)	0.00005	0.0001
K_A (ml/mg)	47	47		K_B (ml/mg)	0.15	15
k_{A1} (ml/mg.s)	0.003	0.0085		k_{B1} (ml/mg.s)	0.00015	0.003
k_{A2} (1/s)	0.00006	0.000181		k_{B2} (1/s)	0.001	0.0002
C_{RAmax} (mg/ml)	72	69		C_{RBmax} (mg/ml)	56	1
n_A	1	1		n_B	1	1
K_d (ml/mg)	400	350-2000				

ε_R = 0.31 and ε_p = 0.72 and 0.9.

6.5.4.1 NaCl simulation

The FD-ML model correctly predicted NaCl exit position using parameters obtained from axial column experiments (Table 6-13), but gave higher peaks than obtained in experimental results and did not predict the tailing. Tailing suggested that NaCl was being held in the resin and then diffusing out. This could be simulated using an unrealistic C_{RBmax} of 56 mg NaCl per ml resin. However, C_{RBmax} itself was insufficient to change the NaCl concentration profile (Figure 6-44) so k_{B1} and k_{B2} parameters were adjusted so NaCl desorbed five times faster (Table 6-13) to give a better fit (Figure 6-43).

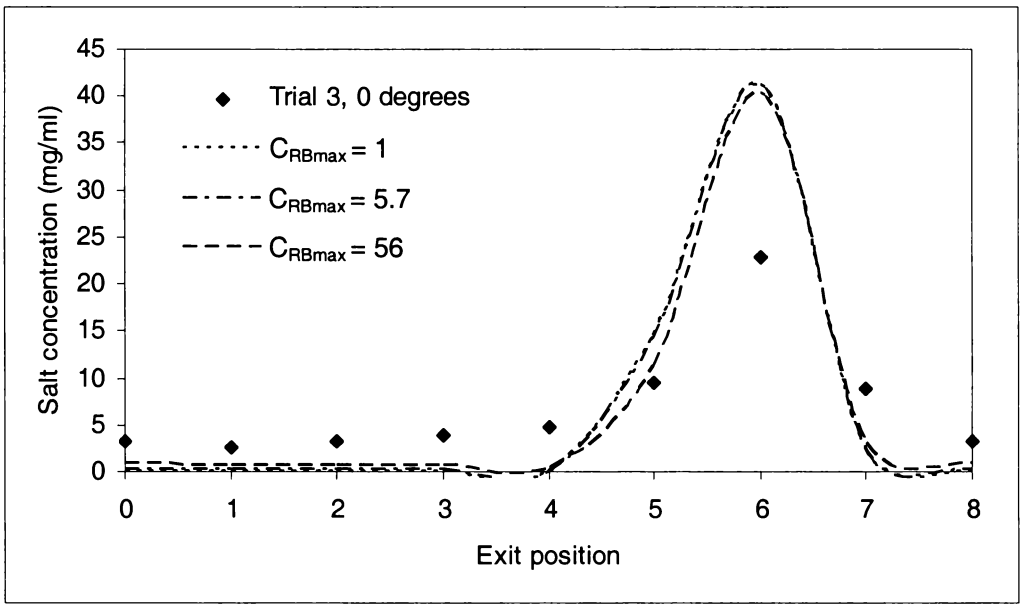

Figure 6-44. Effect of C_{RBmax} on simulated NaCl profiles at 48 min/rev, and divider angle 0 degrees. Model parameters shown in Table 6-13. k_{B1} = 0.003 ml/mg.s, k_{B2} = 0.0002 1/s.

Decreasing the value of diffusion rate k_{fB} broadened the NaCl profile until equal concentrations of NaCl appeared in exit positions 5 and 6, but did not give the tailing found in experimental data (Figure 6-45). A higher ε_p of 0.9 gave a better fit with some experimental data (Figures I.7-1 to I.7-12) which suggests that resin porosity ε_p or external void fraction ε_R was higher than experimentally determined.

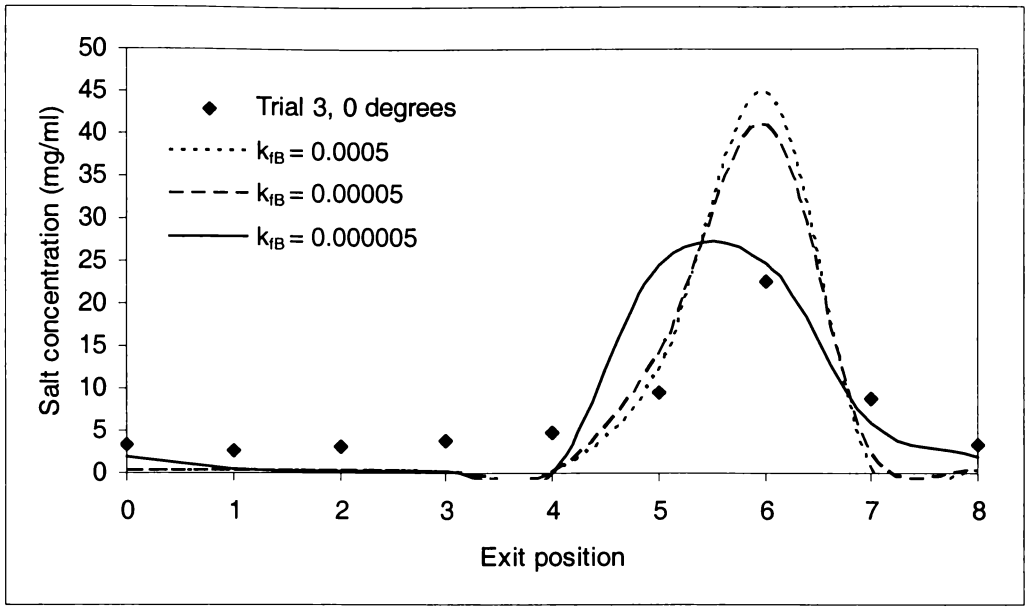

Figure 6-45. Effect of k_{fB} on NaCl concentration profile at 48 min/rev, and divider angle 0 degrees. Model parameters shown in Table 6-13.

The FD-ML model was inaccurate for simulating NaCl profiles from the CRFC in continuous mode because unrealistic Langmuir parameters were needed to obtain a good fit with experimental results. The experimental tailing could be due to pore diffusion or NaCl interaction with bound BSA. This was not apparent in axial column elution studies as 10-CV of NaCl solution was used. Only small volumes of buffer were applied each rotation to a 1-degree segment of the annulus (a repeating cycle of 1.1 CV BSA, 3.3 CV equilibration, 1.1 CV elution, 3.3 CV equilibration at 48 min/rev). In axial column studies, all BSA was eluted before elution buffer was flushed from the column, whereas in the CRFC, mass recoveries show that BSA was accumulating in the resin.

The accuracy of the FD-ML could be checked if an annulus segment was simulated using a 1-ml column. If tailing occurred, then experiments using 1.1 CV pulses of elution buffer could be done without loading BSA to determine if the tailing is due to pore diffusion or BSA-NaCl interaction. The FD-ML could then be revised and used to simulate the CRFC with greater accuracy.

6.5.4.2 BSA simulation

The FD-ML model correctly simulated the BSA exit profile, but gave higher peaks than found experimentally. The disrepency could be due to the BSA dimer accumulating in the resin because it binds more strongly than the monomer. Model parameters obtained from curve fitting were similar to those obtained from small axial column experiments, showing that CRFC protein elution profiles can be predicted from small axial column data. Simulations were done by varying film diffusion k_{fA}, protein uptake k_{A1} and protein desorption K_d values. Decreasing k_{fA} and k_{A1} resulted in more protein appearing in the loading zone and sections after the loading zone and decreasing elution peaks (Figures 6-46 and 6-47) because k_{fA} and k_{A1} were not high enough for the resin to adsorb most of the BSA in the loading zone. Increasing k_{fA} resulted in narrower elution peaks. Increasing the desorption parameter K_d made the resin more sensitive to NaCl so more BSA eluted earlier and BSA elution peak heights decreased (Figure 6-48).

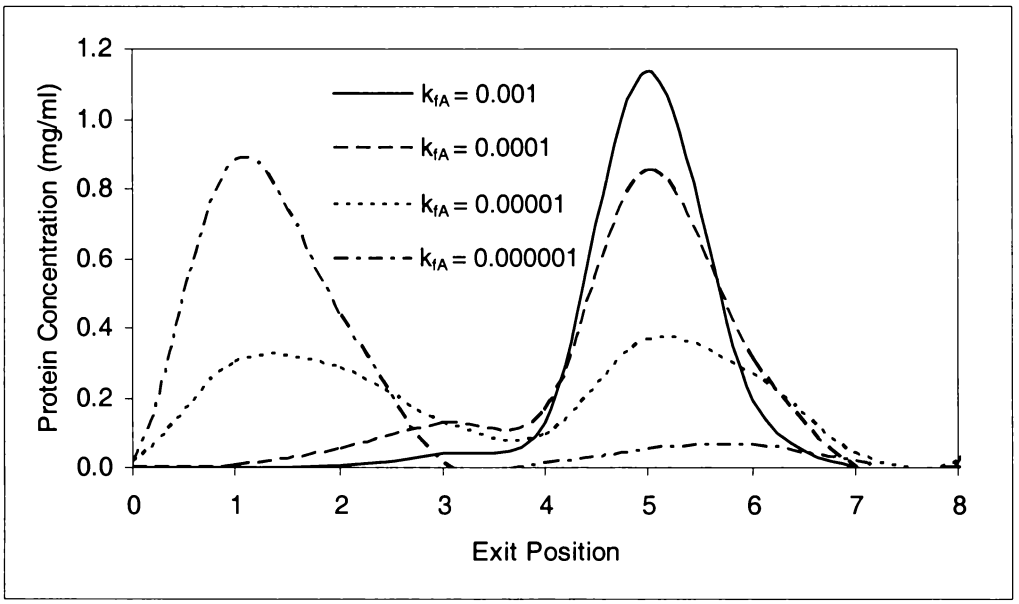

Figure 6-46. Effect of k_{fA} on BSA concentration profiles at 48 min/rev, divider angle 0 degrees. Model parameters shown in Table 6-13.

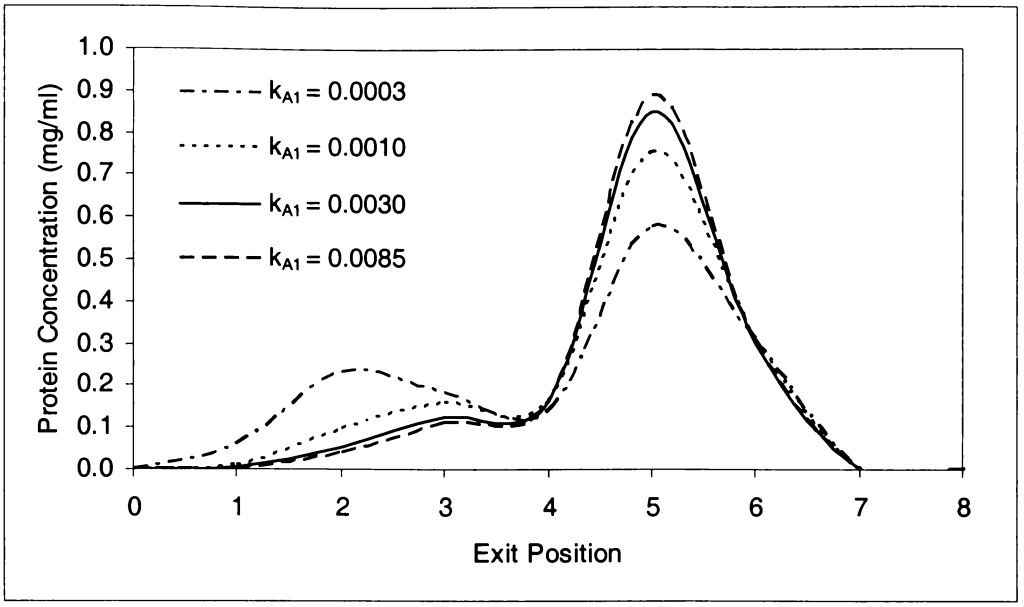

Figure 6-47. Effect of k_{A1} on BSA concentration profiles at 48 min/rev and divider angle 0 degrees. Model parameters shown in Table 6-13.

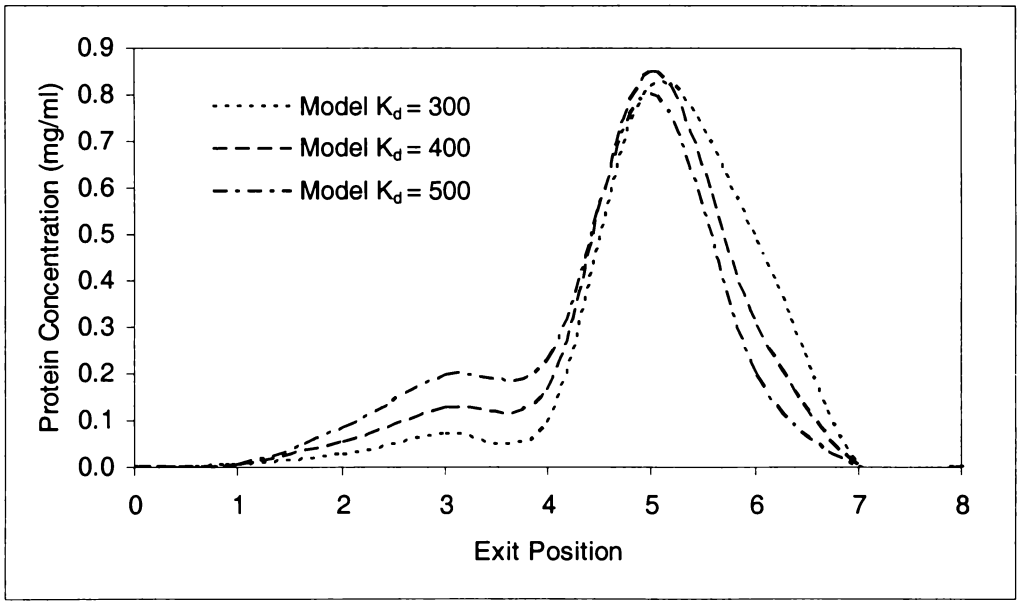

Figure 6-48. Effect of K_d on BSA concentration profiles at 48 min/rev and divider angle 0 degrees. Model parameters shown in Table 6-13.

6.6 Separating BSA and lactoferrin

Results from the continuous trial to separate BSA and lactoferrin showed the CRFC performed well. 85% of the BSA was recovered in the BSA collection zone (arbitrarily assigned to sections 4-7) at 94% purity, and 74% of the lactoferrin was recovered in the lactoferrin collection zone (arbitrarily assigned to sections 1-3 and 8) at 68% purity. The separation factor for BSA (defined as the ratio of BSA to lactoferrin in the feed stream divided by the ratio of BSA to lactoferrin in the BSA collection zone) was 4.79. Mass recovery during collection was 96% for BSA and 92% for lactoferrin. Total mass balances for BSA, lactoferrin and NaCl closed within 3%. A slight increase lactoferrin concentration (section 5 in Figure 6-49) indicates that there was some non-specific binding to the resin.

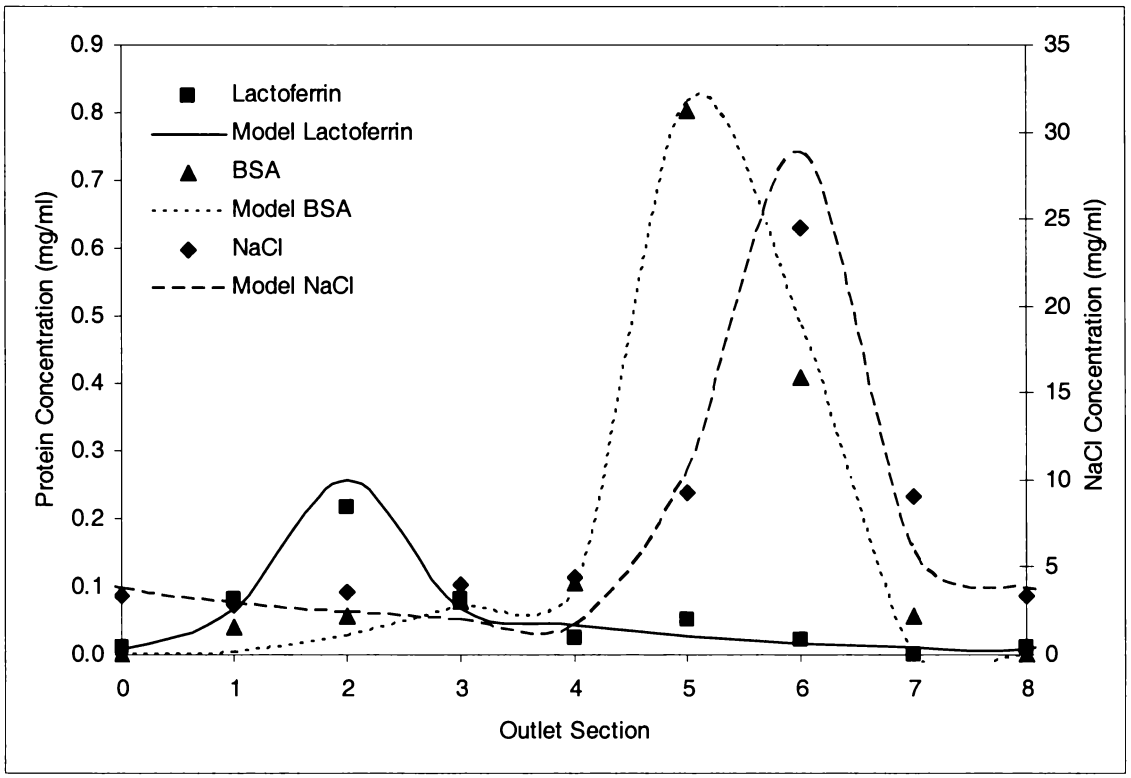

Figure 6-49. Elution profiles of BSA, lactoferrin and NaCl from the CRFC. Feed was 1.6 mg/ml BSA and 0.53 mg/ml lactoferrin, total flow 40 ml/min, feed flow of 5 ml/min to section 1, elution flow 5ml/min to section 5, and rotation speed 49 min/rev.

Table 6-14. Masses of protein recovered and purities from the CRFC for conditions in Figure 6-49.

	Lactoferrin	BSA
Yields (%)		
LF Zone (sections 1-3, 8)	0.74	0.11
BSA Zone (sections 4-7)	0.18	0.85
Total Mass Recovery (%)	0.92	0.96
Purity of fractions recovered (%)		
LF Zone (sections 1-3, 8)	0.68	0.32
BSA Zone (sections 4-7)	0.06	0.94

BSA and NaCl were simulated using the same experimental conditions and parameters given in Table 6-13. Lactoferrin profiles were simulated using C_{RAmax} = 3 mg/ml, k_{fA} = 0.0001 cm/s, K_A = 0.6 ml/mg and k_{A1} = 0.0015 ml/mg.s, obtained by fitting the model to experimental data. Lactoferrin was assumed not to compete with NaCl and BSA for resin binding sites since its pI (pI 9) was above the solution pH (pH 7). Some adsorption did occur however, as there was a slight lactoferrin peak in the elution zone (section 5 in Figure 6-49). Adsorption favoured BSA, which had a K_A = 47 ml/mg compared to K_A = 0.6 ml/mg for lactoferrin. The simulation separation factor value for BSA was 4.73 which is in good agreement with the experimentally determined value of 4.79.

Separation could be improved by increasing the sections (e.g. to 16) in the CRFC outer feed and inner exit chambers, but this would make construction and operation more complex.

Chapter 7

Conclusions and Recommendations

7.1 General findings

A prototype of a continuous radial flow chromatograph (CRFC) was developed. It consisted of

- A radial flow format for low pressure drop and rapid separation.
- A 218-ml annular bed (14.6 cm O.D., 8.6 cm I.D. and 2 cm deep) that rotates at 0.02 to 1 rpm. Cross-current movement of the bed past fixed feed and exit points allowed continuous separation.
- An outer feed chamber divided into eight sections which can independently supply protein laden feed, equilibration and elution buffer to the annulus.
- An inner exit chamber divided into eight sections to receive different buffers.
- A modular format that allowed easy assembly, bed packing and modification.

In batch (fixed bed) and continuous (rotating bed) operation, the CRFC was used to extract BSA from a stock solution. The CRFC was also used to continuously separate BSA from lactoferrin. 85% of BSA was recovered from the mixture at 94% purity, with a separation factor of 4.8.

7.2 Modelling

The CRFC was modelled in batch and continuous modes using two resin-solute interaction models. Adsorption was described in both models by the multicomponent Langmuir-Freundlich isotherm (MLF). In the first model (NP) the resin treated as non-porous and in the second (FD) the resin was porous and mass transfer between flowing solution and resin pores was described by film-diffusion.

MLF was in good agreement with experimental data for adsorption isotherm and batch experiments. However, MLF fitting parameters n_A and n_B caused model instability when simulating breakthrough and elution in axial column experiments, so a multicomponent Langmuir isotherm (ML) was used. FD-ML best described NaCl breakthrough profiles. BSA film diffusion parameters obtained correlated well with

predictions using equations from literature. A modified ML model was used to fit BSA elution profiles and good agreement was found.

FD-ML was used to simulate CRFC batch and continuous operation. BSA uptake parameters from fitting simulations to small axial column and CRFC data matched well, showing that CRFC performance could be predicted using parameters from axial column work. Uptake parameters were 30 times higher than those obtained from CRFC batch operation, showing that further work was needed to account for solute distribution in the CRFC feed and exit chambers during step concentration changes. It is likely the assumptions of instantaneous mixing and distribution in the feed and exit chambers were incorrect. In continuous operation, chamber section concentrations are constant with time, therefore solute distribution does not contribute to column performance. Predicted breakthrough profiles using axial column uptake parameters suggest that batch radial flow chromatography should perform well once solute and flow distribution problems are eliminated.

No changes in batch breakthrough or elution profiles were found when interstitial dispersion constants were varied, due to the predominance of extra-column dispersion and short bed depth of the axial flow column and CRFC.

FD-ML simulated BSA profiles were in good agreement with batch axial and radial flow and continuous radial flow experimental data. However FD-ML did not predict NaCl tailing in the CRFC during continuous operation because the model did not accurately describe NaCl pore diffusion and retention in the resin for small volumes of elution buffer applied. NaCl tailing might be due to equilibrium adsorption of Na^+ and Cl^- ions to BSA accumulated in the resin. This was hidden in batch axial column and CRFC operation because large volumes of elution buffer were applied. Better predictions could be obtained by using a layered resin particle model, simulating NaCl diffusion through the pores rather than using an averaged pore concentration and accounting for BSA-NaCl interaction.

The finite difference method allowed axial flow column and CRFC simulations to be run rapidly. The model was unstable when rapid changes in concentration occurred. This was overcome by increasing the number of simulation steps and reducing the time interval between steps, but at the expense of longer simulation times.

7.3 Technical findings

The CRFC prototype was robust and reliable. Bed channelling was easily detected by passing salt pulses through the CRFC and analysing the concentration profile. Problems that were found include:

- High pressure drops due to resin fouling. But, fouling was removed by leaving regeneration solution in the CRFC overnight.
- Pitting of stainless steel surfaces in contact with o-rings around the annulus due to seal contamination.
- Low column resolution during batch CRFC operation due to slow solute distribution in feed and exit chambers..

The CRFC has potential for continuous step-elution separations of a clarified feed. It should not be used to extract components from fermentation broth or solutions with particulates due to fouling. Because of the short bed depth, the CRFC is not suitable for isocratic separations such as size exclusion or gradient elution. The CRFC could potentially be used as a secondary purification step in large scale separations.

7.4 Recommendations for future work

The following areas for future investigation are suggested to improve CRFC operation, resolution and modelling.

- **Improving CRFC separation**

The effect of further modifying CRFC configuration and operating conditions on CRFC performance should be investigated. This could be done using data already obtained from continuous separation of BSA and lactoferrin and simulating the effect of number of feed and exit chambers, divider angle, feed and elution zone width, and annulus speed, on separation efficiency, yield and purity.

The number of outer feed and inner exit chambers could be increased to 16-32 sections. This would make multi-component separations possible and/or allow a regeneration

zone. The latter would increase the operating cycle between CIP. The effectiveness of this modification could be tested using a three-component feed and the CFRC optimized using models developed in this thesis.

- **Improving column resolution**

Further experimental work should be done to investigate how feed and exit chamber volume and design affect CRFC column resolution. The effect of different feed chamber configurations on dye profiles through the annular bed should be examined by replacing the stainless steel top of the annulus with a Perspex/glass lid and passing dye pulses through the CRFC. The dye profiles would indicate how the continuous three-dimensional model developed can be adapted to allow for solute distribution in the feed and exit chambers, and thus aid in designing radial flow chromatographic systems.

- **Column design**

The current packed bed column has the disadvantages of complex construction (porous walls have to be fabricated and welded to plates), packing and unpacking, the possibility of channelling occurring, and slow flowrates due to slow uptake kinetics. The feasibility of replacing the annular bed and porous walls with a monolithic annular column contructed from a robust material should be investigated. This would simplify construction and the monolithic column flow and kinetic characteristics would allow greatly increased throughputs.

- **Model accuracy**

The FD-ML model did not predict NaCl tailing in the CRFC during continuous operation. Tailing might be due to equilibrium adsorption of Na^+ and Cl^- ions to accumulated BSA in the resin. This should be investigated by simulating an annular segment of the resin bed using a 1-ml column and subjecting it to cyclic pulses of BSA, equilibration, elution, and equilibration buffers. If tailing occurred, then experiments using pulses of elution and equilibration buffer should be done to determine if NaCl tailing is due to pore diffusion (tailing occurs) or BSA-NaCl interaction (no tailing occurs). The FD-ML could then be revised and used to simulate the CRFC with greater accuracy.

References

Akoum, A., M. A. Vijayalakshmi and M. Sigot (1989). "Scale-Up of "Myxalin" Purification by a Pseudoaffinity Method Using a Radial Flow Column." Chromatographia **28**(3/4): 157 - 160.

Barker, P. E. and G. Ganetsos (1988). "Chemical and Biochemical Separations Using Preparative and Large-Scale Batch and Continuous Chromatography." Separation and Purification Methods **17**(1): 1-65.

Bart, H. J., R. C. Messenbock, C. H. Byers, A. Prior and J. Wolfgang (1996). "Continuous Chromatographic Separation of Fructose, Mannitol and Sorbitol." Chemical Engineering and Processing **35**(6): 459-471.

Begovich, J. M., C. H. Byers and W. G. Sisson (1983). "A High-Capacity Pressurized Continuous Chromatograph." Separation Science and Technology **18**(12-13): 1167-1191.

Begovich, J. M. and W. G. Sisson (1984). "A Rotating Annular Chromatograph for Continuous Separations." AIChE Journal **30**(5): 705 - 710.

Bird, R. B., W. E. Steward and E. N. Lightfoot (2002). Transport Phenomena, John Wiley & Sons. 2nd edition.

Bloomingburg, G. F., J. S. Bauer, G. Carta and C. H. Byers (1991). "Continuous Separation of Proteins by Annular Chromatography." Industrial and Engineering Chemistry Research **30**(5): 1061-1067.

Bloomingburg, G. F. and G. Carta (1994). "Separation of Protein Mixtures by Continuous Annular Chromatography with Step Elution." The Chemical Engineering Journal **55**: B19-B27.

Branovic, K., A. Buchacher, M. Barut, A. Strancar and D. Josic (2000). "Application of monoliths for downstream processing of clotting factor IX." Journal of Chromatography A **903**(1-2): 21-32.

Bridges, S. and P. E. Barker (1993). Continuous Cross-Current Chromatographic Refiners. Preparative and Production Scale Chromatography. P. Ganetsos and P. E. Barker, Eds. New York, Marcel Dekker. **63:** 113 - 126.

Brock, J. H. (2002). "The physiology of lactoferrin." Biochemistry and Cell Biology **80:** 1-6

Brown, W. G. (1939). "Micro Separations by Chromatographic Adsorption on Blotting Paper." Nature **143**(3618): 377-378.

Buchacher, A., G. Iberer, A. Jungbauer, H. Schwinn and D. Josic (2001). "Continuous Removal of Protein Aggregates by Annular Chromatography." Biotechnology Progress **17**(1): 140-149.

Byers, C. H., W. G. Sisson, J. P. DeCarli II and G. Carta (1990). "Sugar Separations on a Pilot Scale by Continuous Annular Chromatography." Biotechnology Progress **6**: 13-20.

Byers, C. H., W. G. Sisson, J. P. Decarli and G. Carta (1989). "Pilot-Scale Studies of Sugar Separations by Continuous Chromatography." Applied Biochemistry and Biotechology **20-1**(JAN-): 635-654.

Canon, R. M., J. M. Begovich and W. G. Sisson (1980). "Pressurized Continuous Chromatography." Separation Science and Technology **15**(3): 655-678.

Canon, R. M. and W. G. Sisson (1978). "Operation of an Improved, Continuous Annular Chromatograph." Journal of Liquid Chromatography **1**(4): 427-441.

Carta, G., J. P. DeCarli, C. H. Byers and W. G. Sisson (1989). "Separation of Metals by Continuous Annular Chromatography with Step Elution." Chemical Engineering Commununications **79**: 207-227.

Chen, H.-L. and K. C. Hou (1985). Bioseparation by Cartridge Chromatography. Annual Reports on Fermentation Processes. G. T. Tsao, Ed. New York, Academic Press. **8:** 59-71.

Conder, J. R. and B. O. Hayek (2000). "Adsorption and Desorption Kinetics of Bovine Serum Albumin in Ion Exchange and Hydrophobic Interaction Chromatography on Silica Matrices." Biochemical Engineering Journal **6**(3): 225-232.

Cowan, G. H., I. S. Gosling and W. P. Sweetenham (1989). "Modeling Methods to Aid the Design and Optimization of Batch Stirred-Tank and Packed-Bed Column Adsorption and Chromatography Units." Journal of Chromatography **484**(DEC): 187-210.

DeCarli, J. P., G. Carta and C. H. Byers (1990). "Displacement Separations by Continuous Annular Chromatography." AIChE Journal **36**(8): 1220-1228.

Delaney, R. A. M., J. K. Donnelly and R. D. Kearney (1973). "Industrial Applications of Gel Filtration-1 Whey." Process Biochemistry: 13-16.

Demmer, W. and D. Nussbaumer (1999). "Large-Scale Membrane Adsorbers." Journal of Chromatography A **852**: 73-81.

Deutsch, D. G. and E. T. Mertz (1970). Science **170**: 1095. cited by Planques et al. (1991).

Dinelli, D., S. Polezzo and M. Taramasso (1962). "Rotating Unit for Preparative-Scale Gas Chromatography." Journal of Chromatography **7**: 477-484.

Fahien, R. W. and J. M. Smith (1955). "Mass Transfer in Packed Beds." AIChE Journal **1**(1): 28-37.

Fox, J. B. J. (1969). "Continuous Chromatography Apparatus II. Operation." Journal of Chromatography **43**: 55 - 60.

Fox, J. B. J., R. C. Calhoun and W. J. Eglington (1969). "Continuous Chromatography Apparatus I. Construction." Journal of Chromatography **43**: 48 - 54.

Ghosh, R. (2002). "Protein separation using membrane chromatography: opportunities and challenges." Journal of Chromatography A **952**(1-2): 13-27.

Giddings, J. C. (1962). "Theoretical Basis for a Continuous, Large-Capacity Gas Chromatographic Apparatus." Analytical Chemistry **34**(1): 37-39.

Giovannini, R. and R. Freitag (2001). "Isolation of a Recombinant Antibody from Cell-Culture Supernatant - Continuous Annular Versus Batch and Expanded- Bed Chromatography." Biotechnology and Bioengineering **73**(6): 522-529.

Giovannini, R. and R. Freitag (2002). "Continuous Isolation of Plasmid DNA by Annular Chromatography." Biotechnology and Bioengineering **77**(4): 445-454.

Goto, M. and S. Goto (1987). "Continuous Separation Using an Annular Chromatograph with Rotating Inlet and Outlet." Journal of Chemical Engineering of Japan **20**(6): 598 - 603.

Goto, S. and Y. Takahashi (1993). Continuous Rotating Annular Chromatography. Preparative and Production Scale Chromatography. P. Ganetsos and P. E. Barker, Eds. New York, Marcel Dekker. **63:** 127 - 141.

Gu, T. (1995). Mathematical Modeling and Scale-up of Liquid Chromatography. Germany, Springer-Verlg Berlin Heidelberg.

Gu, T., G. J. Tsai and G. T. Tsao (1992). "Multicomponent Affinity Radial Flow Chromatography." Separation Technology **2**: 176-182.

Gu, T. Y., G. J. Tsai and G. T. Tsao (1991). "A Theoretical-Study of Multicomponent Radial Flow Chromatography." Chemical Engineering Science **46**(5-6): 1279-1288.

Gustavsson, P. E. and P. O. Larsson (2001). "Continuous Superporous Agarose Beds in Radial Flow Columns." Journal of Chromatography A **925**: 69-78.

Hall, L. G. and L. G. Cole (1959). "Chromatography." US Patent 2,891,630.

Heaton, W. B. (1963). "Chromatographic Method and Apparatus." US Patent 3,077,103.

Heft, B. K. (1991). Radial Flow Chromatography in Compressed Pancake-Shaped Beds. PhD Thesis, Louisiana State University, Louisiana. cited by Rice and Heft (1991).

Heftmann, E., J. M. Krochta, D. F. Farkas and S. Schwimmer (1972). "The Chromatofuge, an Apparatus for Preparative Rapid Radial Column Chromatography." Journal of Chromatography **66**: 365-369.

Hopf, P. P. (1947). "Radial Chromatography in Industry." Industrial and Engineering Chemistry **39**: 938 - 940.

Hou, K. C. and R. M. Mandaro (1986). "Bioseparation by Ion Exchange Cartridge Chromatography." BioTechniques **4**(4): 358-367.

Hou, K. C. and R. Zaniewski (1990). "Purification of urokinase by combined cation exchanger and affinity chromatographic cartridges." Journal of Chromatography **525**: 297-306.

Hou, K. C., R. Zaniewski and S. Roy (1991). "Protein A immobilized affinity cartridge for immobilized purification." Biotechnology and Applied Biochemistry **13**: 257-268.

Howard, A. J., G. Carta and C. H. Byers (1988). "Separation of Sugars by Continuous Annular Chromatography." Industrial and Engineering Chemistry Research **27**(10): 1873-1882.

Huang, S. H., W. C. Lee and G. T. Tsao (1988a). "Mathematical Models of Radial Chromatography." The Chemical Engineering Journal **38**(3): 179-186.

Huang, S. H., S. Roy, K. C. Hou and G. T. Tsao (1988b). "Scaling-Up of Affinity Chromatography by Radial-Flow Cartridges." Biotechnology Progress **4**(3): 159-165.

Hunter, A. K. and G. Carta (2000). "Protein Adsorption on Novel Acrylamido-Based Polymeric Ion Exchangers: II. Adsorption Rates and Column Behavior." Journal of Chromatography A **897**(1-2): 81-97.

Hunter, A. K. and G. Carta (2001a). "Effects of Bovine Serum-Albumin Heterogeneity on Frontal Analysis with Anion-Exchange Media." Journal of Chromatography A **937**(1-2): 13-19.

Hunter, A. K. and G. Carta (2001b). "Protein Adsorption on Novel Acrylamido-Based Polymeric Ion-Exchangers: III. Salt Concentration Effects and Elution Behavior." Journal of Chromatography A **930**(1-2): 79-93.

Iberer, G., H. Schwinn, D. Josic, A. Jungbauer and A. Buchacher (2001). "Improved Performance of Protein Separation by Continuous Annular Chromatography in the Size-Exclusion Mode." Journal of Chromatography A **921**(1): 15-24.

Iberer, G., H. Schwinn, D. Josic, A. Jungbauer and A. Buchacher (2002). "Continuous Purification of a Clotting Factor IX Concentrate and Continuous Regeneration by Preparative Annular Chromatography." Journal of Chromatography A **972**(1): 115-129.

Indyk, H. E. and E. L. Filonzi (2004). "Determination of lactoferrin in bovine milk, colostrum and infant formulas by optical biosensor analysis." International Dairy Journal. In Press, Corrected Proof.

James, E. A. and D. D. Do (1991). "Equilibria of Biomolecules on Ion-Exchange Adsorbents." Journal of Chromatography **542**: 19.

Josic, D., A. Buchacher and A. Jungbauer (2001). "Monoliths as Stationary Phases for Separation of Proteins and Polynucleotides and Enzymatic Conversion." J Chromatogr B **752**(2): 191-205.

Josic, D. and A. Strancar (1999). "Application of Membranes and Compact, Porous Units for the Separation of Biopolymers." Industrial and Engineering Chemistry Research **38**: 333-342.

Jungbauer, A., D. Pettauer, A. Buchacher, E. Wenisch, F. Unterluggauer, K. Uhl and F. Steindl (1988). "Scaleup of Monoclonal-Antibody Purification Using Radial Streaming Ion-Exchange Chromatography." Biotechnology and Bioengineering **32**(3): 326-333.

Kaczmarski, K., D. Antos, H. Sajonz, P. Sajonz and G. Guiochon (2001). "Comparative Modeling of Breakthrough Curves of Bovine Serum Albumin in anion-Exchange Chromatography." Journal of Chromatography A **925**: 1-17.

Kaye, L. A. (1978). Fluid Distribution in Radial Flow Vapor Phase, Fixed Bed Reactors. 71st Annual AIChE Meeting, Miami Beach. Cited by Yee (1987).

Kim, Y.-H. and E. K. Lee (1996). "Comparison of axial and radial flow chromatography on protein separation speed and resolution." Korean Journal of Chemical Engineering **13**(5): 466-472.

Kitakawa, A., Y. Yamanishi and T. Yonemoto (1997). "Complete Separation of Amino-Acids Using Continuous Rotating Annular Ion-Exchange Chromatography with Partial Recycle of Effluent." Industrial and Engineering Chemistry Research **36**(9): 3809-3814.

Kitakawa, A., Y. Yamanishi, T. Yonemoto and T. Tadaki (1995). "Modeling and Simulation of Continuous Rotating Annular Ion- Exchange Chromatography for Separation of Amino-Acids." Separation Science and Technology **30**(16): 3089-3110.

Lacoste-Bourgeacq, J. F., C. Desneux and M. Allary (1991). "A new procedure using membrane chromatography for the valorization of Fraction IV from Kistler and Nitschmann's fraction of blood plasma." Chromatographia **32**(1/2): 27-32.

Lanckriet, H. and A. P. J. Middelberg (2004). "Continuous Chromatographic Protein Refolding." Journal of Chromatography A **1022**(1-2): 103-113.

Lane, L., M. L. Koscielny, P. R. Levison, D. W. Toome and E. T. Butts (1990). "Chromatography of Hen Egg-White Proteins on Anion-Exchange Cellulose at high Flow Rates Using a Radial Flow Column." Bioseparation **1**: 141-147.

Lapidus, L. and N. R. Amundson (1950). "Mathematics of Adsorption in Beds. III. Radial Flow." Journal of Physical Chemistry **54**: 821-829.

Lapidus, L. and N. R. Amundson (1952). "The Rate-Determining Steps in Radial Adsorption Analysis." Journal of Physical Chemistry **56**: 373-383.

Lay, M. C. (1998). Continuous Radial Flow Chromatography. MSc Thesis, University of Waikato, Hamilton, New Zealand.

Lee, W. C., G. J. Tsai and G. T. Tsao (1990). "Radial-Flow Affinity Chromatography for Trypsin Purification." ACS Symposium Series **427**: 104-117.

LeVan, A. D., M. Carta and C. M. Yon (1997). Adsorption and ion exchange. Perry's Chemical Engineers' Handbook, 7th Edition. R. H. Perry, D. W. Green and J. O. Maloney, Eds. New York, McGraw-Hill: 16.1-16.66.

Levenspiel, O. (1993). The Chemical Reactor Omnibook. Corvallis, Oregon 97339, OSU Book Stores, Inc.

Levison, P. R. (2003). "Large-scale ion-exchange column chromatography of proteins: Comparison of different formats." Journal of Chromatography B **790**(1-2): 17-33.

Levison, P. R., S. E. Badger, D. W. Toome, E. T. Butts, M. L. Koscielny and L. Lane (1991). Upstream and Downstream Processing in Biotechnology III. R. de Bruyne and A. Huyghebaert, Eds., Royal Flemish Society of Engineers.

Liapis, A. I. (1989). "Theoretical Aspects of Affinity Chromatography." Journal of Biotechnology **11**: 143-160.

Liu, Z., G. Yin, S. Feng, D. Wang, F. Ding and N. Yuan (2001). "Oscillatory Electroosmosis-Enhanced Intra/Inter-Particle Liquid Transport and its Primary applications in the Preparative Electrochromatography of Proteins." Journal of Chromatography A **921**(1): 93-98.

Luft, L. (1962). "Apparatus for Continuous Separation of Volatile Components of a Gaseous Mixture." US Patent 3,016,106.

Mackenzie, J. R. and M. Truesdale (1990). "Radial High-Performance Thin-Layer Chromatography Used to Assess Fetal Lung Maturity." Clinical Chemistry **36**(5): 728-731.

Mandaro, R. M., S. Roy and K. C. Hou (1987). "Filtration Supports for Affinity Separation." Bio/Technology **5**: 928-932.

Martin, A. J. P. (1949). "Summarizing paper." Discussions of the Faraday Society(7): 332 - 336.

McGregor, W. C., D. P. Szesko, R. M. Mandaro and V. R. Rai (1986). "Practicum: High Performance Isolation of a Recombinant Protein on Composite Ion Exchange Media." Bio/Technology **4**: 526-527.

Medellin, P. (1976). Removal of Sulfur Dioxide and Nitrogen Oxides from Flue Gases in Radial-Flow Fixed Bed. PhD Thesis, Washington University, St. Louis, Missouri. Cited by Yee (1987).

Menozzi, F. D., P. Vanderpoorten, C. Dejaiffe and A. O. A. Miller (1987). "One-Step Purification of Mouse Monoclonal Antibodies by Mass Ion Exchange Chromatography on Zetaprep." Journal of Immunological Methods.

Milavec Zmak, P., H. Podgornik, J. Jancar, A. Podgornik and A. Strancar (2003). "Transfer of gradient chromatographic methods for protein separation to Convective Interaction Media monolithic columns." Journal of Chromatography A **1006**(1-2): 195-205.

Mitchell, H. L., W. G. Schrenk and R. E. Silker (1953). "Preparation of Carotene Concentrates from Dehydrated Alfalfa Meal." Industrial and Engineering Chemistry **45**(2): 415-417.

Moore, S. A., B. F. Anderson, C. R. Groom, M. Haridas and E. N. Baker (1997). "Three-dimensional structure of diferric bovine lactoferrin at 2.8 A resolution." Journal of Molecular Biology **274**(Nov): 222-236.

Mosier, L. C. (1963). "Continuous Gas Chromatography." US Patent 3,078,647.

Mueller, G. E. (1999). "Radial Void Fraction Correlation for Annular Packed-Beds." Aiche J **45**(11): 2458-2460.

Munson-McGee, S. H. (2000). "Fluid-Dynamics of Radial-Flow Ion-Exchange in Partially Filled Columns." Separation Science and Technology **35**(15): 2415-2429.

Nelson, P. A. and T. R. Galloway (1975). "Particle-tofluid heat and mass transfer in dense systems of fine particles." Chemical Engineering Science **30**: 1-6.

Ngo, T. T. and N. Khatter (1991). "Rapid and Simple Isolation of Multigram Goat IgG from Serum Using Avid Al and Radial Flow Column." Applied Biochemistry and Biotechnology **30**(1): 111-119.

Nicholas, R. A. and J. B. Fox Jr (1969). "Continuous Chromatography Apparatus III. Application." Journal of Chromatography **43**: 61 - 65.

Peters, E. C., F. Svec and J. M. J. Frechet (1997). "Preparation of Large-Diameter "Molded" Porous Polymer Monliths and the Control of Pore Structure Homogeneity." Chemistry of Materials **9**: 1898-1902.

Pharmacia (1983). Ion Exchange Chromatography: Principles and Methods. Uppsala, Sweden.

Plaigin, M., J. F. Lacoste-Bourgeacq, R. M. Mandaro and C. Lemay (1989). "Purification of Plasma Fractions by Radial Flow Chromatography Cartridges." Colloque INSERM **175**: 169-176.

Planques, Y., H. Pora and F. D. Menozzi (1991). "Affinity Purification of Plasminogen by Radial-Flow Affinity-Chromatography." Journal of Chromatography **539**(2): 531-533.

Podgornik, A., M. Barut, J. Jancar and A. Strancar (1999). "Isocratic separations on thin glycidyl methacrylate-ethylenedimethacrylate monoliths." Journal of Chromatography A **848**(1-2): 51-60.

Podgornik, A., M. Barut and A. Strancar (2000). "Construction of Large-volume Monolithic Columns." Analytical Chemistry **72**: 5693-5699.

Podgornik, A., J. Jancar, M. Merhar, S. Kozamernik, D. Glover, K. Cucek, M. Barut and A. Strancar (2004). "Large-scale methacrylate monolithic columns: design and properties." Journal of Biochemical and Biophysical Methods. In Press, Corrected Proof.

Ponzi, P. R. and L. A. Kaye (1979). "Effect of Flow Maldistribution on Conversion and Selectivity in Radial Flow Fixed-Bed Reactors." AIChE Journal **25**(1): 100-108.

Rachinskii, V. V. (1968). "Basic Principles of Radial Chromatography." Journal of Chromatography **33**: 234 - 241.

Reissner, K., A. Prior, J. Wolfgang, H. J. Bart and C. H. Byers (1997). "Preparative Desalting of Bovine Serum-Albumin by Continuous Annular Chromatography." Journal of Chromatography A **763**(1-2): 49-56.

Rice, R. G. (1982). "Approximate Solutions for Batch, Packed Tube and Radial Flow Adsorbers - Comparison with Experiment." Chemical Engineering Science **37**: 83-91.

Rice, R. G. and B. K. Heft (1990). "Radial Flow Chromatography in Compressed Pancake-Shaped Beds." Chemical Engineering Communications **98**: 231-242. Using Smart Source Parsing.

Rice, R. G. and B. K. Heft (1991). "Separations via Radial Flow Chromatography in Compacted Particle Beds." AIChE Journal **37**(4): 629-632.

Rice, R. G., B. K. Heft, M. Borie and M. Yee (1989). Radial Flow Chromatography. 3rd Fundamentals of Adsorption Conference, Sonthofen, Germany, Technical University of Munich.

Saxena, V. and M. Dunn (1989). "Solving Scale-Up: Radial Flow Chromatography." Bio/Technology **7**(3): 250.

Saxena, V., K. Subramanian, S. Saxena and M. Dunn (1989). "Production-Scale Radial Flow Chromatography." Biopharm(March): 46-50.

Saxena, V. and A. E. Weil (1987). "Radial Flow Columns: A New Approach to Scaling-Up Biopurifications." BioChromatography **2**(2): 90-97.

Saxena, V., A. E. Weil, W. C. Kawahata, W. C. McGregor and M. Chandler (1987). "Applications of Radial Flow Columns for Fast Affinity Chromatography." American Laboratory(October 1987): 112-120.

Schlegl, R., G. Iberer, C. Machold, R. Necina and A. Jungbauer (2003). "Continuous Matrix-Assisted Refolding of Proteins." Journal of Chromatography A **1009**(1-2): 119-132.

Scott, C. D., R. D. Spence and W. G. Sisson (1976). "Pressurized, Annular Chromatograph for Continuous Separations." Journal of Chromatography **126**: 381 - 400.

Sepragen (1998). Press releases: HAYWARD, CA, April 23, May 31, August 25, and October 15, 1998 - Sepragen Corporation.

Sisson, W. G., J. M. Begovich, C. H. Byers and C. D. Scott (1988). "Continuous Chromatography." ChemTech **18**(8): 498-502.

Solms, J. J. (1955). "Process for the Continuous Chromatographic Separation of Mixtures." US Patent 786,896.

Song, X. Q., Y. Jin and Z. Q. Yu (1994). "Influence of Outward Radial Gas-Flow on Particle Movement in an Annular Moving-Bed." Powder Technology **79**(3): 247-256.

Strancar, A., M. Barut, A. Podgornik, P. Koselj, H. Schwinn, P. Raspor and D. Josic (1997). "Application of Compact Porous Tubes for Preparative Isolation of Clotting Factor VIII from Human Plasma." Journal of Chromatography A **760**: 117-123.

Sun, T., G. Chen, Y. Liu, F. Bu and M. Wen (2000a). "Chromatography of Human Prothrombin from Nitschmann Fraction III on Q Sepharose Fast Flow Using Axial and Radial Flow Column." Bioprocess Engineering **23**: 121-125.

Sun, T., G. Chen, Y. Liu, F. Bu and M. Wen (2000b). "Chromatography of Human Prothrombin from Nitschmann Fraction-III on DEAE Sepharose Fast-Flow Using Axial and Radial Flow Column." Biomedical Chromatography **14**(7): 478-482.

Sun, T., G. Chen, Y. Liu, F. Bu and M. Wen (2000c). "Purification of Human Prothrombin from Nitschmann Fraction III Using DEAE Membrane Radial Flow Chromatography." Journal of Chromatography B **742**(1): 109-114.

Sussman, M. V. (1970). "Apparatus for Effecting Interactions of Fluids at Extended Solid Surfaces." US Patent 3,503,712.

Sussman, M. V. (1976). "Continuous Chromatography." ChemTech **6**: 260.

Sussman, M. V., K. N. Astill and R. N. S. Rathore (1974). "Continuous Gas Chromatography." Journal of Chromatographic Science **12**: 91-97.

Sussman, M. V., K. N. Astill, R. Rombach, A. Cerullo and S. S. Chen (1972). "Continuous Surface Chromatography." Industrial and Engineering Chemistry Research Fundamentals **11**(2): 181-190.

Sussman, M. V. and C. C. Huang (1967). "Continuous Gas Chromatography." Science **156**: 974-976.

Sussman, M. V. and R. N. S. Rathore (1975). "Continuous Modes of Chromatography." Chromatographia **8**: 55.

Svec, F. and J. M. J. Frechet (1999). "Molded Rigid Monolithic Porous Polymers: An Inexpensive, Efficient, and Versatile Alternative to Beads for the Design of Materials for Numerous Applications." Industrial and Engineering Chemistry Research **38**: 34-48.

Svensson, H., C.-E. Agrell, S.-O. Dehlen and L. Hagdahl (1955). "An Apparatus for Continuous Chromatographic Separation." Science Tools **2**: 17-21.

Takahashi, Y. and S. Goto (1991a). "Continuous Concentration of Single Component Using an Annular Chromatograph." Journal of Chemical Engineering of Japan **24**(4): 460-465.

Takahashi, Y. and S. Goto (1991b). "Continuous Separation Using an Annular Chromatograph with Non-Isocratic Elution." Journal of Chemical Engineering of Japan **24**(1): 121-123.

Takahashi, Y. and S. Goto (1991c). "Continuous Separations of Amino Acids by Using an Annular Chromatograph with Rotating Inlet and Outlet." Separation Science and Technology **26**(1): 1-13.

Takahashi, Y. and S. Goto (1994). "Continuous Separation of Fructooligosaccharides Using an Annular Chromatograph." Separation Science and Technology **29**(10): 1311 - 1318.

Taramasso, M. and D. Dinelli (1964). "Preparative Scale Gas Chromatography by a Laboratory Rotating Unit." Journal of Gas Chromatography: 150-153.

Tharakan, J. and M. Belizaire (1995a). "Ligand Efficiency in Axial and Radial Flow Immunoaffinity Chromatography of Factor-IX." Journal of Chromatography A **702**(1-2): 191-196.

Tharakan, J. P. and M. Belizaire (1995b). "Protein Band Dispersion in Axial and Radial Flow Chromatography." Journal of Liquid Chromatography **18**(1): 39-49.

Thiele, A., T. Falk, L. Tobiska and A. Seidel-Morgenstern (2001). "Prediction of Elution Profiles in Annular Chromatography." Computers & Chemical Engineering **25**(7-8): 1089-1101.

Tong, X.-D., B. Xue and Y. Sun (2003). "Modeling of expanded-bed protein adsorption by taking into account the axial particle size distribution." Biochemical Engineering Journal **16**(3): 265-272.

Tsaur, Y. (1996). Radial Ion Exchange Processes. PhD Thesis, University of Melbourne, Melbourne, Australia.

Tsaur, Y. and D. C. Shallcross (1997a). "Comparison of Simulated Performance of Fixed Ion-Exchange Beds in Linear and Radial Flow." Solvent Extraction and Ion Exchange **15**(4): 689-708.

Tsaur, Y. and D. C. Shallcross (1997b). "Modeling of Ion Exchange Performance in a Fixed Radial Flow Annular Bed." Industrial Engineering and Chemistry Research **36**: 2359 - 2367.

Tuthill, E. J. (1970). "Apparatus for Continuous Chromatography." US Patent 3,527,350.

Tyn, M. T. and T. W. Gusek (1990). "Prediction of Diffusion Coefficients of Proteins." Biotechnology and Bioengineering **35**: 327-338.

Uretschlager, A., A. Einhauer and A. Jungbauer (2001). "Continuous Separation of Green Fluorescent Protein by Annular Chromatography." Journal of Chromatography A **908**(1-2): 243-250.

Wankat, P. C. (1977). "The Relationship Between One-Dimensional and Two-Dimensional Separation Processes." AIChE Journal **23**(6): 859 - 867.

Weil, H. (1949). Industrial Chromatography, Part 1, Column Chromatography and Radial Chromatography. Canadian Chemistry and Process Industries Toronto, Westman Publications. **33:** 956-959.

Whitley, R. D., R. Wachter, F. Liu and N. H. L. Wang (1989). "Ion-Exchange Equilibria of Lysozyme, Myoglobin and Bovine Serum Albumin. Effective Valence and Exchanger Capacity." Journal of Chromatography **465**: 137-156.

Williams, T. I. (1947). An Introduction to Chromatography. Glasgow, Great Britain, Blackie & Son.pages 36-38.

Wolf, E. and T. Vermeulen (1976). "A Multiple-Layer Cross-Flow Configuration for Preparative Chromatography of Multicomponent Mixtures." Industrial Engineering Chemistry, Process Design Development **15**(4): 485-490.

Yee, M. (1987). Fluid Mechanics and Transient Mass Transfer for Radial Flow in Pancake-Shaped Packed Beds. MSc. Thesis, Louisiana State University, Louisiana.

Yonemoto, T., A. Kitakawa, S. N. Zheng and T. Tadaki (1993). "A Novel Continuous Rotating Annular Liquid Chromatograph with a Multichannel Peristaltic Pump for Variable Eluent Withdrawal." Separation Science and Technology **28**(17-18): 2587-2605.

Appendix A Designs for CRFC Prototype II

A.1 Reference Sheets

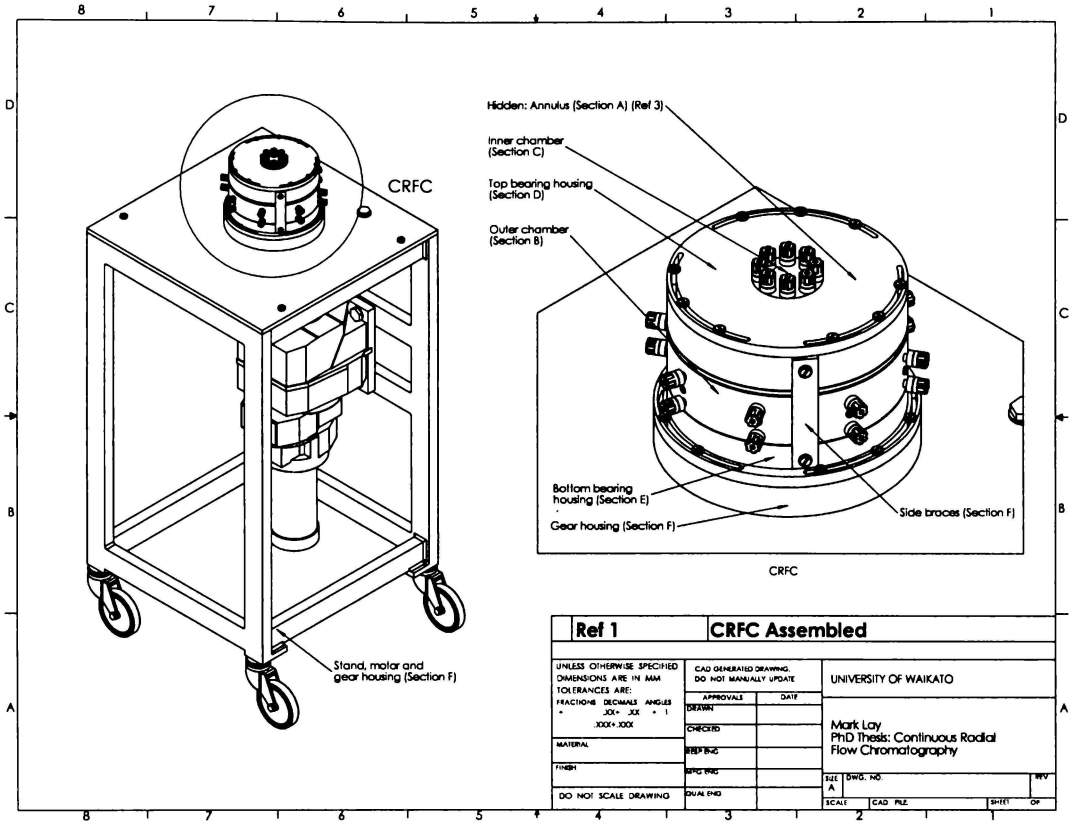

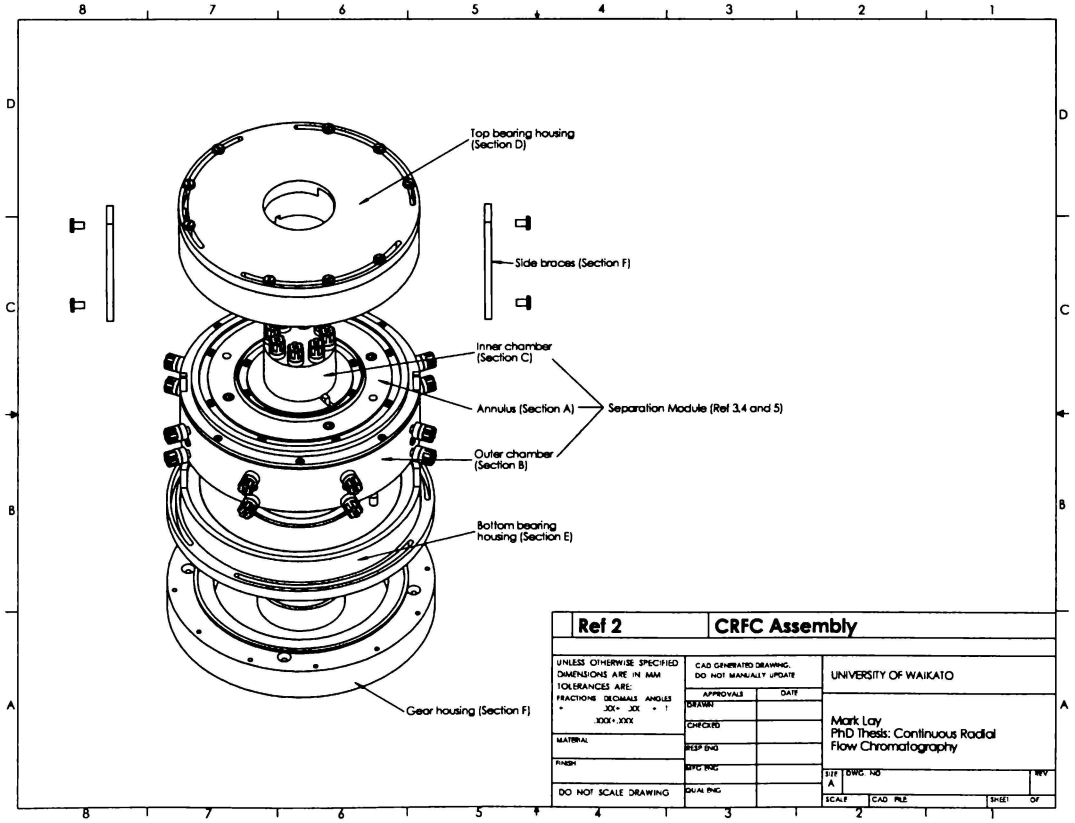

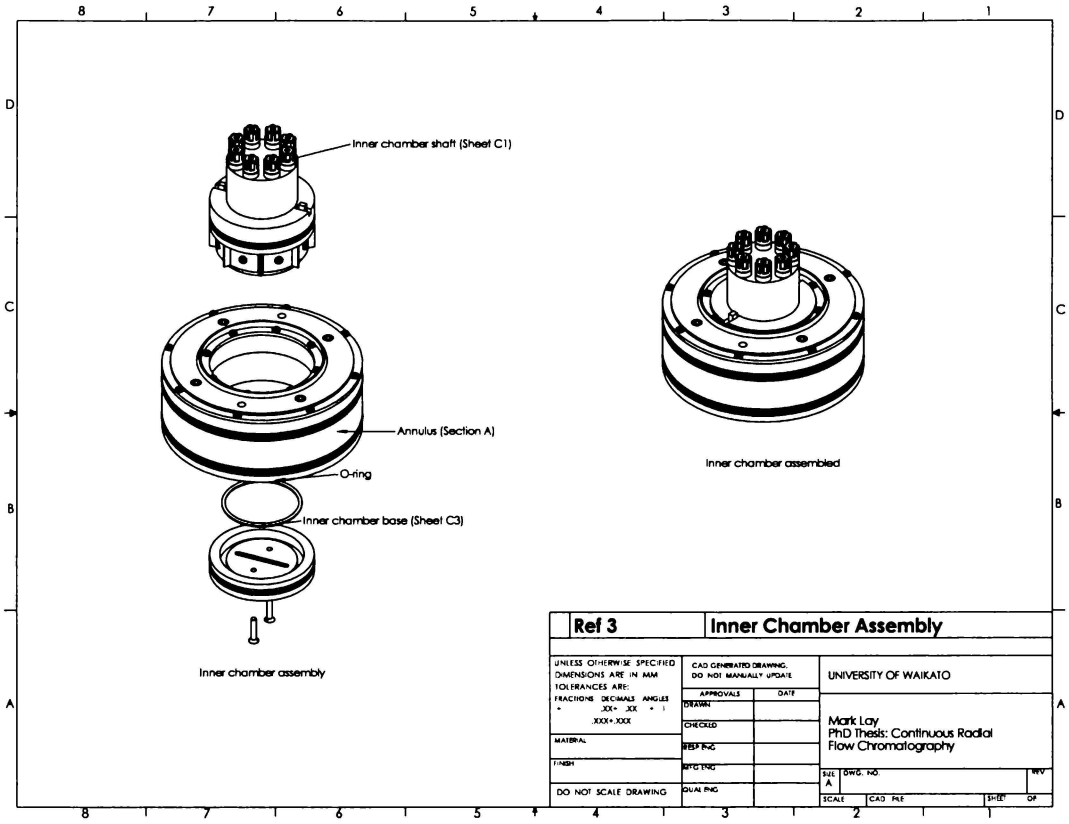
Inner chamber shaft (Sheet C1)
Annulus (Section A)
O-ring
Inner chamber base (Sheet C3)
Inner chamber assembly
Inner chamber assembled
Ref 3
Inner Chamber Assembly
UNLESS OTHERWISE SPECIFIED
DIMENSIONS ARE IN MM
TOLERANCES ARE:
FRACTIONS DECIMALS ANGLES
± .XX± .XX ± 1
.XXX±.XXX
MATERIAL
FINISH
DO NOT SCALE DRAWING
CAD GENERATED DRAWING.
DO NOT MANUALLY UPDATE
APPROVALS
DATE
DRAWN
CHECKED
ENG APP
MFG APP
QUAL ENG
UNIVERSITY OF WAIKATO
Mark Lay
PhD Thesis: Continuous Radial
Flow Chromatography
SIZE
A
DWG. NO.
REV
SCALE
CAD REF
SHEET
OF

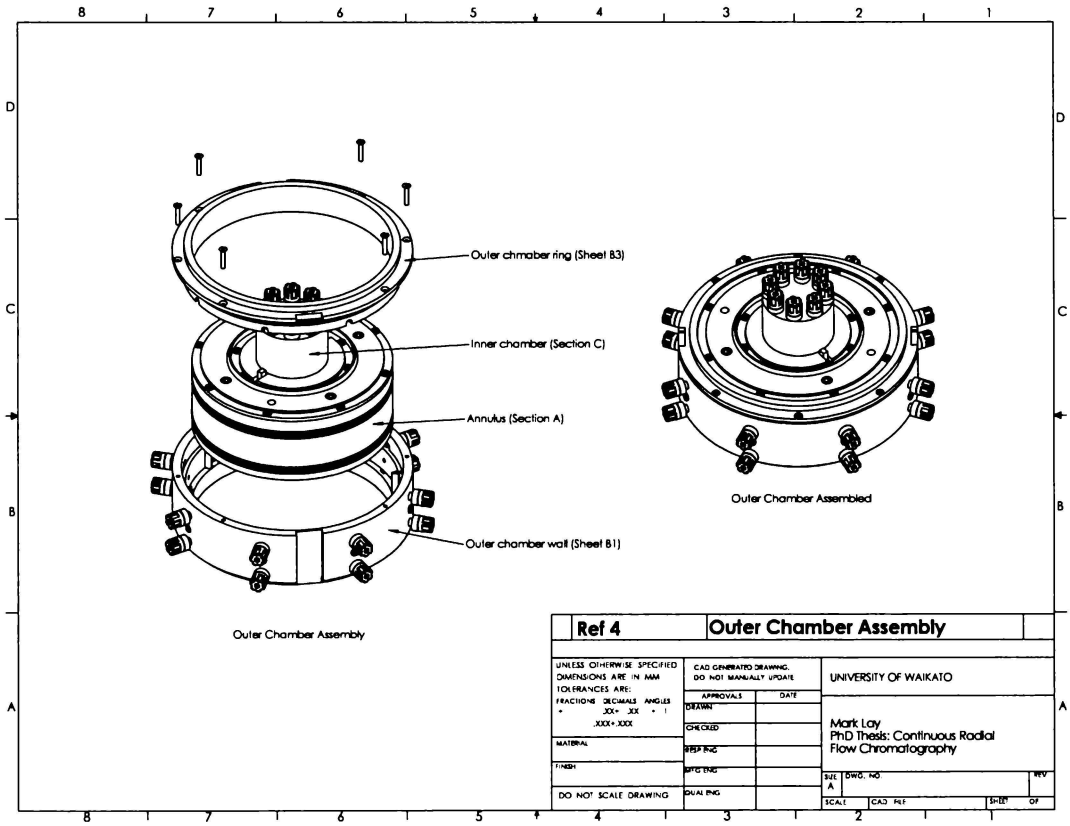
Outer chmaber ring (Sheet B3)
Inner chamber (Section C)
Annulus (Section A)
Outer chamber wall (Sheet B1)
Outer Chamber Assembly
Outer Chamber Assembled
Ref 4
Outer Chamber Assembly
UNLESS OTHERWISE SPECIFIED
DIMENSIONS ARE IN MM
TOLERANCES ARE:
FRACTIONS DECIMALS ANGLES
± .XX± .XX ± 1
.XXX±.XXX
MATERIAL
FINISH
DO NOT SCALE DRAWING
CAD GENERATED DRAWING.
DO NOT MANUALLY UPDATE
APPROVALS
DATE
DRAWN
CHECKED
ENG APP
MFG APP
QUAL ENG
UNIVERSITY OF WAIKATO
Mark Lay
PhD Thesis: Continuous Radial
Flow Chromatography
SIZE
A
DWG. NO.
REV
SCALE
CAD REF
SHEET
OF

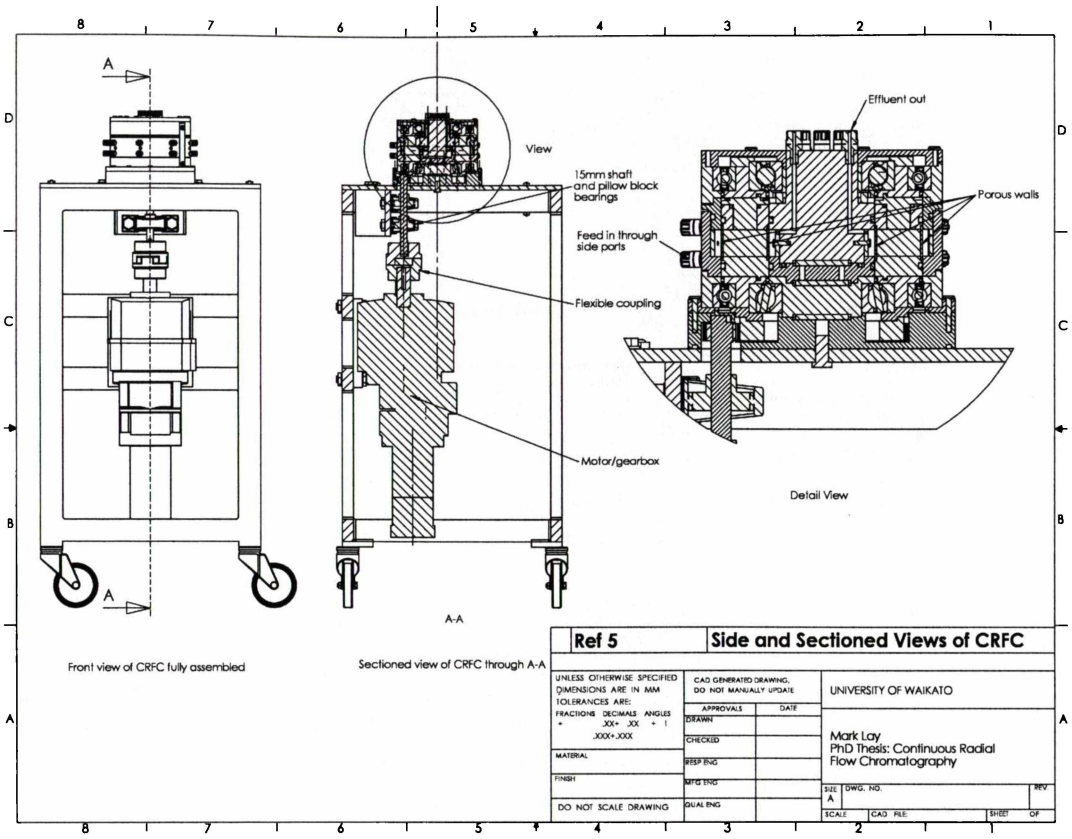
A
A
Front view of CRFC fully assembled
View
15mm shaft and pillow block bearings
Feed in through side ports
Flexible coupling
Motor/gearbox
A-A
Sectioned view of CRFC through A-A
Effluent out
Porous walls
Detail View
Ref 5
Side and Sectioned Views of CRFC
UNLESS OTHERWISE SPECIFIED DIMENSIONS ARE IN MM TOLERANCES ARE: FRACTIONS DECIMALS ANGLES + .XX+ .XX + 1 .XXX+.XXX
CAD GENERATED DRAWING. DO NOT MANUALLY UPDATE
APPROVALS DATE
DRAWN
CHECKED
RESP ENG
MFG ENG
QUAL ENG
MATERIAL
FINISH
DO NOT SCALE DRAWING
UNIVERSITY OF WAIKATO
Mark Lay
PhD Thesis: Continuous Radial Flow Chromatography
SIZE A
DWG. NO.
REV
SCALE
CAD FILE:
SHEET
OF

A.2 Annulus

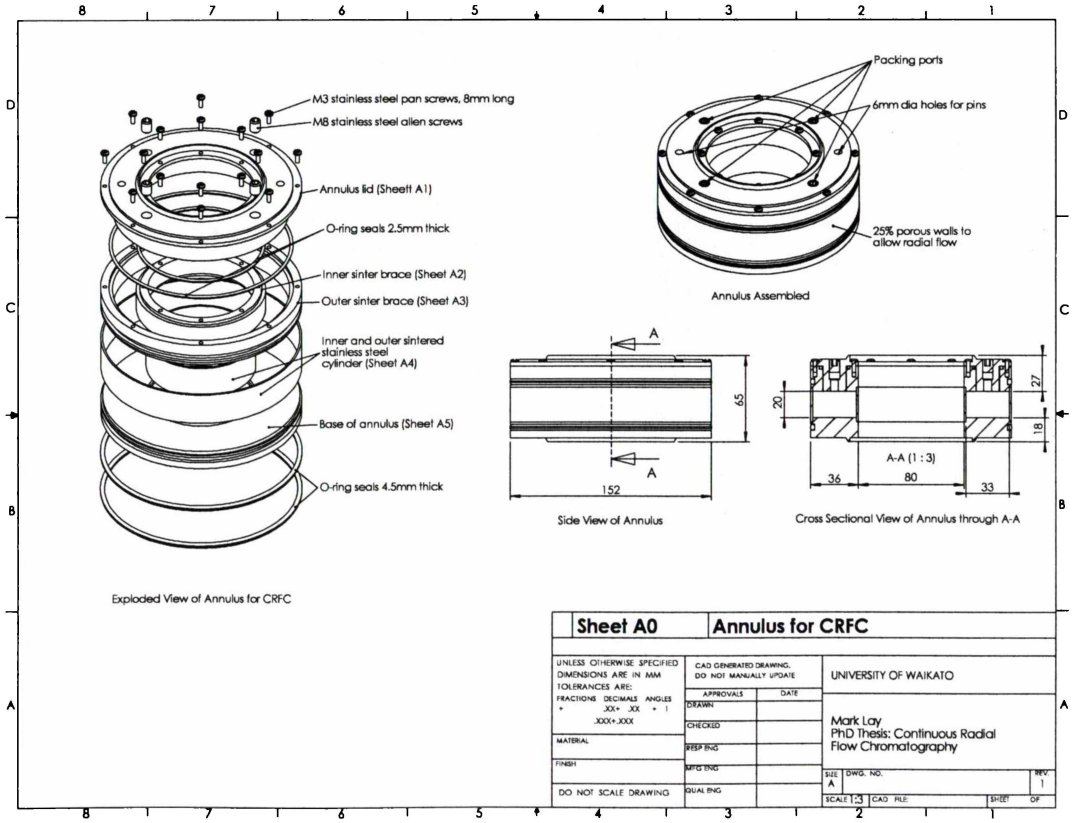
M3 stainless steel pan screws, 8mm long
M8 stainless steel allen screws
Annulus lid (Sheett A1)
O-ring seals 2.5mm thick
Inner sinter brace (Sheet A2)
Outer sinter brace (Sheet A3)
Inner and outer sintered stainless steel cylinder (Sheet A4)
Base of annulus (Sheet A5)
O-ring seals 4.5mm thick
Exploded View of Annulus for CRFC
Packing ports
6mm dia holes for pins
25% porous walls to allow radial flow
Annulus Assembled
A
65
152
A
Side View of Annulus
20
27
18
A-A (1 : 3)
36
80
33
Cross Sectional View of Annulus through A-A
Sheet A0
Annulus for CRFC
UNLESS OTHERWISE SPECIFIED DIMENSIONS ARE IN MM TOLERANCES ARE: FRACTIONS DECIMALS ANGLES + .XX+ .XX + 1 .XXX+.XXX
CAD GENERATED DRAWING. DO NOT MANUALLY UPDATE
APPROVALS DATE
DRAWN
CHECKED
RESP ENG
MFG ENG
QUAL ENG
MATERIAL
FINISH
DO NOT SCALE DRAWING
UNIVERSITY OF WAIKATO
Mark Lay
PhD Thesis: Continuous Radial Flow Chromatography
SIZE A
DWG. NO.
REV 1
SCALE 1:3
CAD FILE:
SHEET
OF

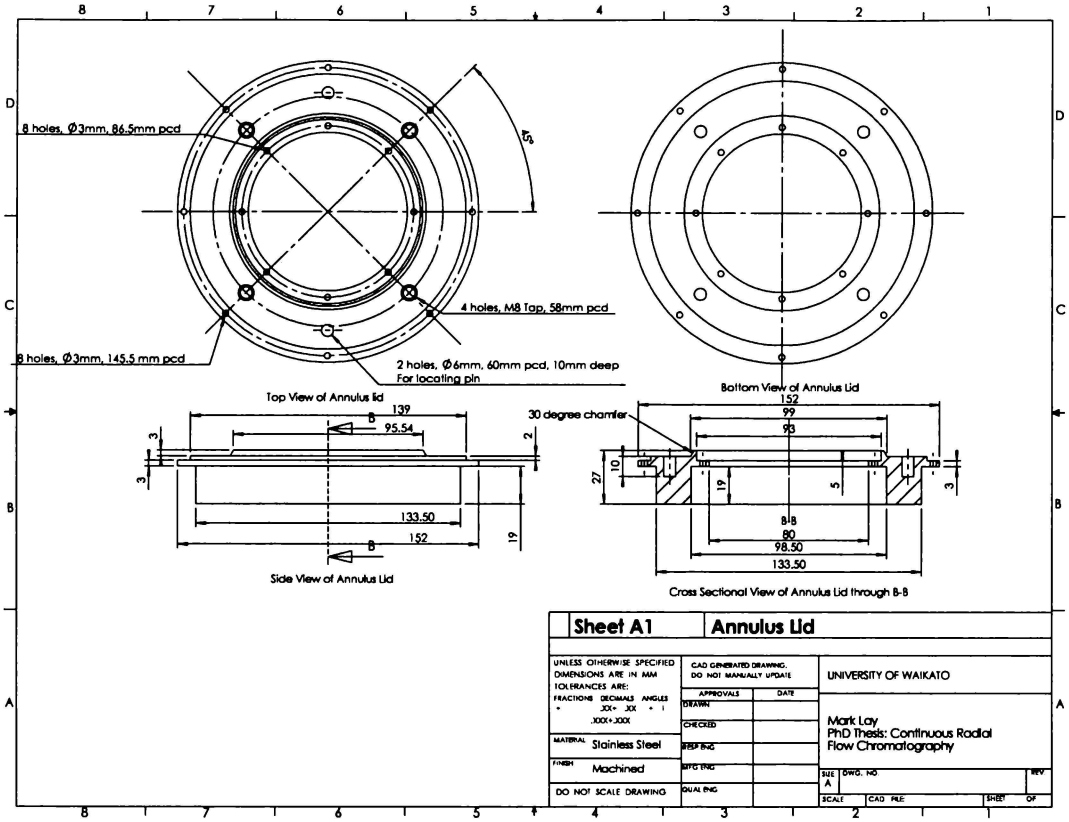
8 holes, Ø3mm, 86.5mm pcd
45°
4 holes, M8 Tap, 58mm pcd
8 holes, Ø3mm, 145.5 mm pcd
2 holes, Ø6mm, 60mm pcd, 10mm deep
For locating pin
Top View of Annulus lid
Bottom View of Annulus Lid
30 degree chamfer
139
95.54
133.50
152
Side View of Annulus Lid
152
99
93
80
98.50
133.50
Cross Sectional View of Annulus Lid through B-B
Sheet A1
Annulus Lid
UNLESS OTHERWISE SPECIFIED DIMENSIONS ARE IN MM TOLERANCES ARE: FRACTIONS DECIMALS ANGLES ± XX± .XX ± 1 .XXX±.XXX
CAD GENERATED DRAWING. DO NOT MANUALLY UPDATE
APPROVALS DATE
DRAWN
CHECKED
ENG APP
MFG ENG
QUAL ENG
MATERIAL Stainless Steel
FINISH Machined
DO NOT SCALE DRAWING
UNIVERSITY OF WAIKATO
Mark Lay
PhD Thesis: Continuous Radial Flow Chromatography
SIZE A
DWG. NO
REV
SCALE
CAD FILE
SHEET
OF

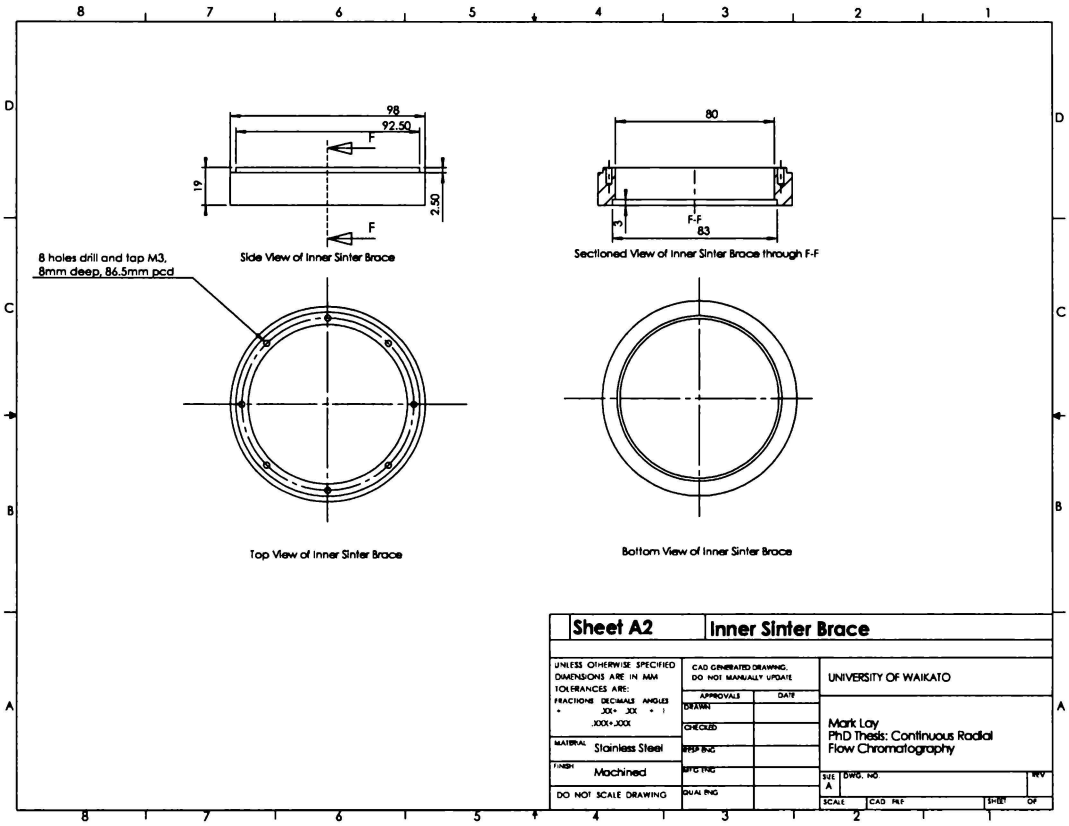
98
92.50
19
2.50
Side View of Inner Sinter Brace
80
3
F-F
83
Sectioned View of Inner Sinter Brace through F-F
8 holes drill and tap M3, 8mm deep, 86.5mm pcd
Top View of Inner Sinter Brace
Bottom View of Inner Sinter Brace
Sheet A2
Inner Sinter Brace
UNLESS OTHERWISE SPECIFIED DIMENSIONS ARE IN MM TOLERANCES ARE: FRACTIONS DECIMALS ANGLES ± XX± .XX ± 1 .XXX±.XXX
CAD GENERATED DRAWING. DO NOT MANUALLY UPDATE
APPROVALS DATE
DRAWN
CHECKED
ENG APP
MFG ENG
QUAL ENG
MATERIAL Stainless Steel
FINISH Machined
DO NOT SCALE DRAWING
UNIVERSITY OF WAIKATO
Mark Lay
PhD Thesis: Continuous Radial Flow Chromatography
SIZE A
DWG. NO
REV
SCALE
CAD FILE
SHEET
OF

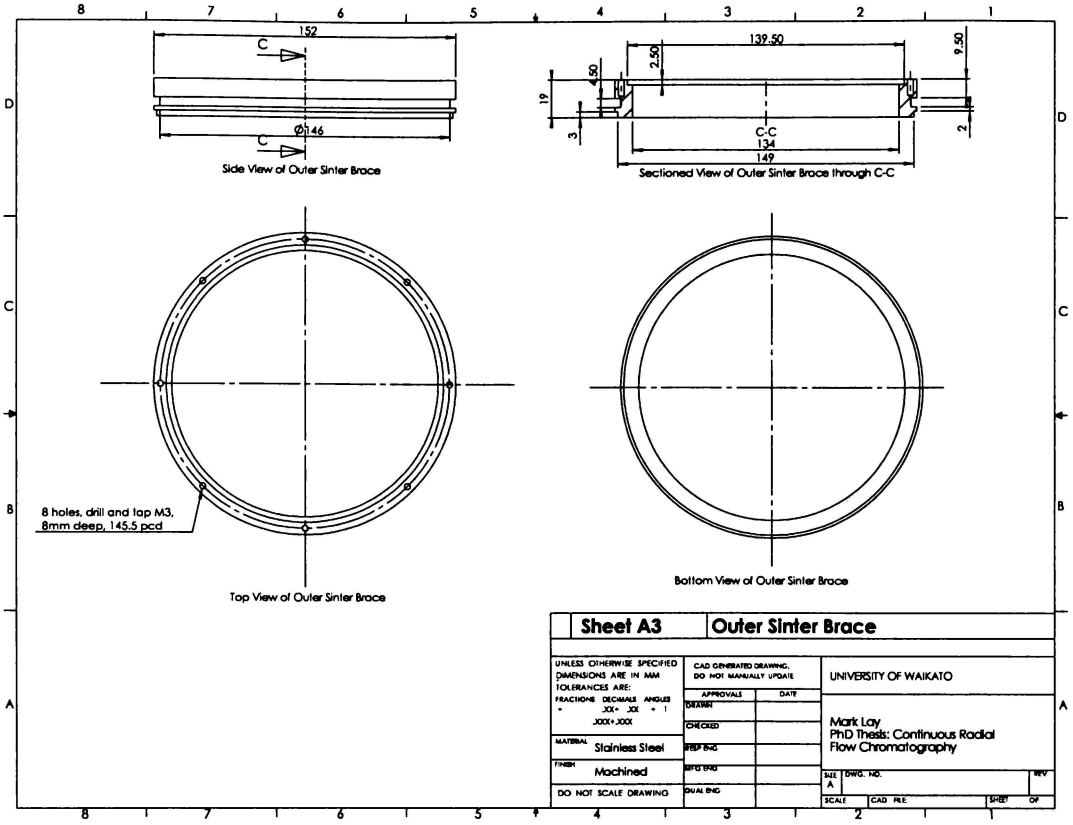
152
C
C
Ø146
Side View of Outer Sinter Brace
139.50
2.50
9.50
4.50
19
3
2
C-C
134
149
Sectioned View of Outer Sinter Brace through C-C
8 holes, drill and tap M3, 8mm deep, 145.5 pcd
Top View of Outer Sinter Brace
Bottom View of Outer Sinter Brace
Sheet A3
Outer Sinter Brace
UNLESS OTHERWISE SPECIFIED DIMENSIONS ARE IN MM TOLERANCES ARE:
FRACTIONS DECIMALS ANGLES
± .XX± .XX ± 1
.XXX± .XXX
MATERIAL Stainless Steel
FINISH Machined
DO NOT SCALE DRAWING
CAD GENERATED DRAWING. DO NOT MANUALLY UPDATE
APPROVALS DATE
DRAWN
CHECKED
MFG ENG
QUAL ENG
UNIVERSITY OF WAIKATO
Mark Lay
PhD Thesis: Continuous Radial Flow Chromatography
SIZE A
DWG. NO.
REV
SCALE
CAD FILE
SHEET
OF

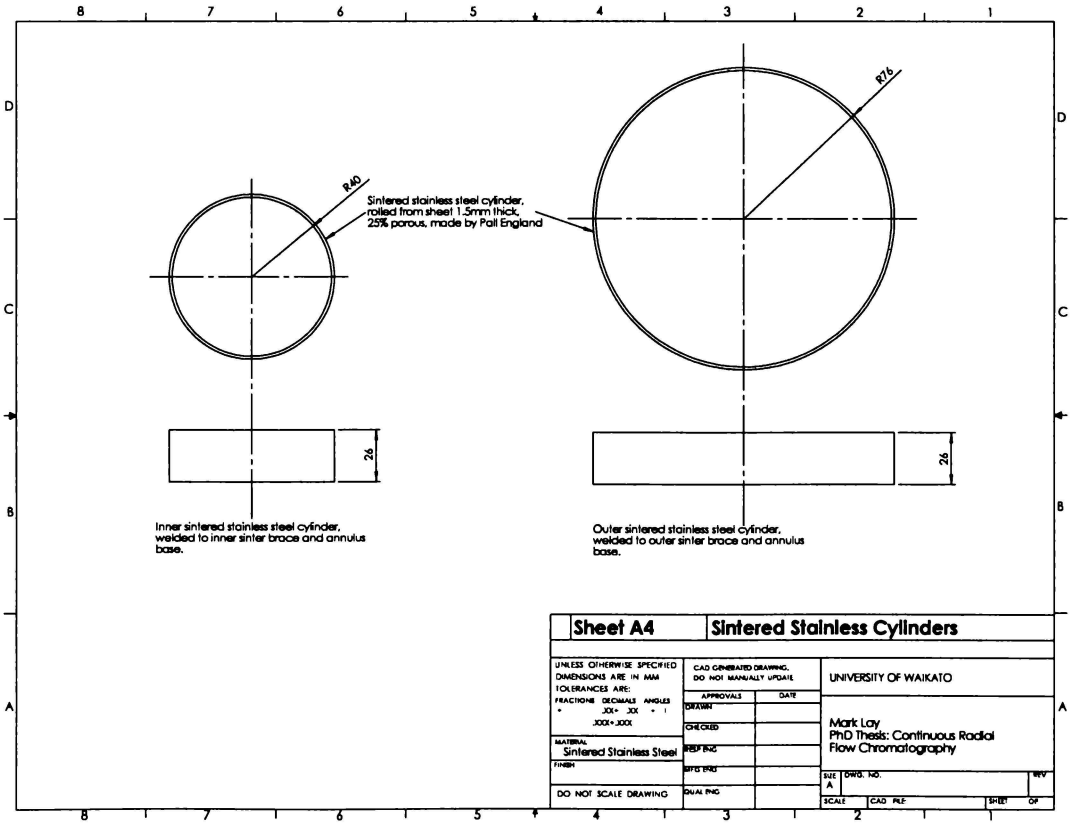
R40
Sintered stainless steel cylinder, rolled from sheet 1.5mm thick, 25% porous, made by Pall England
R76
26
26
Inner sintered stainless steel cylinder, welded to inner sinter brace and annulus base.
Outer sintered stainless steel cylinder, welded to outer sinter brace and annulus base.
Sheet A4
Sintered Stainless Cylinders
UNLESS OTHERWISE SPECIFIED DIMENSIONS ARE IN MM TOLERANCES ARE:
FRACTIONS DECIMALS ANGLES
± .XX± .XX ± 1
.XXX± .XXX
MATERIAL Sintered Stainless Steel
FINISH
DO NOT SCALE DRAWING
CAD GENERATED DRAWING. DO NOT MANUALLY UPDATE
APPROVALS DATE
DRAWN
CHECKED
MFG ENG
QUAL ENG
UNIVERSITY OF WAIKATO
Mark Lay
PhD Thesis: Continuous Radial Flow Chromatography
SIZE A
DWG. NO.
REV
SCALE
CAD FILE
SHEET
OF

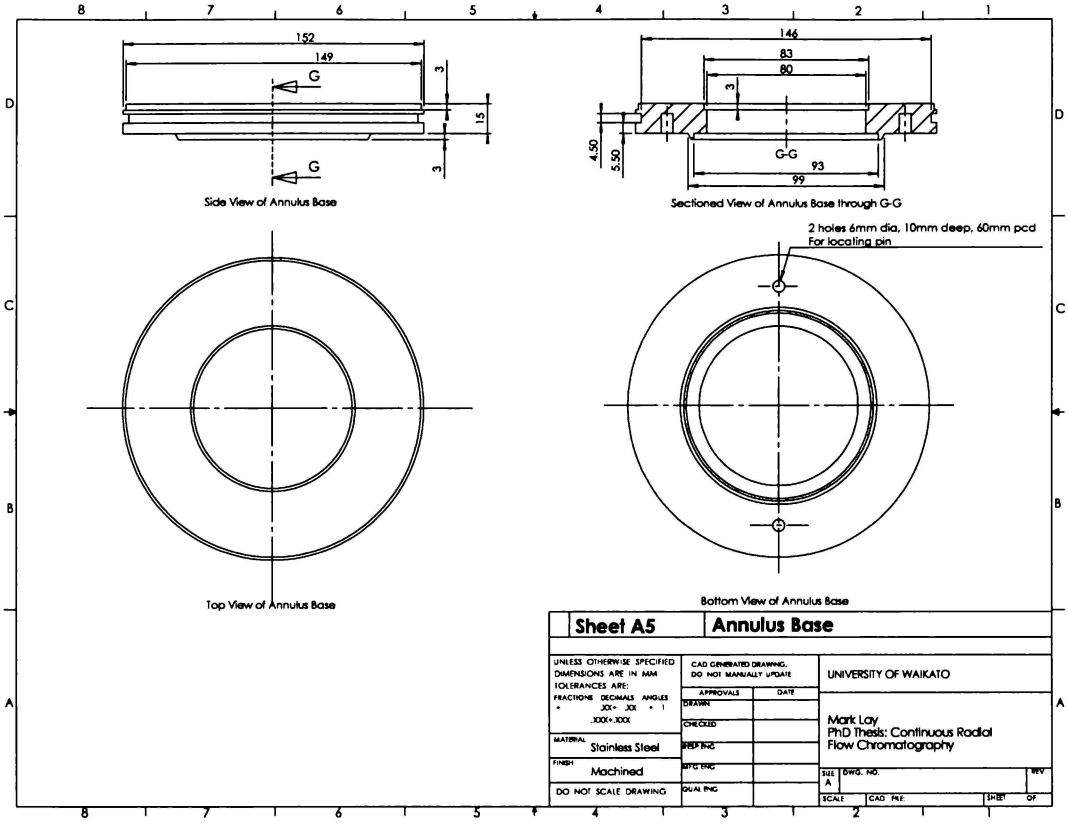

A.3 Outer Chamber

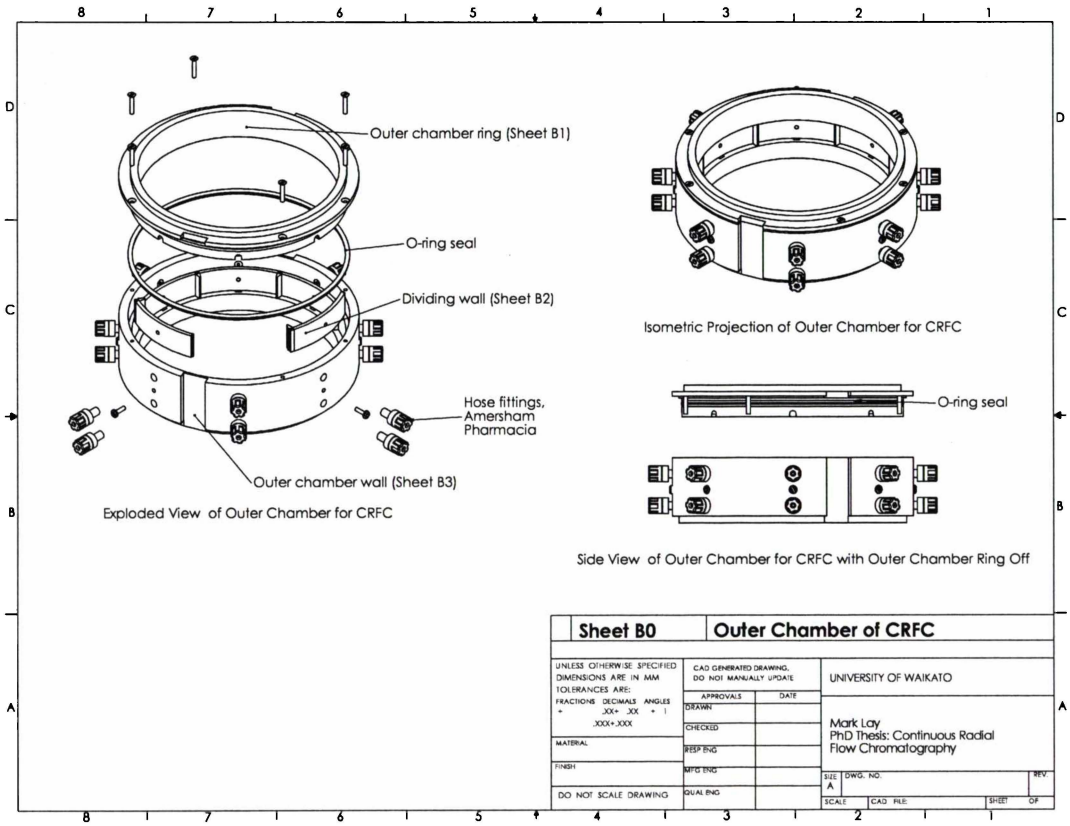

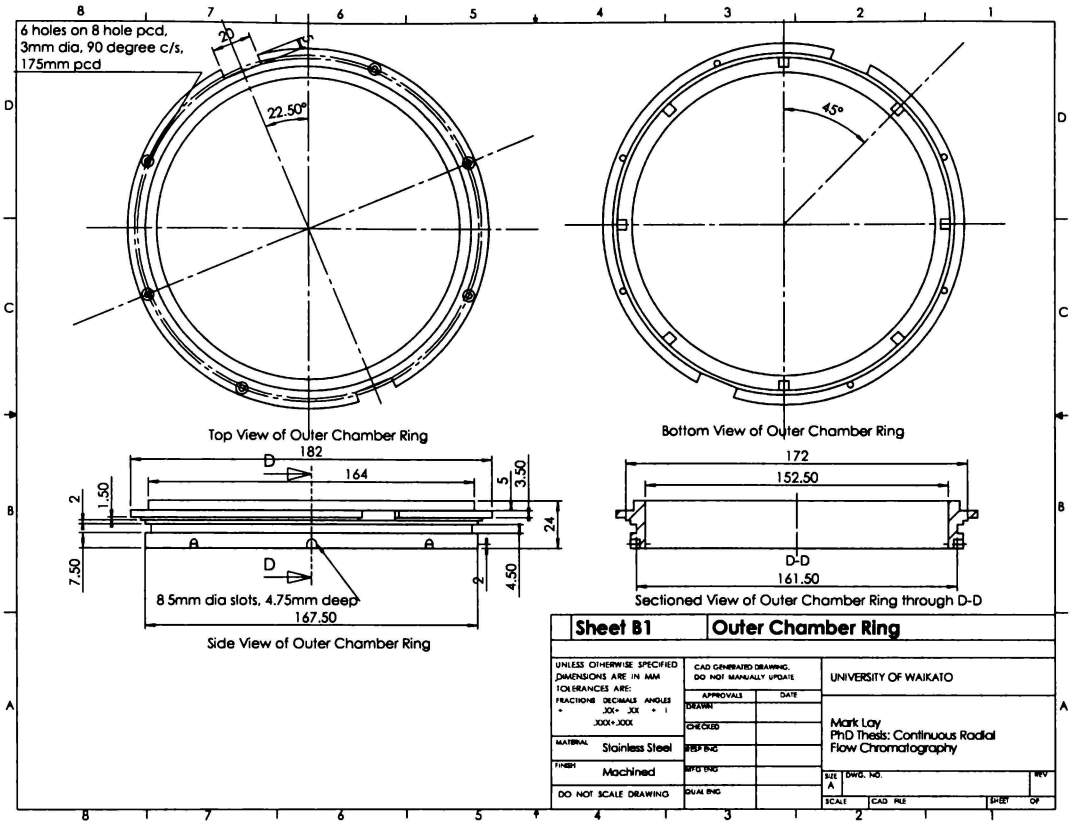
6 holes on 8 hole pcd,
3mm dia, 90 degree c/s,
175mm pcd
20
22.50°
Top View of Outer Chamber Ring
45°
Bottom View of Outer Chamber Ring
182
164
5
3.50
2
1.50
24
7.50
2
4.50
8.5mm dia slots, 4.75mm deep
167.50
Side View of Outer Chamber Ring
172
152.50
D-D
161.50
Sectioned View of Outer Chamber Ring through D-D
Sheet B1
Outer Chamber Ring
UNLESS OTHERWISE SPECIFIED DIMENSIONS ARE IN MM
TOLERANCES ARE:
FRACTIONS DECIMALS ANGLES
± .XX ± .XXX ± 1
MATERIAL Stainless Steel
FINISH Machined
DO NOT SCALE DRAWING
CAD GENERATED DRAWING. DO NOT MANUALLY UPDATE
APPROVALS DATE
DRAWN
CHECKED
MFG ENG
QUAL ENG
UNIVERSITY OF WAIKATO
Mark Lay
PhD Thesis: Continuous Radial Flow Chromatography
SIZE A
DWG. NO.
REV
SCALE
CAD FILE
SHEET OF

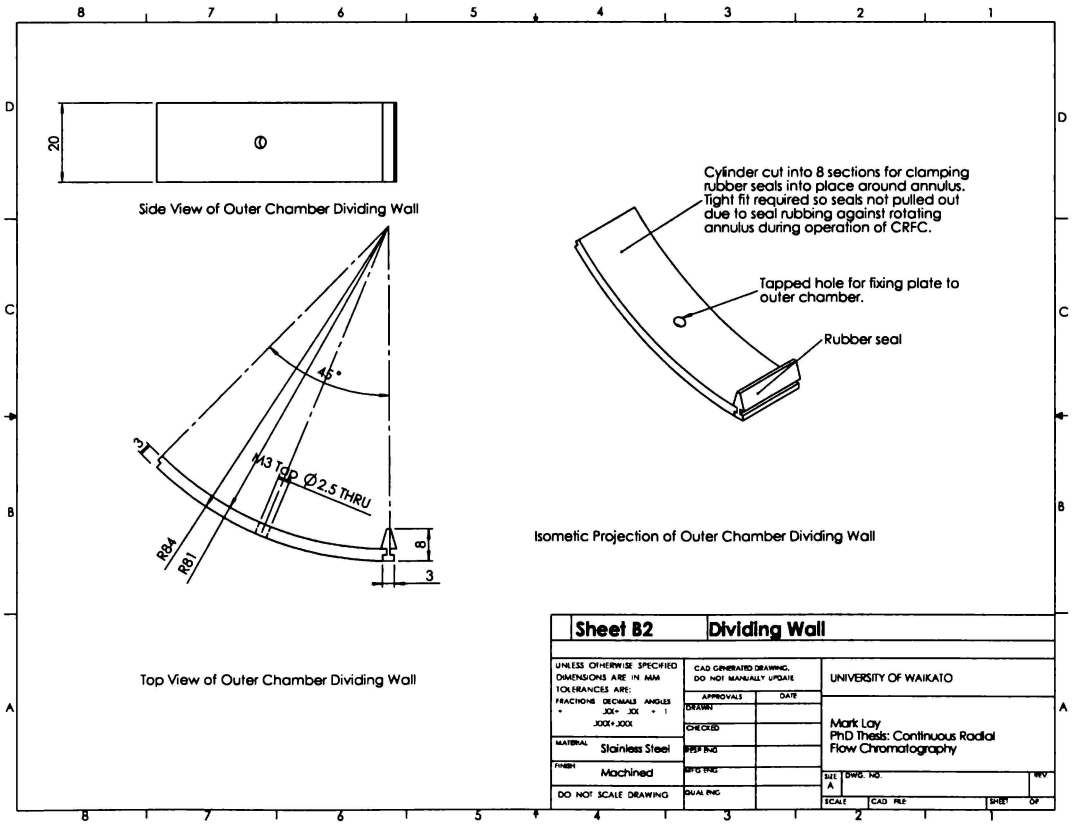
20
Side View of Outer Chamber Dividing Wall
Cylinder cut into 8 sections for clamping rubber seals into place around annulus. Tight fit required so seals not pulled out due to seal rubbing against rotating annulus during operation of CRFC.
Tapped hole for fixing plate to outer chamber.
Rubber seal
45°
M3 TAP Ø2.5 THRU
R84
R81
8
3
Top View of Outer Chamber Dividing Wall
Isometric Projection of Outer Chamber Dividing Wall
Sheet B2
Dividing Wall
UNLESS OTHERWISE SPECIFIED DIMENSIONS ARE IN MM
TOLERANCES ARE:
FRACTIONS DECIMALS ANGLES
± .XX ± .XXX ± 1
MATERIAL Stainless Steel
FINISH Machined
DO NOT SCALE DRAWING
CAD GENERATED DRAWING. DO NOT MANUALLY UPDATE
APPROVALS DATE
DRAWN
CHECKED
MFG ENG
QUAL ENG
UNIVERSITY OF WAIKATO
Mark Lay
PhD Thesis: Continuous Radial Flow Chromatography
SIZE A
DWG. NO.
REV
SCALE
CAD FILE
SHEET OF

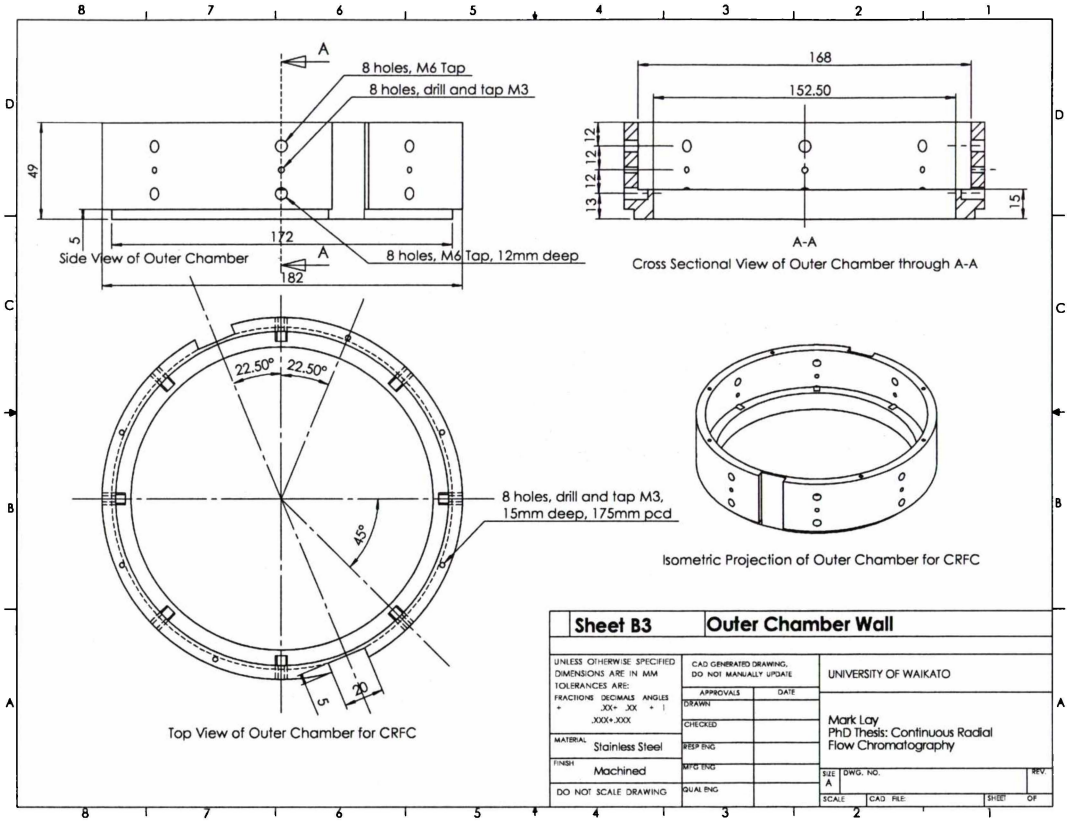

A.4 Inner Chamber

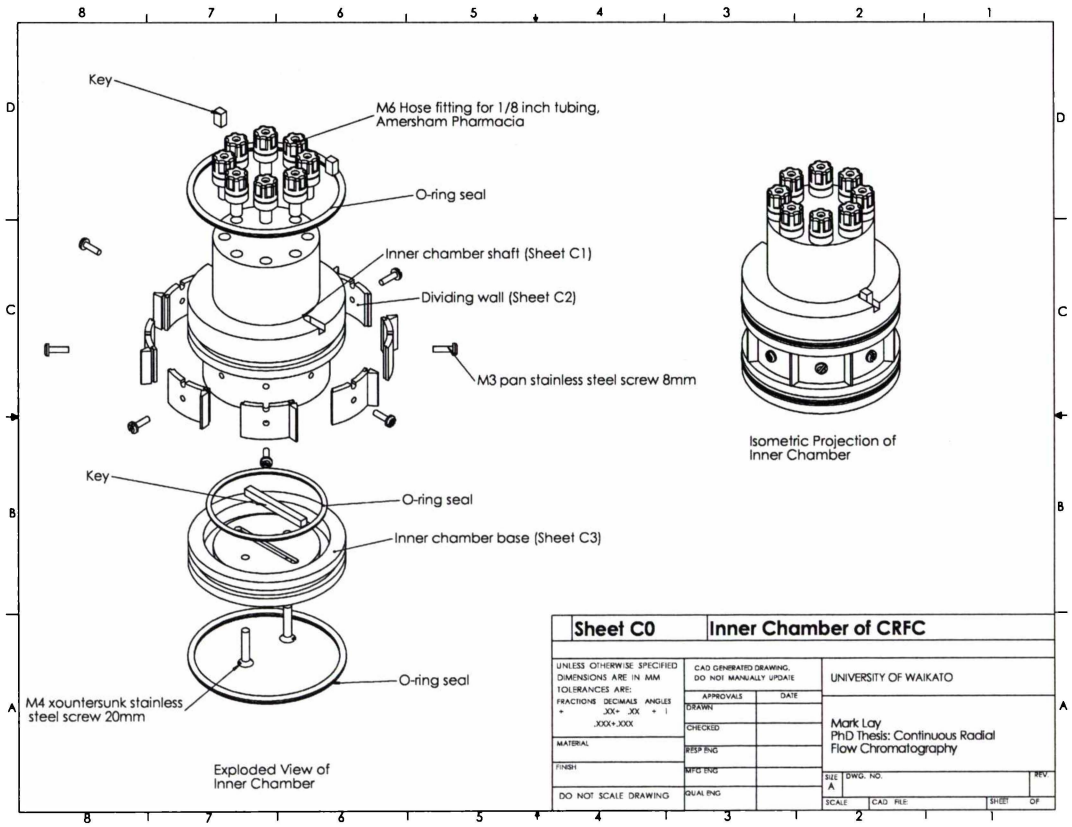

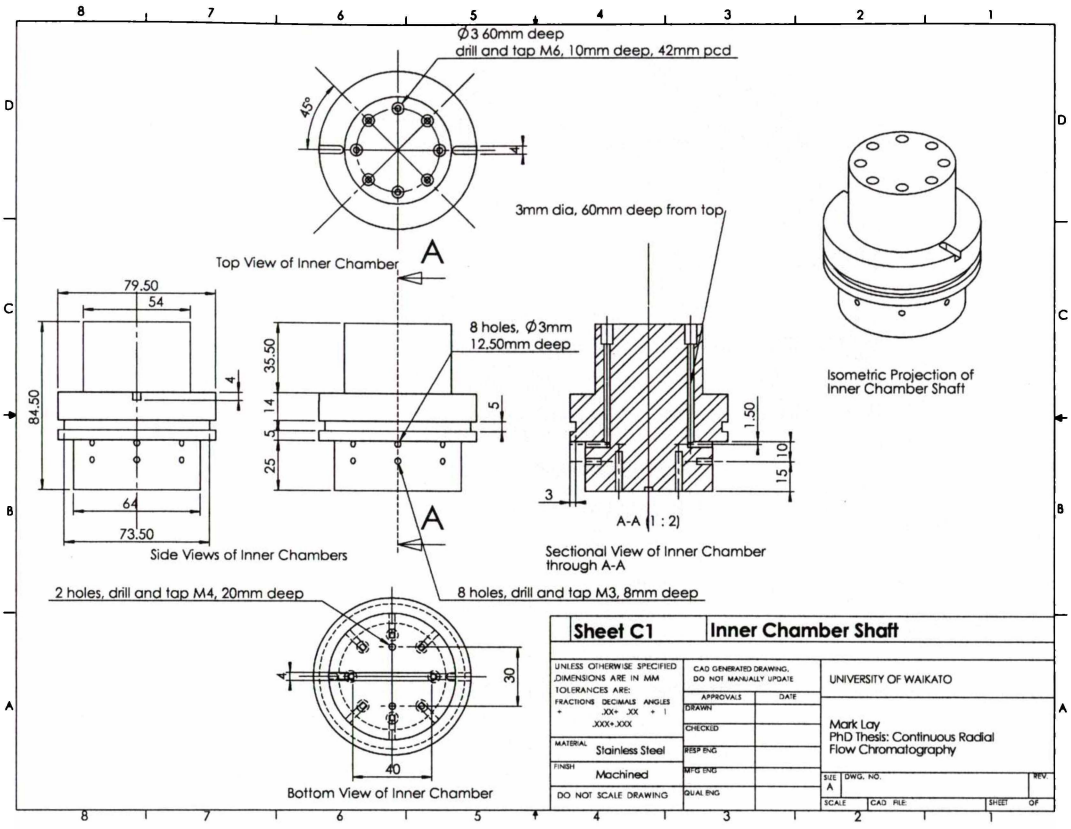
Ø3 60mm deep
drill and tap M6, 10mm deep, 42mm pcd
45°
Top View of Inner Chamber
3mm dia, 60mm deep from top
Isometric Projection of Inner Chamber Shaft
79.50
54
84.50
4
64
73.50
Side Views of Inner Chambers
8 holes, Ø3mm
12.50mm deep
35.50
14
5
25
5
A
A
A-A (1 : 2)
Sectional View of Inner Chamber through A-A
1.50
10
15
3
2 holes, drill and tap M4, 20mm deep
8 holes, drill and tap M3, 8mm deep
30
40
Bottom View of Inner Chamber
Sheet C1
Inner Chamber Shaft
UNLESS OTHERWISE SPECIFIED DIMENSIONS ARE IN MM TOLERANCES ARE: FRACTIONS DECIMALS ANGLES ± .XX± .XX ± 1 .XXX±.XXX
MATERIAL Stainless Steel
FINISH Machined
DO NOT SCALE DRAWING
CAD GENERATED DRAWING. DO NOT MANUALLY UPDATE
APPROVALS DATE
DRAWN
CHECKED
RESP ENG
MFG ENG
QUAL ENG
UNIVERSITY OF WAIKATO
Mark Lay
PhD Thesis: Continuous Radial Flow Chromatography
SIZE A
DWG. NO.
REV.
SCALE
CAD FILE
SHEET
OF

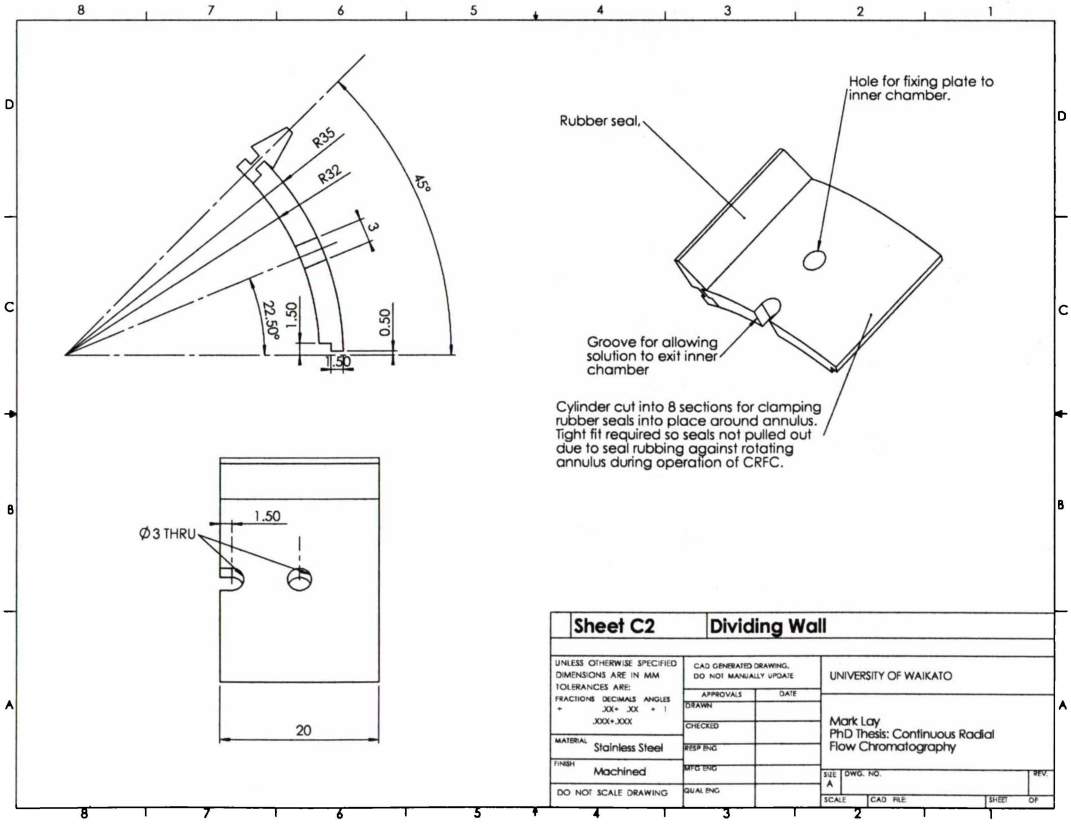
R35
R32
45°
3
22.50°
1.50
0.50
1.50
Hole for fixing plate to inner chamber.
Rubber seal,
Groove for allowing solution to exit inner chamber
Cylinder cut into 8 sections for clamping rubber seals into place around annulus. Tight fit required so seals not pulled out due to seal rubbing against rotating annulus during operation of CRFC.
Ø3 THRU
1.50
20
Sheet C2
Dividing Wall
UNLESS OTHERWISE SPECIFIED DIMENSIONS ARE IN MM TOLERANCES ARE: FRACTIONS DECIMALS ANGLES ± .XX± .XX ± 1 .XXX±.XXX
MATERIAL Stainless Steel
FINISH Machined
DO NOT SCALE DRAWING
CAD GENERATED DRAWING. DO NOT MANUALLY UPDATE
APPROVALS DATE
DRAWN
CHECKED
RESP ENG
MFG ENG
QUAL ENG
UNIVERSITY OF WAIKATO
Mark Lay
PhD Thesis: Continuous Radial Flow Chromatography
SIZE A
DWG. NO.
REV.
SCALE
CAD FILE
SHEET
OF

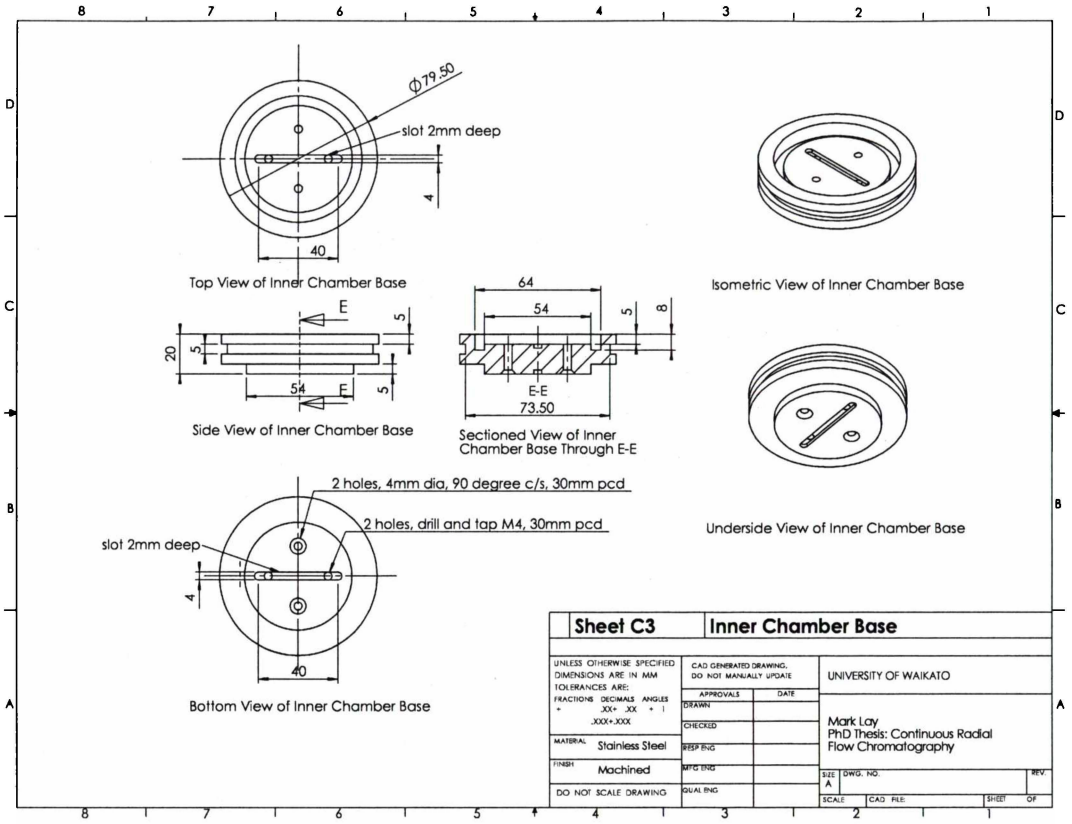

A.5 Top Bearing Housing

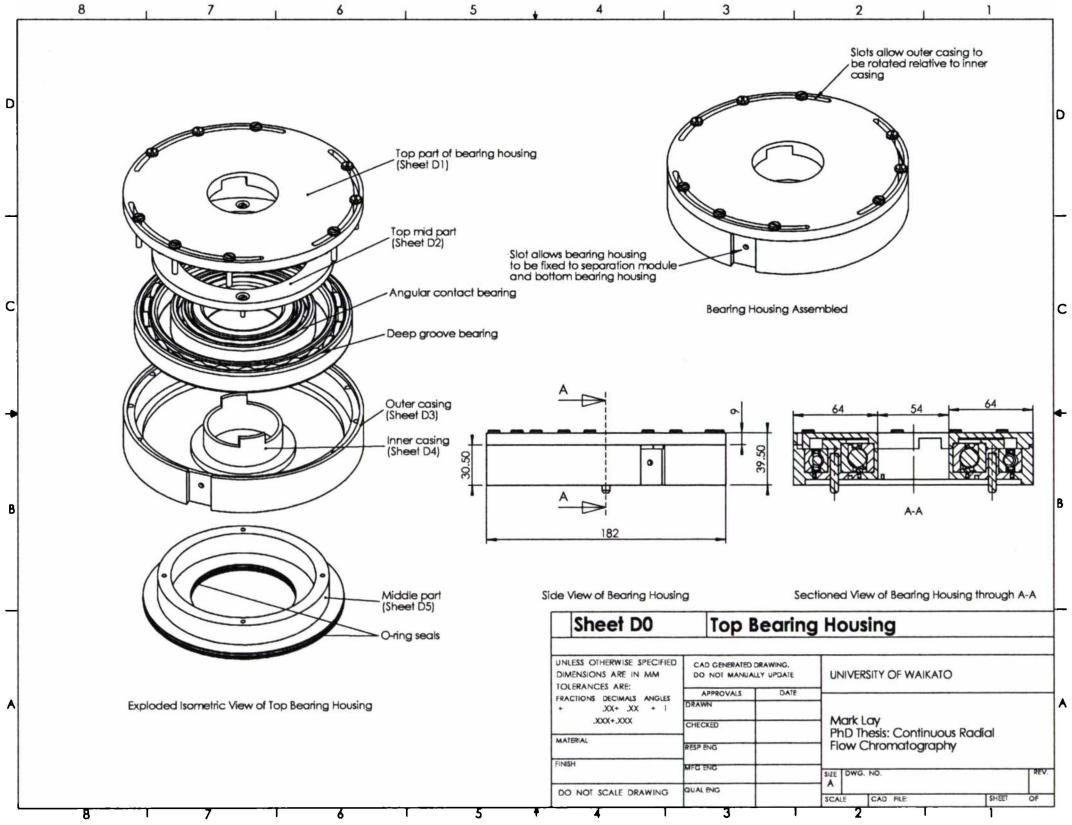

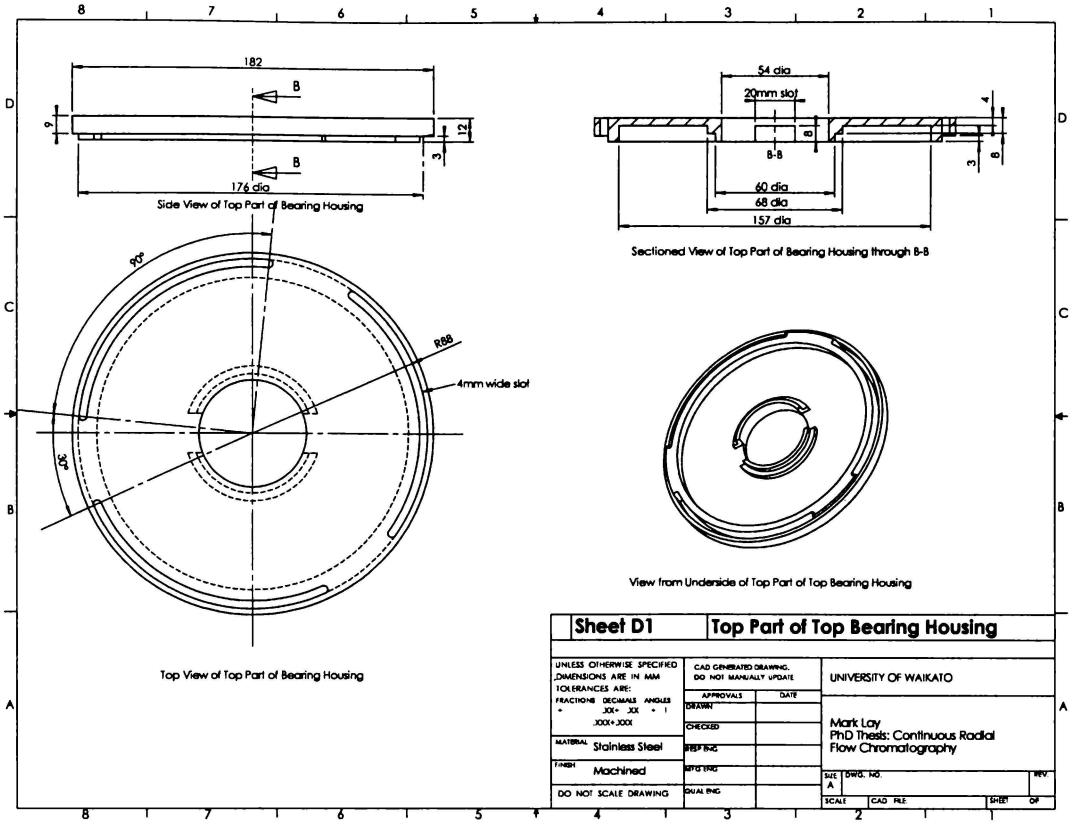
182
B
B
9
12
3
176 dia
Side View of Top Part of Bearing Housing
54 dia
20mm slot
8
4
8-8
3
6
60 dia
68 dia
157 dia
Sectioned View of Top Part of Bearing Housing through B-B
90°
R88
4mm wide slot
30°
Top View of Top Part of Bearing Housing
View from Underside of Top Part of Top Bearing Housing
Sheet D1
Top Part of Top Bearing Housing
UNLESS OTHERWISE SPECIFIED DIMENSIONS ARE IN MM
TOLERANCES ARE:
FRACTIONS DECIMALS ANGLES
± .XX ± .XX ± 1
.XXX ± .XXX
MATERIAL Stainless Steel
FINISH Machined
DO NOT SCALE DRAWING
CAD GENERATED DRAWING. DO NOT MANUALLY UPDATE
APPROVALS DATE
DRAWN
CHECKED
MFG ENG
QUAL ENG
UNIVERSITY OF WAIKATO
Mark Lay
PhD Thesis: Continuous Radial Flow Chromatography
SIZE A
DWG. NO.
REV
SCALE
CAD FILE
SHEET OF

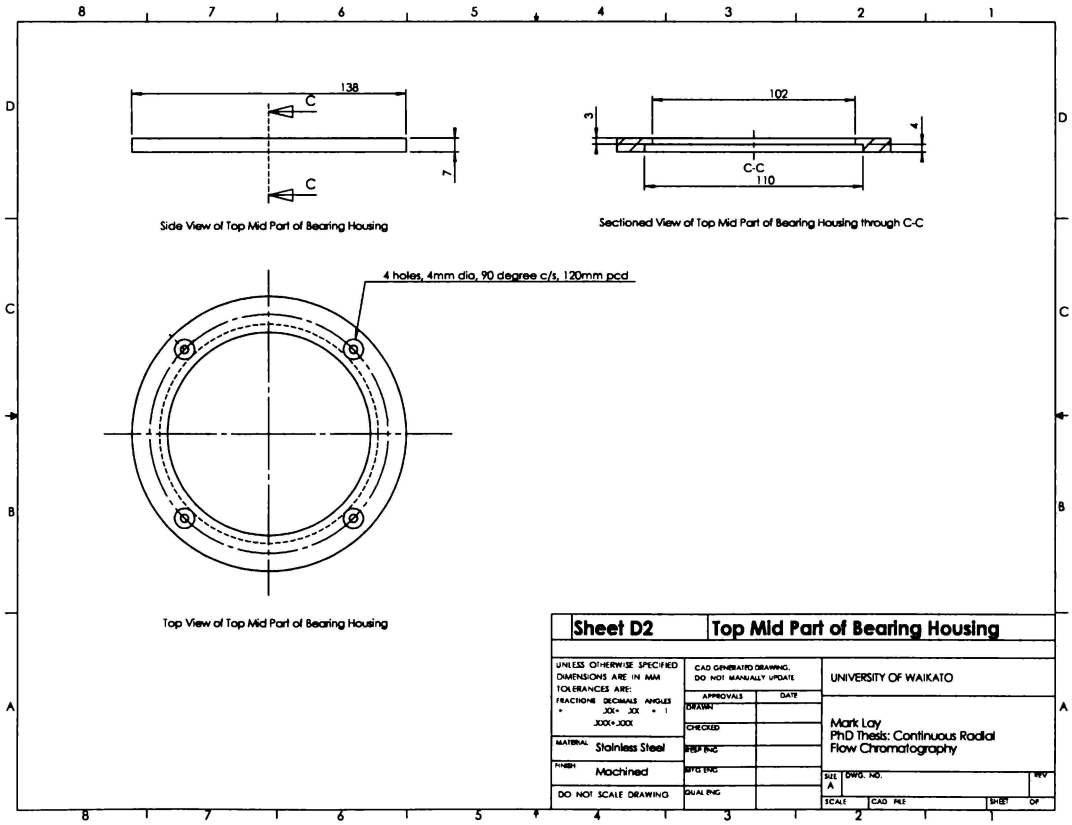
138
C
C
7
Side View of Top Mid Part of Bearing Housing
102
3
4
C-C
110
Sectioned View of Top Mid Part of Bearing Housing through C-C
4 holes, 4mm dia, 90 degree c/s, 120mm pcd
Top View of Top Mid Part of Bearing Housing
Sheet D2
Top Mid Part of Bearing Housing
UNLESS OTHERWISE SPECIFIED DIMENSIONS ARE IN MM
TOLERANCES ARE:
FRACTIONS DECIMALS ANGLES
± .XX ± .XX ± 1
.XXX ± .XXX
MATERIAL Stainless Steel
FINISH Machined
DO NOT SCALE DRAWING
CAD GENERATED DRAWING. DO NOT MANUALLY UPDATE
APPROVALS DATE
DRAWN
CHECKED
MFG ENG
QUAL ENG
UNIVERSITY OF WAIKATO
Mark Lay
PhD Thesis: Continuous Radial Flow Chromatography
SIZE A
DWG. NO.
REV
SCALE
CAD FILE
SHEET OF

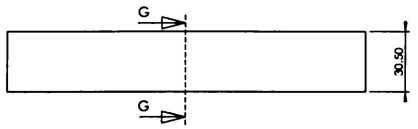

Side View of Outer Casing for Top Bearing Housing

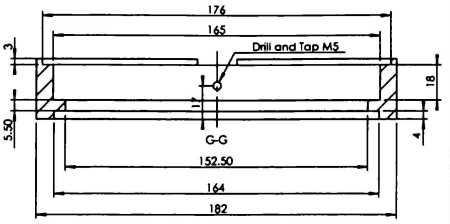

Sectioned View of Outer Casing for Top Bearing Housing through G-G

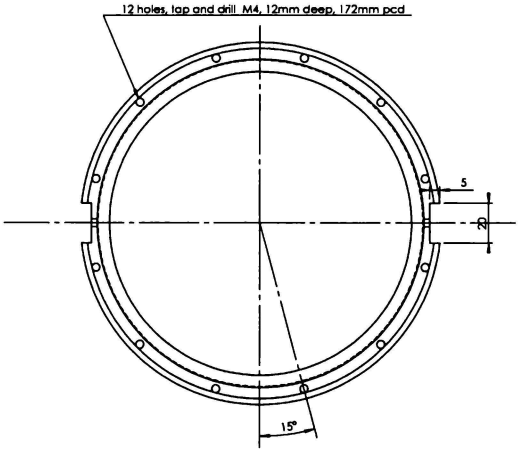

Top View of Outer Casing for Top Bearing Housing

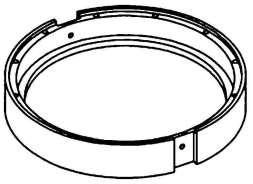

Isometric View of Outer Casing for Top Bearing Housing

Sheet D3	Outer Casing of Top Bearing Housing
UNLESS OTHERWISE SPECIFIED DIMENSIONS ARE IN MM TOLERANCES ARE: FRACTIONS DECIMALS ANGLES ± .XX± .XX ± 1 .XXX±.XXX	CAD GENERATED DRAWING. DO NOT MANUALLY UPDATE
MATERIAL Stainless Steel	APPROVALS DATE
FINISH Machined	DRAWN
DO NOT SCALE DRAWING	CHECKED
	MFG ENG
	QUAL ENG
UNIVERSITY OF WAIKATO	
Mark Lay PhD Thesis: Continuous Radial Flow Chromatography	
SIZE A DWG. NO. REV	
SCALE CAD FILE SHEET OF	

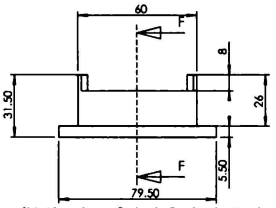

Side View of Inner Casing for Top Bearing Housing

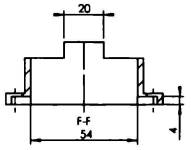

Sectioned View of Inner Casing for Top Bearing Housing through F-F

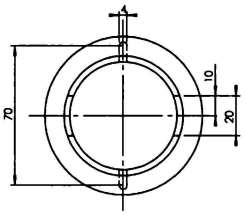

Top View of Inner Casing for Top Bearing Housing

Isometric and Underside View of Inner Casing for Top Bearing Housing

Sheet D4	Inner Casing
UNLESS OTHERWISE SPECIFIED DIMENSIONS ARE IN MM TOLERANCES ARE: FRACTIONS DECIMALS ANGLES ± .XX± .XX ± 1 .XXX±.XXX	CAD GENERATED DRAWING. DO NOT MANUALLY UPDATE
MATERIAL Stainless Steel	APPROVALS DATE
FINISH Machined	DRAWN
DO NOT SCALE DRAWING	CHECKED
	MFG ENG
	QUAL ENG
UNIVERSITY OF WAIKATO	
Mark Lay PhD Thesis: Continuous Radial Flow Chromatography	
SIZE A DWG. NO. REV	
SCALE CAD FILE SHEET OF	

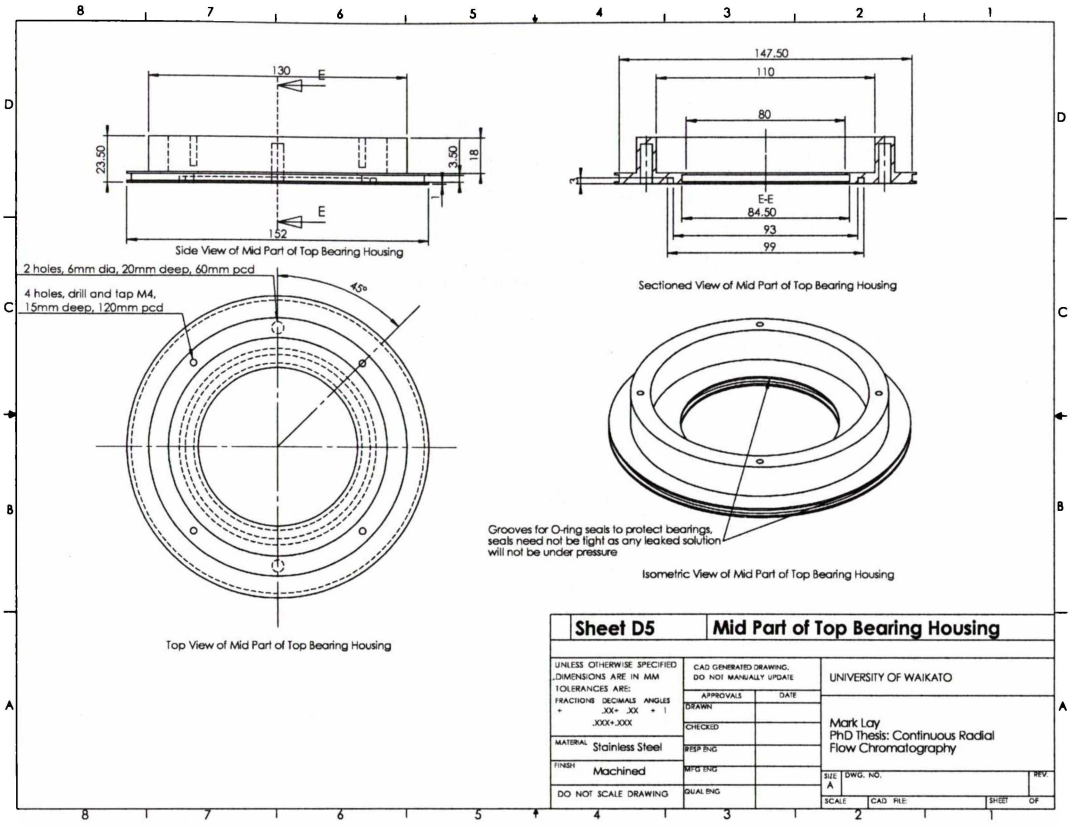
130
E
23.50
3.50
18
E
152
Side View of Mid Part of Top Bearing Housing
147.50
110
80
E-E
84.50
93
99
Sectioned View of Mid Part of Top Bearing Housing
2 holes, 6mm dia, 20mm deep, 60mm pcd
4 holes, drill and tap M4, 15mm deep, 120mm pcd
45°
Top View of Mid Part of Top Bearing Housing
Grooves for O-ring seals to protect bearings, seals need not be tight as any leaked solution will not be under pressure
Isometric View of Mid Part of Top Bearing Housing
Sheet D5
Mid Part of Top Bearing Housing
UNLESS OTHERWISE SPECIFIED DIMENSIONS ARE IN MM TOLERANCES ARE: FRACTIONS DECIMALS ANGLES ± .XX± .XX ± 1 .XXX±.XXX
MATERIAL Stainless Steel
FINISH Machined
DO NOT SCALE DRAWING
CAD GENERATED DRAWING. DO NOT MANUALLY UPDATE
APPROVALS DATE
DRAWN
CHECKED
RESP ENG
MFG ENG
QUAL ENG
UNIVERSITY OF WAIKATO
Mark Lay
PhD Thesis: Continuous Radial Flow Chromatography
SIZE A
DWG. NO.
REV
SCALE
CAD FILE
SHEET
OF

A.6 CRFC Base

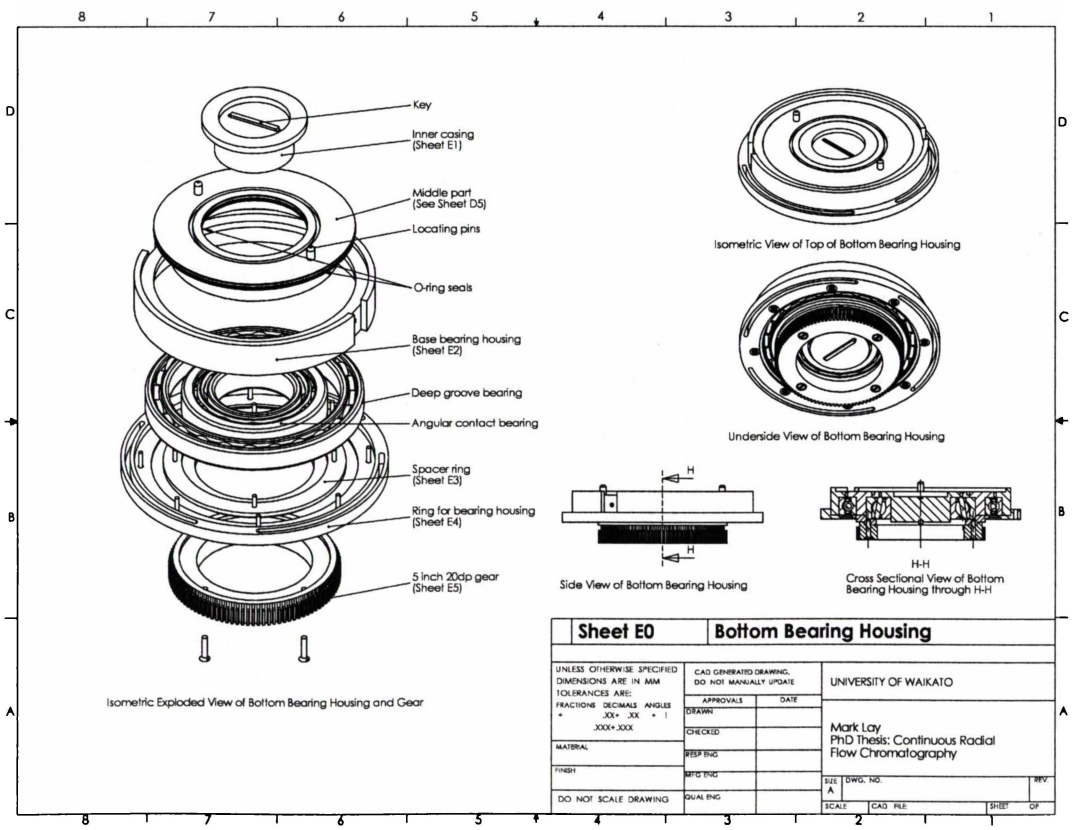
Key
Inner casing (Sheet E1)
Middle part (See Sheet D5)
Locating pins
O-ring seals
Base bearing housing (Sheet E2)
Deep groove bearing
Angular contact bearing
Spacer ring (Sheet E3)
Ring for bearing housing (Sheet E4)
5 inch 20dp gear (Sheet E5)
Isometric Exploded View of Bottom Bearing Housing and Gear
Isometric View of Top of Bottom Bearing Housing
Underside View of Bottom Bearing Housing
H
H
Side View of Bottom Bearing Housing
H-H
Cross Sectional View of Bottom Bearing Housing through H-H
Sheet E0
Bottom Bearing Housing
UNLESS OTHERWISE SPECIFIED DIMENSIONS ARE IN MM TOLERANCES ARE: FRACTIONS DECIMALS ANGLES ± .XX± .XX ± 1 .XXX±.XXX
MATERIAL
FINISH
DO NOT SCALE DRAWING
CAD GENERATED DRAWING. DO NOT MANUALLY UPDATE
APPROVALS DATE
DRAWN
CHECKED
RESP ENG
MFG ENG
QUAL ENG
UNIVERSITY OF WAIKATO
Mark Lay
PhD Thesis: Continuous Radial Flow Chromatography
SIZE A
DWG. NO.
REV
SCALE
CAD FILE
SHEET
OF

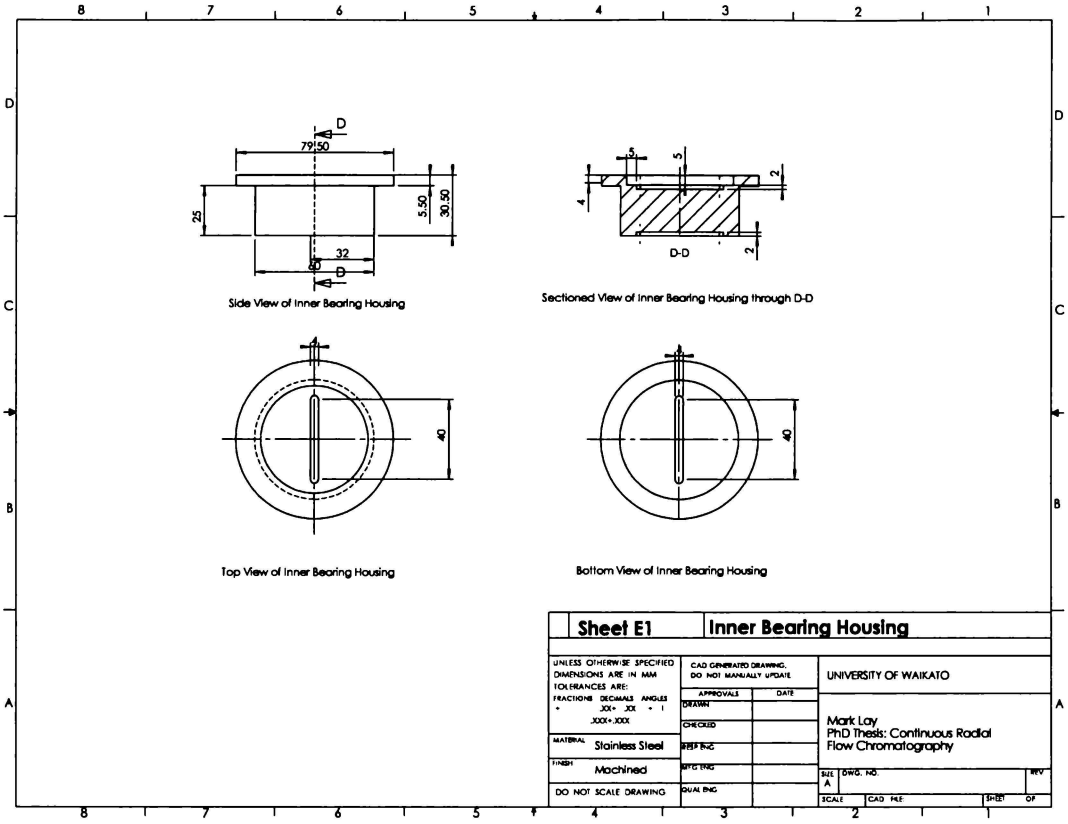
D
79.50
25
5.50
30.50
32
Side View of Inner Bearing Housing
5
5
2
4
2
D-D
Sectioned View of Inner Bearing Housing through D-D
40
Top View of Inner Bearing Housing
40
Bottom View of Inner Bearing Housing
Sheet E1
Inner Bearing Housing
UNLESS OTHERWISE SPECIFIED
DIMENSIONS ARE IN MM
TOLERANCES ARE:
FRACTIONS DECIMALS ANGLES
± .XX± .XX ± 1
.XXX±.XXX
MATERIAL Stainless Steel
FINISH Machined
DO NOT SCALE DRAWING
CAD GENERATED DRAWING.
DO NOT MANUALLY UPDATE
APPROVALS DATE
DRAWN
CHECKED
REQ'D ENG
MFG ENG
QUAL ENG
UNIVERSITY OF WAIKATO
Mark Lay
PhD Thesis: Continuous Radial
Flow Chromatography
SIZE A
DWG. NO.
REV
SCALE
CAD FILE
SHEET
OF

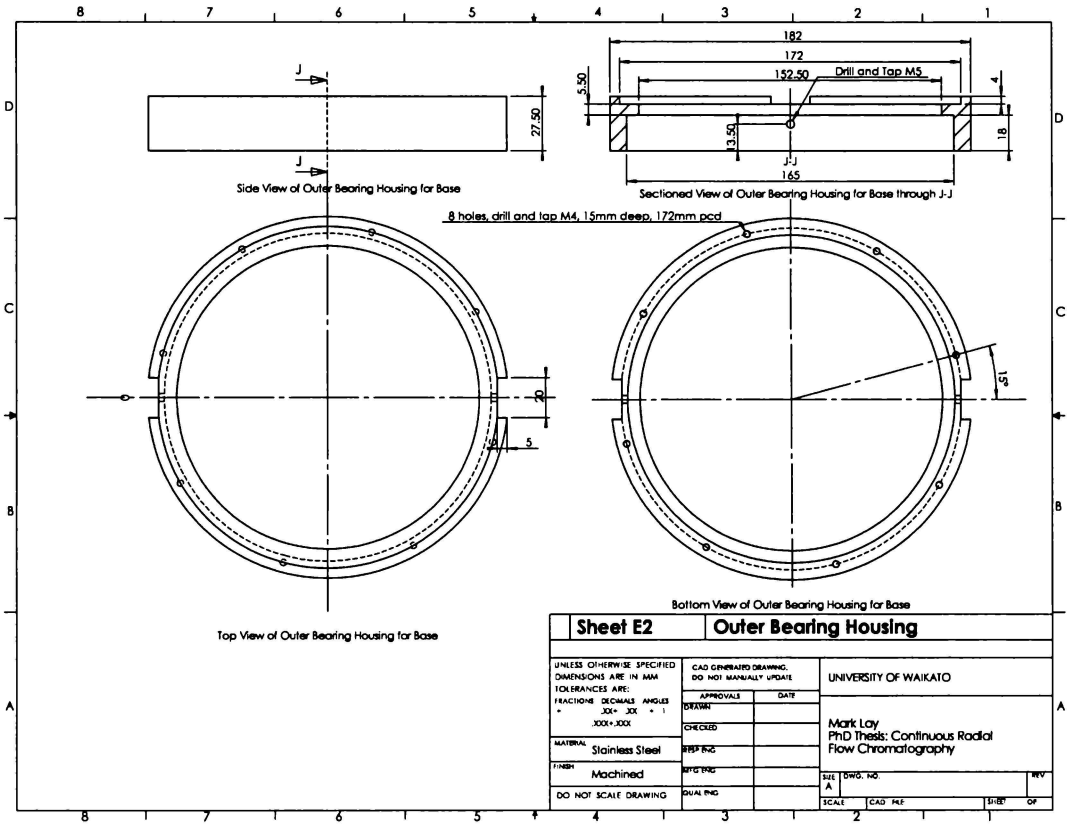
J
J
27.50
Side View of Outer Bearing Housing for Base
182
172
152.50
Drill and Tap M5
5.50
4
13.50
18
J-J
165
Sectioned View of Outer Bearing Housing for Base through J-J
8 holes, drill and tap M4, 15mm deep, 172mm pcd
20
15
5
Top View of Outer Bearing Housing for Base
51
Bottom View of Outer Bearing Housing for Base
Sheet E2
Outer Bearing Housing
UNLESS OTHERWISE SPECIFIED
DIMENSIONS ARE IN MM
TOLERANCES ARE:
FRACTIONS DECIMALS ANGLES
± .XX± .XX ± 1
.XXX±.XXX
MATERIAL Stainless Steel
FINISH Machined
DO NOT SCALE DRAWING
CAD GENERATED DRAWING.
DO NOT MANUALLY UPDATE
APPROVALS DATE
DRAWN
CHECKED
REQ'D ENG
MFG ENG
QUAL ENG
UNIVERSITY OF WAIKATO
Mark Lay
PhD Thesis: Continuous Radial
Flow Chromatography
SIZE A
DWG. NO.
REV
SCALE
CAD FILE
SHEET
OF

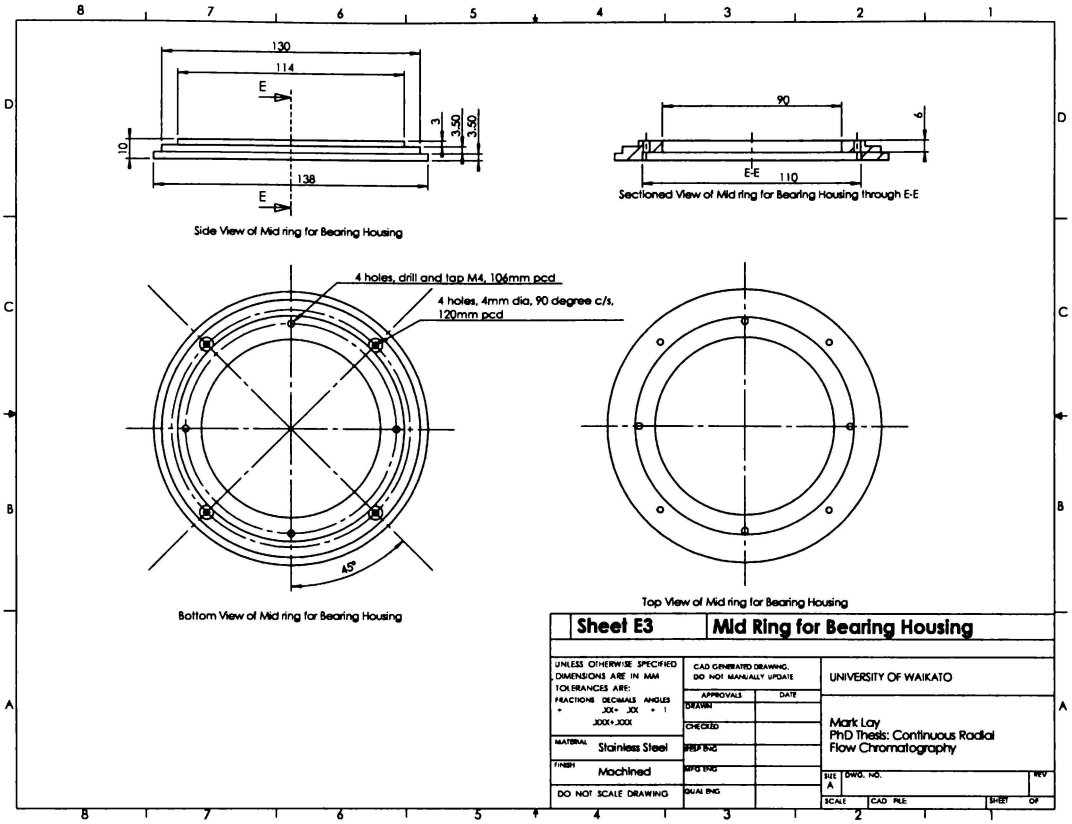
130
114
E
3
3.50
3.50
10
138
E
Side View of Mid ring for Bearing Housing
90
6
E-E
110
Sectioned View of Mid ring for Bearing Housing through E-E
4 holes, drill and tap M4, 106mm pcd
4 holes, 4mm dia, 90 degree c/s, 120mm pcd
45°
Bottom View of Mid ring for Bearing Housing
Top View of Mid ring for Bearing Housing
Sheet E3
Mid Ring for Bearing Housing
UNLESS OTHERWISE SPECIFIED DIMENSIONS ARE IN MM
TOLERANCES ARE:
FRACTIONS DECIMALS ANGLES
± .XX ± .1
.XXX± .XXX
MATERIAL Stainless Steel
FINISH Machined
DO NOT SCALE DRAWING
CAD GENERATED DRAWING. DO NOT MANUALLY UPDATE
APPROVALS DATE
DRAWN
CHECKED
MFG ENG
QUAL ENG
UNIVERSITY OF WAIKATO
Mark Lay
PhD Thesis: Continuous Radial Flow Chromatography
SIZE A
DWG. NO.
REV
SCALE
CAD FILE
SHEET
OF

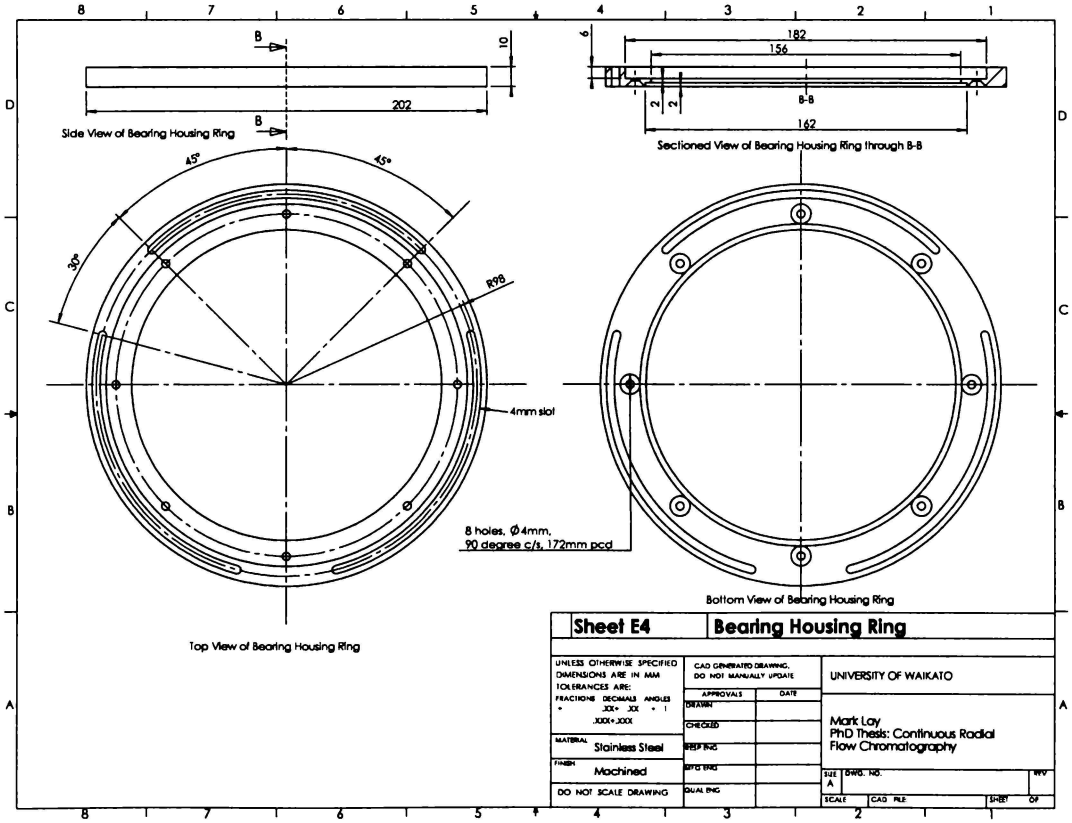
B
10
202
B
Side View of Bearing Housing Ring
6
182
156
2
2
B-B
162
Sectioned View of Bearing Housing Ring through B-B
45°
45°
30°
R98
4mm slot
8 holes, Ø4mm, 90 degree c/s, 172mm pcd
Top View of Bearing Housing Ring
Bottom View of Bearing Housing Ring
Sheet E4
Bearing Housing Ring
UNLESS OTHERWISE SPECIFIED DIMENSIONS ARE IN MM
TOLERANCES ARE:
FRACTIONS DECIMALS ANGLES
± .XX ± .1
.XXX± .XXX
MATERIAL Stainless Steel
FINISH Machined
DO NOT SCALE DRAWING
CAD GENERATED DRAWING. DO NOT MANUALLY UPDATE
APPROVALS DATE
DRAWN
CHECKED
MFG ENG
QUAL ENG
UNIVERSITY OF WAIKATO
Mark Lay
PhD Thesis: Continuous Radial Flow Chromatography
SIZE A
DWG. NO.
REV
SCALE
CAD FILE
SHEET
OF

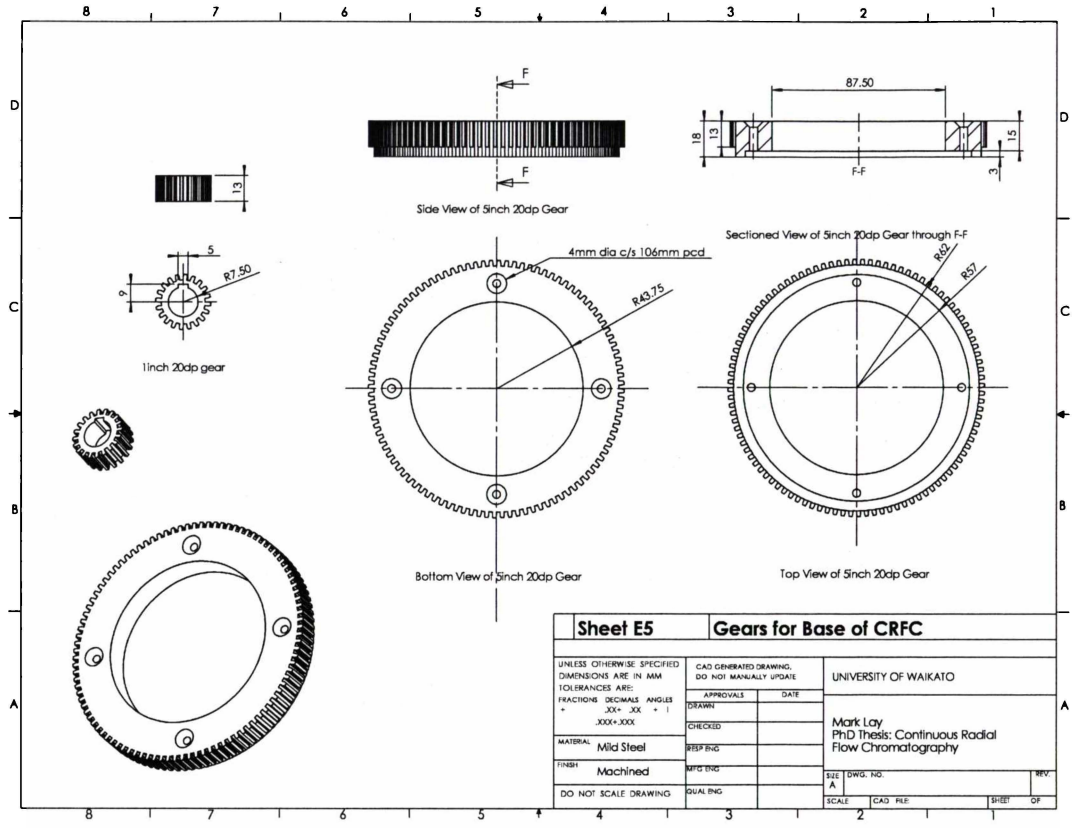

A.7 Stand and Gear Housing

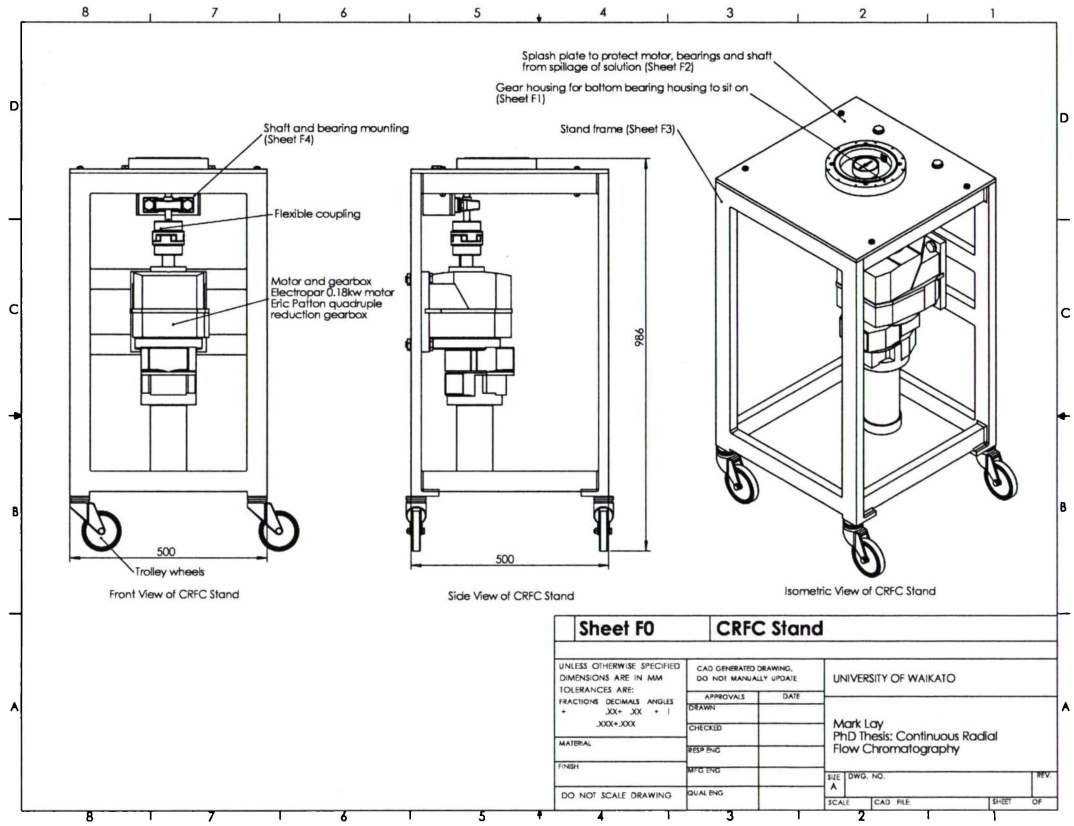

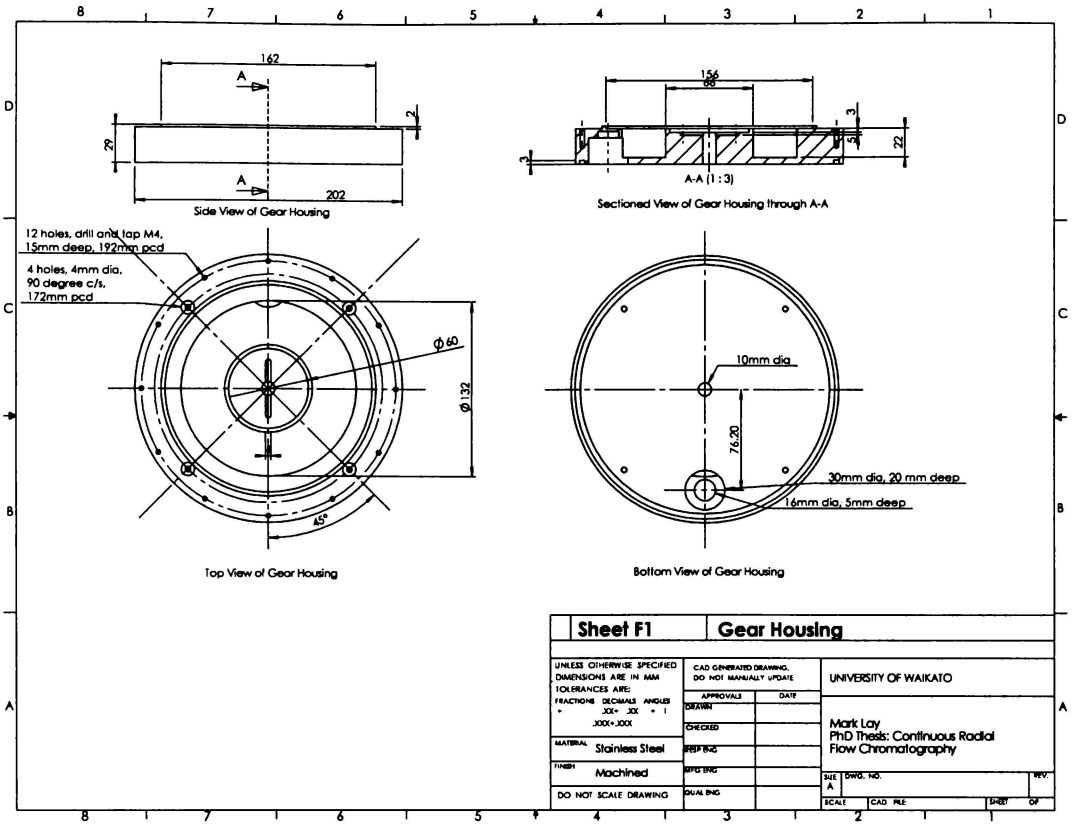
162
A
29
2
202
Side View of Gear Housing
156
66
3
5
22
A-A (1 : 3)
Sectioned View of Gear Housing through A-A
12 holes, drill and tap M4, 15mm deep, 192mm pcd
4 holes, 4mm dia, 90 degree c/s, 172mm pcd
Ø60
Ø132
45°
Top View of Gear Housing
10mm dia
76.20
30mm dia, 20 mm deep
16mm dia, 5mm deep
Bottom View of Gear Housing
Sheet F1
Gear Housing
UNLESS OTHERWISE SPECIFIED DIMENSIONS ARE IN MM
TOLERANCES ARE:
FRACTIONS DECIMALS ANGLES
± .XX ± .01
.XXX±.005
MATERIAL Stainless Steel
FINISH Machined
DO NOT SCALE DRAWING
CAD GENERATED DRAWING. DO NOT MANUALLY UPDATE
APPROVALS DATE
DRAWN
CHECKED
ENG APP
MFG ENG
QUAL ENG
UNIVERSITY OF WAIKATO
Mark Lay
PhD Thesis: Continuous Radial Flow Chromatography
SIZE A
DWG. NO.
REV.
SCALE
CAD FILE
SHEET
OF

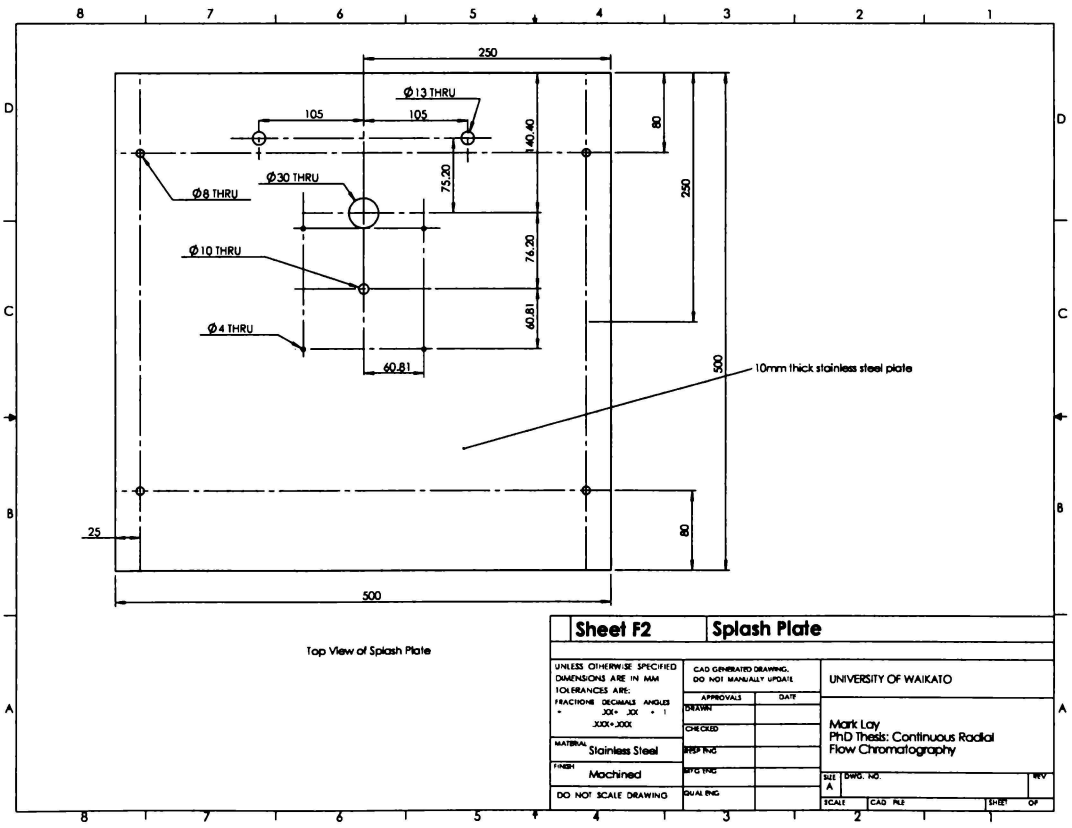
250
Ø13 THRU
105
105
40.40
80
75.20
Ø8 THRU
Ø30 THRU
250
Ø10 THRU
76.20
Ø4 THRU
60.81
60.81
500
10mm thick stainless steel plate
25
80
500
Top View of Splash Plate
Sheet F2
Splash Plate
UNLESS OTHERWISE SPECIFIED DIMENSIONS ARE IN MM
TOLERANCES ARE:
FRACTIONS DECIMALS ANGLES
± .XX ± .01
.XXX±.005
MATERIAL Stainless Steel
FINISH Machined
DO NOT SCALE DRAWING
CAD GENERATED DRAWING. DO NOT MANUALLY UPDATE
APPROVALS DATE
DRAWN
CHECKED
ENG APP
MFG ENG
QUAL ENG
UNIVERSITY OF WAIKATO
Mark Lay
PhD Thesis: Continuous Radial Flow Chromatography
SIZE A
DWG. NO.
REV.
SCALE
CAD FILE
SHEET
OF

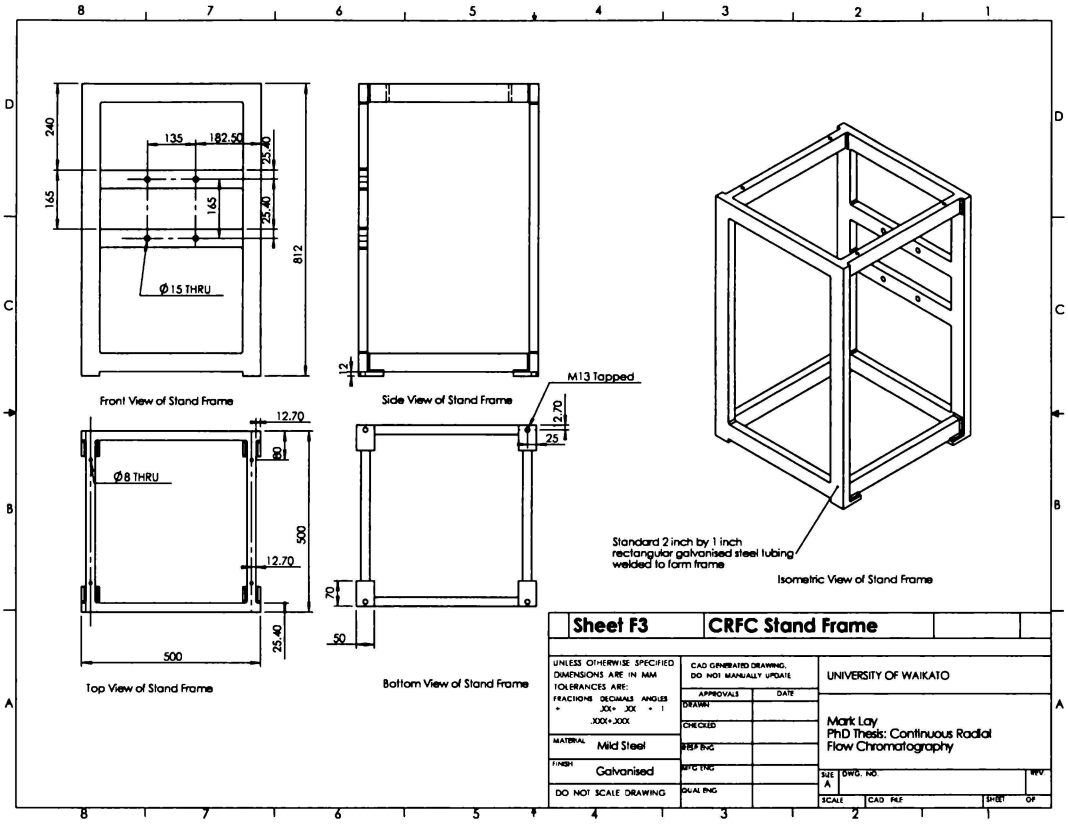
240
135
182.50
25.40
165
165
25.40
812
Ø15 THRU
Front View of Stand Frame
12
Side View of Stand Frame
M13 Tapped
12.70
25
12.70
80
Ø8 THRU
500
12.70
70
50
500
25.40
Top View of Stand Frame
Bottom View of Stand Frame
Standard 2 inch by 1 inch rectangular galvanised steel tubing welded to form frame
Isometric View of Stand Frame
Sheet F3
CRFC Stand Frame
UNLESS OTHERWISE SPECIFIED DIMENSIONS ARE IN MM TOLERANCES ARE:
FRACTIONS DECIMALS ANGLES
± .XX± .XX ± 1
.XXX±.XXX
MATERIAL Mild Steel
FINISH Galvanised
DO NOT SCALE DRAWING
CAD GENERATED DRAWING. DO NOT MANUALLY UPDATE
APPROVALS DATE
DRAWN
CHECKED
ENG APP
MFG APP
QUAL ENG
UNIVERSITY OF WAIKATO
Mark Lay
PhD Thesis: Continuous Radial Flow Chromatography
SIZE A
DWG. NO.
REV
SCALE
CAD REF
SHEET
OF

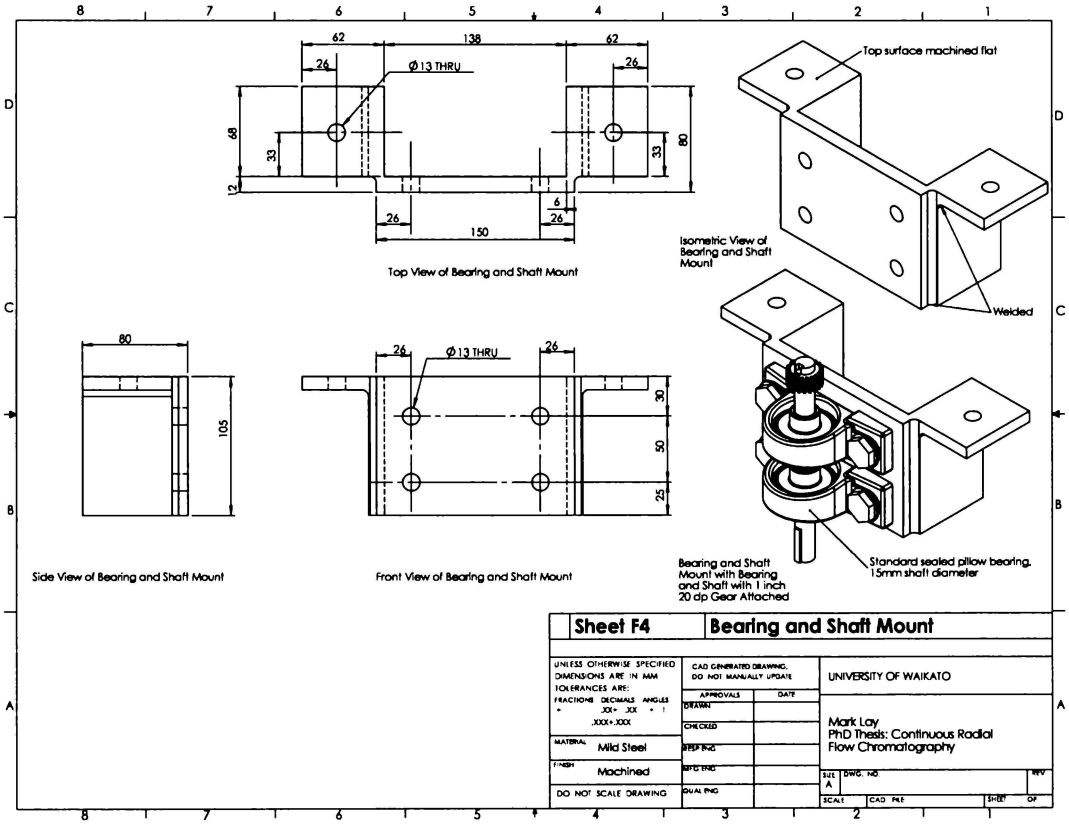
62
138
62
26
26
Ø13 THRU
68
33
33
80
12
6
26
26
150
Top View of Bearing and Shaft Mount
Top surface machined flat
Isometric View of Bearing and Shaft Mount
Welded
80
105
26
Ø13 THRU
26
30
50
25
Side View of Bearing and Shaft Mount
Front View of Bearing and Shaft Mount
Bearing and Shaft Mount with Bearing and Shaft with 1 inch 20 dp Gear Attached
Standard sealed pillow bearing, 15mm shaft diameter
Sheet F4
Bearing and Shaft Mount
UNLESS OTHERWISE SPECIFIED DIMENSIONS ARE IN MM TOLERANCES ARE:
FRACTIONS DECIMALS ANGLES
± .XX± .XX ± 1
.XXX±.XXX
MATERIAL Mild Steel
FINISH Machined
DO NOT SCALE DRAWING
CAD GENERATED DRAWING. DO NOT MANUALLY UPDATE
APPROVALS DATE
DRAWN
CHECKED
ENG APP
MFG APP
QUAL ENG
UNIVERSITY OF WAIKATO
Mark Lay
PhD Thesis: Continuous Radial Flow Chromatography
SIZE A
DWG. NO.
REV
SCALE
CAD REF
SHEET
OF

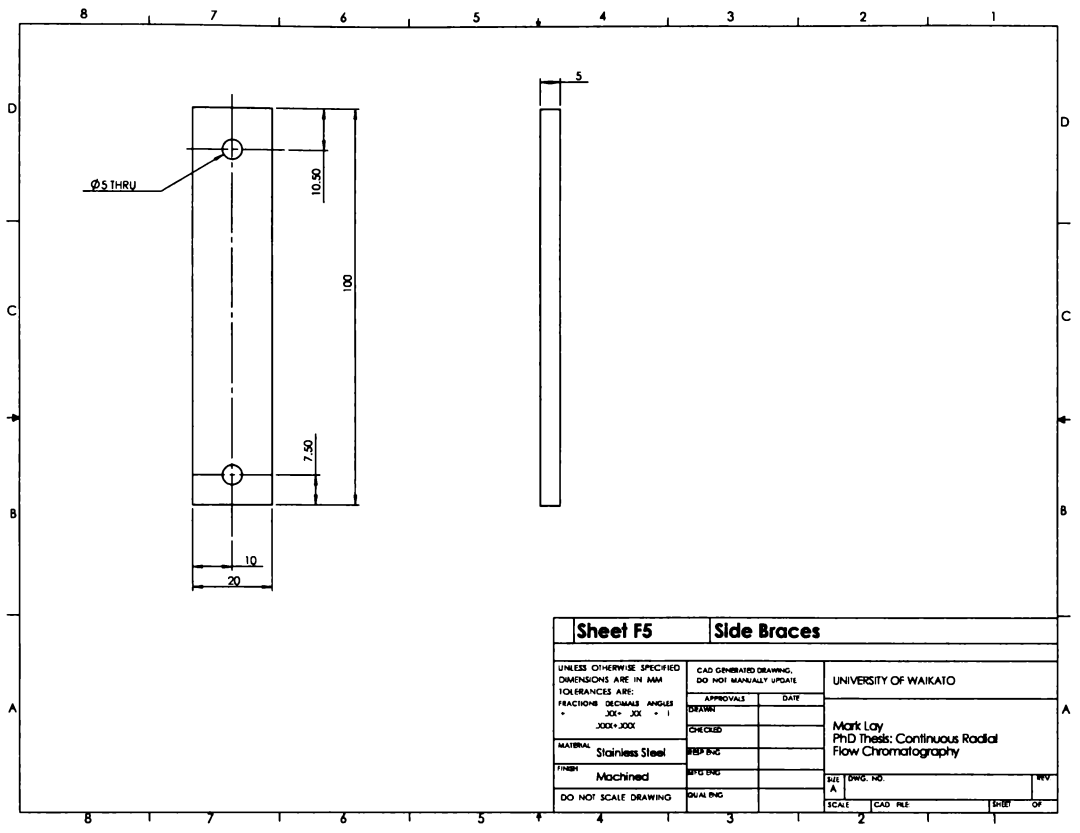
Ø5 THRU
10.50
100
7.50
10
20
5
Sheet F5
Side Braces
UNLESS OTHERWISE SPECIFIED
DIMENSIONS ARE IN MM
TOLERANCES ARE:
FRACTIONS DECIMALS ANGLES
± .XX ± .1
.XXX± .XXX
MATERIAL
Stainless Steel
FINISH
Machined
DO NOT SCALE DRAWING
CAD GENERATED DRAWING,
DO NOT MANUALLY UPDATE
APPROVALS
DATE
DRAWN
CHECKED
ENG APP.
MFG ENG
QUAL ENG
UNIVERSITY OF WAIKATO
Mark Lay
PhD Thesis: Continuous Radial
Flow Chromatography
SIZE
A
DWG. NO.
REV
SCALE
CAD FILE
SHEET
OF

Appendix B Protein and Resin Properties

Table B-1. Properties BSA and lactoferrin.

Protein	MW (kDa)	pI	Residues	Size (Å)	Reference
BSA	67	4.98-5.18	582	141 x 42	(Whitley *et al.* 1989)
Lactoferrin	77-80	8-9	689		(Moore *et al.* 1997)
					(Brock 2002)

Table B-2. Characteristics of DEAE Sepharose Fast Flow resin (Pharmacia 1983).

Characteristic	Specification
Type of gel	Weak anion
Total ionic capacity (umol/mol gel)	110-160
Recommended working flow rate range (cm/h)	100-300
Approx. mean particle size (um)	90
Particle size range (um)	45-165
Working pH range	2-9
pH stability	
short term	1-14
long term	2-13
Dynamic binding capacity (mg/ml resin)*	
Thyroglobulin (MW 669 000)	3.1
HSA (MW 68 000)	110
a-lactalbumin (MW 14 300)	100

*in 0.05M Tris, pH 8.3, flow rate of 75 cm/h.

Appendix C Calibration Data

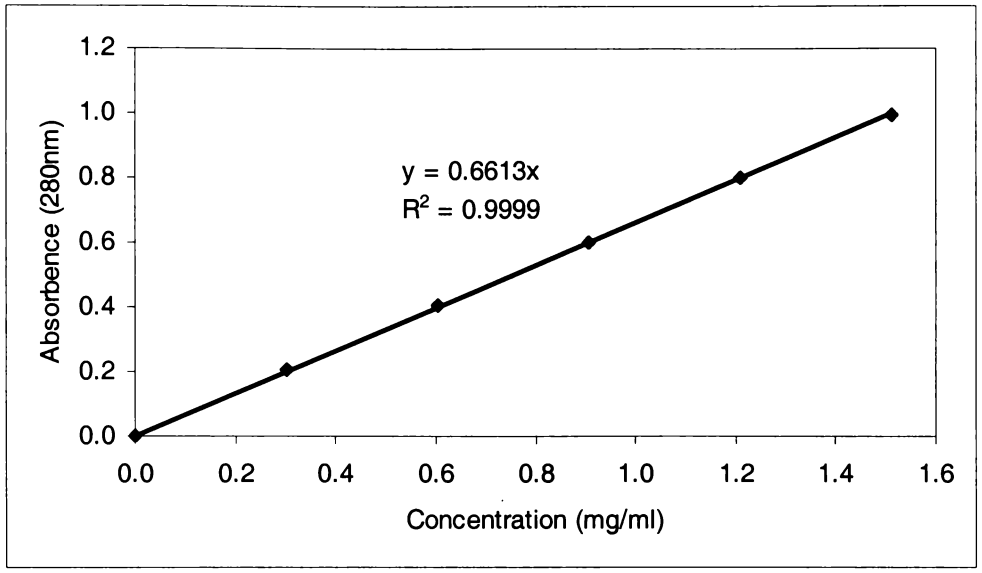

Figure C-1. Calibration data for Ultraspec 2000 UV/Visible spectrophotometer at 280nm using standard solutions of BSA in equilibration buffer.

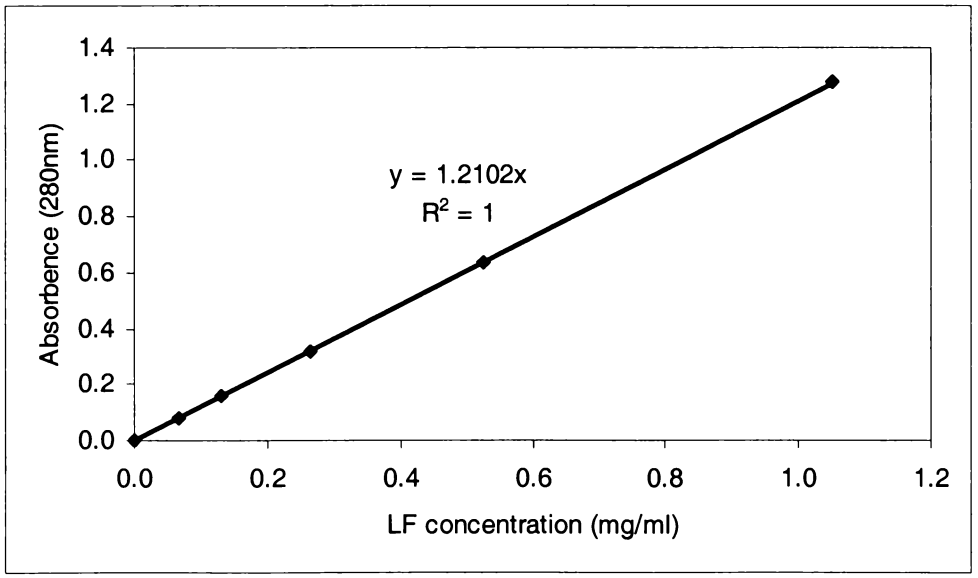

Figure C-2. Calibration data for Ultraspec 2000 UV/Visible spectrophotometer at 280nm using a serially diluted stock solution of lactoferrin in equilibration buffer.

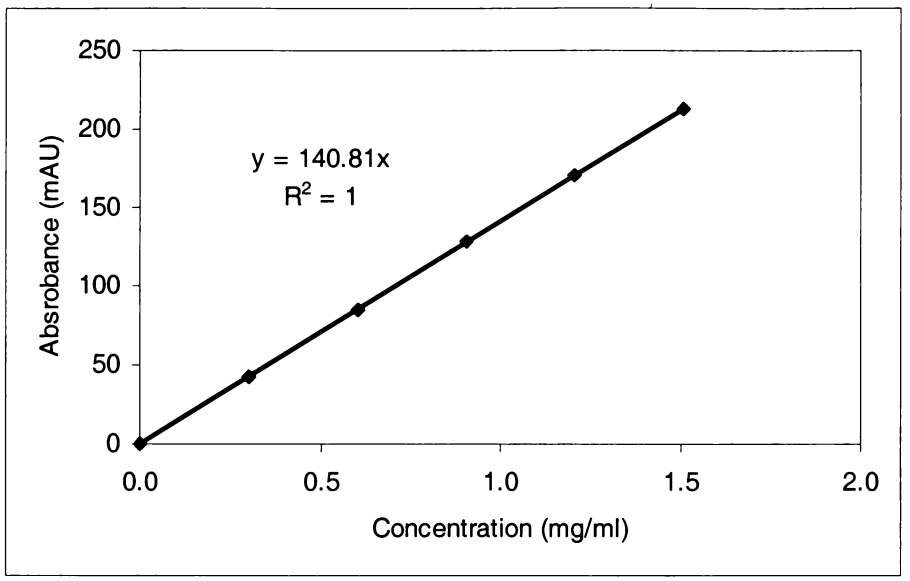

Figure C-3. Calibration data for the AKTAexplorer100 inline UV spectrophotometer at 280 nm using the AKTA to make dilutions of a 1.5 mg/ml stock standard solution of BSA in equilibration buffer.

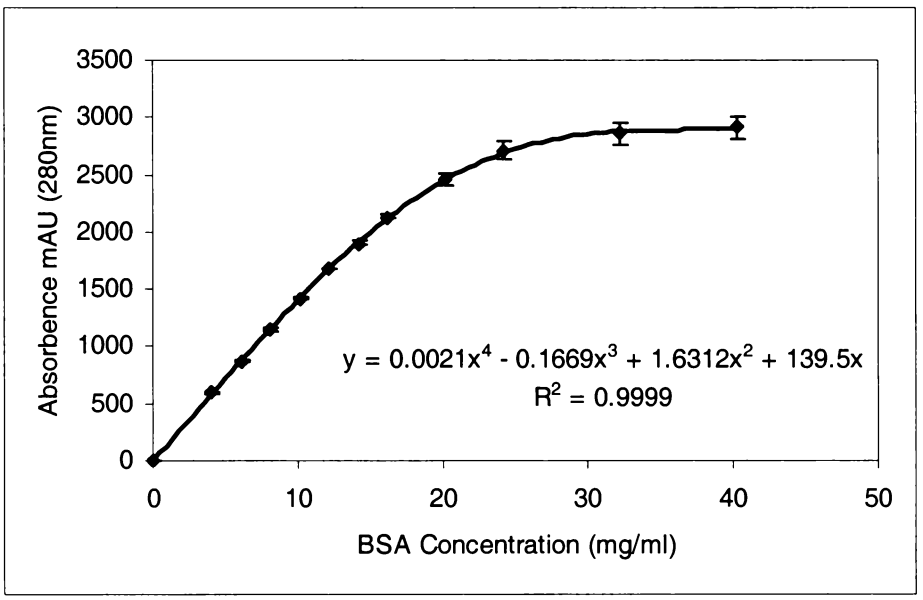

Figure C-4. Calibration data for the AKTAexplorer100 inline UV spectrophotometer at 280 nm using the AKTA to make dilutions of a 43 mg/ml stock standard solution of BSA in equilibration buffer.

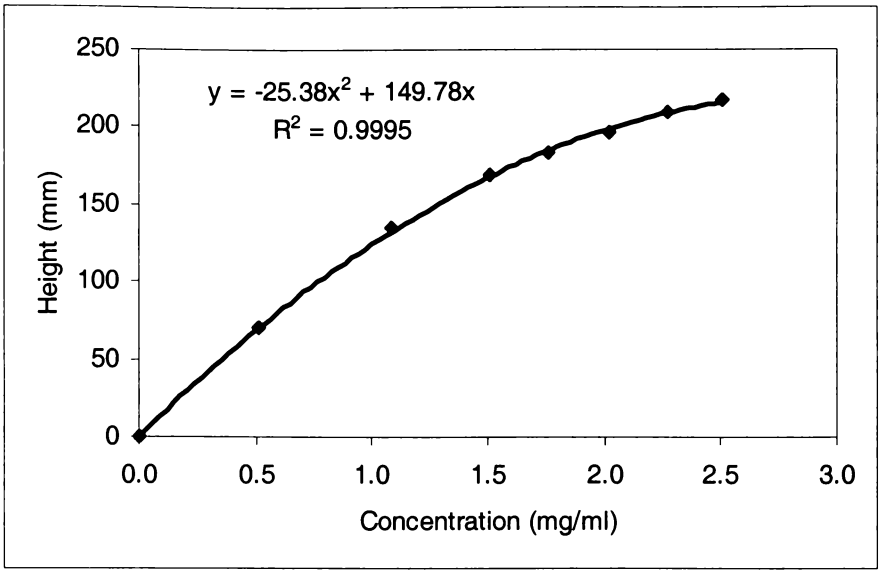

Figure C-5. Calibration data for Optical and Control Unit UV-1 Spectrophotometer (280nm) coupled to a chart recorder, using standard solutions of BSA in equilibration buffer.

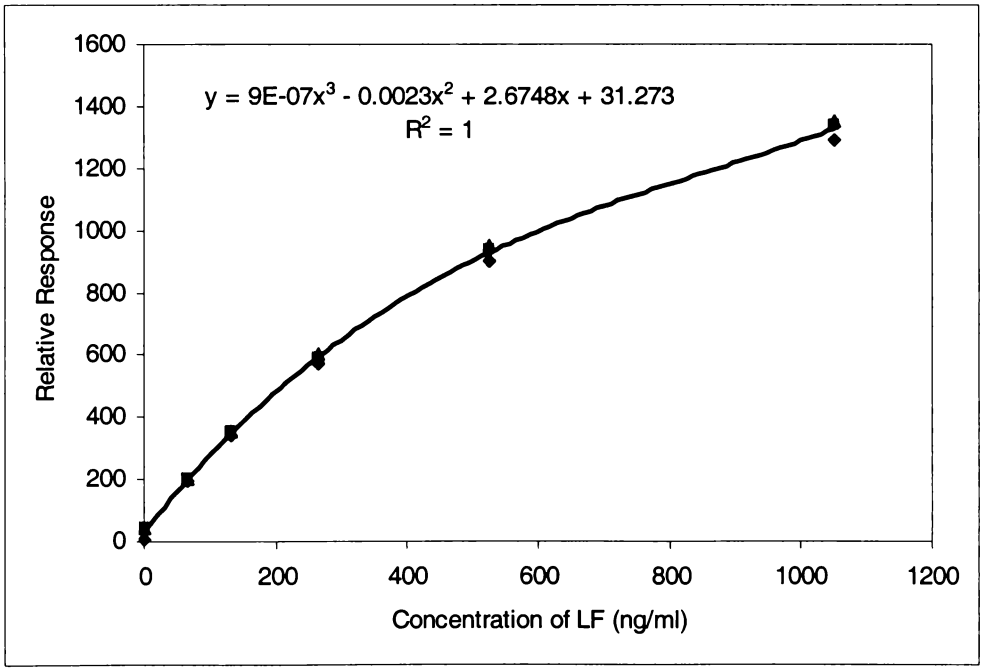

Figure C-6. Calibration data for Biacore SPR CM5 lactoferrin antibody chip using a serially diluted standard solution of lactoferrin in equilibration buffer.

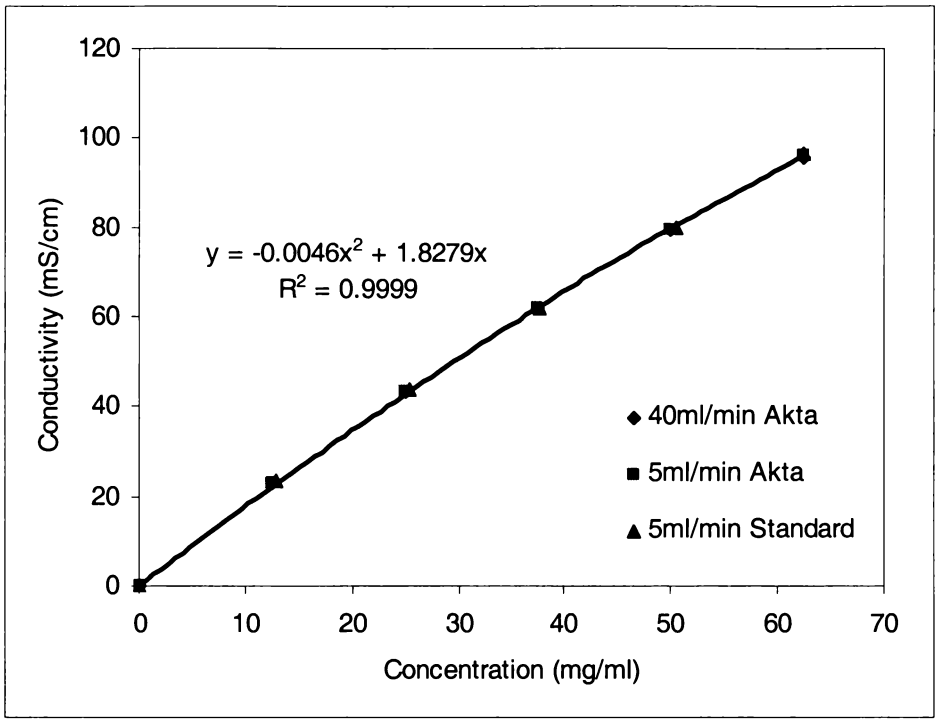

Figure C-7. Calibration data for the AKTAexplorer100 inline conductivity probe using standard solutions of NaCl in distilled water and using the AKTA to make dilutions from a stock standard solution.

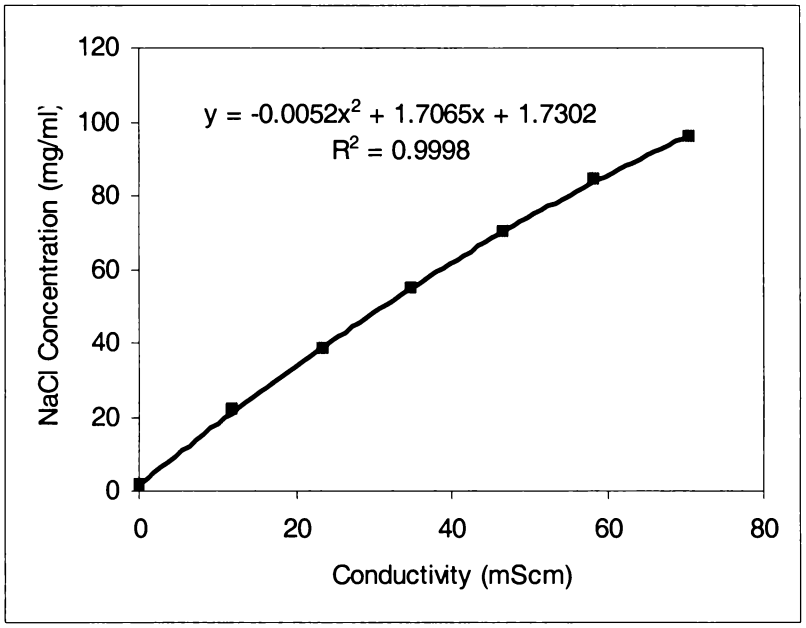

Figure C-8. Calibration data for Cyberscan 100 conductivity probe using standard solutions of NaCl in equilibration buffer.

Appendix D Void Fraction Measurements

D.1 External void fraction

A sample of equilibrated DEAE sepharose FF resin was touch-dried on filter paper. The resin was placed in three 100 ml measuring cylinders with 50 ml of equilibration buffer V_B. The measuring cylinders were sealed to prevent evaporation, and the resin allowed to settle in solution overnight. The volume of settled resin V_{RS} and volume of the mixture, i.e. equilibration buffer and resin V_{R+B} was noted and the void fraction ε_R calculated using the following equation,

$$\varepsilon_R = \frac{V_{RS} + V_S - V_{R+S}}{V_{RS}} \tag{208}$$

To determine if there was any shrinkage of resin due to the presence of salt, NaCl was added to the measuring cyclinders to make the solution up to approximately 1M NaCl concentration. The cylinders were sealed again and the contents of the measuring cylinder well mixed and allowed to settle overnight. The settled volume of resin in salt solution was noted and compared to the settled volume of resin in equilibration buffer.

DEAE Sepharose FF has an external void fraction of 0.31 (Table D.1-1). Spherical resin of a uniform size has a void fraction of 0.4. It was expected that DEAE sepharose FF would have a slightly lower void fraction as the particle size ranges from 45 to 165 um and has an average size of 90um (Amersham Biosciences Catalogue).

Table D.1-1. Results from external void fraction measurements.

Settled resin volume (ml)	Total volume (ml)	Volume solution added (ml)	Resin volume (ml)	Void fraction	Settled resin volume after NaCl addition (ml)	Fraction of original volume
27.0	69.0	50.0	19.0	0.30	26.5	0.98
16.0	61.0	50.0	11.0	0.31	15.7	0.98
17.8	62.3	50.0	12.3	0.31	17.5	0.98

The DEAE Sepharose FF volume decreased by 2% in NaCl solution. Therefore, to prevent channeling occurring in the packed bed due to resin volume changes in salt solutions, the CRFC annulus should be packed with a resin slurry in salt solution.

D.2 Internal pore fraction measurements

Samples of DEAE sepharose FF in equilibration buffer were placed in three 50ml measuring cylinders and allowed to settle. Settled volume of resin and total volume of solution and resin in the measuring cylinder was noted. 5, 10 and 15 ml aliquots of a 50.44 mg/ml NaCl solution made up in equilibration buffer was added to the measuring cylinders and equilibration buffer added so that the total volume of the mixture equalled 40 ml. The measuring cylinders were covered, the contents well mixed and the mixture left overnight. The resin was resuspended several times to evenly distribute NaCl. Conductivity was measured the next day using a conductivity probe and concentration of NaCl determined by comparing results to a calibration data. Internal pore fractions were then calculated. Some chloride ions were expected to absorb as DEAE sepharose FF has a chloride ion capacity C_{RBmax} of 0.11-0.16 mmol per ml resin (Amersham Biosciences Catalogue), or 3.9-5.7 mg per ml resin. Calculations of internal pore fraction were corrected for Cl^- absorption (Table D.2-1 and D.2-2)

Table D.2-1. Average calculated pore fractions for different resin Cl^- capacities

C_{RBmax} (mg/ml)	0	3.9	5.7
ε_P	1.05	0.82	0.72

Researchers have reported ε_P = 0.95 (Whitley *et al.* 1989), 0.78 for NaCl, 0.55 for BSA, and 0.67 for bovine haemoglobin (Bloomingburg *et al.* 1991; Bloomingburg and Carta 1994) for Sepharose resin (Amersham Biosciences). For convenience, ε_P = 0.72 was used in model simulations for both BSA and NaCl. Excellent agreement was found between simulated and NaCl breakthrough curves using ε_P = 0.72 (Figure 6-14).

Table D.2-2. Pore fraction calculation. Parameters used $\varepsilon_R = 0.31$, $C_{RBmax} = 5.7$ mg Cl^- /ml resin.

NaCl solution			
Volume NaCl solution (V_S) (ml)	10.0	15.0	20.0
Concentration NaCl (C_S) (mg/ml)	50.4	50.4	50.4
Mass NaCl (M_S) (mg)	504.4	756.6	1008.8
Mass Cl^- (M_{Cl}) (mg/ml)	306.0	459.0	612.0
Resin solution			
Total volume (V_{R+B}) (ml)	30.0	25.0	20.0
Settled volume of resin (V_{RS}) (ml)	10.3	11.0	11.2
Actual volume resin ($V_R = V_{RS}(1-\varepsilon_R)$) (ml)	7.1	7.6	7.7
Actual volume solution ($V_B = V_{R+B} - V_R$) (ml)	22.9	17.4	12.3
Combined solutions			
Volume bulk solution ($V_{BS} = V_B + V_S$) (ml)	32.9	32.4	32.3
Calculation of mass absorbed by resin			
Bound Cl^- ($M_{RS} = V_R C_{rs\,max}$) (mg)	40.5	43.3	44.0
Mass NaCl in solution ($M_{Sleft} = M_S - M_{RS}$) (mg)	463.9	713.3	964.8
Calculation of pore volume			
Conductivity (mScm)	22.3	32.7	41.8
Concentration NaCl (C_{Sleft}) (mg/ml)	12.2	19.0	25.3
Pore volume $V_P = V_{BS} - (M_{Sleft}/C_{Sleft})$ (ml)	5.0	5.2	5.9
Internal pore fraction ($\varepsilon_P = V_P/V_R$)	0.70	0.68	0.77

Appendix E AKTAexplorer100 Methods

Programmes used for automated AKTAexplorer100 operation are presented in this appendix.

E.1 BSA calibration

```
MAIN_SEPARATION
        0.00 Base Volume
        0.00 Block Normal, Start_Conditions_IX
        0.00 Block Normal, Set_Scale_Cond
        0.00 End_method
END_SEPARATION
SUB_SEPARATION Start_Conditions_IX
        0.00 Base SameAsMain
        0.00 ColumnPosition #Column_position
        0.00 PumpAInlet A1
        0.00 BufferValveA1 A11
        0.00 Flow #Flowrate -(ml/min)-
        0.00 Gradient 100 -(%B)-, 0.00 -(base)-
        0.00 Wavelength #Wavelength_1 -(nm)-, #Wavelength_2 -(nm)-, #Wavelength_3 -(nm)-
        0.00 AveragingTime #UV_Averaging_time -(sec)-
        0.00 Alarm_Pressure Enabled, #Pressure_limit -(MPa)-, 0 -(MPa)-
        0.00 OutletValve WasteF1
        0.00 AutoZeroUV
        0.00 End_block
END_SEPARATION
SUB_SEPARATION Set_Scale_Cond
        0.00 Base SameAsMain
        50 SetCondScale0% 0.00 -(mS/cm)-
        100 AutoZeroUV
        200 BufferValveA1 A15
        200.00 Gradient 50 -(%B)-, 0.00 -(base)-
        300 Gradient 65 -(%B)-, 0.00 -(base)-
        400.00 Gradient 70 -(%B)-, 0.00 -(base)-
        500 Gradient 75 -(%B)-, 0.00 -(base)-
        600.00 Gradient 85 -(%B)-, 0.00 -(base)-
        700.00 Gradient 90 -(%B)-, 0.00 -(base)-
        800.00 Gradient 95 -(%B)-, 0.00 -(base)-
        800.00 End_block
END_SEPARATION
SUB_SEPARATION Column_Equilibration
        0.00 Base SameAsMain
        0.00 Gradient 0.00 -(%B)-, 0.00 -(base)-
        1.00 End_block
END_SEPARATION
END_METHOD
```

E.2 Conductivity calibration using standard solutions

```
MAIN_SEPARATION
        0.00 Base Volume
        0.00 Block Normal, Start_Conditions_IX
        0.00 Block Normal, Set_Scale_Cond
        0.00 End_method
END_SEPARATION
SUB_SEPARATION Start_Conditions_IX
        0.00 Base SameAsMain
        0.00 ColumnPosition #Column_position
        0.00 PumpAInlet A1
        0.00 PumpBInlet B1
        0.00 BufferValveA1 A11
        0.00 Flow #Flowrate -(ml/min)-
        0.00 Gradient 0.00 -(%B)-, 0.00 -(base)-
        0.00 Wavelength #Wavelength_1 -(nm)-, #Wavelength_2 -(nm)-, #Wavelength_3 -(nm)-
        0.00 AveragingTime #UV_Averaging_time -(sec)-
        0.00 Alarm_Pressure Enabled, #Pressure_limit -(MPa)-, 0 -(MPa)-
        0.00 OutletValve WasteF1
        0.00 AutoZeroUV
        0.00 End_block
END_SEPARATION
SUB_SEPARATION Set_Scale_Cond
        0.00 Base SameAsMain
        0.00 Flow 40 -(ml/min)-
        90 Flow 5 -(ml/min)-
        100 ColumnPosition Position4
        100 SampleValve S1
        100 SampleFlow 5 -(ml/min)-
        150.00 SampleValve S2
        200.00 SampleValve S3
        250.00 SampleValve S4
        250.00 Gradient 100 -(%B)-, 0.00 -(base)-
        300.00 SampleFlow 0 -(ml/min)-
        300.00 ColumnPosition Position1Bypass
        410.00 Gradient 0.00 -(%B)-, 0.00 -(base)-
        500.00 ColumnPosition Position4
        500.00 SampleValve S5
        500.00 SampleFlow 5.00 -(ml/min)-
        550.00 End_Block
END_SEPARATION
END_METHOD
```

E.3 Conductivity calibration

```
MAIN_SEPARATION
        0.00 Base Volume
        0.00 Block Normal, Start_Conditions_IX
        0.00 Block Normal, Set_Scale_Cond
        0.00 End_method
END_SEPARATION
SUB_SEPARATION Start_Conditions_IX
        0.00 Base SameAsMain
        0.00 ColumnPosition #Column_position
        0.00 PumpAInlet A1
        0.00 PumpBInlet B1
```

```
        0.00 BufferValveA1 A11
        0.00 Flow #Flowrate -(ml/min)-
        0.00 Gradient 0.00 -(%B)-, 0.00 -(base)-
        0.00 Wavelength #Wavelength_1 -(nm)-, #Wavelength_2 -(nm)-, #Wavelength_3 -(nm)-
        0.00 AveragingTime #UV_Averaging_time -(sec)-
        0.00 Alarm_Pressure Enabled, #Pressure_limit -(MPa)-, 0 -(MPa)-
        0.00 OutletValve WasteF1
        0.00 AutoZeroUV
        0.00 End_block
END_SEPARATION
SUB_SEPARATION Set_Scale_Cond
        0.00 Base SameAsMain
        50 SetCondScale0% 0.00 -(mS/cm)-
        100 Gradient 20 -(%B)-, 0.00 -(base)-
        150.00 Gradient 40 -(%B)-, 0.00 -(base)-
        200.00 Gradient 60 -(%B)-, 0.00 -(base)-
        250.00 Gradient 80 -(%B)-, 0.00 -(base)-
        300.00 Gradient 100 -(%B)-, 0.00 -(base)-
        400.00 SetCondScale100% 100.00 -(mS/cm)-
        410.00 Gradient 0.00 -(%B)-, 0.00 -(base)-
        500.00 End_block
END_SEPARATION
END_METHOD
```

E.4 Step concentration change for BSA and NaCl using primary pumps

```
MAIN_SEPARATION
        0.00 Base Volume
        0.00 ColumnPosition Position3
        0.00 Wavelength  280 -(nm)- [Set UV wavelength]
        0.00 AveragingTime 2.56 -(sec)- [Set averaging time for recording UV adsorbance]
        0.00 Alarm_Pressure Enabled, 4.00 -(MPa)-, 0.00 -(MPa)- [Max, Min pressure]
        0.00 OutletValve WasteF1
        0.00 PumpAInlet A1
        0.00 BufferValveA1 A11 [Equilibration buffer]
        0.00 PumpBInlet B1  [BSA and NaCl solutions]
        0.00 Flow 1.00 -(ml/min)-
        20.00 AutoZeroUV
        21.00 Gradient 20.00 -(%B)-, 0.00 -(base)- [Ratio of BSA, NaCl solution to equilibration
        buffer]
        36.00 Gradient 40.00 -(%B)-, 0.00 -(base)- [0.00 -(base)- is period over which gradient change is
        done]
        46.00 Gradient 60.00 -(%B)-, 0.00 -(base)-
        56.00 Gradient 80.00 -(%B)-, 0.00 -(base)-
        66.00 Gradient 100.00 -(%B)-, 0.00 -(base)-
        76.00 Gradient 0.00 -(%B)-, 0.00 -(base)-
        86.00 End_Method
END_SEPARATION
END_METHOD
```

E.5 Step concentration change using superloop and NaCl solution

MAIN_SEPARATION
0.00 Base Volume
0.00 ColumnPosition Position3
0.00 Alarm_Pressure Enabled, 4.00 -(MPa)-, 0.00 -(MPa)- [Max, Min pressure]
0.00 OutletValve WasteF1
0.00 PumpAInlet A1
0.00 BufferValveA1 A11 [Equilibration buffer]
0.00 Flow 4 -(ml/min)- [Clear lines with equilibration buffer]
10.00 Flow 1 -(ml/min)-
11.00 InjectionValve Inject [Direct flow to top of Superloop which contains NaCl solution]
20.00 InjectionValve Load [Stop flow to Superloop]
30.00 End_Method
END_SEPARATION
END_METHOD

E.6 Small column breakthrough

Notes: A1-A11 Equilibration buffer
A2 1mol NaCl in equilibration buffer
B1 1.5mg/ml BSA in equilibration buffer
Scouting method, can repeat run using different loading and equilibration flowrates and different loading volumes.

MAIN_SEPARATION
0.00 Base Volume, 0.96 -(ml)-, HiTrap_DEAE_Sepharose_FF_1_ml_(kit)
0.00 Block Normal, Start_Conditions_Sys
0.00 Block Normal, Column_Equilibration
0.00 Block Normal, Column_Equilibration_2
0.00 Block Normal, Column_Load
0.00 Block Normal, Column_Wash
0.00 Block Normal, Elution_1
0.00 Block Normal, Column_Equilibration_3
0.00 End_method
END_SEPARATION
SUB_SEPARATION Start_Conditions_Sys
0.00 Base SameAsMain
0.00 ColumnPosition 3
0.00 Wavelength 280 -(nm)-, 0 -(nm)-, 0 -(nm)-
0.00 AveragingTime 2.56 -(sec)-
0.00 Alarm_Pressure Enabled, 0.5 -(MPa)-, 0.00 -(MPa)-
0.00 PumpAInlet A1
0.00 BufferValveA1 A11 [Equilibration buffer]
0.00 PumpBInlet B1 [BSA solution]
0.00 OutletValve WasteF1
0.00 AutoZeroUV
0.00 End_block
END_SEPARATION
SUB_SEPARATION Column_Equilibration [Fast equilibration of column]
0.00 Base SameAsMain
0.00 Flow 1.00 -(ml/min)-
4.00 AutoZeroUV
4.00 End_Block
END_SEPARATION
SUB_SEPARATION Column_Equilibration_2 [Equilibration at loading flowrate]
0.00 Base SameAsMain

0.00 Flow #Flow_Equilibration_2 -(ml/min)- [Adjustable for repeated runs]
1.00 End_Block
END_SEPARATION
SUB_SEPARATION Column_Load [Loading column with BSA]
0.00 Base SameAsMain
0.00 Gradient 100.00 -(%B)-, 0.00 -(base)- [Loading BSA onto column from B1]
#Loading_Volume End_Block [Adjustable for repeated runs]
END_SEPARATION
SUB_SEPARATION Column_Wash [Remove unbound BSA with equilibration buffer]
0.00 Base SameAsMain
0.00 Gradient 0.00 -(%B)-, 0.00 -(base)-
0.00 Flow 1.00 -(ml/min)-
5.00 End_Block
END_SEPARATION
SUB_SEPARATION Elution_1 [Remove bound BSA]
0.00 Base SameAsMain
0.00 PumpWash OFF, ON, OFF, OFF [Flush equilibration solution from Pump A with elution buffer]
10.00 End_Block
END_SEPARATION
SUB_SEPARATION Column_Equilibration_3
0.00 Base SameAsMain
0.00 PumpWash A11, OFF, OFF, OFF [Flush elution buffer from Pump A with equilibration buffer]
5.00 End_Block
END_SEPARATION
END_METHOD

E.7 Small column desorption

Notes: A1-A11, Equilibration buffer
A1-A18, 1.5mg/ml BSA solution in equilibration buffer
B1, 1mol NaCl solution in equilibration buffer
B2, Equilibration buffer

MAIN_SEPARATION
0.00 Base Volume
0.00 Block Normal, Start_Conditions_Sys
0.00 Block Normal, Load_Superloop
0.00 Block Normal, Column_Equilibration
0.00 Block Normal, Column_Equilibration_2
0.00 Block Normal, Column_Load
0.00 Block Normal, Column_Wash
0.00 Block Normal, Elution_1
0.00 Block Normal, Elution_2
0.00 Block Normal, Column_Equilibration_3
10.00 End_method
END_SEPARATION
SUB_SEPARATION Start_Conditions_Sys
0.00 Base SameAsMain
0.00 ColumnPosition Position1Bypass
0.00 FlowDirection Downflow
0.00 InjectionValve Load
0.00 Wavelength #Wavelength_1 -(nm)-, #Wavelength_2 -(nm)-, #Wavelength_3 -(nm)-
0.00 AveragingTime #UV_Averaging_time -(sec)-
0.00 Alarm_Pressure Enabled, 10.00 -(MPa)-, 0.00 -(MPa)-
0.00 OutletValve WasteF1
0.00 Flow 4.00 -(ml/min)-
9.00 AutoZeroUV

```
        10.00 End_Block
END_SEPARATION
SUB_SEPARATION Load_Superloop
        0.00 Base SameAsMain
        0.00 Flow 0.00 -(ml/min)-
        0.00 ColumnPosition Position1Bypass
        0.00 BufferValveA1 A18
        0.00 PumpWash A18, OFF, OFF, OFF
        0.00 Flow 10.00 -(ml/min)-
        10.00 ColumnPosition Position4
        30.00 ColumnPosition Position1Bypass
        30.00 Flow 0.00 -(ml/min)-
        30.00 Gradient 100.00 -(%B)-, 0.00 -(base)-
        30.00 PumpBInlet B2
        30.00 PumpWash OFF, OFF, OFF, ON
        30.00 Flow 10.00 -(ml/min)-
        40.00 InjectionValve Inject
        60.00 InjectionValve Load
        60.00 Gradient 0.00 -(%B)-, 0.00 -(base)-
        70.00 ColumnPosition Position4
        119.00 Flow 1 -(ml/min)-
        120.00 Flow 0.00 -(ml/min)-
        120.00 ColumnPosition Position1Bypass
        120.00 BufferValveA1 A11
        120.00 PumpBInlet B1
        120.00 PumpWash OFF, OFF, ON, OFF
        120.00 PumpWash A11, OFF, OFF, OFF
        120.00 Flow 10.00 -(ml/min)-
        130.00 End_Block
END_SEPARATION
SUB_SEPARATION Column_Equilibration
        0.00 Base Volume, 0.96 -(ml)-, HiTrap_DEAE_Sepharose_FF_1_ml_(kit)
        0.00 Alarm_Pressure Enabled, 0.5 -(MPa)-, 0.00 -(MPa)-
        0.00 Flow 4.00 -(ml/min)-
        0.00 ColumnPosition Position3
        10.00 End_Block
END_SEPARATION
SUB_SEPARATION Column_Equilibration_2
        0.00 Base SameAsMain
        0.00 Flow 0.50 -(ml/min)-
        1.00 End_Block
END_SEPARATION
SUB_SEPARATION Column_Load
        0.00 Base SameAsMain
        0.00 InjectionValve Inject
        50.00 InjectionValve Load
        50.00 End_Block
END_SEPARATION
SUB_SEPARATION Column_Wash
        0.00 Base SameAsMain
        0.00 Gradient 0.00 -(%B)-, 0.00 -(base)-
        10.00 End_Block
END_SEPARATION
SUB_SEPARATION Elution_1
        0.00 Base SameAsMain
        0.00 Flow 0.20 -(ml/min)-
        0.00 Gradient #Gradient_Elution -(%B)-, 0.00 -(base)-
        10.00 End_Block
END_SEPARATION
SUB_SEPARATION Elution_2
```

```
        0.00 Base Volume
        0.00 Gradient 100.00 -(%B)-, 0.00 -(base)-
        0.00 Flow 1.00 -(ml/min)-
        10.00 End_Block
END_SEPARATION
SUB_SEPARATION Column_Equilibration_3
        0.00 Base SameAsMain
        0.00 Gradient 0.00 -(%B)-, 0.00 -(base)-
        0.00 Flow 4.00 -(ml/min)-
        10.00 End_Block
END_SEPARATION
END_METHOD
```

E.8 Bed integrity and flow manifold method

```
MAIN_SEPARATION
        0.00 Base Volume
        0.00 Block Normal, Start_Conditions_IX
        0.00 Block Normal, Set_Scale_Cond
        0.00 Block Normal, Adsorption
        0.00 Block Normal, Clean_After_Adsorption
        0.00 End_method
END_SEPARATION
SUB_SEPARATION Start_Conditions_IX
        0.00 Base SameAsMain
        0.00 ColumnPosition #Column_position
        0.00 PumpAInlet A1
        0.00 PumpBInlet B1
        0.00 BufferValveA1 A11
        0.00 Flow #Flowrate -(ml/min)-
        0.00 Gradient 0.00 -(%B)-, 0.00 -(base)-
        0.00 Wavelength #Wavelength_1 -(nm)-, #Wavelength_2 -(nm)-, #Wavelength_3 -(nm)-
        0.00 AveragingTime #UV_Averaging_time -(sec)-
        0.00 Alarm_Pressure Enabled, #Pressure_limit -(MPa)-, 0 -(MPa)-
        0.00 OutletValve WasteF1
        0.00 AutoZeroUV
        0.00 End_block
END_SEPARATION
SUB_SEPARATION Set_Scale_Cond
        0.00 Base SameAsMain
        50 SetCondScale0% 0.00 -(mS/cm)-
        100 Gradient 20 -(%B)-, 0.00 -(base)-
        150.00 Gradient 40 -(%B)-, 0.00 -(base)-
        200.00 Gradient 60 -(%B)-, 0.00 -(base)-
        250.00 Gradient 80 -(%B)-, 0.00 -(base)-
        300.00 Gradient 100 -(%B)-, 0.00 -(base)-
        400.00 SetCondScale100% 100.00 -(mS/cm)-
        410.00 Gradient 0.00 -(%B)-, 0.00 -(base)-
        500.00 End_block
END_SEPARATION
SUB_SEPARATION Adsorption
        0.00 Base SameAsMain
        0.00 ColumnPosition Position4
        0.00 Gradient 0.00 -(%B)-, 0.00 -(base)-
        300.00 SampleFlow 5 -(ml/min)-
        500.00 Gradient 100 -(%B)-, 0.00 -(base)-
        800.00 Gradient 0 -(%B)-, 0.00 -(base)-
        1100.00 End_block
END_SEPARATION
```

```
SUB_SEPARATION Clean_After_Adsorption
        0.00 Base SameAsMain
        0.00 PumpBInlet B1
        0.00 Gradient #Clean_Conc -(%B)-, 0.00 -(base)-
        1000.00 End_Block
END_SEPARATION
END_METHOD
```

E.9 CRFC breakthrough and elution

Notes: A1-A11 Equilibration buffer
A1-A12 1M NaOH
A1-A13 20% Ethanol
A1-A14 Distilled water
A2 Loading solution
B1 Elution buffer
B2- 20% ethanol

```
MAIN_SEPARATION
        0.00 Base Volume
        0.00 Block Normal, Start_Conditions_IX
        0.00 Block Normal, Set_Scale_Cond
        0.00 Block Normal, Equilibration
        0.00 Block Normal, Loading
        0.00 Block Normal, Wash
        0.00 Block Normal, Elution
        0.00 Block Normal, Clean_Everything
        0.00 End_method
END_SEPARATION
SUB_SEPARATION Start_Conditions_IX
        0.00 Base SameAsMain
        0.00 ColumnPosition #Column_position
        0.00 PumpAInlet A1
        0.00 BufferValveA1 A11
        0.00 Flow #Flowrate -(ml/min)-
        0.00 Gradient 0.00 -(%B)-, 0.00 -(base)-
        0.00 Wavelength #Wavelength_1 -(nm)-, #Wavelength_2 -(nm)-, #Wavelength_3 -(nm)-
        0.00 AveragingTime #UV_Averaging_time -(sec)-
        0.00 Alarm_Pressure Enabled, #Pressure_limit -(MPa)-, 0 -(MPa)-
        0.00 OutletValve WasteF1
        0.00 AutoZeroUV
        0.00 End_block
END_SEPARATION
SUB_SEPARATION Set_Scale_Cond
        0.00 Base SameAsMain
        100 AutoZeroUV
        150.00 PumpAInlet A2
        350.00 PumpAInlet A1
        350.00 BufferValveA1 A11
        550.00 End_block
END_SEPARATION
SUB_SEPARATION Equilibration
        0.00 Base SameAsMain
        0.00 ColumnPosition Position3
        300.00 SampleFlow 5 -(ml/min)-
        800.00 End_block
END_SEPARATION
SUB_SEPARATION Loading
```

```
        0.00 Base SameAsMain
        0.00 PumpAInlet A2
        0.00 OutletValve FracF2
        8000.00 End_block
END_SEPARATION
SUB_SEPARATION Wash
        0.00 Base SameAsMain
        0.00 BufferValveA1 A11
        0.00 OutletValve FracF2
        0.00 PumpAInlet A1
        4000 End_block
END_SEPARATION
SUB_SEPARATION Elution
        0.00 Base Volume
        0.00 OutletValve F3
        0.00 PumpBInlet B1
        0.00 Gradient 100 -(%B)-, 0.00 -(base)-
        4000.00 End_block
END_SEPARATION
SUB_SEPARATION Clean_Everything
        0.00 Base SameAsMain
        0.00 Gradient 0.00 -(%B)-, 0.00 -(base)-
        0.00 OutletValve WasteF1
        0 BufferValveA1 A12
        1000.0 BufferValveA1 A14
        2500.0 BufferValveA1 A13
        2500.00 PumpBInlet B2
        2500.00 Gradient 50 -(%B)-, 0.00 -(base)-
        4000.00 End_block
END_SEPARATION
END_METHOD
```

Appendix F Resin Cleaning

Used resin was sieved through 250 μm mesh to remove large particulate matter, and retained in a glass funnel with a sintered glass filter. The funnel was fixed to a Buchner flask. Solution was drawn through the filter by applying a vacuum in the flask. The resin was washed with 3 litres of 1M solution of sodium acetate adjusted to pH 3, rinsed with distilled water, and washed with 0.5M sodium hydroxide which was left overnight in the resin. It was then rinsed with distilled water, washed with 3 litres of sodium acetate solution as stated above and rinsed again with distilled water.

Appendix G Recycling of BSA

The CRFC required large quantities of bovine serum albumin for the breakthrough experiments. BSA in New Zealand is regarded as a biological hazard that must be sterilized prior to disposal. It is also expensive to obtain, approximately $1000 per kilogram. Therefore BSA used in the experiments performed was recycled using an ultrafiltration membrane.

A Millipore spiral wound PTTK Prep/Scale-TFF 2.5-ft^2 30-KD polyethersulfone membrane unit was set up as shown in Figure F-1. A feed tank supplied the UF membrane with used BSA through a Cole-Palmer Pro-Spense centrifugal pump. Two Wika pressure gauges (1-241 kPa) were used to measure the feed and retentate pressure. The needle valve on the retentate flow line and feed pump were adjusted to maintain a pressure of 103 kPa during operation with an initial permeate flowrate of 300 ml/min. The retentate was returned to the feed tank while permeate was was sent to waste.

Typical volumes of BSA solution recycled were around 25 L at concentrations ranging from 1mg/ml to 5mg/ml of BSA in solution. The BSA was concentrated until the total volume remaining in the feed tank was 500 ml. The BSA was then desalted by adding 3 L of distilled water to the feed tank and concentrating the solution until the remaining volume was 500ml. The desalting step was repeated three times.

The BSA was flushed from the system using distilled water into a 2-L Shott bottle. The membrane was rinsed with 5 L distilled water and cleaned by circulating 1 L of 1M NaOH solution through it for 15 min. The membrane was then rinsed with 10 L of distilled water.

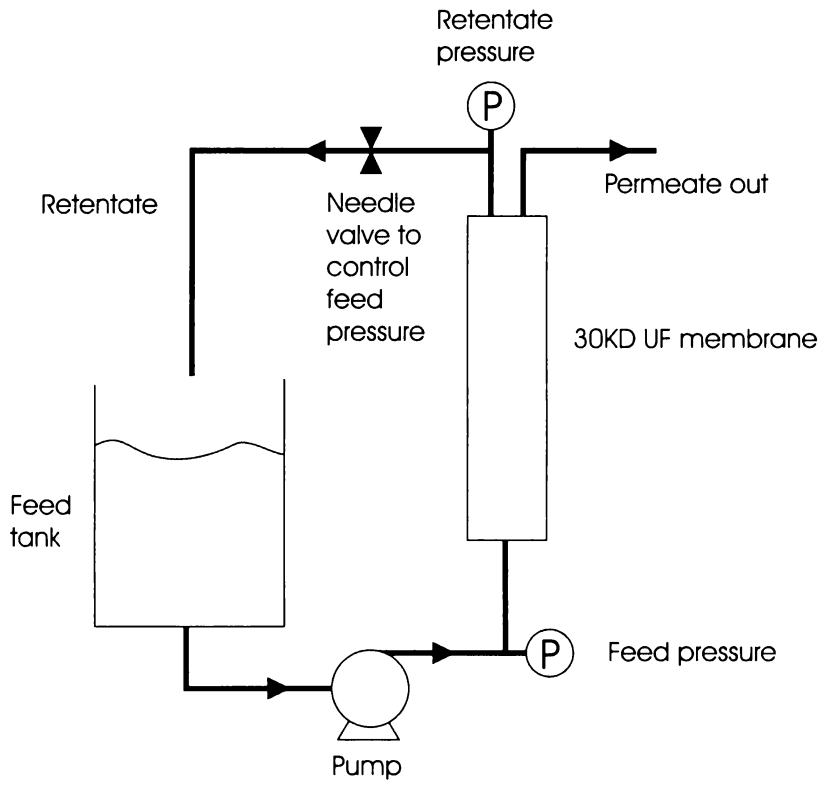

Figure G-1. Setup of ultrafiltration equipment for recycling of BSA.

Appendix H Matlab Models

H.1 Akta dispersion including gradient mixer

```
%Note: for solute injection from superloop, stage n=2 (gradient mixer) is removed.

%Akta system dispersion including gradient mixer

%Experimental Conditions
Qinput=1;%Total flowrate through column (ml/min)
Q=Qinput/60;%Total flowrate through column (ml/s)
cin=56.49;%Concentration of solute entering column (mg/ml)
cin1=0.*cin;
cin2=0.2*cin;
cin3=0.4*cin;
cin4=0.6*cin;
cin5=0.8*cin;
cin6=cin;
cin7=0;

%Times for loading, wash and elution
v1=21;%input('enter volume of equilibration buffer to be put through   ');
v2=15;%input('enter volume of loading solution to be put through   ');
v3=10;%input('enter volume of wash buffer to be put through   ');
v4=10;%input('enter volume of elution buffer to be put through   ');
v5=10;
v6=10;
v7=10;
t1=v1/Q;
t2=(v2/Q)+t1;
t3=(v3/Q)+t2;
t4=(v4/Q)+t3;
t5=(v5/Q)+t4;
t6=(v6/Q)+t5;
t7=(v7/Q)+t6;

%Model Conditions
N=2;%63;%Number of stages in radial direction annulus divided into
J=3;%input('Please enter time divider   ');%Time divider, used for determining delt
Ve=0.13;%Volume element (ml)
vdelay=2.0;
delt=1;%change in time (s)
T=ceil(t7./delt)%total number of time steps

for t=1;
   for n=1:7;
      c(t,n)=0;

   end
end

for t=2:T;
   time(t)=t.*delt;
   for n=1;
      if time(t)<t1;
         c(t,n)=cin1;

      elseif time(t)<t2;
```

```
        c(t,n)=cin2;

      elseif time(t)<t3;
        c(t,n)=cin3;

      elseif time(t)<t4;
        c(t,n)=cin4;

      elseif time(t)<t5;
        c(t,n)=cin5;

      elseif time(t)<t6;
        c(t,n)=cin6;
      else
        c(t,n)=0;

      end
    end
    for n=2
      %equation for gradient mixer, the 2.2 is the volume of the mixer
      c(t,n)=c(t-1,n)+(((Q.*(c(t-1,n-1)-c(t-1,n))).*delt)./(2.2));
    end
    for n=3:7;
      c(t,n)=c(t-1,n)+(((Q.*(c(t-1,n-1)-c(t-1,n))).*delt)./(Ve));
    end

    cnorm(t)=c(t,7);
    vapp(t)=(time(t).*Q)+vdelay;

    Ex(1,t)=vapp(t);
    Ex(2,t)=cnorm(t);

end

C=cnorm(1:T);
V=vapp(1:T);

figure;%creates a new figure
plot(V,C);
ylabel('Concentration');
xlabel('Volume applied');
title('Concentration of protein leaving system over volume applied');

%Save results to a datafile that can be imported into Microsoft Excel
%Change Ex from a row to a column (Excel has a limited number of columns)

Exc=Ex';
csvwrite('csvlist.dat',Exc);
```

H.2 Axial column NP-MLF breakthrough model

```
%Loading model for 1ml axial flow column, DEAE sepharose FF, Langmuir isotherm only

%Bed Dimensions
r=0.35;%Bed radius (cm)
L=2.5;%length of bed (cm)
Ac=pi.*r.*r;%cross sectional area of column (cm2)
Vc=Ac.*L;%volume of column (ml)
Vdelay1=1; %volume delay if solution coming from superloop (ml)
```

```
Vdelay2=2; %volume delay if solution coming from primary pumps (ml)
Vmix=2.2;%volume mixer on Akta (ml)
Vmix2=0.13;%volume mixers after column to simulate dispersion generated by the system (ml)


%Resin properties
Kp=47;%langmuir coeff (ml/mg)
kp1=0.003;%Rate of uptake of solute by resin (ml/mg.s)
kp2=kp1./Kp;%Rate of disassociation of solute from resin (1/s)
np=1;%fitting parameter
CRAmax=73;%Max solute concentration in resin at saturation (mg/ml)
er=0.31;%Void space of resin (dimensionless)
Rp=0.0045;%Radius of resin (cm)

%Experimental Conditions
Qload=0.1;%Total flowrate through column (ml/min)
Q=Qload/60;%Total flowrate through column (ml/s)
cin=1.51;%Concentration of solute entering column (mg/ml)

ym=0.0;%Molecular dispersion coefficient in length direction for protein
yt=0;%Turbulent dispersion coefficient in length direction for protein
Dm=0.000000611;%Molecular diffusivity of BSA (cm^2/s)

%Times for loading, wash and elution
v1=0;%volume of equilibration buffer to be put through (ml);
v2=80;%volume of loading solution to be put through (ml);
t1=(v1+Vdelay2)/(Qload/60);
t2=((v2)/(Qload/60))+t1;

%Model Conditions
N=30;%Number of stages in radial direction annulus divided into
J=3;%input('Please enter time divider  ');%Time divider, used for determining delt
Ve=Vc./N;%Volume element (ml)
Tres=(Ve.*er)/Q;%Residence time in element (s)
delt=Tres./J;%change in time (s)
delL=L/N;%change in length(cm)
T=ceil(t2./delt)%total number of time steps

%Dispersion factors

Dis=(ym.*Dm)+(yt.*2.*Rp.*(Q./(Ac.*er)));

for t=1;
   vapp(t)=(delt.*Q);
   for n=1:N+7;
      c(t,n)=0;
      CRA(t,n)=0;
   end
end

for t=2:T;
   time(t)=t.*delt;
   for n=1;
      if time(t)<t1;
         c(t,n)=0;
         Q=Qload./60;
      elseif time(t)<t2;
         c(t,n)=cin;
         Q=Qload./60;
      else
```

```
        c(t,n)=0;
        Q=Qload./60;
      end
    end
    for n=2;
      c(t,n)=c(t-1,n)+(((Q.*(c(t-1,n-1)-c(t-1,n))).*delt)./(Vmix));
    end
    for n=3;
      c(t,n)=c(t-1,n)+(((Q.*(c(t-1,n-1)-c(t-1,n))).*delt)./(Ve.*er))-(Dis.*Ac.*delt.*(c(t-1,n)-c(t-
1,n+1))./(delL.*Ve))-(kp1.*(c(t-1,n).^(1./np)).*delt.*(CRAmax-CRA(t-1,n)))+(kp2.*delt.*CRA(t-1,n));
      CRA(t,n)=CRA(t-1,n)+((er./(1-er)).*((kp1.*(c(t-1,n).^(1./np)).*delt.*(CRAmax-CRA(t-1,n)))-
(kp2.*delt.*CRA(t-1,n))));
    end
    for n=4:N+1;
      c(t,n)=c(t-1,n)+(((Q.*(c(t-1,n-1)-c(t-1,n))).*delt)./(Ve.*er))+(Dis.*Ac.*delt.*(c(t-1,n-1)-c(t-
1,n))./(delL.*Ve))-(Dis.*Ac.*delt.*(c(t-1,n)-c(t-1,n+1))./(delL.*Ve))-(kp1*(c(t-
1,n).^(1./np)).*delt.*(CRAmax-CRA(t-1,n)))+(kp2.*delt.*CRA(t-1,n));
      CRA(t,n)=CRA(t-1,n)+((er./(1-er)).*((kp1.*(c(t-1,n).^(1./np)).*delt.*(CRAmax-CRA(t-1,n)))-
(kp2.*delt.*CRA(t-1,n))));
    end
    for n=N+2;
      c(t,n)=c(t-1,n)+(((Q.*(c(t-1,n-1)-c(t-1,n))).*delt)./(Ve.*er))+(Dis.*Ac.*delt.*(c(t-1,n-1)-c(t-
1,n))./(delL.*Ve))-(kp1.*(c(t-1,n).^(1./np)).*delt.*(CRAmax-CRA(t-1,n)))+(kp2.*delt.*CRA(t-1,n));
      CRA(t,n)=CRA(t-1,n)+((er./(1-er)).*((kp1.*(c(t-1,n).^(1./np)).*delt.*(CRAmax-CRA(t-1,n)))-
(kp2.*delt.*CRA(t-1,n))));
    end
    for n=N+3:N+7;
      c(t,n)=c(t-1,n)+(((Q.*(c(t-1,n-1)-c(t-1,n))).*delt)./(Vmix2));
    end

    cnorm(t)=c(t,N+7);
    vapp(t)=vapp(t-1)+(delt.*Q);
    mass(t)=(vapp(t)-vapp(t-1)).*((c(t,N+7)+c(t-1,N+7))./2);

    Ex(1,t)=vapp(t);
    Ex(2,t)=cnorm(t);

end

C=cnorm(1:T);
V=vapp(1:T);

figure;%creates a new figure
plot(V,C);
ylabel('Concentration');
xlabel('Volume applied');
title('Concentration of protein leaving column over volume applied');

%Save results to a datafile that can be imported into Microsoft Excel
%Change Ex from a row to a column (Excel has a limited number of columns)

Exc=Ex';
csvwrite('csvlist.dat',Exc);
```

H.3 Axial column FD-MLF breakthrough model

```
%Loading model for 1ml axial flow column, DEAE sepharose FF, film diffusion

%Bed Dimensions
r=0.35;%Bed radius (cm)
L=2.5;%length of bed (cm)
Ac=pi.*r.*r;%cross sectional area of column (cm2)
Vc=Ac.*L;%volume of column (ml)
Vdelay1=1;
Vdelay2=2;%2;
Vmix=2.2;%volume mixer on Akta (ml)
Vmix2=0.13;%

%Resin properties
Kp=47;%47;%langmuir coeff
kp1=0.0085;%Rate of uptake of solute by resin (s^-1)
kp2=kp1./Kp;%Rate of disassociation of solute from resin (s^-1)
np=1;
CRAmax=70;%Max solute concentration in resin at saturation (mg/ml)
er=0.31;%Void space of resin (dimensionless)
ep=0.72;%Internal porosity of resin
Rp=0.0045;%Radius of resin (cm)
kf=0.0012;% film diffusion coeff (cm)

%Experimental Conditions
Qload=1;%Total flowrate through column (ml/min)
Q=Qload/60;%Total flowrate through column (ml/s)
cin=1.51;%Concentration of solute entering column (mg/ml)

ym=0.0;%Molecular dispersion coefficient in length direction for protein
yme=0.0;%Molecular dispersion coefficient in length direction for elution buffer
yt=0.00;%Turbulent dispersion coefficient in length direction for protein
yte=0.0;%Turbulent dispersion coefficient in length direction for elution buffer
Dm=0.000000611;%Molecular diffusivity of BSA (cm^2/s)

%Times for loading, wash and elution
v1=0;%input('enter volume of equilibration buffer to be put through  ');
v2=50;%input('enter volume of loading solution to be put through  ');
t1=(v1+Vdelay2)/(Qload/60);
t2=((v2)/(Qload/60))+t1;

%Model Conditions
N=30;%63;%Number of stages in axial direction column divided into
J=3;%input('Please enter time divider  ');%Time divider, used for determining delt
Ve=Vc./N;%Volume element (ml)
Tres=(Ve.*er)/Q;%Residence time in element (s)
delt=Tres./J;%change in time (s)
delL=L/N;%change in length(cm)
T=ceil(t2./delt)%total number of time steps

T1=ceil((t1-(Vdelay2/(Qload/60)))/delt);
T2=ceil((t2-(Vdelay2/(Qload/60)))/delt);

%Dispersion factors

Dis=(ym.*Dm)+(yt.*2.*Rp.*(Q./(Ac.*er)));

for t=1;
  vapp(t)=(delt.*Q);
```

```
   for n=1:N+7;
      c(t,n)=0;
      crp(t,n)=0;
      CRA(t,n)=0;
   end
end

for t=2:T;
   time(t)=t.*delt;
   for n=1;
      if time(t)<t1;
         c(t,n)=0;
         Q=Qload./60;
      elseif time(t)<t2;
         c(t,n)=cin;
         Q=Qload./60;
      else
         c(t,n)=0;
         Q=Qload./60;
      end
   end
   for n=2;
      c(t,n)=c(t-1,n)+(((Q.*(c(t-1,n-1)-c(t-1,n))).*delt)./(Vmix));
   end
   for n=3;
      c(t,n)=c(t-1,n)+(((Q.*(c(t-1,n-1)-c(t-1,n))).*delt)./(Ve.*er))-(Dis.*Ac.*delt.*(c(t-1,n)-c(t-
1,n+1))./(delL.*Ve))-(((1-er)./er).*((3.*kf)./Rp).*(c(t-1,n)-crp(t-1,n)).*delt);
      crp(t,n)=crp(t-1,n)+(((3.*kf)./(Rp.*ep)).*(c(t-1,n)-crp(t-1,n)).*delt)-(kp1.*(crp(t-
1,n).^(1./np)).*delt.*(CRAmax-CRA(t-1,n)))+(kp2.*delt.*CRA(t-1,n));
      CRA(t,n)=CRA(t-1,n)+(ep.*((kp1.*(crp(t-1,n).^(1./np)).*delt.*(CRAmax-CRA(t-1,n)))-
(kp2.*delt.*CRA(t-1,n))));
   end
   for n=4:N+1;
      c(t,n)=c(t-1,n)+(((Q.*(c(t-1,n-1)-c(t-1,n))).*delt)./(Ve.*er))+(Dis.*Ac.*delt.*(c(t-1,n-1)-c(t-
1,n))./(delL.*Ve))-(Dis.*Ac.*delt.*(c(t-1,n)-c(t-1,n+1))./(delL.*Ve))-(((1-er)./er).*((3.*kf)./Rp).*(c(t-
1,n)-crp(t-1,n)).*delt);
      crp(t,n)=crp(t-1,n)+(((3.*kf)./(Rp.*ep)).*(c(t-1,n)-crp(t-1,n)).*delt)-(kp1.*(crp(t-
1,n).^(1./np)).*delt.*(CRAmax-CRA(t-1,n)))+(kp2.*delt.*CRA(t-1,n));
      CRA(t,n)=CRA(t-1,n)+(ep.*((kp1.*(crp(t-1,n).^(1./np)).*delt.*(CRAmax-CRA(t-1,n)))-
(kp2.*delt.*CRA(t-1,n))));
   end
   for n=N+2;
      c(t,n)=c(t-1,n)+(((Q.*(c(t-1,n-1)-c(t-1,n))).*delt)./(Ve.*er))+(Dis.*Ac.*delt.*(c(t-1,n-1)-c(t-
1,n))./(delL.*Ve))-(((1-er)./er).*((3.*kf)./Rp).*(c(t-1,n)-crp(t-1,n)).*delt);
      crp(t,n)=crp(t-1,n)+(((3.*kf)./(Rp.*ep)).*(c(t-1,n)-crp(t-1,n)).*delt)-(kp1.*(crp(t-
1,n).^(1./np)).*delt.*(CRAmax-CRA(t-1,n)))+(kp2.*delt.*CRA(t-1,n));
      CRA(t,n)=CRA(t-1,n)+(ep.*((kp1.*(crp(t-1,n).^(1./np)).*delt.*(CRAmax-CRA(t-1,n)))-
(kp2.*delt.*CRA(t-1,n))));
   end
   for n=N+3:N+7;
      c(t,n)=c(t-1,n)+(((Q.*(c(t-1,n-1)-c(t-1,n))).*delt)./(Vmix2));
   end

   cnorm(t)=c(t,N+7);
   vapp(t)=vapp(t-1)+(delt.*Q);
   mass(t)=(vapp(t)-vapp(t-1)).*((c(t,N+3)+c(t-1,N+3))./2);

   Ex(1,t)=vapp(t);
   Ex(2,t)=cnorm(t);
```

```
end

C=cnorm(1:T);
V=vapp(1:T);

figure;%creates a new figure
plot(V,C);
ylabel('Concentration');
xlabel('Volume applied');
title('Concentration of protein leaving column over volume applied');

%Save results to a datafile that can be imported into Microsoft Excel
%Change Ex from a row to a column (Excel has a limited number of columns)

Exc=Ex';
csvwrite('csvlist.dat',Exc);
```

H.4 NaCl breakthrough NP-MLF model

```
%NaCl NP-MLF model for 1ml axial flow column, DEAE sepharose FF, Langmuir isotherm only

%Bed Dimensions
r=0.35;%Bed radius (cm)
L=2.5;%length of bed (cm)
Ac=pi.*r.*r;%cross sectional area of column (cm2)
Vc=Ac.*L;%volume of column (ml)
Vdelay1=1;
Vdelay2=2;
Vmix=2.2;%volume mixer on Akta (ml)
Vmix2=0.13;%
Vstartelute=60;%

%Resin properties
Kp=15;%langmuir coeff (ml/mg)
kp1=0.003;%Rate of uptake of solute by resin (ml/mg.s)
kp2=kp1./Kp;%Rate of disassociation of solute from resin (1/s)
np=1;%fitting parameter
CRSmax=1;%Max solute concentration in resin at saturation (mg/ml)
er=0.31;%Void space of resin (dimensionless)
Rp=0.0045;%Radius of resin (cm)

%Experimental Conditions
Qload=0.25;%Total flowrate through column (ml/min)
Q=Qload/60;%Total flowrate through column (ml/s)
Qelute1=0.2;%First elution flowrate (ml/min)
Qelute2=1;%Second elution flowrate (ml/min)
Qelute3=4;%Third elution flowrate (ml/min)
cin=56.4;%Concentration of solute entering column (mg/ml)
dilution=0.1;%dilution factor for salt buffer
cindil=cin.*dilution;%diluted elution buffer concentration (mg/ml)

ym=0.0;%Molecular dispersion coefficient in length direction for protein
yt=0;%Turbulent dispersion coefficient in length direction for protein
Dm=0.000000611;%Molecular diffusivity of BSA (cm^2/s)

%Times for loading, wash and elution
v0=0;%volume of equilibration buffer to be put through (ml);
v1=10;%volume of diluted salt buffer to be put through (ml);
v2=10;%volume of 100% salt buffer to be put through (ml);
```

```
v3=10;%volume of equilibration buffer to be put through (ml);
t0=((v0)/(Qelute1/60));
t1=((v1)/(Qelute1/60))+t0;
t2=((v2)/(Qelute2/60))+t1;
t3=((v3)/(Qelute3/60))+t2;

%Model Conditions
N=30;%63;%Number of stages in radial direction annulus divided into
J=3;%input('Please enter time divider  ');%Time divider, used for determining delt
Ve=Vc./N;%Volume element (ml)
Tres1=(Ve.*er)/(Qelute1./60);%Residence time in element (s)
delt1=Tres1./J;%change in time (s)
Tres2=(Ve.*er)/(Qelute2./60);%Residence time in element (s)
delt2=Tres2./J;%change in time (s)
Tres3=(Ve.*er)/(Qelute3./60);%Residence time in element (s)
delt3=Tres3./J;%change in time (s)
delL=L/N;%change in length(cm)
T=ceil((t1./delt1)+((t2-t1)./delt2)+((t3-t2)./delt3))%total number of time steps

%Dispersion factors

Dis=(ym.*Dm)+(yt.*2.*Rp.*(Q./(Ac.*er)));

delt=delt1;

for t=1;
   time(t)=delt;
   vapp(t)=((delt.*Q)+Vdelay2+Vstartelute);
   for n=1:N+7;
      c(t,n)=0;
      CRS(t,n)=0;
   end
end

for t=2:T;
   time(t)=time(t-1)+delt;
   for n=1;
      if time(t)<t0;
         c(t,n)=0;
         Q=Qelute1./60;
         delt=delt1;
      elseif time(t)<t1;
         c(t,n)=cindil;
         Q=Qelute1./60;
         delt=delt1;
      elseif time(t)<t2;
         c(t,n)=cin;
         Q=Qelute2./60;
         delt=delt2;
      else
         c(t,n)=0;
         Q=Qelute3./60;
         delt=delt3;
      end
   end
   for n=2;
      c(t,n)=c(t-1,n)+(((Q.*(c(t-1,n-1)-c(t-1,n))).*delt)./(Vmix));
   end
   for n=3;
```

```
    c(t,n)=c(t-1,n)+(((Q.*(c(t-1,n-1)-c(t-1,n))).*delt)./(Ve.*er))-(Dis.*Ac.*delt.*(c(t-1,n)-c(t-
1,n+1))./(delL.*Ve))-(kp1.*(c(t-1,n).^(1./np)).*delt.*(CRSmax-CRS(t-1,n)))+(kp2.*delt.*CRS(t-1,n));
    CRS(t,n)=CRS(t-1,n)+((er./(1-er)).*((kp1.*(c(t-1,n).^(1./np)).*delt.*(CRSmax-CRS(t-1,n)))-
(kp2.*delt.*CRS(t-1,n))));
  end
  for n=4:N+1;
    c(t,n)=c(t-1,n)+(((Q.*(c(t-1,n-1)-c(t-1,n))).*delt)./(Ve.*er))+(Dis.*Ac.*delt.*(c(t-1,n-1)-c(t-
1,n))./(delL.*Ve))-(Dis.*Ac.*delt.*(c(t-1,n)-c(t-1,n+1))./(delL.*Ve))-(kp1*(c(t-
1,n).^(1./np)).*delt.*(CRSmax-CRS(t-1,n)))+(kp2.*delt.*CRS(t-1,n));
    CRS(t,n)=CRS(t-1,n)+((er./(1-er)).*((kp1.*(c(t-1,n).^(1./np)).*delt.*(CRSmax-CRS(t-1,n)))-
(kp2.*delt.*CRS(t-1,n))));
  end
  for n=N+2;
    c(t,n)=c(t-1,n)+(((Q.*(c(t-1,n-1)-c(t-1,n))).*delt)./(Ve.*er))+(Dis.*Ac.*delt.*(c(t-1,n-1)-c(t-
1,n))./(delL.*Ve))-(kp1.*(c(t-1,n).^(1./np)).*delt.*(CRSmax-CRS(t-1,n)))+(kp2.*delt.*CRS(t-1,n));
    CRS(t,n)=CRS(t-1,n)+((er./(1-er)).*((kp1.*(c(t-1,n).^(1./np)).*delt.*(CRSmax-CRS(t-1,n)))-
(kp2.*delt.*CRS(t-1,n))));
  end
  for n=N+3:N+7;
    c(t,n)=c(t-1,n)+(((Q.*(c(t-1,n-1)-c(t-1,n))).*delt)./(Vmix2));
  end

  cnorm(t)=c(t,N+7);
  vapp(t)=vapp(t-1)+(delt.*Q);
  mass(t)=(vapp(t)-vapp(t-1)).*((c(t,N+3)+c(t-1,N+3))./2);

  Ex(1,t)=vapp(t);
  Ex(2,t)=cnorm(t);

end

C=cnorm(1:T);
V=vapp(1:T);

figure;%creates a new figure
plot(V,C);
ylabel('Concentration');
xlabel('Volume applied');
title('Concentration of protein leaving column over volume applied');


%Save results to a datafile that can be imported into Microsoft Excel
%Change Ex from a row to a column (Excel has a limited number of columns)

Exc=Ex';
csvwrite('csvlist.dat',Exc);
```

H.5 Axial elution FD-MLF model

```
%FD-MLF elution model for 1ml axial flow column, DEAE sepharose FF

%Bed Dimensions
r=0.35;%Bed radius (cm)
L=2.5;%length of bed (cm)
Ac=pi.*r.*r;%cross sectional area of column (cm2)
Vc=Ac.*L;%volume of column (ml)
Vdelay1=1;
Vdelay2=2;
```

```
Vmix=2.2;%volume mixer on Akta (ml)
Vmix2=0.13;%
Vstartelute=60;%

%Resin properties for salt
Ks=15;%langmuir coeff (ml/mg)
ks1=0.003;%Rate of uptake of solute by resin (ml/mg.s)
ks2=ks1./Ks;%Rate of disassociation of solute from resin (1/s)
ns=1;%fitting parameter
CRSmax=1;%10;%Max solute concentration in resin at saturation (mg/ml)
er=0.31;%Void space of resin (dimensionless)
ep=0.72;%Pore fraction of resin
kfs=0.0001;%film diffusion coefficient (cm/s)
Rp=0.0045;%Radius of resin (cm)

%Resin properties
Kp=47;%langmuir coeff (ml/mg)
kp1=0.0085;%Rate of uptake of solute by resin at loading flowrate (ml/mg.s)
kp2=kp1./Kp;%Rate of disassociation of solute from resin (1/s) at loading flowrate
np=1;%fitting parameter
CRPmax=69;%10;%Max solute concentration in resin at saturation (mg/ml)
er=0.31;%Void space of resin (dimensionless)
ep=0.72;%Pore fraction of resin
kfp=0.0001;%film diffusion coefficient for BSA (cm/s)
Rp=0.0045;%Radius of resin (cm)
Kd=8;%Desorption parameter

%Experimental Conditions
Qload=0.5;%Loading flowrate through column (ml/min)
Qwash=0.5;%Wash flowrate (ml/min)
Qelute1=0.2;%First elution flowrate (ml/min)
Qelute2=1;%Second elution flowrate (ml/min)
Qelute3=4;%Third elution flowrate (ml/min)
csin=56.4;%Concentration of solute entering column (mg/ml)
cpin=1.51;%Concentration of protein (mg/ml)
dilution=0.02;%dilution factor for salt buffer
csindil=csin.*dilution;%diluted elution buffer concentration (mg/ml)

ym=0.0;%Molecular dispersion coefficient in length direction for protein
yt=0;%Turbulent dispersion coefficient in length direction for protein
Dm=0.000000611;%Molecular diffusivity of BSA (cm^2/s)

%Times for loading, wash and elution
v1=50;%volume of feed solution to be put through (ml) buffer coming from superloop
v2=(10+(Vdelay2-Vdelay1));%volume of equilibration buffer to be put through (ml);
v3=10;%volume of diluted salt buffer to be put through (ml), Vdelay inclusion to account for elution
buffer now coming from primary pumps, no need for equilibration buffer as buffer already in tubes up to
injection valve;
v4=10;%volume of 100% salt buffer to be put through (ml);
v5=10;%volume of equilibration buffer to be put through (ml);
t1=((v1)/(Qload/60));
tsalt=((1)/(Qload/60))+t1;
t2=((v2)/(Qwash/60))+t1;
t3=((v3)/(Qelute1/60))+t2;
t4=((v4)/(Qelute2/60))+t3;
t5=((v5)/(Qelute3/60))+t4;

%Model Conditions
N=30;%63;%Number of stages in radial direction annulus divided into
J=3;%input('Please enter time divider  ');%Time divider, used for determining delt
```

```
Ve=Vc./N;%Volume element (ml)
Tres1=(Ve.*er)/(Qload./60);%Residence time in element (s)
delt1=Tres1./J;%change in time (s)
T1=ceil(t2./delt1);
Tres2=(Ve.*er)/(Qelute1./60);%Residence time in element (s)
delt2=Tres2./12;%change in time (s)
T2=ceil((t3-t2)./delt2);
Tres3=(Ve.*er)/(Qelute2./60);%Residence time in element (s)
delt3=Tres3./12;%change in time (s)
T3=ceil((t4-t3)./delt3);
Tres4=(Ve.*er)/(Qelute3./60);%Residence time in element (s)
delt4=Tres4./12;%change in time (s)
T4=ceil((t5-t4)./delt4);
delL=L/N;%change in length(cm)
T=ceil(T1+T2+T3+T4);%total number of time steps

%Dispersion factors

Dis=(ym.*Dm)+(yt.*2.*Rp.*((Qload./60)./(Ac.*er)));

delt=delt1;

for t=1;
   time(t)=delt;
   vapp(t)=((delt.*(Qload./60))+Vdelay1);
   for n=1:N+7;
      cs(t,n)=0;
      crps(t,n)=0;
      CRS(t,n)=0;
      cp(t,n)=0;
      crpp(t,n)=0;
      CRP(t,n)=0;
   end
end

for t=2:T;
   time(t)=time(t-1)+delt;
   for n=1;
      if time(t)<t1;
         cp(t,n)=cpin;
         cs(t,n)=0;
         Q=Qload./60;
         delt=delt1;
         kfp=0.0004;
         Ks=10;
      elseif time(t)<tsalt;
         cp(t,n)=0;
         cs(t,n)=0.2;
         Q=Qload./60;
         delt=delt1;
         kfp=0.0004;
         Ks=30;
      elseif time(t)<t2;
         cp(t,n)=0;
         cs(t,n)=0;
         Q=Qwash./60;
         delt=delt1;
         kfp1=0.0004;
         Ks=10;
      elseif time(t)<t3;
```

```
        cp(t,n)=0;
        cs(t,n)=csindil;
        Q=Qelute1./60;
        delt=delt2;
        kfp=0.00016;
        Ks=Kse;
      elseif time(t)<t4;
        cp(t,n)=0;
        cs(t,n)=csin;
        Q=Qelute2./60;
        delt=delt3;
        kfp=0.0012;
        Ks=2000;
      else
        cp(t,n)=0;
        cs(t,n)=0;
        Q=Qelute3./60;
        delt=delt4;
        kfp=0.0048;
        Ks=Kse;
      end
    end
    for n=2;
      if time(t)<tsalt;
        cs(t,n)=cs(t-1,n-1);
      else
        cs(t,n)=cs(t-1,n)+(((Q.*(cs(t-1,n-1)-cs(t-1,n))).*delt)./(Vmix));
      end
      cp(t,n)=cp(t-1,n-1);
    end
     for n=3;
      %salt concentration
      cs(t,n)=cs(t-1,n)+(((Q.*(cs(t-1,n-1)-cs(t-1,n))).*delt)./(Ve.*er))-(Dis.*Ac.*delt.*(cs(t-1,n)-cs(t-
1,n+1))./(delL.*Ve))-(((1-er)./er).*((3.*kfs)./Rp).*(cs(t-1,n)-crps(t-1,n)).*delt);
      crps(t,n)=crps(t-1,n)+(((3.*kfs)./(Rp.*ep)).*(cs(t-1,n)-crps(t-1,n)).*delt)-(ks1.*(crps(t-
1,n)).*delt.*(CRSmax-CRS(t-1,n)))+(ks2.*delt.*CRS(t-1,n));
      CRS(t,n)=CRS(t-1,n)+(ep.*((ks1.*(crps(t-1,n)).*delt.*(CRSmax-CRS(t-1,n)))-(ks2.*delt.*CRS(t-
1,n))));
      %protein concentration
      cp(t,n)=cp(t-1,n)+(((Q.*(cp(t-1,n-1)-cp(t-1,n))).*delt)./(Ve.*er))-(Dis.*Ac.*delt.*(cp(t-1,n)-cp(t-
1,n+1))./(delL.*Ve))-(((1-er)./er).*((3.*kfp)./Rp).*(cp(t-1,n)-crpp(t-1,n)).*delt);
      crpp(t,n)=crpp(t-1,n)+(((3.*kfp)./(Rp.*ep)).*(cp(t-1,n)-crpp(t-1,n)).*delt)-(kp1.*(crpp(t-
1,n)).*delt.*(CRPmax-CRP(t-1,n)))+(kp2.*(1+((crps(t-1,n).^(1./ns)).*Kd)).*delt.*CRP(t-1,n));
      CRP(t,n)=CRP(t-1,n)+(ep.*((kp1.*(crpp(t-1,n).^(1./np)).*delt.*(CRPmax-CRP(t-1,n)))-
(kp2.*(1+((crps(t-1,n).^(1./ns)).*Kd)).*delt.*CRP(t-1,n))));
    end
    for n=4:N+1;
      %salt concentration
      cs(t,n)=cs(t-1,n)+(((Q.*(cs(t-1,n-1)-cs(t-1,n))).*delt)./(Ve.*er))+(Dis.*Ac.*delt.*(cs(t-1,n-1)-cs(t-
1,n))./(delL.*Ve))-(Dis.*Ac.*delt.*(cs(t-1,n)-cs(t-1,n+1))./(delL.*Ve))-(((1-er)./er).*((3.*kfs)./Rp).*(cs(t-
1,n)-crps(t-1,n)).*delt);
      crps(t,n)=crps(t-1,n)+(((3.*kfs)./(Rp.*ep)).*(cs(t-1,n)-crps(t-1,n)).*delt)-(ks1.*(crps(t-
1,n)).*delt.*(CRSmax-CRS(t-1,n)))+(ks2.*delt.*CRS(t-1,n));
      CRS(t,n)=CRS(t-1,n)+(ep.*((ks1.*(crps(t-1,n)).*delt.*(CRSmax-CRS(t-1,n)))-(ks2.*delt.*CRS(t-
1,n))));
      %protein concentration
      cp(t,n)=cp(t-1,n)+(((Q.*(cp(t-1,n-1)-cp(t-1,n))).*delt)./(Ve.*er))+(Dis.*Ac.*delt.*(cp(t-1,n-1)-cp(t-
1,n))./(delL.*Ve))-(Dis.*Ac.*delt.*(cp(t-1,n)-cp(t-1,n+1))./(delL.*Ve))-(((1-
er)./er).*((3.*kfp)./Rp).*(cp(t-1,n)-crpp(t-1,n)).*delt);
```

```
    crpp(t,n)=crpp(t-1,n)+(((3.*kfp)./(Rp.*ep)).*(cp(t-1,n)-crpp(t-1,n)).*delt)-(kp1.*(crpp(t-
1,n)).*delt.*(CRPmax-CRP(t-1,n)))+(kp2.*(1+((crps(t-1,n).^(1./ns)).*Kd)).*delt.*CRP(t-1,n));
    CRP(t,n)=CRP(t-1,n)+(ep.*((kp1.*(crpp(t-1,n).^(1./np)).*delt.*(CRPmax-CRP(t-1,n)))-
(kp2.*(1+((crps(t-1,n).^(1./ns)).*Kd)).*delt.*CRP(t-1,n))));
  end
  for n=N+2;
    %salt concentration
    cs(t,n)=cs(t-1,n)+(((Q.*(cs(t-1,n-1)-cs(t-1,n))).*delt)./(Ve.*er))+(Dis.*Ac.*delt.*(cs(t-1,n-1)-cs(t-
1,n)).*(delL.*Ve))-(((1-er)./er).*((3.*kfs)./Rp).*(cs(t-1,n)-crps(t-1,n)).*delt);
    crps(t,n)=crps(t-1,n)+(((3.*kfs)./(Rp.*ep)).*(cs(t-1,n)-crps(t-1,n)).*delt)-(ks1.*(crps(t-
1,n)).*delt.*(CRSmax-CRS(t-1,n)))+(ks2.*delt.*CRS(t-1,n));
    CRS(t,n)=CRS(t-1,n)+(ep.*((ks1.*(crps(t-1,n)).*delt.*(CRSmax-CRS(t-1,n)))-(ks2.*delt.*CRS(t-
1,n))));
    %protein concentration
    cp(t,n)=cp(t-1,n)+(((Q.*(cp(t-1,n-1)-cp(t-1,n))).*delt)./(Ve.*er))+(Dis.*Ac.*delt.*(cp(t-1,n-1)-cp(t-
1,n)).*(delL.*Ve))-(((1-er)./er).*((3.*kfp)./Rp).*(cp(t-1,n)-crpp(t-1,n)).*delt);
    crpp(t,n)=crpp(t-1,n)+(((3.*kfp)./(Rp.*ep)).*(cp(t-1,n)-crpp(t-1,n)).*delt)-(kp1.*(crpp(t-
1,n)).*delt.*(CRPmax-CRP(t-1,n)))+(kp2.*(1+((crps(t-1,n).^(1./ns)).*Kd)).*delt.*CRP(t-1,n));
    CRP(t,n)=CRP(t-1,n)+(ep.*((kp1.*(crpp(t-1,n).^(1./np)).*delt.*(CRPmax-CRP(t-1,n)))-
(kp2.*(1+((crps(t-1,n).^(1./ns)).*Kd)).*delt.*CRP(t-1,n))));
  end
  for n=N+3:N+7;
    cs(t,n)=cs(t-1,n)+(((Q.*(cs(t-1,n-1)-cs(t-1,n))).*delt)./(Vmix2));
    cp(t,n)=cp(t-1,n)+(((Q.*(cp(t-1,n-1)-cp(t-1,n))).*delt)./(Vmix2));

  end

  cnorm(t)=cp(t,N+7);
  enorm(t)=cs(t,N+7);
  vapp(t)=vapp(t-1)+(delt.*Q);
  mass(t)=(vapp(t)-vapp(t-1)).*((cp(t,N+7)+cp(t-1,N+7))./2);
end

C=cnorm(1:T);

V=vapp(1:T);

%figure;%creates a new figure
%plot(V,C);
%ylabel('Concentration');
%xlabel('Volume applied');
%title('Concentration of protein leaving column over volume applied');


for i=1:T1;
  Fx(1,i)=vapp(i);
  Fx(2,i)=cnorm(i);
end

Fxc=Fx';

csvwrite('feedlist.dat',Fxc);

for i=1:T2+T3;
  Ex(1,i)=vapp(i+T1);
  Ex(2,i)=cnorm(i+T1);
  Ex(3,i)=enorm(i+T1);
end

%Save results to a datafile that can be imported into Microsoft Excel
```

```
%Change Ex from a row to a column (Excel has a limited number of columns)

Exc=Ex';
csvwrite('elutelist.dat',Exc);
```

H.6 Flow manifold

```
%CRFC flow manifold

%Experimental Conditions
Qinput=45;%Total flowrate through column (ml/min)
Q=Qinput/60;%Total flowrate through column (ml/s)
cin=1;%Concentration of solute entering column (mg/ml)
cin1=0.*cin;
cin2=1*cin;
cin3=0*cin;
cin4=0*cin;
cin5=0*cin;
cin6=0;
cin7=0;

%Times for loading, wash and elution
v1=0;%input('enter volume of equilibration buffer to be put through   ');
v2=300;%input('enter volume of loading solution to be put through   ');
v3=300;%input('enter volume of wash buffer to be put through   ');
v4=0;%input('enter volume of elution buffer to be put through   ');
v5=0;
v6=0;
v7=0;
t1=v1/Q;
t2=(v2/Q)+t1;
t3=(v3/Q)+t2;
t4=(v4/Q)+t3;
t5=(v5/Q)+t4;
t6=(v6/Q)+t5;
t7=(v7/Q)+t6;

%Model Conditions
N=2;%63;%Number of stages in radial direction annulus divided into
J=3;%input('Please enter time divider   ');%Time divider, used for determining delt
Ve=0.13;%Volume element (ml)
vdelay=721.0;
delt=0.1;%change in time (s)
T=ceil(t7./delt)%total number of time steps

for t=1;
   for n=1:3;
      c(t,n)=0;

   end
end

for t=2:T;
   time(t)=t.*delt;
   for n=1;
      if time(t)<t1;
         c(t,n)=cin1;

      elseif time(t)<t2;
```

```
        c(t,n)=cin2;

      elseif time(t)<t3;
        c(t,n)=cin3;

      elseif time(t)<t4;
        c(t,n)=cin4;

      elseif time(t)<t5;
        c(t,n)=cin5;

      elseif time(t)<t6;
        c(t,n)=cin6;
      else
        c(t,n)=0;

      end
    end
    %for n=2
      %equation for gradient mixer, the 2.2 is the volume of the mixer
    %   c(t,n)=c(t-1,n)+(((Q.*(c(t-1,n-1)-c(t-1,n))).*delt)./(2.2));
    %end
    %for n=3
     %   c(t,n)=c(t-1,n)+(((Q.*(c(t-1,n-1)-c(t-1,n))).*delt)./(0.5));
     %end
    for n=2:3
      %equation for gradient mixer, the 13 is the volume of the mixer
      c(t,n)=c(t-1,n)+(((Q.*(c(t-1,n-1)-c(t-1,n))).*delt)./(13));
    end
    %for n=6
     %   c(t,n)=c(t-1,n)+(((Q.*(c(t-1,n-1)-c(t-1,n))).*delt)./(0.5));
     %end
    %for n=5:9;
     %   c(t,n)=c(t-1,n)+(((Q.*(c(t-1,n-1)-c(t-1,n))).*delt)./(Ve));
     %end

    cnorm(t)=c(t,3);
    vapp(t)=(time(t).*Q)+vdelay;

    Ex(1,t)=vapp(t);
    Ex(2,t)=cnorm(t);

end

C=cnorm(1:T);
V=vapp(1:T);

%figure;%creates a new figure
%plot(V,C);
%ylabel('Concentration');
%xlabel('Volume applied');
%title('Concentration of protein leaving system over volume applied');

%Save results to a datafile that can be imported into Microsoft Excel
%Change Ex from a row to a column (Excel has a limited number of columns)

Exc=Ex';
csvwrite('csvlist.dat',Exc);
```

H.7 Akta pump solution change

```
%Akta pump solution change

%Experimental Conditions
Qinput=45;%Total flowrate through column (ml/min)
Q=Qinput/60;%Total flowrate through column (ml/s)
cin=1;%Concentration of solute entering column (mg/ml)
cin1=0.*cin;
cin2=1.*cin;
cin3=0.0*cin;
cin4=0.0*cin;
cin5=0.0*cin;
cin6=0*cin;
cin7=0;

%Times for loading, wash and elution
v1=150;%input('enter volume of equilibration buffer to be put through   ');
v2=200;%input('enter volume of loading solution to be put through   ');
v3=100;%input('enter volume of wash buffer to be put through   ');
v4=0;%input('enter volume of elution buffer to be put through   ');
v5=0;
v6=0;
v7=0;
t1=v1/Q;
t2=(v2/Q)+t1;
t3=(v3/Q)+t2;
t4=(v4/Q)+t3;
t5=(v5/Q)+t4;
t6=(v6/Q)+t5;
t7=(v7/Q)+t6;

%Model Conditions
N=2;%63;%Number of stages in radial direction annulus divided into
J=3;%input('Please enter time divider   ');%Time divider, used for determining delt
Ve=0.13;%Volume element (ml)
vdelay=5.0;
delt=0.1;%change in time (s)
T=ceil(t7./delt)%total number of time steps

for t=1;
   for n=1:8;
      c(t,n)=0;

   end
end

for t=2:T;
   time(t)=t.*delt;
   for n=1;
      if time(t)<t1;
         c(t,n)=cin1;

      elseif time(t)<t2;
         c(t,n)=cin2;

      elseif time(t)<t3;
         c(t,n)=cin3;

      elseif time(t)<t4;
```

```
        c(t,n)=cin4;

      elseif time(t)<t5;
        c(t,n)=cin5;

      elseif time(t)<t6;
        c(t,n)=cin6;
      else
        c(t,n)=0;

      end
    end
    for n=2
      %equation for pump, the 2 is the volume of the pump
      c(t,n)=c(t-1,n)+(((Q.*(c(t-1,n-1)-c(t-1,n))).*delt)./(2));
    end
    for n=3
      %equation for gradient mixer, the 2.2 is the volume of the mixer
      c(t,n)=c(t-1,n)+(((Q.*(c(t-1,n-1)-c(t-1,n))).*delt)./(2.2));
    end
    for n=4:8;
      c(t,n)=c(t-1,n)+(((Q.*(c(t-1,n-1)-c(t-1,n))).*delt)./(Ve));
    end

    cnorm(t)=c(t,8);
    vapp(t)=(time(t).*Q)+vdelay;

    Ex(1,t)=vapp(t);
    Ex(2,t)=cnorm(t);

end

C=cnorm(1:T);
V=vapp(1:T);

%figure;%creates a new figure
%plot(V,C);
%ylabel('Concentration');
%xlabel('Volume applied');
%title('Concentration of protein leaving system over volume applied');

%Save results to a datafile that can be imported into Microsoft Excel
%Change Ex from a row to a column (Excel has a limited number of columns)

Exc=Ex';
csvwrite('csvlist.dat',Exc);
```

H.8 Akta sample pump

```
%Akta sample pump

%Experimental Conditions
Qinput=5;%Total flowrate through column (ml/min)
Q=Qinput/60;%Total flowrate through column (ml/s)
cin=1;%Concentration of solute entering column (mg/ml)
cin1=0*cin;
cin2=0.2*cin;
cin3=0.4*cin;
cin4=0.6*cin;
cin5=0.8*cin;
```

```
cin6=1*cin;
cin7=0;

%Times for loading, wash and elution
v1=100;%input('enter volume of equilibration buffer to be put through   ');
v2=50;%input('enter volume of loading solution to be put through   ');
v3=50;%input('enter volume of wash buffer to be put through   ');
v4=50;%input('enter volume of elution buffer to be put through   ');
v5=50;
v6=50;
v7=10;
t1=v1/Q;
t2=(v2/Q)+t1;
t3=(v3/Q)+t2;
t4=(v4/Q)+t3;
t5=(v5/Q)+t4;
t6=(v6/Q)+t5;
t7=(v7/Q)+t6;

%Model Conditions
N=5;%63;%Number of stages in radial direction annulus divided into
J=3;%input('Please enter time divider   ');%Time divider, used for determining delt
Ve=0.13;%Volume element (ml)
vdelay=3.33;
delt=1;%change in time (s)
T=ceil(t7./delt)%total number of time steps

for t=1;
   for n=1:6;
      c(t,n)=0;

   end
end

for t=2:T;
   time(t)=t.*delt;
   for n=1;
      if time(t)<t1;
         c(t,n)=cin1;

      elseif time(t)<t2;
         c(t,n)=cin2;

      elseif time(t)<t3;
         c(t,n)=cin3;

      elseif time(t)<t4;
         c(t,n)=cin4;

      elseif time(t)<t5;
         c(t,n)=cin5;

      elseif time(t)<t6;
         c(t,n)=cin6;
      else
         c(t,n)=0;

      end
   end
   for n=2:6;
```

```
    c(t,n)=c(t-1,n)+((((Q.*(c(t-1,n-1)-c(t-1,n))).*delt)./(Ve));
  end

  cnorm(t)=c(t,N+1);
  vapp(t)=(time(t).*Q)+vdelay;

  Ex(1,t)=vapp(t);
  Ex(2,t)=cnorm(t);

end

C=cnorm(1:T);
V=vapp(1:T);

%figure;%creates a new figure
%plot(V,C);
%ylabel('Concentration');
%xlabel('Volume applied');
%title('Concentration of protein leaving system over volume applied');


%Save results to a datafile that can be imported into Microsoft Excel
%Change Ex from a row to a column (Excel has a limited number of columns)

Exc=Ex';
csvwrite('csvlist.dat',Exc);
```

H.9 Batch CRFC operation

```
%Model for batch CRFC operation

Vdelay1=1371;

%Annular Bed Dimensions
r1=7.3;%Outside annular bed radius (cm)
r2=4.3;%Inside annular bed radius (cm)
H=2;%Depth of annular bed (cm)
oswt=0.3;%Outer sinter wall thickness (cm)
iswt=0.3;%Inner sinter wall thickness (cm)
esw=0.25;%void space of sintered walls (dimensionless)

%Chamber allocations
%n=1=imaginary chamber for setting feed input concentrations
%n=2=flow splitter feed chamber
%n=3=crfc outer feed chamber
%n=4=annulus outer sinter wall
%n=5...N+4=annulus bed
%n=N+5=annulus inner sinter wall
%n=N+6=crfc inner exit chamber
%n=N+7=flow splitter exit chamber

%CRFC feed and exit chamber properties
ofc=0.5;%width of chamber surrounding annulus (cm)
iec=0.5;%width of chamber inside inside wall of annulus (cm)
sv=13;%volume of flow splitter feed and exit chambers (ml)
vofc=pi.*H.*(((r1+oswt+ofc).^2)-((r1+oswt).^2));%volume of outer feed chamber (ml)
viec=pi.*H.*(((r2-iswt).^2)-((r2-iswt-iec).^2));%volume of inner exit chamber (ml)

%NaCl Resin Properties
```

```
Ks=15;%NaCl equilibrium constant
ks1=0.003;%Rate of uptake of solute by resin
ks2=ks1/Ks;%Rate of disassociation of solute from resin
crsmax=1;%Max solute concentration in resin at saturation (mg/ml)
ns=1;
er=0.31;%Void space of resin (dimensionless)
ep=0.72;
kfs=0.000005;%Diffusion coefficient
Rp=0.0045;%Resin particle radius

%BSA Resin Properties
Kp=47;%equilibrium constant (ml/mg)
kp1=0.00035;%Rate of uptake of solute by resin (ml/mg.s)
kp2=kp1/Kp;%Rate of disassociation of solute from resin (ml/mg)
crpmax=110;%Max solute concentration in resin at saturation (mg/ml)
er=0.31;%Void space of resin (dimensionless)
ep=0.72;
kfp=0.0005;%Diffusion coefficient (cm2)
Rp=0.0045;%Resin particle radius (cm)
Kd=45;%Desorption parameter (ml/mg.s)

%Experimental Conditions
Qin=45;%Total flowrate through annulus (ml/min)
Q=Qin;
Qe=Qin/60;%Total flowrate through annulus (ml/s)
csin=55;%Concentration of solute entering annulus (mg/ml)
cpin=2.152;
y2p=0.0;
y2s=0;

%Times for loading, wash and elution
v1=8000;%volume of feed solution to be put through (ml) buffer coming from superloop
v2=4000;%volume of equilibration buffer to be put through (ml);
v3=2000;%volume of diluted salt buffer to be put through (ml), Vdelay inclusion to account for elution
buffer now coming from primary pumps, no need for equilibration buffer as buffer already in tubes up to
injection valve;
t1=((v1)/(Q/60));
t2=((v2)/(Q/60))+t1;
t3=((v3)/(Q/60))+t2;

%bed properties

N=33;%63;%Number of stages in radial direction annulus divided into
Nosw=6;
Nisw=6;
delrosw=oswt./Nosw;
delrisw=iswt./Nisw;
delr=(r1-r2)/N;

for n=2;
   ve(n)=sv;
end
for n=3;
   ve(n)=vofc;
   r(n)=r1+oswt;
end
for n=4:Nosw+3;
   r(n)=r1+oswt-((n-3).*delrosw);
   ve(n)=(pi.*((r(n-1).^2)-(r(n).^2)).*H).*esw;
end
```

```
for n=Nosw+4:Nosw+N+3;
   r(n)=r1-((n-(Nosw+3)).*delr);
   ve(n)=(pi.*((r(n-1).^2)-(r(n).^2)).*H);
end
for n=Nosw+N+4:Nosw+N+Nisw+3;
   r(n)=r2-((n-(Nosw+N+3)).*delrisw);
   ve(n)=(pi.*((r(n-1).^2)-(r(n).^2)).*H).*esw;
end
for n=Nosw+N+Nisw+4;
   ve(n)=viec;
end
for n=Nosw+N+Nisw+5;
   ve(n)=sv;
end

%delt calculation
J=6;%input('Please enter time divider  ');%Time divider, used for determining delt
Tres=(ve(Nosw+N+3).*er)./(Q./60);%Residence time in element (s)
delt=Tres./J;%change in time (s)
T=ceil(t3./delt)

te=round(t2./delt);
tw=round(t1./delt);

%Calculate concentrations

for t=1;
   time(t)=delt;
   vapp(t)=((delt.*(Q./60))+Vdelay1);
   for n=1:Nosw+N+Nisw+5;
      cs(t,n)=0;
      crps(t,n)=0;
      crs(t,n)=0;
      cp(t,n)=0;
      crpp(t,n)=0;
      crp(t,n)=0;
   end
end


for t=2:T;
   time(t)=time(t-1)+delt;
   for n=1;
      if time(t)<t1;
         cp(t,n)=cpin;
         cs(t,n)=0;
      elseif time(t)<t2;
         cp(t,n)=0;
         cs(t,n)=0;
      else
         cp(t,n)=0;
         cs(t,n)=csin;
      end
   end
   for n=2:Nosw+3;
      cs(t,n)=cs(t-1,n)+(((cs(t-1,n-1)-cs(t-1,n)).*Qe.*delt)./(ve(n)));
      cp(t,n)=cp(t-1,n)+(((cp(t-1,n-1)-cp(t-1,n)).*Qe.*delt)./(ve(n)));
   end
   for n=Nosw+4;
      %NaCl concentration
```

```
    cs(t,n)=cs(t-1,n)+(((cs(t-1,n-1)-cs(t-1,n)).*Qe.*delt)./(ve(n).*er))-
(((y2s.*(2.*Rp).*Qe.*delt)./(ve(n).*er.*delr)).*(cs(t-1,n)-cs(t-1,n+1)))-(3.*kfs.*(cs(t-1,n)-crps(t-
1,n)).*delt.*((1-er)./(Rp.*er)));
    crps(t,n)=crps(t-1,n)+(3.*kfs.*(cs(t-1,n)-crps(t-1,n)).*delt.*(1/(Rp.*ep)))-(ks1.*crps(t-1,n).*(crsmax-
crs(t-1,n)).*delt)+(ks2.*crs(t-1,n).*delt);
    crs(t,n)=crs(t-1,n)+(ep.*((ks1.*crps(t-1,n).*(crsmax-crs(t-1,n)).*delt)-(ks2.*crs(t-1,n).*delt)));
    %BSA concentration
    cp(t,n)=cp(t-1,n)+(((cp(t-1,n-1)-cp(t-1,n)).*Qe.*delt)./(ve(n).*er))-
(((y2p.*(2.*Rp).*Qe.*delt)./(ve(n).*er.*delr)).*(cp(t-1,n)-cp(t-1,n+1)))-(3.*kfp.*(cp(t-1,n)-crpp(t-
1,n)).*delt.*((1-er)./(Rp.*er)));
    crpp(t,n)=crpp(t-1,n)+(3.*kfp.*(cp(t-1,n)-crpp(t-1,n)).*delt.*(1/(Rp.*ep)))-(kp1.*crpp(t-
1,n)*(crpmax-crp(t-1,n)).*delt)+(kp2.*(1+Kd.*(crps(t-1,n).^(1/ns))).*crp(t-1,n).*delt);
    crp(t,n)=crp(t-1,n)+(ep.*((kp1.*crpp(t-1,n).*(crpmax-crp(t-1,n)).*delt)-(kp2.*(1+Ks.*(crps(t-
1,n).^(1/ns))).*crp(t-1,n).*delt)));
  end
  for n=Nosw+5:Nosw+N+2;
    %NaCl concentration
    cs(t,n)=cs(t-1,n)+(((cs(t-1,n-1)-cs(t-
1,n)).*Qe.*delt)./(ve(n).*er))+(((y2s.*(2.*Rp).*Qe.*delt)./(ve(n).*er.*delr)).*(cs(t-1,n-1)-(2.*cs(t-
1,n))+cs(t-1,n+1)))-(3.*kfs.*(cs(t-1,n)-crps(t-1,n)).*delt.*((1-er)./(Rp.*er)));
    crps(t,n)=crps(t-1,n)+(3.*kfs.*(cs(t-1,n)-crps(t-1,n)).*delt.*(1/(Rp.*ep)))-(ks1.*crps(t-1,n).*(crsmax-
crs(t-1,n)).*delt)+(ks2.*crs(t-1,n).*delt);
    crs(t,n)=crs(t-1,n)+(ep.*((ks1.*crps(t-1,n).*(crsmax-crs(t-1,n)).*delt)-(ks2.*crs(t-1,n).*delt)));
    %BSA concentration
    cp(t,n)=cp(t-1,n)+(((cp(t-1,n-1)-cp(t-
1,n)).*Qe.*delt)./(ve(n).*er))+(((y2p.*(2.*Rp).*Qe.*delt)./(ve(n).*er.*delr)).*(cp(t-1,n-1)-(2.*cp(t-
1,n))+cp(t-1,n+1)))-(3.*kfp.*(cp(t-1,n)-crpp(t-1,n)).*delt.*((1-er)./(Rp.*er)));
    crpp(t,n)=crpp(t-1,n)+(3.*kfp.*(cp(t-1,n)-crpp(t-1,n)).*delt.*(1/(Rp.*ep)))-(kp1.*crpp(t-
1,n).*(crpmax-crp(t-1,n)).*delt)+(kp2.*(1+Ks.*(crps(t-1,n).^(1/ns))).*crp(t-1,n).*delt);
    crp(t,n)=crp(t-1,n)+(ep.*((kp1.*crpp(t-1,n).*(crpmax-crp(t-1,n)).*delt)-(kp2.*(1+Ks.*(crps(t-
1,n).^(1/ns))).*crp(t-1,n).*delt)));
  end
  for n=Nosw+N+3;
    %NaCl concentration
    cs(t,n)=cs(t-1,n)+(((cs(t-1,n-1)-cs(t-
1,n)).*Qe.*delt)./(ve(n).*er))+(((y2s.*(2.*Rp).*Qe.*delt)./(ve(n).*er.*delr)).*(cs(t-1,n-1)-cs(t-1,n)))-
(3.*kfs.*(cs(t-1,n)-crps(t-1,n)).*delt.*((1-er)./(Rp.*er)));
    crps(t,n)=crps(t-1,n)+(3.*kfs.*(cs(t-1,n)-crps(t-1,n)).*delt.*(1/(Rp.*ep)))-(ks1.*crps(t-1,n).*(crsmax-
crs(t-1,n)).*delt)+(ks2.*crs(t-1,n).*delt);
    crs(t,n)=crs(t-1,n)+(ep.*((ks1.*crps(t-1,n).*(crsmax-crs(t-1,n)).*delt)-(ks2.*crs(t-1,n).*delt)));
    %BSA concentration
    cp(t,n)=cp(t-1,n)+(((cp(t-1,n-1)-cp(t-
1,n)).*Qe.*delt)./(ve(n).*er))+(((y2p.*(2.*Rp).*Qe.*delt)./(ve(n).*er.*delr)).*(cp(t-1,n-1)-cp(t-1,n)))-
(3.*kfp.*(cp(t-1,n)-crpp(t-1,n)).*delt.*((1-er)./(Rp.*er)));
    crpp(t,n)=crpp(t-1,n)+(3.*kfp.*(cp(t-1,n)-crpp(t-1,n)).*delt.*(1/(Rp.*ep)))-(kp1.*crpp(t-
1,n).*(crpmax-crp(t-1,n)).*delt)+(kp2.*(1+Ks.*(crps(t-1,n).^(1/ns))).*crp(t-1,n).*delt);
    crp(t,n)=crp(t-1,n)+(ep.*((kp1.*crpp(t-1,n).*(crpmax-crp(t-1,n)).*delt)-(kp2.*(1+Ks.*(crps(t-
1,n).^(1/ns))).*crp(t-1,n).*delt)));
  end
  for n=Nosw+N+4:Nosw+N+Nisw+5;
    cs(t,n)=cs(t-1,n)+(((cs(t-1,n-1)-cs(t-1,n)).*Qe.*delt)./(ve(n)));
    cp(t,n)=cp(t-1,n)+(((cp(t-1,n-1)-cp(t-1,n)).*Qe.*delt)./(ve(n)));
  end
  cnorm(t)=cp(t,Nosw+N+Nisw+5);
  enorm(t)=cs(t,Nosw+N+Nisw+5);
  vapp(t)=vapp(t-1)+(delt.*Qe);

end

C=cnorm(1:T);
```

```
V=vapp(1:T);

%figure;%creates a new figure
plot(V,C);
ylabel('Concentration');
xlabel('Volume applied');
title('Concentration of protein leaving column over volume applied');

B=T/10;

for i=1:B;
   Ex(1,i)=vapp(i.*10);
   Ex(2,i)=cnorm(i.*10);
   Ex(3,i)=enorm(i.*10);
end

Massapp=v1.*cpin;
Masslostload=((mean(cnorm(1:tw))).*(v1));
Masslostwash=((mean(cnorm(1:te))).*(v1+v2));
Massretained=Massapp-Masslostwash;

Ex(4,1)=Massapp;
Ex(4,2)=Masslostload;
Ex(4,3)=Masslostwash;
Ex(4,4)=Massretained;

%Save results to a datafile that can be imported into Microsoft Excel
%Change Ex from a row to a column (Excel has a limited number of columns)

Exc=Ex';
csvwrite('elutelist.dat',Exc);
```

H.10 CRFC model, continuous operation

```
%Model for CRFC under continuous operation

%Annular Bed Dimensions
r1=7.3;%Outside annular bed radius (cm)
r2=4.3;%Inside annular bed radius (cm)
H=2;%Depth of annular bed (cm)
oswt=0.3;%Outer sinter wall thickness (cm)
iswt=0.3;%Inner sinter wall thickness (cm)
esw=0.25;%void space of sintered walls (dimensionless)

%NaCl Resin Properties

ks1=0.00015;%Rate of uptake of solute by resin
ks2=0.001;%Rate of disassociation of solute from resin
crsmax=56;%56;%Max solute concentration in resin at saturation (mg/ml)
ns=1;
er=0.31;%Void space of resin (dimensionless)
ep=0.72;
kfs=0.00005;%Diffusion coefficient
Rp=0.0045;%Resin particle radius

%BSA Resin Properties
Kp=47;
kp1=0.0003;%Rate of uptake of solute by resin
kp2=kp1/Kp;%Rate of disassociation of solute from resin
```

```
crpmax=72;%Max solute concentration in resin at saturation (mg/ml)
er=0.31;%Void space of resin (dimensionless)
ep=0.72;
kfp=0.0001;%Diffusion coefficient
Rp=0.0045;%Resin particle radius
Kd=400; Desorption coefficient

%Experimental Conditions
Qin=40;%Total flowrate through annulus (ml/min)
Q=Qin/60;%Total flowrate through annulus (ml/s)
csin=58;%Concentration of solute entering annulus (mg/ml)
cpin=1.5;
trev=48;%Time taken for annulus to do one revolution (min)
W=360/(trev*60);%Rotation speed (degrees per second)

%Outer Dividing Plate Settings
AO0=0;%Angle for starting equilibration (degrees)
AO1=0;%Angle for starting loading (degrees)
AO2=45;%Angle for starting wash (degrees)
AO3=180;%Angle for starting elution (degrees)
AO4=225;%Angle for finishing elution (degrees)

%Inner Dividing Plate Settings
Ad=0;%Angle of inner plates clockwise relative to outer plates (degrees)
Ndiv=8;%Number of dividers for exit chamber


%Model Conditions
Nosw=6;%Number of stages in radial direction outer wall divided into
delrosw=oswt/Nosw;
N=40;%Number of stages in radial direction annulus divided into
delr=(r1-r2)/N;%Width of element in radial direction (cm)
Nisw=6;%Number of stages in radial direction inner wall divided into
delrisw=iswt/Nisw;
Nas=360;%Number of angular sections
dela=360/Nas;%change in angle
Qe=Q/Nas;%flow per element (ml/s)
delt=0.5;%(s)
Mrev=((trev.*60)./delt)
Nrev=8;
M=Nrev.*Mrev;
Mad=(Ad/360).*Mrev;
Msecwidth=Mrev/Ndiv;%Space between dividing plates (degrees)

%Starting Conditions
%Set everything in matrix to zero

%bed properties

for n=1;
   r(n)=r1+oswt;
end
for n=2:Nosw+1;
   r(n)=r1+oswt-((n-1).*delrosw);
   ve(n)=(pi.*((r(n-1).^2)-(r(n).^2)).*H)./Nas;
end
for n=Nosw+2:Nosw+N+1;
   r(n)=r1-((n-(Nosw+1)).*delr);
   ve(n)=(pi.*((r(n-1).^2)-(r(n).^2)).*H)./Nas;
end
```

```
for n=Nosw+N+2:Nosw+N+Nisw+1;
    r(n)=r2-((n-(Nosw+N+1)).*delrisw);
    ve(n)=(pi.*((r(n-1).^2)-(r(n).^2)).*H)./Nas;
end

%Calculate concentrations

for m=1;
  for n=1:Nosw+N+Nisw+1;
    cs(m,n)=0;
    crps(m,n)=0;
    crs(m,n)=0;
    cp(m,n)=0;
    crpp(m,n)=0;
    crp(m,n)=0;
  end
end

for m=2:M+1;
  for n=1;
    ar(m)=(m-1).*delt.*W;
    ap(m)=360.*(0.5+((atan(tan(((ar(m)./360).*pi)+(pi./2))))./pi));
    if (ap(m)>AO1 & ap(m)<=AO2);
      cp(m,n)=cpin;
    else
      cp(m,n)=0;
    end
    if (ap(m)>AO3 & ap(m)<=AO4);
      cs(m,n)=csin;
    else
      cs(m,n)=0;
    end

  end
  for n=2:Nosw+1;
    cs(m,n)=cs(m-1,n)+(((cs(m-1,n-1)-cs(m-1,n)).*Qe.*delt)./(ve(n).*esw));
    cp(m,n)=cp(m-1,n)+(((cp(m-1,n-1)-cp(m-1,n)).*Qe.*delt)./(ve(n).*esw));
  end
  for n=Nosw+2:Nosw+N+1;
    %NaCl concentration
    cs(m,n)=cs(m-1,n)+(((cs(m-1,n-1)-cs(m-1,n)).*Qe.*delt)./(ve(n).*er))-(3.*kfs.*(cs(m-1,n)-crps(m-
1,n)).*delt.*((1-er)./(Rp.*er)));
    crps(m,n)=crps(m-1,n)+(3.*kfs.*(cs(m-1,n)-crps(m-1,n)).*delt.*(1/(Rp.*ep)))-(ks1.*crps(m-
1,n).*(crsmax-crs(m-1,n)).*delt)+(ks2.*crs(m-1,n).*delt);
    crs(m,n)=crs(m-1,n)+(ep.*((ks1.*crps(m-1,n).*(crsmax-crs(m-1,n)).*delt)-(ks2.*crs(m-1,n).*delt)));
    %BSA concentration
    cp(m,n)=cp(m-1,n)+(((cp(m-1,n-1)-cp(m-1,n)).*Qe.*delt)./(ve(n).*er))-(3.*kfp.*(cp(m-1,n)-crpp(m-
1,n)).*delt.*((1-er)./(Rp.*er)));
    crpp(m,n)=crpp(m-1,n)+(3.*kfp.*(cp(m-1,n)-crpp(m-1,n)).*delt.*(1/(Rp.*ep)))-(kp1.*crpp(m-
1,n).*(crpmax-crp(m-1,n)).*delt)+(kp2.*(1+Kd.*(crps(m-1,n).^(1/ns))).*crp(m-1,n).*delt);
    crp(m,n)=crp(m-1,n)+(ep.*((kp1.*crpp(m-1,n).*(crpmax-crp(m-1,n)).*delt)-(kp2.*(1+Kd.*(crps(m-
1,n).^(1/ns))).*crp(m-1,n).*delt)));
  end
  for n=Nosw+N+2:Nosw+N+Nisw+1;
    cs(m,n)=cs(m-1,n)+(((cs(m-1,n-1)-cs(m-1,n)).*Qe.*delt)./(ve(n).*esw));
    cp(m,n)=cp(m-1,n)+(((cp(m-1,n-1)-cp(m-1,n)).*Qe.*delt)./(ve(n).*esw));
  end
end

Arev=(Nrev-1)*Mrev;
```

```
for d=1:Ndiv;
   secstart(d)=Arev+((d-1).*Msecwidth)-Mad+2;
   secfin(d)=Arev+((d).*Msecwidth)-Mad+1;
   cps(d)=mean(cp(secstart(d):secfin(d),Nosw+N+Nisw+1));
   ces(d)=mean(cs(secstart(d):secfin(d),Nosw+N+Nisw+1));
   fx(d,1)=d;
   fx(d,2)=cps(d);
   fx(d,3)=ces(d);
end

B=floor(M/10);

for i=1:B;
   ex(i,1)=(ar(i.*10)./360);
   ex(i,2)=cp((i.*10),Nosw+N+Nisw+1);
   ex(i,3)=cs((i.*10),Nosw+N+Nisw+1);
end

csvwrite('exlist.dat',ex);
csvwrite('fxlist.dat',fx);

figure;%creates a new figure
plot(cps);%produces graph of cps results
ylabel('Average Protein Concentration (mg/ml)');
xlabel('Section');
title('Average concentration of protein leaving each exit section');
```

Appendix I Additional Results

I.1 Fitting parameters to James and Do's (1991) adsorption equilibria data

Table I.1-1. Model parameters obtained by James and Do (1991).

Parameter	pH 8.1	pH 9.1
C_{RAmax} (mg/ml resin)	85.1	107.8
K_A (M^{-nA})	$4.7*10^5$	$1.2*10^8$
K_B (M^{-nB})	$2.3*10^3$	$8.1*10^4$
n_B	0.60	0.86
n_A	1.78	16.6

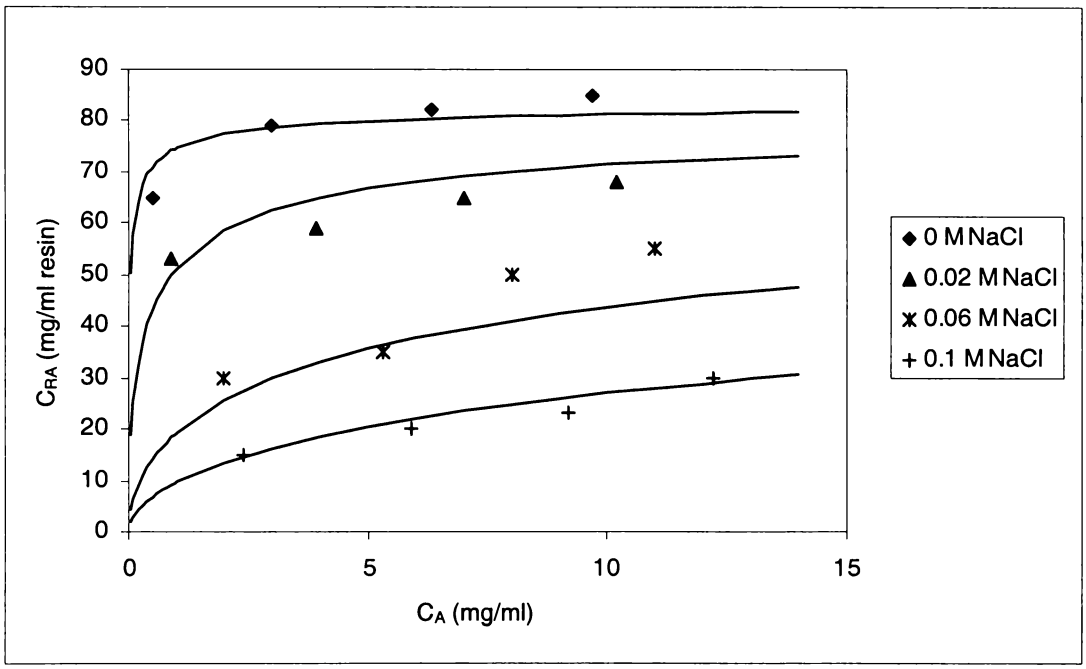

Figure I.1-1. Adsorption isotherm of BSA for DEAE Sepharose Fast Flow resin at a solution pH of 8.1. Model parameters were C_{RAmax} = 84 mg/ml resin, K_A = 8 ml/mg.s, K_B = 3.2 ml/mg.s, n_B = 0.6, and n_A = 1.78. Experimental data taken from James and Do (1991).

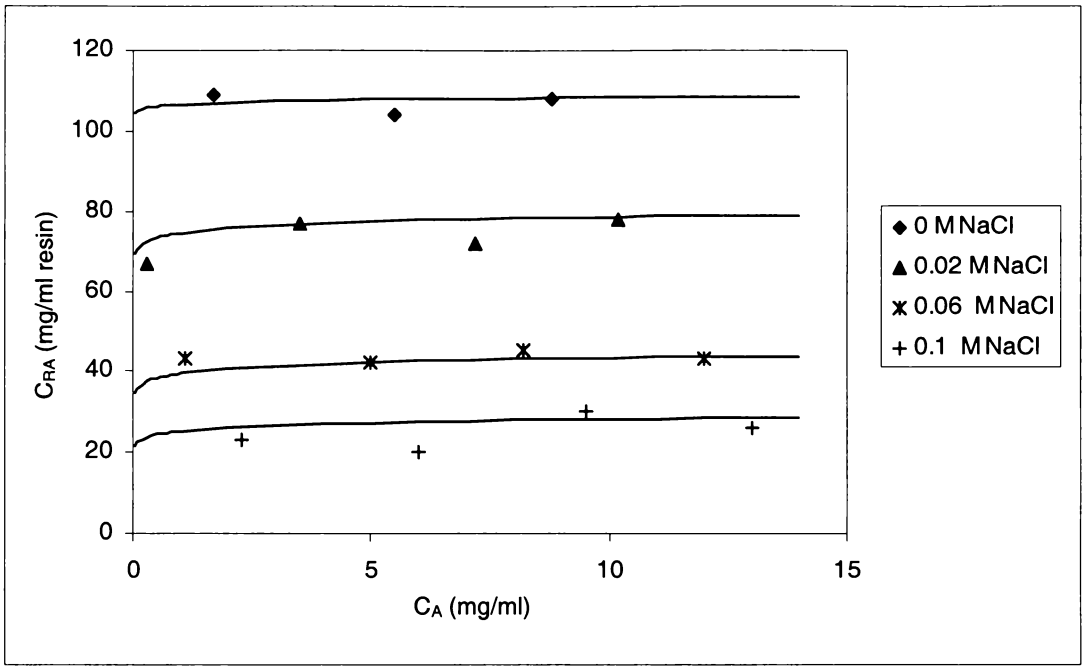

Figure I.1-2. Adsorption isotherm of BSA for DEAE Sepharose Fast Flow resin at a solution pH of 9.1. Model parameters were C_{RAmax} = 120.00 mg/ml resin, K_A = 8 ml/mg.s, K_B = 3.2 ml/mg.s, n_B = 0.8, and n_A = 16. Experimental data taken from James and Do (1991).

I.2 Uptake kinetics

Table I.2-1. k_{A1} parameters assuming a fixed resin capacity at saturation for fitting individual results from Figure 6-4. R^2 values are regression coefficients indicating goodness of fit.

Starting concentration (mg/ml)	k_{A1} (ml/mg.s)	C_{RAmax} (mg/ml)	R^2
1.07	1.30E-04	86	1
1.49	1.10E-04	86	1
1.74	9.00E-05	86	1
2.00	8.40E-05	86	1
2.25	1.30E-04	86	1
2.47	8.40E-05	86	1

Table I.2-2. k_{fA} parameters for each starting concentration.

Starting feed concentration (mg/ml)	k_{fA} (cm/s)
1.07	3.00E-03
1.49	1.00E-03
1.74	8.00E-04
2	5.00E-04
2.25	8.00E-04
2.47	4.00E-04

I.3 AKTAexplorer100 set-up

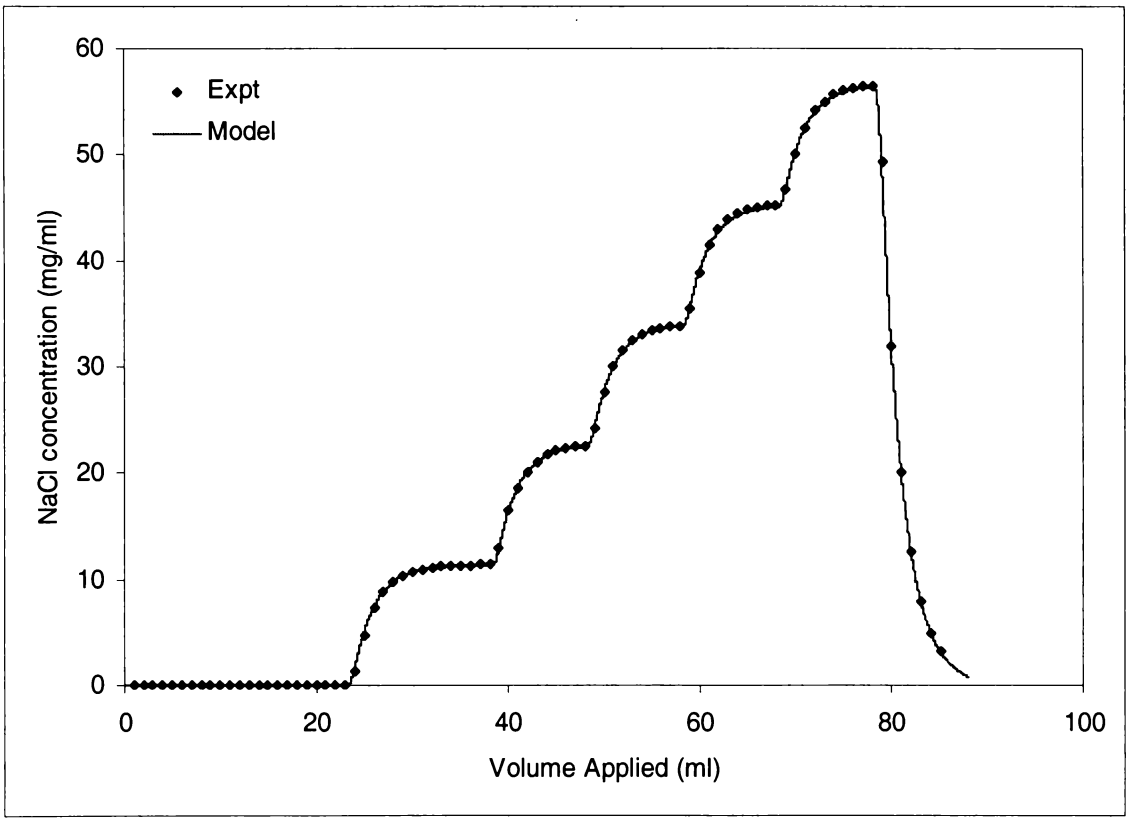

Figure I.3-1. Concentration profile from Akta using gradient mixer and solutions from primary pumps. Solution used was 1M NaCl in 0.02M Tris pH 7.

I.4 Small column breakthrough

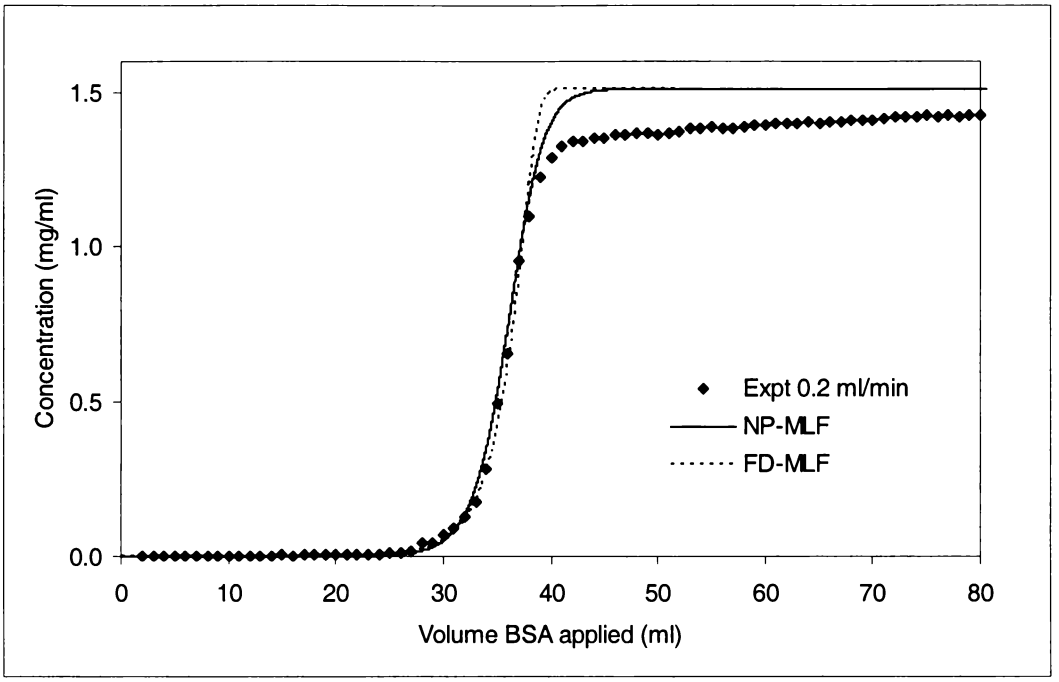

Figure I.4-1. Breakthrough curve for 1ml DEAE Sepharose FF Hitrap column for a flowrate of 0.2 ml/min. Model parameters shown in Table I.4-2 and I.4-3.

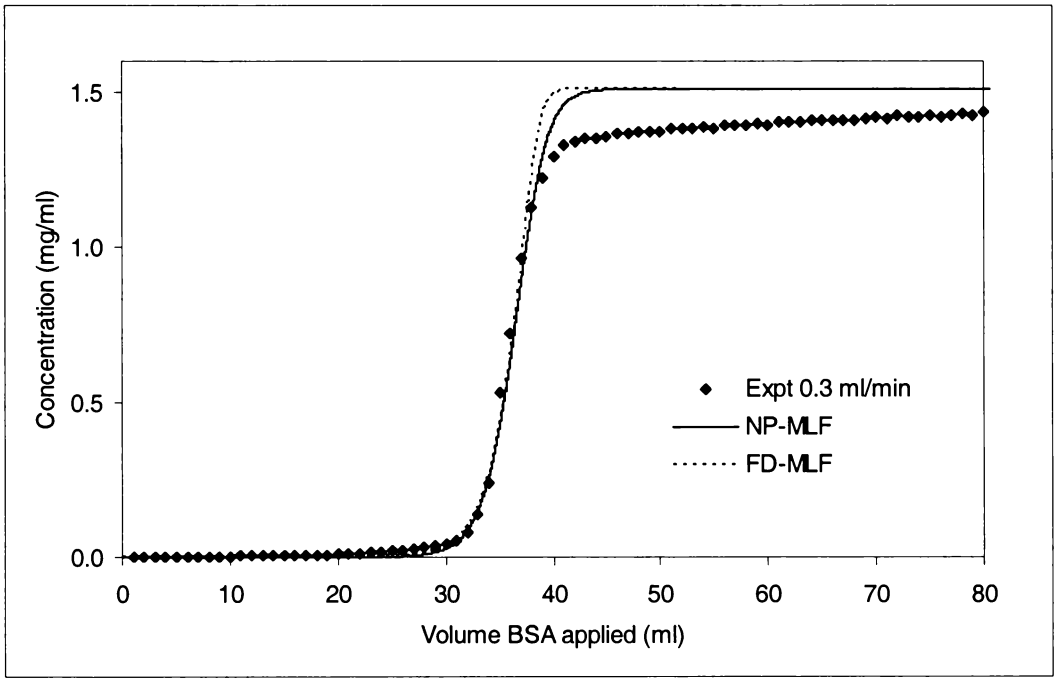

Figure I.4-2. Breakthrough curve for 1ml DEAE Sepharose FF Hitrap column for a flowrate of 0.3 ml/min. Model parameters shown in Table I.4-2 and I.4-3.

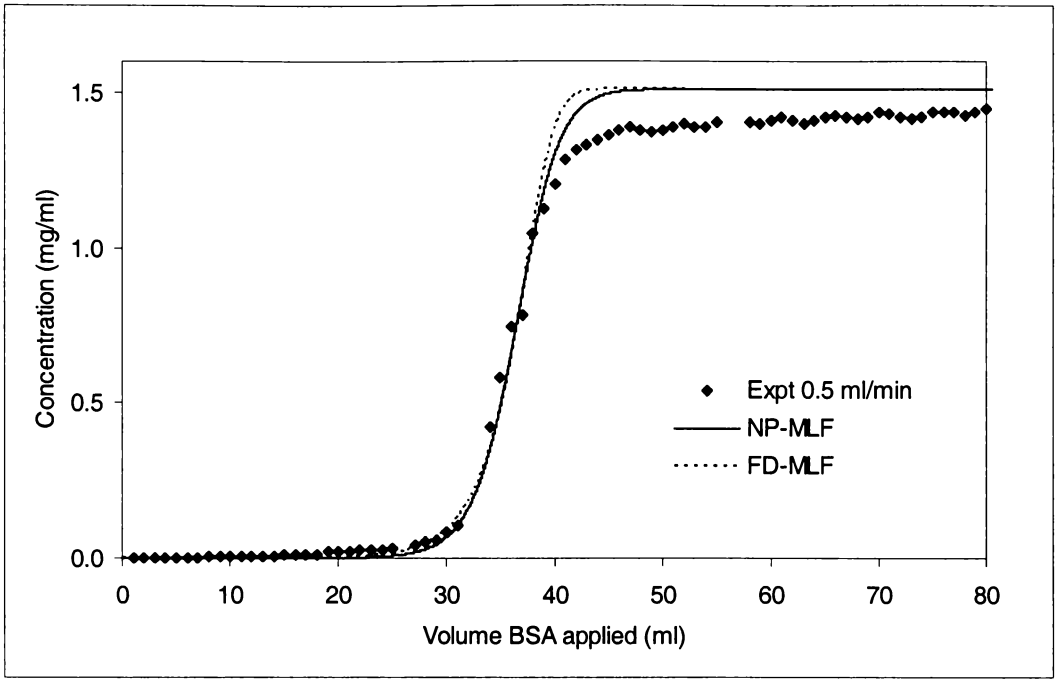

Figure I.4-3. Breakthrough curve for 1ml DEAE Sepharose FF Hitrap column for a flowrate of 0.5ml/min. Model parameters shown in Table I.4-2 and I.4-3.

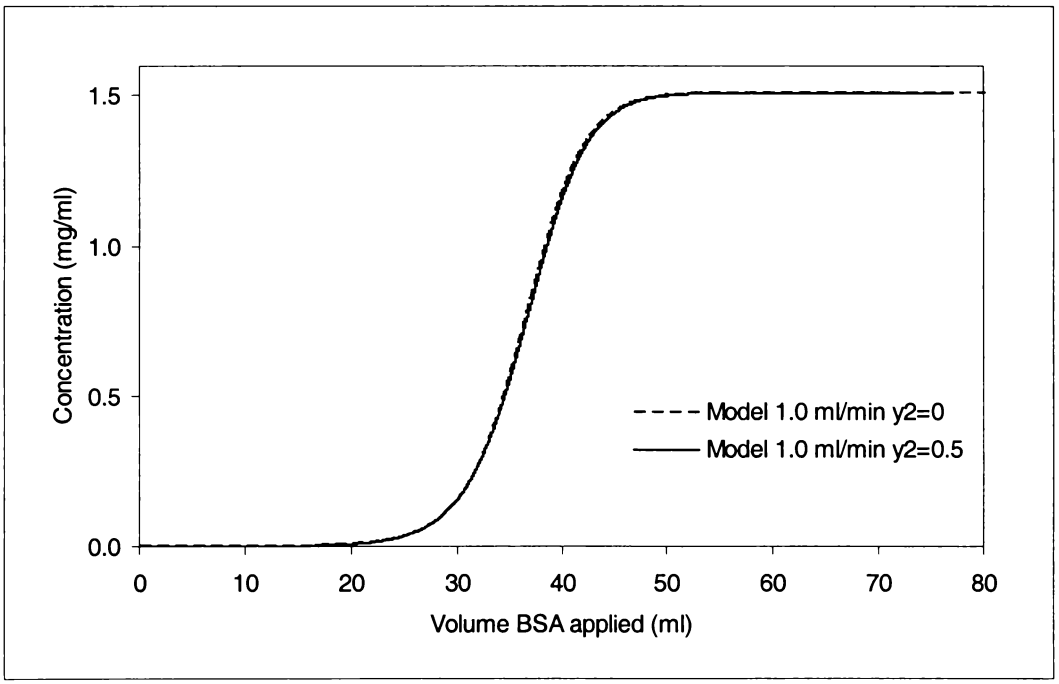

Figure I.4-4. Model results for breakthrough curves at flowrate of 1ml/min at y_2=0 and y_2=0.5, J=3. Parameters shown in Table I.4-2.

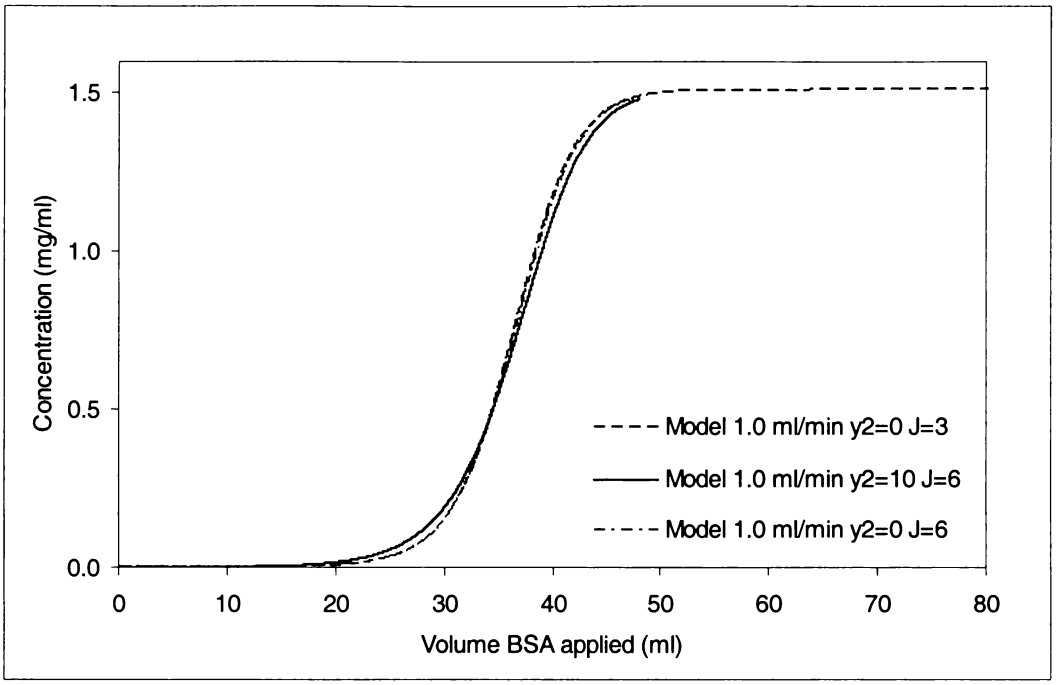

Figure I.4-5. Model results for breakthrough curves at flowrate of 1ml/min at y_2=0, J=3; y_2=0, J=6; and y_2=10, J=6. Parameters shown in Table I.4-2.

Table I.4-1. Parameters used for the calculation of k_{ext} and k_{fA}.

Parameter	Value
D_m BSA (m²/s)	6.11E-11
η (kg/(m*s))	9.82E-04
ρ (kg/m³)	1.00E+03
ε_R	0.31
ε_p	0.72
d_p (m)	9.00E-05
ID column (m)	7.00E-03
Cross sectional area (m2)	3.85E-05

Table I.4-2. Parameters used for fitting the NP-MLF model curves to breakthrough results.

Flowrate (ml/min)	Feed concentration (mg/ml)	C_{RAmax} (mg/ml resin)	K_A (ml/mg)	k_{A1} (ml/mg.s)	k_{A2} (1/s)	n_A	n_{stages}	Time divider J	Δt (s)
0.1	1.51	73	47	3.00E-03	6.38E-05	1	30	3	2
0.2	1.51	71	47	3.50E-03	7.45E-05	1	30	3	1
0.3	1.51	72	47	6.00E-03	1.28E-04	1	30	3	0.66
0.5	1.51	72	47	7.00E-03	1.49E-04	1	30	3	0.4
1	1.51	72	47	9.50E-03	2.02E-04	1	30	3	0.2

Table I.4-3. Parameters used for fitting the FD-MLF model curves to breakthrough results.

Flowrate (ml/min)	Feed concentration (mg/ml)	C_{RAmax} (mg/ml resin)	k_{fA} (cm/s)	K_A (ml/mg)	k_{A1} (ml/mg.s)	k_{A2} (1/s)	n_A	n_{stages}	Time divider J	Δt (s)
0.1	1.51	71	0.00012	47	0.0085	0.000181	1	30	3	2
0.2	1.51	70	0.00016	47	0.0085	0.000181	1	30	3	1
0.3	1.51	70	0.00035	47	0.0085	0.000181	1	30	3	0.66
0.5	1.51	70	0.0004	47	0.0085	0.000181	1	30	3	0.4
1	1.51	70	0.0012	47	0.0085	0.000181	1	30	3	0.2

I.5 Elution experiments

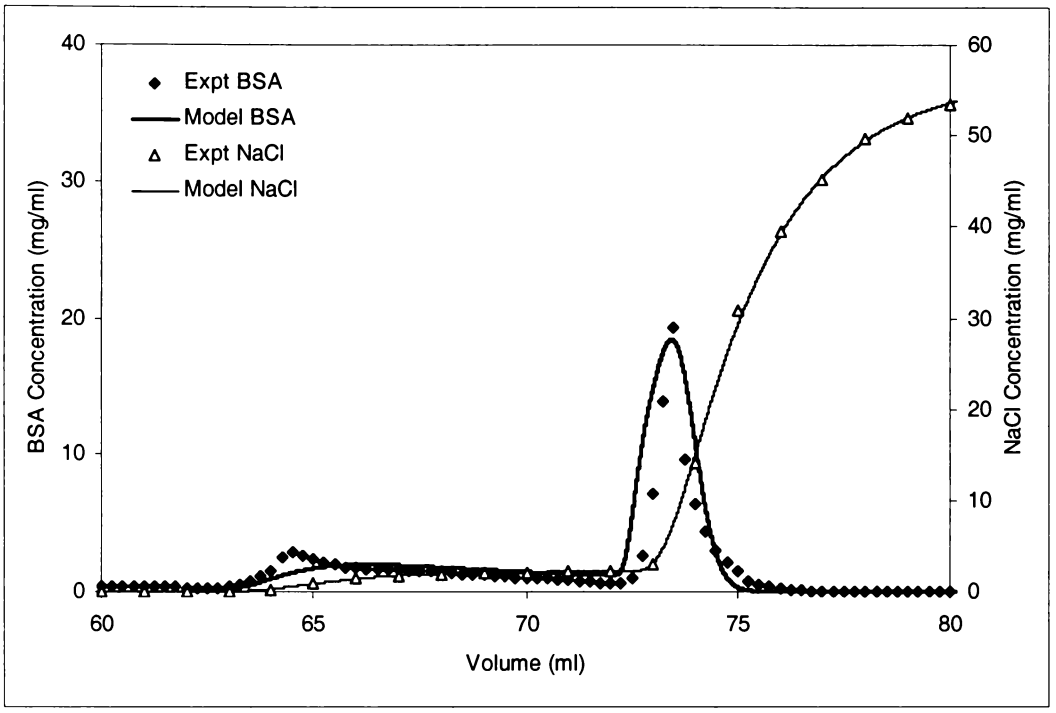

Figure I.5-1. Elution profiles at 0.04M NaCl for the first step in elution and 1M NaCl for the second step. Parameters shown in Table 6-5.

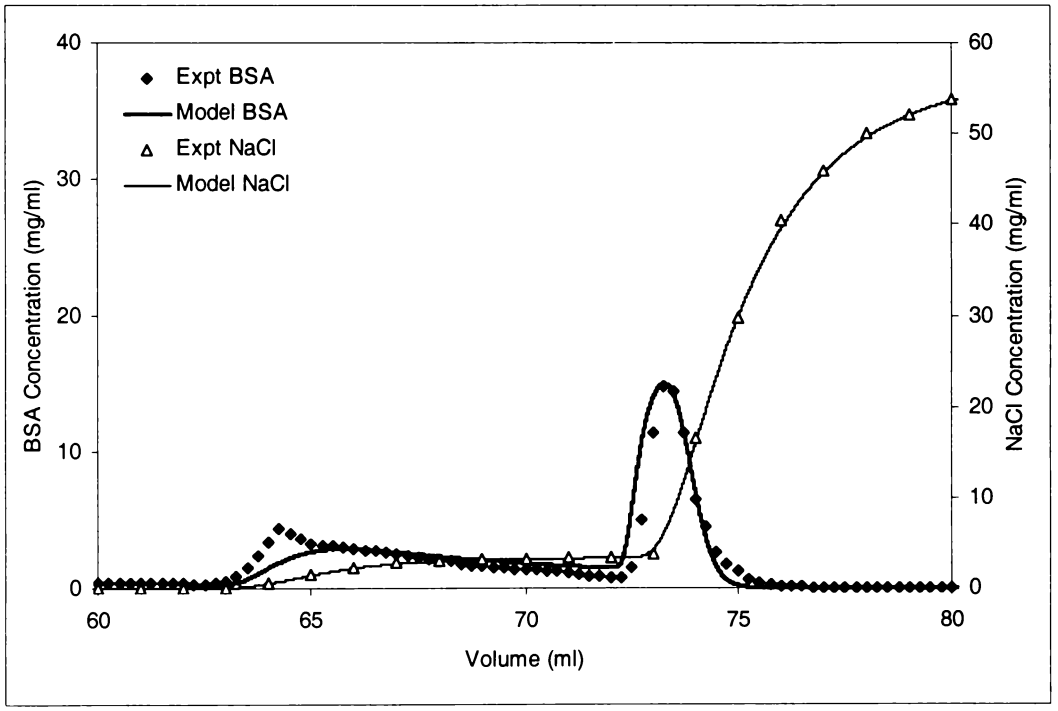

Figure I.5-2. Elution profiles at 0.06M NaCl for the first step in elution and 1M NaCl for the second step. Parameters shown in Table 6-5.

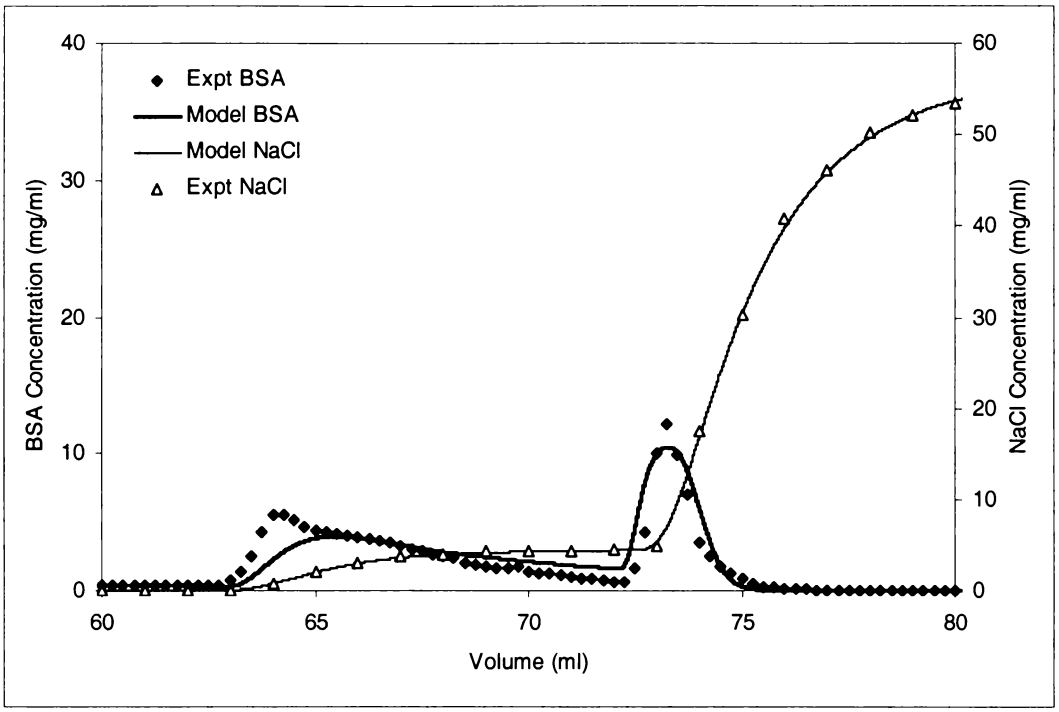

Figure I.5-3. Elution profiles at 0.08M NaCl for the first step in elution and 1M NaCl for the second step. Parameters shown in Table 6-5.

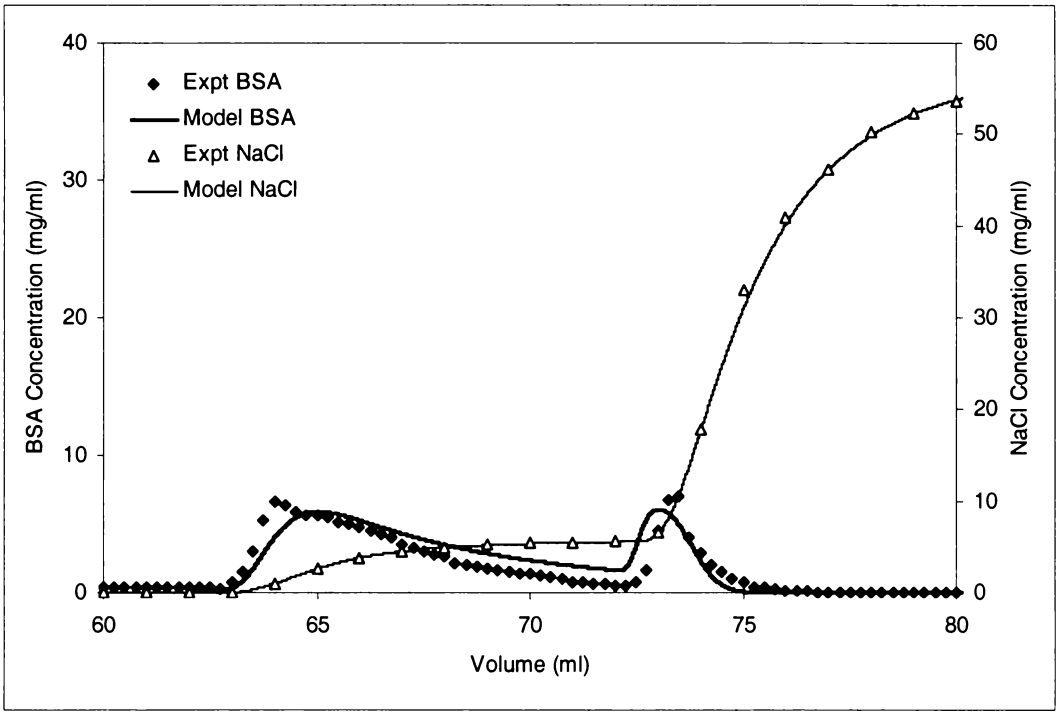

Figure I.5-4. Elution profiles at 0.1M NaCl for the first step in elution and 1M NaCl for the second step. Parameters shown in Table 6-5.

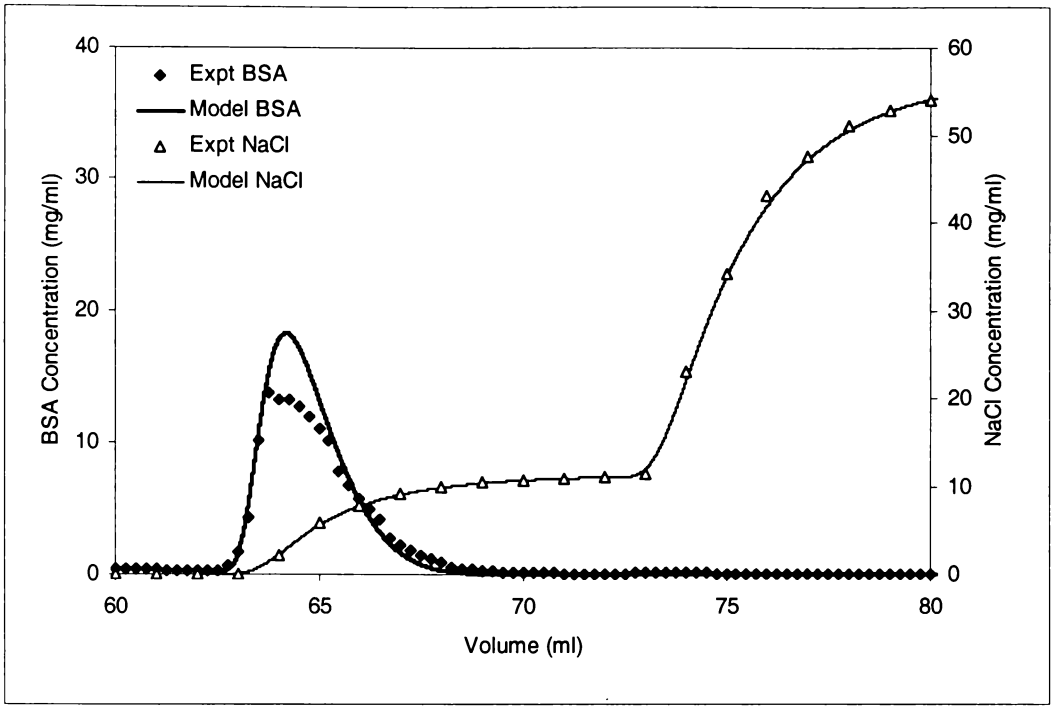

Figure I.5-5. Elution profiles at 0.2M NaCl for the first step in elution and 1M NaCl for the second step. Parameters shown in Table 6-5.

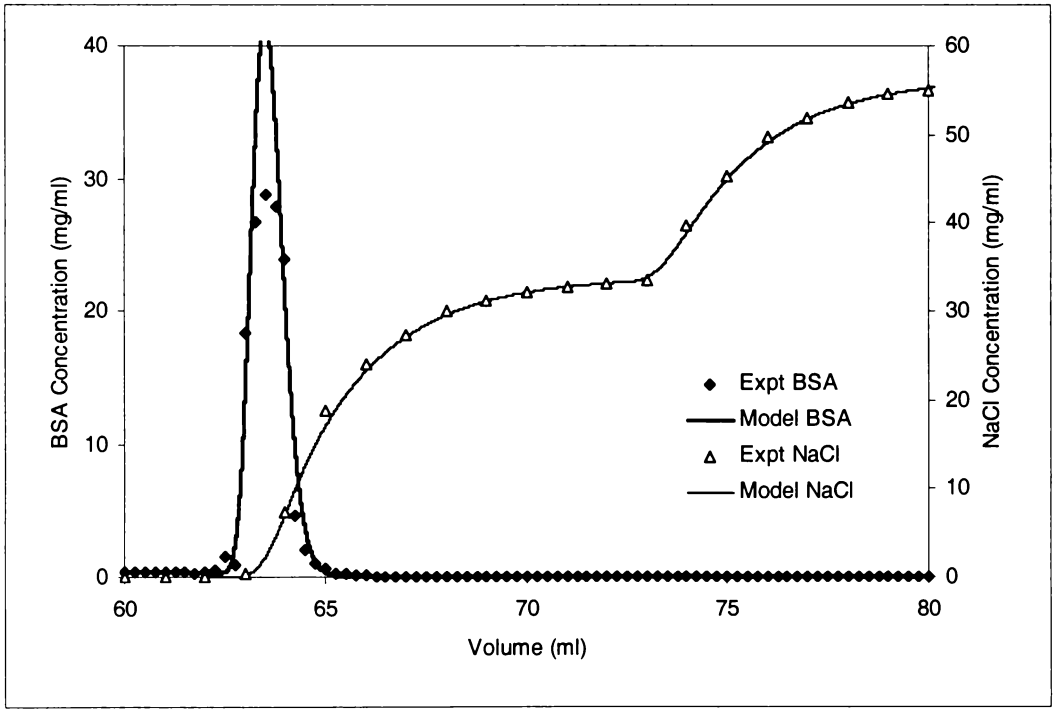

Figure I.5-6. Elution profiles at 0.6M NaCl for the first step in elution and 1M NaCl for the second step. Parameters shown in Table 6-5.

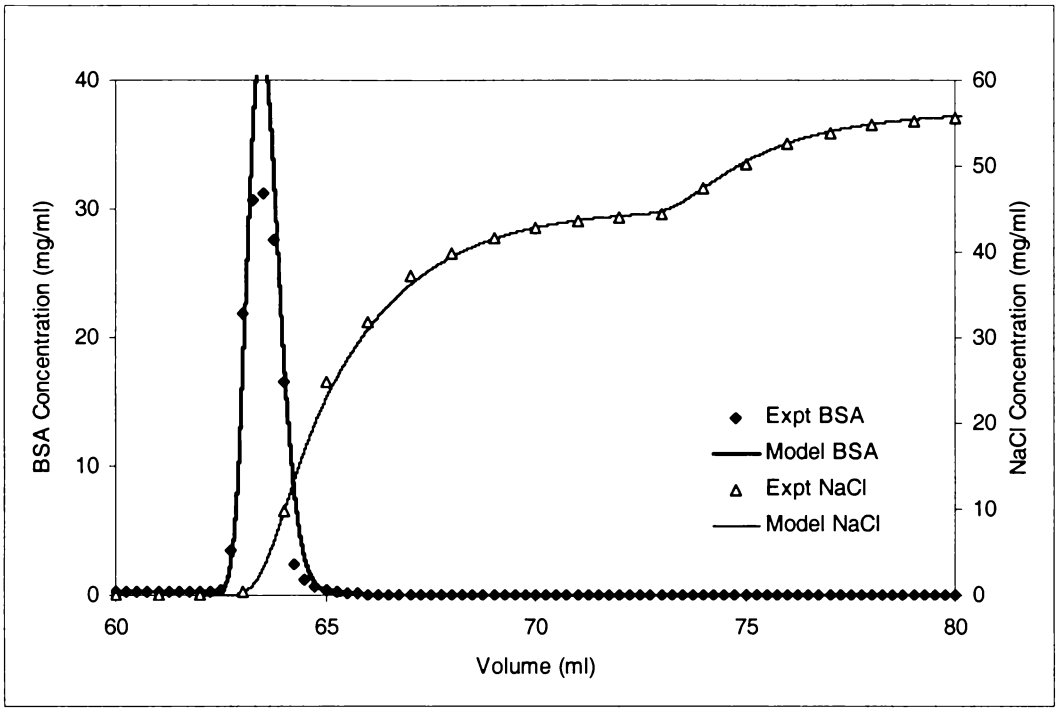

Figure I.5-7. Elution profiles at 0.8M NaCl for the first step in elution and 1M NaCl for the second step. Parameters shown in Table 6-5.

Table I.5-1. Desorption parameters at different salt concentrations using $n_B = 0.4$.

Dilution	NaCl concentration C_B (mg/ml)	C_{RPB}^{1/n_B} (mg/ml)	$k_{A2(eff)}$ (ml/mg.s)
0.02	1.13	1.35E+00	3.85E-03
0.04	2.26	7.64E+00	2.09E-02
0.06	3.38	2.11E+01	5.73E-02
0.08	4.51	4.32E+01	1.17E-01
0.10	5.64	7.55E+01	2.05E-01
0.20	11.28	4.27E+02	1.16E+00
0.40	22.56	2.42E+03	6.56E+00
0.60	33.84	6.66E+03	1.81E+01
0.80	45.12	1.37E+04	3.71E+01
1.00	56.4	2.39E+04	6.48E+01

I.6 Batch radial flow results

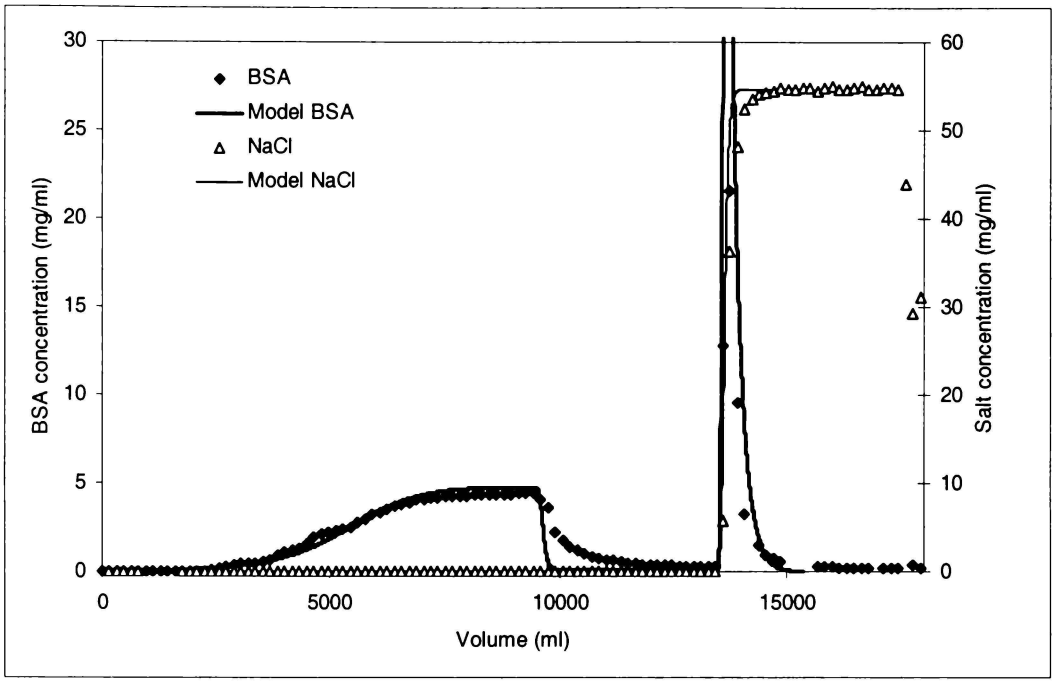

Figure I.6-1. Breakthrough and elution profile for feed concentration of 4.5 mg/ml and 20 ml/min (Column 1 of Table 6-7).

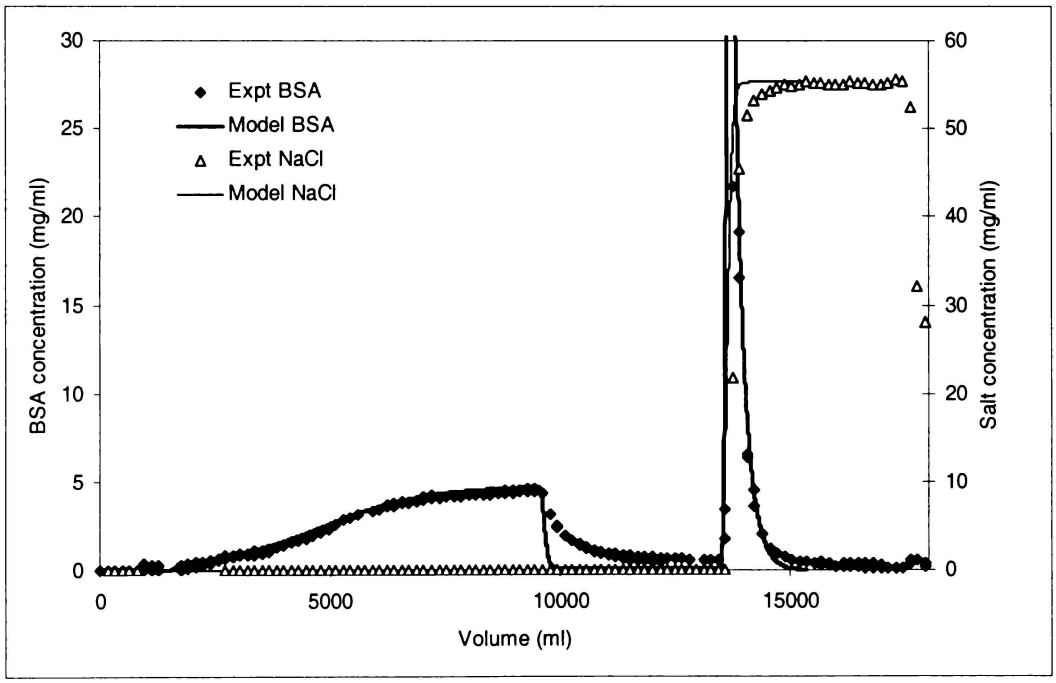

Figure I.6-2. Breakthrough and elution profile for feed concentration of 4.5 mg/ml and 80 ml/min (Column 3 of Table 6-7).

I.7 Model comparisons for single component continuous extraction

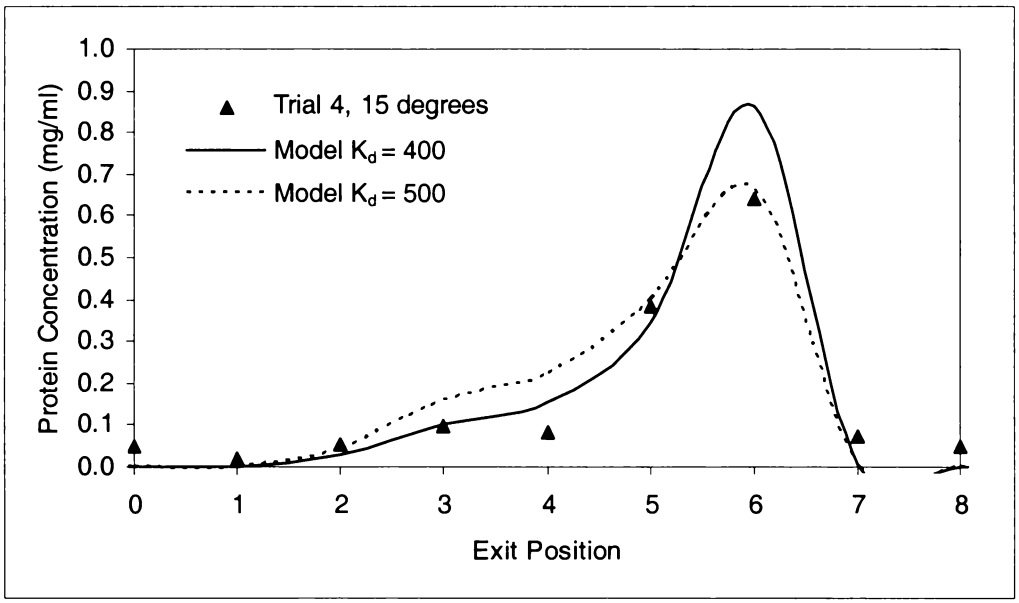

Figure I.7-1. Comparison of model results to experimental results for the BSA elution profile for a rotation speed of 48 min/rev and 15 degree outer plate angle, ε_p = 0.72. Model parameters given in Table 6-13.

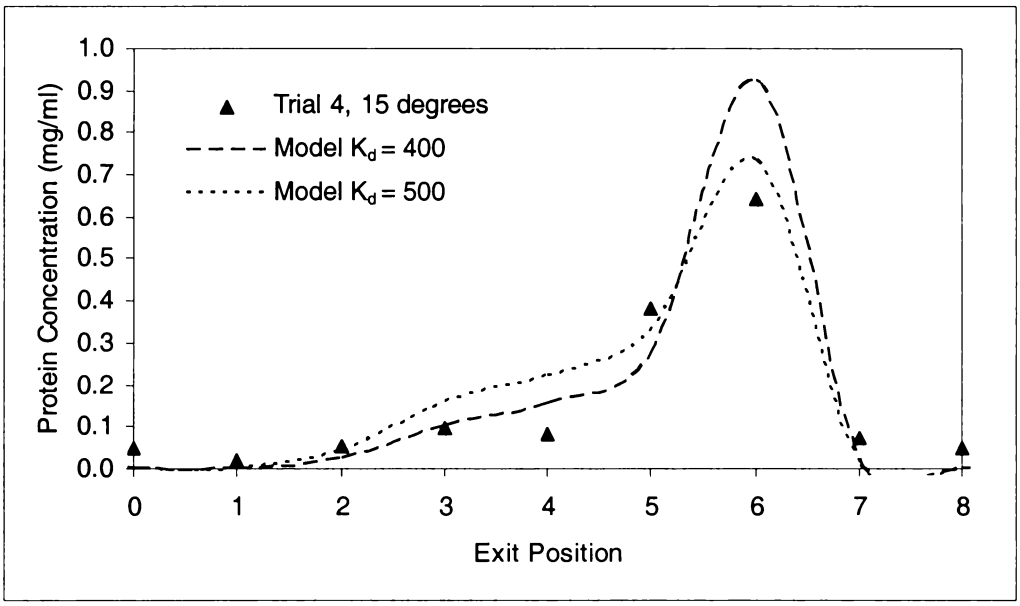

Figure I.7-2. Comparison of model results to experimental results for the BSA elution profile for a rotation speed of 48 min/rev and 15 degree outer plate angle, ε_p = 0.9. Model parameters given in Table 6-13.

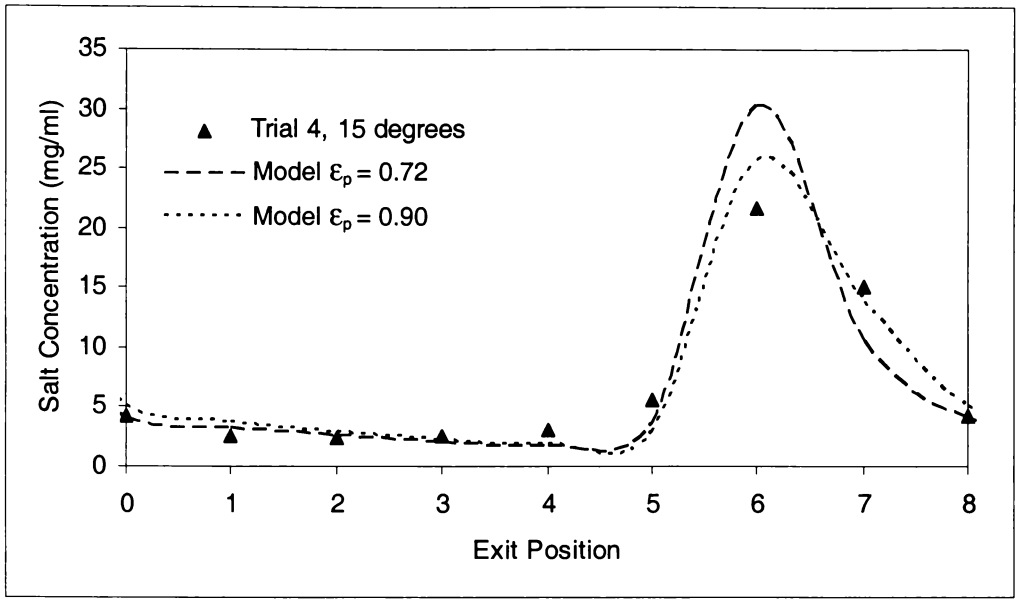

Figure I.7-3. Comparison of model results to experimental results for the NaCl elution profile for a rotation speed of 48 min/rev and 15 degree outer plate angle, ε_p = 0.72 and 0.9. Model parameters given in Table 6-13.

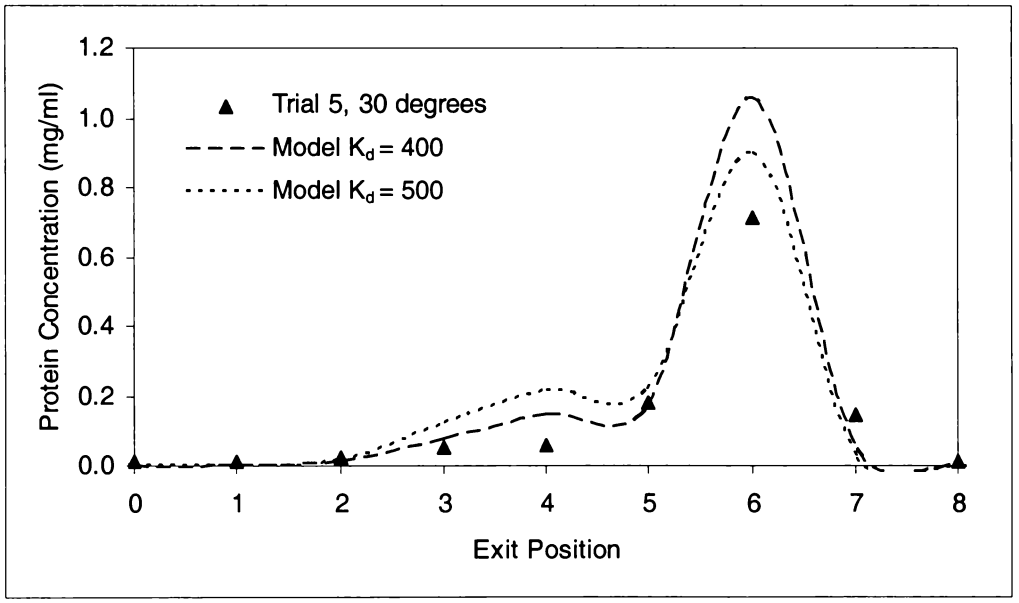

Figure I.7-4. Comparison of model results to experimental results for the BSA elution profile for a rotation speed of 48 min/rev and 30 degree outer plate angle, ε_p = 0.72. Model parameters given in Table 6-13.

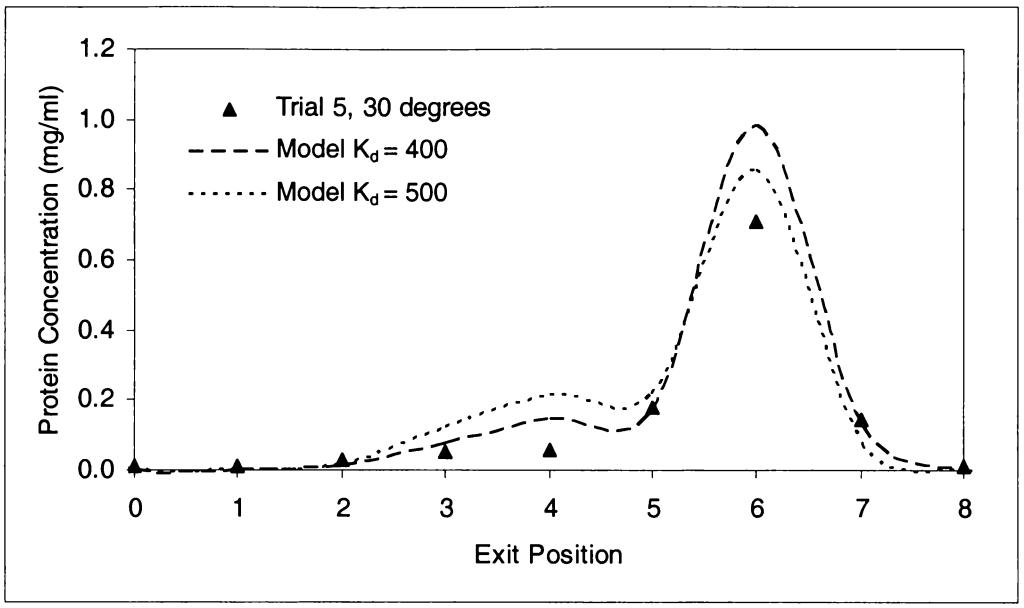

Figure I.7-5. Comparison of model results to experimental results for the BSA elution profile for a rotation speed of 48 min/rev and 30 degree outer plate angle, ε_p = 0.9. Model parameters given in Table 6-13.

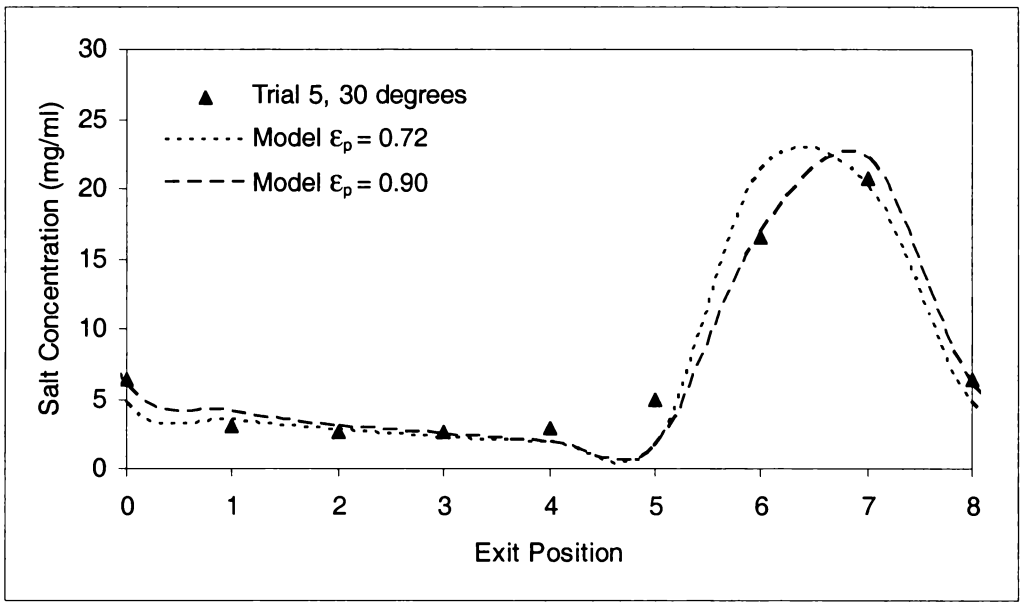

Figure I.7-6. Comparison of model results to experimental results for the NaCl elution profile for a rotation speed of 48 min/rev and 30 degree outer plate angle, ε_p = 0.72 and 0.9. Model parameters given in Table 6-13.

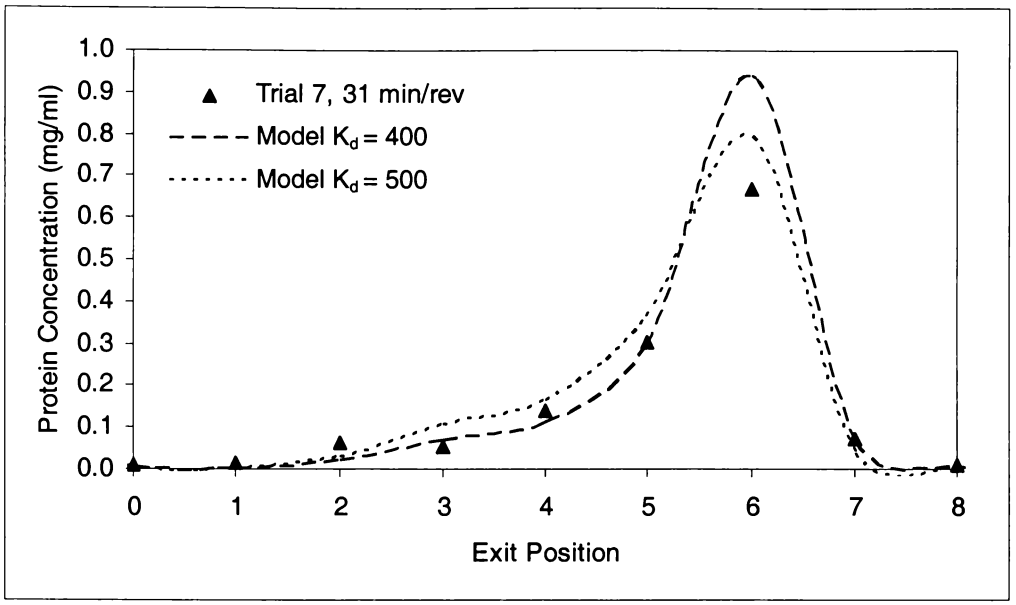

Figure I.7-7. Comparison of model results to experimental results for the BSA elution profile for a rotation speed of 31 min/rev and 0 degree outer plate angle, ε_p = 0.72. Model parameters given in Table 6-13.

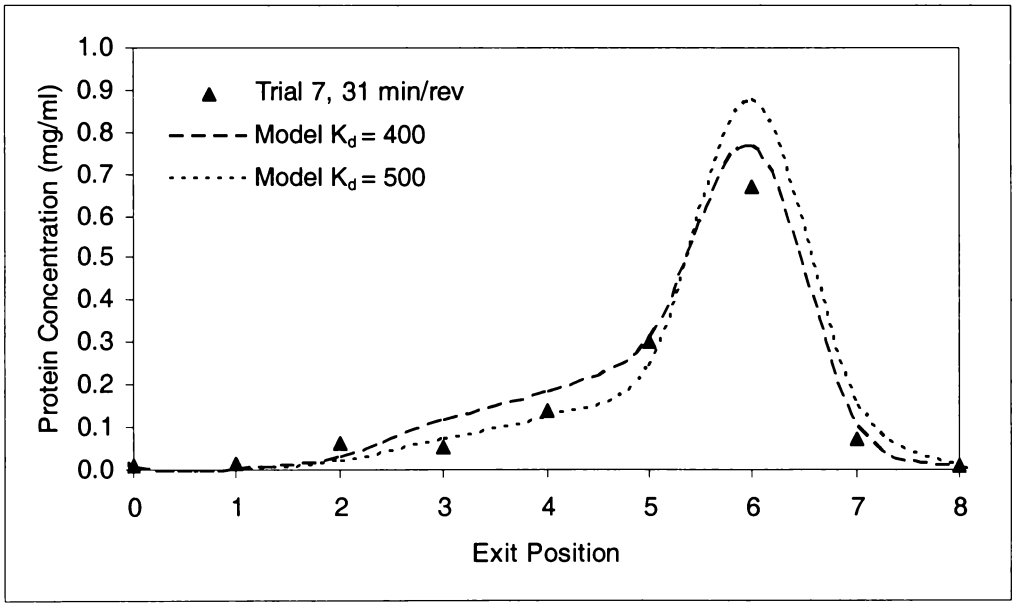

Figure I.7-8. Comparison of model results to experimental results for the BSA elution profile for a rotation speed of 31 min/rev and 0 degree outer plate angle, ε_p = 0.9. Model parameters given in Table 6-13.

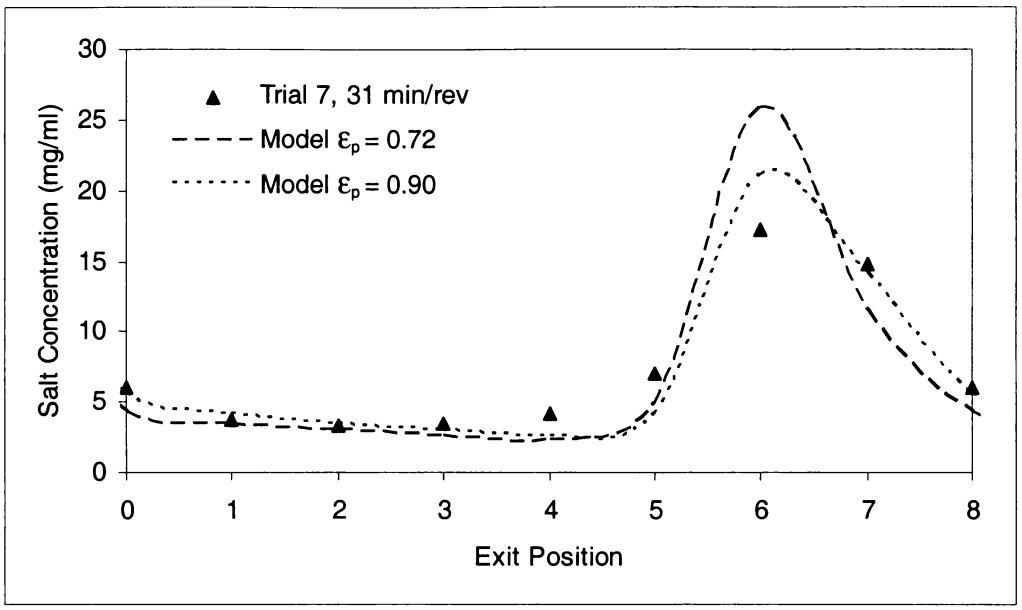

Figure I.7-9. Comparison of model results to experimental results for the NaCl elution profile for a rotation speed of 31 min/rev and 0 degree outer plate angle, ε_p = 0.72 and 0.9. Model parameters given in Table 6-13.

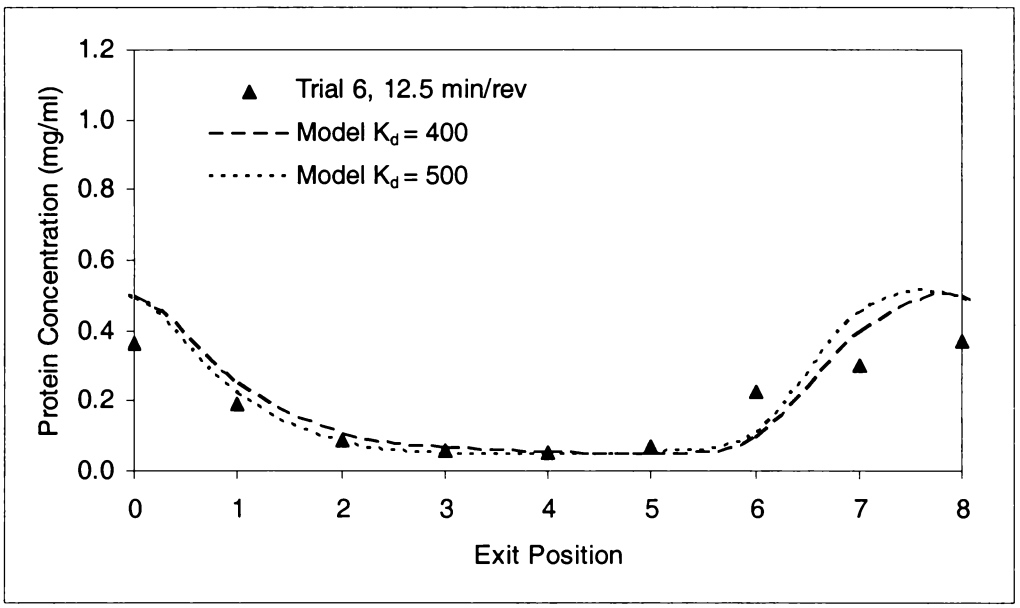

Figure I.7-10. Comparison of model results to experimental results for the BSA elution profile for a rotation speed of 12.5 min/rev and 0 degree outer plate angle, ε_p = 0.72. Model parameters given in Table 6-13.

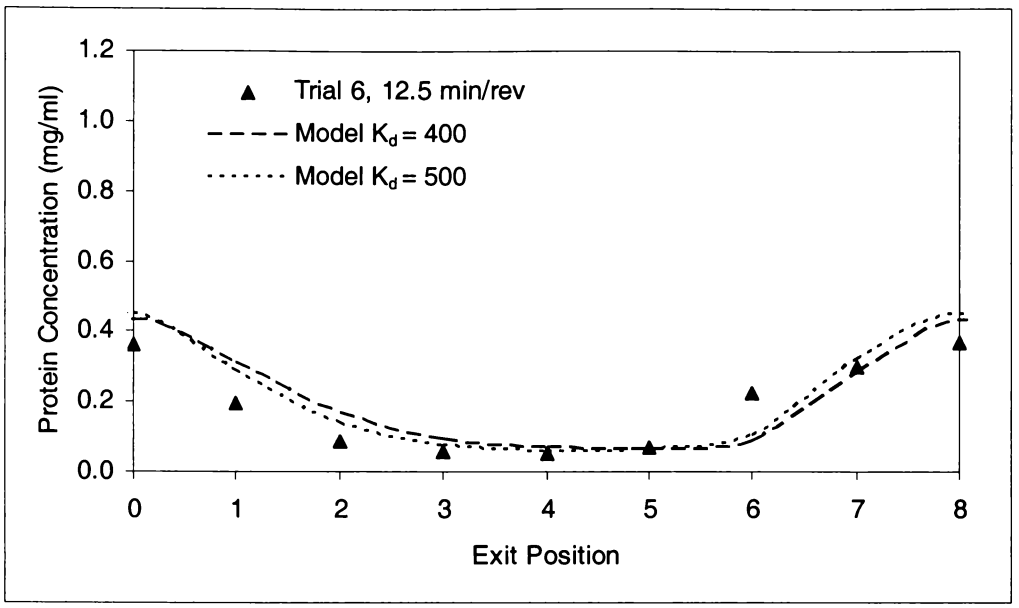

Figure I.7-11. Comparison of model results to experimental results for the BSA elution profile for a rotation speed of 12.5 min/rev and 0 degree outer plate angle, ε_p = 0.9. Model parameters given in Table 6-13.

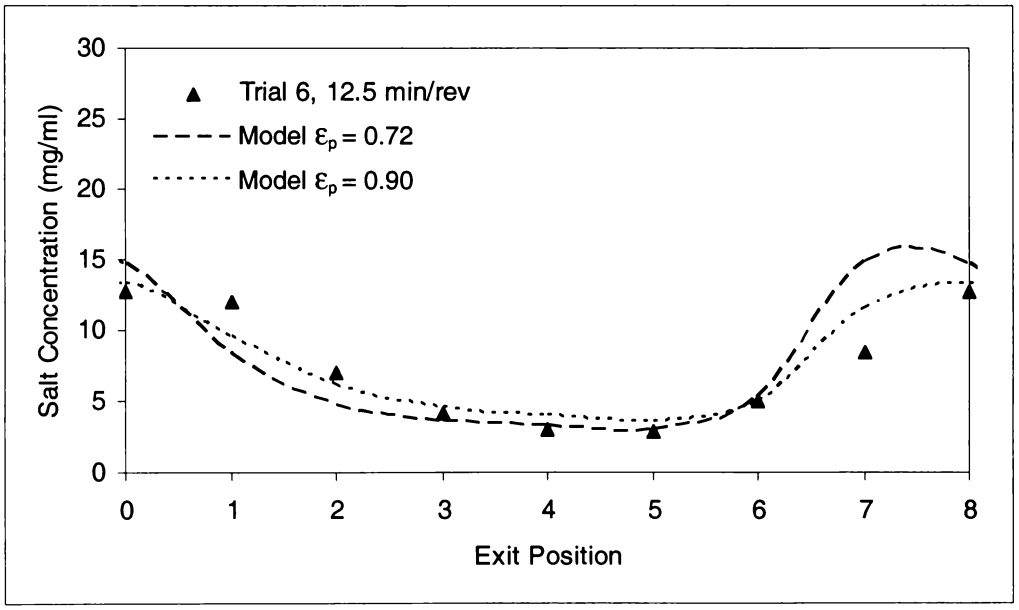

Figure I.7-12. Comparison of model results to experimental results for the NaCl elution profile for a rotation speed of 12.5 min/rev and 0 degree outer plate angle, ε_p = 0.72 and 0.9. Model parameters given in Table 6-13.

Appendix J Outer Feed Chamber Section Model

An outer feed chamber section is divided into N stages in the angular direction. N is chosen so

$$\frac{(N-1)}{2} = \text{integer} \tag{209}$$

Each stage has the same volume V_s given by

$$V_s = \frac{\pi\left(\left(r_1 + T_{osw} + T_{ofc}\right)^2 - \left(r_1 + T_{osw}\right)^2\right)H - V_{div}}{N} \tag{210}$$

V_{div} is volume occupied by the section divider. Feed is introduced at $n = \frac{(N-1)}{2} + 1$ at concentration C_{feed}. Flow goes towards n = 1 and n = N from $n = \frac{(N-1)}{2} + 1$. Each stage has one flow input (Q_{in}) and two flow outputs (Q_{out} and $Q_{annulus}$) except for the feed stage which has one input $Q_{section}$ and three outputs ($2Q_{out}$ and $Q_{annulus}$).

Flow from each stage to the annulus $Q_{annulus}$ is given by

$$Q_{annulus} = \frac{Q_{section}}{N} \tag{211}$$

Concentrations for time step m are calculated by

for $$2 \le m \le M \ , \ 1 \le n \le \frac{(N-1)}{2}$$

$$Q_{in}\big|_n = \frac{\left(Q_{section} - Q_{annulus}\right)}{2} - \left(\frac{(N-1)}{2} - n\right)Q_{annulus} \tag{212}$$

$$Q_{out}\big|_n = Q_{in}\big|_n - Q_{annulus} \tag{213}$$

$$C_A\big|_{n,m} = C_A\big|_{n,m-1} + \frac{Q_{in}\big|_n C_A\big|_{n+1,m-1} - \left(Q_{annulus} + Q_{out}\big|_n\right) C_A\big|_{n,m-1}}{V_s}\Delta t \tag{214}$$

for $$n = \frac{(N-1)}{2} + 1$$

$$Q_{out}\big|_n = Q_{section} - Q_{annulus} \tag{215}$$

$$C_A\big|_{n,m} = C_A\big|_{n,m-1} + \frac{Q_{section} C_{feed} - \left(Q_{annulus} + Q_{out}\big|_n\right) C_A\big|_{n,m-1}}{V_s}\Delta t \tag{216}$$

for $$\frac{(N-1)}{2} + 2 \le n \le N$$

$$Q_{in}\big|_n = \frac{\left(Q_{section} - Q_{annulus}\right)}{2} - \left(n - \frac{(N-1)}{2} - 2\right) Q_{annulus} \tag{217}$$

$$Q_{out}\big|_n = Q_{in}\big|_n - Q_{annulus} \tag{218}$$

$$C_A\big|_{n,m} = C_A\big|_{n,m-1} + \frac{Q_{in}\big|_n C_A\big|_{n-1,m-1} - \left(Q_{annulus} + Q_{out}\big|_n\right) C_A\big|_{n,m-1}}{V_s}\Delta t \tag{219}$$

Simulation steps M is given by

$$M = \frac{t_{run}}{\Delta t} \tag{220}$$

Time is given by

$$t\big|_m = (m-1)\Delta t \tag{221}$$

Boundary conditions are

for $$m=1,\ 1 \le n \le N,\ C_A\big|_n = 0 \tag{222}$$